SYNTHESES AND PHOTOPHYSICAL STUDIES OF NEUTRAL GOLD COMPLEXES FOR POTENTIAL APPLICATIONS IN LIGHT EMITTING DEVICES

DISSERTATION

zur

Erlangung der natturwissenschaftlichen Doktorwürde

(Dr. sc. nat.)

Vorgelegt der

Mathematisch- natturwissenschaftlichen Fakultät

der

Universität Zürich

von

N. JAI ANAND GARG

aus

Indien

Promotionskomitee

Prof. Dr. Heinz Berke (Vorsitz)

Dr. Koushik Venkatesan (Leitung)

Prof. Dr. Roger Alberto

Zürich 2012

TABLE OF CONTENTS

LIST OF ABBREVIATIONS

2-MeTHF	2-methyltetrahydrofuran
B3LYP	Becke-Lee-Yang-Parr hybrid functional
C.N.	coordination number
CT	charge transfer
CV	cyclic voltammetry
DCM	dichloromethane
DFT	density function theory
DMF	*N*,*N*-dimethylformamide
DMSO	dimethylsulfoxide
DIPA	diisopropylamine
ESI-MS	electrospray ionization mass spectroscopy
GC	gas chromatography
HOMO	highest occupied molecular orbital
HRMS	high resolution mass spectroscopy
ILCT	intra ligand charge transfer
IR	infrared (spectroscopy)
LCD	liquid-crystal display
LF	ligand field
LMCT	ligand-to-metal charge transfer
LUMO	lowest unoccupied molecular orbital
MC	metal centered
MLCT	metal-to-ligand charge transfer
MMCT	metal-to-metal charge tansfer
MO	molecular orbital
NHC	*N*-heterocyclic carbene
NMR	nuclear magnetic resonance
NOE	nuclear Overhauser effect (spectroscopy)

OLED	organic light-emitting device
PMMA	poly(methyl methacrylate)
QY	quantum yield
ref.	reference
RT (or r.t.)	room temperature (20-25°C)
RTP	room temperature phosphoresecnce
SOC	spin-orbit coupling
SOMO	singly occupied molecular orbital
TCSPC	time correlated single photon counting
TD-DFT	time dependent density function theory
TGA	thermogravimetric analysis
THF	tetrahydrofuran
TIPS	triisopropylsilyl
TLC	thin layer chromatography
TMS	trimethylsilyl
TMSA	trimethylsilylacetylene
UV-vis	ultraviolet-visible (spectroscopy)
XRD	X-ray diffraction

Chapter 1. Introduction

1.0 Overview of Dissertation

The following report represents the part of the work done by the author during the course of his doctoral studies in the ACI, University of Zürich. Within this compilation of studies, some of them have been published and some have been submitted for publication in peer-reviewed scientific journals. The current chapter (Chapter 1) provides an introductory background to the rest of the chapters. Section 2.0 of this chapter presents a general introduction about the various photophysical aspects of organo-transition metal complexes. The following section (Section 3.0) explains in a rough chronological order, the evolution of various synthetic methodologies and certain subtler aspects of gold chemistry relevant to the authors work in the dissertation. It also provides sufficient insight into the photophysical attributes of Au(I) and Au(III) complexes and the state-of-art of the research in this area. The chapter ends with delineating the motivation and formulation of goals for the thesis. In addition to this introductory chapter, more specific literature support is provided in the beginning of all the chapters. Chapter 2, 3 and 4 comprises of the authors publication 1, 2 and 3 respectively. Chapters 2 and 3 deals with a new class of neutral (C^N) cyclometalated Au(III) diaryl and dialkynyl compexes respectively and their detailed photophysical and theoretical evaluation (DFT studies). In Chapter 4, a systematic study on the various photophysical aspects of σ-alkynyl Au(I) *N*-heterocyclic carbenes complexes is presented. Chapter 5 explores synthetic routes for the construction of non-cyclometalated (N^N) ligated Au(III) dihalide and diaryl complexes and attempts to examine the non-luminescent behavior of some of the synthesized compounds. Based on the knowledge obtained from Chapter 4, synthesis of Au(I) alkynyl complexes with sterically demanding *N*-heterocyclic carbene ligands suitable as monomers for the construction of conjugated polymers is presented in Chapter 6. In Chapter 7, the photoluminescence (PL) behavior of β-Iminoenamine boron difluoride complexes has been explored. A part of this work has been submitted for publication. Unpublished results pertaining to the published chapters (2, 3 and 4) are included in their corresponding appendix sections. The summary section gives in a nut shell the various targets and achievements accomplished during the course of dissertation.

2.0 General overview: Light emission in organo transition-metal complexes.

Light emitting devices a historical perspective.

Sustainable energy is undoubtedly of imminent necessity today. In order to achieve this goal, one needs to minimize the energy requirements of the objects which are used in everyday life. Sun is a perennial source of light energy, therefore several strategies to harness it, and convert it into other forms of energy is of great importance. Initiated by sunlight, the natural photosynthetic systems enable sequential multi-step electron transfer processes to produce high-energy biological fuel namely the adenosine triphosphate (ATP). In the realm of creating artificial photosystems, chemists all over the world have been captured by the photophysics and photochemistry of molecules, especially those with long-lived excited state lifetimes. By the year 1960, the principles of spontaneous decay established by Albert Einstein were extrapolated and applied to radiative transitions (electronic absorption principles) in organic chromophores.[1] Around the same time, a theoretical framework for describing non-radiative relaxation of the excited state, also called as the energy-gap law or the 'golden-rule' behavior was established.[2] In the organometallic research front, Crosby and others found that the second and third row transition-metal complexes with metal-to-ligand charge transfer (MLCT) characteristics exhibited intense luminescence both in solution and in the solid state at room-temperature.[3] These initial findings provoked intense research efforts into photophysics and photochemistry of organo transition-metal complexes. The decade of 1980 was also marked with notable discoveries in the application of luminescent molecules in emerging display technology. Tang and VanSlyke for the first time described a new electroluminescent device with a double-layered architecture employing organic chromophore as the emitting component[4] operating with a driving voltage of less than 10 V.

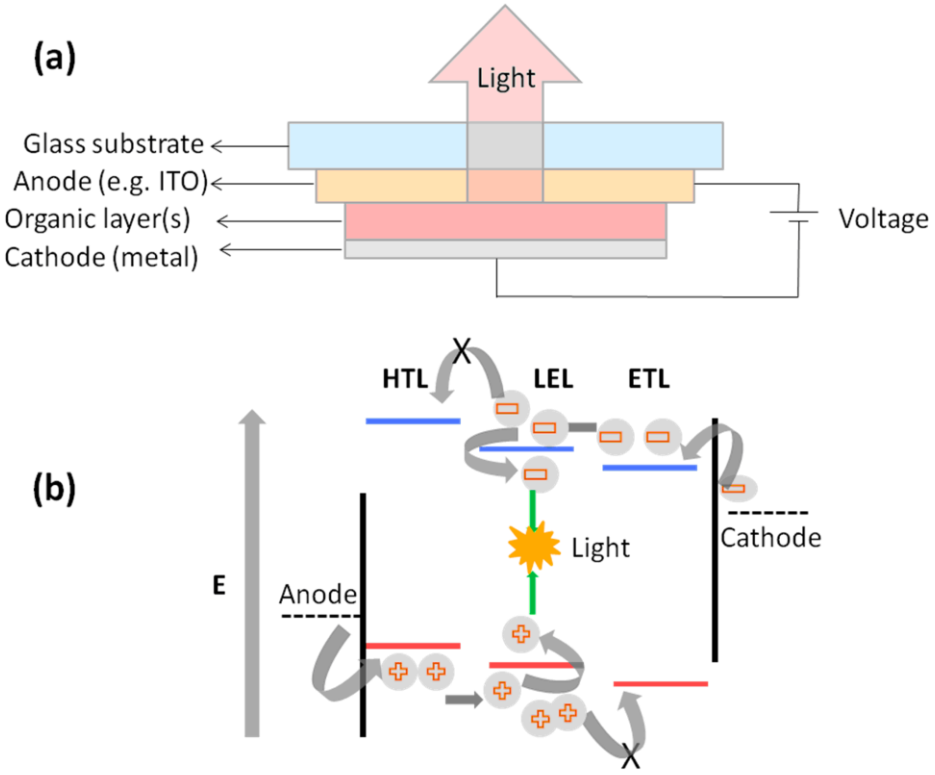

Figure 1. (**a**) Basic setup of an organic light emitting diode (OLED), (**b**) Working principle of OLED described schematically.[4]

Figure 1 schematically describes the basic set-up (**a**) and the working principle (**b**) of OLEDs. The device consist of a system of organic layer(s), sandwiched between an 'indium tin oxide' (ITO) anode and a low-work function metal cathode (Al or Ca). When a drive voltage typically between 2 and 20 V is applied, electrons from the cathode and holes from the anode are injected into the emitting organic layer(s). Due to the electric field, the electrons and holes migrate towards each other eventually forming a pairwise bound state called excitons. The decay of the excitons by photon emission is then perceived as visible light. This key invention marked the birth of what are now commercially available as Organic Light Emitting Devices (OLED). Friend et al. used poly(*p*-phenylene-vinylene) (PVV) as light emitting polymer introducing a separate branch of single layer thin-film technology.[5] Since then, research directed towards

OLED technology saw exponential growth and is now set to replace the traditional liquid-crystalline display (LCD) technology. Among the host of advantages of OLEDS,[6] the most significant and relevant to energy sustainability is its power consumption. Whereas the LCD displays require background lighting which consumes extra power, OLEDs due to its inherent emissive nature consume less power. Alongside this development, the experimental verification of "the inverted region" concept put forth by Rudolf A. Marcus in the famous electron-transfer theory[7a] was achieved by Miller and Closs in 1984 using steroid bridged Donor-Acceptor (D-A) systems.[7b] The room temperature phosphorescence (RTP) shown by certain class of organo transition-metal complexes at that time prompted their use as a replacement for purely organic based fluorescent molecules both in OLEDs[8] and also in D-A supramolecular 'antenna' systems.[9] However, the most compelling reasons for using such phosphorescence based emitters were far beyond mere curiosity. The theoretical treatment of spin-orbit coupling predicts maximum quantum efficiency for the molecules with heavier atomic mass and it has a tremendous bearing on the photophysical nature of the molecule. In the following paragraphs, the relevance of spin-orbit coupling in triplet emission and also the effect of spatial orientation of the molecule on the nature of emission are briefly discussed.

Photoluminescence from the triplet excited state and its dependence on spin-orbit coupling.

Some of the key factors realized in controlling the phenomenon of excited-state relaxation in a chemical species are: (1) the spin and symmetry of the molecular ensemble in its ground and excited states, (2) the energy difference (ΔE) between the two states, (3) the presence of other isoenergetic states capable of providing alternate relaxation pathways. Phosphorescence is principally forbidden according to the selection rules since it involves the change in the orientation of electrons' spin. It only gains certain degree of 'allowedness' when the emitting triplet state acquires some contribution from the singlet state. The relatively large effective nuclear charge of the metal in the organo transition-metal complexes induces a partial mixing of the single and triplet states through spin-orbit coupling (SOC) process. This phenomenon then circumvents the

forbidden nature of optical transition from T_1 to the electronic ground states S_0 to a certain extent.[10] With the rate of non-radiative decay being constant, the effectiveness of SOC decides the rate of radiative decay which is in turn reflected in the photoluminescence quantum yield of the molecule. Additionally, strong back-bonding to the metal as seen in most organo transition-metal complexes enhances ultrafast intersystem crossing (order of 10^{12}-10^{13} s^{-1}) leading to generation of triplet states.[11]

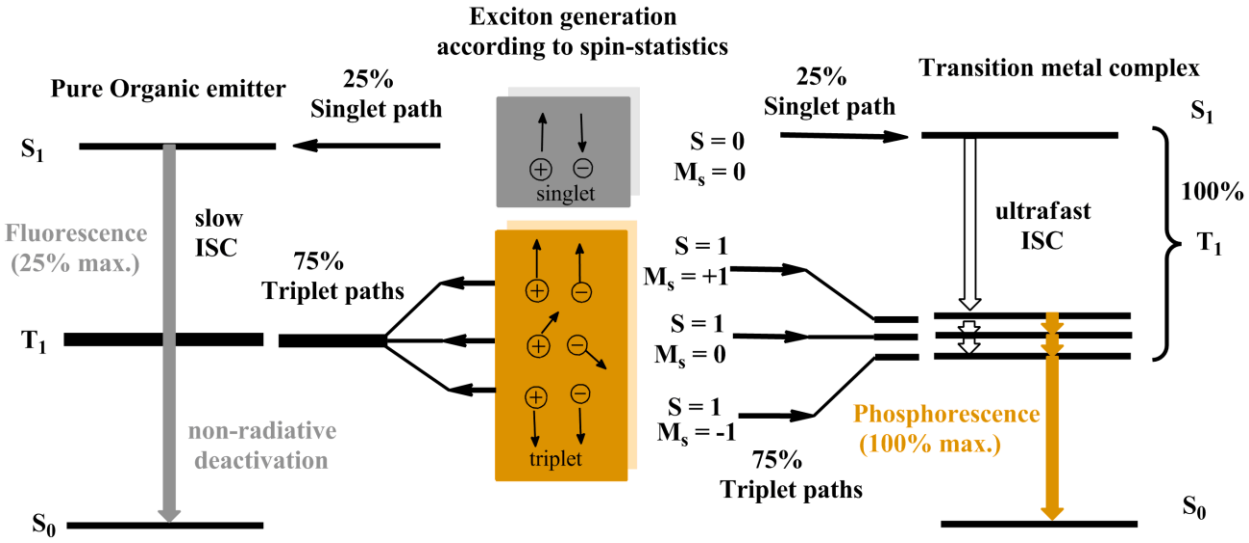

Figure 2. Schematic representations of singlet and triplet harvesting pathways[11]

Ideally, the electroluminescence spectrum resembles the photoluminescence (PL) profile of the emitter. In a conventional OLED set up (Figure 1), if the electron and hole combination to generate excitons takes place statistically then, 25% of excitons lead to the generation of pure singlet states and rest 75% produces triplet states. Owing to effective SOC in heavier metals, this rule is relaxed and the generated excited-state is not a 'pure' singlet or a triplet state. This phenomenon is also termed as 'heavy-metal' effect. Since both singlet and triplet states are utilized, this may in theory lead to maximum internal quantum efficiency (IQE) of 100% as against 25% for purely fluorescent luminophores. [10],[11] A rough schematic representation of this process is shown in Figure 2.

As mentioned earlier, the spin and symmetry of the molecule intricately influences the photophysical nature. Among the 4d and 5d transition metal complexes, those with octatahedral geometry like the tris-Ir(III)phenylpyridine [Ir(*ppy*)$_3$] are considered to be most suited as phosphorescent emitters because of their high degree of symmetry. Nevertheless, square planar d^8 complexes such as Pt(II) are also well investigated (Figure 3, part **a**).[12] Neutral complexes are preferred in a conventional OLED set-up to avoid any charge migration in the applied potential. In recent days cationic complexes (Figure 3, part **b**) are however becoming increasingly popular in the fabrication of solid-state light emitting electrochemical cells (LECs).[13]

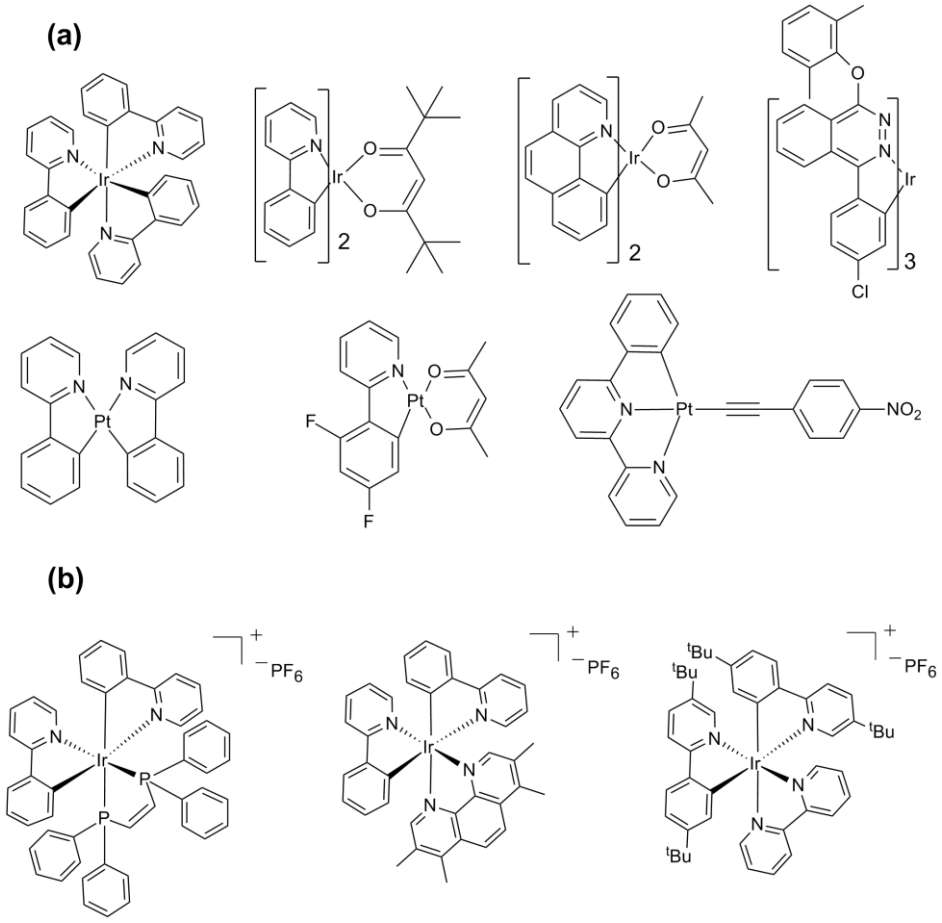

Figure 3. Some examples of popular organo transition-metal complexes used in OLEDs.

Under all circumstances, the PL properties closely rely on the molecular orbitals (MOs) responsible for the T_1 and S_0 states. With judicious choice of ligand surrounding the

metal, one can now design complexes where the identity of the triplet state is predetermined. In a transition metal complex, the electronic states generated due to photo-excitation can be primarily classified as, (1) *d*-*d* or metal-centred (MC) states: which arise due to the splitting of the *d* orbital of the metal, (2) $d\pi^*$ states (metal-to-ligand charge transfer (MLCT) states): occurs due to the promotion of electron from filled metal *d* orbital to the π^* orbital of the ligand,

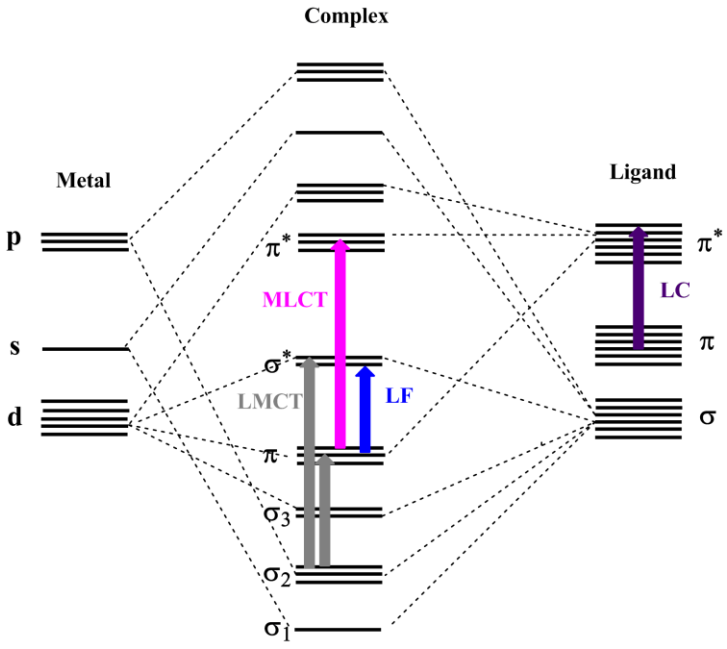

Figure 4. Simplified molecular orbital scheme of an octahedral metal complex depicting most common transitions.[13c]

(3) $\pi\pi^*$ or $n\pi^*$ intraligand (IL) states: with transitions involving the filled bonding or non-bonding orbitals of the ligand to its higher antibonding orbitals, (4) πd^* (ligand-to-metal charge-transfer (LMCT) states): which happens due to electron transfer from the ligand systems to a metal centered orbital. In the case Pd(II), Pt(II) and Au(III) square planar complexes (d^8 systems), the interplay of factors due to both 'heavy-atom' and the relative positioning of the molecular orbitals determine the photophysical outcome. Owing to a low SOC factor in Pd(II) complexes, most of them are emissive only at cryogenic temperatures.[14] On the other hand Pt(II) complexes are however known to exhibit RT phosphorescence due to their efficient SOC. Au(III) complexes are generally non

emissive at RT. The *d-d* ligand field (LF) states (metal-centered) are believed to be low-lying for gold and therefore thermal population at ambient temperature leads to deactivation by non-radiative pathways. It is important at this point to qualitatively discuss certain aspects concerning the relative positioning of *d-d* orbitals in organo transition-metal complexes. Upon photoexcitation, the strongly antibonding $d_{x^2-y^2}$ orbitals can get populated, this then can cause a shift in the excited state potential energy horizontally which physically implies the weakening of metal ligand (M-L) bond (Figure 5, **a**). Such a situation can lead to an isoenergetic cross over points which can act as effective channels of radiationless decay by either internal conversion or intersystem crossing. In a different scenario (Figure 5, **b**), when organic ligands are involved, transitions such as MLCT (d-π^*) or intra- or inter ligand charge transfer (LC, π-π^* or $n\pi^*$) can come into play, in such cases the separation between them and *d-d* levels (ΔE) becomes crucial. If the difference between them is comparable to the energy supplied at ambient temperature (kT), the *d-d* transition can still provide a concrete pathway for non-radiative decay.[12b]

In complexes containing heavier metal like Ir(III), the large atomic mass of the metal alone is sufficiently huge to cause large *d-d* separation. Therefore thermal energy (at ambient temperature) is not sufficient to populate these levels. Comparatively, in Au(III) complexes which have low lying *d-d* states, promotion of electron into the anti-bonding orbital of the metal induces a significant excited state distortion along with the weakening of the metal-ligand (M-L) bond. These states are detrimental to radiative pathways and sometimes termed as ‘dissociative states’.

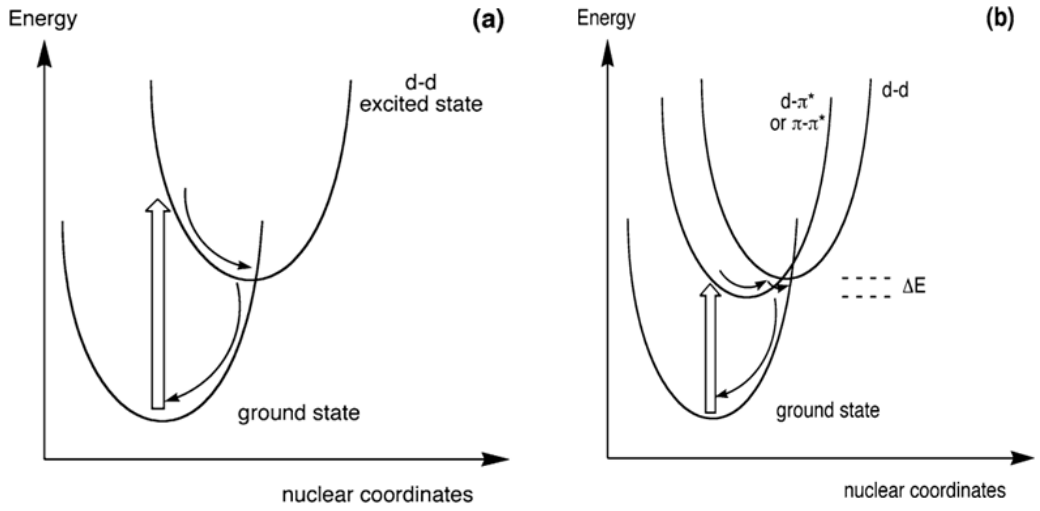

Figure 5. Displacement of the potential energy surface for the d-d excited state in a square planar d^8 complex formed due to population of antibonding $d_{x^2-y^2}$ orbital is illustrated, (**b**) Illustrates the possibility of thermally accessible d-d states, even though the transition originally involves metal-to-ligand or only ligand orbitals. Figure adapted from ref. 12b.

It is pertinent to mention here that, in rare cases of Au(I) complexes, depending on the geometry of the molecule, relaxations from the metal-centered states have been known to be emissive.[15] Along with the high crystal-field stabilization energy due to the heaviness of the atomic nuclei, the geometry adopted by the metal ion in a coordination complex also plays a crucial role. Detailed investigations from the group of Yersin has revealed that mixing of MLCT states is more effective in a quasi octahedral environment than in quasi square planar environment. Therefore an effective Zero Field Splitting (ZFS) of the T_1 state is achieved in the former case. The magnitude of ZFS directly influences the radiative decay rates and emission quantum yields. For a competitively faster radiative decay rate from the triplet state, a ZFS value of greater than 10 cm^{-1} (1.2 x 10^{-3} eV) has been suggested.[11] Quasi octahedral complexes such as Re(I), Os(II) and Ir(III) or even second row transition metals like Ru(II) have been experimentally observed to have large ZFS values. Such large values (sometimes to the extent 40 cm^{-1}) have not yet been reported for the square planar complexes. The square planar nature of the d^8 systems can

lead to additional complications; for example in the absence of sterically bulky substituents, close interplanar metal-metal interaction with the overlaying of dz^2 orbitals can occur. This often leads to the formation of weakly bound $d\sigma$ and $d\sigma^*$ states leading to excimeric emissions which are red shifted, and results in lower quantum yields. With a fair balance of pros and cons, research efforts into luminescent d^8 square planar systems are still being pursued unflinchingly.

3.0 General overview: Chemistry of gold

"Gold is where you find it" so goes a saying, gold is arguably the oldest metal known to mankind. It shows a rich chemistry, and continues to feature strongly as a metal of choice for research due to its unique physical and chemical properties.[16]

Oxidation states of Gold.

Gold chemistry is principally dominated by +I and +III oxidation states corresponding to the electronic configurations [Xe]5d^{10} and [Xe]5d^8 respectively. Other less common oxidation states are nevertheless known, some of them include -I (e.g. CsAu, RbAu), +II (e.g. $Au_2Cl_2(CH_2PMe_2CH_2)_2$), and +V (e.g. $[XeF_5][AuF_6]$).[17] The observation of +II oxidation state in either mononuclear, planar or pseudo-octahedral forms of 5d^9 Au(II) systems is quite rare. When compared to those of Cu(II) systems, Au(II) is perceived to be unstable because of the high energy requirement of the unpaired electron occupying the $d_{x^2-y^2}$ orbital. The first and only structurally characterized mononuclear Au(II) compound is one containing the bis(1,4,7-trithiacyclononane)gold dication.[18] Most gold complexes which suggest the presence of Au(II) oxidation state according to their empirical formulae are not paramagnetic, but often contain a mixture of Au(I) and Au(III) units, *viz.* AuS, $Cs[AuCl_3]$, $K[AuI_3]$ and $K_5[Au_5(CN)_{10}I_2]$.[19] Metal-metal bond formation by a dimeric Au_2 (+IV) species are known to be greatly stabilized[20] among gold complexes. Similarly, non-integer oxidation states have also been observed in gold cluster complexes. For example, complex such as $[Au_9\{P(p\text{-}C_6H_4CH_3)_3\}_8][PF_6]_3$ implies an average formal oxidation state of +0.33 for each gold atom.[21] Au(I) complexes in general exhibits linear two coordinate geometry (e.g. PPh_3AuCl).[22] Trigonal planar

(C.N. = 3) and tetrahedral geometries (C.N. = 4) have also been observed in the cases such as $[AuCl(PPh_3)_2]$ and $[Au(diars)_2]^+$ respectively.[23] Au(III) complexes (e.g. $Na[AuCl_4]$, Au_2Cl_6, and $[(C_2H_5)_2AuBr]_2$) are normally four coordinate and adopts a square planar geometry. However, sometimes they tend towards geometries which can be described as highly distorted octahedral, for instance, the complex $[AuCl_2(py)_2]Cl{\cdot}H_2O$ contains the square planar $[AuCl_2(py)_2]^+$ fragment with closely associated ionic H_2O and Cl^- in the axial positions assuming a distorted octahedral solely due to the nature of crystal packing.[24]

Brief introduction to Organogold complexes

As early as in 1907, Pope and Gibson prepared dialkylgold(III) halides of the type $[R_2AuX]$[R = alkyl group, X = halide] by reacting gold trihalides/tetrahaloauric acid with an excess of a Grignard reagent.[25] Thereafter, it was not until early 1950s, the chemistry of alkylgold(I) and trialkylgold(III) witnessed dramatic developments fuelled by the discovery of organolithium reagents and the use of tertiary phosphines as stabilizing ligands.[26] Until today, the preparation of organogold(I) compounds largely rely on replacement of halides from complexes such as [AuX(L)] (L = PR_3, SR_2) using Grignard or organolithium reagents.[27] Alternative to the use of phosphine Au(I) halide, an isolated high yielding method employing tris(triphenylphosphine)Au(I)oxonium tetrafluoroborate has also been reported.[28] Organogold complexes in the +III oxidation state are generally derived from their corresponding inorganic salts such as $NaAuCl_4$. Other than this method, the +III oxidation state in gold can also be achieved by an oxidative addition process. This reaction is particularly considered to be important in the reactivity of Au(I) complexes since the oxidized products are often more thermodynamically stable.[29] Mononuclear Au(I) complexes typically undergo oxidative addition with small molecules such as halogens, alkyl halides and dialkyl disulfides. As an illustrative example, when iodomethane is reacted with $[Au(CH_3)(PPh_3)]$, it initially forms the oxidative addition product $[(CH_3)_2AuI(PPh_3)]$ which further undergoes ligand exchange with the starting material to give $[AuI(PPh_3)]$ and the trimethyl compound $[(CH_3)_3Au(PPh_3)]$ (Figure 6, part **a**)

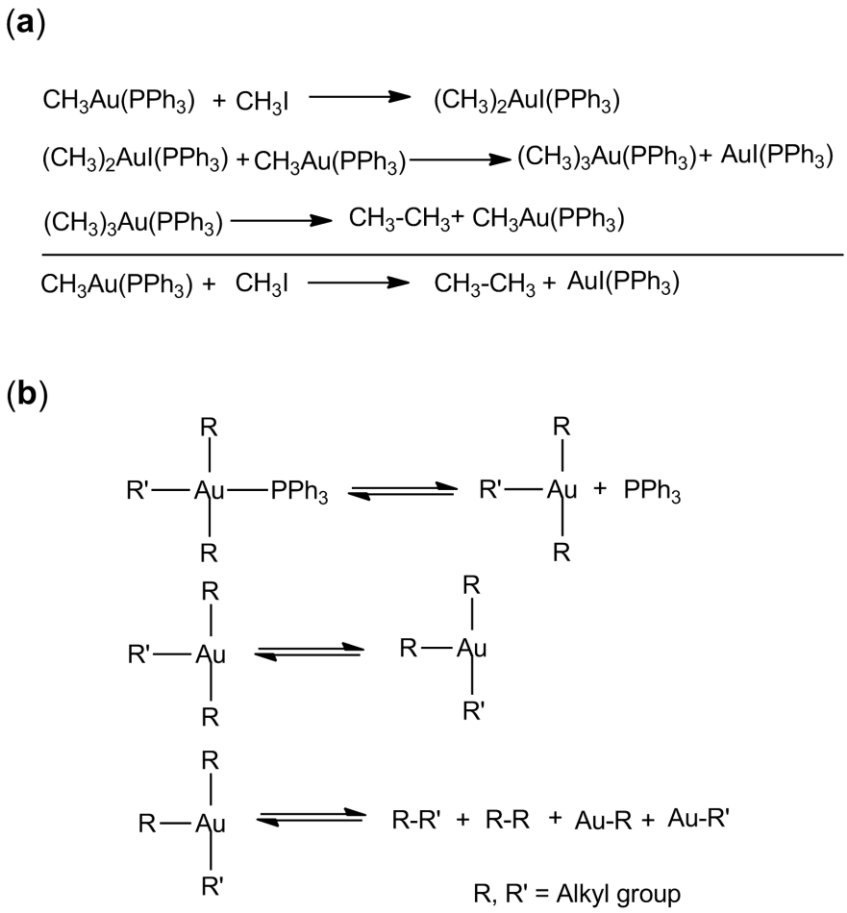

Figure 6. (**a**) Reaction sequence leading to the reductive elimination of ethane from dimethyl Au(III) complex. (**b**) Proposed mechanism involving a T-shaped intermediate.

Reductive elimination processes from such a trialkyl Au(III) species leads to the generation of ethane. Based on careful studies, an intra-molecular reductive elimination mechanism involving initial dissociation of the ligand generating a T-shaped intermediate which is further capable of undergoing *cis-trans* isomerization has been proposed[30] (Figure 6, part **b**). Early mechanistic investigations such as this, served to introduce gold into the field of homogeneous catalysis.[31] A lot of attention since then has been laid on the synthesis of organometallic species of gold. Comprehensive treatises[27],[32a] on gold have been appearing regularly. Review articles devoted to specific topics like syntheses and reactivity[32c-d] and also applications of organogold compounds [32e] have also been published.

Closed-shell metallophilic interactions in gold compounds.

In the late 80's, solid-state structural investigations of molecular gold compounds in its +I oxidation state led to an interesting observation; in the absence of any type of steric hindrance, it was found that shorter-than-normal intra/inter-molecular equilibrium Au···Au attractive interactions of the order approx. 2.5-3.5 Å existed between formally closed-shell $5d^{10}$ gold centers[33] This unique ability of gold to form weak bonds with itself which could not be rationalized by conventional concepts of chemical bonding was named as 'aurophilicity' in 1989. Aurophilicity may be described as a correlation effect enhanced by relativistic effects.[34] In heavier atoms, the increased nuclear charge causes an increase in the average velocity of electrons that penetrate to the nucleus (the *s* electrons), this in turn leads to increase in the mass of the electron under relativistic considerations (when velocity of the orbiting electron approaches the speed of light)

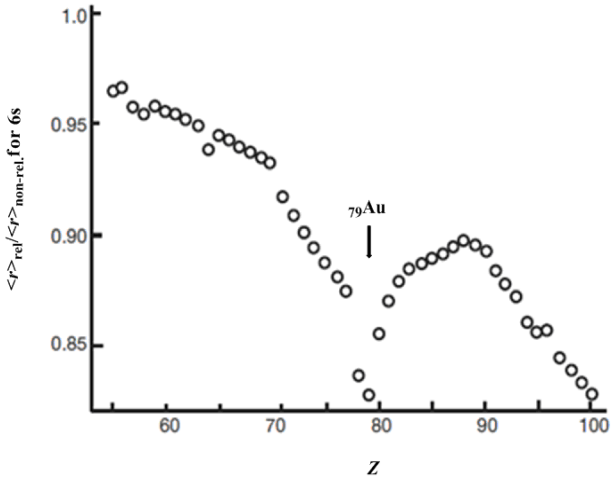

Figure 7. The relativistic contraction of the *6s* shell in the elements Cs (*Z* = 55) to Fm (*Z* = 100), showing the pronounced maximum of the contraction at gold (*Z* = 79) (reproduced from ref. 34).

The increase in mass results in a decrease in orbital radius, since orbital radius is inversely proportional to electron mass. In addition to the contraction of the *s* orbitals,

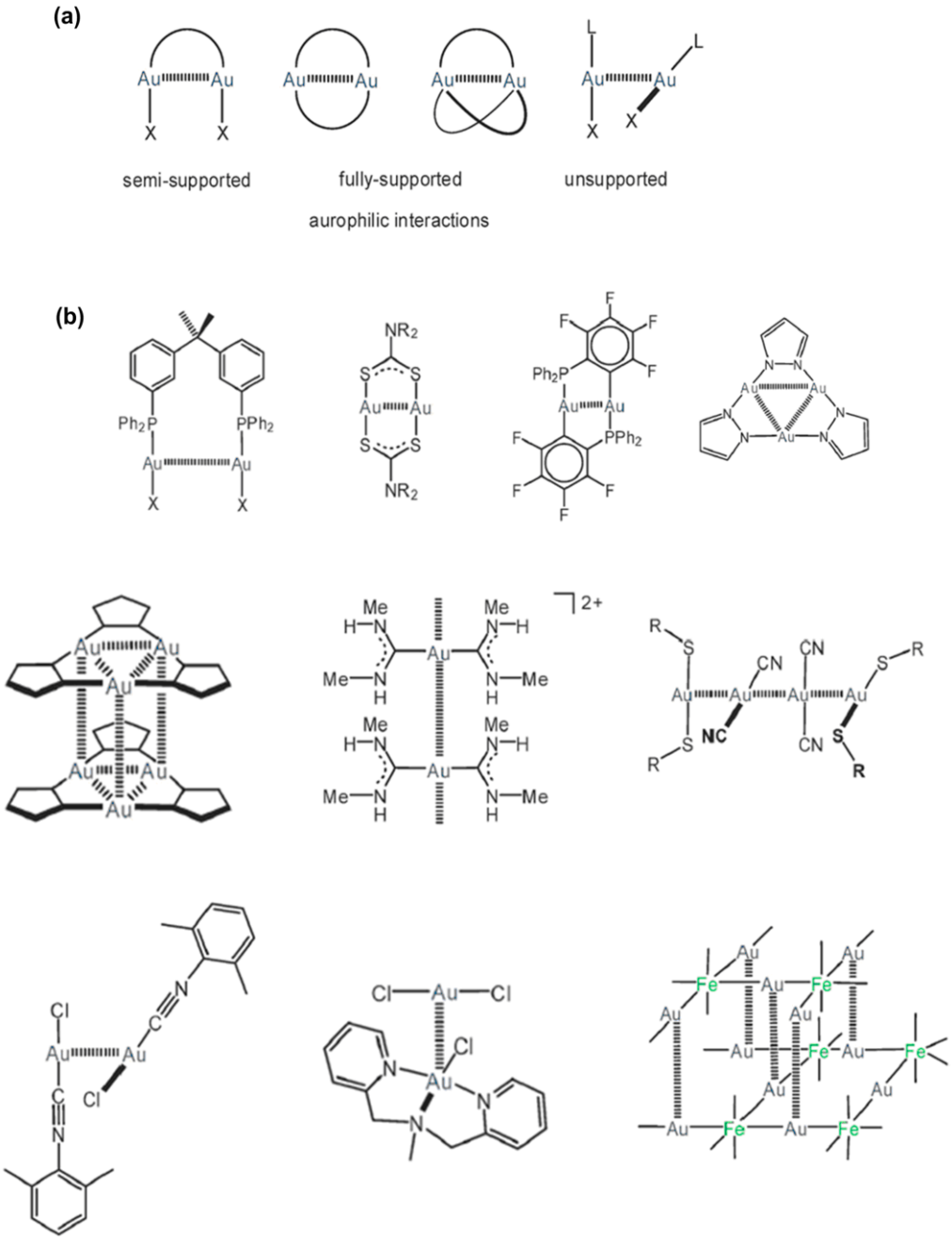

Figure 8. (**a**) Schematic diagram illustrating types of aurophilic interactions in gold compounds (**b**) Some example of Au(I) complexes showing Au···Au interactions. (figure adapted from ref. 33e)

radial expansion of the *5d* orbitals also occurs, which allows closed-shell $5d^{10}$ Au(I) compounds to interact with the gold atoms in other complexes. The relativistic contraction of the *6s* shells is at a maximum for gold (Figure 7),[34c] and therefore, the van der Waals radius of the gold atom (1.66 Å) is less than that of silver (1.72 Å), which is in contrast to that expected for a heavier atom. Relativistic effects also explain the high resistance of gold to oxidation and the attainment of higher oxidation states as compared to silver[34d] Au···Au contacts (defined in the dz^2 plane) lowers the energy of the $\sigma^*(dz^2)\rightarrow\sigma(6p)$ transition and are therefore believed to modulate the PL properties of many Au(I) complexes.[35]

3.1 Chemistry of Cyclometalated Gold(III) complexes.

Cyclometalated transition-metal complexes.

Organometallic complexes containing a covalently linked metal-carbon σ-bond along with another metal-donor atom encompassed in a cyclic structure are broadly described in various terms as *ortho*-metalated, cyclometalated or as intramolecular coordination compounds.[36] Various methods for the preparation of such complexes are known *viz.* cyclometalation, oxidative addition, transmetalation, trans-cyclometalation, expansion of the cyclometalated ring, external nucleophilic attack on a coordinated ligand. Among these, the term cyclometalation is used for the reaction process, which involves intramolecular activation of sigma C-X bond (where X is an atom of a non-metallic element) of a transition metal complex. Normally, cyclometalation occurs due to the interaction of the ligand with the metal leading to hydride transfer to the metal centre with a subsequent elimination of the proton with a suitable leaving group (Figure 9, Part **a**).

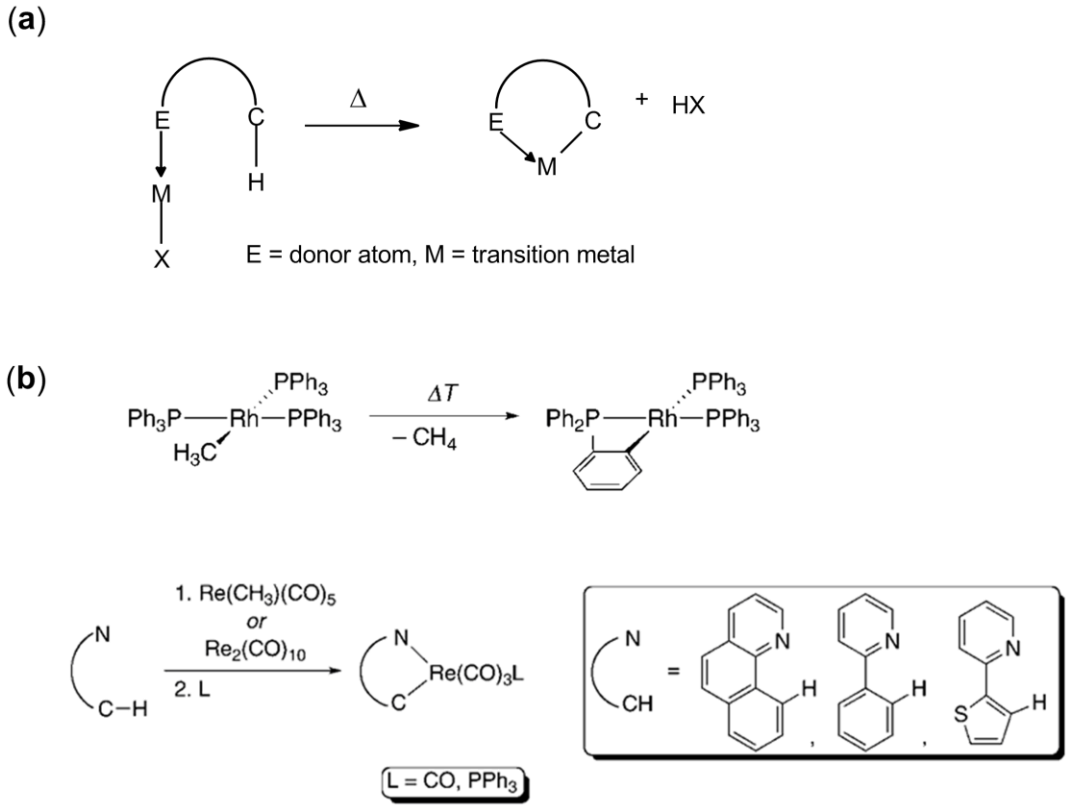

Figure 9. (**a**) Representation of a simple cyclometation process. (**b**) Selected examples of cyclometalation reactions. (figure adapted from ref. 36e.)

Cyclometalation in gold complexes: Synthetic routes to C^N gold(III)di-, halides, aryls and acetylides.

Compared to enormous literature precedence available on the cyclometalation chemistry of Pt(II) and Pd(II) complexes, relatively less is known about its isoelectronic Au(III) congeners. The earliest report concerning direct activation of arene C-H bond by Au(III) chloride to give $(ArAuCl_2)_2$ type of complexes dates back to 1931.[37] Only a few scattered reports followed thereafter until last two decades which however saw a renewed activity in this area. The current impetus in creating σ-bonded carbon-gold (C-Au) activated systems such as $(C^N)AuCl_2$ (C^N = cyclometalated ligand) is perhaps due to the magnitude of knowledge acquired on Pt(II) d^8-square planar systems (e.g. L_2PtCl_2

systems) and their application as potential anti-tumor leads. From an entropic point of view, cyclometalation helps to stabilize Au(III) centre towards reduction to lower oxidation states (+I and 0) and it is therefore desirable to create such complexes. Once stable, these complexes can be explored for various other properties like photoluminescence, optical non-linearity etc. In the following paragraphs, a brief overview on the methods adopted for achieving C^N cyclometalated gold complexes with particular emphasis on halides as ancillary ligands is presented. A more elaborate account on various aspects of cyclometalation in gold has been elegantly dealt by Henderson.[38] Among the cyclometalated mononuclear Au(III) complexes, the ones containing nitrogen atom as donor ligand are more frequently encountered when compared to phosphorus. Typically, cyclometalation results in products containing five- or less common strained six membered ring systems[38] which may or may not contain a Au(III)-aryl bond. Some representative examples are shown in Figure 10.

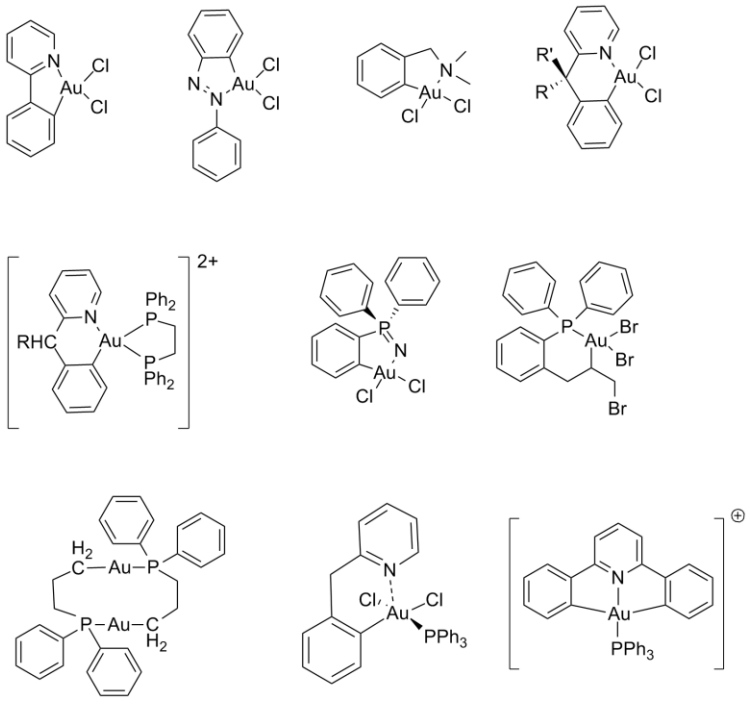

Figure 10. Representative examples of cyclometalated gold complexes.

There are two prominent commonly applied strategies to achieve cyclometalation in Au(III) complexes: (1) Direct cycloauration method.[39] (2) Transmetallation from corresponding organo- mercury,[40] lithium,[41] tin[42] and zinc[43] reagents. Direct cycloauration was first attempted by Constable and Leese by treating 2-phenylpyridine with $HAuCl_4/NaAuCl_4$.[44] A yellow *N*-bonded complex **1** was obtained initially (Scheme 1). Thermolysis of **1** either in solution[44] or in the solid-state[45] afforded the C-H activated five membered cycloaurated product **2**.

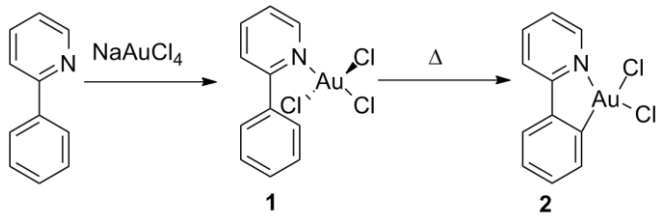

Scheme 1.

Heterocyclic derivatives also underwent direct cycloauration (Scheme 2); 2-(3-thienyl)pyridine and 2-(2-thienyl)pyridine reacted with $Na[AuCl_4]\cdot 2H_2O$ to form the corresponding *N*-bonded $AuCl_3$ adducts similar to **1** under ambient conditions. Upon heating the 3-thienyl $AuCl_3$ adduct, it underwent direct cycloauration to yield **3**, whereas the 2-thienyl$AuCl_3$ adduct could be cycloaurated to **4** only with the assistance of silver salts like $AgBF_4$.[39h]

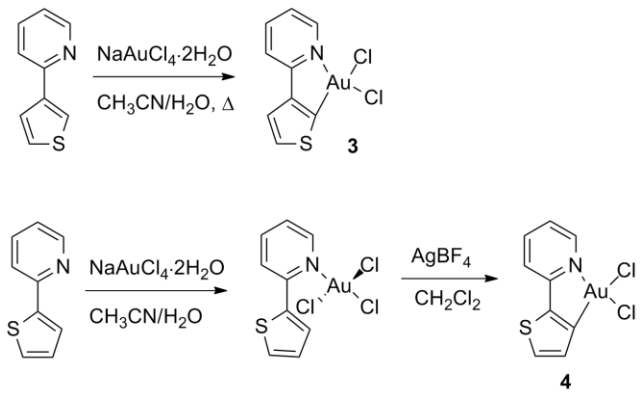

Scheme 2.

Silver salts often assists the cycloauration process by abstracting one of the halide and thereby creating a reactive coordination site. As a modified version of the direct cycloauration procedure, a number of silver-assisted reactions were subsequently reported. [39b],[39g] As mentioned earlier, cycloauration reaction involving the activation of sp^3 C-H bond rather than sp^2 C-H has also been demonstrated, but to a limited extent. Some examples which involves activation of methylene[46] and methyl groups[47] are seen in complexes **5** and **6** (Scheme 3).

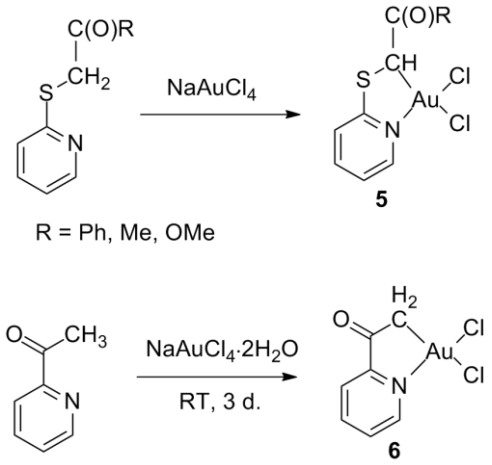

Scheme 3.

Direct cycloauration method has also been exploited to form strained six-membered ring complexes. For instance, the reaction of 2-anilinopyridine with $NaAuCl_4$ in boiling water yielded **7** [39a] and was structurally characterized.

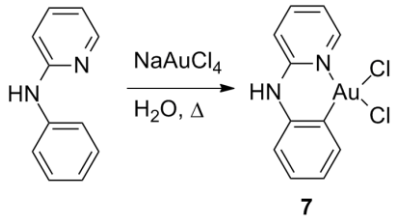

Scheme 4.

Over the years, several improvements[39e] and variations[48] of this method resulted in generating a wide library of such complexes, some examples are shown in Figure 11 below.

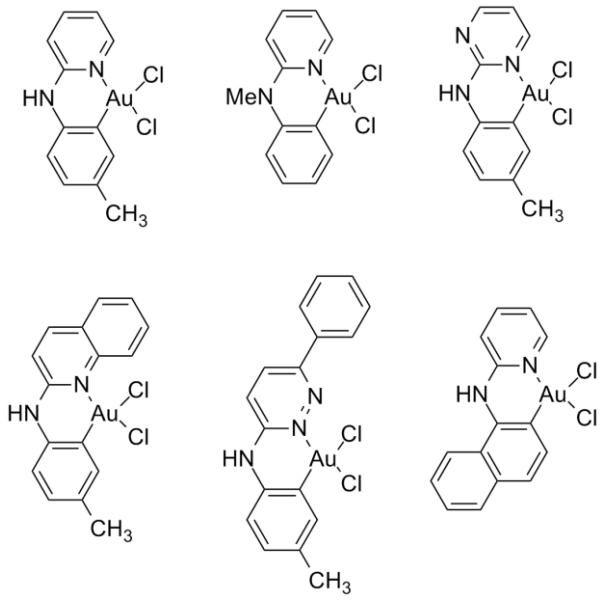

Figure 11. Selected examples of cycloaurated complexes with strained six-membered ring

Cycloauration in the cases of 2-benzylpyridines and closely related derivatives such as 2-phenoxypyridine and 2-(phenylsulfanyl)pyridine by the direct method were observed to proceed *via* different isolable intermediates such as salts $[H_2L][AuCl_4]$ or neutral adducts $[LAuCl_3]$ of the respective ligands. Often by subjecting such intermediates to elevated temperatures (approx. 150°C) in appropriate solvent media leads to the generation of the cyclometalated products.[48a] In a similar fashion 6-benzyl-substituted 2,2'-bipyridines also readily form complexes containing six-membered cycloaurated rings.[49]

Yet another versatile methodology to achieve cyclometalation (especially of those which fail under direct methods) is through transmetallation. Reaction of Au(III) precursors (invariably an $AuCl_4$ salt or $LAuCl_3$ adduct) and an organomercury substrate leads to the transfer of the organic group from mercury to gold. These reactions are often carried out with added tetramethylammonium chloride salt which results in the formation of the

relatively insoluble chloromercurate salt $[Me_4N]_2[Hg_2Cl_6]$, which can be easily separated from the cyclometalated product. 1,2-Diphenyldiazene was cyclometalated to [(*pap*)$AuCl_2$][*pap* = phenylazophenyl] (**8**) starting to from its Hg(II) chloride by treating with [(*tht*)$AuCl_3$] (*tht* = tetrahydrothiophene) in the presence of $[Me_4]NCl$[40c] (Scheme 5).

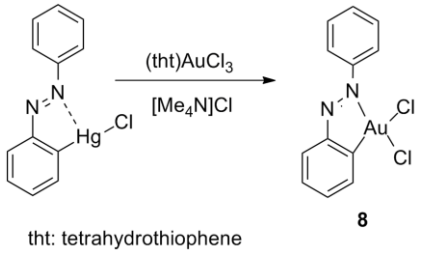

Scheme 5.

The mechanism of transmetalation is believed to take place in the following steps as proposed in the exemplary case of [*damp*$AuCl_2$] [*damp* = 2-(dimethylaminomethyl)phenyl] complex (Figure 12, part **a**): First, there is an initial coordination of the amine donor to gold, forming a bimetallic intermediate; the organomercury precursor generally has a weak (if any) interaction between the metal and the amine donor and then the transfer of the aryl group from mercury to gold occurs, with concomitant elimination of $HgCl_2$ giving the cyclometalated product. Groups of Bonnardel and Parish have greatly extended the organomercury transmetalation chemistry by synthesizing a variety of suitable precursors. Numerous pyridyl substituted derivatives of cyclometalated phenylpyridine Au(III) complexes were prepared through this method.[50] Examples of certain Au(III) complexes prepared by the mercury chloride route is shown in part **b** of Figure 12.

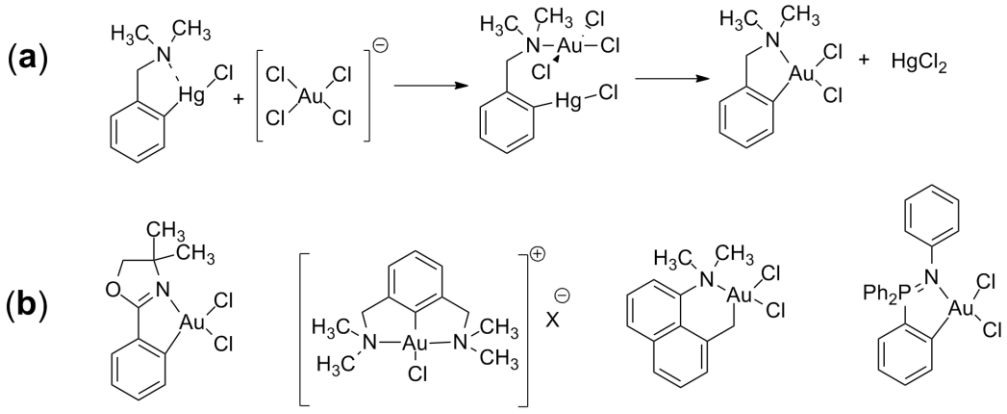

Figure 12. (**a**) Scheme depicting transmetalation sequence in [*damp*$AuCl_2$]. (**b**) Examples of complexes synthesized by transmetalation [50]

Chloromercurial derivative of 2,6-diphenylpyridine when reacted with gold precursors form charge neutral tridentate C^N^C gold(III) complexes.[51] Chemical functionalization of these complexes results in several tridentate Au(III) complexes with interesting PL properties which would be discussed later in this chapter. Similarly, conversion of 6-phenyl-2,2'-bipyridine to its organomercury derivative followed by reaction with Na[$AuCl_4$] gave the cycloaurated product as a [$AuCl_4$] salt.[51c]

Replacement of halides in (C^N)AuX_2 complexes with aryl and alkynyl ancillary ligands.

The coordinated halides have been effectively replaced by aryl ligands by transmercuration. Reaction of $HgPh_2$ with [(*damp*)$AuCl_2$] [*damp* = 2-(dimethylaminomethyl)phenyl] in chloroform gave monophenyl complex [(*damp*)Au(Ph)Cl] (**9**) (Figure 13). When Hg($C_6H_4CF_3$-*o*) was used instead under the same conditions, it was found to yield the corresponding unstable bis(aryl) complex (**10**) as confirmed by NMR studies.[40d] The mono(pentafluorophenyl) complex (**11**) was analogously obtained by the reaction of *damp*$AuCl_2$ with Hg(C_6F_5)$_2$ and [Me_4N]Cl.[52]

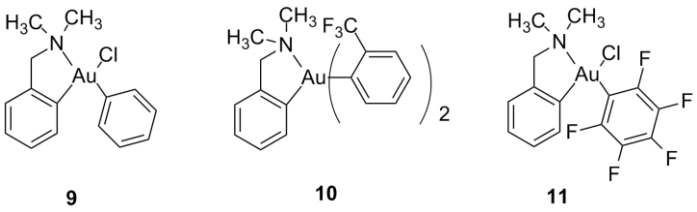

Figure 13. Examples of previously known mono-, diaryl Au(III) complexes.

Yam and co-workers were successful in introducing various alkynyl ligands in the diphenylpyridine complexes. Reaction of (C^N^C)AuCl with various terminal acetylides in CH_2Cl_2 with Et_3N and catalytic amount of CuI gave a range of Au(III) σ-acetylides.[53] In an alternative method, NaOH in refluxing methanol was used to obtain the same alkynyl substituted products but in a comparatively lower yields. Treatment of the tridentate gold halide with several *N*-heterocyclic azolium salts yielded the corresponding cationic gold complexes.[54] Both the imidazole substituted **13** and phenylacetylide substituted **14** exemplary complexes (Scheme 6) showed room temperature phosphorescence (RTP). Interesting photophysical and electrochemical attributes of these classes of complexes would be dealt in the succeeding paragraphs.

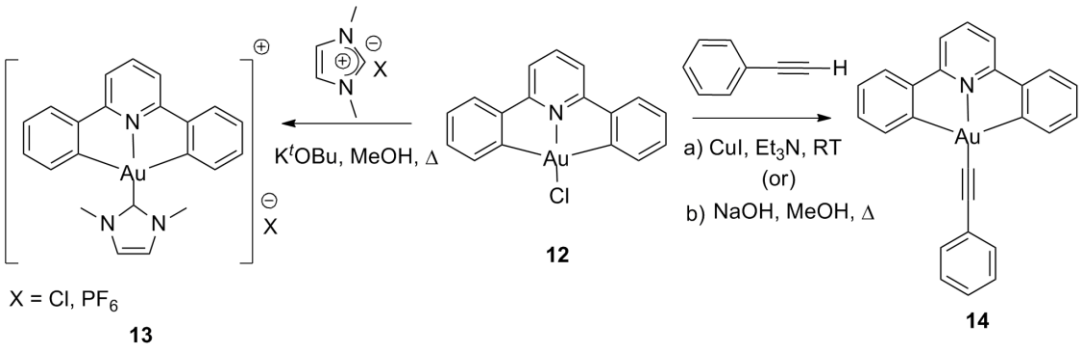

Scheme 6.

3.2 Photophysics of Gold complexes.

Photophysics of cylometalated Au(III) complexes.

Two definitive reviews have appeared until now on the topic of luminescent Au(III) cyclometalated complexes.[55] The overall stability of tridentate cyclometalated complexes prompted investigations into the photophysical aspects of such complexes. Monocationic cyclometalated chlorogold(III) complexes such as $[Au(N^N^C)Cl]^+$ (**15)** shown in Figure 14, were reported to be luminescent in the solid state, in fluid solution at RT and in 77 K rigidified glass matrices by Che and co-workers.[56] The PL spectrum of **15** showed a vibronic-structured profile with progressional spacings of ~1400 cm^{-1} in various media. Its excited state lifetime was in microseconds and the emission wavelength was insensitivity to solvent variation. These features firmly suggested the triplet nature of the lowest emitting state. With an excited state-reduction potential of 2.2 V *vs* NHE, **15** was also found to induce oxidative ring cleavage in tetrahydrofuran molecule. Further, in a photochemical experiment involving 1,4-dimethoxybenzene, the corresponding radical cation was observed also suggesting strong photo oxidizing nature of the complex. Later in 1998, the same group reported a monochloro gold(III) complex [(C^N^C)AuCl] (**12**) based on a dianionic bis-cyclometalated diarylpyridine chelate as shown in Scheme 6.[57] The chloro complex **12** was non-luminescent at RT but showed luminescence in acetonitrile solvent at 77 K. The absorption and emission characteristics were found to be dominated by IL [$\pi\rightarrow\pi^*$] transitions and metal-perturbed IL [$\pi\rightarrow\pi^*$] emission from a triplet state respectively. In the similar study, the emission energies of the binuclear complex **16** (Figure 14) prepared by reaction of bisphosphine ligand (*dppm*) with **12** were found to be red-shifted presumably due to the excimeric emission caused by intramolecular π–π stacking of the {Au(C^N^C)} moieties.

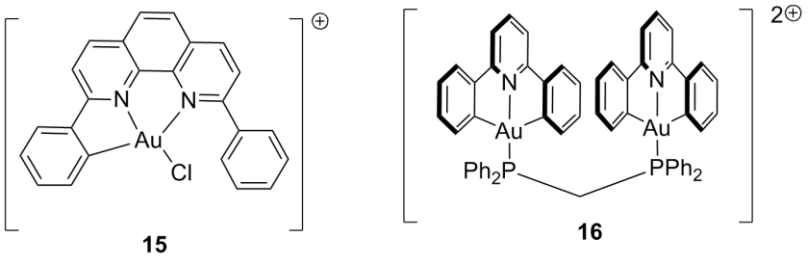

Figure 14. Examples of luminescent cyclometalated Au(III) complexes prepared by Che and co-workers.

The above studies by Che group firmly established the ligand centered dominance of the bis cyclometalated Au(III) complexes. As mentioned above the chloro complexes of the type **12** are generally non-emissive in fluid media at RT. Yam and co-workers came out with a strategy of introducing strongly σ-donating alkynyl ligands so as to raise the energy of the *d-d* states and also to decrease the electrophilicity of the Au(III) center. In line with this hypothesis, and as a significant break-through, a series of [(C^N^C)Au(III)L][L = aryl alkynes] complexes of the type **14** were demonstrated to be room temperature emissive (Scheme 6).[53] The emission maxima in the region 474-476 nm was attributed to metal-perturbed intra ligand [$\pi \rightarrow \pi^*$(C^N^C)] phosphorescence. Cyclic voltammetry showed that the first reduction process in such complexes involves the cyclometalated portion of the ligand (-1.52 V and -1.59 V *vs* SCE). The electrochemical potentials of the first anodic waves were noted to be quite sensitive to the nature of the alkynyl ligands.[53d] Theoretical studies (TDDFT calculations) by Zhang [58] and co-workers on such complexes was in conformity with the experimental observations of Yam and suggested the lowest emitting state in the complexes of the type **14** to be of ^{3}IL (intraligand) nature. Later in 2009,[54] the same group replaced the halide in **12** with neutral ligands such as *N*-heterocyclic carbenes (**14**) affording cationic complexes which were an effective replacement of the earlier known mononuclear phosphine complexes such $[Au(C^N^C)PPh_3]^+$ (Scheme 6). While the phosphine complexes were emissive only at cryogenic temperatures, for instance as in the case of **16**, the NHC bearing complexes were emissive both at 77 K and at ambient temperatures further highlighting the

importance of σ-donating carbanionic ligand. The emission energies in these classes of complexes were largely insensitive to the nature of the NHC ligand and require the variation in the functional groups in the cyclometalate core to bring about tuning over the visible wavelengths. Several binuclear NHC complexes were also studied and their emission was found to be red shifted approximately by 10 nm. No Au(III)···Au(III) interactions were observed in the crystal packing structures of these complexes, however, short interplanar C^N^C distances (~3.4 Å) were observed indicating π-π stacking in these complexes. Some of these complexes (Figure 15, **17** and **18**)

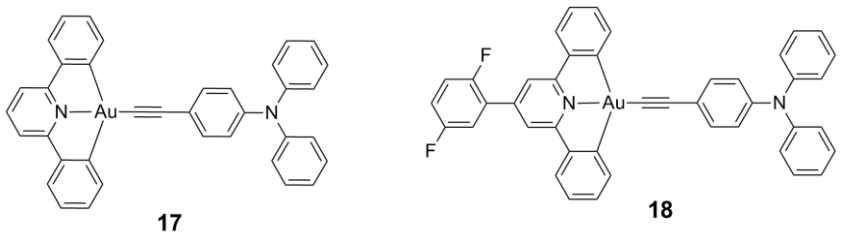

Figure 15. Examples of cyclometalated Au(III) acetylides incorporated into OLEDs.

were incorporated into OLEDS as dopants and were found to be emission tunable by varying the doping concentration. Maximum external quantum efficiency (EQE) of 5.5% and a luminescence power efficiency of 14.5 lm W^{-1} were achieved in the case of **17**.[53b] Further improving on this model, **18** was developed with a *p*-difluorophenyl unit attached to the C^N^C core. The LLCT emission in this complex was bathochromically shifted to 669 nm from 620 nm observed for **17**. When doped on a poly(methyl methacrylate) (PMMA) host matrix with increasing weight% concentrations, the PL wavelength of this compound was found to shift towards red. This observation was attributed to excimeric emission originating due to π-π stacking of the cyclometalate unit. As a significant milestone, the OLED device fabricated incorporating **18** showed an EQE value of 11.5% and an power efficiency of 26.2 lm W^{-1}, which are in the comparable range with the popular tris-cyclometalated Ir(III) phenylpyridine complexes.[53c]

3.3 Chemistry of Gold(I) complexes

Synthetic routes to σ-bonded mononuclear phosphine or N-heterocyclic gold(I) halides, aryls and acetylides.

The +I oxidation state in gold is by far the most investigated among others. Complexes bearing one, two or multiple gold atoms supported by different types of ligands have been described. An elaborate classification on the basis of nuclearity has been elegantly presented by Gimeno[16] and the various synthetic aspects of the Au(I) chemistry have been dealt by Schmidbaur and others in a book chapter.[59] Only selective methodologies adopted specifically for the generation of σ-bonded mononuclear phosphine or *N*-heterocyclic Au(I) anionic substrates (*viz*. alkyl, aryl and acetylides) relevant to the dissertation will be discussed here.

Although the linear two coordinate geometry in Au(I) complexes (e.g. AuXL) has been known since long time, it is only in the recent decades this field has attracted more attention, driven primarily due to the discovery of aurophilicity. The neutral ligand attached to the gold center can be derived from a variety of functional groups such as phosphine, arsine, isocyanide, carbene, ylides etc. Again, the anionic ancillary part can include a halide, alkyl or aryl, chalcogenolate, acetylides and so on. In certain cases, the complexes of the type [LAuX][L = neutral ligand, X = halide] may undergo ligand redistribution in solution and crystallize as homoleptic isomeric forms $[AuL_2]^+[AuX_2]^-$.[60] Mononuclear tertiary phosphine Au(I) chlorides have been often used as suitable precursor complexes for further derivatizations. They can be classically prepared by reducing chloroauric acid with triphenylphosphine in 95% ethanol.[61] Complexes such as [AuCl(CO)] or [$AuCl(SR_2)$, R = alkyl group] also constitutes an important class of precursors for the preparation of various dinuclear (chloro)gold(I) complexes such as $[Au_2Cl_2\{\mu\text{-}(PPh_2)_2(CH_2)_n\}]$ (n = 1-8) upon reaction with various corresponding bidentate phosphines.[59]

Alkyl Au(I)phosphines are usually prepared by the reaction of an alkyllithium or a Grignard reagent with a complex Au(I) halides[62] (Scheme 7, equation 1). Tris(phosphinegold(I))oxonium tetrafluoroborates have also been used sometimes instead

of (phosphine)Au(I) halides (Scheme 7, equation 2). The low solubility of the oxonium salts in ether and tetrahydrofuran solvents enables easier isolation of the product.[63] Similar to alkylgold(I)phosphines, aryl gold complexes [ArAuL] (L being a neutral donor ligand) can also be prepared *via* organolithium and Grignard routes.[64] Displacement of weakly coordinating ligands such as THT (tetrahydrothiophene, SC_4H_8) with a variety of more strongly coordinating donors have also been employed to synthesize Au(I) aryl complexes[65] (Scheme 7, equation 3).

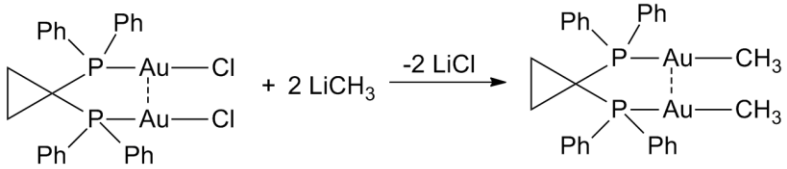

(1)

$[(Ph_3PAu)_3O][BF_4]$ $\xrightarrow[\text{(ii) } H_2O]{\text{(i) RLi (or) RMgCl}}$ $[AuR(PPh_3)]$ (2)

$[AuCl(SMe_2)] + CH_3MgCl + CH_3CN \xrightarrow{-MgCl_2,\ -S(CH_3)_2} [AuCH_3(CNCH_3)]$ (3)

$[Au(TPA)_3]Cl + Na[BPh_4] \longrightarrow [AuPh(TPA)] + NaCl + 2TPA + BPh_3$ (4)

TPA = 1,3,5-triaza-7-phosphaadamantane

$[(t\text{-}Bu_3PAu)_3O][BF_4] + Na[BPh_4] \longrightarrow 3[AuPh(PBu\text{-}t_3)] + Na[BPh_4] + PhBO$ (5)

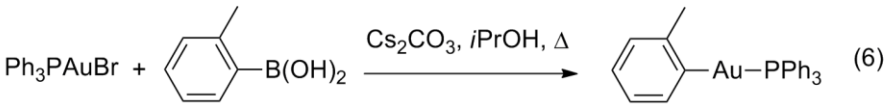

(6)

Scheme 7

Borate salts can be used to prepare arylAu(I) species. When (phosphine)Au(I) halides or tris(phosphineAu(I))oxonium salts are treated with sodium tetraphenylborate, it gives arylAu(I) phosphines through an unusual phenyl transfer reaction as shown in (Scheme 7, equation 5).[66] Recently, Gray and co-workers have employed aryl boronic acids to obtain arylgold(I)phospines[67] (equation 6).

Au(I)alkynyl complexes has been widely explored due to its rigid-rod nature, polarizibilty, luminescence behavior and for numerous other aspects.[68] Early methods for synthesizing them involved reduction of $HAuCl_4$ by SO_2 in the presence of acetate, followed by the addition of terminal alkynes. Polymeric Au(I) acetylides $[Au(C{\equiv}CR)]_n$ were obtained by this way. Alternative methods using $[Au(NH_3)_2]^+$ have also been described for obtaining such oligomeric species.[69] In the later years, the use of Cu(I) salts in diethylamine or sodium alkoxide in alcoholic medium to achieve alkynylation gained prominence (Scheme 8, equation 2).[70] Electrochemical oxidation of gold metal in acetonitrile solution of the acetylene also proved to be an alternative high-yielding preparatory method[71] (Scheme 8, equation 3). Vicente et al. employed acetylacetonato Au(I) derivatives to obtain Au(I) acetylides[72a] and others have used alkylgold(I) complexes[72b] and *N*-substituted (phosphine)gold(I) imidazoles [72c] to achieve the same. A variety of bifunctional alkynyl ligands like $R_2PC{\equiv}CH$ or *p*-$C{\equiv}N\text{-}C_6H_4\text{-}C{\equiv}CH$ have been used in the synthesis of novel classes of metal-containing polymers. More on this class of molecules has been discussed in the introduction section of Chapter 5 in this thesis.

$$[AuCl(PPh_3)] + HC{\equiv}CC_6F_5 \xrightarrow[-[Et_2NH_2]Cl]{Et_2NH/Cu(I)Cl} [Au(C{\equiv}CC_6F_5)(PPh_3)] \quad (1)$$

$$[AuCl\{P(C_6H_4Me\text{-}4)_3\}] + HC{\equiv}CMe \xrightarrow[-HCl]{EtOH/NaOEt} [Au(C{\equiv}CMe)\{P(C_6H_4Me\text{-}4)_3\}] \quad (2)$$

$$\text{Cathode:} \quad e^- + (PhC{\equiv}CH) \longrightarrow (PhC{\equiv}C)^- + 1/2H_2(g)$$

$$\text{Anode:} \quad Au \longrightarrow Au^+ + e^-$$

$$\text{Overall reaction:} \quad Au + (PhC{\equiv}CH) \longrightarrow (PhC{\equiv}C)Au + 1/2H_2(g) \quad (3)$$

$$[AuCl(Ph_2PC{\equiv}CH)] \xrightarrow{NaOMe} [\{Au(Ph_2PC{\equiv}C-\}_x] \quad (4)$$

Scheme 8.

Au(I)carbene complexes can be achieved through several routes, some notable methods involve: (1) Nucleophilic addition of alcohols or amines to gold isocyanides.[73a] (2) Nucleophilic carbene transfer from electron-rich olefins.[73b] (3) Alkylation or protonation of gold azolyl compounds. [74] (4) Reaction of gold sources with Ag-NHC or free NHC/ generated *in situ*.[75] (Scheme 9). Among these various methods, the last method is of relevance to our work. In the year 1997, a series of liquid crystalline Au(I)-NHC were obtained by reacting *N,N'*-dialkyl benzimidazolium salts with [Au(SMe_2)Cl] under basic phase-transfer catalysis conditions.[76] Later, an alternative strategy using Ag(I)-NHC as carbene transfer agent was reported by the same group.[77] The silver carbenes can be generated either from the imidazolium salts with a silver base such as Ag_2O or by reacting free NHC with suitable silver source. Transmetalation of the thus obtained silver carbenes with Au(I) precursor complexes having a labile neutral ligand turned out to be a method of choice for obtaining Au(I)-NHC complexes (Scheme 9).

1) Routes for preparation of silver carbene complex

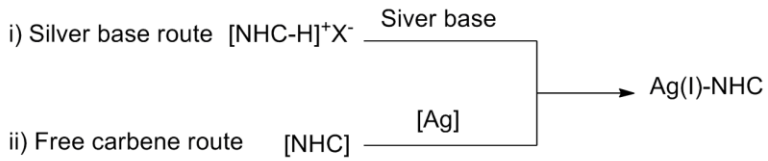

[NHC-H] = azolium moiety
Silver base = Ag_2O, Ag_2CO_3, AgOAc
[Ag] = silver source

2) Transmetallation of silver carbene complex to Au(I) carbene complex

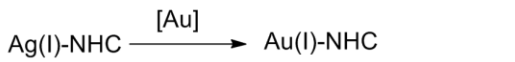

[Au] = gold(I) sources containing labile ligands
e.g. [AuCl(SMe_2)] or [AuCl(CO)]

Scheme 9.

Typically, the reactivity of NHC Au(I) halides towards substitution reactions were similar to the phosphine gold(I) counterparts[78] with an added advantage of the increase in electron density on the gold due to the good σ-donating nature of NHC. Therefore, syntheses of aryl,[79] acetylide[80] and hydroxyl bearing NHC Au(I) complexes[81] appeared in literature following analogous routes.

Photoluminescence in mononuclear gold(I) alkynyl complexes.

Exploration of photoluminescence in Au(I) complexes was mainly driven by the curiosity for short intermolecular Au···Au contacts. The first Au(I) alkynyl moieties to be studied for luminescence[68] were $[N(PPh_3)_2]$-$[Au(C{\equiv}CPh)_2]$, $[Au(PPh_3)(C{\equiv}CPh)]$ (**19**) and $[Au_2(\mu\text{-}dppe)(C{\equiv}CPh)_2]$[*dppe* = 1,2-bis(diphenylphosphino)ethane] (**20**) (Figure 16). Among these, the structurally characterized $[Au_2(\mu\text{-}dppe)(C{\equiv}CPh)_2]$(**20**) displayed aurophilic contacts to the extent of 3.153(2) Å. It showed PL in CH_2Cl_2 at 298 K and also a red-shifted solid state emission attributed to intraligand $[(d\delta^*)^1(p\sigma)^1]$ phosphorescence. Later in 1994, groups from Mingos and Yam evaluated the photophysics of a series of alkynyl-bridged binuclear complexes *viz.* $[(Ph)_n(Np)_{3-n}PAuC{\equiv}CAuP(Ph)_n(Np)_{3-n}$(*n* = 0-3)][Np = naphthalene] and $Fc_2PhPAuC{\equiv}CAuPPhFc_2$. A bathochromic shift in the emission wavelengths in the 77 K rigid matrices corresponding to increase in the number of Np groups on the phosphine suggested the existence of a $^3[\sigma(Au–P){\rightarrow}\pi^*(Np)]$ excited state.[70d] A well resolved vibronic structured emission bands in the region 400-600 nm with progressional spacings of ~2100 cm^{-1} was also observed indicating its $^3[\pi{\rightarrow}\pi^*(C{\equiv}C)]$ intra-ligand nature of transition. In a related paper[78] a series of Au(I) complexes bearing bridging phosphine or alkynyl ligands were investigated and were found to be phosphorescent. The PL of $[Au_3(dmmp)(C{\equiv}CPh)_3]$ [*dmmp* = bis(dimethylphosphinomethy1)-methylphosphine] was quenched in the presence of electron acceptors such as 4-methoxycarbonyl-*N*-methylpyridinium ion, with a bimolecular quenching rate constant of $4.98{\times}10^9$ dm^3 mol^{-1} s^{-1}. Oxidative quenching of $[Au_2(dppn)(C{\equiv}C\text{-}4\text{-}C_6H_4OMe)_2]$ [*dppn* = 1,8-bis(diphenylphosphino)naphthalene] with MV^{2+}, was investigated employing *pump-probe* nanosecond transient absorption

spectroscopy. Photophysics of mono- and diynyl complexes with nuclearity ranging from one to three have also been described. [78a], [82]

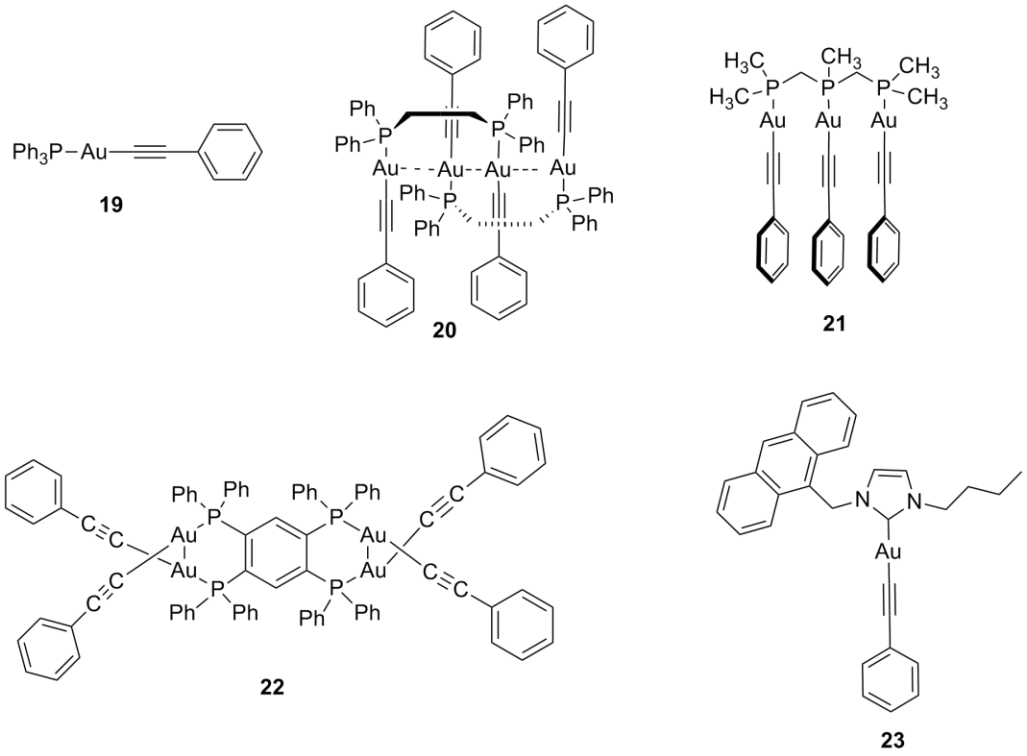

Figure 16. Selected examples of phosphine and NHC Au(I) acetylides

The high-energy absorption bands in such complexes were ascertained to IL phosphine-centered and [$\pi \rightarrow \pi^*$(C≡C)] IL transitions, whereas the low-energy absorption bands were assigned as [σ(Au–P)$\rightarrow\pi^*$(C≡C)] or metal-perturbed [$\pi \rightarrow \pi^*$(C≡C)] IL mixed with [5*d*(Au)$\rightarrow\pi^*$(C≡C)] MLCT transitions. Both the UV-vis and PL were attributed to the nature of the acetylide ligands as well as the nuclearity of the metal complexes. Similar to phosphine Au(I) alkynes, the PL properties of NHC bearing Au(I) alkynes (e.g Figure 16, **23**) have also been probed on several occasions by groups of Lin, Gray, Nolan and Che and are explained in the introduction to Chapter 4. Unlike tertiary phosphines, NHCs as neutral ligand offers more scope for varying the electronic features of the molecule. With this advantage, numerous reports on the topic continue to throng the literature hoping to

find application in optical light emitting devices. Two of the most distinctive aspects of Au(I) photophysics nevertheless relies on the relaxation of spin-forbidden nature of the lowest-energy $^3[\pi\rightarrow\pi^*$(alkynyl)] excited states owing to heavy-metal induced spin-orbit coupling (SOC) and also their modification due to the presence of aurophilic contacts.

4.0 Motivation of the Thesis.

From the preceding discussions, one can appreciate the recent surge of interest in developing energy sustainable metal based phosphorescent optoelectronic devices. It was seen that, one of the key aspects in acquiring edge over fluorescence based emitters lies in the tuning of the excited state lifetime towards an optimal[83] interval of ~5-50 μs at 298 K. Further, it was also understood that the choice of transition metal and its primary coordination sphere decides the photoluminescence attributes such as the quantum yield, wavelength and color purity.

The quantum mechanical basis of the 'spin-orbit' coupling recommends the construction of metal-organic fragments incorporating those metals which have more of its own direct influence (metal-participation) in the lowest emitting state. With this background, cyclometalated complexes based on Ir(III) and Pt(II) metal centers are currently heavily investigated by various research groups. Adding to this fact, the popularity of these privileged metals is further augmented by their overall stability and ease of synthesis. Gold belongs to the same row as Ir and Pt in the periodic table; however its utility as a room temperature emissive phosphor is largely limited in stark contrast to Ir and Pt complexes. In the following paragraphs, some of the reasons for the under-exploration of gold complexes and the motivation to pursue exploration in gold chemistry are discussed.

The atomic ion of Au^+ possesses a spin-orbit constant (ξ) value of 5104 cm^{-1} which is larger than that calculated for platinum ξ = 4481 cm^{-1}. Also, the extent of spin-orbit splitting of the low-lying ^{3}D microstates is to the extent of 13000 cm^{-1}.[84] Therefore one could expect that organometallic complexes incorporating gold ion would also show large SOC values effecting ultrafast intersystem crossing. However, this fact is largely overshadowed due to several other reasons: (1) First is the ligand dominated

photophysics in gold complexes; most of the previous studies concerning photoluminescence in gold complexes have shown limited participation of the metal in the emission process, which means that the internal conversion (IC) is principally a faster process leading to non emissivity at RT. (2) The commonly believed low-lying *d-d* metal orbitals in organogold complexes are also thought to be prominent channel for increased non-radiative decay rates. (3) The chemical nature of gold complexes; the strong oxidizing and electrophilic aspects of organogold compounds has led to a perception that gold complexes are unstable and therefore unsuitable for PL applications, and finally (4) the scarcity of robust synthetic routes for acquiring stable luminescent organometallic gold fragments.

With the passage of time, newer applications have emerged which do not strictly require all the 'theoretically ideal' aspects to be fulfilled. For example broad and structured emission profiles of a ligand dominated triplet emission are now acceptable for white light emitting devices (WOLED). Charged complexes are now growingly important in light emitting electrochemical cell (LECs) technology. In this changing scenario we thought that gold can be a suitable metal for further exploration. Much more importantly we believed that establishing newer routes and stabilization of both Au(I) and Au(III) complexes with judicious choice of ligand environment can result in stable room temperature phosphorescent molecules.

At the time of the start of the dissertation in 2008, the tridentate (C^N^C) cyclometalated gold acetylides[53] (scheme 6, example **14**) were the sole class of charge neutral Au(III) complexes, which were found to be emissive at room temperature. Similarly, there was not a single thorough report describing synthesis and photophysical aspects of *N*-heterocyclic carbene bearing Au(I) σ-acetylides, although the photoluminescence of phosphine ligated Au(I) complexes were previously dealt in the groups of Che and Yam. In this regard, we were prompted to pursue investigations in this area primarily with three broad visions in mind. First our aim was to develop novel routes to access stable and charge neutral Au(I) and Au(III) organometallic units which are phosphorescent at room temperature. Secondly we aimed to understand the photoluminescence properties of the

synthesized molecules in depth and thirdly our interest was directed in exploring the possibility of applying the organogold fragments as small molecule phosphors or incorporating them as modular monomer units in phosphorescent oligomers/polymers.

5.0 References

[1] (a) Birks, J. B. In *Photophysics of Aromatic Molecules*, Wiley: NY, 1970. (b) Strickler, S. J.; Berg, R. A. *J. Chem. Phys*. **1962**, *37*, 814.

[2] (a) Avouris, P.; Gelbart, W. M.; El-Sayed, M. A. *Chem. Rev.* **1977**, *77*, 793. (b) Freed, K. F.; Jortner, J. *J. Chem. Phys*. **1970**, 52, 6272. (c) Bixon, M.; Jortner, J. *J. Chem. Phys.* **1968**, 48, 715.

[3] (a) Harrigan, R. W.; Crosby, G. A. *J. Chem. Phys.* **1973**, *59*, 3468. (b) Hipps, K.W.; Crosby, G. A. *J. Am. Chem. Soc.* **1975**, *97*, 7042.

[4] (a) Tang, C. W.; Vanslyke, S. A. *Appl. Phys. Lett.* **1987**, *51*, 913. (b) Weiss, J. O.; Krause, R.; Paetzold, R. *Adv. in Solid State Phys.* **2008**, *46*, 321.

[5] Burroughes, J. H.; Bradley, D. D. C.; Brown, A. R.; Marks, R. N.; Mackay, K.; Friend, R. H.; Burns, P. L.; Holmes, A. B. *Nature* **1990**, *347*, 539.

[6] Geffroy, B.; Roy, P.-L.; Prat, C. *Polym. Int.* **2006**, 55, 572.

[7] (a) Marcus, R. A. *Angew. Chem., Int. Ed. Engl.* **1993**, *32*, 1111. (b) Miller, J. R.; Calcaterra, L. T.; Closs, G. L. *J. Am. Chem. Soc.* **1984**, *106*, 3047.

[8] Baldo, M. A.; O'Brien, D. F.; You, Y.; Shoustikov, A.; Sibley, S.; Thompson, M. E.; Forrest, S. R. *Nature* **1998**, *395*, 151.

[9] (a) Chen, P. Y.; Duesing, R.; Graff, D. K.; Meyer, T. J. *J. Phys. Chem.* **1991**, *95*, 5850. (b) Chen, P. Y.; Westmoreland, T. D.; Danielson, E.; Schanze, K. S.; Anthon, D.; Neveux, P. E.; Meyer, T. J. *Inorg. Chem.* **1987**, *26*, 1116.

[10] (a) Wilson, J. S.; Dhoot, A. S.; Seeley, A. J. A. B.; Khan, M. S.; Köhler, A.; Friend, R. H. *Nature* **2001**, *413*, 828. (b) Baldo, M. A.; O'Brien, D. F.; Thompson, M. E.; Forrest, S. R. *Phys. Rev. B* **1999**, *60*, 14422.

[11] (a) Yersin, H. *Topics in Current Chemistry* **2004**, 241, 1. (b) Yersin, H.; Finkenzeller, W. J. In *Highly Efficient OLEDs with Phosphorescent Materials*;

Yersin, H., Ed.; Wiley-VCH: Weinheim, 2007. (c) Yersin, H. In *Transition Metal and Rare Earth Compounds III*, 2004; Vol. 241.

[12] (a) Brooks, J.; Babayan, Y.; Lamansky, D.; Djurovich, P.; Tsyba, I.; Bau, R.; Thompson, M. E.; *Inorg. Chem.,* **2002**, *41*, 3055. (b) Williams, J. A. G. *Top. Curr. Chem.* **2007**, *281*, 205.

[13] (a) Goldsmith, J. I.; Hudson, W. R.; Lowry, M. S.; Anderson, T. H.; Bernhard, S. *J. Am. Chem. Soc.* **2005**, *127*, 7502. (b) Tinker, L. L.; McDaniel, N. D.; Curtin, P. N.; Smith, C. K.; Ireland, M. J.; Bernhard, S. *Chem.–Eur. J.* **2007**, *13*, 8726. (c) Gade, L. H. *Koordinationschemie*; Wiley-VCH: Verlag GmbH: Weinheim, 1998.

[14] (a) Neve, F.; Crispini, A.; Pietro, C. D.; Campagna, S. *Organometallics* **2002**, *21*, 3511. (b) Harvey, P.D.; Gray, H. B. *J. Am. Chem. Soc.* **1988**, *110*, 2145.

[15] Sinha, P.; Wilson, A. K.; Omary, M. A. *J. Am. Chem. Soc*, **2005**, *127*, 12488.

[16] Gimeno, M. C. In *Modern Supramolecular Gold Chemistry: Gold-Metal Interactions and Applications*; Laguna. A., Ed.; Wiley-VCH: Weinheim, 2008, Chap. 1.

[17] Schmidbaur, H.; Grohmann, A.; Olmos, M. E. In *Gold: Progress in Chemistry, Biochemistry and Technology*; Schmidbaur, H., Ed.; Wiley: NewYork, 1999.

[18] Blake, A. J.; Greig, J. A.; Holder, A. J.; Hyde, T. I.; Taylor, A.; Schröder, M. *Angew. Chem., Int. Ed. Engl*. **1990**, *29*, 197.

[19] (a) Bergendahl, T. J. *J. Chem. Edu*. **1975**, *52*, 731. (b) Eijndhoven, J. C. M. T.; Verschoor, G. C. *Mater. Res. Bull*. **1974**, *9*, 1667. (c) Berthold, H. J.; Ludwig, W. Z. *Naturforsch. Teil B* **1980**, *35*, 970. (d) Strähle, J.; Gelinek, J.; Kölmel, M.; Nemcek, A. M. *Z. Naturforsch. Teil B* **1979**, *34*, 1047. (e) Calderazzo, F.; Dell'Amico, D. B. *Inorg. Chem*. **1982**, *21*, 3639. (f) Bertinotti, C.; Bertinotti, A. *Acta Crystallogr.* **1972**, *B28*, 2635.

[20] Laguna, A.; Laguna, M. *Coord. Chem. Rev*. **1999**, *193-195*, 837.

[21] Schmidbaur, H. *Angew. Chem., Int. Ed. Engl*. **1976**, *15*(12), 728

[22] Anderson, G. K. *Adv. Organomet. Chem*. **1982**, *20*, 39.

[23] Cotton, F. A.; Wilkinson, G.; Murillo, C. A.; Bochmann, M. *Advanced Inorganic Chemistry, 6th Ed*.; Wiley: New York, 1999, p. 1085.

[24] (a) Jones, P. G. *Gold Bull*. **1981**, *14*, 159. (b) Jones, P. G. *Gold Bull*. **1983**, *16*, 114. (c) Jones, P. G. *Gold Bull*. **1986**, *19*, 46.

[25] Pope, W. J.; Gibson, C. S. *J. Chem. Soc*. **1907**, 2061.

[26] (a) Gilman, H.; Woods, L. A. *J. Am. Chem. Soc*. **1948**, *70*, 550. (b) Coates, G. E.; Parkin, C. *J. Chem. Soc*. **1963**, 421.

[27] Grohmann, A.; Schmidbaur, H. In *Comprehensive Organometallic Chemistry II;* Abel, E. W.; Stone, F. G. A.; Wilkinson, G., Eds.; Pergamon: Oxford, 1995.

[28] (a) Perevalova, E. G.; Bolesov, I. G.; Kalyuzhnaya, Y. S.; Voyevodskaya, T. I.; Kuzmina, L. G.; Korsunsky, V. I.; Grandberg, K. I.; *J. Organomet. Chem.* **1989**, *369*, 267. (b) Perevalova, E. G.; Grandberg, K. I.; Smyslova, E. I.; Kalyuzhnaya, E. S. *Bull. Acad. Sci. USSR, Chem. Ser*. **1985**, 191.

[29] Novak, I. In *The Chemistry of Organic Derivatives of Gold and Silver*; Patai, S.; Rappoport, Z., Eds.; Wiley: 1999, Chap. 5.

[30] (a) Dyadchenko, V. P. *Russ. Chem. Rev*. **1982**, *51*, 265. (b) Tamaki, A.; Kochi, J. K. *J. Organomet. Chem*. **1972**, *40*, C81. (c) Tamaki, A.; Kochi, J. K. *J. Organomet. Chem*. **1976**, *64*, 411. (d) Tamaki, A.; Magennis, S. A.; Kochi, J. K. *J. Am. Chem. Soc*. **1974**, *96*, 6140. (e) Kochi, J. K. *Organometallic Mechanisms and Catalysis*; Academic Press: New York, 1978. (f) Komiya, S.; Albright, T. A.; Hoffmann, R.; Kochi, J. K. *J. Am. Chem. Soc*. **1976**, *98*, 7255.

[31] Hashmi, A. S. K.; Hutchings, G. J. *Angew. Chem. Int. Ed.* **2006**, *45*, 7896.

[32] (a) Schmidbaur, H.; Schier, A. In *Comprehensive Organometallic Chemistry III*; Mingos, D. M. P.; Crabtree, R. H., Eds.; Elsevier: Amesterdam, 2007. (c) Parish, R. V. *Gold Bull*. **1997**, *30*, 3. (d) Parish, R. V. *Gold Bull*. **1997**, *30*, 55. (e) Parish, R. V. *Gold Bull*. **1998**, *31*, 14.

[33] Jones, P. G. *Gold Bull*. **1981**, *14*, 102. (b) Schmidbaur, H.; Pollok, T.; Herr, R.; Wagner, F. E.; Bau, R.; Riede, J.; Müller, G. *Organometallics* **1986**, *5*, 566. (c) Scherbaum, F.; Grohmann, A.; Huber, B.; Krüger, C.; Schmidbaur, H. *Angew. Chem., Int. Ed. Engl.* **1988**, *27*, 1544. (d) Schmidbaur, H.; Graf, E.; Müller, G.

Angew. Chem., Int. Ed. Engl. **1988**, *27*, 417. (e) Schmidbaur, H.; Schier, A. *Chem. Soc. Rev.* **2012**, *41*, 370.

[34] Pyykkö, P.; *Angew. Chem. Int. Ed*. **2004**, *43*, 4412. (b) Barysz, M.; Pyykkö, P. *Chem. Phys. Lett*. **2000**, *325*, 225. (c) Pyykkö, P.; Desclaux, J. P. *Acc. Chem. Res*. **1979**, *12*, 276. (d) Bartlett, N. *Gold Bull*. **1998**, *31*, 22.

[35] (a) King, C.; Wang, J. C.; Khan, M. N. I.; Fackler, J. P., Jr. *Inorg. Chem*. **1989**, *28*, 2145. (b) Che, C. M.; Kwong, H-L.; Poon, C -K.; Yam, V. W-W. *J. Chem. Soc., Dalton Trans*. **1990**, 3215. (c) Nagasundaram, N.; Roper. G.; Biscoe, J.; Chai, J. W.; Patterson, H. H.; Blom, N.; Ludi, A. *Inorg. Chem*. **1986**, *25*, 2947. (d) Schwerdtfeger, P.; Bruce, A. E.; Bruce, M. R. M. *J. Am. Chem. Soc*. **1998**, *120*, 6587. (e) Gade. L. H. *Angew. Chem., Int. Ed. Engl.* **1997**, *36*, 1171. (f) Pintado-Alba, A.; De la Riva, H.; Nieuwhuyzen, M.; Bautista, D.; Raithby, P. R.; Sparkes, H. A.; Teat, S. J.; López-de-Luzuriaga, J. M.; Lagunas, M. C. *Dalton Trans*. **2004**, 3459. (g) Lee,Y. A.; McGarrah, J. E.; Lachicotte, R. J.; Eisenberg, R. *J. Am. Chem. Soc*. **2002**, *124*, 10662. (h) Pan, Q. J.; Zhang, H. X. *Organometallics* **2004**, *23*, 5198.

[36] (a) Parshall, G. W. *Acc. Chem. Res*. **1970**, *3*, 139. (b) Dehand, J.; Pfeffer, M. *Coord. Chem. Rev*. **1976**, *18*, 327. (c) Bruce, M. I. *Angew. Chem., Int. Ed. Engl.* **1977**, *16*, 73. (d) Omae, I. In *Organometallic Intramolecular Coordination Compounds*; Elsevier: Amsterdam, 1986. (e) Albrecht, M. *Chem. Rev*. **2010**, *110*, 576-623. (f) Omae, I. *Chem. Rev*. **1979**, *79*, 287. (g) Omae, I. *Coord. Chem. Rev*. **1982**, *42*, 245. (h) Omae, I. *Coord. Chem. Rev*. **1979**, *28*, 97.

[37] Kharasch, M. S.; Isbell, H. S. *J. Am. Chem. Soc*. **1931**, *53*, 3053.

[38] Henderson, W. *Adv. Organomet. Chem*. **2006**, *54*, 207.

[39] (a) Nonoyama, M.; Nakajima, K.; Nonoyama, K. *Polyhedron* **1997**, *16*, 4039. (b) Ieda, H.; Fujiwara, H.; Fuchita, Y. *Inorg. Chim. Acta* **2001**, *319*, 203. (c) Constable, E. C.; Sousa, L. R. *J. Organomet. Chem*. **1992**, *427*, 125. (d) Fuchita, Y.; Ieda, H.; Tsunemune, Y.; Kinoshita-Nagaoka, J.; Kawano, H. *J. Chem. Soc., Dalton Trans*. **1998**, 791. (e) Fuchita, Y.; Ieda, H.; Kayama, A.; Kinoshita-Nagaoka, J.; Kawano, H.; Kameda, S.; Mikuriya, M. *J. Chem. Soc., Dalton*

Trans. **1998**, 4095. (f) Constable, E. C.; Leese, T. A. *J. Organomet. Chem*. **1989**, *363*, 419. (g) Fuchita, Y.; Ieda, H.; Yasutake, M. *J. Chem. Soc., Dalton Trans*. **2000**, 271. (h) Fuchita, Y.; Ieda, H.; Wada, S.; Kameda, S.; Mikuriya, M. *J. Chem. Soc., Dalton Trans.* **1999**, 4431. (i) Cinellu, M. A.; Zucca, A.; Stoccoro, S.; Minghetti, G.; Manassero, M.; Sansoni, M. *J. Chem. Soc., Dalton Trans*. **1995**, 2865. (j) Brown, S. D. J.; Henderson, W.; Kilpin, K. J.; Nicholson, B. K. *Inorg. Chim. Acta* **2007**, *360*, 1310. (k) Bennett, M. A.; Hoskins, K.; Kneen, W. R.; Nyholm, R. S.; Hitchcock, P. B.; Mason, R.; Robertson, G. B.; Towl, A. D. C. *J. Am. Chem. Soc*. **1971**, *93*,4591.

[40] Vicente, J.; Chicote, M. T.; Bermúdez, M. D. *J. Organomet. Chem*. **1984**, *268*, 191. (b) Parish, R. V.; Wright, J. P.; Pritchard, R. G. *J. Organomet. Chem*. **2000**, *596*, 165. (c) Vicente, J.; Chicote, M. T. *Inorg. Chim. Acta*. **1981**, *54*, L259. (d) Vicente, J.; Bermúdez, M. D.; Carrión, F. J.; Jones, P. G. *Chem. Ber*. **1996**, *129*, 1301. (e) Bonnardel, P. A.; Parish, R. V. *J. Organomet. Chem*. **1996**, *515*, 221.

[41] Bennett, M. A.; Bhargava, S. K.; Hockless, D. C. R.; Welling, L. L.; Willis, A. C. *J. Am. Chem. Soc*. **1996**, *118*, 10469. (b) Bhargava, S. K.; Mohr, F.; Bennett, M. A.; Welling, L. L.; Willis. A. C. *Organometallics* **2000**, *19*, 5628.

[42] Usón, R.; Vicente, J.; Cirac, J. A.; Chicote, M. T. *J. Organomet.Chem.* **1980**, *198*, 105-112.

[43] Dekker, J.; Münninghoff, J. W.; Boersma, J. *Organometallics* **1987**, *6*, 1236.

[44] Constable, E. C.; Leese, T. A. *J. Organomet. Chem.* **1989**, *363*, 419-424.

[45] (a) Mansour, M. A.; Lachicotte, R. J.; Gysling, H. J.; Eisenberg, R. *Inorg. Chem*. **1998**, *37*, 4625. (b) Ivanov, M. A.; Puzyk, M. V. *Russian J. Gen. Chem*. **2001**, 71, 1660 (Transl. from *Zh. Obsch. Khim*. **2001**, *71*, 1751).

[46] Vicente, J.; Chicote, M. T.; Lozano, M. I.; Huertas, S. *Organometallics* **1999**, *18*, 753.

[47] Fan, D.; Meléndez, E.; Ranford, J. D.; Lee, P. F.; Vittal, J. J. J. *Organomet. Chem.* **2004**, *689*, 2969.

[48] Nonoyama, M.; Nakajima, K. *Transition Met. Chem*. **1999**, *24*, 449.

[49] Cinellu, M. A.; Zucca, A.; Stocoro, S.; Minghetti, G.; Manassero, M.; Sansoni, M. *J. Chem. Soc., Dalton Trans.* **1996**, 4217.

[50] (a) Parish, R. V.; Wright, J. P.; Pritchard, R. G. *J. Organomet. Chem*. **2000**, *596*, 165. (b) Bonnardel, P. A.; Parish, R. V. *J. Organomet. Chem.* **1996**, *515*, 221. (c) Bonnardel, P. A.; Parish, R. V.; Pritchard, R. G. *J. Chem. Soc., Dalton Trans.* **1996**, 3185.

[51] Wong, K.-H.; Cheung, K.-K.; Chan, M. C.-W.; Che, C.-M. *Organometallics* **1998**, *17*, 3505. (b) Yam, V. W.-W.; Wong, K. M.-C.; Hung, L.-L.; Zhu, N. *Angew. Chem. Int. Ed.* **2005**, 44, 3107. (c) Constable, E. C.; Henney, R. P. G.; Leese, T. A.; Tocher, D. A. *J. Chem. Soc., Dalton Trans.* **1990**, 443.

[52] Vicente, J.; Bermúdez, M. D.; Chicote, M. T.; Sanchez-Santano, M. J. *J. Organomet. Chem.* **1989**, *371*, 129.

[53] (a) Yam, V. W.-W.; Wong, K. M.-C.; Hung, L.-L.; Zhu, N. *Angew. Chem. Int. Ed.*, **2005**, 44, 3107. (b) Wong, K. M.-C.; Zhu, X.; Hung, L.-L.; Zhu, N.; Yam, V. W.-W.; Kwok, H.-S. *Chem. Commun*. **2005**, 2906. (c) Au, V. K.-M.; Wong, K. M.-C.; Tsang, D. P.-K.; Chan, M.-Y.; Zhu, N.; Yam, V. W.-W. *J. Am. Chem. Soc*. **2010**, *132*, 14273. (d) Wong, K. M.-C.; Hung, L. L.; Lam, W. H.; Zhu, N. Y.; Yam, V. W. -W. *J. Am. Chem. Soc.* **2007,** *129*, 4350.

[54] Yam, V. W.-W.; Au, V. K.-M.; Wong, K. M.-C.; Zhu, N. *J. Am. Chem. Soc*. **2009**, *131*, 9076.

[55] (a) Yam, V.W.-W.; Cheng, E. C. C. *Top. Curr. Chem.* **2007**, *281*, 269. (b) Bronner, C.; Wenger O. S. *Dalton Trans.* **2011**, *40*, 12409.

[56] (a) Chan, C. W.; Wong, W. T.; Che C.-M. *Inorg. Chem.* **1994**, *33*, 1266. (b) Liu, H. Q.; Cheung, T. C.; Peng, S. M.; Che C.-M. *J. Chem. Soc., Chem. Commun*. **1995**, 1787.

[57] Wong, K.-H.; Cheung, K.-K.; Chan, M. C.-W.; Che, C.-M. *Organometallics*, **1998**, *17*, 3505.

[58] Yang, B.-Z.; Zhou, X.; Liu, Y.; Bai, F.-Q.; Zhang, H. -X. *J. Phys. Chem. A*, **2009**, *113*, 9396.

[59] Schmidbaur, H.; Grohmann, A.; Olmos, M. E.; Schier, A. In *The Chemistry of Organic Derivatives of Gold and Silver*: Patai, S.; Rappaport, Z., Eds.; Wiley: 1999. Chap. 8.

[60] Teo, B. K.; Zhang, H.; Shi, X. *J. Am. Chem. Soc.* **1990**, *112*, 8552.

[61] Braunstein, P.; Lehner, H.; Matt. D. *Inorg. Syntheses* **1990**, *27*, 218.

[62] (a) Puddephatt, R. J.; Treurnicht, I.; *J. Organomet. Chem.* **1987**, *319*, 129. (b) Schmidbaur, H.; Pollok, T.; Herr, R.; Wagner, F. E.; Bau, R.; Riede, J.; Müller, G. *Organometallics*, **1986**, *5*, 566.

[63] Perevalova, E. G.; Bolesov, I. G.; Kalyuzhnaya, Y. S.; Voyevodskaya, T. I.; Kuzmina, L. G.; Korsunsky, V. I.; Grandberg, K. I. *J. Organomet. Chem.***1989**, *369*, 267.

[64] (a) Kadish, K.; Davis, D. G.; Fuhrhop, J. H. *Angew. Chem., Int. Ed. Engl.* **1972**, *11*, 1014. (b) Hay, C. H.; Johnson, B. F. G.; Lewis, J.; McQueen, R. C. S.; Raithby, P. R.; Sorrell, R. M.; Taylor, M. J. *Organometallics*, **1985**, *4*, 202.

[65] (a) Usón, R.; Laguna, A.; Villacampa, M. D. *Inorg. Chim. Acta* **1984**, *81*, 25. (b) Usón, R.; Laguna, A.; Laguna, M.; Fraile, M. N.; Jones, P. G.; Sheldrick, G. M. *J. Chem. Soc., Dalton Trans.* **1986**, 291.

[66] Forward, J. M.; Fackler, Jr. J. P.; Staples, R. J. *Organometallics*, **1995**, *14*, 4194. (b) Sladek, A.; Hofreiter, S.; Paul, M.; Schmidbaur, H.; *J. Organomet. Chem.* **1995**, *501*, 47.

[67] Partyka, D. V.; Zeller, M.; Hunter, A. D.; Gray, T. G. *Angew.Chem. Int. Ed.* **2006**, *45*, 8188.

[68] Li, D.; Hong, X.; Che, C.-M.; Lo, W.-C.; Peng, S.-M. *J. Chem. Soc., Dalton Trans*. **1993**, 2929.

[69] (a) Mingos, D. M. P.; Yau, J.; Menzer, S.; Williams, D. J. *Angew. Chem., Int. Ed. Engl.* **1995**, *34*, 1894. (b) Grohmann, A. *Angew. Chem., Int. Ed. Engl.* **1995**, *34*, 2107.

[70] (a) Bruce, M. I.; Horn, E.; Matisons, J. G.; Snow, M. R. *Aust. J. Chem.* **1984**, *37*, 1163. (b) Cross, R. J.; Davidson, M. F.; *J. Chem. Soc., Dalton Trans.* **1986**, 411. (c) Cross, R. J.; Davidson, M. F.; Mclennan, A. J. *J. Organomet. Chem.* **1984**,

265, C37-C39. (d) Müller, T. E.; Choi, S. W. K.; Mingos, D. M. P.; Murphy, D.; Williams, D. J.; Yam, W. -W. V. *J. Organomet. Chem.* **1994**, *484*, 209.

[71] Casey A. T.; Vecchio, A. M. *Appl. Organomet. Chem.* **1990**, *4*, 513.

[72] (a) Vicente, J.; Chicote, M. T.; Abrisqueta, M. D. *J. Chem. Soc., Dalton Trans.* **1995**, 497. (b) Murakami, M.; Inouye, M.; Suginome, M.; Ito, Y. *Bull. Chem. Soc. Jpn.* **1988**, *61*, 3649. (c) Bonati, F.; Burini, A.; Pietroni, B. R.; Giorgini, E.; Bovio, B.; *J. Organomet. Chem.* **1988**, *344*, 119

[73] (a) Bonati, F.; Minghetti, G. *Synth. React. Inorg. Metal-Org. Chem.* **1971**, *1*, 299. (b) Cetinkaya, B.; Dixneuf. P.; Lappert, M. F.; *J. Chem. Soc., Dalton Trans.* **1974**, 1827.

[74] (a) Bonati, F.; Burini, A.; Pietroni, B. R.; Bovio, B. *J. Organomet. Chem.* **1989**, *375*, 147. (b) Raubenheimer, H. G.; Scott, F.; Roos, M.; Otte, R. *J. Chem. Soc., Chem. Commun.* **1990**, 1722.

[75] Lin, J. C. Y.; Huang, R. T. W.; Lee, C. S.; Bhattacharyya, A.; Hwang, W. S.; Lin, I. J. B. *Chem. Rev.* **2009**, *109* (8), 3561.

[76] Lee, K. M.; Lee, C. K.; Lin, I. J. B. *Angew. Chem., Int. Ed. Engl.* **1997**, *36*, 1850.

[77] Wang, H. M. J.; Lin, I. J. B. *Organometallics* **1998**, *17*, 972.

[78] Yam, V. W.-W.; Choi, S. W. K. *J. Chem. Soc., Dalton Trans.* **1996**, 4227.

[79] Raubenheimer, H. G.; Lindeque, L.; Cronje, S. *J. Organomet. Chem*. **1996**, *511*, 177.

[80] (a) Gao, L.; Partyka, D. V.; Updegraff, J. B.; Deligonul, N.; Gray, T. G. *Eur. J. Inorg. Chem.* **2009**, 2711. (b) Partyka, D. V.; Gao, L.; Teets, T. S.; Updegraff, J. B.; Deligonul, N.; Gray, T. G. *Organometallics* **2009**, *28*, 6171.

[81] Fortman, G. C.; Poater, A.; Levell, J. W.; Gaillard, S.; Slawin, A. M. Z.; Samuel, I. D. W.; Cavallo, L.; Nolan, S. P. *Dalton Trans.* **2010**, *39*, 10382.

[82] (a) Yam, V. W. -W.; Choi, S. W. K.; Cheung, K. K. *Organometallics* **1996**, *15*, 1734. (b) Yam, V. W. -W.; Choi, S. W. K.; Cheung, K. K. *J. Chem. Soc., Dalton Trans*. **1996**, 3411.

[83] Evans, R. C.; Douglas, P.; Winscom, C. J. *Coord. Chem. Rev.* **2006**, *250*, 2093.

[84] Griffith, J. S. In *The Theory of Transition Metals*; Cambridge University Press: Cambridge, 1964. (b) Fraga, S.; Saxena, K. M. S.; Karwowski, J. In *Handbook of Atomic Data. Physical Sciences Data*; Elsevier: Amsterdam (The Netherlands), 1976, *5*, 551.

Chapter 2.

Stable and Tunable Phosphorescent Neutral Cyclometalated Au(III) Diaryl Complexes

Publication 1. Garg, J. A.; Blacque, O.; Fox, T.; Venkatesan, K. *Inorg. Chem.* **2010**, *49*, 11463-11472.

Inorganic Chemistry
Article

Inorg. Chem. **2010**, *49*, 11463–11472 **11463**
DOI: 10.1021/ic101437h

Stable and Tunable Phosphorescent Neutral Cyclometalated Au(III) Diaryl Complexes

Jai Anand Garg, Olivier Blacque, Thomas Fox, and Koushik Venkatesan*

Institute of Inorganic Chemistry, University of Zürich, Winterthurerstrasse 190, CH-8057, Zürich, Switzerland

Received July 19, 2010

A series of novel luminescent cyclometalated Au(III) neutral complexes of the type *cis*-[(N^C)AuL] [N^C = 2-phenylpyridine (*ppy*), L = 1,1′-biphenyl (**1**)] and *cis*-[(N^C)AuL$_2$] [N^C = 2-phenylpyridine (*ppy*), L = C_6H_5 (**2**), C_6F_5 (**3**), C_6H_4-CF_3-*p* (**4**), 2-C_4H_3S (**5**)]; [N^C = 2-(2-thienyl)pyridine (*thpy*), L = C_6H_5 (**6**), C_6F_5 (**7**)]; [N^C = 2-(5-methyl-2-thienyl)pyridine (*5 m-thpy*), L = C_6F_5 (**8**)] were successfully synthesized. The X-ray crystal structures of all compounds except **3** have been determined. These complexes were found to show long-lived emission in solution at room temperature. The emission origins of the complexes have been tentatively assigned to be derived from triplet states predominantly bearing intraligand (IL) character with some perturbation from the metal center. Density functional theory (DFT) calculations were performed to evaluate the stability associated with the complexes and TD-DFT calculations to ascertain the nature of the excited state. Variation of the cyclometalated ligands in the complexes readily leads to the tuning of the nature of the lower energy emissive states.

Introduction

The search for tunable room-temperature phosphorescent neutral metal complexes has gained tremendous impetus following the near-commercialization of cyclometalated Ir(III) complexes as OLEDs.[1−4] Recently, interest in understanding the basic photoluminescence (PL) properties of previously under-explored Au(III) complexes has gained attention with a long-term vision of using them as efficient small molecule phosphors.[5] Although, gold is significantly a "heavy-metal" with spin−orbit coupling constant $\zeta = 5100\ cm^{-1}$ for its 5d electrons,[6,7] thermally accessible, low-lying metal-centered (d-d) states and the photoreactivity exhibited by these complexes are perhaps much to the disfavor of the metal being considered for OLED applications.[8−10] However, early report of a cationic diimine Au(III) complex[9] and more recently biscyclometalated complexes of the type [Au(C^N^C)L] where L = aryl alkynyl[11,12] as well as [Au(C^N^C)(NHC)]-[PF_6][13] has led to the cognition that strong σ-donating ligands are key for populating the emissive states and also for reducing the electrophilicity at the Au(III) metal center. We hypothesized that cyclometalation, by the way of employing strong field aromatic stabilized carbanions as ligands, would sufficiently destabilize the metal centered (MC) transition to higher energies thereby creating a conducive metal−ligand environment for effective mixing of singlet−triplet states and radiative relaxation from the triplet manifold.

Pertinent to our aim of creating Au(III) complexes enriched with gold−carbon bonds and evaluating their photophysical properties, methods for the syntheses of di- or triaryl Au(III) complexes were of interest. Vicente and co-workers have reported extensive investigations, notably devoted toward development of synthetic methodologies for the creation of diaryl Au(III) complexes.[14−38] Triaryl Au(III) complexes are relatively less common, nevertheless, not completely unknown;

*To whom correspondence should be addressed. E-mail: venkatesan.koushik@aci.uzh.ch.

(1) Baldo, M. A.; O'Brien, D. F.; You, Y.; Shoustikov, A.; Sibley, S.; Thompson, M. E.; Forrest, S. R. *Nature* **1998**, *395*, 151–154.
(2) Yersin, H. *Highly efficient OLEDs with Phosphorescent Materials*; Wiley-VCH: Weinheim, 2008.
(3) Nazeeruddin, M. K.; Grätzel, M. *Struct. Bonding (Berlin)* **2007**, *123*, 113–175.
(4) Chou, P.-T.; Chi, Y. *Chem.—Eur. J.* **2007**, *13*, 380–395.
(5) Wong, K. M.-C.; Zhu, X. L.; Hung, L.-L.; Zhu, N. Y.; Yam, V. W.-W.; Kwok, H.-S. *Chem. Commun*. **2005**, 2906–2908.
(6) Griffith, J. S. *The Theory of Transition Metals*; Cambridge University Press: Cambridge, 1964.
(7) Gao, L.; Partyka, D. V.; Updegraff, J. B.; Deligonul, N.; Gray, T. G. *Eur. J. Inorg. Chem*. **2009**, 2711–2719.
(8) Vogler, A.; Kunkely, H. *Coord. Chem. Rev*. **2001**, *211*, 223–233.
(9) Yam, V. W.-W.; Choi, S. W.-K.; Lai, T.-F.; Lee, W.-K. *J. Chem. Soc., Dalton Trans*. **1993**, 1001–1002.
(10) Chan, C.-W.; Wong, W.-T.; Che, C.-M. *Inorg. Chem*. **1994**, *33*, 1266–1272.
(11) Wong, K. M.-C.; Hung, L.-L.; Lam, W. H.; Zhu, N. Y.; Yam, V. W.-W. *J. Am. Chem. Soc*. **2007**, *129*, 4350–4365.
(12) Yam, V. W.-W.; Wong, K. M.-C.; Hung, L.-L.; Zhu, N. Y. *Angew. Chem., Int. Ed*. **2005**, *44*, 3107–3110.
(13) Au, V. K.-M.; Wong, K. M.-C.; Zhu, N. Y.; Yam, V. W.-W. *J. Am. Chem. Soc*. **2009**, *131*, 9076–9085.
(14) Usón, R.; Laguna, A.; Vicente, J. *J. Organomet. Chem*. **1975**, *86*, 415–421.
(15) Usón, R.; Laguna, A.; Vicente, J. *J. Organomet. Chem*. **1977**, *131*, 471–475.
(16) Usón, R.; Laguna, A.; Vicente, J.; García, J.; Bergareche, B.; Brun, P. *Inorg. Chim. Acta* **1978**, *28*, 237–243.

Published on Web 11/12/2010

interesting transmetallating procedures using organomercurials have been reported by the same group for obtaining such complexes.[39−43] It is therefore of interest to investigate these established classes of complexes as potential photoactive materials.

Our initial experiments to substitute halides in monocyclometalated Au(III) complexes using lithiated aryls were promising and encouraged us to proceed further in these lines. However, we noticed that some of these complexes showed signs of decomposition during reaction and in solid state after isolation. Complexes with two aryl ligands disposed *cis* to each other in a square planar environment could be unstable because of their ability for facile reductive elimination either forming Au(I) species or metallic gold;[10,39,44−46] this could also be understood in light of the fact that Au(III) complexes tend to have large positive redox potentials. The instability could also be reminiscent to the phenomenon of Aryl/PPh_3 "*transphobia*" commonly used in palladium chemistry.[47,48] We thought that utilization of aryl ligands bearing fluorinated substituents could render the Au(III) complexes stable because of the possible increase in the π-back-donation from the metal. Indeed, in our case, complexes synthesized with such substituents were found to be more stable.

Scheme 1

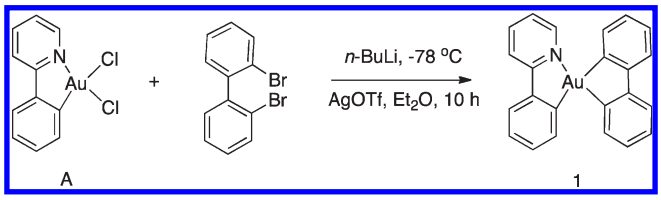

Results and Discussion

Syntheses and Characterization of Complexes. Our initial aim was to synthesize a planar (π-delocalized) cyclometalated complex using dicarbanionic chelate like 2,2′-biphenyl dianion as an ancillary ligand and evaluate its PL properties. We hoped that incorporation of biphenyl ligand would create appropriately placed intermediate electronic states below the dissociative MC states leading to interesting photophysical properties. Lithium-halogen exchange was adopted to be a general synthetic protocol for generating aryl anions suitable to substitute gold halides at low temperatures (−78 °C). Creation of complex **1** (Scheme 1) was realized with difficulty overcoming synthetic impediments to the best of 12% yield following some optimization experiments. Addition of catalytic amount of AgOTf significantly aided the formation of desired product. It needs to be mentioned here that the desired product could possibly be obtained following a transmetalation sequence described in literature and was not investigated by us.[17] Much to our encouragement the complex showed room temperature (RT) phosphorescence in fluid medium. In efforts to further improve the yield, we surmised that complexes bearing aryl carbanions as ligands but having less constrained arrangement around the metal center can be a better alternative and may exhibit better properties. Also, from a mechanistic standpoint, ligand substitution in square planar Au(III) complexes (d^8 systems) as in our case is likely to follow an associative pathway by a stepwise nucleophilic substitution sequence leading to a five coordinated ionic square planar or trigonal bipyrimidal intermediate in the transition state. It is therefore probable that the bidentate coordination modes in the later transition states would require greater activation energy than for the monodentate ones. However, on the other hand the products of the latter case provide greater risk of reductive elimination, which have been largely circumvented by utilization of perfluorinated ligands in the study presented here.

In this paper, we describe the syntheses, structural characterization, and tunable emission properties of a series of neutral cycloaurated complexes of the type *cis*-[(N^C)AuL$_n$]

(17) Usón, R.; Vicente, J.; Cirac, J. A.; Chicote, M. T. *J. Organomet. Chem.* **1980**, *198*, 105–112.
(18) Vicente, J.; Chicote, M. T.; Arcas, A.; Artigao, M. *Inorg. Chim. Acta* **1982**, *65*, L251–L253.
(19) Vicente, J.; Chicote, M. T.; Arcas, A.; Artigao, M.; Jiménez, R. *J. Organomet. Chem.* **1983**, *247*, 123–129.
(20) Vicente, J.; Chicote, M. T.; Bermúdez, M. D.; Solans, X.; Font-Altaba, M. *J. Chem. Soc., Dalton Trans.* **1984**, 557–562.
(21) Vicente, J.; Chicote, M. T.; Cayuelas, J. A.; Fernandez-Baeza, J.; Jones, P. G.; Sheldrick, G. M.; Espinet, P. *J. Chem. Soc., Dalton Trans.* **1985**, 1163–1168.
(22) Vicente, J.; Chicote, M. T.; Bermúdez, M. D.; Sanchez-Santano, M. J.; Jones, P. G.; Fittschen, C.; Sheldrick, G. M. *J. Organomet. Chem.* **1986**, *310*, 401–409.
(23) Vicente, J.; Chicote, M. T.; Saura-Llamas, I.; Turpin, J.; Fernandez-Baeza, J. *J. Organomet. Chem.* **1987**, *333*, 129–137.
(24) Vicente, J.; Chicote, M. T.; Bermúdez, M. D.; Sanchez-Santano, M. J.; Jones, P. G. *J. Organomet. Chem.* **1988**, *354*, 381–390.
(25) Vicente, J.; Chicote, M. T.; Saura-Llamas, I.; Jones, P. G.; Meyer-Bäse, K.; Erdbrügger, C. F. *Organometallics* **1988**, *7*, 997–1006.
(26) Vicente, J.; Bermúdez, M. D.; Chicote, M. T.; Sanchez-Santano, M. J. *J. Chem. Soc., Chem. Commun.* **1989**, 141–142.
(27) Vicente, J.; Bermúdez, M. D.; Chicote, M. T.; Sanchez-Santano, M. J. *J. Organomet. Chem.* **1989**, *371*, 129–135.
(28) Vicente, J.; Bermúdez, M. D.; Chicote, M. T.; Sanchez-Santano, M. J. *J. Organomet. Chem.* **1990**, *381*, 285–292.
(29) Vicente, J.; Bermúdez, M. D.; Chicote, M. T.; Sanchez-Santano, M. J. *J. Chem. Soc., Dalton Trans.* **1990**, 1945–1950.
(30) Vicente, J.; Bermúdez, M. D.; Escribano, J.; Carrillo, M. P.; Jones, P. G. *J. Chem. Soc., Dalton Trans.* **1990**, 3083–3089.
(31) Vicente, J.; Bermúdez, M. D.; Sanchez-Santano, M. J.; Payá, J. *Inorg. Chim. Acta* **1990**, *174*, 53–56.
(32) Vicente, J.; Chicote, M. T.; Saura-Llamas, I. *J. Chem. Soc., Dalton Trans.* **1990**, 1941–1944.
(33) Vicente, J.; Chicote, M. T.; Lagunas, M. C.; Jones, P. G. *J. Chem. Soc., Dalton Trans.* **1991**, 2579–2583.
(34) Vicente, J.; Bermúdez, M. D.; Carrillo, M. P.; Jones, P. G. *J. Chem. Soc., Dalton Trans.* **1992**, 1975–1980.
(35) Vicente, J.; Bermúdez, M. D.; Carrillo, M. P.; Jones, P. G. *J. Organomet. Chem.* **1993**, *456*, 305–312.
(36) Vicente, J.; Bermúdez, M. D.; Carrión, F. J. *Inorg. Chim. Acta* **1994**, *220*, 1–3.
(37) Vicente, J.; Bermúdez, M. D.; Carrión, F. J.; Jones, P. G. *J. Organomet. Chem.* **1996**, *508*, 53–57.
(38) Vicente, J.; Chicote, M. T. *Coord. Chem. Rev.* **1999**, *195*, 1143–1161.
(39) Vicente, J.; Bermúdez, M. D.; Escribano, J. *Organometallics* **1991**, *10*, 3380–3384.
(40) Vicente, J.; Bermúdez, M. D.; Carrión, F. J.; Jones, P. G. *Chem. Ber.* **1996**, *129*, 1301–1306.
(41) Vicente, J.; Bermúdez, M. D.; Carrión, F. J.; Jones, P. G. *Chem. Ber.* **1996**, *129*, 1395–1399.
(42) Bardaji, M.; Laguna, A. *Inorg. Chim. Acta* **2001**, *318*, 38–44.
(43) Bardaji, M.; Laguna, A.; Vicente, J.; Jones, P. G. *Inorg. Chem.* **2001**, *40*, 2675–2681.
(44) Komiya, S.; Albright, T. A.; Hoffmann, R.; Kochi, J. K. *J. Am. Chem. Soc.* **1976**, *98*, 7255–7265.
(45) Cinellu, M. A.; Zucca, A.; Stoccoro, S.; Minghetti, G.; Manassero, M.; Sansoni, M. *J. Chem. Soc., Dalton Trans.* **1996**, 4217–4225.
(46) Kar, A.; Mangu, N.; Kaiser, H. M.; Beller, M.; Tse, M. K. *Chem. Commun.* **2008**, 386–388.
(47) Vicente, J.; Arcas, A.; Bautista, D.; Jones, P. G. *Organometallics* **1997**, *16*, 2127–2138.
(48) Vicente, J.; Abad, J. A.; Frankland, A. D.; de Arellano, M. C. R. *Chem.—Eur. J.* **1999**, *5*, 3066–3075.

Scheme 2

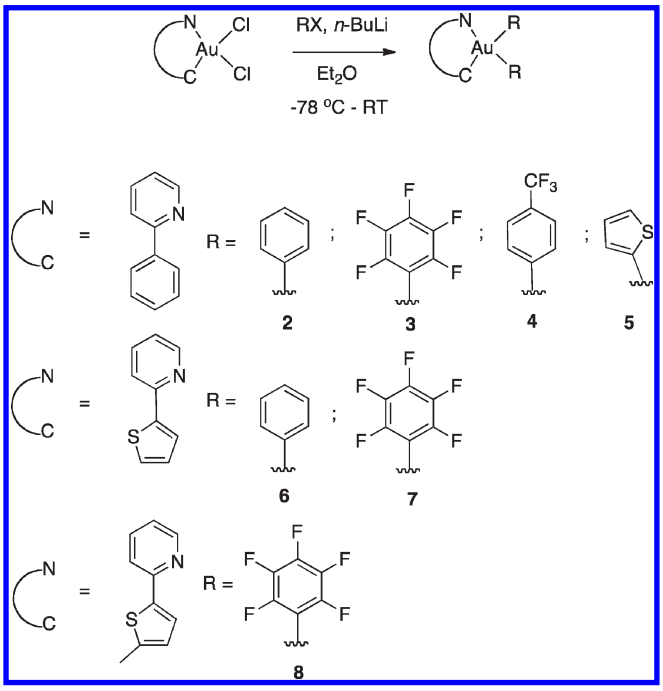

(L = aryl, n = 1, 2) most of which (**1**, **3**, **4**, **6**−**8**) exhibits good stability in common organic solvents and are also stable in the solid state for months under ambient conditions. Au(III) complexes, namely, *cis*-[(N^C)AuL] [N^C = 2-phenylpyridine (*ppy*), L = 1,1′-biphenyl (**1**)]; *cis*-[(N^C)-AuL_2] [N^C = 2-phenylpyridine, L = C_6H_5 (**2**), C_6F_5 (**3**), C_6H_4-CF_3-*p* (**4**), 2-C_4H_3S (**5**)]; [N^C = 2-(2-thienyl)-pyridine (*thpy*), L = C_6H_5 (**6**), C_6F_5 (**7**)]; [N^C = 2-(5-methyl-2-thienyl)pyridine (*5 m-thpy*), L = C_6F_5 (**8**)] were prepared from their corresponding cycloaurated Au(III) dichlorides (Scheme 2). Yields for complexes **2**−**8** were modest in the range 25−56% owing to the concomitant biaryl formation via reductive elimination as confirmed by ^{1}H NMR study. To our knowledge this is the first report of structurally characterized Au(III) monocyclometalated complexes with diaryl ligands. A cycloauration method described earlier in literature[49] was followed for obtaining dichloride precursor *cis*-[(N^C)$AuCl_2$] [N^C = 2-phenylpyridine (*ppy*)] for the synthesis of **1**−**5**. Complexes **6** and **7** were obtained from *cis*-[(N^C)$AuCl_2$] [N^C = 2-(2-thienyl)pyridine (*thpy*)] by following a procedure[50] which was also analogously adopted for synthesizing previously unknown *cis*-[(N^C)$AuCl_2$] [N^C = 2-(5-methyl-2-thienyl)pyridine (*5 m-thpy*)], the dihalide precursor for **8**. It is important to note that these starting materials do not exhibit RT phosphorescence.[51]

The stability of these complexes were found to depend significantly on the nature of the aryl ligands. Complexes containing nonperfluorinated groups showed signs of gradual decomposition in the solid state. The thermal stability of complexes **2** and **3** in solid state were studied using thermogravimetric analysis (TGA) (See Supporting Information, Figure S2). **2** and **3** showed initial weight loss ($\sim T_{10\%}$) in the interval 100−185 °C and 133−242 °C, respectively; the onset of total degradation (T_d) of **3** was observed at relatively higher temperature (T_d = 250 °C) than **2** (T_d = 180 °C).

Structural and Photophysical Characterization. X-ray single crystal structures were determined for all complexes except **3**. The perspective views of **1**, **2**, **5**, and **8** are shown in Figure 1 (for others see Figures S3−S5 in Supporting Information). As expected the Au(III) atom adopts a distorted square planar environment, the average Au−N bond distance is 2.102 Å and the mean Au−C_{aryl} bond distance of non-cyclometalated ligands (both *cis* and *trans* to nitrogen) was found to be 2.043 Å, values which correspond closely with those reported for similar [Au(C^N^C)] complexes[11,12] and the cationic diimine complexes.[9] The N−Au−C bite angles in **1**−**8** are restricted in the interval of 79.3−80.8° because of the steric requirements of the cyclometalating N^C ligands; consequently the respective *trans* angle to the ancillary carbons also deviates accordingly. The effect is more pronounced in **1** where there is an imposing steric congestion of both the *ppy* and biphenyl. Further, the molecular packing in the crystal structures of these complexes showed no Au···Au interactions; the shortest intermolecular Au···Au distance is 4.8022(1) Å in **1**. It is important to note that the crystal structures did not reveal the presence of any kind of solvent coordination to the metal center. Concentration dependent absorption studies of all the complexes in CH_2Cl_2 ($c \approx 10^{-6}$−10^{-4} mol dm^{-3}) did not change either the peak maxima or generate an additional low energy band confirming the absence of Au···Au interactions in solution and also precludes any excimeric (MMLCT) transitions.

Complexes **1**−**8** showed emission both in fluid solution at RT and in rigidified glass media (2-MeTHF) at 77 K. The spectroscopic data for complexes **1**−**8** are given in Table 1, and the absorption and emission profiles of complexes **1**−**3** and **6**−**8** are shown in Figure 2, respectively. Cyclometalated complexes with a *ppy* core exhibited intense absorption with lowest energy absorption maxima in the range λ = 316−338 nm. The *thpy* complexes **6** and **7** showed bathochromic shifts ($\lambda \sim 40$ nm) as expected for compounds, which inherently possess donor−acceptor (D-A) properties.[52] The red shift was more pronounced for the *5 m-thpy* complex **8** with the effect arising from the methyl substituent.[53] In general, the shape and position of absorption bands in electronic spectra resemble the skeletal vibrations of their respective ligands with a slight red shift (5−9 nm). This indicates that the π-conjugation is preserved through the metal site by mixing of the contributing frontier orbitals of the gold atom and the ligand.

Varying ligands ancillary to the cyclometalating (N^C) gold center had no marked effect on the absorption wavelengths. Increasing solvent polarity from toluene to tetrahydrofuran (THF) showed a slight hypsochromic shift ($\lambda \sim 6$ nm) for complexes **3**−**5** and for **7**−**8** indicating the ground state has more polar character as compared to the excited state. The emission spectra of the *ppy* complexes

(49) Constable, E. C.; Leese, T. A. *J. Organomet. Chem.* **1989**, *363*, 419–424.
(50) Fuchita, Y.; Ieda, H.; Wada, S.; Kameda, S.; Mikuriya, M. *J. Chem. Soc., Dalton Trans.* **1999**, 4431–4435.
(51) Mansour, M. A.; Lachicotte, R. J.; Gysling, H. J.; Eisenberg, R. *Inorg. Chem.* **1998**, *37*, 4625–4632.
(52) Tsuboyama, A.; Iwawaki, H.; Furugori, M.; Mukaide, T.; Kamatani, J.; Igawa, S.; Moriyama, T.; Miura, S.; Takiguchi, T.; Okada, S.; Hoshino, M.; Ueno, K. *J. Am. Chem. Soc.* **2003**, *125*, 12971–12979.
(53) Thomas, S. W., III; Venkatesan, K.; Müller, P.; Swager, T. M. *J. Am. Chem. Soc.* **2006**, *128*, 16641–16648.

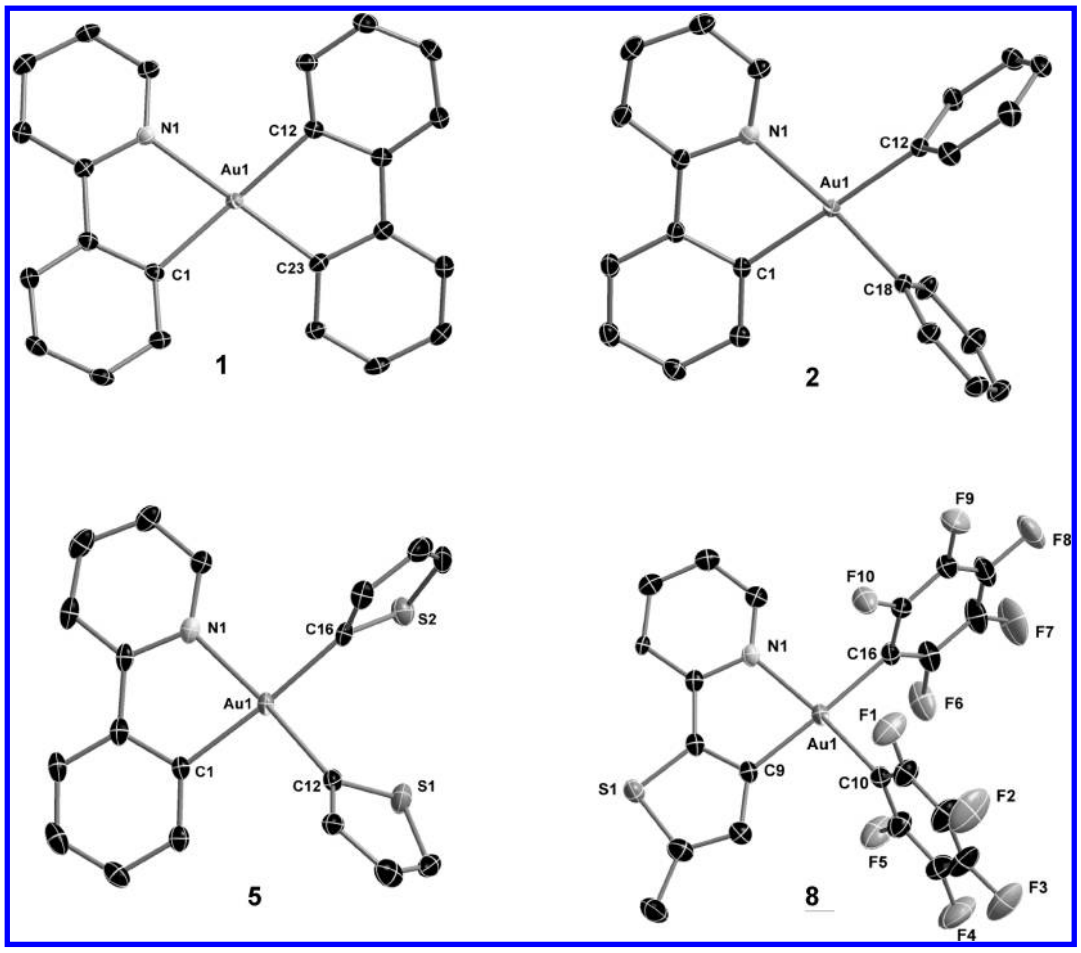

Figure 1. X-ray crystal structures of **1**, **2**, **5**, and **8** with selective atomic numbering scheme. Thermal ellipsoids are drawn at the 30% probability level. Hydrogen atoms and solvent molecules are omitted for clarity.

Table 1. Photophysical Properties of Complexes **1**−**8**

	room temperature solution (CH_2Cl_2)						
complex	absorption λ_{max}[nm] (ε_{max}/[dm^3 mol^{-1}cm^{-1}])	emission λ_{max}[nm]	τ [μs]	Φ_P[a]	k_r [s^{-1}] × 10^3	k_{nr} [s^{-1}] × 10^5	77 K glass[b] (2-MeTHF)
1	308 (5145), 317 (5385)	484, 506	1.10	3.7×10^{-3}	3.4	9.1	478, 513, 540
2	316 (8480)	467 (sh), 490, 519 (sh)	0.33	9.5×10^{-3}	28.7	30.0	453, 485, 512
3	324 (7214), 338 (5254, sh)	471 (sh), 493, 529 (sh)	4.41	1.0×10^{-3}	0.2	2.3	457, 489, 528
4	321 (8623)	470 (sh), 490, 522 (sh)	1.23	9.9×10^{-3}	8.0	8.1	452, 486, 517
5	319 (7884)	472 (sh), 492, 526 (sh)	0.53	1.9×10^{-2}	35.8	18.5	453, 489, 515
6	287 (13700), 357 (8070)	537, 569	1.15	2.5×10^{-3}	2.7	8.6	522, 541, 563
7	286 (12610), 363 (8540)	544, 577	1.12	1.5×10^{-3}	1.3	8.9	527, 545, 570
8	294 (8810), 380 (5760)	548, 592	1.21	2.0×10^{-3}	1.6	8.2	548, 593

[a] PL quantum yield determined with quinine sulfate as standard at 298 K. [b] Vibronic structured emission bands.

1−**5** in CH_2Cl_2 exhibit a low vibronic structured band with λ_{max} centered around 490 nm and more resolved progressive vibrational progression spacings of ∼1500 cm^{-1} at 77 K (2-MeTHF), which is close to stretching modes of C═C in pyridine systems. Again, the emission wavelengths did not change with different ancillary ligands like phenyl, pentafluorophenyl, *p*-trifluoromethylphenyl, and thienyl. Emission spectra of the *thpy* cyclometalates **6**−**8** depicted the same trend as for the *ppy* ones but systematically red-shifted in line with their respective absorption profiles. Vibrational spacings of about ∼1400 cm^{-1} were also observed here. On the basis of the above observations and considering the low radiative rate constant[54] $k_r \sim 10^3$−10^4 s^{-1} (see Table 1), the origin of the emission is assigned to intraligand charge transfer (^{3}ILCT) [π−π*] perturbed by the metal center. Stokes shifts of the lower lying emission in the range of 174−220 nm and lifetimes in the sub microsecond regime together with the observation of a 5 to 10-fold decrease in PL intensities upon exposure to molecular dioxygen suggest that the emission occurs from the triplet state. Isoelectronic biscyclometalated platinum(II) systems reported possess emission properties with more metal contribution in contrast to these Au(III)diaryl complexes.[55,56]

(54) Radiative (k_r) and non-radiative (k_{nr}) decay rates were estimated from the lifetime data (τ) using the formula $k_r = \Phi_P/\tau$ and $k_{nr} = (1 - \Phi_P)/\tau$ assuming radiative rate constants do not show significant temperature dependence from 77 to 298 K and k_{isc} is considered as unity.

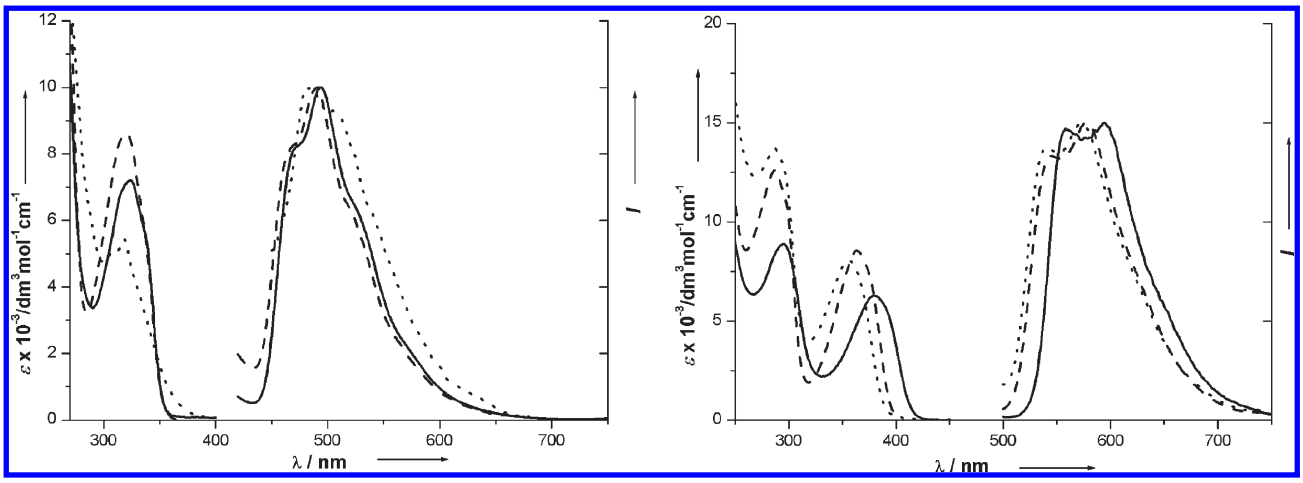

Figure 2. (left) Electronic absorption and normalized emission (*I*) spectra of **1** (dotted line), **2** (dashed line), **3** (solid line) in degassed CH_2Cl_2 at 298 K and (right) electronic absorption and normalized emission (*I*) spectra of **6** (dotted line), **7** (dashed line), **8** (solid line) in degassed CH_2Cl_2 at 298 K.

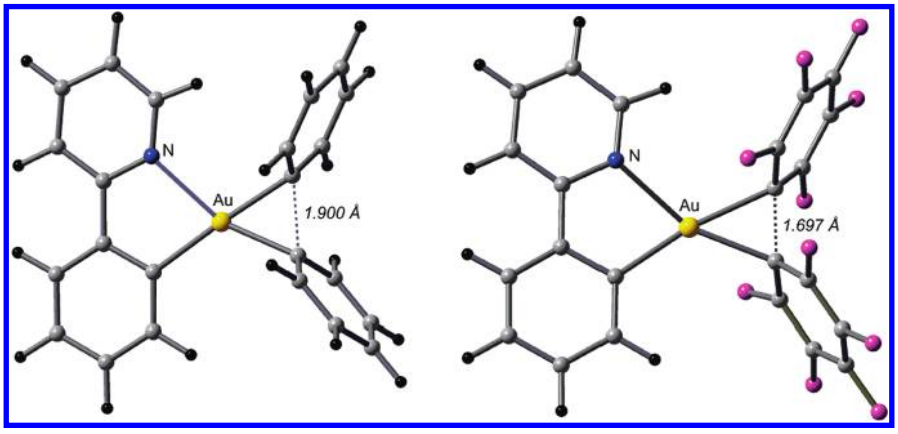

Figure 3. DFT optimized transition states **TS-2** (left) and **TS-3** (right).

DFT calculations. To gain insight into the properties of our Au(III) complexes, density functional theory (DFT) studies were carried out with the Gaussian03 program package[57] using the hybrid functional PBE1PBE[58] in conjunction with the Stuttgart/Dresden effective core potentials (SDD) basis set[59] for the Au center augmented with one f-polarization function (α = 1.050) and the standard 6-31+G(d) basis set[60] for the remaining atoms. The relative stability of the compounds bearing different ancillary aryl ligands was first investigated. The transition states (**TS**) encountered during the intramolecular dimerization of C_6H_5 in **2** and C_6F_5 in **3** were successfully optimized and characterized (Figure 3). The $C_{aryl}\cdots C_{aryl}$ distance of 1.900 for **TS-2** and 1.697 Å for **TS-3** clearly indicates that the C−C bond formation in **2** occurs in an earlier stage in comparison with **3**. Furthermore, the electronic energies reveal decomposition barrier heights of 21.9 and 40.7 kcal/mol respectively and therefore confirm that the decomposition of the Au(III) complexes leading to the formation of corresponding biphenyl is significantly faster in **2**. This is also consistent with the experimental observation for these complexes.

Time-dependent density functional theory (TD-DFT)[61−63] combined with the conductive polarizable continuum model (CPCM)[64,65] was used to produce the ten lowest singlet−singlet and singlet−triplet vertical excitations calculated

(55) Chassot, L.; Muller, E.; von Zelewsky, A. *Inorg. Chem*. **1984**, *23*, 4249–4253.
(56) Chassot, L.; von Zelewsky, A. *Inorg. Chem*. **1987**, *26*, 2814–2818.
(57) Frisch, M. J.; Trucks, G. W.; Schlegel, H. B.; Scuseria, G. E.; Rob, M. A.; Cheeseman, J. R.; Montgomery Jr., J. A.; Vreven, T.; Kudin, K. N.; Burant, J. C.; Millam, J. M.; Iyengar, S. S.; Tomasi, J.; Barone, V.; Mennucci, B.; Cossi, M.; Scalmani, G.; Rega, N.; Petersson, G. A.; Nakatsuji, H.; Hada, M.; Ehara, M.; Toyota, K.; Fukuda, R.; Hasegawa, J.; Ishida, M.; Nakajima, T.; Honda, Y.; Kitao, O.; Nakai, H.; Klene, M.; Li, X.; Knox, J. E.; Hratchian, H. P.; Cross, J. B.; Bakken, V.; Adamo, C.; Jaramillo, J.; Gomperts, R.; Stratmann, R. E.; Yazyev, O.; Austin, A. J.; Cammi, R.; Pomelli, C.; Ochterski, J. W.; Ayala, P. Y.; Morokuma, K.; Voth, G. A.; Salvador, P.; Dannenberg, J. J.; Zakrzewski, V. G.; Dapprich, S.; Daniels, A. D.; Strain, M. C.; Farkas, O.; Malick, D. K.; Rabuck, A. D.; Raghavachari, K.; Foresman, J. B.; Ortiz, J. V.; Cui, Q.; Baboul, A. G.; Clifford, S.; Cioslowski, J.; Stefanov, B. B.; Liu, G.; Liashenko, A.; Piskorz, P.; Komaromi, I.; Martin, R. L.; Fox, D. J.; Keith, T.; Al-Laham, M. A.; Peng, C. Y.; Nanayakkara, A.; Challacombe, M.; Gill, P. M. W.; Johnson, B.; Chen, W.; Wong, M. W.; Gonzalez, C.; Pople, J. A. *Gaussian 03*; Gaussian, Inc.: Wallingford, CT, 2003.
(58) Adamo, C.; Barone, V. *J. Chem. Phys*. **1999**, *110*, 6158–6170.
(59) Dunning, T. H., Jr.; Hay, P. J. *Modern Theoretical Chemistry*; Plenum: New York, 1976; Vol. *3*.
(60) Ditchfie, R.; Hehre, W. J.; Pople, J. A. *J. Chem. Phys*. **1971**, *54*, 724–728.
(61) Stratmann, R. E.; Scuseria, G. E.; Frisch, M. J. *J. Chem. Phys*. **1998**, *109*, 8218–8224.
(62) Bauernschmitt, R.; Ahlrichs, R. *Chem. Phys. Lett*. **1996**, *256*, 454–464.
(63) Casida, M. E.; Jamorski, C.; Casida, K. C.; Salahub, D. R. *J. Chem. Phys*. **1998**, *108*, 4439–4449.
(64) Barone, V.; Cossi, M. *J. Phys. Chem. A* **1998**, *102*, 1995–2001.
(65) Cossi, M.; Rega, N.; Scalmani, G.; Barone, V. *J. Comput. Chem*. **2003**, *24*, 669–681.

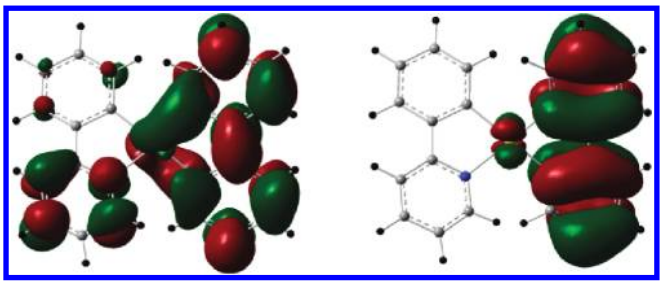

Figure 4. TD-DFT/CPCM calculated LUMO+2 (left) and HOMO (right) of the ground state geometry of **1**.

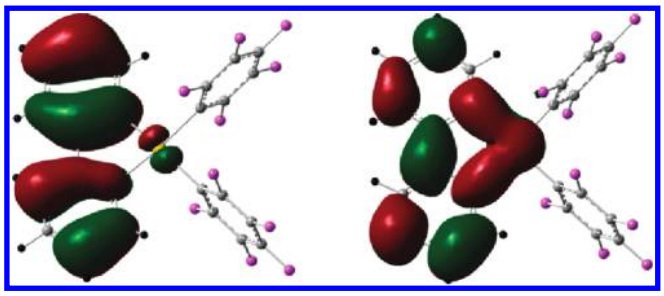

Figure 5. TD-DFT/CPCM calculated HOMO (left) and LUMO (right) of the ground state geometry of **3**.

at the ground state singlet S_0 optimized geometries. Despite the PBE1PBE[64] calculations having systematically provided underestimated absorption maxima λ_{max} by 17−20 nm (**5**−**8**) or 26−45 nm (**1**−**4**), the absorption properties of **1**−**8** and the trend observed in the experiments are well reproduced by the calculations (see Supporting Information, Table S5). For **2**−**8**, the lowest significant singlet transition $S_0 \rightarrow S_n$ (n = 1 for **3**, **6**, **7**, **8**; n = 2 for **2**, **4**; n = 3 for **5**) is the one showing the largest coefficient of the calculated excited states. The frontier molecular orbitals involved in the dominant excitation are almost exclusively located on the N^C ligands, *ppy* for **2**−**5** or *thpy* for **6**−**8** as expected. This can be attributed to a transition with an intraligand charge transfer ^{1}ILCT [$\pi \rightarrow \pi^*$] character. For **1**, the picture is different since three low energy transitions of similar intensity at 311, 288, and 282 nm were calculated. The two lowest-lying transitions $S_0 \rightarrow S_3$ and $S_0 \rightarrow S_6$ at 311 and 288 nm are due to the one-electron excitations from HOMO-2→LUMO and HOMO-4→LUMO, respectively (hereafter H = HOMO, L = LUMO). H-2 and H-4 are mainly composed of π orbitals of biphenyl (*bip*) and *ppy*, whereas L is dominantly localized on *ppy* (86%), consequently the corresponding band can be attributed to a transition with an admixture of ligand-to-ligand ^{1}LLCT [π(*bip*)→π^*(*ppy*)] and intraligand ^{1}ILCT [$\pi \rightarrow \pi^*$ (*ppy*)] characters. The $S_0 \rightarrow S_8$ transition at 282 nm with the most relevant contribution from H→L+3 accounts for an inverse charge transfer since H is at 97% on *bip* and L+3 is totally delocalized over the whole molecule.

The lowest vertical triplet S_0-T_1 transition of **1** is $\pi-\pi^*$ type defined by the configuration H→L+2 where H is mainly a π orbital localized at the *bip* ligand (97%) and L+2 is a π^* orbital delocalized at 75% on the *bip*, 17% on the *ppy* ligand, and at 8% on the metal center (Figure 4). This indicates that the excited state contains both ^{3}LLCT [π(*bip*)→π^*(*ppy*)] and ^{3}ILCT [π(*bip*)→π^*(*bip*)] characters. The DFT optimized triplet state is in agreement with the lowest-lying $\pi-\pi^*$ transition since the main variations of the geometrical parameters relative to the ground state of **1** correspond well to the electronic transition from H to L+2, especially for the C−C bond bridging the two rings of the *bip*, the bond distance of which is hardly shortened by 0.081 Å in the triplet state, a consequence of the π antibonding character of the C−C bond in H and π bonding in L+2 (which became the lower- and higher-energy singly occupied molecular orbital of the optimized triplet state). All bond distances around the metal center are also slightly shortened in the triplet state. The emission maximum of **1** was estimated by the solvent-corrected (CH_2Cl_2) energy difference between the optimized ground and triplet states. The calculated λ_{max} of 486 nm is in good agreement with the experimental data of 506 nm. In the other *ppy*-containing compounds **2**−**5**, the optimized triplet states also correspond very well to the lowest vertical singlet−triplet transitions S_0-T_1. The main difference in comparison with **1** is that the orbitals involved in the $\pi-\pi^*$ transition are mainly located on the *ppy* ligand: H-1→L (83→94%), H→L (98→92%), H-1→L (92→95%), H-2→L (95→95%) for **2**−**5**, respectively. This indicates that the excited state exhibits a ^{3}ILCT [$\pi \rightarrow \pi^*$ (*ppy*)] character, only slightly perturbed by the metal center (2−6%) (Figure 5). As a result, it was found that the main geometric changes appear in the *ppy* group where the bond distance of the C−C linker is shortened by 0.078−0.079 Å compared to the ground state parameters. The estimated emission maxima based on the calculated ground and triplet state energies correlate successfully with the experimental emission wavelengths (in parentheses) with 466 (490), 472 (493), 468 (490), and 470 (492) nm for **2**−**5**, respectively.

The same study was adopted for the *thpy* species **6**−**8**. For all the three compounds, the lowest vertical triplet S_0-T_1 transition corresponds to the H→L excitation. H and L orbitals are at 96−99% and 92−93% located on the *thpy* ligand respectively, indicating a ^{3}ILCT [$\pi \rightarrow \pi^*$ (*thpy*)] character of the triplet state. The main variations in the geometry of the optimized triplet states are no longer observed on the C−C bridge (only −0.049 to −0.056 Å) but rather in the five-membered thienyl ring with significant elongations of four over five bond distances (+0.011 to +0.096 Å), in agreement with the shape of the π/π^* H and L orbitals. The significant red-shifted emission of **6**−**8** in comparison with **1**−**5** is also well reproduced by our calculations with 569 (569), 572 (577), and 604 (592) nm for **6**−**8**, respectively.

Conclusion

We have shown for the first time that cyclometalated compounds of the type *cis*-[(N^C)AuL$_n$] (L = aryl, n = 2) are stable with the incorporation of fluorinated functional groups on the aryl rings. They show phosphorescence emission at RT in fluid solution and their emission wavelengths can be tuned by changing the cyclometalating ligand. DFT calculations in conjunction with experimental work have ascertained the relative stability of the complexes and the nature of the triplet excited state. The stability and ease of tunability demonstrated in this work make these systems amenable for the development of efficient neutral triplet phosphors for OLED applications. Several strategies are currently being pursued in

our group for the improvement of quantum yields and to obtain blue triplet emitters based on these Au(III) complexes.

Experimental Section

Materials and General Methods. Commercially available reagents were purchased from Aldrich and were used as such without further purification. Diethylether used in reactions was dried by distillation under N_2 atmosphere using sodium benzophenone ketyl radical prior to use. Sodium tetrachloroaurate (III) dihydrate was purchased from Strem chemicals. Gold(III) dichloride precursor complex [(N^C)$AuCl_2$][N^C = 2-phenylpyridine (*ppy*)] (**A**) was prepared according to a known procedure[49] and [(N^C)$AuCl_2$][N^C = 2-(2-thienyl)pyridine (*thpy*)] (**B**) was synthesized based on a different cycloauration procedure.[50] A procedure analogous to the latter was adopted for preparing precursor complex [N^C = 2-(5-methyl-2-thienyl)pyridine (*5 m-thpy*)][$AuCl_2$] (**C**), which is described below. All manipulations requiring an inert atmosphere were carried out using standard Schlenk techniques under dinitrogen. ^{1}H, ^{13}C{^{1}H}, and ^{19}F NMR spectra were recorded on Bruker AV2−400 (400 MHz) or AV-500 (500 MHz) spectrometers. Chemical shifts (δ) are reported in parts per million (ppm) referenced to tetramethylsilane (δ 0.00 ppm) using the residual proton solvent peaks as internal standards (^{1}H NMR experiments) or the characteristic resonances of the solvent nuclei (^{13}C NMR experiments). ^{19}F NMR was referenced to $CFCl_3$ (δ 0.00 ppm). Coupling constants (*J*) are quoted in hertz (Hz), and the following abbreviations are used to describe the signal multiplicities: s (singlet); d (doublet); t (triplet); q (quartet); m (multiplet); dd (doublet of doublet); td (triplet of doublet); dm (doublet of multiplet). Proton and carbon assignments have been made using routine one and two-dimensional NMR spectroscopies where appropriate. Infrared (IR) spectra were recorded on a Perkin-Elmer 1600 Fourier Transform spectrophotometer using KBr pellet with frequencies (ν_{max}) quoted in wavenumbers (cm^{-1}). Elemental microanalysis was carried out with Leco CHNS-932 analyzer. Mass spectra were run on a Finnigan-MAT-8400 mass spectrometer. TLC analysis was performed on precoated Merck Silica Gel 60F_{254} slides and visualized by luminescence quenching either at (short wavelength) 254 nm or (long wavelength) 365 nm. Chromatographic purification of products was performed on a short column (length 15.0 cm: diameter 1.5 cm) using silica gel 60, 230−400 mesh using a forced flow of eluent. UV−vis measurements were carried out on a Perkin-Elmer Lambda 19 UV/vis spectrophotometer. Emission spectra were acquired on Perkin-Elmer spectrophotometer using 450 W xenon lamp excitation by exciting at the longest-wavelength absorption maxima. All samples for emission spectra were degassed by at least three freeze−pump−thaw cycles in an anaerobic cuvette and were pressurized with N_2 following each cycle. 77 K emission spectra were acquired in frozen 2-methyltetrahydrofuran (2-MeTHF) glass. Luminescence quantum yields of (ϕ) were determined at 298 K (estimated uncertainty ±15%) using standard methods;[66] wavelength-integrated intensities (*I*) of the corrected emission spectra were compared to iso-absorptive spectra of quinine sulfate standard (ϕ_r = 0.54 in 1N H_2SO_4 air-equilibrated solution) and were corrected for solvent refractive index. Phosphorescence lifetime measurements were performed on an Edinburgh FLS920 spectrophotometer, using nF900 with 30000 Hz frequency, with 15 nm excitation and 15 nm emission slit widths. Thermogravimetric analysis (TGA) was done using a NETZSCH STA 449C instrument. The thermal stability of the samples under a nitrogen atmosphere was determined by measuring their weight loss while heating at a rate of 1 °C min^{-1} from 25 to 600 °C.

Computational Details. All calculations were performed with the Gaussian 03 program package[57] using the hybrid functional PBE1PBE[58] in conjunction with the Stuttgart/Dresden effective core potentials (SDD) basis set[59] for the Au center augmented with one f-polarization function (exponent α = 1.050) and the standard 6-31+G(d) basis set[60] for the remaining atoms. Several exchange-correlation functionals (B3LYP,[67−69] MPW1K,[70,71] BB1K,[67,72,73] PBE1PBE,[58] G96LYP,[68,72] TPSS[74,75] and TPSSLYP1W[75]) were tested on the geometry structures of **1** and **2**; the hybrid PBE1PBE provided the best match with the geometrical X-ray data and was selected for our study (see Supporting Information). Full geometry optimizations without symmetry constraints were carried out in the gas phase for both the singlet ground states (S_0) and the lowest triplet excited states (T_1). The optimized geometries were confirmed to be potential energy minima by vibrational frequency calculations at the same level of theory, as no imaginary frequencies were found. The first 10 singlet−singlet and singlet−triplet transition energies were computed at the optimized S_0 geometries, by using the time-dependent DFT (TDDFT) methodology.[61−63] Solvent effects were taken into account using the conductive polarizable continuum model (CPCM)[64,65] with dichloromethane as solvent for single-point calculations on all optimized gas-phase geometries.

X-ray Diffraction Analyses. Relevant details about the structure refinements are given in Supporting Information, Tables S1 and S2, and selected geometrical parameters are included in the captions of the corresponding figures (Supporting Information, Figures S3, S4, and S5). Intensity data were collected at 183(2) K an Oxford Xcalibur diffractometer (4-circle kappa platform, Ruby CCD detector, and a single wavelength Enhance X-ray source with Mo K_α radiation, λ = 0.71073 Å)[76] The selected suitable single crystals were mounted using polybutene oil on the top of a glass fiber fixed on a goniometer head and immediately transferred to the diffractometer. Pre-experiment, data collection, data reduction, and analytical absorption corrections[77] were performed with the Oxford program suite CrysAlisPro.[78] The crystal structures were solved with SHELXS-97[79] using direct methods. The structure refinements were performed by full-matrix least-squares on F^2 with SHELXL-97.[79] All programs used during the crystal structure determination process are included in the WINGX software.[80] The program PLATON[81] was used to check the result of the X-ray analyses. CCDC-778147−778153 contain the supplementary crystallographic data (excluding structure factors) for this paper. These data can be obtained free of charge from The Cambridge Crystallographic Data Center via www.ccdc.cam.ac.uk/data_request/cif.

[N^C = 2-(5-Methyl-2-thienyl)pyridine][$AuCl_3$]. 2-(5-methyl-2-thienyl)pyridine (0.150 g, 0.856 mmol) in acetonitrile (3.5 mL) was added to Na[$AuCl_4$]·$2H_2O$ (0.313 g, 0.787 mmol) in H_2O (3.5 mL), and the resulting mixture was stirred at room temperature for 12 h. The orange solids that precipitated out were

(66) Demas, J. N.; Crosby, G. A. *J. Phys. Chem.* **1971**, *75*, 991–1024.
(67) Becke, A. D. *Phys. Rev. A* **1988**, *38*, 3098–3100.
(68) Lee, C. T.; Yang, W. T.; Parr, R. G. *Phys. Rev. B* **1988**, *37*, 785–789.
(69) Stephens, P. J.; Devlin, F. J.; Chabalowski, C. F.; Frisch, M. J. *J. Phys. Chem.* **1994**, *98*, 11623–11627.
(70) Lynch, B. J.; Fast, P. L.; Harris, M.; Truhlar, D. G. *J. Phys. Chem. A* **2000**, *104*, 4811–4815.
(71) Lynch, B. J.; Zhao, Y.; Truhlar, D. G. *J. Phys. Chem. A* **2003**, *107*, 1384–1388.
(72) Gill, P. M. W. *Mol. Phys.* **1996**, *89*, 433–445.
(73) Zhao, Y.; Lynch, B. J.; Truhlar, D. G. *J. Phys. Chem. A* **2004**, *108*, 2715–2719.
(74) Tao, J. M.; Perdew, J. P.; Staroverov, V. N.; Scuseria, G. E. *Phys. Rev. Lett.* **2003**, *91*, 146401.
(75) Dahlke, E. E.; Truhlar, D. G. *J. Phys. Chem. B* **2005**, *109*, 15677–15683.
(76) *Xcalibur CCD System*; Oxford Diffraction Ltd: Abingdon, Oxfordshire, England, 2007.
(77) Clark, R. C.; Reid, J. S. *Acta Crystallogr., Sect. A* **1995**, *51*, 887–897.
(78) *CrysAlisPro*, Versions 1.171.32.34d-55; Oxford Diffraction Ltd: Abingdon, Oxfordshire, England.
(79) Sheldrick, G. M. *Acta Crystallogr., Sect. A* **2008**, *64*, 112–122.
(80) Farrugia, L. J. *J. Appl. Crystallogr.* **1999**, *32*, 837.
(81) Spek, A. L. *J. Appl. Crystallogr.* **2003**, *36*, 7–13.

filtered off, and the precipitate was successively washed with water and diethylether to give the title product. Yield = 0.278 g, 68%. Positive EI-MS: m/z: 476 $[M]^+$; IR (KBr): ν(Au−Cl) 363 cm^{-1}; ^1H NMR (500 MHz, CD_3CN, 298 K) δ 2.63 (s, 3H), 7.06 (d, J = 4.0 Hz, 1H), 7.72 (t, J = 5.5 Hz, 1H), 7.76 (d, J = 4.0 Hz, 1H), 7.79 (d, J = 6.5 Hz, 1H), 8.22 (t, J = 5.5 Hz, 1H), 8.93 (d, J = 6.0 Hz, 1H); ^{13}C NMR (125 MHz, CD_3CN, 298 K) δ 15.2, 127.2, 128.0, 130.4, 132.6, 136.2, 143.4, 147.6, 150.9, 153.4; elemental analysis (%) calcd for $C_{10}H_9AuCl_3NS$: C, 25.10; H, 1.90; N, 2.93. Found: C, 25.00; H, 1.88; N, 2.99.

[N^C = 2-(5-Methyl-2-thienyl)pyridine][$AuCl_2$] (C). Silver(I) tetrafluoroborate (0.084 g, 0.431 mmol) was added to [N^C = 2-(5-methyl-2-thienyl)pyridine][$AuCl_3$] (0.200 g, 0.418 mmol) in dichloromethane (60 mL), and the resulting mixture was refluxed for 4 h. After filtration under hot condition, the filtrate was evaporated to dryness, and the residue was washed with a minimum amount of acetonitrile (3.0 mL) to remove silver salts, giving the title complex **C** as a green solid. Yield = 0.073 g, 40%. Positive EI-MS: m/z: 405 $[M - Cl]^+$; IR (KBr): ν (Au−Cl) 304, 354 cm^{-1}; ^1H NMR (500 MHz, DMSO-d_6, 298 K): δ 2.60 (s, 3H), 7.07 (s, 1H), 7.56 (td, J = 6.0, 1.5 Hz, 1H), 7.86 (d, J = 7.5 Hz, 1H), 8.25 (td, J = 6.0, 1.5 Hz, 1H), 9.25 (d, J = 5.5 Hz, 1H); ^{13}C NMR (125 MHz, DMSO-d_6, 298 K): δ 15.6, 120.3, 122.4, 126.0, 137.0, 144.0, 144.2, 147.8, 150.3, 158.3; elemental analysis (%) calcd for $C_{10}H_8AuCl_2NS$; C, 27.17; H, 1.82; N, 3.17 Found: C, 27.32; H, 1.94; N, 3.19.

***cis*-[(N^C)AuL][N^C = 2-phenylpyridine, L = 2,2′-biphenyl] (1).** To 2,2′-Dibromobiphenyl (88.0 mg, 0.28 mmol) in dry diethylether (5.0 mL), *n*-BuLi (0.35 mL, 0.55 mmol, 1.6 M in hexanes) was added slowly via syringe at −78 °C and then stirred for 1 h at RT. The dilithiated solution was then transferred into a flask containing diethylether suspension of **A** (100.0 mg, 0.23 mmol) and AgOTf (4.6 mg, 0.018 mmol) maintained at −78 °C. The cold bath was removed immediately after addition, and the mixture was allowed to stir for 10 h. It was then quenched by addition of water (5.0 mL) and extracted with dichloromethane (2 × 15 mL). The separated organic layers were combined and dried over $MgSO_4$. Filtration followed by concentration of the solvent in vacuo gave the crude product as a light brown solid. It was washed with pentane (5.0 mL), and the residue was purified by flash column chromatography using silica gel (eluent: Hexane/EtOAc = 3/2) to afford **1** as an off-white solid. Single crystals suitable for X-ray diffraction analysis were obtained from slow evaporation by layering of pentane over concentrated solution of the complex in dichloromethane at 0−5 °C. Yield = 15.0 mg, 12%. IR: (KBr) ν_{max} 3414, 2924, 2853, 1638, 1618, 1605, 1581, 1482, 1429, 1160, 1104, 1013, 736, 734, 726, 615, 479 cm^{-1}; ^1H NMR (500 MHz, CD_2Cl_2, 298 K): δ 7.11 (td, J = 6.0, 1.0 Hz, 1H), 7.18−7.25 (m, 3H), 7.36 (td, J = 6.5, 1.0 Hz, 1H), 7.50−7.57 (m, 4H), 7.62 (d, J = 6.5 Hz, 1H), 7.92 (d, J = 8.5 Hz, 1H), 7.95 (d, J = 8.5 Hz, 1H), 8.08 (d, J = 6.5 Hz, 2H), 8.19 (d, J = 7.0 Hz, 1H), 9.2 (d, J = 5.5 Hz, 1H); $^{13}C\{^1H\}$ NMR (125 MHz, CD_2Cl_2, 298 K): δ 121.1, 121.3, 121.7, 123.8, 125.0, 126.5, 126.9, 127.0, 127.1, 127.5, 131.1, 132.0, 134.0, 135.7, 140.7, 147.3, 148.5, 149.4, 154.0, 155.8, 167.3, 171.4, 174.1; elemental analysis (%) calcd for $C_{23}H_{16}AuN$; C, 54.88; H, 3.20; N, 2.78; Found: C, 54.60; H, 3.12; N, 2.68 (Note: ^1H NMR and IR analyses of late eluting fractions from the column (eluent:ethyl acetate) suggest the presence of about 10% of monocoordinated biphenyl Au(III) chloride complex, characterization details of which are not presented here).

General Procedure for the Synthesis of Cyclometalated Au (III) Complexes (2−8). *n*-BuLi (0.52 mmol, 1.6 M in hexanes) was added via syringe to a cooled (−78 °C) solution of the aryl halide (0.50 mmol) in dry diethylether under nitrogen atmosphere and stirred for 20 min at that temperature. It was then transferred via cannula into a flask containing an diethylether suspension of cycloaurated Au(III)dichloride (0.22 mmol) precooled at −78 °C. This temperature was maintained for 20 min and then the mixture was allowed to warm to RT and stirred further for 1 h. (Note: At this stage the reaction mixture turns dark (violet coloration), more in the case of non-fluorinated analogues indicating partial decomposition of the product to metallic gold). TLC examination (EtOAc/Hexane = 1/5) of the reaction mixture at this stage usually showed two major spots, the first ($R_f \sim 0.7$) corresponding to the homocoupled diaryl and the second being the desired organometallic product ($R_f \sim 0.4$) which also gets faintly illuminated in UV lamp longwave (365 nm). The reaction was quenched by addition of water (5 mL) followed by extraction with ethyl acetate/dichloromethane. After separation, the organic layer was dried over $MgSO_4$ and concentrated in vacuo to obtain the crude product. Purification on a short silica gel column (eluent: EtOAc and hexane mixture) was adopted to obtain analytically pure products. Some derivatives were prepared with modifications in the general procedure and are described individually.

***cis*-[(N^C)AuL_2][N^C = 2-phenylpyridine, L = C_6H_5] (2).** Phenyllithium (0.61 mL, 0.746 mmol, 1.8 M soln. in di-*n*-butylether) was syringed into a Schlenk flask containing cooled (−78 °C) suspension of **A** (150.0 mg, 0.35 mmol) in diethylether (5.0 mL) under N_2 atmosphere. The cold bath was removed 15 min after addition, and the reaction mixture was allowed to warm up to RT and stirred for 12 h. The reaction was then quenched by adding H_2O (8.0 mL) and extracted with dichloromethane (2 × 10 mL). The combined dichloromethane layers were dried over $MgSO_4$, filtered, and concentrated in vacuo to yield the crude product. Further purification by flash column chromatography using silica gel (eluent: Hexane/EtOAc = 3/1) afforded **2** as off-white solid. Single crystals suitable for X-ray diffraction analysis were obtained from slow evaporation by layering of pentane over concentrated solution of the complex in dichloromethane at 0−5 °C. Yield = 100.0 mg, 55.0%. IR (KBr): ν_{max} 3413, 2924, 2853, 1638, 1618, 1605, 1571, 1478, 1422, 1163, 1062, 1019, 751, 734, 695, 631, 471 cm^{-1}; ^1H NMR (500 MHz, $CDCl_3$, 298 K): δ 7.03−7.09 (m, 3H), 7.15 (t, J = 8.0 Hz, 2H), 7.19 (t, J = 7.0 Hz, 1H), 7.22−7.31 (m, 4H), 7.45 (d, J = 8.0 Hz, 2H), 7.49 (d, J = 7.0 Hz, 2H), 7.80 (d, J = 7.5 Hz, 1H), 7.92−7.98 (m, 2H), 8.18 (d, J = 5 Hz, 1H); $^{13}C\{^1H\}$NMR (125 MHz, $CDCl_3$, 298 K): δ 119.9, 123.1, 124.1, 124.6, 126.2, 127.1, 127.2, 128.7, 131.1, 132.4, 135.2, 135.9, 140.1, 142.0, 145.8, 149.2, 166.7, 166.9, 169.6; elemental analysis (%) calcd for $C_{23}H_{18}AuN$; C, 54.66; H, 3.59; N, 2.77; Found: C, 54.52; H, 3.42; N, 2.80.

***cis*-[(N^C)AuL_2][N^C = 2-phenylpyridine, L = C_6F_5] (3).** This reaction was performed according to the general procedure. To iodopentafluorobenzene (153.2 mg, 0.521 mmol) in diethylether (5.0 mL), *n*-BuLi (0.33 mL, 0.541 mmol, 1.6 M soln. in hexanes) was added. The lithiated product was transferred to a flask containing **A** (100.0 mg, 0.237 mmol) in diethylether. The crude product thus obtained after workup was purified by flash column chromatography using silica gel (eluent: Hexane/EtOAc = 5/1) to obtain an off-white solid. The solid was further recrystallized from a mixture of ether and pentane to obtain **3** as a white solid. Yield = 66 mg, 40%. IR (KBr): ν_{max} 3414, 2923, 2853, 1738, 1637, 1610, 1509, 1462, 1477, 1365, 1309, 1263, 1073, 967, 906, 885, 812, 785, 757, 732, 629, 466 cm^{-1}; ^1H NMR (500 MHz, $CDCl_3$, 298 K): δ 6.83 (d, J = 7.5 Hz, 1H), 7.29 (td, J = 6.5, 1.5 Hz, 1H), 7.37 (t, J = 7.0 Hz, 2H), 7.78 (d, J = 7.5 Hz, 1H), 8.04 (d, J = 8.0 Hz, 1H), 8.12 (td, J = 8.0, 1.5 Hz, 1H), 8.25 (d, J = 8.0 Hz, 1H); $^{13}C\{^1H\}$ NMR (125 MHz, $CDCl_3$, 298 K): δ 120.8, 124.3, 125.2, 127.8, 132.3, 133.8, 137.5 (dm, $^1J_{C-F}$ = 251.0 Hz), 138.1 (dm, $^1J_{C-F}$ = 251.0 Hz), 139.5 (dm, $^1J_{C-F}$ = 251.0 Hz), 141.8, 144.1 (dm, $^1J_{C-F}$ = 232.0 Hz), 145.1, 146.5 (dm, $^1J_{C-F}$ = 232.0 Hz), 149.3, 158.0, 165.8, 166.7, (note: resonances for 2C submerged in baseline); ^{19}F NMR (470 MHz, $CDCl_3$, 298 K): δ −122.2 (m, 2F, *o*-C_6F_5), −122.3 (m, 2F, *o*-C_6F_5), −157.8 (t, J = 20.2 Hz, 1F, *p*-C_6F_5), −158.7 (t, J = 20.2 Hz, 1F, *p*-C_6F_5), −161.5 (t, J = 19.2 Hz, 2F, *m*-C_6F_5), −162.5

(t, J = 19.7 Hz, 2F, *m*-C_6F_5); elemental analysis (%) calcd. for: $C_{23}H_8AuF_{10}N \cdot CH_3C(O)OC_2H_5$: C, 41.93; H, 2.09; N, 1.81; Found: C, 41.86; H, 2.00; N, 1.97.

***cis*-[(N^C)AuL$_2$][N^C = 2-phenylpyridine, L = C_6H_4-CF_3-*p*] (4).** This reaction was performed according to the general procedure. To 1-bromo-4-(trifluoromethyl)benzene (117.2 mg, 0.521 mmol) in diethylether (5.0 mL), *n*-BuLi (0.33 mL, 0.541 mmol, 1.6 M soln. in hexanes) was added. The lithiated product was then transferred to a flask containing **A** (100.0 mg, 0.237 mmol) in diethylether. The crude product thus obtained after workup was purified by flash column chromatography using silica gel (eluent: Hexane/EtOAc = 5/1) to obtain **4** as off-white solid. Single crystals suitable for X-ray diffraction analysis were obtained from slow evaporation by layering of pentane over concentrated solution of the complex in dichloromethane at 0−5 °C. Yield = 51.0 mg, 33%. IR (KBr): ν_{max} 3413, 3064, 1637, 1607, 1482, 1439, 1390, 1327, 1157, 1120, 1087, 1078, 1066, 1050, 1013, 906, 820, 755, 733, 679, 666, 648, 599, 478 cm^{-1}; ^{1}H NMR (500 MHz, CD_2Cl_2, 298 K): δ 6.89 (dd, J = 8.5, 1.5 Hz, 1H), 7.23−7.30 (m, 3H), 7.41 (d, J = 8.5 Hz, 2H), 7.48 (d, J = 8 Hz, 2H), 7.60 (d, J = 9.0 Hz, 2H), 7.66 (d, J = 8.5 Hz, 2H), 7.82 (dd, J = 8.5, 1.5 Hz, 1H), 7.99−8.03 (m, 2H), 8.05 (d, J = 8.0 Hz, 1H); ^{13}C{^{1}H} NMR (125 MHz, CD_2Cl_2, 298 K): δ 120.7, 121.9, 123.9, 124.0, 124.8, 125.2, 125.3 (q, $^2J_{C-F}$ = 3.8 Hz), 125.6 (q, $^2J_{C-F}$ = 3.9 Hz), 126.5 (q, $^1J_{C-F}$ = 32.0 Hz), 127.2 (q, $^1J_{C-F}$ = 31.6 Hz), 131.5, 133.0, 135.7, 135.8, 141.3, 146.2, 147.0, 149.5, 167.0, 167.1, 172.4; ^{19}F NMR (376 MHz, $CDCl_3$, 298 K): δ −62.19 (s, 3H), −62.22 (s, 3H); elemental analysis (%) calcd for: $C_{25}H_{16}AuF_6N$: C, 46.82; H, 2.51; N, 2.18 Found: C, 46.70; H, 2.65; N, 2.18.

***cis*-[(N^C)AuL$_2$][N^C = 2-phenylpyridine, L = C_4H_3S] (5).** This reaction was performed according to the general procedure. To 2-bromothiophene (0.83 mL, 0.52 mmol) in diethylether (5.0 mL), *n*-BuLi (0.33 mL, 0.541 mmol, 1.6 M soln. in hexanes) was added, and this mixture was transferred to flask containing **A** (100.0 mg, 0.237 mmol) in diethylether. The crude product thus obtained after workup was purified by column chromatography on silica gel (eluent: Hexane/EtOAc = 5/1) to obtain **5** as off-white solid. Single crystals suitable for X-ray diffraction analysis were obtained from slow evaporation by layering of pentane over concentrated solution of the complex in dichloromethane at 0−5 °C. Yield = 68 mg, 55%. IR (KBr): ν_{max} 3413, 1638, 1617, 1481, 1437, 1402, 1259, 1202, 1064, 1028, 834, 806, 751, 690, 626, 471 cm^{-1}; ^{1}H NMR (500 MHz, $CDCl_3$, 298 K): δ 6.98 (d, J = 5.0 Hz, 1H), 7.04 (d, J = 5.0 Hz, 1H), 7.12−7.14 (m, 1H), 7.16−7.18 (m, 1H), 7.24−7.28 (m, 2H), 7.29−7.32 (m, 2H), 7.47 (d, J = 5.0 Hz, 1H), 7.61 (d, J = 5.0 Hz, 1H), 7.75−7.77 (m, 1H), 7.95−8.00 (m, 2H), 8.35 (d, J = 5.0 Hz, 1H); ^{13}C{H} NMR (125 MHz, $CDCl_3$, 298 K): δ 119.9, 123.4, 124.3, 125.0, 125.6, 127.9, 129.4, 131.5, 132.3, 135.3, 140.8, 145.5, 149.4, 151.7, 158.7, 160.3, 163.2, 164.7, 166.8; elemental analysis (%) calcd for $C_{19}H_{14}AuNS_2$: C, 44.10; H, 2.73; N, 2.71; Found: C, 43.90; H, 2.87; N, 2.63.

***cis*-[(N^C)AuL$_2$] [N^C = 2-(2-thienyl)pyridine, L = C_6H_5] (6).** Phenyllithium (0.64 mL, 0.780 mmol, 1.8 M soln. in di-*n*-butyl ether) was slowly syringed into a Schlenk flask containing cooled (−78 °C) suspension of **B** (100.0 mg, 0.233 mmol) in diethylether (5.0 mL) under N_2 atmosphere. The cold bath was removed after 15 min, and the reaction mixture was allowed to warm up to RT and stirred further for 1 h. H_2O (8.0 mL) was added to quench the reaction mixture and was then extracted with ethyl acetate (20.0 mL). The organic layer was dried over $MgSO_4$, filtered, and concentrated in vacuo to obtain the crude product. It was washed with pentane (2 × 2.0 mL), and the residue was then extracted by adding toluene (2 × 5.0 mL). The toluene layer was concentrated, and further recrystallization of the residue with diethylether and pentane mixture (2:1) and storing at −30 °C afforded **6** as a light green solid. Single crystals suitable for X-ray diffraction analysis were obtained from slow evaporation by layering of pentane over concentrated solution of the complex in dichloromethane at 0−5 °C. Yield = 30.0 mg, 25%. ^{1}H NMR (500 MHz, CD_2Cl_2, 298 K): δ 6.71 (d, J = 4.5 Hz, 1H), 7.06 −7.12 (m, 3H), 7.16 (t, J = 7.5 Hz, 2H), 7.26 (t, J = 7.5 Hz, 2H), 7.43−7.46 (m, 3H), 7.50 (d, J = 7.5 Hz, 2H), 7.64 (d, J = 7.5 Hz, 1H) 7.90 (td, J = 8.0, 1.5 Hz, 1H), 7.97 (d, J = 5.5 Hz, 1H); ^{13}C{^{1}H} NMR (125 MHz, CD_2Cl_2, 298 K): δ 119.0, 121.4, 124.5, 125.0, 128.5, 128.7, 129.0, 133.1, 134.1, 135.0, 136.3, 140.9, 147.0, 148.8, 161.0, 164.1, 178.9; elemental analysis (%) calculated for $C_{21}H_{16}AuNS$: C, 49.32; H, 3.15; N, 2.74; Found: C, 49.17; H, 3.00; N, 2.80.

***cis*-[(N^C)AuL$_2$] [N^C = 2-(2-thienyl)pyridine, L = C_6F_5] (7).** This reaction was performed according to the general procedure. To iodopentafluorobenzene (151.0 mg, 0.514 mmol) in diethylether (5.0 mL), *n*-BuLi (0.33 mL, 0.537 mmol, 1.6 M soln. in hexanes) was added, and this was transferred to a flask containing **B** (100.0 mg, 0.233 mmol) in diethylether. The crude product thus obtained was purified by flash column chromatography using silica gel (eluent: Hexane/EtOAc = 5/1) to obtain **7** as light yellow solid. Single crystals suitable for X-ray diffraction analysis were obtained from slow evaporation by layering of pentane over a concentrated solution of the complex in diethylether at 0−5 °C. Yield = 61 mg, 38%. IR (KBr): ν_{max} 3414, 2923, 2853, 1738, 1637, 1610, 1509, 1477, 1462, 1365, 1309, 1263, 1163, 1073, 967, 906, 885, 812, 785, 757, 732, 629, 466 cm^{-1}; ^{1}H NMR (500 MHz, $CDCl_3$, 298 K): δ 6.55 (d, J = 4.5 Hz, 1H), 7.24 (td, J = 4.5, 1.5 Hz, 1H), 7.47 (d, J = 5 Hz, 1H), 7.67 (d, J = 8 Hz, 1H), 8.02 (td, J = 6.5, 1.5 Hz, 1H), 8.07 (d, J = 5.5 Hz, 1H); ^{13}C{H} NMR (125 MHz, $CDCl_3$, 298 K): δ 119.7, 122.5, 130.2, 132.0, 137.5 (dm, $^1J_{C-F}$ = 251.0 Hz), 138.0 (dm, $^1J_{C-F}$ = 251.0 Hz), 139.5 (dm, $^1J_{C-F}$ = 251.0 Hz), 142.4, 145.6 (dm, $^1J_{C-F}$ = 250.0 Hz), 146.0, 146.5 (dm, $^1J_{C-F}$ = 250.0 Hz), 149.0, 161.1, 162.4, (note: resonances for 3C submerged in baseline); ^{19}F NMR (376 MHz, $CDCl_3$, 298 K): δ −120.5 (m, 2F, *o*-C_6F_5), −120.6 (m, 2F, *o*-C_6F_5), −156.0 (t, $^3J_{F-F}$ = 18.8 Hz, 1F, *p*-C_6F_5), −156.9 (t, $^3J_{F-F}$ = 18.6 Hz, 1F, *p*-C_6F_5), −160.1 (t, $^3J_{F-F}$ = 18.8 Hz, 2F, *m*-C_6F_5), −161.2 (t, $^3J_{F-F}$ = 19.1 Hz, 2F, *m*-C_6F_5); elemental analysis (%) calcd for $C_{21}H_6AuF_{10}NS$: C, 36.49; H, 0.87; N, 2.03; Found: C, 36.77; H, 0.89; N, 1.97.

***cis*-[N^C = 2-(5-methyl-2-thienyl)pyridine, L = C_6F_5] (8).** This reaction was performed according to the general procedure. To iodopentafluorobenzene (146.3 mg, 0.497 mmol) in diethylether (5.0 mL), *n*-BuLi (0.33 mL, 0.537 mmol, 1.6 M soln. in hexanes) was added, and this mixture was transferred to a flask containing **C** (100.0 mg, 0.226 mmol) in diethylether. The crude product thus obtained after workup was purified by flash column chromatography using silica gel (eluent Hexane/EtOAc = 5:1) to obtain **8** as yellow-green solid. Yield = 90 mg, 56%. Alternatively, direct recrystallization of the crude product using ether and pentane mixture also afforded analytically pure compound. Single crystals suitable for X-ray diffraction analysis were obtained from slow evaporation by layering of pentane over concentrated solution of the complex in diethylether at 0−5 °C. IR (KBr): ν_{max} 3413, 2925, 2027, 1637, 1615, 1508, 1463, 1477, 1366, 1264, 1250, 1160, 1072, 967, 880, 842, 812, 789, 765, 620, 473 cm^{-1}; ^{1}H NMR (500 MHz, CD_2Cl_2, 298 K): δ 2.49 (d, J = 1.0 Hz, 3H), 6.19 (d, J = 1.0 Hz, 1H), 7.13 (td, J = 6.0, 1.5 Hz, 1H), 7.52 (dd, J = 6.0, 1.5 Hz, 1H), 7.95 (td, J = 6.0, 1.5 Hz, 1H), 7.97 (dd, J = 6.0,1.5 Hz, 1H); ^{13}C{^{1}H}NMR (125.MHz, CD_2Cl_2, 298 K): δ 15.4, 119.6, 122.2, 130.6, 137.5 (dm, $^1J_{C-F}$ = 251.6 Hz), 138.0 (dm, $^1J_{C-F}$ = 251.0 Hz), 140.0 (dm, $^1J_{C-F}$ = 251.0 Hz), 143.0, 143.8, 145.0 (dm, $^1J_{C-F}$ = 251.0 Hz), 147.0, 147.1 (dm, $^1J_{C-F}$ = 251.0 Hz), 148.0 (dm, $^1J_{C-F}$ = 251.0 Hz), 149.0, 161.4, 163.0, (note: resonances for 2C submerged in baseline); ^{19}F NMR (376 MHz, $CDCl_3$, 298 K): δ −120.5 (m, 2F, *o*-C_6F_5), −120.6 (m, 2F, *o*-C_6F_5), −156.2 (t, $^3J_{F-F}$ = 18.8 Hz, 1F, *p*-C_6F_5), −157.1 (t, $^3J_{F-F}$ = 21.5 Hz, 1F, *p*-C_6F_5), −160.20 (t, $^3J_{F-F}$ = 18.8 Hz, 2F, *m*-C_6F_5), −161.21 (t, $^3J_{F-F}$ = 22.5 Hz,

2F, *m*-C_6F_5); elemental analysis (%) calcd for $C_{22}H_8AuF_{10}NS$: C, 37.46; H, 1.14; N, 1.99; Found: C, 37.63; H, 1.27; N, 2.06.

Acknowledgment. We thank S. V. Rocha and Dr. N. Finney for help with excited-state lifetime measurements. K.V. is grateful to the University of Zürich and Prof. H. Berke for generous support.

Supporting Information Available: X-ray crystallographic data for complexes **1**−**2** and **4**−**8** in CIF format, absorbance and emission spectra of **4** and **5** (Figure S1), thermogravimetric analysis of **2** and **3** (Figure S2); ORTEP plots of **4**, **6**, and **7** (Figures S3−S5); crystallographic details of all X-ray structures (Tables S1 and S2); and computational details. This material is available free of charge via the Internet at http://pubs.acs.org.

Supporting Information

Stable and Tunable Phosphorescent Neutral Cyclometalated Au(III) Diaryl Complexes

*Jai Anand Garg, Olivier Blacque, Thomas Fox and Koushik Venkatesan**

Institute of Inorganic Chemistry, University of Zürich, Winterthurerstrasse 190, CH-8057, Zürich, Switzerland

Table of contents

1. Electronic absorption and emission spectra

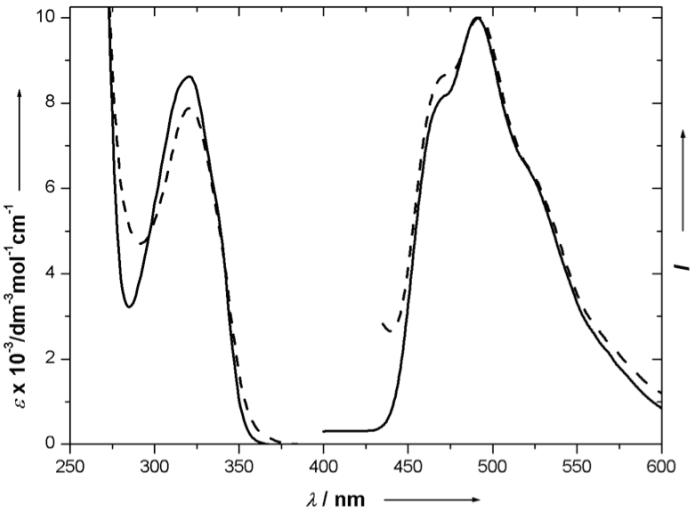

Figure S1. Electronic absorption and normalized emission (*I*) spectra of **4** solid (——), **5** dash (----) in degassed CH_2Cl_2 at 298 K.

2. Thermogravimetric Analysis (TGA)

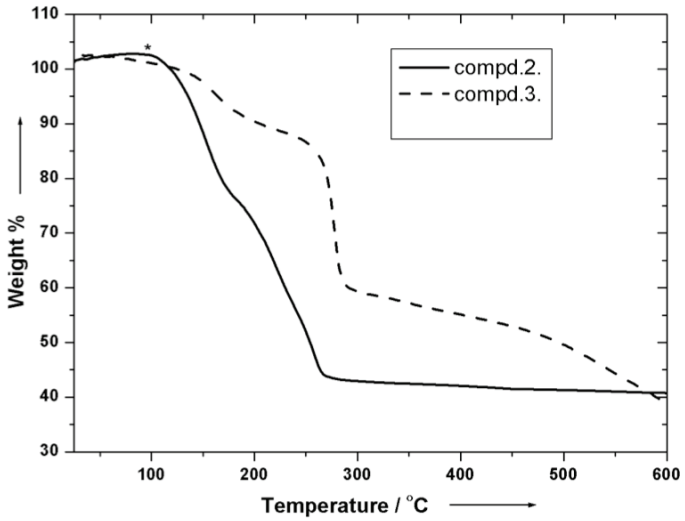

Figure S2. Thermal gravimetric traces of the complexes measured under N_2 atmosphere, rate of heating 1°C/min from 25 °C to 600 °C. * denotes instrumental artefact.

3. X-ray diffraction studies of 4, **6** and **7**

*Single crystal X-ray structure of complex **4***

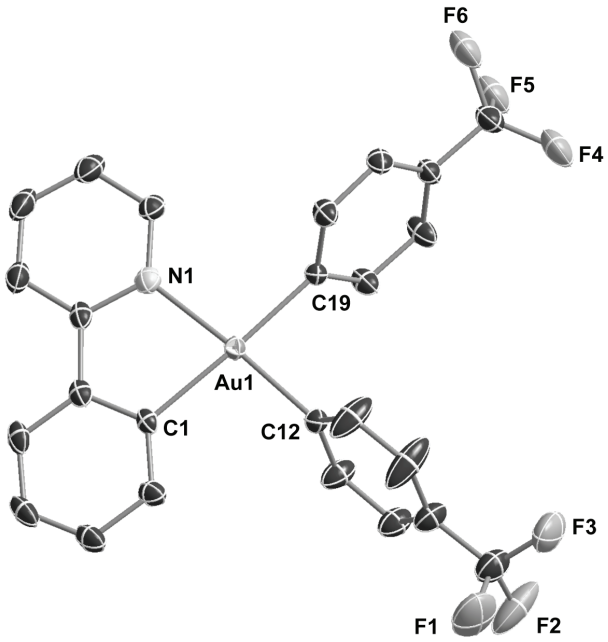

Figure S3. Thermal ellipsoid plot of **4** (30% probability level of thermal ellipsoids) with selective atomic numbering scheme. Hydrogen atoms and solvent molecules are omitted for clarity. Selected bond lengths (Å) and angles (°): Au1-C1 2.087(3), Au1-N1 2.080(3), Au1-C12 2.049(4), Au1-C19 2.030(3); C1-Au1-N1 79.81(14), C12-Au1-C19 86.56(14).

Single crystal X-ray structure of complex ***6***

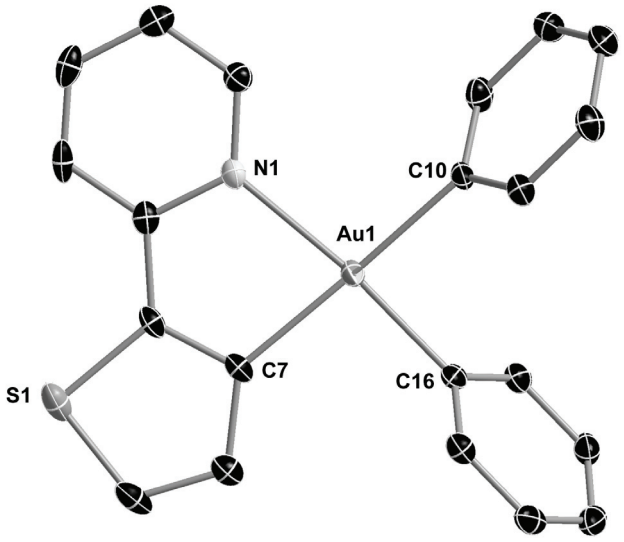

Figure S4. Thermal ellipsoid plot of **6** (30% probability level of thermal ellipsoids) with selective atomic numbering scheme. Hydrogen atoms are omitted for clarity. Selected bond lengths (Å) and angles (°): Au1-C7 2.064(3), Au1-N1 2.156(3), Au1-C10 2.073(3), Au1-C16 2.011(3); C7-Au1-N1 79.35(12), C10-Au1-C16 87.77(13).

Single crystal X-ray structure of complex 7

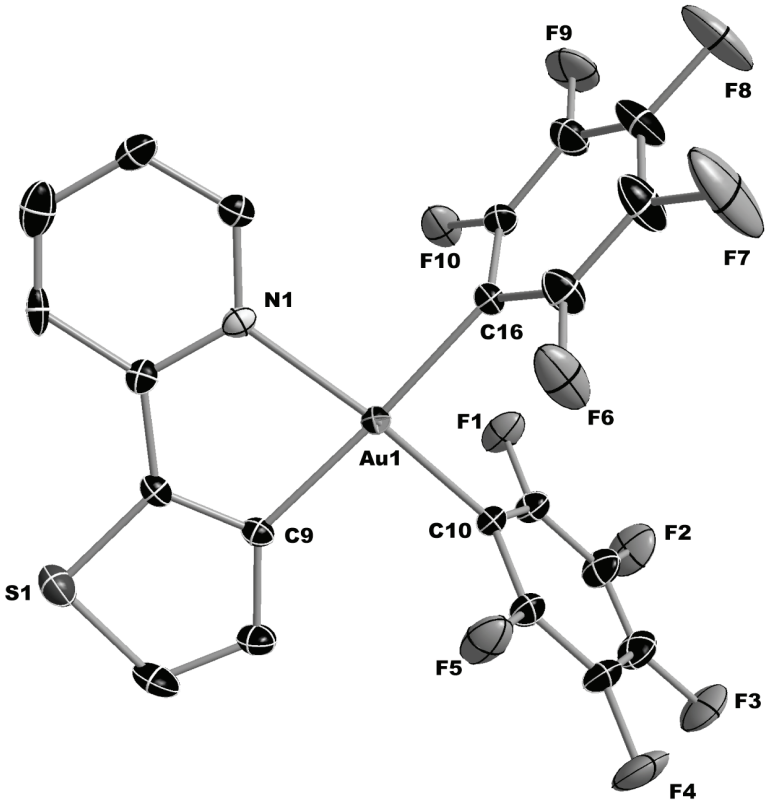

Figure S5. Thermal ellipsoid plot of **7** (30% probability level of thermal ellipsoids) with selective atomic numbering scheme. Hydrogen atoms are omitted for clarity. Selected bond lengths (Å) and angles (°): Au1-C9 2.051(3), Au1-N1 2.094(3), Au1-C10 2.028(4), Au1-C16 2.072(3); C9-Au1-N1 80.33(12), C10-Au1-C16 90.15(14).

Table S1. Crystallographic data for compounds **1**, **2**, **4** and **5**.

	1	**2**	**4**	**5**
empirical formula	C_{23} H_{16} Au N	C_{23} H_{18} Au N, C H_2 Cl_2	2(C_{25} H_{16} Au F_6 N), C H_2 Cl_2	C_{19} H_{14} Au N S_2
formula weight ($g \cdot mol^{-1}$)	503.34	590.28	1367.64	517.42
temperature (K)	183(2)	183(2)	183(2)	183(2)
wavelength (Å)	0.71073	0.71073	0.71073	0.71073
crystal system, space group	monoclinic, $P\,2_1/n$	triclinic, P -1	triclinic, P -1	triclinic, P -1
a (Å)	12.9330(1)	9.2059(2)	10.2601(1)	9.6459(1)
b (Å)	7.2609(1)	9.8567(2)	11.2177(2)	12.2106(2)
c (Å)	17.8058(2)	12.3049(2)	12.0695(3)	15.2673(2)
α (deg)	90	82.599(2)	66.219(2)	71.165(1)
β (deg)	99.795(1)	77.215(2)	70.755(2)	75.545(1)
γ (deg)	90	79.161(2)	83.596(1)	83.295(1)
volume ($Å^3$)	1647.68(3)	1065.00(4)	1199.79(4)	1646.77(4)
Z, density (calcd) ($Mg \cdot m^{-3}$)	4, 2.029	2, 1.841	1, 1.893	4, 2.087
abs coefficient (mm^{-1})	8.932	7.167	6.303	9.184
F(000)	960	568	654	984
crystal size (mm^3)	0.26 x 0.11 x 0.04	0.42 x 0.36 x 0.25	0.36 x 0.16 x 0.10	0.40 x 0.19 x 0.06
θ range (deg)	3.0 to 30.5	2.6 to 32.6	2.6 to 30.5	2.6 to 30.5
reflections collected	24140	26821	18261	50352
reflections unique	5035 / [R_{int} = 0.0544]	7746 / [R_{int} = 0.0223]	7324 / [R_{int} = 0.0229]	10053 / [R_{int} = 0.0394]
completeness to θ (%)	99.9	100.0	99.9	100.0
absorption correction	analytical	analytical	analytical	analytical
max/min transmission	0.731 and 0.270	0.274 and 0.113	0.556 and 0.239	0.587 and 0.133
data / restraints / parameters	3985 / 0 / 226	7018 / 0 / 253	6257 / 24 / 338	7610 / 12 / 429
goodness-of-fit on F^2	0.907	1.114	1.037	0.956
final R_1 and wR_2 indices [$I > 2\sigma(I)$]	0.0209, 0.0420	0.0185, 0.0456	0.0308, 0.0779	0.0248, 0.0485
R_1 and wR_2 indices (all data)	0.0311, 0.0432	0.0221, 0.0460	0.0389, 0.0794	0.0414, 0.0504

The unweighted R-factor is $R_1 = \sum(Fo - Fc)/\sum Fo$; $I > 2\,\sigma(I)$ *and the weighted R-factor is* $wR_2 = \{\sum w(Fo^2 - Fc^2)^2/\sum w(Fo^2)^2\}^{1/2}$

Table S2. Crystallographic data for compounds **6**, **7** and **8**.

	6	**7**	**8**
empirical formula	C_{21} H_{16} Au N S	2(C_{21} H_6 Au F_{10} N S), C_5 H_{12}	4(C_{22} H_8 Au F_{10} N S), C_4 H_{10} O
formula weight ($g \cdot mol^{-1}$)	511.37	1454.76	2895.46
temperature (K)	183(2)	183(2)	183(2)
wavelength (Å)	0.71073	0.71073	0.71073
crystal system, space group	triclinic, *P* -1	monoclinic, *P* 2_1/c	monoclinic, *P* 2_1/c
a (Å)	7.1806(3)	13.5299(2)	13.7962(3)
b (Å)	10.0899(7)	7.0529(1)	7.0262(1)
c (Å)	12.5115(7)	24.4528(4)	25.1853(4)
α (deg)	73.057(5)	90	90
β (deg)	80.072(4)	94.083(1)	91.636(2)
γ (deg)	80.953(5)	90	90
volume ($Å^3$)	848.62(8)	2327.49(6)	2440.34(7)
Z, density (calcd) ($Mg \cdot m^{-3}$)	2, 2.001	2, 2.076	1, 1.970
abs coefficient (mm^{-1})	8.791	6.504	6.203
F(000)	488	1380	1370
crystal size (mm^3)	0.15 x 0.09 x 0.02	0.34 x 0.21 x 0.17	0.23 x 0.21 x 0.07
θ range (deg)	2.9 to 28.3	3.0 to 32.56	2.9 to 30.5
reflections collected	10934	32577	37165
reflections unique	4219 / [R_{int} = 0.0361]	8481 / [R_{int} = 0.0261]	7417 / [R_{int} = 0.0266]
completeness to θ (%)	99.9	100.0	99.9
absorption correction	analytical	analytical	analytical
max/min transmission	0.848 and 0.361	0.414 and 0.256	0.684 and 0.329
data / restraints / parameters	3682 / 0 / 217	5018 / 9 / 325	5892 / 55 / 330
goodness-of-fit on F^2	0.939	1.008	0.980
final R_1 and wR_2 indices [$I > 2\sigma(I)$]	0.0240, 0.0413	0.0271, 0.0690	0.0261, 0.0704
R_1 and wR_2 indices (all data)	0.0301, 0.0420	0.0674, wR2 = 0.0763	0.0351, 0.0720

The unweighted R-factor is $R_1 = \sum(Fo - Fc)/\sum Fo$; $I > 2\,\sigma(I)$ *and the weighted R-factor is* $wR_2 = \{\sum w(Fo^2 - Fc^2)^2/\sum w(Fo^2)^2\}^{1/2}$.

Relevant details about the structure refinements are given in Tables S1 and S2, and selected geometrical parameters are included in the captions of the corresponding figures (Figures S3-S5). Intensity data were collected at 183(2) K an Oxford Xcalibur diffractometer (4-circle kappa platform, Ruby CCD detector, and a single wavelength Enhance X-ray source with MoK_α radiation, λ = 0.71073 Å).[1] The selected suitable single crystals were mounted using polybutene oil on the top of a glass fiber fixed on a goniometer head and immediately transferred to the diffractometer. Pre-experiment, data collection, data reduction and analytical absorption corrections[2] were performed with the Oxford program suite *CrysAlisPro*.[3] The crystal structures were solved with SHELXS-97[4] using direct methods. The structure refinements were performed by full-matrix least-squares on F^2 with SHELXL-97.[4] All programs used during the crystal structure determination process are included in the WINGX software.[5] The program PLATON[6] was used to check the result of the X-ray analyses. CCDC-778147-778153 contain the supplementary crystallographic data (excluding structure factors) for this paper. These data can be obtained free of charge from The Cambridge Crystallographic Data Centre via www.ccdc.cam.ac.uk/data_request/cif.

Solvent molecules co-crystallized with the cyclometalated Au(III) complexes **2**, **4**, **7** and **8** in proportions 1/1 (CH_2Cl_2), 2/1 (CH_2Cl_2), 2/1 (C_5H_{12}), and 4/1 ($C_4H_{10}O$), respectively. In the crystal structure of **4** the solvent molecules lie about a center of inversion and are disordered over several sets of positions. Some distance restraints were used to correct the geometry. The fluorine atoms F4-F6 of one CF_3 group were also disordered over two sets of positions A and B with site occupancy factors of 0.568-0.432(6). Constraints were used to make the anisotropic displacement parameters of these atoms equal. There are two crystallographically independent Au(III) molecules in the asymmetric unit of the crystal structure of **5**. Furthermore, two thiophene ligands are rotationally disordered with site occupancy factors of 0.653-0.347(3) and 0.788-0.212(3). Many restraints (12) were used to refine correctly the model. In the crystal structures of **7** and **8** the solvent molecules of pentane and diethylether lie on centers of inversion and are disordered over two sets of positions with sof of 0.5 and 0.25 in **7** and **8**, respectively. In 8 the diethylether atoms were only isotropically refined. All hydrogen atoms were calculated after each cycle of refinement using a riding model, with C-H = 0.93 Å + U_{iso}(H) = 1.2U_{eq}(C) for aromatic H atoms, with C-H = 0.97 Å + U_{iso}(H) = 1.2U_{eq}(C) for methylene H atoms, and with C-H = 0.96 Å + U_{iso}(H) = 1.5U_{eq}(C) for methyl H atoms.

4. Computational details

All calculations were performed with the Gaussian 03 program package[7] using the hybrid functional PBE1PBE[8] in conjunction with the Stuttgart/Dresden effective core potentials (SDD) basis set[9] for the Au center augmented with one f-polarization function (exponent α = 1.050) and the standard 6-31+G(d) basis set[10] for the remaining atoms. Several exchange-correlation functionals (B3LYP,[11] MPW1K,[12] BB1K,[11a,13] PBE1PBE,[8] G96LYP,[11b,14] TPSS[15] and TPSSLYP1W[16]) were tested on the geometry structures of **1** and **2**, the hybrid PBE1PBE provided the best match with the geometrical X-ray data and was selected for our study. Full geometry optimizations without symmetry constraints were carried out in the gas phase for both the singlet ground states (S_0) and the lowest triplet excited states (T_1). The optimized geometries were confirmed to be potential energy minima by vibrational frequency calculations at the same level of theory, as no imaginary frequency was found. The transition-state structures TS-2 and TS-3 were located using Synchronous Transit-Guided Quasi-Newton (STQN) methods[17] until the Hessian matrix had only one imaginary eigenvalue. The identity of the transition states was confirmed by visualizing the corresponding vibration with GaussView.[18] The first 10 singlet-singlet and singlet-triplet transition energies were computed at the optimized S_0 geometries, by using the time-dependent DFT (TDDFT) methodology.[19] Solvent effects were taken into account using the conductor-like polarizable continuum model (CPCM)[20] with dichloromethane as solvent for single-point calculations on all optimized gas-phase geometries.

5. DFT results

Energies and cartesian coordinates of the optimized ground-state structure of 1

H	-4.87451100	3.22388900	-1.18105300	C	2.85666500	0.73337000	0.19157900
H	2.64818400	-4.36459200	-1.37096400	H	-4.96667800	-0.98251000	0.49734600
H	-2.66403500	4.34919600	-1.39141900	Au	0.03572400	0.01244400	-0.01080800
H	4.87822100	-3.30163200	-1.08208400	C	-2.84833100	-0.73363700	0.19137400
C	-3.96083200	2.69289800	-0.92726700	C	3.97085400	1.52468300	0.48235700
C	2.72411200	-3.33798600	-1.01878400	N	-1.63364100	-1.33440500	0.23858900
C	-2.72122800	3.32123700	-1.03975600	C	1.56402500	1.29447200	0.28703600
C	3.97195400	-2.74173500	-0.86408800	C	-3.99504700	-1.46237400	0.53133700
H	0.60447700	-3.09491900	-0.91280800	C	3.81525500	2.84521700	0.89847600
H	-4.98197500	0.87016800	-0.46991700	C	-3.88366600	-2.78136600	0.94284200
C	-4.01629100	1.36809900	-0.51459700	H	4.69071500	3.44873000	1.12554000
C	1.56236800	-2.61084800	-0.73327800	C	-1.52222400	-2.59498400	0.67622800
H	-0.60122500	3.14541600	-0.84950900	C	1.41489400	2.59824600	0.75117200
H	5.03314500	-0.93901500	-0.37903400	H	-4.77262200	-3.34544300	1.21264500
C	4.05615200	-1.41109700	-0.45731500	H	-0.51375800	-2.98602400	0.74639600
C	-1.55026000	2.63391900	-0.71683200	H	0.42794400	3.01903100	0.90855500
C	2.89598200	-0.68525200	-0.17869600	C	2.53832300	3.37684100	1.04961700
C	-2.83689600	0.68055200	-0.19366000	C	-2.62027400	-3.36239900	1.03211600
C	1.62515300	-1.29458100	-0.27520100	H	2.40617400	4.39532200	1.40743900
C	-1.57250400	1.31325100	-0.25770000	H	-2.48034000	-4.38217400	1.37512900
H	4.97048400	1.10320000	0.40567300				

After PCM corrections, the SCF energy is -1075.489338 a.u.

Zero-point correction=	0.323245 (Hartree/Particle)
Thermal correction to Energy=	0.342474
Thermal correction to Enthalpy=	0.343418
Thermal correction to Gibbs Free Energy=	0.274912
Sum of electronic and zero-point Energies=	-1075.145415
Sum of electronic and thermal Energies=	-1075.126186
Sum of electronic and thermal Enthalpies=	-1075.125242
Sum of electronic and thermal Free Energies=	-1075.193748

Energies and cartesian coordinates of the optimized triplet-state structure of 1

H	4.86106300	3.29312300	1.05139100	C	-2.87836000	0.69777400	-0.12071200
H	-2.65086300	-4.34819100	1.35662600	H	4.98069400	-1.01068800	-0.34994200
H	2.63950800	4.40108600	1.26228700	Au	-0.01855000	0.00917900	-0.00619600
H	-4.89422600	-3.34927300	0.90062700	C	2.85498900	-0.72580400	-0.16064700
C	3.94975900	2.74414500	0.82890900	C	-4.02895600	1.55387200	-0.29036900
C	-2.71856700	-3.33181400	0.97677000	N	1.62965400	-1.31591500	-0.24624700
C	2.70331200	3.36381700	0.94022500	C	-1.53785600	1.27575100	-0.28263700
C	-3.99966700	-2.75331500	0.73725100	C	4.00612000	-1.48106900	-0.41919900
H	-0.59572500	-3.08336500	0.93023200	C	-3.87341200	2.83882200	-0.72216200
H	4.98552800	0.92260900	0.41047000	C	3.90295600	-2.81165000	-0.78965800
C	4.01427600	1.40916500	0.45815900	H	-4.74186900	3.47576400	-0.87021700
C	-1.54786000	-2.59921800	0.72384000	C	1.53020700	-2.59414800	-0.64900300
H	0.58488300	3.15832000	0.79220800	C	-1.43018400	2.57300900	-0.75716500
H	-5.08120600	-1.01602200	0.14998300	H	4.79694400	-3.39348100	-0.99681500
C	-4.10299800	-1.45783300	0.32050700	H	0.52309300	-2.97635900	-0.76558700
C	1.53734600	2.65465500	0.65628500	H	-0.45588900	2.99945500	-0.97056000
C	-2.91092700	-0.66443500	0.12997700	C	-2.57168200	3.35289100	-0.99432500
C	2.83902700	0.69442400	0.17551300	C	2.63339600	-3.38214000	-0.92009600
C	-1.59005900	-1.29232600	0.25910000	H	-2.46161100	4.36084300	-1.38571400
C	1.56791200	1.31914600	0.23726500	H	2.49730900	-4.41087400	-1.23729700
H	-5.02238300	1.16105300	-0.09144900				

After PCM corrections, the SCF energy is -1075.391210 a.u.

Zero-point correction=	0.318882 (Hartree/Particle)
Thermal correction to Energy=	0.338653
Thermal correction to Enthalpy=	0.339597
Thermal correction to Gibbs Free Energy=	0.269110
Sum of electronic and zero-point Energies=	-1075.053228
Sum of electronic and thermal Energies=	-1075.033456
Sum of electronic and thermal Enthalpies=	-1075.032512
Sum of electronic and thermal Free Energies=	-1075.102999

Energies and cartesian coordinates of the optimized ground-state structure of 2

H	3.53310900	3.19134800	-2.12350700	H	1.87597400	1.37032600	-2.12686000
C	3.06493500	2.89249900	-1.18806700	C	1.50711200	1.46360600	0.00060300
C	2.12347500	1.86218000	-1.18920900	H	4.14580500	4.33147400	0.00180700
C	3.40970800	3.53131600	0.00175700	C	2.80360700	3.13275500	1.19161900

C	1.85660100	2.10691700	1.19222500	C	3.12687300	-2.86399800	1.21926300
Au	0.10204100	0.03212100	-0.00060600	H	1.84782500	-1.42250300	2.15888300
H	3.06490300	3.62125000	2.12797000	C	-3.87530200	-1.63225900	0.01154100
H	1.38963100	1.81652800	2.13056200	H	-0.33846000	-3.06138900	0.02843700
C	-1.51723300	1.32227600	-0.01694000	C	-2.44922900	-3.56618500	0.03508600
C	1.61995600	-1.37335300	0.00886900	H	-2.67925800	4.53167300	-0.06755200
N	-1.51211400	-1.37386900	0.00721100	C	-3.93461100	2.78115900	-0.04881100
C	-1.51493500	2.71814200	-0.03634400	H	-4.93014700	0.88845500	-0.02955700
C	-2.76842000	0.66278400	-0.01559800	H	3.38952500	-3.37791600	-2.12679100
C	2.08513700	-1.94233800	-1.18574100	C	3.56932200	-3.42260800	0.02096200
C	2.16665100	-1.84980900	1.20895100	H	3.53479700	-3.21296700	2.16601000
C	-2.74439100	-0.80665900	0.00130600	H	-4.86588200	-1.19166900	0.00702400
C	-1.36380700	-2.70316900	0.02414400	C	-3.72768200	-3.01143200	0.02841300
C	-2.70691700	3.44413400	-0.05202000	H	-2.28983200	-4.63927400	0.04871600
H	-0.56722600	3.25170300	-0.03961600	H	-4.86406200	3.34457300	-0.06117700
C	-3.96624400	1.39190300	-0.03074200	H	4.32020300	-4.20930300	0.02583000
H	1.69837500	-1.59249700	-2.14268200	H	-4.60641100	-3.65117600	0.03672400
C	3.04617200	-2.95604900	-1.18407400				

After PCM corrections, the SCF energy is -1076.678059 a.u.

Zero-point correction=	0.343481 (Hartree/Particle)
Thermal correction to Energy=	0.364502
Thermal correction to Enthalpy=	0.365446
Thermal correction to Gibbs Free Energy=	0.289569
Sum of electronic and zero-point Energies=	-1076.314834
Sum of electronic and thermal Energies=	-1076.293814
Sum of electronic and thermal Enthalpies=	-1076.292870
Sum of electronic and thermal Free Energies=	-1076.368746

Energies and cartesian coordinates of the optimized triplet-state structure of 2

H	-3.79438400	-2.93300300	-2.07974700	H	0.53882900	-3.24853200	-0.09903200
C	-3.23108800	-2.73243600	-1.17085000	C	4.01653800	-1.42815600	-0.04535300
C	-2.27041900	-1.72033300	-1.16686900	H	-1.40327100	1.88694900	-2.08379700
C	-3.47787400	-3.47566400	-0.01753800	C	-2.88605000	3.11675000	-1.14352300
H	-2.10683500	-1.14015900	-2.07165300	C	-3.27712200	2.71442100	1.19626600
C	-1.53034500	-1.44571700	-0.01215200	H	-2.11876300	1.15200100	2.09919800
H	-4.23120300	-4.25969700	-0.02026800	C	3.93701200	1.60067800	0.03657400
C	-2.75246000	-3.20067500	1.13979300	H	0.38236900	3.06086600	0.09894300
C	-1.78257500	-2.19585400	1.14210800	C	2.50308100	3.52418200	0.11453700
Au	-0.10298100	-0.03023900	-0.00233300	H	2.65402900	-4.54422500	-0.15031800
H	-2.93654300	-3.77045700	2.04827600	C	3.94574100	-2.78721800	-0.09000900
H	-1.21933400	-2.00545100	2.05309300	H	4.98554900	-0.93844900	-0.02963400
C	1.48627300	-1.33783500	-0.03479600	H	-3.10827800	3.65866700	-2.06091700
C	-1.60871600	1.38488000	0.01204900	C	-3.56694200	3.42594100	0.03273700
N	1.49965800	1.35065300	0.03037400	H	-3.80801800	2.94080800	2.11892500
C	1.48741700	-2.71680400	-0.08339300	H	4.92278900	1.14850400	0.01572900
C	2.79625900	-0.64123600	-0.02188200	C	3.80564100	2.96128900	0.08645200
C	-1.91923300	2.10818100	-1.14951600	H	2.34629000	4.59644500	0.15825400
C	-2.31388100	1.70367200	1.18097000	H	4.86002300	-3.37545700	-0.10985500
C	2.77947500	0.74907800	0.01274600	H	-4.32105700	4.20951300	0.04123500
C	1.39566500	2.66723700	0.08328100	H	4.68248200	3.60172400	0.10521900
C	2.68247600	-3.45867100	-0.11195300				

After PCM corrections, the SCF energy is -1076.575702 a.u.

Zero-point correction=	0.338940 (Hartree/Particle)
Thermal correction to Energy=	0.360585
Thermal correction to Enthalpy=	0.361529
Thermal correction to Gibbs Free Energy=	0.283826
Sum of electronic and zero-point Energies=	-1076.218215
Sum of electronic and thermal Energies=	-1076.196570
Sum of electronic and thermal Enthalpies=	-1076.195626
Sum of electronic and thermal Free Energies=	-1076.273329

Energies and cartesian coordinates of the optimized ground-state structure of 3

C	-2.22250100	2.82621100	1.32345300	C	3.54433900	0.41082400	0.05295500
C	-1.31594100	1.77433800	1.24722300	C	-1.30261000	-2.14365500	0.99678400
C	-2.45513600	3.60987200	0.19950800	C	-1.78750500	-1.45998000	-1.20472500
C	-0.62411100	1.47692000	0.08016400	C	3.43317800	-1.04315900	-0.08677000
C	-1.77846800	3.33637900	-0.98309500	C	1.93383700	-2.83893000	-0.27467900
C	-0.87507500	2.27932100	-1.02649100	C	3.62884100	3.17897000	0.32254200
Au	0.67239500	-0.05303200	-0.01626300	H	1.48516300	3.10973100	0.28689500
C	2.33481400	1.13936900	0.10278800	C	4.77696200	1.07137500	0.13616000
C	-0.96203300	-1.35404300	-0.09372700	C	-2.39900200	-2.99963900	1.00036300
N	2.16502400	-1.52677900	-0.14025200	C	-2.89298300	-2.30317200	-1.24737000
C	2.39874000	2.52400500	0.24096500	C	4.50779400	-1.93426500	-0.16883400

H	0.89143900	-3.13544400	-0.31272700		F	-0.23575900	2.05796000	-2.18126100
C	2.96221400	-3.76277300	-0.36071200		F	-1.99669100	4.09027800	-2.06042000
H	3.65722900	4.26081400	0.42819800		F	-3.31985000	4.62015500	0.25654000
C	4.81823600	2.45381500	0.26999900		F	-2.86749400	3.08948400	2.45988400
H	5.71111900	0.51693500	0.09917600		F	-1.12052200	1.04178000	2.35120900
C	-3.19978900	-3.07593100	-0.13314400		F	-1.53098200	-0.73201900	-2.30437200
H	5.52354500	-1.55806200	-0.12726400		F	-3.65864400	-2.38284600	-2.33688500
C	4.27328400	-3.29442200	-0.30495100		F	-4.25216600	-3.89132100	-0.15415700
H	2.73384400	-4.81774300	-0.46738900		F	-2.68858300	-3.74721400	2.06713000
H	5.77548100	2.96376000	0.33429500		F	-0.54527800	-2.11353900	2.10938500
H	5.10897400	-3.98601600	-0.36859400					

After PCM corrections, the SCF energy is -2068.158509 a.u.

Zero-point correction=	0.262583 (Hartree/Particle)
Thermal correction to Energy=	0.292524
Thermal correction to Enthalpy=	0.293468
Thermal correction to Gibbs Free Energy=	0.198936
Sum of electronic and zero-point Energies=	-2067.876142
Sum of electronic and thermal Energies=	-2067.846200
Sum of electronic and thermal Enthalpies=	-2067.845256
Sum of electronic and thermal Free Energies=	-2067.939788

Energies and cartesian coordinates of the optimized triplet-state structure of 3

C	-2.30886000	2.76846400	1.32208900		H	0.97577700	-3.11738000	-0.30626700
C	-1.37430900	1.74126200	1.24687500		C	3.06661800	-3.67583600	-0.34732700
C	-2.55756000	3.54849800	0.19908700		H	3.57020000	4.33392000	0.43453000
C	-0.66901200	1.46348300	0.08270200		C	4.79561500	2.53842100	0.24976900
C	-1.86862100	3.29566400	-0.98088300		H	5.76010200	0.65729000	0.05741600
C	-0.93765000	2.26256600	-1.02245500		C	-3.12400000	-3.15112100	-0.14709100
Au	0.66912600	-0.03610300	-0.01121300		H	5.60186400	-1.43569900	-0.11066700
C	2.28757800	1.19478300	0.10797600		C	4.39602300	-3.18376500	-0.28826500
C	-0.92996900	-1.37377800	-0.09241300		H	2.85486600	-4.73407400	-0.45261900
N	2.17291900	-1.46472200	-0.13523900		H	5.73117300	3.08890900	0.30409100
C	2.33419500	2.56243600	0.25131800		H	5.23829500	-3.86617000	-0.34618800
C	3.56388200	0.44780700	0.04223800		F	-0.28896500	2.06237300	-2.17638000
C	-1.25899500	-2.17061400	0.99670200		F	-2.10172000	4.04663800	-2.05754700
C	-1.74439600	-1.50124000	-1.20958500		F	-3.44847400	4.53607300	0.25478600
C	3.48377000	-0.93162900	-0.08042600		F	-2.96511500	3.01241800	2.45664000
C	2.00394400	-2.77138000	-0.26495800		F	-1.16467400	1.01297100	2.35129800
C	3.55979300	3.25352300	0.32422800		F	-1.49875100	-0.76778200	-2.30782200
H	1.41130600	3.13274700	0.30847500		F	-3.58332200	-2.47099000	-2.35486600
C	4.81285500	1.18445100	0.11237800		F	-4.15583200	-3.99233700	-0.17497800
C	-2.33394600	-3.05354000	0.99216300		F	-2.61330300	-3.80652700	2.05791300
C	-2.82805200	-2.37188500	-1.25959200		F	-0.51333200	-2.12056400	2.11564900
C	4.59550600	-1.83737000	-0.15761700					

After PCM corrections, the SCF energy is -2068.057374 a.u.

Zero-point correction=	0.258117 (Hartree/Particle)
Thermal correction to Energy=	0.288684
Thermal correction to Enthalpy=	0.289628
Thermal correction to Gibbs Free Energy=	0.192786
Sum of electronic and zero-point Energies=	-2067.779960
Sum of electronic and thermal Energies=	-2067.749393
Sum of electronic and thermal Enthalpies=	-2067.748449
Sum of electronic and thermal Free Energies=	-2067.845291

Energies and cartesian coordinates of the optimized ground-state structure of 4

H	-2.15201600	3.41912200	-2.12418800		C	-0.42132400	-3.82941300	0.01266300
C	-2.03549700	2.86604100	-1.19633500		C	1.81722200	-3.12722800	0.03200900
C	-1.36576600	1.64508600	-1.19501900		C	-4.43627400	-2.43485800	-0.05316100
C	-2.55945600	3.37577600	-0.00870000		H	-3.57180900	-0.46964100	-0.05587300
H	-0.96153400	1.26695700	-2.13022300		C	-2.89478300	-4.28428400	-0.01605200
C	-1.21567400	0.91469900	-0.01172900		H	1.82019000	-0.01064700	-2.14077200
C	-2.40672700	2.66187700	1.17880100		C	3.49142300	0.91794800	-1.18647200
C	-1.74229700	1.43743700	1.17428700		C	3.34528200	1.18427300	1.20725800
Au	-0.30671500	-0.87175200	-0.00878100		H	1.55404500	0.47491300	2.13231600
H	-2.81503400	3.05371400	2.10620900		C	0.00004500	-5.16412700	0.03430500
H	-1.64869100	0.88784400	2.10751700		H	2.48746600	-2.27318600	0.03039500
C	-2.04650500	-1.98755300	-0.01960100		C	2.28786800	-4.43084600	0.05425800
C	1.50675000	0.12961700	-0.00255200		H	-5.45736000	-2.06040700	-0.07267400
N	0.50962900	-2.84179000	0.01053700		C	-4.20075800	-3.80955900	-0.03841800
C	-3.36697800	-1.53741100	-0.04378100		H	-2.72636100	-5.35833800	-0.00584800
C	-1.82061800	-3.38349800	-0.00781400		H	4.03712300	1.04707400	-2.11757700
C	2.23334000	0.31767000	-1.18794700		C	4.05242300	1.34665300	0.01626800
C	2.08743300	0.58421500	1.18970800		H	3.77680900	1.52244200	2.14541500

H	-0.73394700	-5.96189900	0.03605200		F	-4.16456500	4.80823500	0.97300600
C	1.35390600	-5.46514800	0.05491800		F	-3.85600500	4.97902500	-1.16678000
H	3.35562600	-4.62195700	0.07119400		F	-2.36124500	5.72355100	0.20686300
H	-5.03187500	-4.50974600	-0.04522700		F	5.27622700	3.36085800	-0.19828900
H	1.67931200	-6.50196100	0.07227300		F	6.03215000	1.88703900	1.19274700
C	-3.23602900	4.71287500	0.00031900		F	6.20391700	1.55580200	-0.94343900
C	5.38579900	2.03077300	0.01845400					

After PCM corrections, the SCF energy is -1750.176271 a.u.

Zero-point correction=	0.353137 (Hartree/Particle)
Thermal correction to Energy=	0.381465
Thermal correction to Enthalpy=	0.382409
Thermal correction to Gibbs Free Energy=	0.286562
Sum of electronic and zero-point Energies=	-1749.801268
Sum of electronic and thermal Energies=	-1749.772940
Sum of electronic and thermal Enthalpies=	-1749.771996
Sum of electronic and thermal Free Energies=	-1749.867843

Energies and cartesian coordinates of the optimized triplet-state structure of 4

H	-0.95895600	3.91588600	-2.11801000		C	3.53787000	0.20158900	1.20249300
C	-1.04295500	3.35204700	-1.19308600		H	1.61139500	0.09549600	2.12248500
C	-0.76746900	1.98705500	-1.18387100		C	-1.55823100	-4.97091200	0.02007100
C	-1.42957800	3.99330200	-0.01649000		H	1.69335400	-2.92410000	0.04679000
H	-0.46248000	1.50710700	-2.11000700		C	0.84056300	-4.91663100	0.05496200
C	-0.88051800	1.24079500	-0.00573400		H	-5.82205500	-0.36086200	-0.08584500
C	-1.53256600	3.26490300	1.16753100		C	-5.14067400	-2.43293500	-0.05056700
C	-1.26322900	1.89780500	1.16934900		H	-4.23644500	-4.35256000	-0.01612500
Au	-0.54889500	-0.74069400	0.00058600		H	4.17822800	-0.29636400	-2.09800800
H	-1.83325500	3.75958800	2.08695900		C	4.26856100	0.09039400	0.02000800
H	-1.36404800	1.34516400	2.10019400		H	4.04407900	0.44327200	2.13309500
C	-2.53349500	-1.27187300	-0.01617800		H	-2.49858700	-5.51128500	0.01065600
C	1.47785700	-0.32525800	0.00549100		C	-0.37248300	-5.65234900	0.04270600
N	-0.35097400	-2.83837600	0.01702800		H	1.80614100	-5.40999600	0.07450200
C	-3.65584200	-0.47129400	-0.04500800		H	-6.15057200	-2.83521400	-0.06327500
C	-2.72544500	-2.74255500	-0.00967000		H	-0.35752400	-6.73802500	0.05143500
C	2.23455200	-0.41773500	-1.17254300		C	-1.67913700	5.47087700	-0.01357600
C	2.15924400	-0.00279500	1.18726000		C	5.74441800	0.35038200	0.01707300
C	-1.58294600	-3.53421800	0.00883700		F	-2.56845000	5.83611600	0.93177200
C	0.78364700	-3.51843000	0.04067400		F	-2.15525200	5.91025100	-1.19580600
C	-4.95445700	-1.01433200	-0.06276700		F	-0.55173100	6.17683500	0.22995700
H	-3.54071900	0.60994800	-0.05392900		F	6.03439100	1.63958000	-0.26956700
C	-4.07478600	-3.27909500	-0.02418600		F	6.31241200	0.08756500	1.21081800
H	1.74815500	-0.65893400	-2.11673000		F	6.39143700	-0.39684600	-0.90136500
C	3.61335200	-0.21326700	-1.17310600					

After PCM corrections, the SCF energy is -1750.074306 a.u.

Zero-point correction=	0.348544 (Hartree/Particle)
Thermal correction to Energy=	0.377545
Thermal correction to Enthalpy=	0.378490
Thermal correction to Gibbs Free Energy=	0.279570
Sum of electronic and zero-point Energies=	-1749.704903
Sum of electronic and thermal Energies=	-1749.675902
Sum of electronic and thermal Enthalpies=	-1749.674958
Sum of electronic and thermal Free Energies=	-1749.773877

Energies and cartesian coordinates of the optimized ground-state structure of 5

Au	-0.06882300	-0.05001800	-0.01765600		H	4.93929100	-3.27943000	-0.01999000
C	1.55990900	-1.31431600	0.00349100		H	4.54617100	3.71752500	0.03614400
N	1.50412700	1.37245500	-0.04483100		C	-1.43943900	-1.49450300	0.08945800
C	1.57935500	-2.70893000	-0.02255500		C	-1.60132000	-2.42314200	1.08972700
C	2.79952800	-0.63300000	0.00467300		S	-2.64904700	-1.70219700	-1.12727600
C	2.74875200	0.83308400	-0.00283600		C	-2.69561600	-3.30940000	0.86112000
C	1.32549300	2.69898200	-0.05425600		H	-0.95871100	-2.47550300	1.96295200
C	2.78435600	-3.41370300	-0.02912400		C	-3.34964500	-3.04746100	-0.31113200
H	0.64121900	-3.25656300	-0.04023500		H	-2.97895400	-4.10729700	1.54059100
C	4.00870200	-1.34209400	-0.00027500		H	-4.20016000	-3.56575100	-0.73632000
C	3.86025500	1.68256500	0.02587800		C	-1.58420100	1.34388300	-0.10313300
H	0.29206200	3.03133700	-0.08821300		C	-1.99977400	2.09316200	-1.18283000
C	2.39256000	3.58375100	-0.02905100		S	-2.50896800	1.78417800	1.28939000
H	2.77365900	-4.50129200	-0.04928300		C	-3.04544900	3.01714600	-0.88057300
C	4.00067900	-2.73153600	-0.01439500		H	-1.57871100	1.98050500	-2.17875400
H	4.96298200	-0.82105800	0.00138400		C	-3.42414900	2.96737600	0.43326700
H	4.85923400	1.26304400	0.06155200		H	-3.49774300	3.68300400	-1.60957300
C	3.68236600	3.05828600	0.01243600		H	-4.18730800	3.55013900	0.93439200
H	2.20916200	4.65296500	-0.03917600					

After PCM corrections, the SCF energy is -1718.084024 a.u.

Zero-point correction=	0.276695 (Hartree/Particle)
Thermal correction to Energy=	0.296855
Thermal correction to Enthalpy=	0.297799
Thermal correction to Gibbs Free Energy=	0.224460
Sum of electronic and zero-point Energies=	-1717.787098
Sum of electronic and thermal Energies=	-1717.766938
Sum of electronic and thermal Enthalpies=	-1717.765994
Sum of electronic and thermal Free Energies=	-1717.839333

Energies and cartesian coordinates of the optimized triplet-state structure of 5

Au	-0.07581800	-0.04490600	-0.01179000	H	4.92266100	-3.31688500	0.03719600
C	1.52168600	-1.32703300	0.00350600	H	4.62240200	3.66948600	-0.02575000
N	1.48871500	1.35139100	-0.04293600	C	-1.46252000	-1.47988600	0.08635800
C	1.54066400	-2.70421700	-0.05142900	C	-1.64247200	-2.40873900	1.08377500
C	2.81995800	-0.61125700	0.02388300	S	-2.65738700	-1.68438500	-1.14577700
C	2.78042900	0.77668000	-0.00685200	C	-2.73789600	-3.29045500	0.84189000
C	1.35524000	2.66710400	-0.05738100	H	-1.01283400	-2.46214500	1.96645900
C	2.74811000	-3.42822000	-0.04664600	C	-3.37640200	-3.02532900	-0.33815900
H	0.59996100	-3.24695500	-0.08998000	H	-3.03459700	-4.08588700	1.51865400
C	4.05083000	-1.38107200	0.05936400	H	-4.22622100	-3.53752600	-0.77208900
C	3.91972700	1.65192500	-0.00545600	C	-1.57660900	1.36091600	-0.09376100
H	0.33268100	3.03554800	-0.08099100	C	-1.97759100	2.12550000	-1.16793500
C	2.44570300	3.54531400	-0.04971600	S	-2.51436100	1.78644700	1.29476200
H	2.73439000	-4.51395800	-0.08397500	C	-3.02312100	3.04923900	-0.86472200
C	4.00071300	-2.74090300	0.01995700	H	-1.54573600	2.02406200	-2.16035200
H	5.01058200	-0.87572800	0.10750400	C	-3.41608300	2.98374400	0.44424700
H	4.91413800	1.21904500	0.01189800	H	-3.46492900	3.72646300	-1.58967800
C	3.75956500	3.01018900	-0.02687800	H	-4.18176000	3.56349900	0.94501900
H	2.26627400	4.61481400	-0.05997400				

After PCM corrections, the SCF energy is -1717.982421 a.u.

Zero-point correction=	0.272149 (Hartree/Particle)
Thermal correction to Energy=	0.292954
Thermal correction to Enthalpy=	0.293898
Thermal correction to Gibbs Free Energy=	0.218106
Sum of electronic and zero-point Energies=	-1717.690792
Sum of electronic and thermal Energies=	-1717.669988
Sum of electronic and thermal Enthalpies=	-1717.669044
Sum of electronic and thermal Free Energies=	-1717.744836

Energies and cartesian coordinates of the optimized ground-state structure of 6

H	-4.11463900	-2.72026700	-1.91044100	C	-3.37085100	2.65378900	1.19263800
C	-3.42255200	-2.63059500	-1.07596400	H	-2.26019700	1.04150300	2.06854100
C	-2.47547900	-1.60578400	-1.07721200	C	3.86717400	1.54794800	0.06434200
C	-3.49430800	-3.52470400	-0.00907000	H	0.36784700	3.08401600	0.13112000
H	-2.45271100	-0.90159100	-1.90447600	C	2.49388400	3.51950300	0.16270800
C	-1.57321000	-1.47569300	-0.01720300	H	-3.05579400	3.75263600	-2.00500900
H	-4.23873100	-4.31713400	-0.00667500	C	-3.60700700	3.42149700	0.05288300
C	-2.60583400	-3.39132300	1.05584000	H	-3.94146800	2.83846900	2.10065800
C	-1.64517200	-2.37791100	1.04976300	H	4.84004800	1.06593700	0.04553200
Au	-0.16397600	-0.04596900	-0.00638500	C	3.75722800	2.92844800	0.13514500
H	-2.65210800	-4.08088600	1.89611000	H	2.36732400	4.59533700	0.22105100
H	-0.94810600	-2.30047200	1.88087300	H	-4.35857500	4.20738000	0.06598900
C	-1.65667500	1.37489400	0.02062100	H	4.65309700	3.54287700	0.17109700
N	1.48358600	1.36162000	0.04136900	C	1.44291600	-1.34525300	-0.05668600
C	-1.91207500	2.15470900	-1.11781500	C	2.65401700	-0.67650600	-0.04332700
C	-2.41168600	1.63946200	1.17166300	C	1.64266300	-2.75019500	-0.12337900
C	2.70637400	0.76522900	0.02020300	S	4.01986200	-1.74792100	-0.10633100
C	1.38061600	2.69167400	0.11436000	C	2.96821200	-3.10799800	-0.15411200
H	-1.35513200	1.97678900	-2.03787700	H	0.83647200	-3.47652500	-0.15015700
C	-2.87602800	3.16608900	-1.10601000	H	3.39062800	-4.10478800	-0.20648300

After PCM corrections, the SCF energy is -1397.37657 a.u.

Zero-point correction=	0.309927 (Hartree/Particle)
Thermal correction to Energy=	0.330619
Thermal correction to Enthalpy=	0.331564
Thermal correction to Gibbs Free Energy=	0.256916
Sum of electronic and zero-point Energies=	-1397.048903
Sum of electronic and thermal Energies=	-1397.028211
Sum of electronic and thermal Enthalpies=	-1397.027266
Sum of electronic and thermal Free Energies=	-1397.101914

Energies and cartesian coordinates of the optimized triplet-state structure of 6

H	-4.10875600	-2.69306400	-1.96447100	C	-3.34822800	2.67930300	1.19856300
C	-3.43733400	-2.60304400	-1.11327500	H	-2.24176700	1.06629600	2.07852200
C	-2.47633300	-1.59154000	-1.10099100	C	3.91102000	1.52975700	0.03919400
C	-3.54877600	-3.48432400	-0.03895600	H	0.38893300	3.06349000	0.13495200
H	-2.42177300	-0.89826100	-1.93610000	C	2.51685400	3.48281200	0.14442100
C	-1.59991300	-1.45920300	-0.01936700	H	-3.03911500	3.76077600	-2.00545200
H	-4.30370300	-4.26674600	-0.04704800	C	-3.58480100	3.44248900	0.05589800
C	-2.68700200	-3.34965300	1.04739800	H	-3.91423500	2.87146700	2.10791100
C	-1.71385500	-2.34785200	1.05560800	H	4.88305700	1.04531200	0.01027000
Au	-0.16725400	-0.04858800	0.00103100	C	3.80175000	2.89662800	0.10485800
H	-2.76525500	-4.02795000	1.89452600	H	2.38521300	4.55797300	0.20074600
H	-1.04099900	-2.26692900	1.90618000	H	-4.33224300	4.23231800	0.06789600
C	-1.64516000	1.38601100	0.02651400	H	4.69127800	3.51959000	0.12803500
N	1.47621600	1.33026300	0.04084600	C	1.39797600	-1.37256800	-0.04532900
C	-1.90073600	2.16121200	-1.11483200	C	2.69793700	-0.66495300	-0.03839800
C	-2.39427100	1.66011100	1.17913000	C	1.59960200	-2.73580900	-0.10592600
C	2.73680300	0.72267300	0.01102400	S	4.06626500	-1.75950900	-0.09446300
C	1.39538000	2.65429300	0.10965300	C	2.94605200	-3.12796100	-0.13771000
H	-1.34763100	1.97578400	-2.03554700	H	0.79377800	-3.46374900	-0.12871700
C	-2.85931200	3.17760800	-1.10428100	H	3.34664000	-4.13347300	-0.18682500

After PCM corrections, the SCF energy is -1397.292598 a.u.

Zero-point correction=	0.306169 (Hartree/Particle)
Thermal correction to Energy=	0.327436
Thermal correction to Enthalpy=	0.328380
Thermal correction to Gibbs Free Energy=	0.251599
Sum of electronic and zero-point Energies=	-1396.969230
Sum of electronic and thermal Energies=	-1396.947962
Sum of electronic and thermal Enthalpies=	-1396.947018
Sum of electronic and thermal Free Energies=	-1397.023800

Energies and cartesian coordinates of the optimized ground-state structure of 7

F	3.64743200	-2.43795600	-2.35722700	C	-3.41745300	0.51337600	0.06280400
F	1.58117300	-0.71077800	-2.29299400	C	-3.08887900	-3.65289500	-0.35523800
F	0.25967300	2.14471500	-2.13061100	C	-3.41719900	-0.92172600	-0.07376600
F	2.04437000	4.15554800	-1.98884700	C	0.96920100	-1.37852900	-0.10766700
C	2.87482600	-2.36265800	-1.27267200	C	-2.22583900	1.21361200	0.10621300
C	1.80074200	-1.48087200	-1.21467500	N	-2.16885800	-1.46378300	-0.13919800
C	0.93556500	2.31852100	-0.98869000	C	-2.01079500	-2.78461400	-0.27767100
C	1.85200100	3.36371900	-0.93425400	H	-0.98596100	-3.13676500	-0.32635600
F	4.16484300	-4.03012000	-0.21501500	Au	-0.61077000	-0.02696300	-0.01427800
C	3.14262400	-3.17817000	-0.17899300	C	0.71280500	1.47729700	0.09460200
H	-4.22612200	3.91122700	0.38973900	F	3.44655800	4.58321000	0.30222200
S	-4.79988000	1.54896300	0.18169900	C	2.56905000	3.58500100	0.23542000
C	-3.78092700	2.92823400	0.29203900	C	2.33452300	-3.10588900	0.94961900
H	-5.24436000	-3.76856400	-0.34204100	C	1.26996500	-2.21077300	0.96268300
H	-5.53393300	-1.30993100	-0.09170300	C	1.44335700	1.72259900	1.25005000
H	-1.66104100	3.35292700	0.29598800	C	2.36401800	2.76138700	1.33594400
C	-2.44673200	2.60740700	0.24009300	F	2.58708700	-3.89339100	1.99650900
C	-4.37542500	-3.11860100	-0.28564400	F	0.50493200	-2.18286400	2.06944900
C	-4.54260200	-1.74932000	-0.14533900	F	1.27410100	0.95045300	2.33075600
H	-2.91732000	-4.71807500	-0.46559100	F	3.04790600	2.97448000	2.45975600

After PCM corrections, the SCF energy is -2388.855596 a.u.

Zero-point correction=	0.228924 (Hartree/Particle)
Thermal correction to Energy=	0.258581
Thermal correction to Enthalpy=	0.259525
Thermal correction to Gibbs Free Energy=	0.165340
Sum of electronic and zero-point Energies=	-2388.608598
Sum of electronic and thermal Energies=	-2388.578940
Sum of electronic and thermal Enthalpies=	-2388.577996
Sum of electronic and thermal Free Energies=	-2388.672181

Energies and cartesian coordinates of the optimized triplet-state structure of 7

F	3.56455500	-2.53384200	-2.36978100	C	3.05835100	-3.24879500	-0.18337500
F	1.54344700	-0.75567400	-2.30043000	H	-4.13304500	4.00919400	0.38489100
F	0.33605900	2.14235300	-2.13343100	S	-4.83149600	1.63749500	0.17497400
F	2.18224800	4.09375800	-1.98985800	C	-3.72434800	3.01065100	0.28889300
C	2.80235900	-2.43343500	-1.27986000	H	-5.34070200	-3.66045200	-0.33096700
C	1.75108600	-1.52474000	-1.21928100	H	-5.60006000	-1.20095200	-0.08135900
C	1.01420100	2.29354900	-0.98927000	H	-1.57877900	3.37393400	0.29723200
C	1.96381500	3.30896600	-0.93475600	C	-2.37367400	2.63736600	0.23867600
F	4.05901000	-4.12592600	-0.22167200	C	-4.46962600	-3.01444100	-0.27685900

C	-4.61595000	-1.65726800	-0.13858800	C	0.76215100	1.46014400	0.09396000
H	-3.00669000	-4.62749500	-0.45983200	F	3.59573100	4.47779900	0.30207800
C	-3.45917800	0.56006500	0.05963300	C	2.68682500	3.50796000	0.23506200
C	-3.16853700	-3.56095300	-0.34913500	C	2.26097400	-3.14938800	0.95069300
C	-3.46611800	-0.81990200	-0.06882300	C	1.21883400	-2.22820100	0.96697300
C	0.93041700	-1.39526700	-0.10669600	C	1.50030700	1.68365500	1.24937400
C	-2.17002700	1.28123300	0.11010400	C	2.45419700	2.69196500	1.33577200
N	-2.18662800	-1.39033200	-0.13707100	F	2.50234100	-3.93609500	2.00079800
C	-2.07049400	-2.70858900	-0.27409600	F	0.46488100	-2.17523500	2.07955900
H	-1.05688800	-3.09293100	-0.32646900	F	1.30617900	0.91906100	2.33131900
Au	-0.61099000	-0.00439100	-0.01270400	F	3.14347800	2.88386100	2.46026200

After PCM corrections, the SCF energy is -2388.772102 a.u.

Zero-point correction= 0.225229 (Hartree/Particle)
Thermal correction to Energy= 0.255450
Thermal correction to Enthalpy= 0.256394
Thermal correction to Gibbs Free Energy= 0.160116
Sum of electronic and zero-point Energies= -2388.529040
Sum of electronic and thermal Energies= -2388.498819
Sum of electronic and thermal Enthalpies= -2388.497875
Sum of electronic and thermal Free Energies= -2388.594153

Energies and cartesian coordinates of the optimized ground-state structure of 8

F	4.50256500	-0.72827900	-2.33330500	C	1.62021300	-0.87177200	-0.09100000
F	1.89156900	-0.06721700	-2.29907800	C	-2.38730500	0.07064200	0.08107600
F	-0.57325000	1.97361300	-2.15157400	N	-1.16348800	-2.31275100	-0.14601000
F	0.14480200	4.56483300	-2.03786700	C	-0.44229100	-3.43236700	-0.27083200
C	3.76905900	-0.96538100	-1.24467100	H	0.63414900	-3.30140900	-0.30200100
C	2.41872800	-0.63453600	-1.20139500	Au	-0.39195400	-0.34100500	-0.01917000
C	-0.03572600	2.43648200	-1.01638700	C	0.13977200	1.59222800	0.07343200
C	0.32664700	3.77896800	-0.97653800	F	1.22723400	5.58777900	0.23913700
F	5.64945900	-1.88124100	-0.15412500	C	0.87869800	4.30437800	0.18544300
C	4.35886700	-1.55486900	-0.13231300	C	3.59403400	-1.80936500	1.00012300
S	-4.84654500	-0.74180400	0.12668500	C	2.24685900	-1.46338900	0.99794100
C	-4.54299400	0.95641000	0.24514200	C	0.69343000	2.14564600	1.22066700
H	-2.91985800	-5.72946500	-0.37192100	C	1.06301600	3.48449600	1.29225100
H	-4.25837000	-3.64528100	-0.14483200	F	4.15802200	-2.38204900	2.06516200
H	-2.80418900	2.23868300	0.26809800	F	1.53996000	-1.74160800	2.10860000
C	-3.19221300	1.22657500	0.20701200	F	0.88603900	1.38981900	2.30882000
C	-2.42305600	-4.76511200	-0.30847300	F	1.58900800	3.98739000	2.40895000
C	-3.17398300	-3.60723300	-0.18129900	C	-5.67420300	1.92728000	0.36884700
H	-0.40951500	-5.56785700	-0.45470600	H	-5.59157300	2.50142200	1.29883400
C	-3.15209000	-1.08086800	0.02684800	H	-5.66545100	2.63925100	-0.46455500
C	-1.03071700	-4.68443800	-0.35571400	H	-6.64669500	1.42660400	0.37059200
C	-2.52535500	-2.36907200	-0.10057300				

After PCM corrections, the SCF energy is -2428.124292 a.u.

Zero-point correction= 0.256621 (Hartree/Particle)
Thermal correction to Energy= 0.287375
Thermal correction to Enthalpy= 0.288319
Thermal correction to Gibbs Free Energy= 0.192127
Sum of electronic and zero-point Energies= -2427.851498
Sum of electronic and thermal Energies= -2427.820745
Sum of electronic and thermal Enthalpies= -2427.819801
Sum of electronic and thermal Free Energies= -2427.915992

Energies and cartesian coordinates of the optimized triplet-state structure of 8

F	4.42644200	-0.97610600	-2.38243600	H	-0.59205800	-5.52577200	-0.41456800
F	1.84114800	-0.21972000	-2.33425700	C	-3.22474600	-1.01364200	0.04384100
F	-0.51639700	2.02190500	-2.14031800	C	-1.19388900	-4.62889200	-0.31736100
F	0.32876500	4.57265600	-2.02886400	C	-2.63892200	-2.26948600	-0.06545000
C	3.70331400	-1.14376800	-1.27379900	C	1.57652400	-0.93269400	-0.09473200
C	2.36718300	-0.75988500	-1.22247300	C	-2.36823900	0.19303800	0.08050400
C	0.07018100	2.44844700	-1.01453800	N	-1.24093000	-2.24494800	-0.12541400
C	0.49248300	3.77360100	-0.97400000	C	-0.56748400	-3.38790000	-0.24960500
F	5.56491400	-2.09397400	-0.17957200	H	0.51391100	-3.30217000	-0.29955300
C	4.28791800	-1.71772600	-0.15047300	Au	-0.40735800	-0.31653000	-0.02020700
S	-4.91917200	-0.60534600	0.13173000	C	0.21867400	1.59197200	0.07079300
C	-4.52366700	1.11760200	0.22488500	F	1.48555600	5.53629700	0.23756300
H	-3.11559100	-5.64136100	-0.31474300	C	1.08219700	4.26906300	0.18269800
H	-4.40513100	-3.52289000	-0.09633400	C	3.53166600	-1.90348700	1.00114100
H	-2.72924400	2.34505300	0.22920900	C	2.19790200	-1.50804900	1.00657200
C	-3.13154900	1.33777100	0.17860800	C	0.80477900	2.11910400	1.21587200
C	-2.60339400	-4.68536100	-0.25746000	C	1.23888600	3.43858100	1.28589700
C	-3.31970000	-3.51789600	-0.13537100	F	4.09207300	-2.45409800	2.07968300

F	1.50530800	-1.70657700	2.14217200	H	-6.33297900	1.98161900	-0.49781800
F	0.97553100	1.35422600	2.30114200	H	-5.23370400	3.11069900	0.35565400
F	1.79573200	3.91463000	2.39949300	H	-6.20663400	1.93480800	1.27125300
C	-5.63605700	2.09341600	0.34478800				

After PCM corrections, the SCF energy is -2428.045634 a.u.

Zero-point correction=	0.253448 (Hartree/Particle)
Thermal correction to Energy=	0.285406
Thermal correction to Enthalpy=	0.286350
Thermal correction to Gibbs Free Energy=	0.186477
Sum of electronic and zero-point Energies=	-2427.776106
Sum of electronic and thermal Energies=	-2427.744148
Sum of electronic and thermal Enthalpies=	-2427.743204
Sum of electronic and thermal Free Energies=	-2427.843077

Energies and cartesian coordinates of the optimized transition state TS-2

H	3.90800000	-2.72920300	2.15279000	H	-0.49954200	-3.32785100	-0.00311600
C	3.54024600	-2.34467800	1.20406900	C	-3.98923100	-1.66394300	-0.00029600
C	2.56620400	-1.35279100	1.20732700	H	1.88913200	1.23987700	2.15515900
C	4.04163500	-2.84831200	0.00348900	C	2.61606500	3.01492000	1.20244600
H	2.19400200	-0.98349500	2.15906200	C	2.61573400	3.01346100	-1.20626300
C	2.05928900	-0.82760000	0.00065400	H	1.88860200	1.23731100	-2.15670800
H	4.80641300	-3.62012900	0.00456500	C	-4.12379200	1.34259200	0.00218200
C	3.54242700	-2.34588100	-1.19849200	H	-0.71545900	3.04751400	0.00038200
C	2.56838500	-1.35398400	-1.20454100	C	-2.85779200	3.38804500	0.00206900
Au	0.08596800	-0.15810500	-0.00047300	H	-2.53153300	-4.72899700	-0.00334300
H	3.91191200	-2.73134900	-2.14615600	C	-3.88330700	-3.04996300	-0.00140500
H	2.19799700	-0.98557300	-2.15731800	H	-4.98122500	-1.21848200	0.00035800
C	-1.55058500	-1.44944400	-0.00106700	H	2.82151000	3.51124700	2.14822100
C	1.80669500	1.05529100	-0.00061500	C	2.89029800	3.66363600	-0.00234100
N	-1.75252000	1.27431300	0.00037900	H	2.82088600	3.50866600	-2.15269000
C	-1.47626500	-2.84678600	-0.00225900	H	-5.07912500	0.82968100	0.00275900
C	-2.83640300	-0.86417800	-0.00010200	C	-4.08701700	2.73016200	0.00276200
C	2.08310500	1.72949200	1.20397700	H	-2.78780700	4.47128400	0.00242900
C	2.08281900	1.72800600	-1.20611700	H	-4.78139400	-3.66272600	-0.00155100
C	-2.92494300	0.61332100	0.00089900	H	3.31806600	4.66283100	-0.00300900
C	-1.71044000	2.60514900	0.00090200	H	-5.01491200	3.29678300	0.00377400
C	-2.62135000	-3.64439900	-0.00242300				

Frequencies --	-334.8110	16.9313	35.8856
Frequencies --	37.7744	56.2376	66.6777
Frequencies --	70.1175	83.1527	114.6695 …

Zero-point correction=	0.341638 (Hartree/Particle)
Thermal correction to Energy=	0.362346
Thermal correction to Enthalpy=	0.363290
Thermal correction to Gibbs Free Energy=	0.289466
Sum of electronic and zero-point Energies=	-1076.279851
Sum of electronic and thermal Energies=	-1076.259144
Sum of electronic and thermal Enthalpies=	-1076.258199
Sum of electronic and thermal Free Energies=	-1076.332023

Energies and cartesian coordinates of the optimized transition state TS-3

C	3.11835200	-2.12708600	1.10979100	C	-3.84266400	3.06843900	-0.59554600
C	2.17003500	-1.11855600	1.16267500	H	-2.99554200	-4.91077900	0.70897900
C	3.34536400	-2.81906500	-0.07206700	C	-4.44448600	-3.34140100	0.41958500
C	1.39262700	-0.71241700	0.04908800	H	-5.65175000	-1.60902500	0.11024300
C	2.58595000	-2.49041300	-1.18999200	C	2.08380200	3.66602200	0.07672800
C	1.64520200	-1.47944800	-1.12541500	H	-5.87508300	0.38294900	-0.24477200
Au	-0.69570500	-0.23421400	0.02194300	C	-5.02153400	2.32825000	-0.52185200
C	-2.22137600	-1.62205400	0.19842700	H	-3.84767000	4.14022700	-0.76593200
C	1.13405200	0.96338100	-0.01914200	H	-5.30372600	-4.00149200	0.50494800
N	-2.59027800	1.06901800	-0.23102200	H	-5.98624800	2.81584600	-0.63590300
C	-2.05571900	-2.99065100	0.42321200	F	0.35848100	1.36452300	2.21694900
C	-3.53473900	-1.11940900	0.08364900	F	1.31450900	3.81402600	2.29335500
C	1.02051600	1.78456800	1.13633900	F	2.52950800	4.91405100	0.12122700
C	1.71725300	1.61806100	-1.13057400	F	2.75236200	3.45854900	-2.16976700
C	-3.71427000	0.33021800	-0.15464500	F	1.90867900	0.96397900	-2.27252700
C	-2.64555000	2.38364000	-0.44207400	F	2.05275000	-0.47885200	2.32765200
C	-3.15078100	-3.84841700	0.53386200	F	3.83159200	-2.42000100	2.19598200
H	-1.05289400	-3.40307100	0.51448300	F	4.26127400	-3.77990000	-0.13198100
C	-4.63474000	-1.98296400	0.19519800	F	2.73541000	-3.18851000	-2.31424800
C	1.48538700	3.08952300	1.19028600	F	0.86987400	-1.32140700	-2.20275600
C	2.18727300	2.92101400	-1.09166100				
C	-4.95915800	0.95981600	-0.30170000				
H	-1.68917600	2.90072700	-0.48839500				

```
Frequencies --  -143.8807               15.9248               24.8195
Frequencies --    28.4019               40.5209               51.8972
Frequencies --    59.5470               66.8951               81.2713 …

Zero-point correction=                           0.260372 (Hartree/Particle)
Thermal correction to Energy=                    0.289889
Thermal correction to Enthalpy=                  0.290833
Thermal correction to Gibbs Free Energy=         0.198196
Sum of electronic and zero-point Energies=          -2067.811349
Sum of electronic and thermal Energies=             -2067.781832
Sum of electronic and thermal Enthalpies=           -2067.780888
Sum of electronic and thermal Free Energies=        -2067.873525
```

Table S3. Selected bond distances (Å), bond angles and dihedral angles (°) for **1**.

	X-ray	B3LYP	MPW1K	BB1K	PBE1PBE	G96LYP	TPSS	TPSSLYP1W
Au1-C1	2.089(3)	2.109	2.075	2.073	2.083	2.122	2.104	2.135
Au1-C12	2.077(3)	2.099	2.065	2.062	2.075	2.114	2.097	2.125
Au1-C23	2.030(3)	2.040	2.007	2.005	2.017	2.055	2.038	2.064
Au1-N1	2.125(2)	2.199	2.149	2.150	2.159	2.212	2.178	2.222
C6-C7	1.474(4)	1.471	1.463	1.462	1.466	1.475	1.470	1.477
C17-C18	1.473(4)	1.472	1.463	1.462	1.467	1.477	1.472	1.478
mean unsigned error		***0.022***	***0.016***	***0.017***	***0.011***	***0.031***	***0.017***	***0.039***
ranking		***5/7***	***2/7***	***3/7***	***1/7***	***6/7***	***3/7***	***7/7***
N1-Au1-C1	79.43(10)	78.27	78.91	78.73	78.83	78.13	78.53	77.89
C12-Au1-C23	80.75(11)	80.44	80.73	80.63	80.72	80.36	80.55	80.21
C1-Au1-C12	164.46(10)	166.20	166.01	165.99	164.84	165.62	165.73	166.35
N1-Au1-C23	167.56(10)	164.91	164.86	164.61	165.86	164.50	164.95	165.34
mean unsigned error		***1.50***	***1.22***	***1.36***	***0.70***	***1.53***	***1.27***	***1.62***
ranking		***5/7***	***2/7***	***4/7***	***1/7***	***6/7***	***3/7***	***7/7***
Au-C1-N1-C12	-9.84	-8.56	-8.70	-8.71	-8.80	-8.91	-8.90	-8.49

Table S4. Selected bond distances (Å), bond angles and dihedral angles (°) for **2**.

	X-ray	B3LYP	MPW1K	BB1K	PBE1PBE
Au1-C1	2.066(2)	2.095	2.061	2.061	2.070
Au1-C12	2.068(2)	2.094	2.060	2.058	2.069
Au1-C18	2.010(2)	2.028	1.997	1.996	2.006
Au1-N1	2.1106(18)	2.175	2.129	2.133	2.141
C6-C7	1.481(3)	1.475	1.467	1.466	1.470
mean unsigned error		***0.029***	***0.012***	***0.013***	***0.010***
ranking		***4/4***	***2/4***	***3/4***	***1/4***
N1-Au1-C1	80.02(8)	79.07	79.70	79.59	79.61
C12-Au1-C18	86.83(8)	88.53	88.27	88.21	88.33
C1-Au1-C12	178.35(8)	175.30	176.01	176.06	175.75
N1-Au1-C18	174.58(7)	175.24	175.42	175.30	175.52
mean unsigned error		***1.59***	***1.23***	***1.20***	***1.36***
ranking		***4/4***	***2/4***	***1/4***	***3/4***
Au1-C1-N1-C12	-0.59(5)	-0.05	-0.07	-0.28	-0.14
Au1-N1-C1-C18	-0.18(5)	-0.07	-0.13	-0.11	-0.19
N1-Au1-C12-C13	93.46(18)	87.19	86.95	87.43	85.40
C1-Au1-C18-C23	-92.98(18)	-92.01	-92.11	-104.74	-97.24
mean unsigned error		***1.97***	***1.99***	***4.54***	***3.19***
ranking		***1/4***	***2/4***	***4/4***	***3/4***

Table S5. Selected singlet-singlet (S_n) and singlet-triplet (T_1) excited states with TDDFT/CPCM vertical excitation energies (nm), transition coefficients, orbitals involved in the transitions, and oscillator strengths for compounds **1-8**.

	1	**2**	**3**	**4**	**5**	**6**	**7**	**8**
				Absorption				
Exp. λ_{max}	317	316	338	321	319	357	365	380
Calctd λ_{max} [a]	291	288	304	276	302	339	346	360
S_0-S_n	*n* = 2 325 (0.059) H-1->L (0.63)	*n* = 2 311 (0.217) H-1->L (0.65)	*n* = 1 313 (0.219) H->L (0.66)	*n* = 2 311 (0.221) H-1->L (0.64)	*n* = 3 311 (0.209) H-2->L (0.65)	*n* = 1 343 (0.248) H->L (0.65)	*n* = 1 347 (0.239) H->L (0.65)	*n* = 1 361 (0.268) H->L (0.65)
S_0-S_n	*n* = 3 311 (0.133) H-2->L (0.59)	*n* = 4 286 (0.102) H-5->L (0.44)	*n* = 2 287 (0.097) H-2->L (0.42)	*n* = 3 286 (0.108) H-2->L (0.60)	*n* = 6 288 (0.077) H-5->L (0.48)	*n* = 4 284 (0.144) H->L+1 (0.61)	*n* = 3 285 (0.089) H-2->L (0.51)	*n* = 3 288 (0.155) H->L+2 (0.66)
S_0-S_n	*n* = 6 288 (0.150) H-4->L (0.55)	*n* = 9 274 (0.200) H-1->L+1 (0.59)	*n* = 8 313 (0.067) H-1->L+1 (0.41)	*n* = 6 272 (0.186) H-1->L+1 (0.59)		*n* = 6 280 (0.127) H-5->L (0.57)	*n* = 4 282 (0.074) H-4->L (0.47)	*n* = 4 284 (0.104) H-2->L (0.54)
S_0-S_n	*n* = 7 285 (0.059) H->L+1 (0.43)			*n* = 10 264 (0.167) H->L+2 (0.59)			*n* = 6 278 (0.133) H->L+2 (0.59)	*n* = 5 280 (0.069) H-4->L (0.48)
S_0-S_n	*n* = 8 282 (0.135) H->L+3 (0.38)						*n* = 9 273 (0.050) H-4->L+1 (0.65)	
				Emission				
Exp. λ_{max}	506	490	493	490	492	569	577	592
Calctd λ_{max} [b]	486	466	472	468	470	569	572	604
S_0-T_1	454 H->L+2 (0.59)	437 H-1->L (0.66)	441 H->L (0.69)	438 H-1->L (0.66)	439 H-2->L (0.68)	514 H->L (0.74)	516 H->L (0.74)	537 H->L (0.74)

[a] The calculated values are obtained from the TDDFT/CPCM Uv-vis spectra drawn by Gaussview [b] Solvent-corrected energy difference between the optimized ground state and the lowest-lying triplet state.

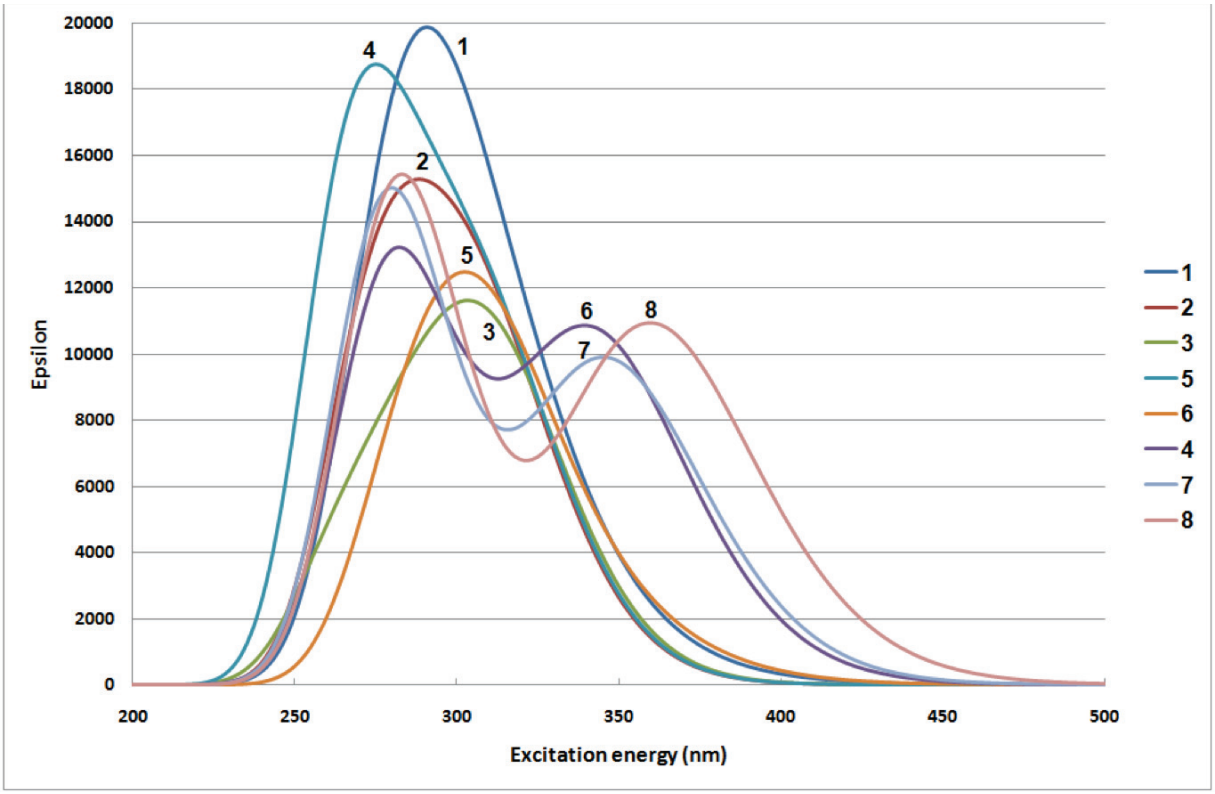

Figure S6. TDDFT/CPCM calculated UV-vis absorption spectra for compound **1**-**8** (in CH_2Cl_2).

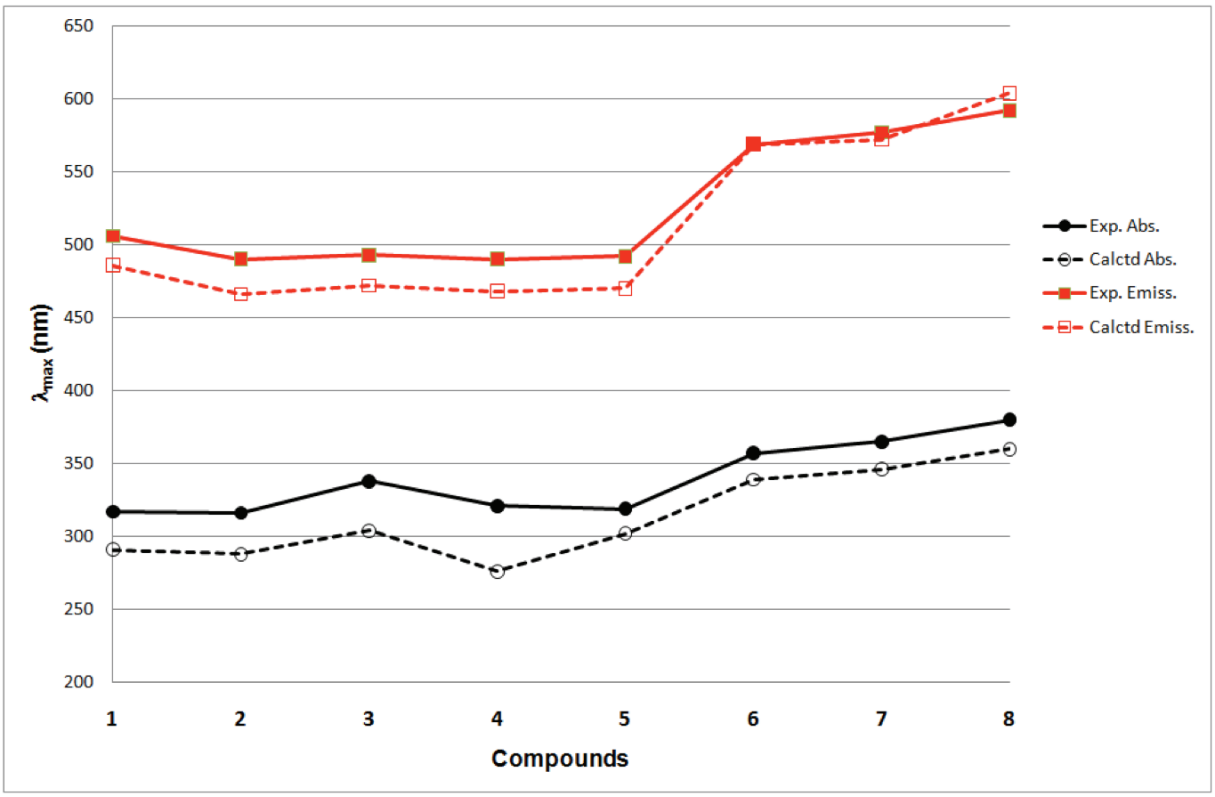

Figure S7. Comparison between experimental and TDDFT/CPCM calculated absorption and emission maxima for compound **1-8** (the mean underestimations are 26 and 16 nm, for the calculated absorption and emission data respectively).

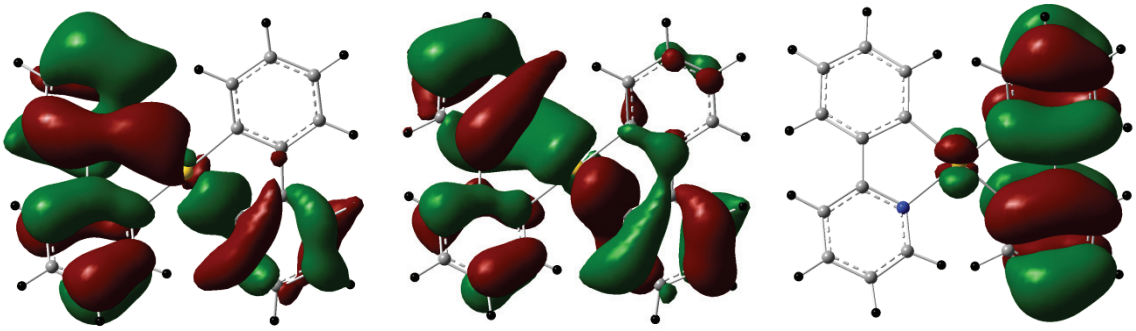

HOMO -2 HOMO -1 HOMO

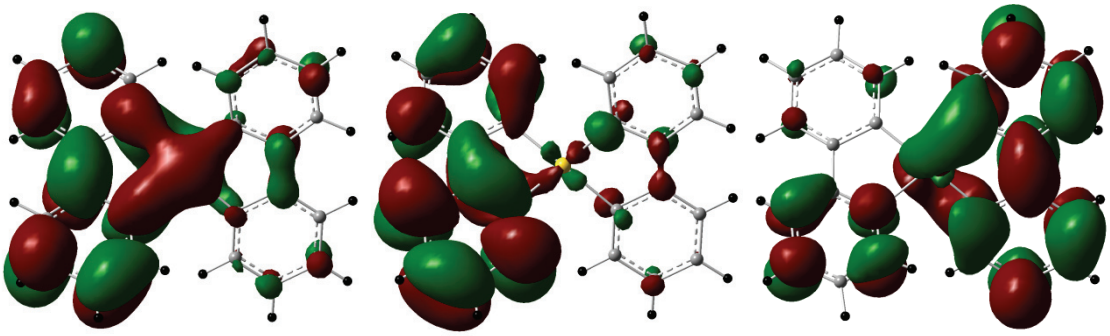

LUMO LUMO +1 LUMO +2

Energy (eV)		Composition (%)		
		biphenyl	phenylpyridine	Au
L+2	-1.07	75	17	8
L+1	-1.24	6	91	3
LUMO	-1.95	6	86	8
HOMO	-6.12	97	1	2
H-1	-6.68	31	60	9
H-2	-6.86	20	76	4
H-3	-6.99	91	4	5
H-4	-7.13	41	54	5
H-5	-7.30	48	48	4

Figure S8. Spatial plots, energies (eV) and compositions (%) of selected frontier molecular orbitals of **1**.

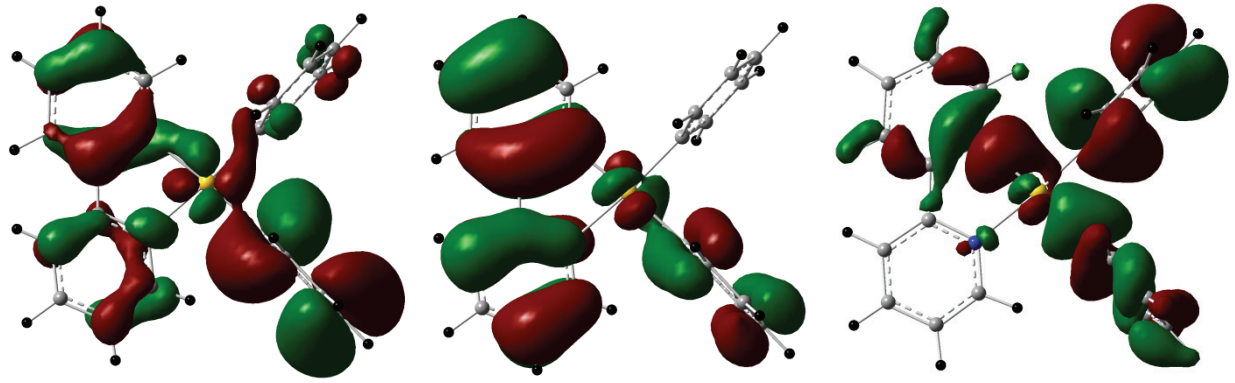

HOMO -2 HOMO -1 HOMO

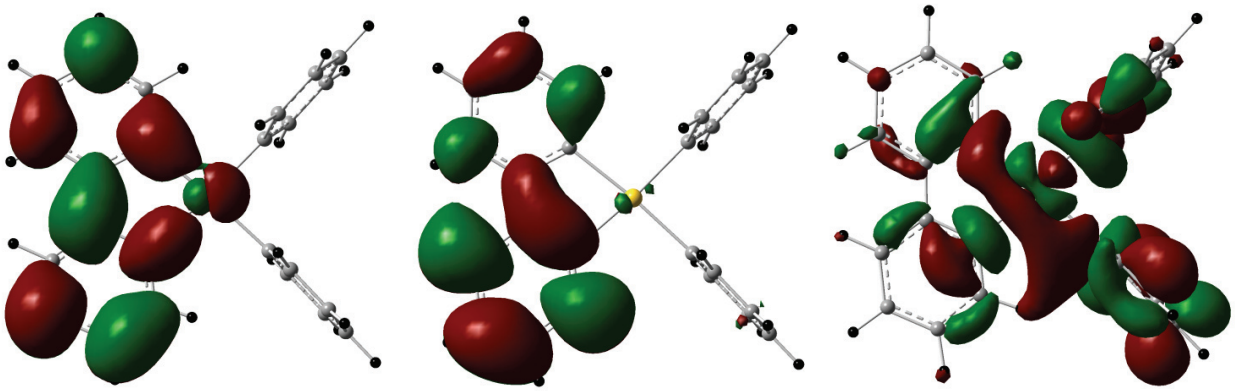

LUMO LUMO +1 LUMO +2

Energy (eV)		Composition (%)		
		C_6H_5	phenylpyridine	Au
L+2	-0.25	42	16	41
L+1	-1.19	1	98	1
LUMO	-1.86	0	94	6
HOMO	-6.38	74	22	4
H-1	-6.71	14	83	3
H-2	-6.72	79	16	5
H-3	-6.92	96	4	0
H-4	-7.03	73	26	1
H-5	-7.13	30	67	4

Figure S9. Spatial plots, energies (eV) and compositions (%) of selected frontier molecular orbitals of **2**.

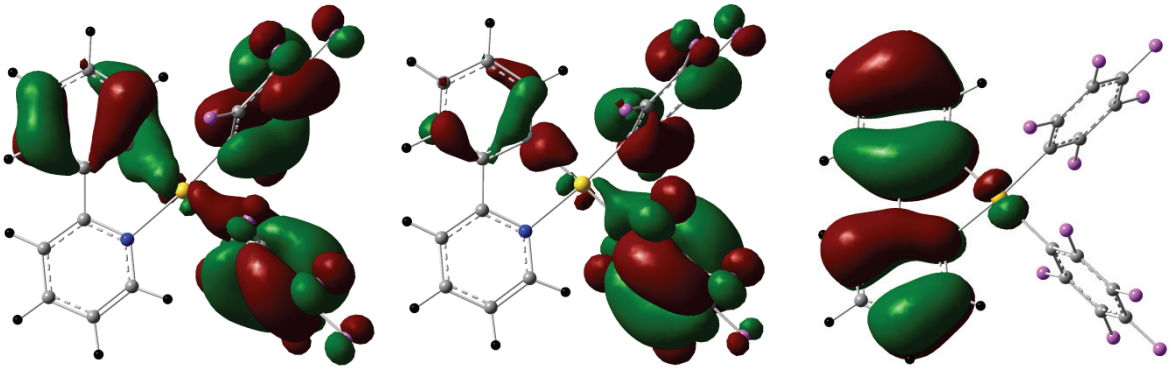

HOMO -2 HOMO -1 HOMO

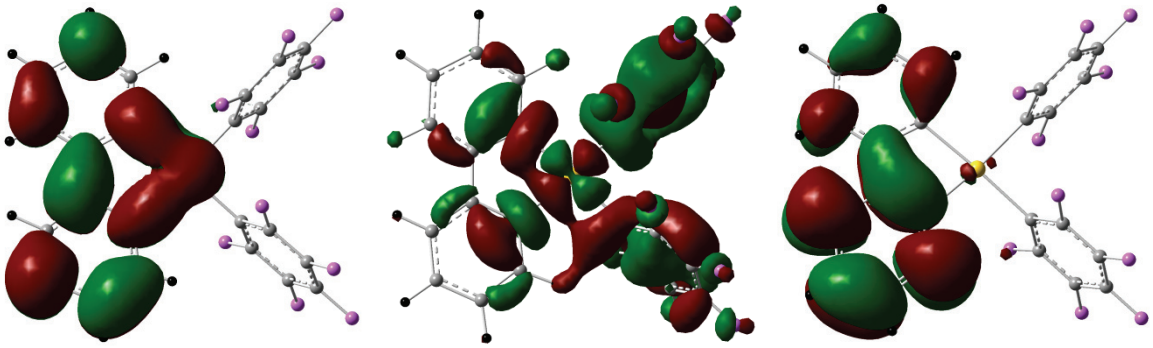

LUMO LUMO +1 LUMO +2

Energy (eV)		Composition (%)		
		C_6F_5	phenylpyridine	Au
L+2	-1.45	1	98	1
L+1	-1.54	52	18	29
LUMO	-2.21	2	92	6
HOMO	-7.04	0	98	2
H-1	-7.31	93	6	1
H-2	-7.35	82	16	2
H-3	-7.41	95	4	1
H-4	-7.46	54	42	4
H-5	-7.52	55	41	3

Figure S10. Spatial plots, energies (eV) and compositions (%) of selected frontier molecular orbitals of **3**.

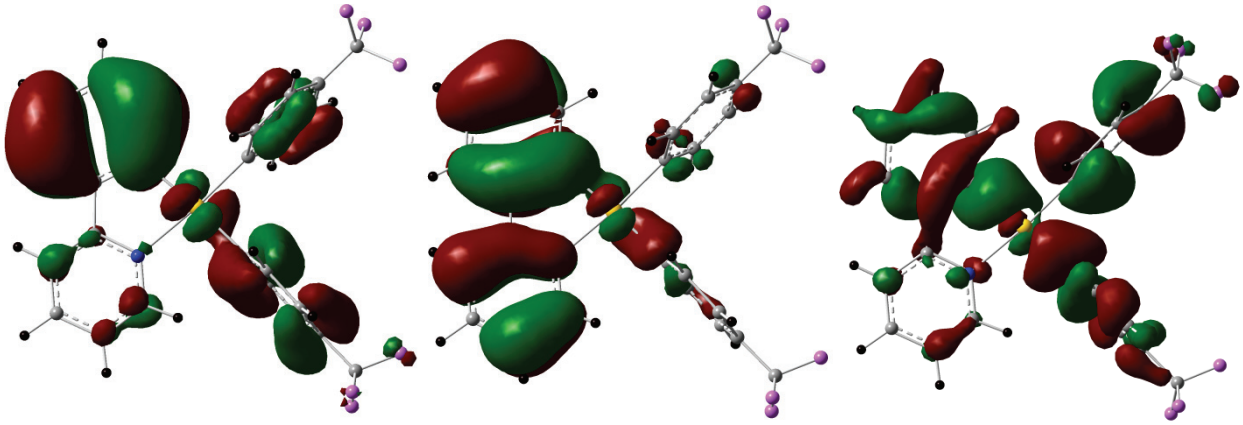

HOMO -2 HOMO -1 HOMO

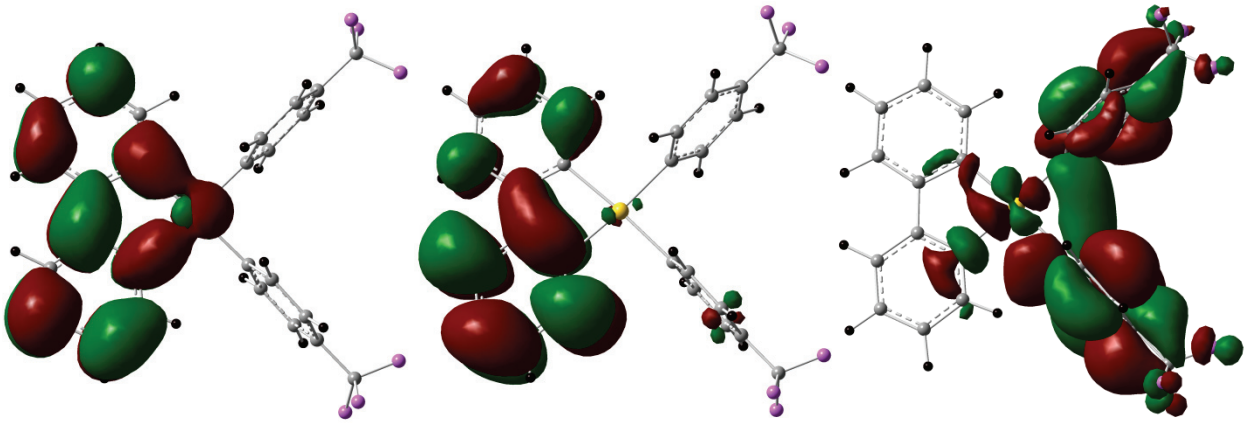

LUMO LUMO +1 LUMO +2

Energy (eV)		Composition (%)		
		$C_6H_4CF_3$	phenylpyridine	Au
L+2	-0.75	92	3	5
L+1	-1.29	2	97	1
L	-1.97	0	95	5
H	-6.81	60	36	4
H-1	-6.82	5	92	3
H-2	-7.20	19	77	4
H-3	-7.27	76	18	6
H-4	-7.38	98	2	0
H-5	-7.51	97	2	1

Figure S11. Spatial plots, energies (eV) and compositions (%) of selected frontier molecular orbitals of **4**.

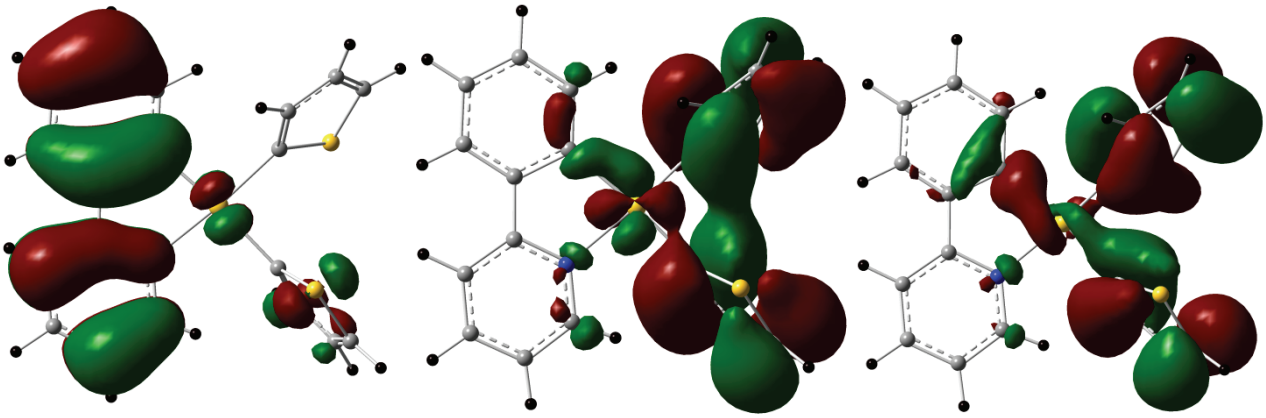

HOMO -2 HOMO -1 HOMO

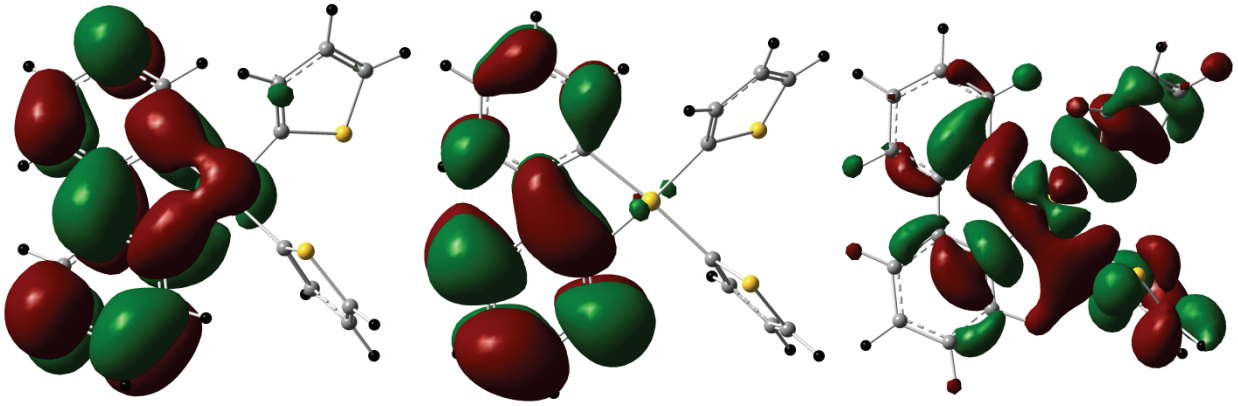

LUMO LUMO +1 LUMO +2

Energy (eV)		Composition (%)		
		C_4H_3S	phenylpyridine	Au
L+2	-0.57	43	25	32
L+1	-1.26	1	99	0
L	-1.98	0	95	5
H	-6.23	93	5	2
H-1	-6.31	91	1	8
H-2	-6.82	3	95	2
H-3	-6.96	95	4	1
H-4	-7.02	96	3	1
H-5	-7.23	3	93	4

Figure S12. Spatial plots, energies (eV) and compositions (%) of selected frontier molecular orbitals of **5**.

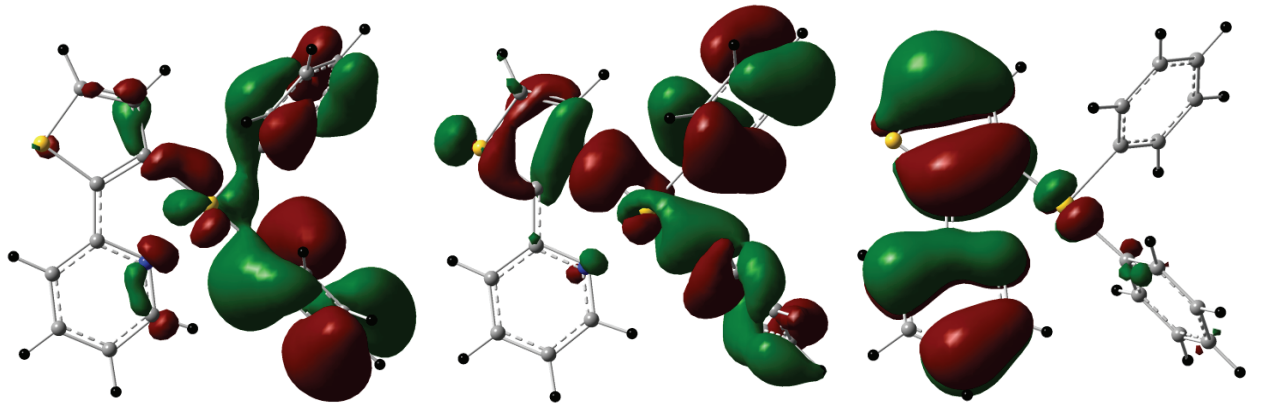

HOMO -2 HOMO -1 HOMO

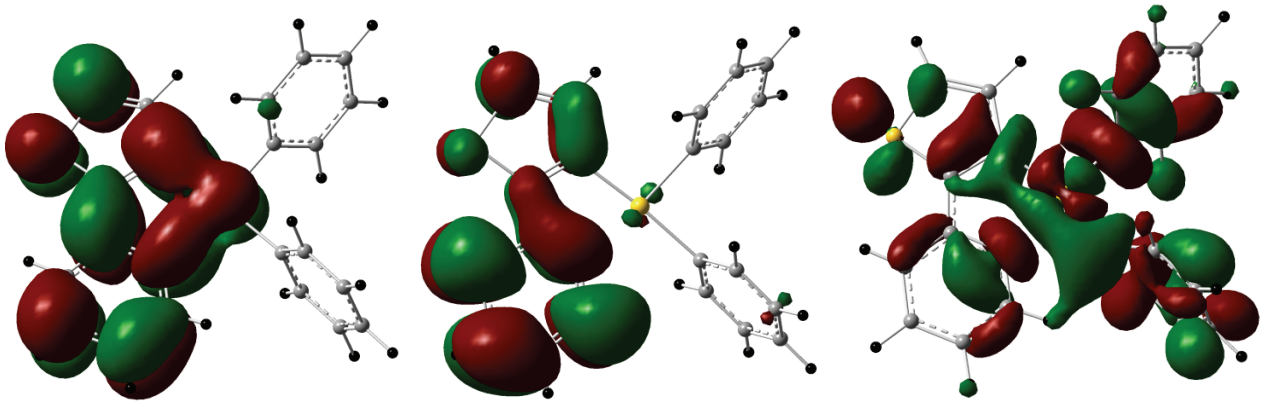

LUMO LUMO +1 LUMO +2

Energy (eV)		Composition (%)		
		C_6H_5	thienylpyridine	Au
L+2	-0.44	47	27	26
L+1	-1.16	2	97	1
L	-1.93	0	93	7
H	-6.36	2	96	2
H-1	-6.53	77	19	4
H-2	-6.76	89	4	7
H-3	-7.00	99	1	0
H-4	-7.09	93	6	1
H-5	-7.20	8	88	4

Figure S13. Spatial plots, energies (eV) and compositions (%) of selected frontier molecular orbitals of **6**.

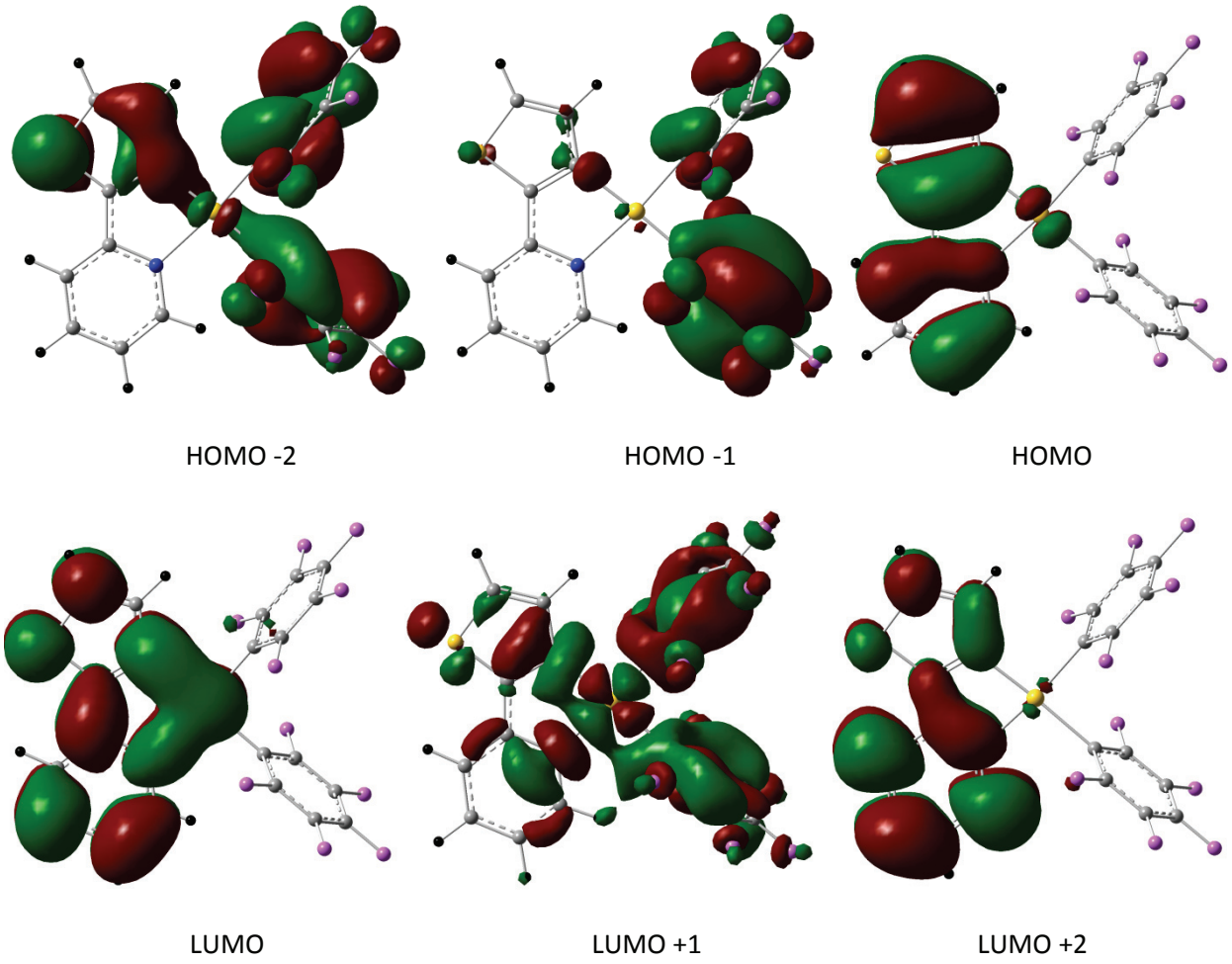

Energy (eV)		Composition (%)		
		C_6F_5	thienylpyridine	Au
L+2	-1.42	2	98	0
L+1	-1.65	54	20	26
L	-2.28	0	92	8
H	-6.68	0	98	2
H-1	-7.34	98	2	0
H-2	-7.40	81	18	1
H-3	-7.43	97	2	1
H-4	-7.49	69	26	5
H-5	-7.56	39	59	3

Figure S14. Spatial plots, energies (eV) and compositions (%) of selected frontier molecular orbitals of **7**.

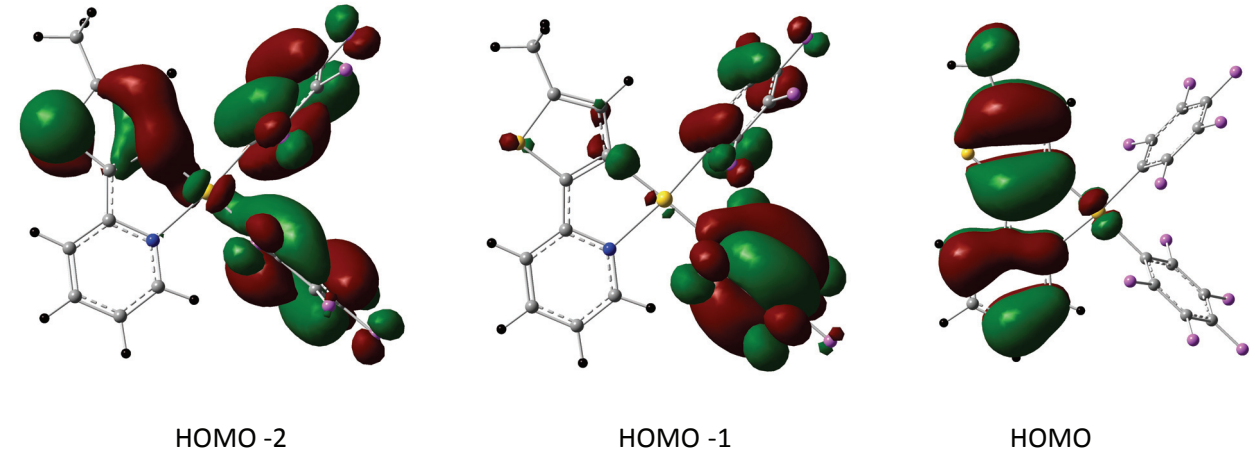

HOMO -2 HOMO -1 HOMO

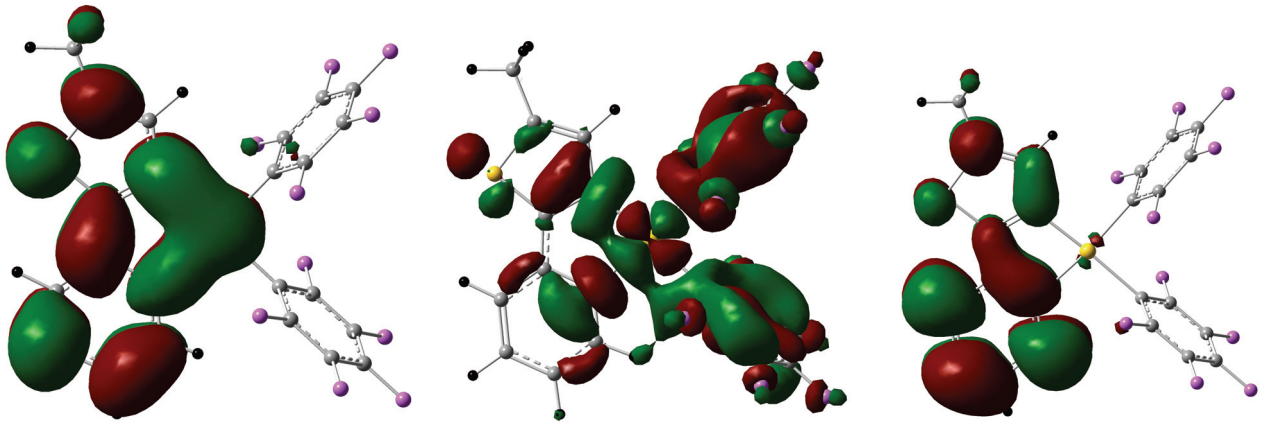

LUMO LUMO +1 LUMO +2

Energy (eV)		Composition (%)		
		C_6F_5	methylthienylpyridine	Au
L+2	-1.38	1	99	0
L+1	-1.63	55	21	94
L	-2.23	0	93	7
H	-6.48	0	99	1
H-1	-7.33	98	2	0
H-2	-7.39	77	21	2
H-3	-7.43	97	2	1
H-4	-7.48	67	28	5
H-5	-7.55	43	54	3

Figure S15. Spatial plots, energies (eV) and compositions (%) of selected frontier molecular orbitals of **8**.

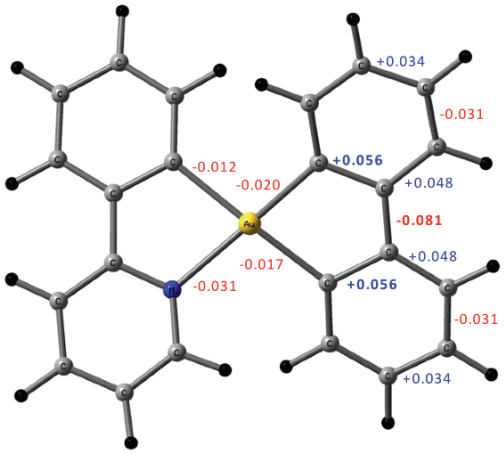
+0.034
-0.031
-0.012
-0.020
+0.056
+0.048
-0.081
-0.017
+0.048
-0.031
+0.056
-0.031
+0.034

1

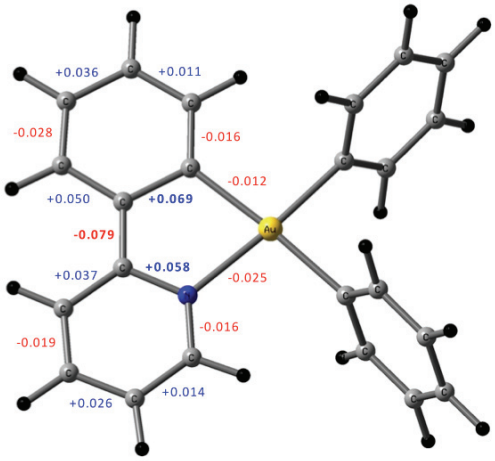
+0.036
+0.011
-0.028
-0.016
-0.012
+0.050
+0.069
-0.079
+0.037
+0.058
-0.025
-0.016
-0.019
+0.026
+0.014

2

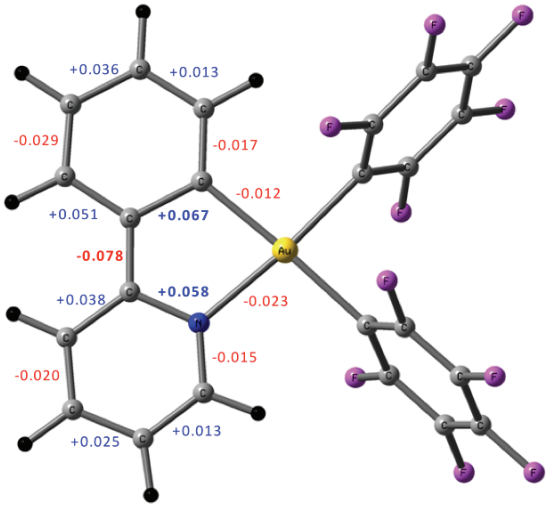
+0.036
+0.013
-0.029
-0.017
-0.012
+0.051
+0.067
-0.078
+0.038
+0.058
-0.023
-0.015
-0.020
+0.025
+0.013

3

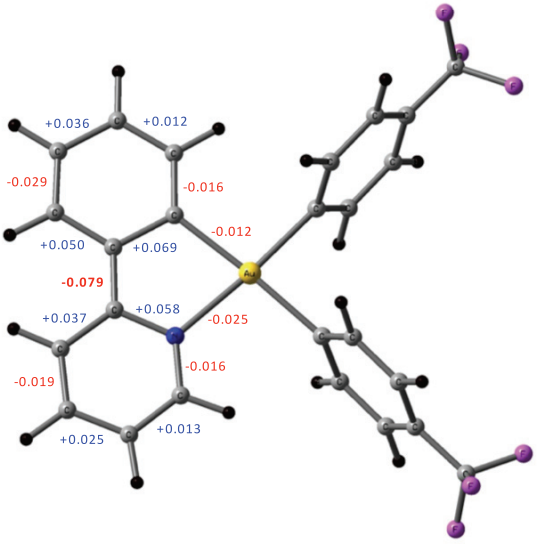
+0.036
+0.012
-0.029
-0.016
-0.012
+0.050
+0.069
-0.079
+0.037
+0.058
-0.025
-0.016
-0.019
+0.025
+0.013

4

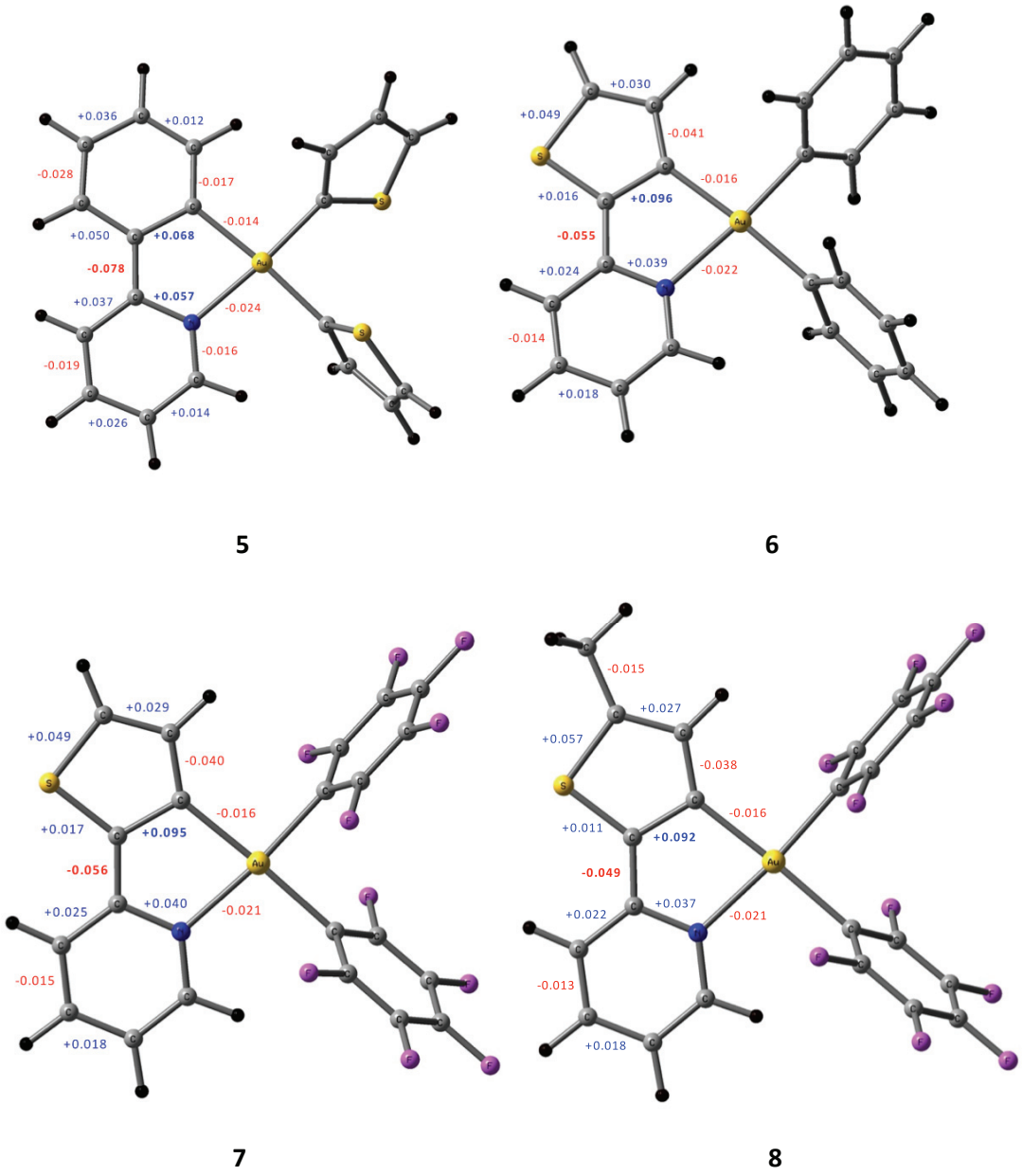

Figure S16. DFT optimized structures of the excited triplet states of **1-8** with the main differences in bond distances (larger than 0.01 Å) in comparison with the corresponding DFT optimized ground states.

6. References

[1] Xcalibur CCD System; Oxford Diffraction Ltd: Abingdon, Oxfordshire, England, 2007.

[2] Clark, R. C.; Reid, J. S. *Acta Cryst*. **1995**, *A51*, 887-897.

[3] *CrysAlisPro* (versions 1.171.32.34d-55), Oxford Diffraction Ltd, Abingdon, Oxfordshire, England.

[4] Sheldrick, G. M. *Acta Cryst*. **2008**, *A64*, 112-122.

[5] Farrugia, L. J. *J. Appl. Cryst*. **1999***, 32,* 837.

[6] Spek, A. L. *J. Appl. Cryst*. **2003**, *36*, 7-13.

[7] Frisch, M. J.; Trucks, G. W.; Schlegel, H. B.; Scuseria, G. E.; Rob, M. A.; Cheeseman, J. R.; Montgomery Jr., J. A.; Vreven, T.; Kudin, K. N.; Burant, J. C.; Millam, J. M.; Iyengar, S. S.; Tomasi, J.; Barone, V.; Mennucci, B.; Cossi, M.; Scalmani, G.; Rega, N.; Petersson, G. A.; Nakatsuji, H.; Hada, M.; Ehara, M.; Toyota, K.; Fukuda, R.; Hasegawa, J.; Ishida, M.; Nakajima, T.; Honda, Y.; Kitao, O.; Nakai, H.; Klene, M.; Li, X.; Knox, J. E.; Hratchian, H. P.; Cross, J. B.; Bakken, V.; Adamo, C.; Jaramillo, J.; Gomperts, R.; Stratmann, R. E.; Yazyev, O.; Austin, A. J.; Cammi, R.; Pomelli, C.; Ochterski, J. W.; Ayala, P. Y.; Morokuma, K.; Voth, G. A.; Salvador, P.; Dannenberg, J. J.; Zakrzewski, V. G.; Dapprich, S.; Daniels, A. D.; Strain, M. C.; Farkas, O.; Malick, D. K.; Rabuck, A. D.; Raghavachari, K.; Foresman, J. B.; Ortiz, J. V.; Cui, Q.; Baboul, A. G.; Clifford, S.; Cioslowski, J.; Stefanov, B. B.; Liu, G.; Liashenko, A.; Piskorz, P.; Komaromi, I.; Martin, R. L.; Fox, D. J.; Keith, T.; Al-Laham, M. A.; Peng, C. Y.; Nanayakkara, A.; Challacombe, M.; Gill, P. M. W.; Johnson, B.; Chen, W.; Wong, M. W.; Gonzalez, C.; Pople, J. A. Gaussian 03 (Gaussian, Inc., Wallingford, CT, **2003**).

[8] Adamo, C.; Barone, V. *J. Chem. Phys*. **1999**, *110*, 6158.

[9] Dunning Jr, T. H.; Hay, P. J. *Modern Theoretical Chemistry*; Schaefer, H. F., III, Ed.; Plenum: New York, **1976**; Vol. 3, pp 1– 28.

[10] Ditchfield, R.; Hehre, W. J.; Pople, J. A. *J. Chem. Phys*. **1971**, *54*, 724.

[11] a) Becke, A. D. *Phys. Rev. A* **1988**, *38*, 3098; b) Lee, C.; Yang, W.; Parr, R. G. *Phys. Rev. B* **1988**, *37*, 785; c) Stephens, P. J.; Devlin, F. J.; Chabalowski, C. F.; Frisch, M. J. *J. Phys. Chem*. **1994**, *98*, 11623.

[12] a) Lynch, B. J.; Fast, P. L.; Harris, M.; Truhlar, D. G. *J. Phys. Chem. A* **2000**, *104*, 4811; b) Lynch, B. J.; Zhao, Y.; Truhlar, D. G. *J. Phys. Chem. A* **2003**, *107*, 1384.

[13] a) Becke, A. D.; *J. Chem. Phys*. **1996**, 104, 1040; b) Zhao, Y.; Lynch, B. J.; Truhlar, D. G.; *J. Phys. Chem. A* **2004**, 108, 2715.

[14] Gill, P. M. W. *Mol. Phys*. **1996**, 89, 433.

[15] Tao, J.; Perdew, J. P.; Staroverov, V. N.; Scuseria, G. E. *Phys. Rev. Lett*. **2003**, 91, 146401.

[16] Dahlke, E. E.; Truhlar, D. G. *J. Phys. Chem. B* **2005**, 109, 15677.

[17] a) Peng, C.; Ayala, P. Y.; Schlegel, H. B.; Frisch, M. J. *J. Comp. Chem.* **1996**, *17*, 49-56; b) Peng, C.; Schlegel, H. B. *Israel J. Chem.* **1993**, *33*, 449-454.

[18] GaussView 4.1; Gaussian Inc.: Wallingford, CT, 2006.

[19] a) Stratmann, R. E.; Scuseria, G. E.; Frisch, M. J. *J. Chem. Phys.* **1998**, 109, 8218-24; b) Bauernschmitt, R.; Ahlrichs, R. *Chem. Phys. Lett.* **1996**, *256*, 454-64; c) Casida, M. E.; Jamorski, C.; Casida, K. C.; Salahub, D. R. *J. Chem. Phys.* **1998**, *108*, 4439-49.

[20] a) Barone, V.; Cossi, M. *J. Phys. Chem. A* **1998**, 102, 1995-2001; b) Cossi, M.; Rega, N.; Scalmani, G.; Barone, V. *J. Comp. Chem.* **2003**, 24, 669-81.

APPENDIX (Chapter 2)

In view of preparing Au(III) diaryl complexes with 2-(benzo[*b*]thiophen-2-yl)pyridine as the (N^C) cyclometalating core, the corresponding Au(III) trichloride namely [N^C = 2-(benzo[*b*]thiophen-2-yl)pyridine][$AuCl_3$] was prepared in 45% yield by reacting with $NaAuCl_4 \cdot 2H_2O$. Cycloauration to Au(III) dichloride [N^C = 2-(benzo[*b*]thiophen-2-yl)pyridine][$AuCl_2$] (**D**) was achieved using silver(I) tetrafluoroborate in CH_2Cl_2 in a meager yield of 11%. Single crystals suitable for X-ray analysis was obtained by slow diffusion of pentane in concentrated solution of **D** in CH_2Cl_2. Owing to the low overall yields of the compounds, arylation of the dichloride complexes was not pursued. However, the synthetic and X-ray characterization details are presented. Diaryl complex **9** incorporating 1,2,3-trimethoxy benzene as ancillary ligand on *ppy* core was prepared in 37% according to the general procedure.

In an different attempt to create constrained five membered auracycle with a bidentate dicarbanionic chelate in similar to **1** (see main text), 1,8-diiodonaphthalene was reacted with *ppy*Au(III)Cl_2 using the optimized lithation procedure. Contrary to our expectation we could only obtain the mono-iodosubstituted product namely *cis*-[(N^C)AuClL][N^C = 2-phenylpyridine, L = naphthalene] (**10**) as confirmed by ESI-MS, ^{1}H NMR and single-crystal XRD studies. The synthetic and crystallographic details are also presented here.

Experimental section.

[N^C = 2-(benzo[*b*]thiophen-2-yl)pyridine][$AuCl_3$].

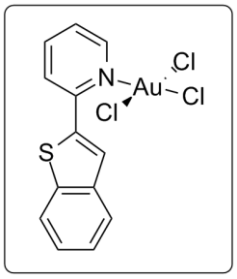

This reaction was carried out analogous to a literature known procedure (Chapter 2, ref. no. 50 in the main text). Accordingly, 2-(benzo[*b*]thiophen-2-yl)pyridine (350.0 mg, 1.65 mmol) was reacted with $NaAuCl_4 \cdot 2H_2O$ (626.0 mg, 1.57 mmol) in a 1:1 mixture of acetonitrile (5.5 mL) and water (5.5 mL) to obtain the title product. Yield: 383.0 mg (45%); ^{1}H NMR (500 MHz, CD_2Cl_2, 298 K): δ = 7.55-7.61 (m, 2H), 7.77 (t, J = 6.5 Hz, 1H), 8.03-8.08 (m, 3H), 8.15 (s, 1H), 8.26 (t, J = 6.5 Hz, 1H), 8.88 (d, J = 5.0 Hz, 1H); ^{13}C{^{1}H}NMR (125 MHz, CD_2Cl_2, 298 K): δ = 119.9, 121.9, 122.8, 123.0, 124.6, 125.0, 125.8, 126.9, 136.5, 140.2, 140.6, 148.0, 150.9;

elemental analysis (%) calcd. for $C_{13}H_9AuCl_3NS$; C, 30.34; H, 1.76; N, 2.72. Found: C, 30.09; H, 1.73; N, 2.77.

[N^C = 2-(benzo[*b*]thiophen-2-yl)pyridine][$AuCl_2$] (D)

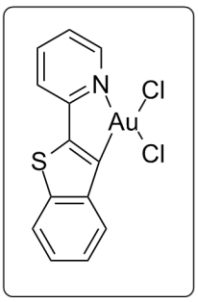

This reaction was carried out analogous to a literature known procedure (Chapter 2, ref. no. 50 in the main text). Accordingly, $AgBF_4$ (107.1 mg, 0.55 mmol) was added to [N^C = 2-(benzo[*b*]thiophen-2-yl)pyridine][$AuCl_3$] (270.0 mg, 0.524 mmol) in CH_2Cl_2 (90.0 mL), and the resulting mixture was refluxed for 2 h. After filtration under hot condition, the filtrate was evaporated to dryness, and the residue was washed with a minimum amount of cold acetonitrile (3.0 mL) to afford the crude product, which was recrystallized from THF to obtain the product as dark red crystals. Yield = 27.5 mg, (11%). ^{1}H NMR (500 MHz, DMSO-d_6, 298 K): δ = 7.49 (dt, J = 5.5, 12.5 Hz, 2H), 7.67 (t, J = 6.5 Hz, 1H), 8.0 (d, J = 7.5 Hz, 1H), 8.13 (d, J = 7.5 Hz, 1H), 8.34 (t, J = 6.5 Hz, 1H), 9.06 (d, J = 7.5 Hz, 1H), 9.44 (d, J = 5.0 Hz, 1H); ^{13}C{^{1}H}NMR (125 MHz, DMSO-d_6, 298 K): δ = 122.6, 123.9, 124.4, 126.0, 126.3, 127.2, 139.5, 140.0, 145.0, 148.7, 159.1; elemental analysis (%) calcd. for $C_{13}H_8AuCl_2NS$; C, 32.66; H, 1.69; N, 2.93; Found: C, 32.58; H, 1.65; N, 2.87.

***cis*-[(N^C)AuL_2][N^C = 2-phenylpyridine, L = 1,2,3-trimethoxybenzene] (9)**

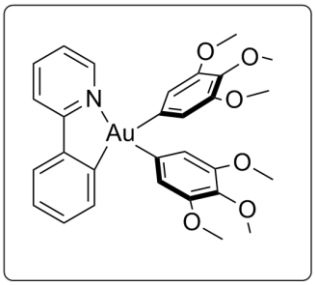

Following the general procedure, to a solution of 5-bromo-1,2,3-trimethoxybenzene (100.0 mg, 0.52 mmol) in Et_2O (5.0 mL), *n*-BuLi (0.33 mL, 0.537 mmol, 1.6 M soln. in hexanes) was added, and this was transferred to a flask containing **B** [(N^C)$AuCl_2$] (100.0 mg, 0.236 mmol) in Et_2O. The crude product thus obtained was purified by column chromatography using silica gel (eluent: Hexane/EtOAc = 5/1) to obtain complex **9** as an off-white solid. Yield = 60.0 mg (37.0%); ^{1}H NMR (500 MHz, CD_2Cl_2, 298 K): δ = 3.71 (s, 3H). 3.72 (s, 3H), 3.77 (s, 6H), 3.79 (s, 6H), 6.72 (s, 2H), 6.74 (s, 2H), 7.28-7.38 (m, 2H), 7.41 (t, J = 6.5 Hz, 1H), 7.69 (d, J = 7.5 Hz, 1H), 7.90 (d, J = 7.5 Hz, 1H), 8.04 (t, J = 7.5 Hz, 1H), 8.17 (d, J = 7.0 Hz, 1H), 9.59 (d, J = 7.0 Hz, 1H); ^{13}C{^{1}H}NMR (125 MHz, CD_2Cl_2, 298 K): δ = 56.7, 61.1, 99.7, 104.5, 109.5, 117.0, 121.0, 121.3, 121.4, 124.9, 125.4, 128.2, 132.4,

136.2, 142.4, 146.1, 151.5, 153.7, 156.6, 167.5; elemental analysis (%) calcd. for $C_{29}H_{30}AuNO_6$: C, 50.81; H, 4.41; N, 2.04; Found: C, 50.61; H, 4.40; N, 2.22.

***cis*-[(N^C)AuClL][N^C = 2-phenylpyridine, L = naphthalene] (10)**

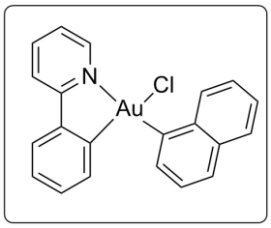

Following the general procedure, to a solution of 1,8-diiodonapthalene (148.5 mg, 0.390 mmol) in Et_2O (5.0 mL) *n*-BuLi (0.5 mL, 0.816 mmol, 1.6 M soln. in hexanes) was added, and this mixture was transferred to a flask containing **B** [(N^C)$AuCl_2$] (150.0 mg, 0.355 mmol) in Et_2O. The crude product thus obtained was purified by column chromatography using silica gel (eluent: Hexane/EtOAc = 5/1), the product thus obtained was again recrystallized in CH_2Cl_2 to get **10** as light yellow solid. Yield: 40.0 mg (22%). Single crystals suitable for X-ray analysis was obtained by slow diffusion of pentane in concentrated solution of the product in CH_2Cl_2. ESI-MS: *m/z*= 478.0 $[M\text{-}Cl]^+$; ^{1}H NMR (300 MHz, $CDCl_3$, 298 K): δ = 7.35-7.58 (m, 6H), 7.68-7.86 (m, 4H), 7. 99-8.01 (m, 2H), 8.1 (d, *J* = 6.5 Hz, 2H), 8.72-8.84 (m, 2H);$^{13}C\{^1H\}$NMR (125 MHz, $CDCl_3$, 298 K): δ = 119.9, 120.2, 123.3, 124.1, 124.4, 124.5, 124.6, 126.2,126.5, 128.0, 128.7, 129.3, 130.6, 131.2, 131.5, 132.4,136.2, 140.2, 152.8; elemental analysis (%) calcd. for $C_{21}H_{15}AuClN$: C, 49.09; H, 2.94; N, 2.73; Found: C, 48.89; H, 2.70; N, 2.98.

Solid-state photoluminescence studies of complexes 4 and 7.

Thin films of complexes **4** and **7** were prepared on glass substrate with 2 wt% loading on PMMA host matrix. The absolute solid-state quantum yields calculated using an integrating-sphere set-up on a Horiba Jobin Yvon spectrophotometer. Complexes **4** and **7** showed values of 2.1% and 2.0% respectively.

Crystallographic studies.

The perspective views of the benzo[*b*]thiophen-2-yl)pyridine gold(III) dichloride **D** and napthyl substituted phenylpyridine mono chloro complex **10** are shown in Figure A1. The various metric details of these complexes are given in Table A1 and A2.

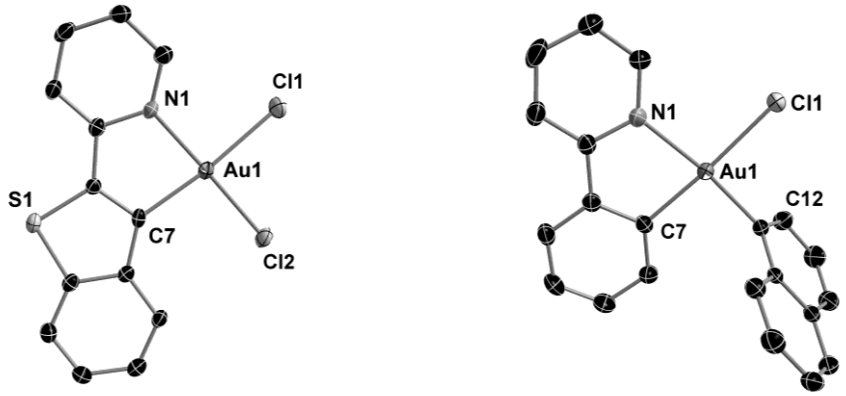

D **10**

Figure A1. X-ray crystal structures of **D**, and **10** with selective atomic numbering scheme. Thermal ellipsoids are drawn at the 50% probability level. Hydrogen atoms are omitted for clarity.

Table A1. Selected bond distances (Å) and angles (°) data of **D** and **10**.

Complex **D**			
N(1)-Au(1)	2.047(3)	C(7)-Au(1)	2.030(4)
Cl(1)-Au(1)	2.3640(12)	Cl(2)-Au(1)	2.2711(11)
N(1)-Au(1)-C(7)	81.89(16)	N(1)-Au(1)-C(1)	92.87(11)
C(7)-Au(1)-Cl(2)	96.48(12)	Cl(1)-Au(1)-Cl(2)	88.88(4)
N(1)-Au(1)-Cl(2)	177.39(11)	C(7)-Au(1)-Cl(1)	173.72(12)

Complex **10**			
N(1)-Au(1)	2.101(2)	C(7)-Au(1)	2.019(3)
C(12)-Au(1)	2.011(3)	Cl(1)-Au(1)	2.3653(7)
N(1)-Au(1)-C(7)	80.83(10)	C(12)-Au(1)-Cl(1)	91.05(7)
N(1)-Au(1)-Cl(1)	95.58(6)	C(7)-Au(1)-C(12)	92.55(10)

Table A2. Crystallographic data for compounds **D** and **10.**

	D	**10**
empirical formula	C_{13} H_8 Au Cl_2 N S	C_{21} H_{15} Au Cl N
formula weight ($g \cdot mol^{-1}$)	478.14	513.76
temperature (K)	183(2)	183(2)
wavelength (Å)	0.71073	0.71073
crystal system, space group	Monoclinic, *P* 21/n	Monoclinic, *P* 21/c
a (Å)	11.6024(3)	9.9968(2)
b (Å)	8.2573(1)	18.9034(3)
c (Å)	13.6508(3)	9.3750(2
α (deg)	90	90
β (deg)	106.129(2)	107.197(2)
γ (deg)	90	90
volume ($Å^3$)	1256.33(5)	1692.42(6)
Z, density (calcd) ($Mg \cdot m^{-3}$)	4, 2.528	4, 2.016
abs coefficient (mm^{-1})	12.278	8.851
F(000)	888	976
crystal size (mm^3)	0.43 x 0.31 x 0.18	0.40 x 0.27 x 0.17
θ range (deg)	2.71 to 30.49	2.83 to 30.51
reflections collected	14244	18572
reflections unique	3830 [R(int) = 0.0636]	5168 [R(int) = 0.0246]
completeness to θ (%)	99.9	99.9
absorption correction	Analytical	Analytical
max/min transmission	0.16 and 0.05	0.374 and 0.152
data / restraints / parameters	3830 / 0 / 163	5168 / 0 / 217
goodness-of-fit on F^2	1.067	0.981
final R_1 and wR_2 indices [$I > 2\sigma(I)$]	R_1 = 0.0298, wR_2 = 0.0823	R_1 = 0.0198, wR_2 = 0.0434
R_1 and wR_2 indices (all data)	R_1 = 0.0360, wR_2 = 0.0838	R_1 = 0.0297, wR_2 = 0.0444
Largest diff. peak and hole ($e/Å^3$)	2.367 and -2.252	1.256 and -0.801

The unweighted R-factor is $R_1 = \sum(Fo - Fc)/\sum Fo$; $I > 2\,\sigma(I)$ *and the weighted R-factor is* $wR_2 = \{\sum w(Fo^2 - Fc^2)^2/\sum w(Fo^2)^2\}^{1/2}$

Chapter 3.

Syntheses and Photophysical Properties of Luminescent Mono-cyclometalated Gold(III) *cis*-Dialkynyl Complexes

Publication 2. Garg, J. A.; Blacque, O.; Fox, T.; Venkatesan, K. *Inorg. Chem.* **2011**, *50*, 5430-5441.

Inorganic Chemistry

ARTICLE

pubs.acs.org/IC

Syntheses and Photophysical Properties of Luminescent Mono-cyclometalated Gold(III) *cis*-Dialkynyl Complexes

Jai Anand Garg, Olivier Blacque, and Koushik Venkatesan*

Institute of Inorganic Chemistry, University of Zürich, Winterthurerstrasse 190, CH-8057 Zürich, Switzerland

Supporting Information

ABSTRACT: A series of novel luminescent neutral cyclometalated gold(III) complexes of the type *cis*-[(N^C)Au(C≡CR)$_2$] (R = aryl, silyl groups) having different cyclometalating cores (N^C) have been synthesized by CuI promoted halide to alkynyl metathesis with NEt_3 as in situ deprotonating agent. Along with spectroscopic characterizations (nuclear magnetic resonance and infrared spectroscopies and electrospray ionization mass spectrometry) and elemental analysis, the molecular structures of some of the complexes have been established by single-crystal X-ray diffraction studies. Photophysical studies reveal that the complexes exhibit room-temperature phosphorescence (RTP). Experimental observations and density functional theory calculations qualitatively suggest limited participation of the metal and alkynyl ligands in the lowest energy emitting state. The nature of the emission is mainly governed by metal-perturbed ^{3}IL($\pi-\pi^*$) transitions originating from the cyclometalate part of the molecule, and its variation readily leads to the tuning of the emission wavelengths. Cyclic voltammetry measurements of selected complexes showed irreversible redox behavior with near-equivalent cathodic peak potential ($E_{p,c}$) assigned to the C^N core.

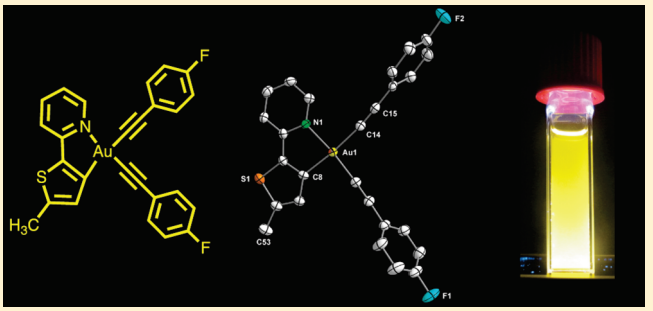

INTRODUCTION

Organogold(I) σ-alkynyl complexes are widely investigated for their interesting luminescence, nonlinear optical (NLO) properties and their ability to build metallo-macromolecular entities.[1−9] In sharp contrast, gold(III) alkynyl complexes are relatively less explored. Notables among the few known examples include mononuclear gold(III) complexes containing one alkynyl ligand, viz., [Au(C≡CCF$_3$)Me$_2$(L)] and [Au(C≡CR)Me$_2$(PPh$_3$)],[10,11] [Au(C^N^C)(C≡CR)],[2,12,13] and three alkynyl ligands [Au(C≡CR)$_3$(L)] and four alkynyl ligands [ER$_4$]$^+$[Au(C≡CR)$_4$]$^-$.[14,15] Dinuclear gold(I)−gold(III) complexes bearing two alkynyl ligands, viz., [Au^I(μ-{CH$_2$}PPh$_2$)$_2$Au^{III}(C≡CR)$_2$], have also been reported[16] (Figure 1). In general, gold(III) complexes tend to exhibit relatively large positive reduction potentials,[17,18] and the consequent instability is a probable reason for their scarcity. Except for the cyclometalated systems (C^N^C) in the above-noted examples that have been studied for luminescence properties, the other gold alkynyls have been chiefly explored, either for catalysis or for studying reductive elimination processes.[10,11,14,15] In recent years, extensive investigations carried out by Yam and co-workers has revealed that cyclometalated gold(III) monoalkynyl complexes with terdentate ligands can exhibit room-temperature phosphorescence.[2,12,13] Also, external quantum efficiency (EQE) to the order of 11.5% in an organic light emitting diode (OLED) device which is well comparable to cyclometalated Ir(III) systems has been achieved.[19]

In the past few years, we have been interested in a relatively less explored class of mononuclear cyclometalated neutral diaryl/dialkynyl gold(III) complexes. Gold(III) alkynyls, similar to isoelectronic platinum(II) alkynyl systems (d^8-configuration) could possibly offer tunable electronic and luminescent properties due to their electron-richness, rigid-rod nature, and polarizability.[8,20] In our previous study, we have shown that diaryl complexes of the type *cis*-[(N^C)AuL$_n$] (L = aryl, n = 1, 2) containing perfluorinated aryl groups can be quite stable and offer interesting photophysical properties.[21] Very recently, investigations into gold(III) dialkynyl systems have appeared in literature further exemplifying their importance.[22]

From a photophysical standpoint, anionic acetylenic carbon ($^-$C≡) is desirable since strong σ-donating ligands are required for "lifting" the energy levels of the otherwise low-lying metal-centered (MC) orbitals. These orbitals are quite susceptible for thermal population at ambient temperatures which then follows rapid nonradiative relaxation pathways.[2] Here in this work we report the syntheses of stable mononuclear cyclometalated *cis*-gold(III)-σ-dialkynyl complexes and their luminescent properties.

RESULTS AND DISCUSSION

Syntheses and Characterization of Complexes. Dichlorogold(III) complexes (**A**−**E**) with different cyclometalating cores **1**−**5** (Scheme 1) were first prepared as precursors to obtain the desired dialkynyls. Complex [(N^C)AuCl$_2$] [N^C = 2-phenylpyridine

Received: November 4, 2010
Published: May 23, 2011

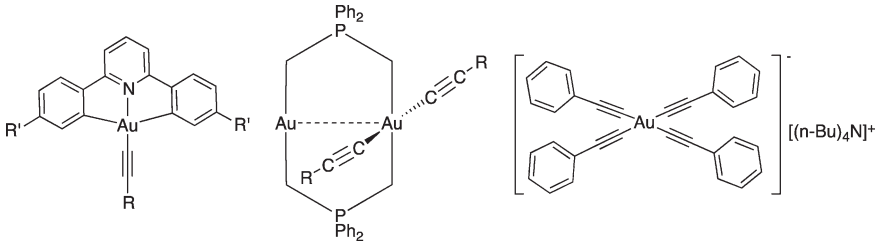

Figure 1. Known gold(III) mono-, di-, and tetraalkynyl complexes.

Scheme 1

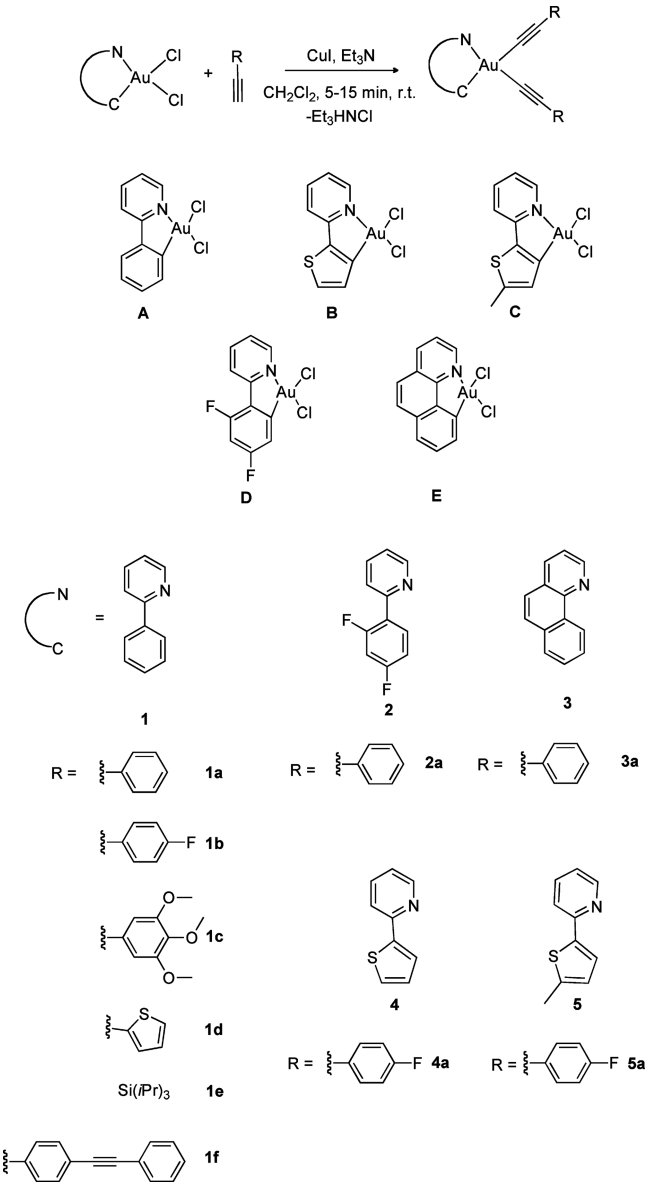

(ppy)] (**A**) was prepared according to the procedure reported by Constable and Leese involving transmetalation reaction of ortho-activated ppyHg^{II} chloride with sodium tetrachloroaurate,[23] [(N^C)-AuCl$_2$] [N^C = 2-(2-thienyl)pyridine (thpy); **B**] and [N^C = 2-(5-methyl-2-thienyl)pyridine (5-me-thpy)][AuCl$_2$; **C**] were synthesized on the basis of direct cycloauration methods.[21,24] The remaining precursor dihalides which were unknown, namely, [(N^C)AuCl$_2$] [N^C = 2-(2,4-difluorophenyl)pyridine (dfppy); **D**] and [(N^C)-AuCl$_2$] [N^C = benzo[*h*]quinoline (bzq); **E**], were prepared via analogous[25,26] literature known transmetalation sequences from mercury derivatives. The method essentially takes advantage of the propensity of mercury(II) salts toward electrophilic substitution for attaining ortho-activation. The ortho-mercurated dfppy was obtained in rather low yield of 11% after repeated recrystallization from ethanol (see Supporting Information for step 1 of **D**). A single resonance signal in ^{199}Hg NMR at $\delta = -1000$ ppm coupled to fluorine $^4J_{Hg-F}$ (248.0 Hz) was observed; the same coupling constant to mercury nucleus was observed in ^{19}F NMR, which showed two sets of signals at −108.3 and −110.1 ppm. A characteristic IR absorption at 342 cm^{-1} assignable to ν(Hg−Cl) was also found. These preceding observations unambiguously establish the identity of the expected ortho-activated [(dfppy)Hg^{II}Cl] and ruled out the possibility of any multiple mercuration which is sometimes encountered in this chemistry.[25,26] Transmetalation of ortho-mercurated bzq (see Experimental Section) required long reaction times (4 days) under optimized conditions of reflux in a 1:1 mixture of dichloromethane and acetonitrile. The ^{1}H NMR spectra of the aurated dichlorides **D** and **E** showed diagnostic downfield shifts (mean difference ($\Delta\delta$), ca. 2.0 ppm) for aromatic proton attached to carbon α to N of the pyridyl ring when compared to those of their respective free dfppy and bzq. In addition IR spectra showed two characteristic stretching vibrations ν(Au−Cl) in the region of 300−415 cm^{-1}.

Utilizing the above precursor complexes, various gold(III) dialkynyls of the type [Au(C^N)(C≡CR)$_2$] [N^C = ppy, R = phenyl (**1a**), 4-fluorophenyl (**1b**), 3,4,5-trimethoxyphenyl (**1c**), 2-thienyl (**1d**), Si(*i*Pr)$_3$ (**1e**), 4-(phenylethynyl)phenyl (**1f**); N^C = dfppy, R = phenyl (**2a**); N^C = bzq, R = phenyl (**3a**); N^C = thpy, R = 4-fluorophenyl (**4a**); and N^C = 5-me-thpy, R = 4-fluorophenyl (**5a**)] were synthesized (Scheme 1). Et$_3$N served as a mild enough base for in situ deprotonation of the relatively acidic acetylenic proton, and the substitution was aided with the addition of a catalytic amount of CuI. It is pertinent to mention here that Yam et al. have recently reported the synthesis of the same class of compounds by a lithiation protocol.[22a]

The reaction proceeds smoothly to completion in less than 20 min at room temperature (RT). Generally, products were obtained in modest yields (25−60%) following simple workup and flash-column purification using neutral Al$_2$O$_3$. Longer reaction times, especially for complexes with thienyl C^N units **4a** and **5a**, lead to an increased amount of unidentified impurities. In the case of **1e**, the reaction was notably clean and complete within 5 min. This could well be expected in light of investigations upon various silyl acetylenes having similar deprotonation rates as compared to aryl acetylenes despite the electronegativity considerations of silicon and carbon.[27] All of the products were completely characterized by ^{1}H, ^{13}C, and ^{19}F NMR and IR spectroscopies and elemental microanalyses. ^{1}H and ^{13}C NMR

dx.doi.org/10.1021/ic102216v |*Inorg. Chem.* 2011, 50, 5430–5441

of all complexes showed two sets of resonances due to the nonequivalent alkynyl ligands. The shift of the proton α to the nitrogen of the pyridyl ring appeared in the range δ = 9.34−9.81 ppm. The higher end values of this interval were notably observed for complexes with bzq and dfppy cores. Such shifts have also been noted with benzoquinoline platinum(II) dialkynyl cyclometalated complexes described in the literature.[28] From the ^{1}H−^{1}H and ^{1}H−^{13}C COSY experiments done for **2a**, the aurated carbon Au−C(sp^2) appeared at 159.0 ppm, which falls in the range previously observed in the literature for five-membered gold(III) metalacycles containing N as one of the donor atoms.[29] Although the chemical shifts for the metalated α-acetylenic carbons ($\delta C_\alpha\equiv$) could not be assigned with certainty, the two C_β signals were observed at δ = 99.0 and 104.0 ppm. In the cases of benzoquinoline platinum(II) dialkynyls the C_α have been unambiguously identified by taking advantage of ^{195}Pt satellites. IR spectra of the prepared complexes showed the expected two acetylenic bands ν(C≡C) characterized by weak absorption in the region of 2100−2200 cm^{-1}.

Stability and Thermogravimetric Studies. During the initial stages of the study, examination of the emission properties of complexes **1a** and **1b** showed no marked variation, and this prompted us to prepare complexes with varied cyclometalating ligands. We chose to use fluorinated aryl acetylides in most of the complexes, with an anticipation they will improve the stability of the complexes on similar lines of thought as explained for gold(III) biaryl complexes presented in our previous study.[21] All complexes synthesized were found to be stable to air and moisture in the solid state under ambient conditions. Homocoupled products, namely, the butadiynes formed through reductive elimination, were observed as byproduct (confirmed by ^{1}H NMR and GC-MS studies) in some cases such as for **1a** and **3a** but were not observed in others, especially for the fluorinated analogues. In comparison with the gold(III) diaryl complexes,[21] these complexes exhibit enhanced stability which could be partly understood on the basis of hybridization considerations of Au−C(sp) vs Au−C(sp^2).

It was interesting to note that while **1c** containing electron-rich alkynyl was quite stable both in solid state and in organic solvents, a dichloromethane solution of **1d** showed discernible decomposition in a few days, and attempts to isolate a complex with 4-ethynyl-*N*,*N*-dimethylaniline as an ancillary ligand with a ppy core (**1**) was unsuccessful because of its instability. Thermogravimetric analysis (TGA) of **1a** and **1b** showed the final decomposition temperature (T_d) of the latter occurs at a much higher temperature around 500 °C than the former at around 290 °C (see Supporting Information Figure S1). This can be probably attributed to the resulting increase in the stability of the complex due to the electron withdrawing nature of fluorine.

Structural Characterization. Single-crystal X-ray structures were determined for seven complexes (**1a**−**1c**, **1e**, **3a**, **4a**, and **5a**). They were obtained from slow evaporation by layering of pentane over concentrated solution of the complexes in dichloromethane at 0−5 °C. The perspective views of **1a**, **1e**, **3a**, and **5a** are shown in Figure 2 (for others, see Supporting Information, Figures S2−S4), and some relevant bond distances and angles are given in Table 1. Crystallographic details are provided in the Supporting Information (Table S1 and Table S2). The structural analysis indicates the coordination environment around the gold metal center as a distorted square-planar geometry which is generally observed for square-planar d^8 complexes with non-equivalent coordination environment. The cyclometalated part is essentially flat, and the largest deviations from the main plane defined by the C^NAuCC metallacycle atoms were 0.072(1) Å observed for **1b** and 0.063(9) Å for **1e**. The maximum twist angle between the planes comprising N^CAu and AuCC was 5.85(14)° in **1b**. The metalated Au−C(sp^2) distances, irrespective of different cyclometalating cores were found to lie in a narrow range of 2.027(3)−2.067(2) Å without much deviation from those reported for their precursor dihalides and other analogous complexes. The N−Au−C_{aryl} chelate bite angles of the complexes were found to range between 80.33(9) and 81.93(9)° with the consequent enlargement of the opposite $C_{alkynyl}$−Au−$C_{alkynyl}$ angle which falls in the range of 88.47(6)−95.28(14)°. The deviation from the idealized 90° is commonly observed in related systems[21,22] and can be attributed to the steric requirements of the cyclometalating ligands. For complexes **1a**−**1c**, **4a**, and **5a** the Au−$C_{alkynyl}$ distances trans to nitrogen of the pyridyl ring lie in the range of 1.965(3)−2.006(2) Å while the distances to other metalated acetylenic carbon fall in the range of 1.993(2)−2.052(2) Å, and this slight but distinct variation could be understood due to the greater trans influence exerted by C(sp^2); however, for complexes **1e** and **3a** the distances were nearly the same within the limits of experimental uncertainty. Deviations from collinearity in the range of 168.2(2)−179.6(3)° were observed for the interatomic angles comprising Au−$C_\alpha\equiv C_\beta$ trans to both N and the metalated carbon. The other angles connecting the aryl or silyl part ($C_\alpha\equiv C_\beta$—$C_{aryl/silyl}$) however did not show large variations. The intermolecular Au···Au distance for **1c** (3.7285(1) Å) was found to be the shortest among the others, which fall in the range of 4.1468(2)−7.6181(1) Å (see Supporting Information Table S3). Since the Au···Au distances are no shorter than the sum of the van der Waals radii between the gold atoms in the crystal lattice, significant aurophilic interactions could be ruled out.

UV−Vis Absorption Studies. The UV−vis profiles of the complexes (see Figure 3 and in Supporting Information Figure S5) with ppy cyclometalate (**1a**−**1f**) and also **2a** exhibit a low-energy absorption band centered around 317−323 nm. Thpy-cyclometalated complex (**4a**) and 5-me-thpy (**5a**) featured bands at lower energies of 368 and 381 nm, respectively, due to their inherent internal charge-transfer nature.[30,31] Understandably, π-delocalization causes lower energy absorptions of bzq (**3a**) at 383 nm. Typically, the complexes showed molar absorptivities in the order of 10^3 to 10^4 dm^3 mol^{-1} cm^{-1}, notably greater in the case of **1f**. In general, the shape of the absorption bands resembled those of the respective free ligands with bathochromic shifts due to metal coordination.

Emission Studies. Complexes except **1c** and **1d** showed intense long-lived phosphorescence at RT. While **1d** showed weak emission at RT (not shown in figures), **1c** was non-emissive (not shown in figures). Nevertheless, all of the complexes showed emission at 77 K (me-THF) rigidified media (see Supporting Information Figure S6). The non-emissive nature of **1c** could be because of thermal equilibrium with deactivating excited states or due to photoinduced electron transfer, presumably from the electron rich methoxy substituents. The latter phenomenon with methoxy-phenylacetylene ligands was also observed previously with Pt(II) cyclometalated complexes.[32] Further studies are due for definitive conclusions. As mentioned earlier, with initial observation that **1a** and **1b** emitting at nearly the same wavelengths (see Table 2), we also thought that either extending the conjugation or changing the cyclometalated ligand can offer tuning of emission wavelengths. Accordingly, **1f** and **2a**−**5a**

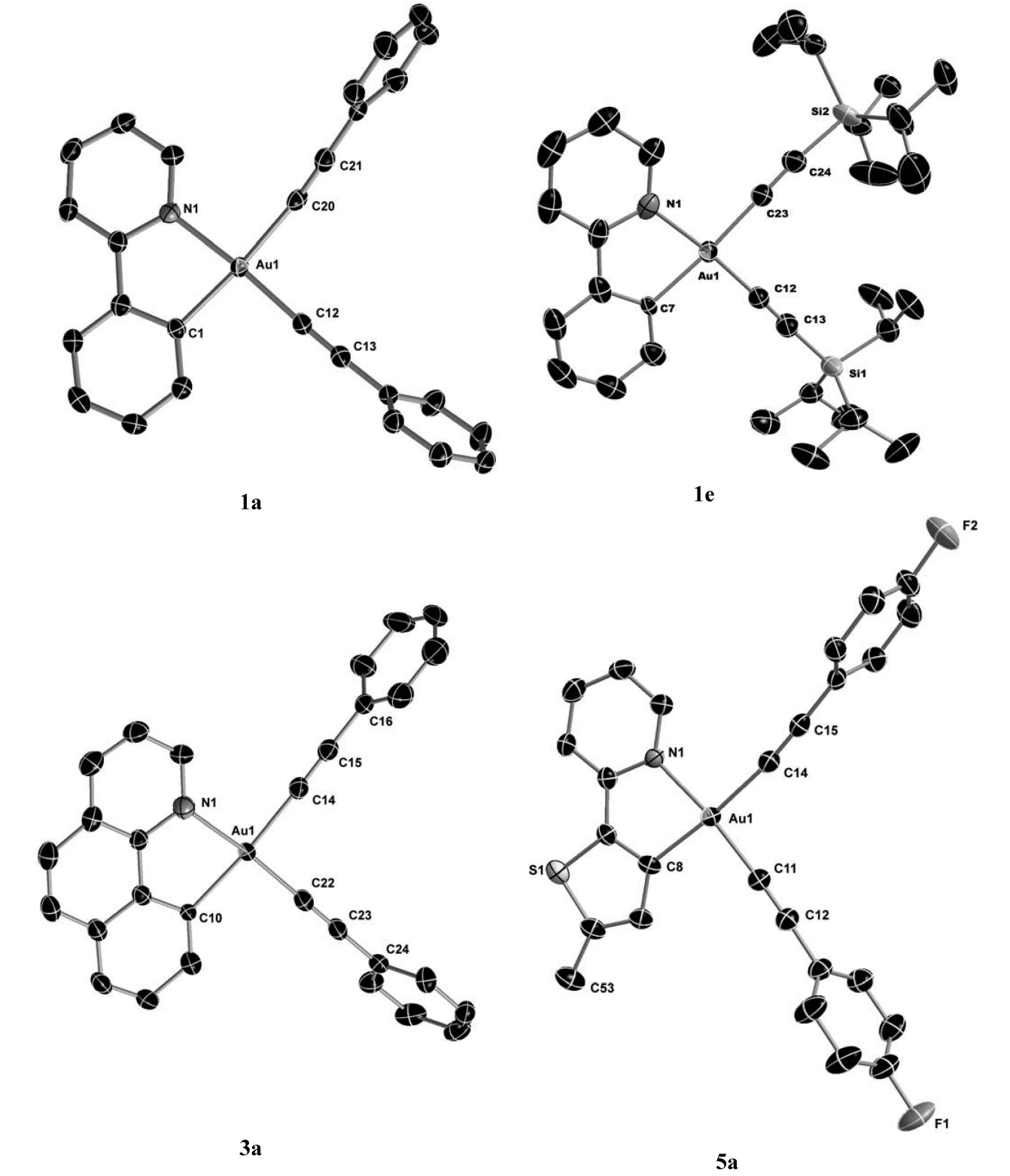

Figure 2. X-ray crystal structures of **1a**, **1e**, **3a**, and **5a** with selective atomic numbering scheme. Thermal ellipsoids are drawn at the 50% probability level. Hydrogen atoms and solvent molecules are omitted for clarity.

did show variation in their lowest energy emission maxima. Interestingly, the structural variation of the cyclometalate such as in **4a** and **5a** was more efficient in tuning emission toward longer wavelengths than that achieved by increasing conjugation by one alkyne unit in the ancillary ligand, such as in **1f**. This suggests the enhanced participation of cyclometalate in the excited state and emission tuning could be achieved by the choice of cyclometalated unit with different $\pi-\pi^*$ energies.

dx.doi.org/10.1021/ic102216v |*Inorg. Chem.* 2011, 50, 5430–5441

Vibrational structured emission profiles even at RT strongly suggest ligand centered (^{3}IL) dominance as in most cases of luminescent gold(III) complexes.[2,12] Emission spectra measured at 77 K generally featured strong bands with vibrational progressions of 1200−1250 cm^{-1} due to the participating ligands (see Supporting Information Figure S6). These values relate more closely to C═N and C═C stretching frequencies and to rocking aromatic C−H modes. Vibrational progressions corresponding to ν(C≡C) stretching modes around 2200 cm^{-1} were comparatively less prominent. No significant residual fluorescence from the ligands was observed in these complexes. It is worth mentioning here that the emission of the fluorescent chromophore benzo[*h*]quinoline λ_{em} = 363 nm shifted to 488 nm in **3a**. The quantum yields (Φ_p) were generally found to lie in the order of 10^{-2} and were notably greater for **1e**; this is also qualitatively in agreement with the quantum yield values observed for Au(III) complexes described recently in literature.[22] As anticipated, there was an increase in the quantum yield of **3a** as compared to **1a**, which could be explained in terms of a partial decrease in nonradiative decay rates (k_{nr}) due to structural rigidification. The decrease in quantum yield of **5a** as compared to **4a** could be understood on the basis of the excited-state structural distortions associated with complexes accompanying a larger Stokes shift. Utilization of dfppy ligand **2**, popular for blue emission in Ir(III) [33] and Pt(II) [34] complexes in **2a**, did show a hypsochromic shift of 8 nm as compared to **1a**. Longer emission wavelengths of **5a** as compared to that of **4a** are due to the lowering of the $\pi-\pi^*$ band gap consequent from the increased electron richness of the thienyl unit. The Stokes shift for these complexes are large, and the excited-state lifetime is in the microsecond regime, indicating the phosphorescent nature of emission. Considering the above observations, and also from the longer excited-state lifetimes (τ), in line with the increasing internal charge-transfer nature of the C^N unit, **5a** > **4a** > **2a**, the emission is assigned to originate from the ^{3}IL ($\pi-\pi^*$) state of the cyclometalate perturbed by the metal.

Table 1. Selected Bond Distances (Å) and Angles (deg) Data of Complexes 1a, 1e, 3a, and 5a

	distance		angle
		Complex **1a**	
C(12)−Au(1)	1.971(2)	C(1)−Au(1)−N(1)	81.33(9)
C(20)−Au(1)	2.052(2)	C(12)−Au(1)−C(20)	90.39(9)
C(1)−Au(1)	2.038(2)	C(1)−Au(1)−C(12)	94.19(9)
N(1)−Au(1)	2.0596(19)	N(1)−Au(1)−C(20)	94.09(8)
		Complex **1e**	
C(7)−Au(1)	2.052(2)	C(7)−Au(1)−N(1)	80.33(9)
N(1)−Au(1)	2.0515(19)	C(23)−Au(1)−C12	89.93(9)
C(23)−Au(1)	1.993(2)	C(23)−Au(1)−N(1)	94.99(9)
C(12)−Au(1)	2.006(2)	C(12)−Au(1)−C(7)	94.75(9)
		Complex **3a**	
C(10)−Au(1)	2.067(2)	N(1)−Au(1)−C(10)	81.93(9)
N(1)−Au(1)	2.061(2)	C(22)−Au(1)−C(14)	92.64(10)
C(14)−Au(1)	2.008(3)	C(14)−Au(1)−N(1)	92.25(9)
C(22)−Au(1)	2.003(3)	C(22)−Au(1)−C(10)	93.14(9)
		Complex **5a**	
N(1)−Au(1)	2.082(2)	C(8)−Au(1)−N(1)	81.07(10)
C(8)−Au(1)	2.032(3)	C(11)−Au(1)−C(14)	92.61(11)
C(14)−Au(1)	2.040(3)	C(14)−Au(1)−N(1)	94.16(10)
C(11)−Au(1)	1.965(3)	C(11)−Au(1)−C(8)	92.20(11)

Cyclic Voltammetry Studies. Cyclic voltammetry for selected complexes **1a**−**1c**, **1f**, **4a**, and **5a** (see Supporting Information Table S4) showed irreversible oxidation peaks in the range from +0.29 to +0.70 V (vs Fc$^{0/+}$ couple) and irreversible cathodic peak potentials in the range from −2.29 to −2.48 V (vs Fc$^{0/+}$ couple) in CH_2Cl_2 at RT. Both processes are assignable to ligand-centered electrochemical events. Due to the similarity of the reduction peak potentials within the same C^N cyclometalate, the reduction process is attributed to origination from the cyclometalated part of the complex and the oxidation from the electron rich alkynyl unit. On the basis of precedences of CV studies of related complexes,[12,22,35] and due to the oxidizing nature of the gold(III) complexes, the metal is less likely to be involved in the redox process. The large electrochemical band gap with oxidation and the reduction peaks widely separated, along with the absence of redox activity from the metal, further corroborates our photophysical observation of the limited participation of the metal in the frontier orbitals.

Density Functional Theory and Time-Dependent Density Functional Theory Calculations. To better understand the absorption and emission properties of the synthesized compounds, density functional theory (DFT) calculations were carried out for selected molecules with the Gaussian 03 program package.[36] The

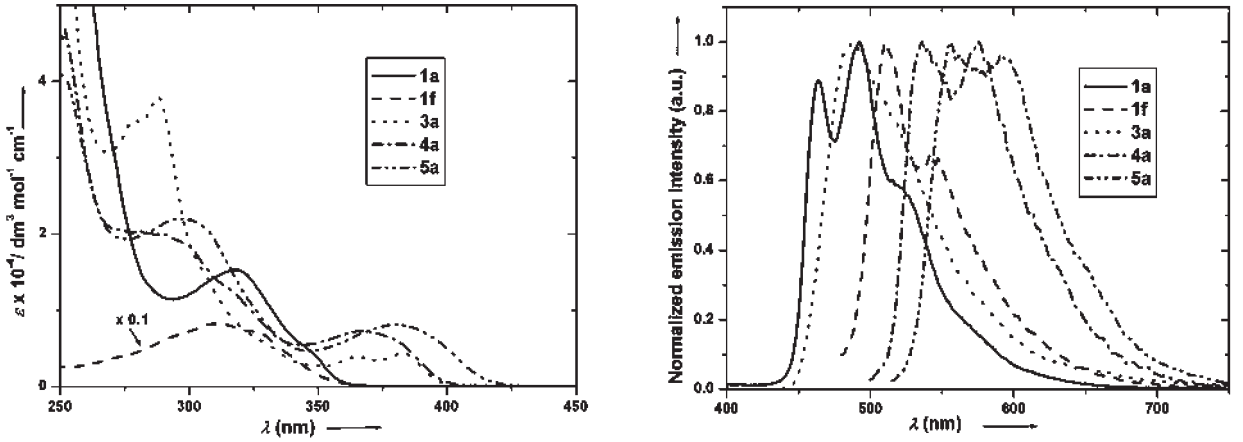

Figure 3. (Left) Electronic absorption spectra in CH_2Cl_2 at RT and (right) normalized emission (I) spectra in degassed CH_2Cl_2 at RT.

Table 2. Photophysical Properties of Complexes 1a−1f and 2a−5a

	room-temperature solution (CH_2Cl_2)				
complex	absorption λ_{max} (nm; ε_{max}/(dm^3 mol^{-1}cm^{-1}))	emission λ_{max} (nm)	τ (μs)	Φ_p [a]	77 K glass[b] (2-me-THF; nm)
1a	318 (15 310)	463, 491, 524 sh	4.4	6.0×10^{-3}	457, 491, 518
1b	318 (13 681)	467, 493, 526 sh	4.5	4.0×10^{-2}	456, 490, 522
1c	321 (15 340)	non-emissive			458, 492, 520
1d	261 (21 290), 323 (10 551)	weakly emissive			486, 505, 525
1e	250 (22 394), 319 (8550), 341 sh (5278)	461, 492, 521 sh	1.4	0.11	459, 486, 528
1f	310 (82 244), 327 sh (71 261)	510, 542	13.0	5.9×10^{-2}	502, 533, 563
2a	317 (1825)	462, 483	1.4	1.6×10^{-2}	457, 522, 555
3a	289 (38 030), 365 (3910), 383 (4374)	488, 515 sh	11.2	1.2×10^{-2}	487, 520
4a	281 (20 314), 368 (7320)	534, 575	7.4	4.4×10^{-2}	452, 574, 590
5a	295 (21 950), 381 (8120)	556, 591	19.1	1.5×10^{-2}	545, 570, 598

[a] Photoluminescence quantum yield determined with quinine sulfate in 1 N H_2SO_4 as standard at 298 K. [b] Vibronic structured emission bands.

Table 3. Selected Singlet−Singlet (S_0-S_n) and Singlet−Triplet (S_0-T_m) Excited States with TDDFT/CPCM Vertical Excitation Energies (nm), Transition Coefficients, Orbitals Involved in the Transitions, and Oscillator Strengths *f* for Compounds 1a, 1b, 1e, and 4a (with $f > 0.015$)

	1a	**1b**	**1e**	**4a**
exp abs λ_{max}	318	318	319	368
S_0-S_n	$n = 3$	$n = 2$	$n = 1$	$n = 1$
	318 (0.175) H-2 → L (0.67)	339 (0.083) H-1 → L (0.66)	323 (0.079) H → L (0.63)	353 (0.038) H → L (0.62)
S_0-S_n	$n = 4$	$n = 3$	$n = 4$	$n = 2$
	292 (0.192) H-3 → L (0.65)	318 (0.182) H-2 → L (0.67)	302 (0.150) H-3 → L (0.64)	351 (0.138) H-2 → L (0.57)
S_0-S_n	$n = 6$	$n = 4$	$n = 5$	$n = 3$
	278 (0.123) H → L+2 (0.53)	292 (0.181) H-3 → L (0.65)	299 (0.215) H-4 → L (0.63)	337 (0.267) H-1 → L (0.68)
S_0-S_n	$n = 7$	$n = 6$	$n = 7$	$n = 5$
	276 (0.032) H-6 → L (0.45)	280 (0.054) H-4 → L (0.65)	274 (0.139) H → L+1 (0.58)	293 (0.199) H-3 → L (0.68)
S_0-S_n	$n = 8$	$n = 7$		$n = 7$
	276 (0.034) H-1 → L+1 (0.46)	280 (0.028) H-1 → L+2 (0.61)		290 (0.248) H → L+2 (0.57)
S_0-S_n	$n = 9$	$n = 8$		$n = 8$
	274 (0.311) H-1 → L+2 (0.50)	275 (0.291) H → L+2 (0.64)		284 (0.059) H → L+1 (0.60)
S_0-S_n	$n = 10$	$n = 9$		$n = 9$
	265 (0.143) H-7 → L (0.44)	273 (0.051) H-1 → L+1 (0.63)		284 (0.133) H-2 → L+1 (0.54)
S_0-S_n		$n = 10$		
		265 (0.161) H-7 → L (0.49)		
exptl emiss λ_{max}	491	493	492	575
calcd λ_{max} [a]	471 (2.63 eV)	468 (2.65 eV)	468 (2.65 eV)	571 (2.17 eV)
T_1-S_0	441 H-2 ← L (0.66)	442 H-2 ← L (0.66)	441 H-4 ← L (0.51) H ← L (0.41)	518 H-2 ← L (0.73)

[a] Solvent-corrected (CH_2Cl_2) energy difference between the optimized ground state and lowest triplet state.

molecular structures of the electronic ground states and lowest triplet states of compounds **1a**, **1b**, **1e**, and **4a** were exemplarily studied. On the basis of the optimized geometries, time-dependent DFT (TD-DFT) calculations[37] combined with the conductive polarizable continuum model (CPCM)[38,39] were used to produce the molecular orbital energy levels and compositions, the absorption spectra, and the lowest singlet−singlet and singlet−triplet electronic transitions in CH_2Cl_2 media.

Selected TD-DFT singlet−singlet electronic transitions, excitation energies, and oscillator strengths of **1a**, **1b**, **1e**, and **4a** are given in Table 3. For **1a**, the lowest lying absorption transition $S_0 \rightarrow S_3$ at 318 nm ($f < 0.175$, the oscillator strengths for the $S_0 \rightarrow S_1$ and $S_0 \rightarrow S_2$ transitions being very small: $f < 0.005$) is in good agreement with the low-energy absorption band experimentally centered at 318 nm. This transition is derived from the HOMO-2 → LUMO excitation. As shown in Figure 4, both frontier orbitals are distributed predominantly over the organic ligand ppy (about 90%) with some contributions from the metal center and the alkynyl ligands (see Supporting Information for molecular orbital compositions). The absorption band can then be ascribed to a transition with a metal-perturbed intraligand charge-transfer $^1IL_{\pi\rightarrow\pi^*(ppy)}CT$ character. Other significant higher transitions at 292 nm ($S_0 \rightarrow S_4$, $f = 0.192$), 278 nm ($S_0 \rightarrow S_6$, $f = 0.123$), and 274 nm ($S_0 \rightarrow S_9$, $f = 0.311$) are better related to the intense high-energy band centered around 250−260 nm. They involve frontier molecular orbitals located either on the alkynyl ligands (HOMO-1, HOMO, and LUMO+2) or on the phenylpyridine (HOMO-3 and LUMO) with a small contribution from the metal center (less than 5%)

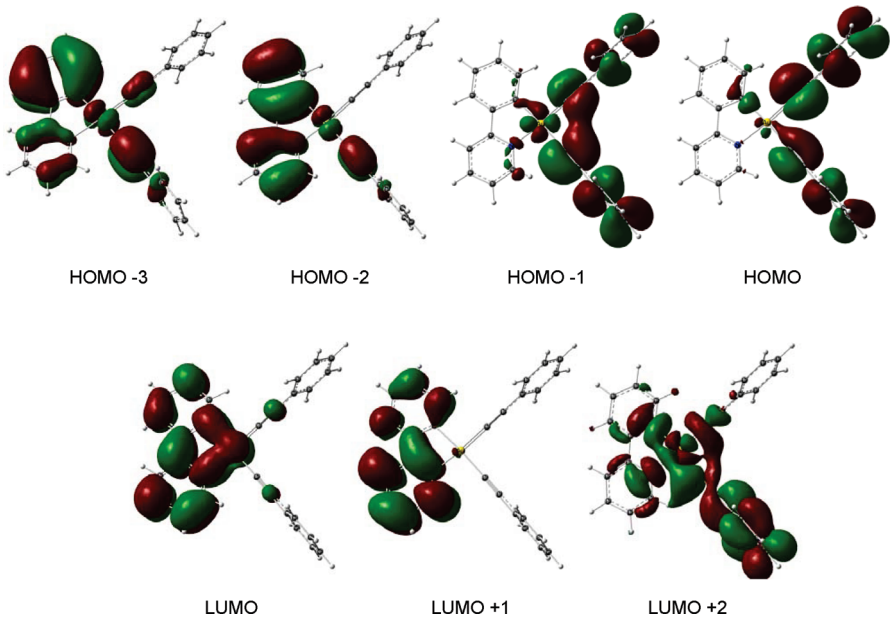

Figure 4. Isodensity plots of selected frontier orbitals of the ground state of **1a** (isodensity value, 0.02).

except for LUMO+2, which displays 25% of the electron density on the gold atom (Figure 4). The corresponding absorption band can be characterized as a transition with an admixture of intraligand charge-transfer $^1IL_{\pi\rightarrow\pi^*(ppy)}CT$ and metal-perturbed ligand-to-ligand $^1LL_{\pi(alk)\rightarrow\pi^*(alk)}CT$ characters.

For **1b**, the lowest significant singlet−singlet transitions $S_0 \rightarrow S_2$, $S_0 \rightarrow S_3$, and $S_0 \rightarrow S_4$ (f = 0.083, 0.182, 0.181; $S_0 \rightarrow S_1$ with $f < 0.010$) at 339, 318, and 292 nm are derived from the HOMO-1 → LUMO, HOMO-2 → LUMO, and HOMO-3 → LUMO excitations, respectively. Except HOMO-1 which is mainly located on the alkynyl ligands with a small contribution of the metal, the other four orbitals are a π/π^* combination of the phenylpyridine ligand. The main absorption band experimentally observed at 318 nm can be attributed to these three transitions characterized by metal-perturbed intraligand charge-transfer $^1IL_{\pi\rightarrow\pi^*(ppy)}CT$ and ligand-to-ligand $^1LL_{\pi(alk)\rightarrow\pi^*(ppy)}CT$ characters. The calculated electronic transitions for compound **1e** show the same general picture as that for **1b**. The influence of the terminal F atom in **1b** and the $SiMe_3$ group in **1e** on the alkynyl ligands is established by the lowest and significant singlet−singlet $\pi(alk) \rightarrow \pi^*(ppy)$ transitions with f = 0.083 and 0.079 at 339 and 323 nm, respectively. Nevertheless, the main character of the lowest absorption band of **1e** remains $\pi \rightarrow \pi^*(ppy)$ as shown by the $S_0 \rightarrow S_4$ and $S_0 \rightarrow S_5$ transitions calculated at 302 and 299 nm with the larger oscillator strengths f = 0.150 and 0.215, respectively. Compound **4a** differs from **1b** by the presence of 2-(2-thienyl)pyridine (thpy) instead of phenylpyridine. Experimentally, thpy is responsible of a lower energy absorption band at 368 nm for **4a** in comparison with **1a**−**1f**. The lowest transitions at 353, 351, and 337 nm calculated for **4a** (f = 0.038, 0.138, 0.267) are in good agreement with the experimental trend. As in **1a**, **1b**, and **1e**, the LUMO is localized on the N^C ligand with a small contribution from the metal center. HOMO and HOMO-1 are π-alkynyl based orbitals, and HOMO-2 distributes over thpy; consequently the corresponding HOMO → LUMO, HOMO-2 → LUMO, and HOMO-1 → LUMO excitations give rise to the main experimental absorption bands with an admixture of the metal-perturbed $^1IL_{\pi\rightarrow\pi^*(thpy)}CT$ and $^1LL_{\pi(alk)\rightarrow\pi^*(thpy)}CT$ characters.

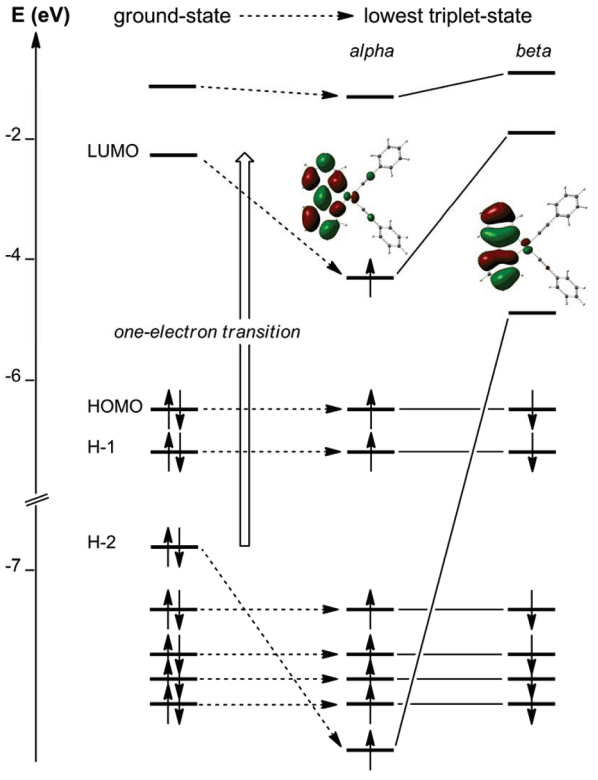

Figure 5. MO diagrams for the ground state and lowest triplet state of **1a**.

It is worth noting that the lowest TD-DFT excited states are calculated to be of triplet character at 441, 442, 441, and 518 nm for **1a**, **1b**, **1e**, and **4a**, respectively (Table 3). These calculated transitions are not observed in the visible region of the experimental absorption spectra, confirming the spin-forbidden character of these singlet−triplet transitions. For all compounds the calculated wavelengths corresponding to the $T_1 \rightarrow S_0$ transitions

dx.doi.org/10.1021/ic102216v |Inorg. Chem. 2011, 50, 5430–5441

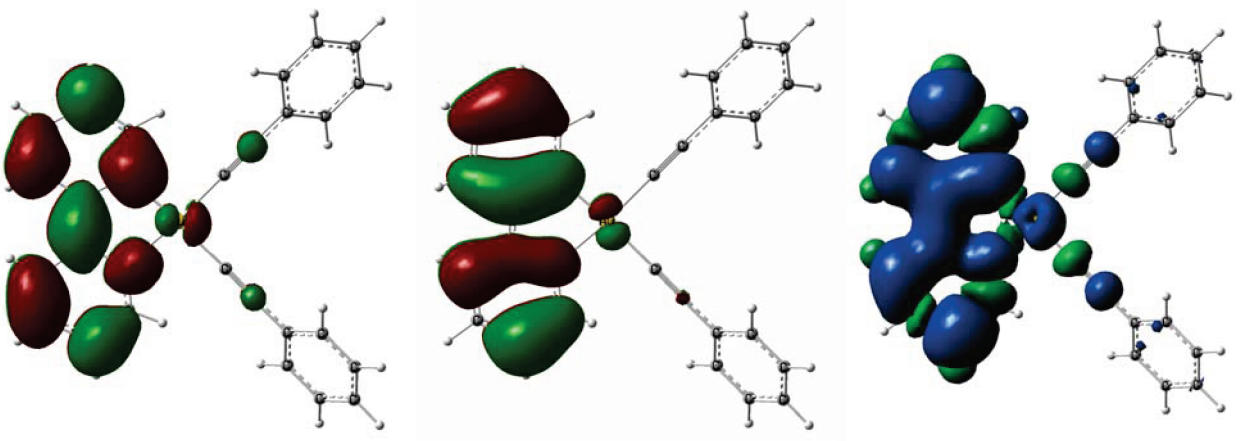

Figure 6. Isodensity plots of the singlet HOMO (left), singlet LUMO (middle), and the triplet spin density surface of the lowest triplet state of **1a** (isodensity value, 0.02).

are in line with the experimental emission wavelengths (in parentheses) with 441 (491), 442 (493), 441 (492), and 518 (575) nm for **1a**, **1b**, **1e**, and **4a**, respectively (Table 3). Nevertheless, the calculated emission maxima are more reliable when based on the energy difference between the optimized emissive triplet state and the optimized ground state. Indeed, the calculated values reported in Table 3 as calculated λ_{max} of 471 (**1a**), 468 (**1b**), 468 (**1e**), and 571 (**4a**) are in good agreement with the experimental values even still underestimated by 4−25 nm. Careful analyses of the molecular orbital diagrams of the optimized closed-shell ground state and open-shell triplet state of **1a** (Figure 5) confirm that the calculated transition LUMO → HOMO-2 is responsible of the experimental emission at 491 nm. They also reveal some inversion in the order of the orbitals with geometrical consequences. The ground-state HOMO-2 (−6.90 eV) is greatly affected by the one-electron HOMO-2 → LUMO excitation since the derived singly occupied α orbital of the triplet state is found at −7.47 eV as HOMO-7(α) while the corresponding unoccupied β orbital is the singlet LUMO of the system (−4.83 eV). The population of the ground-state LUMO (−2.13 eV) by one electron stabilized the singlet molecular orbital which becomes HOMO(α) in the triplet -state MO diagram (at −4.22 eV), while the corresponding unoccupied orbital is only slightly destabilized as LUMO+1(β) at −1.91 eV (Figure 5). The electronic density of the HOMO-2 and LUMO being mainly localized on the phenylpyridine ligand with a π-antibonding character of the central C−C bridge for the former and contrastingly a π-bonding character of the central C−C bridge for the latter orbital, the main variation observed in the optimized excited state with respect to the ground-state geometry is a significant shortening of the central C−C bond by 0.076 Å (1.388 Å vs 1.464 Å). The singlet HOMO, singlet LUMO, and the triplet spin density surface of the lowest triplet state of **1a** (Figure 6) visually identify the emission from a transition with a ^{3}ILCT character originated by the phenylpyridine ligand. Comparable studies were carried out for the other selected compounds **1b**, **1e**, and **4a** with no major differences in comparison with **1a** since the frontier orbitals involved in the calculated emissions and the triplet spin density surfaces of the lowest triplet states are similar in shape. For all studied compounds, the calculated phosphorescences are the reverse processes of the lowest lying absorptions because of the same transition characters.

CONCLUSIONS

In conclusion, we have developed a facile synthetic access toward tunable phosphorescent gold(III) *cis*-dialkynyl complexes. As demonstrated, the method can be applied quite generally to various gold(III) cyclometalated complexes bearing different alkynyls. This might help further to understand fundamental photophysics associated with gold(III) alkynyl complexes and design molecules with increased quantum yields suitable for OLEDs. The basic square-planar gold(III) dialkynyl motif could also be advantageously used for the development of macromolecules which are limited until now as compared to the isoelectronic platinum(II) systems.

EXPERIMENTAL SECTION

Material and Methods. All manipulations were carried out without special precautions for excluding air and moisture. ^{1}H and ^{13}C{^{1}H} NMR were recorded on Bruker AV2-400 or AV-500 spectrometers. ^{19}F NMR spectra were recorded on either a Varian Mercury spectrometer or Bruker AV2-400 spectrometers. Chemical shifts (δ) are reported in parts per million (ppm) referenced to tetramethylsilane (δ 0.00 ppm) using the residual protio solvent peaks as internal standards (^{1}H NMR experiments) or the characteristic resonances of the solvent nuclei (^{13}C NMR experiments). ^{19}F NMR was referenced to $CFCl_3$ (δ 0.00 ppm). Coupling constants (J) are quoted in hertz, and the following abbreviations are used to describe the signal multiplicities: s (singlet); d (doublet); t (triplet); q (quartet); m (multiplet); dd (doublet of doublet); td (triplet of doublet); dt (doublet of triplet). Proton and carbon assignments have been made using routine one- and two-dimensional NMR spectroscopies where appropriate. Infrared (IR) spectra were recorded on a Perkin-Elmer 1600 Fourier transform spectrophotometer using KBr pellet with frequencies (ν) quoted in wavenumbers (cm^{-1}). Elemental microanalysis was carried out with a Leco CHNS-932 analyzer. Mass spectra were run on a Finnigan-MAT-8400 mass spectrometer. Thin-layer chromatography (TLC) analysis was performed on precoated Merck silica gel $60F_{254}$ slides and visualized by luminescence quenching either at (short wavelength) 254 nm or (long wavelength) 365 nm. Chromatographic purification of products was performed on a short column (length, 15.0 cm; diameter, 1.5 cm) using forced flow of eluent. UV−vis measurements were carried out on a Perkin-Elmer Lambda 19 UV/vis spectrophotometer. Emission spectra were acquired on Perkin-Elmer spectrophotometer using 450 W xenon lamp excitation by exciting at the longest wavelength absorption maxima. All samples for emission spectra

were degassed by at least three freeze−pump−thaw cycles in an anaerobic cuvette and were pressurized with N_2 following each cycle. Emission spectra at 77 K were acquired in frozen 2-methyltetrahydrofuran (2-me-THF) glass. Luminescence quantum yields (Φ_p) were determined at 298 K (estimated uncertainty, ±15%) using standard methods;[40] wavelength-integrated intensities (I) of the corrected emission spectra were compared to isoabsorptive spectra of quinine sulfate standard (Φ_{ref} = 0.546 in 1 N H_2SO_4 air-equilibrated solution) and was corrected for solvent refractive index. Phosphorescence lifetimes were measured by time-correlated single-photon counting method (TCSPC) performed on an Edinburgh FLS920 spectrophotometer, using nF900 lamp source at 30 000 Hz frequency with 15 nm excitation and 15 nm emission slit widths. Thermogravimetric analysis (TGA) was done using a NETZSCH STA 449C instrument. Cyclic voltammograms were obtained with BAS 100W voltammetric analyzer. The cell was equipped with a gold working electrode, a Pt counter electrode, and a nonaqueous reference electrode. All sample solutions (CH_2Cl_2) were approximately 5×10^{-3} M in substrate and 0.1 M in Bu_4NPF_6 and were prepared under nitrogen. Ferrocene was subsequently added and the calibration of voltammograms recorded. The BAS 100W program was employed for data analysis.

Commercially available reagents were purchased from Aldrich and were used as such without further purification. Sodium tetrachloroaurate-(III) dihydrate was purchased from Strem Chemicals. All terminal alkynes described were either commercially purchased or synthesized by established sonogashira cross-coupling protocol.

*Synthesis of [(N^C)AuCl$_2$] [N^C = 2-(2,4-Difluorophenyl)pyridine] (**D**).* (3,5-Difluoro-2-(pyridin-2-yl)phenyl)mercury(II) chloride (0.170 g, 0.398 mmol) was added as a suspension in dichloromethane (DCM) (15.0 mL) to a solution of sodium tetrachloroaurate(III) dihydrate (0.158 g, 0.397 mmol) in acetonitrile (15.0 mL), and the mixture was stirred for 4 h at RT. It was then filtered and washed with cold acetonitrile (4.0 mL) and dried in vacuo to obtain off-white solid. Yield = 0.087 g, 48%. Positive ESI-MS: m/z 421.0 $[M - Cl]^+$. IR (KBr): ν(Au−Cl) 301, 320 cm^{-1}. ^1H NMR (500 MHz, DMSO-d_6, 298 K): δ 7.35 (td, J = 10.0 Hz, 2.5 Hz, 1H), 7.53 (d, J = 7.0 Hz, 1H), 7.77 (t, J = 7.0 Hz, 1H), 8.26 (d, J = 8.0 Hz, 1H), 8.37 (t, J = 7.5 Hz, 1H), 9.61 (d, J = 7.0 Hz, 1H). $^{13}C\{^1H\}$ NMR (125 MHz, DMSO-d_6, 298 K): δ 105.2 (t, $^2J_{C-F}$ = 26.0 Hz), 113.5 (d, $^2J_{C-F}$ = 26.0 Hz), 124.3 (d, $^2J_{C-F}$ = 19.5 Hz), 125.1, 127.0, 144.4, 148.4, 150.3, 158.8 (dd, $^1J_{C-F}$ = 260.0 Hz, 12.3 Hz), 160.5, 161.2 (dd, $^1J_{C-F}$ = 260.0 Hz, 12.5 Hz). ^{19}F NMR (282 MHz, DMSO-d_6, 298 K): δ −107.0, −102.2. Anal. Calc for $C_{11}H_6AuCl_2F_2N$ (%): C, 28.84; H, 1.32; N, 3.06. Found: C, 28.62; H, 1.26; N, 3.19.

*Synthesis of [(N^C)AuCl$_2$] [N^C = Benzo[h]quinoline][AuCl$_2$] (**E**).* Benzo[h]quinolin-10-ylmercury(II) chloride (0.15 g, 0.362 mmol) in DCM (20 mL) was added to a solution of sodium tetrachloroaurate(III) dihydrate (0.143 g, 0.360 mmol) in acetonitrile (20 mL), and the mixture was refluxed for 4 days. The pale violet solid that separated out was collected by filtration, washed with cold acetonitrile (15 mL), and dried under reduced pressure. Yield = 0.093 g, 58%. Positive ESI-MS: m/z 467.8 $[M + Na]^+$. IR (KBr): ν(Au−Cl) 378, 412 cm^{-1}. ^1H NMR (400 MHz, DMSO-d_6, 298 K): δ 7.71 (t, J = 7.5 Hz, 1H), 7.80 (d, J = 7.5 Hz, 1H), 7.9−8.0 (m, 4H), 8.93 (d, J = 8.5 Hz, 1H), 9.63 (d, J = 5.6 Hz, 1H); $^{13}C\{^1H\}$ NMR (125 MHz, DMSO-d_6, 298 K): δ 125.1, 126.3, 128.5, 128.9, 129.0, 130.0, 130.3, 131.4, 136.3, 143.4, 149.0, 152.2, 155.7. Anal. Calc for $C_{13}H_8AuCl_2N$ (%): C, 35.00; H, 1.81; N, 3.14. Found: C, 34.79; H, 1.83; N, 2.97.

*General Procedure for the Synthesis of Cyclometalated Gold(III) σ-Dialkynyl Complexes (**1a**−**1f**, **2a**, **3a**, **4a**, and **5a**).* To the suspension of respective cycloaurated gold(III) dichlorides (1.0 equiv.) in DCM (ca. 5.0 mL) are sequentially added the corresponding alkynes (2.3 equiv), triethylamine (0.055 equiv), and CuI (0.15 equiv) at RT. The suspension quickly turns into clear homogeneous solution, which is then further stirred for 15 min. Removal of solvents in vacuo, followed by sufficient pentane wash, yields the crude material. Purification by flash column chromatography (neutral Al_2O_3:eluent:EtOAc and hexane mixture) yields respective products as off-white to yellow solids. In some cases the purification procedures are slightly modified and are described below individually along with characterization data.

Note: During initial optimization experiments, aqueous workup protocol was followed and compounds were found to be quite stable to addition of water; later a direct purification procedure as described above was adopted because it gave improved yields.

*Synthesis of [(N^C)AuL$_2$] [N^C = 2-Phenylpyridine, L = Phenylacetylene] (**1a**).* The reaction of **A** (0.10 g, 0.236 mmol) with phenylacetylene (0.06 mL, 0.538 mmol) following the general procedure yielded **1a** as an off-white solid after column chromatography (neutral Al_2O_3; eluent, hexane/EtOAc = 5:1). Yield = 0.072 g, 55%. Positive ESI-MS: m/z 553.0 $[M^+]$. IR (KBr): ν(C≡C) 2132, 2160 cm^{-1}. ^1H NMR (500 MHz, $CDCl_3$, 298 K): δ 7.33−7.48 (m, 8H), 7.50−7.54 (m, 1H), 7.58−7.63 (m, 4H), 7.81 (d, J = 10.0 Hz, 1H), 8.02 (d, J = 10.0 Hz, 1H), 8.16 (t, J = 10.0 Hz, 1H), 8.32 (d, J = 10.0 Hz, 1H), 9.74 (d, J = 5.0 Hz, 1H). $^{13}C\{^1H\}$ NMR (125 MHz, $CDCl_3$, 298 K): δ 80.8, 99.5, 104.3, 118.3, 121.0, 124.8, 125.4, 126.4, 126.5, 127.6, 128.1, 128.7, 128.8, 132.2 (2C), 132.3, 132.4, 136.2, 142.3, 146.1, 151.4, 156.6, 167.4. Anal. Calc for $C_{27}H_{18}AuN$ (%): C, 58.60; H, 3.28; N, 2.53. Found: C, 58.39; H, 3.46; N, 2.40.

*Synthesis of [(N^C)AuL$_2$] [N^C = 2-Phenylpyridine, L = 1-Ethynyl-4-fluorobenzene] (**1b**).* The reaction of **A** (0.20 g, 0.473 mmol) with 1-ethynyl-4-fluorobenzene (0.124 mL, 1.08 mmol) following the general procedure yielded **1b** as an off-white solid which was purified by column chromatography (neutral Al_2O_3; eluent, hexane/EtOAc = 1:1). Yield = 0.175 g, 63%. Positive ESI-MS: m/z 612.0 $[M + Na]^+$. IR (KBr): ν(C≡C) 2137, 2165 cm^{-1}. ^1H NMR (500 MHz, CD_2Cl_2, 298 K): δ 7.05−7.11 (m, 4H), 7.40−7.47 (m, 2H), 7.51 (t, J = 7.5 Hz, 1H), 7.55−7.61 (m, 4H), 7.78 (d, J = 7.5 Hz, 1H), 8.00 (d, J = 7.5 Hz, 1H), 8.14 (t, J = 7.5 Hz 1H), 8.25 (d, J = 10.0 Hz, 1H), 9.66 (d, J = 5.5 Hz, 1H). $^{13}C\{^1H\}$ NMR (125 MHz, $CDCl_3$, 298 K): δ 79.6, 97.8, 102.6, 115.1, 115.3, 117.1, 120.5, 121.9, 122.0, 124.3, 124.9, 127.6, 131.8, 133.4, 133.5, 135.6, 141.8, 145.5, 150.9, 155.8, 162.0 (d, $^1J_{C-F}$ = 246.0 Hz), 161.7 (d, $^1J_{C-F}$ = 246.0 Hz), 166.8. ^{19}F NMR (282 MHz, CD_2Cl_2, 298 K): δ −115.3, −114.9. Anal. Calc for $C_{27}H_{16}AuF_2N$ (%): C, 55.02; H, 2.74; N, 2.38. Found: C, 54.94; H, 2.70; N, 2.25.

*Synthesis of [(N^C)AuL$_2$] [N^C = 2-Phenylpyridine, L = 5-Ethynyl-1,2,3-trimethoxybenzene] (**1c**).* The reaction of **A** (0.10 g, 0.236 mmol) with 5-ethynyl-1,2,3-trimethoxybenzene (0.104 g, 0.542 mmol) following the general procedure yielded **1c** as a yellow crystalline solid after chromatographic purification (neutral Al_2O_3; eluent, hexane/EtOAc = 1:1). Yield = 0.089 g, 50%. IR (KBr): ν(C≡C) 2161, 2171 cm^{-1}. ^1H NMR (500 MHz, CD_2Cl_2, 298 K): δ 3.82 (s, 6H), 3.83 (s, 6H), 3.89 (s, 3H), 3.90 (s, 3H), 6.84 (s, 2H), 6.86 (s, 2H), 7.41−7.49 (m, 2H), 7.53 (t, J = 10.0 Hz, 1H), 7.80 (d, J = 10.0 Hz, 1H), 8.00 (d, J = 10.0 Hz, 1H), 8.16 (t, J = 10.0 Hz, 1H), 8.28 (d, J = 5.0 Hz. 1H), 9.70 (d, J = 5.0 Hz, 1H). $^{13}C\{^1H\}$ NMR (125 MHz, CD_2Cl_2, 298 K): δ 56.0, 60.5, 79.0, 99.0, 103.9, 108.8, 108.9, 116.4, 120.5, 120.7, 120.9, 124.3, 124.9, 127.6, 128.5, 131.6, 135.6, 138.0, 138.2, 141.8, 142.5, 145.5, 147.8, 150.8, 153.0, 155.9, 166.7. Anal. Calc for $C_{33}H_{30}AuNO_6$ (%): C, 54.03; H, 4.12; N, 1.91. Found: C, 53.95; H, 4.01; N, 1.78.

*Synthesis of [(N^C)AuL$_2$] [N^C = 2-Phenylpyridine, L = 2-Ethynylthiophene] (**1d**).* The reaction of **A** (0.10 g, 0.236 mmol) with 2-ethynylthiophene (0.058 g, 0.542 mmol) following the general procedure yielded **1d** as a light brown solid after successive purification by column chromatography (neutral Al_2O_3; eluent, hexane/EtOAc = 2:1), and crystallization at −30 °C in DCM/pentane mixtures (1:1). Yield = 0.033 g, 25%. IR (KBr): ν(C≡C) 2145, 2155 cm^{-1}. ^1H NMR (500 MHz, $CDCl_3$, 298 K): δ 6.95 (dt, J = 9.0 Hz, 3.2 Hz, 2H), 7.13−7.21 (m, 3H), 7.30−7.37 (m, 3H), 7.47 (t, J = 5.5 Hz, 1H), 7.78 (d, J = 7.5 Hz, 1H), 7.79 (d, J = 7.5 Hz, 1H), 8.05 (t, J = 5.0 Hz, 1H), 8.09 (d, J = 5.2 Hz, 1H), 9.5 (d, J = 5.5 Hz, 1H). $^{13}C\{^1H\}$ NMR (125 MHz, $CDCl_3$, 298 K):

δ 85.2, 91.3, 96.1, 98.4, 120.6, 122.7, 124.3, 125.1, 125.2, 125.8, 126.0, 126.2, 126.8, 127.7, 130.5, 130.9, 131.7, 135.4, 141.8, 145.3, 150.7, 155.4, 166.5. Anal. Calc for $C_{23}H_{14}AuNS_2$ (%): C, 48.85; H, 2.50; N, 2.48. Found: C, 48.61; H, 2.44; N, 2.42.

*Synthesis of [(N^C)AuL$_2$] [N^C = 2-Phenylpyridine, L = Ethynyltrisopropylsilane] (**1e**).* The reaction of **A** (0.072 g, 0.170 mmol) with ethynyltrisopropylsilane (0.088 mL, 0.390 mmol) following the general procedure yielded **1e** as a white crystalline solid after chromatographic purification. (neutral Al_2O_3; eluent, hexane/EtOAc = 2:1). Yield = 0.072 g, 60.0%. Positive EI-MS: m/z 736.3 $[M + Na]^+$. IR (KBr): ν(C≡C) 2095, 2071 cm^{-1}. ^1H NMR (500 MHz, CD_2Cl_2, 298 K): δ 1.14 (s, 18H), 1.17 (s, 18H), 1.22 (s, 3H), 1.23 (s, 3H), 7.40−7.45 (m, 3H), 7.74 (d, J = 7.5 Hz, 2.0 Hz 1H), 7.96 (d, J = 7.5 Hz, 1H), 8.10 (t, J = 7.5 Hz, 1H), 8.31 (dd, J = 7.5 Hz, 2.0 Hz, 1H), 9.78 (d, J = 7.5 Hz, 1H). $^{13}C\{^1H\}$ NMR (125 MHz, CD_2Cl_2, 298 K): δ 11.6, 11.7, 18.6, 18.7, 96.6, 99.0, 102.8, 120.2, 123.7, 124.6, 127.3, 131.3, 136.0, 138.0, 141.7, 145.5 150.7, 156.4, 166.8. Anal. Calc for $C_{33}H_{50}AuNSi_2$ (%): C, 55.52; H, 7.06; N, 1.96. Found: C, 55.60; H, 6.96; N, 1.76.

*Synthesis of [(N^C)AuL$_2$] [N^C = 2-Phenylpyridine, L = 1-Ethynyl-4-(phenylethynyl)benzene] (**1f**).* The reaction of **A** (0.10 g, 0.236 mmol) with 1-ethynyl-4-(phenylethynyl)benzene (0.109 g, 0.542 mmol) following the general procedure yielded **1f** as a yellow solid which was further purified by column chromatography (acidic Al_2O_3; eluent, hexane/EtOAc = 2:1). Yield = 0.1 g, 56.0%. IR (KBr): ν(C≡C) 2129, 2159 cm^{-1}. ^1H NMR (500 MHz, $CDCl_3$, 298 K): δ 7.41−7.44 (m, 7H), 7.45−7.62 (m, 14H), 7.81 (d, J = 10.0 Hz, 1H), 8.02 (d, J = 10 Hz, 1H), 8.17 (t, J = 10 Hz, 1H), 8.27 (d, J = 5.5 Hz, 1H), 9.70 (d, J = 5.5 Hz, 1H). $^{13}C\{^1H\}$NMR (125 MHz, CD_2Cl_2, 298 K): δ 82.8, 89.2, 90.5, 98.8, 103.6, 120.7, 120.3, 120.5, 121.6, 122.0, 123.0, 124.2, 124.4, 124.5, 124.9, 125.2, 125.8, 125.9, 127.4, 127.6, 128.4, 128.5, 131.1, 131,3, 131.5, 131.6, 131.7, 131.7, 131.9, 135.6, 141.9, 145.5, 150.9, 156.7, 166.9. Anal. Calc for $C_{43}H_{26}AuN$ (%): C, 68.53; H, 3.48; N, 1.86. Found: C, 68.56; H, 3.58; N, 1.62.

*Synthesis of [(N^C)AuL$_2$] [N^C = 2-(2,4-Difluorophenyl)pyridine, L = Phenylacetylene] (**2a**).* The reaction of **D** (0.060 g, 0.131 mmol) with phenylacetylene (0.032 mL, 0.298 mmol) following the general procedure yielded **2a** as an off-white solid after chromatographic purification (neutral Al_2O_3; eluent, hexane/EtOAc = 1:1). Yield = 0.032 g, 41%. IR (KBr): ν(C≡C) 2137, 2165, cm^{-1}. ^1H NMR (500 MHz, CD_2Cl_2, 298 K): δ 6.86 (td, J = 8.0 Hz, 2.5 Hz, 1H), 7.30−7.39 (m, 6H), 7.50 (t, J = 8.0 Hz, 1H), 7.59−7.64 (m, 4H), 7.97 (dd, J = 8.0 Hz, 2.5 Hz, 1H), 8.14 (t, J = 7.5 Hz, 1H), 8.35 (d, J = 8.0 Hz, 1H), 9.80 (dd, J = 8.0 Hz, 2.5 Hz, 1H). $^{13}C\{^1H\}$ NMR (125 MHz, CD_2Cl_2, 298 K): δ 99.0, 103.8, 104.0 (t, $^2J_{C-F}$ = 26.2 Hz), 114.1, 118.8, 119.0, 124.2, 124.4, 124.6, 125.6, 125.8, 127.6, 127.9, 128.5, 128.6, 130.7, 132.0, 132.1, 142.7, 151.6, 161.2 (d, $^1J_{C-F}$ = 275.0 Hz), 163.9, 164.1(d, $^1J_{C-F}$ = 275.0 Hz). ^{19}F NMR (188 MHz, CD_2Cl_2, 298 K): δ −109.2, −105.4. Anal. Calc for $C_{27}H_{16}AuF_2N.H_2O$ (%): C, 53.39; H, 2.99; N, 2.31. Found: C, 53.20; H, 2.91; N, 2.31. (Note: The elemental analysis was measured on a sample obtained by aqueous workup which was confirmed to be identical to the above-described in all respects.)

*Synthesis of [(N^C)AuL$_2$] [N^C = Benzo[h]quinoline, L = Phenylacetylene] (**3a**).* The reaction of **E** (0.085 g, 0.190 mmol) with phenylacetylene (0.048 mL, 0.430 mmol) following the general procedure yielded **3a** as an off-white solid after chromatographic purification. (neutral Al_2O_3; eluent, hexane/EtOAc = 2:1). Yield = 0.070 g, 64.0%. IR (KBr): ν(C≡C) 2135, 2160 cm^{-1}. ^1H NMR (500 MHz, CD_2Cl_2, 298 K): δ 7.34−7.44 (m, 6H), 7.64−7.68 (m, 4H), 7.57−7.82 (m, 3H), 7.87 (d, J = 8.0 Hz, 1H), 7.94 (d, J = 8.5 Hz, 1H), 8.37 (d, J = 7.0 Hz, 1H), 8.60 (d, J = 8.0 Hz, 1H), 9.81 (d, J = 5.5 Hz, 1H). $^{13}C\{^1H\}$ NMR (125 MHz, $CDCl_3$, 298 K): δ 78.3, 99.0, 103.6, 116.2, 122.9, 123.9, 125.8, 125.9, 127.0, 127.4, 128.2, 128.2, 128.4, 130.2, 130.8, 131.6, 131.7, 131.8, 133.5, 134.8, 140.5, 141.2, 149.7, 154.7, 155.7. Anal. Calc for $C_{29}H_{18}AuN$ (%): C, 60.32; H, 3.14; N, 2.43. Found: C, 60.23; H, 3.27; N, 2.33.

*Synthesis of [(N^C)AuL$_2$] [N^C = 2-(2-Thienyl)pyridine, L = 1-Ethynyl-4-fluorobenzene] (**4a**).* The reaction of **B** (0.10 g, 0.233 mmol) with 1-ethynyl-4-fluorobenzene (0.061 mL, 0.532 mmol) following the general procedure yielded **4a** as an off-white solid after chromatographic purfication (neutral Al_2O_3; eluent, hexane/EtOAc = 1:1). Yield = 0.08 g, 57%. IR (KBr): ν(C≡C) 2120, 2160 cm^{-1}. ^1H NMR (500 MHz, $CDCl_3$, 298 K): δ 7.05−7.10 (m, 4H), 7.36 (t, J = 8.5 Hz, 1H), 7.54−7.64 (m, 7H), 8.05 (t, J = 8.5 Hz, 1H), 9.43 (d, J = 8.0 Hz, 1H). $^{13}C\{^1H\}$ NMR (125 MHz, $CDCl_3$, 298 K): δ 99.0, 102.8, 112.5, 115.1, 115.3, 119.6, 121.7, 122.0, 122.4, 130.0, 133.0, 133.4, 133.5, 133.6, 133.7, 142.3, 145.7, 150.5, 160.3, 161.9 ($^1J_{C-F}$ = 245.0 Hz), 162.4 ($^1J_{C-F}$ = 245.0 Hz). ^{19}F NMR (282 MHz, CD_2Cl_2, 298 K): δ −115.1, −114.8. Anal. Calc for $C_{25}H_{14}AuF_2NS$ (%): C, 50.43; H, 2.37; N, 2.35. Found: C, 50.35; H, 2.38; N, 2.22.

*Synthesis of [(N^C)AuL$_2$] [N^C = 2-(5-Methyl-2-thienyl)pyridine, L = 1-Ethynyl-4-fluorobenzene] (**5a**).* The reaction of **C** (0.178 g, 0.402 mmol) with 1-ethynyl-4-fluorobenzene (0.105 mL, 0.924 mmol) following the general procedure, but worked up after 5 min after addition of CuI, yielded **5a** as an off-white solid after chromatographic purification (neutral Al_2O_3; eluent, hexane/EtOAc = 1:1). Yield = 0.10 g, 41%. Positive EI-MS: m/z 632.1 $[M + Na]^+$. IR (KBr): ν(C≡C) 2129, 2165 cm^{-1}. ^1H NMR (500 MHz, CD_2Cl_2, 298 K): δ 2.62 (s, 3H), 7.05−7.10 (m, 4H), 7.16 (s, 1H), 7.27 (t, J = 8.5 Hz, 1H), 7.47 (d, J = 8.5, 1H) 7.54−7.58 (m, 4H), 8.05 (t, J = 8.5 Hz, 1H), 9.34 (d, J = 5.5 Hz, 1H). $^{13}C\{^1H\}$ NMR (125 MHz, $CDCl_3$, 298 K): δ 15.4, 71.4, 98.9, 102.2, 113.0, 115.1, 115.3, 118.8, 121.5, 121.7, 121.9, 131.5, 133.4, 133.7, 142.1, 143.1, 146.0, 150.2, 160.4, 161.3, 161.7 ($^1J_{C-F}$ = 267 Hz), 162.0 ($^1J_{C-F}$ = 248 Hz). ^{19}F NMR (188 MHz, CD_2Cl_2, 298 K): δ −115.1, −114.7. Anal. Calc for $C_{26}H_{16}AuF_2NS$ (%): C, 51.24; H, 2.65; N, 2.30. Found: C, 51.15; H, 2.77; N, 2.18.

Computational Details. All calculations were performed with the Gaussian 03 program package[36] using the hybrid functional PBE1PBE[41] in conjunction with the Stuttgart/Dresden effective core potentials (SDD) basis set[42] for the Au center augmented with one f-polarization function (exponent α = 1.050) and the standard 6-31+G(d) basis set[43] for the remaining atoms. Full geometry optimizations without symmetry constraints were carried out in the gas phase for the singlet ground states (S_0) and the lowest triplet excited states (T_1). The optimized geometries were confirmed to be potential energy minima by vibrational frequency calculations at the same level of theory, because no imaginary frequency was found. The first 10 singlet−singlet and singlet−triplet transition energies were computed at the optimized S_0 geometries, by using the time-dependent DFT methodology.[37] Solvent effects were taken into account using the conductor-like polarizable continuum model (CPCM)[39] with dichloromethane as solvent for single-point calculations on all optimized gas-phase geometries.

X-ray Diffraction Analyses. Relevant details about the structure refinements are given in Tables S1 and S2 of the Supporting Information, and selected geometrical parameters are included in Table 1 and the captions of the corresponding figures (Figures S2−S4 in the Supporting Information). Intensity data were collected at 183(2) K on an Oxford Xcalibur diffractometer (four-circle kappa platform, Ruby CCD detector, and a single-wavelength Enhance X-ray source with Mo Kα radiation; λ = 0.710 73 Å)[44] The selected suitable single crystals were mounted using polybutene oil on the top of a glass fiber fixed on a goniometer head and immediately transferred to the diffractometer. Preexperiment, data collection, data reduction, and analytical absorption corrections were performed with the Oxford program suite CrysAlisPro.[45] The crystal structures were solved with SHELXS-97[46] using direct methods. The structure refinements were performed by full-matrix least squares on F^2 with SHELXL-97.[46] All programs used during the crystal structure determination process are included in the WINGX software.[47] The program PLATON[48] was used to check the result of the X-ray analyses. CCDC-798717-798723 contains the supplementary crystallographic data

(excluding structure factors) for this paper. These data can be obtained free of charge from The Cambridge Crystallographic Data Center via www.ccdc.cam.ac.uk/data_request/cif.

■ ASSOCIATED CONTENT

Supporting Information. Text describing synthetic details and spectroscopic data of **D**, XRD details, and computational details as well as a reference list, figures showing step 1 for **D**, thermogravimetric analysis of **1a** and **1b**, ORTEP plots of **1b**, **1c**, and **4a**, absorption and emission spectra of **1b**−**1e** and **2a**, cyclic voltammograms of **1a**, **1b**, and **1d**, spatial plots, energies, and compositions of frontier molecular orbitals, singlet HOMO and LUMO of the lowest triplet state of **1a**, and triplet spin density surfaces, and tables listing crystallographic details of all X-ray structures (Table S1 and Table S2), summary of interplanar Au−Au distances, summary of cyclic voltammetry, and computational details and X-ray crystallographic data for complexes **1a**−**1c**, **1e**, **3a**, **4a**, and **5a** (pdf). This material is available free of charge via the Internet at http://pubs.acs.org.

■ AUTHOR INFORMATION

Corresponding Author
*E-mail: venkatesan.koushik@aci.uzh.ch.

■ ACKNOWLEDGMENT

We thank S. V. Rocha and Dr. N. Finney for help with lifetime measurements. K.V. is grateful to the University of Zürich and Prof. H. Berke for generous support.

■ REFERENCES

(1) Yam, V. W.-W.; Cheung, K. L.; Yip, S. K.; Cheung, K. K. *J. Organomet. Chem.* **2003**, *681*, 196–209.
(2) Yam, V. W.-W.; Wong, K. M.-C.; Hung, L.-L.; Zhu, N. Y. *Angew. Chem., Int. Ed.* **2005**, *44*, 3107–3110.
(3) Vicente, J.; Chicote, M. T.; Alvarez-Falcon, M. M.; Bautista, D. *Organometallics* **2004**, *23*, 5707–5712.
(4) Irwin, M. J.; Vittal, J. J.; Puddephatt, R. J. *Organometallics* **1997**, *16*, 3541–3547.
(5) Vicente, J.; Chicote, M. T.; Alvarez-Falcon, M. M.; Abrisqueta, M. D.; Hernandez, F. J.; Jones, P. G. *Inorg. Chim. Acta* **2003**, *347*, 67–74.
(6) Vicente, J.; Chicote, M. T.; Alvarez-Falcon, M. M.; Jones, P. G. *Chem. Commun. (Cambridge, U.K.)* **2004**, 2658–2659.
(7) Schuster, O.; Schmidbaur, H. *Inorg. Chim. Acta* **2006**, *359*, 3769–3775.
(8) Yam, V. W.-W. *Acc. Chem. Res.* **2002**, *35*, 555–563.
(9) Vicente, J.; Gil-Rubio, J.; Barquero, N.; Jones, P. G.; Bautista, D. *Organometallics* **2008**, *27*, 646–659.
(10) Johnson, A.; Puddephatt., R. J.; Quirk, J. L. *J. Chem. Soc., Chem. Commun.* **1972**, 938–939.
(11) Johnson, A.; Puddephatt, R. J. *J. Chem. Soc., Dalton Trans.* **1977**, 1384–1388.
(12) Wong, K. M.-C.; Hung, L. L.; Lam, W. H.; Zhu, N. Y.; Yam, V. W.-W. *J. Am. Chem. Soc.* **2007**, *129*, 4350–4365.
(13) Wong, K. M.-C.; Zhu, X. L.; Hung, L.-L.; Zhu, N. Y.; Yam, V. W.-W.; Kwok, H.-S. *Chem. Commun. (Cambridge, U.K.)* **2005**, 2906–2908.
(14) Schuster, O.; Liau, R. Y.; Schier, A.; Schmidbaur, H. *Inorg. Chim. Acta* **2005**, *358*, 1429–1441.
(15) Schuster, O.; Schmidbaur, H. *Organometallics* **2005**, *24*, 2289–2296.
(16) Méndez, L. A.; Jiménez, J.; Cerrada, E.; Mohr, F.; Laguna, M. *J. Am. Chem. Soc.* **2005**, *127*, 852–853.
(17) Luquin, A.; Cerrada, E.; Laguna, M., *Gold Chemistry—Applications and Future Directions in the Life Sciences*. Wiley-VCH: Weinheim, Germany, 2009.
(18) Chan, C.-W.; Wong, W.-T.; Che, C.-M. *Inorg. Chem.* **1994**, *33*, 1266–1272.
(19) Au, V. K.-M.; Wong, K. M.-C.; Tsang, D. P.-K.; Chan, M.-Y.; Zhu, N.; Yam, V. W.-W. *J. Am. Chem. Soc.* **2010**, *132*, 14273–14278.
(20) Yam, V. W.-W.; Tang, R. P.-L.; Wong, K. M.-C.; Lu, X.-X.; Cheung, K.-K.; Zhu, N. *Chem.—Eur. J.* **2002**, *8*, 4066–4076.
(21) Garg, J. A.; Blacque, O.; Fox, T.; Venkatesan, K. *Inorg. Chem.* **2010**, *49*, 11463–11472.
(22) (a) Au, V. K.-M.; Wong, K. M.-C.; Zhu, N. Y.; Yam, V. W.-W. *Chem.—Eur. J.* **2011**, *17*, 130–142. (b) Yam, V. W.-W.; Choi, S. W.-K.; Lai, T.-F.; Lee, W.-T. *J. Chem. Soc., Dalton Trans.* **1993**, 1001–1002.
(23) Constable, E. C.; Leese, T. A. *J. Organomet. Chem.* **1989**, *363*, 419–424.
(24) Fuchita, Y.; Ieda, H.; Wada, S.; Kameda, S.; Mikuriya, M. *J. Chem. Soc., Dalton Trans.* **1999**, 4431–4435.
(25) Black, D. S.; Deacon, G. B.; Edwards, G. L.; Gatehouse, B. M. *Aust. J. Chem.* **1993**, *46*, 1323–1336.
(26) Parish, R. V.; Wright, J. P.; Pritchard, R. G. *J. Organomet. Chem.* **2000**, *596*, 165–176.
(27) Kresge, A. J.; Pruszynski, P. *J. Org. Chem.* **1991**, *56*, 4811–4815.
(28) Fernández, S.; Forniés, J.; Gil, B.; Gómez, J.; Lalinde, E. *Dalton Trans.* **2003**, 822–830.
(29) Henderson, W. *Adv. Organomet. Chem.*, **2006**, *54*, 207−265, and references therein.
(30) Tsuboyama, A.; Iwawaki, H.; Furugori, M.; Mukaide, T.; Kamatani, J.; Igawa, S.; Moriyama, T.; Miura, S.; Takiguchi, T.; Okada, S.; Hoshino, M.; Ueno, K. *J. Am. Chem. Soc.* **2003**, *125*, 12971–12979.
(31) Thomas, S. W., III; Venkatesan, K.; Müller, P.; Swager, T. M. *J. Am. Chem. Soc.* **2006**, *128*, 16641–16648.
(32) Tang, W.-S.; Lu, X.-X.; Wong, K. M.-C.; Yam, V. W.-W. *J. Mater. Chem.* **2005**, *15*, 2714–2720.
(33) Li, J.; Djurovich, P. I.; Alleyne, B. D.; Yousufuddin, M.; Ho, N. N.; Thomas, J. C.; Peters, J. C.; Bau, R.; Thompson, M. E. *Inorg. Chem.* **2005**, *44*, 1713–1727.
(34) Brooks, J.; Babayan, Y.; Lamansky, S.; Djurovich, P. I.; Tsyba, I.; Bau, R.; Thompson, M. E. *Inorg. Chem.* **2002**, *41*, 3055–3066.
(35) Au, V. K.-M.; Wong, K. M.-C.; Zhu, N. Y.; Yam, V. W.-W. *J. Am. Chem. Soc.* **2009**, *131*, 9076–9085.
(36) Frisch, M. J.; Trucks, G. W.; Schlegel, H. B.; Scuseria, G. E.; Rob, M. A.; Cheeseman, J. R.; Montgomery, J. A., Jr.; Vreven, T.; Kudin, K. N.; Burant, J. C.; Millam, J. M.; Iyengar, S. S.; Tomasi, J.; Barone, V.; Mennucci, B.; Cossi, M.; Scalmani, G.; Rega, N.; Petersson, G. A.; Nakatsuji, H.; Hada, M.; Ehara, M.; Toyota, K.; Fukuda, R.; Hasegawa, J.; Ishida, M.; Nakajima, T.; Honda, Y.; Kitao, O.; Nakai, H.; Klene, M.; Li, X.; Knox, J. E.; Hratchian, H. P.; Cross, J. B.; Bakken, V.; Adamo, C.; Jaramillo, J.; Gomperts, R.; Stratmann, R. E.; Yazyev, O.; Austin, A. J.; Cammi, R.; Pomelli, C.; Ochterski, J. W.; Ayala, P. Y.; Morokuma, K.; Voth, G. A.; Salvador, P.; Dannenberg, J. J.; Zakrzewski, V. G.; Dapprich, S.; Daniels, A. D.; Strain, M. C.; Farkas, O.; Malick, D. K.; Rabuck, A. D.; Raghavachari, K.; Foresman, J. B.; Ortiz, J. V.; Cui, Q.; Baboul, A. G.; Clifford, S.; Cioslowski, J.; Stefanov, B. B.; Liu, G.; Liashenko, A.; Piskorz, P.; Komaromi, I.; Martin, R. L.; Fox, D. J.; Keith, T.; Al-Laham, M. A.; Peng, C. Y.; Nanayakkara, A.; Challacombe, M.; Gill, P. M. W.; Johnson, B.; Chen, W.; Wong, M. W.; Gonzalez, C.; Pople, J. A. *Gaussian 03*; Gaussian: Wallingford, CT, 2003.
(37) (a) Stratmann, R. E.; Scuseria, G. E.; Frisch, M. J. *J. Chem. Phys.* **1998**, *109*, 8218–8224. (b) Bauernschmitt, R.; Ahlrichs, R. *Chem. Phys. Lett.* **1996**, *256*, 454–464. (c) Casida, M. E.; Jamorski, C.; Casida, K. C.; Salahub, D. R. *J. Chem. Phys.* **1998**, *108*, 4439–4449.
(38) Barone, V.; Cossi, M. *J. Phys. Chem. A* **1998**, *102*, 1995–2001.
(39) Cossi, M.; Rega, N.; Scalmani, G.; Barone, V. *J. Comput. Chem.* **2003**, *24*, 669–681.
(40) Demas, J. N.; Crosby, G. A. *J. Phys. Chem.* **1971**, *75*, 991–1024.
(41) Adamo, C.; Barone, V. *J. Chem. Phys.* **1999**, *110*, 6158–6170.

(42) Dunning, T. H., Jr.; Hay, P. J. In *Modern Theoretical Chemistry*; Schaefer, H. F., III, Ed.; Plenum: New York, 1976; Vol. 3, pp 1− 28.
(43) Ditchfield, R.; Hehre, W. J.; Pople, J. A. *J. Chem. Phys.* **1971**, *54*, 724–728.
(44) *Xcalibur CCD System*; Oxford Diffraction: Abingdon, Oxfordshire, England, 2007.
(45) *CrysAlisPro*, Versions 1.171.32.34d-55; Oxford Diffraction: Abingdon, Oxfordshire, England.
(46) Sheldrick, G. M. *Acta Crystallogr., Sect. A* **2008**, *64*, 112–122.
(47) Farrugia, L. J. *J. Appl. Crystallogr.* **1999**, *32*, 837–838.
(48) Spek, A. L. *J. Appl. Crystallogr.* **2003**, *36*, 7–13.

Syntheses and Photophysical Properties of Luminescent Monocyclometalated Gold(III) *cis*-Dialkynyl Complexes

*Jai Anand Garg, Olivier Blacque and Koushik Venkatesan**

Institute of Inorganic Chemistry, University of Zürich, Winterthurerstrasse 190, CH-8057, Zürich, Switzerland

Table of contents

Synthetic details and spectroscopic data.

(3,5-difluoro-2-(pyridin-2-yl)phenyl)mercury(II) chloride (step-1for **D**)

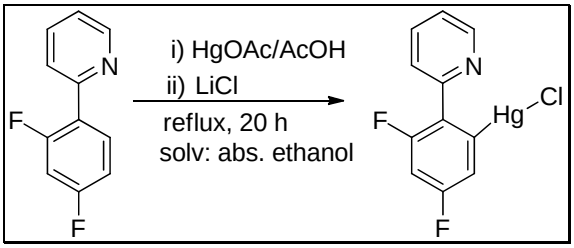

2-(2,4-difluorophenyl)pyridine (1.0 g, 5.23 mmol) in absolute ethanol (6.0 mL) was added to a stirred solution of mercuric acetate (1.8 g, 5.64 mmol) in ethanol (30.0 mL) containing acetic acid (0.4 mL). After being stirred at RT overnight, the reaction mixture was refluxed for 20 h, filtered hot and evaporated to dryness under reduced pressure. The residue thus obtained was re-dissolved in warm ethanol (15 mL) and filtered into a solution of lithium choride (0.554 g, 13.0 mmol) in ethanol (35 mL). The mixture was allowed to stand at RT overnight and filtered, the collected solids were finally washed with cold water (30.0 mL). Recrystallization from ethanol twice gave the title product as colorless needles, Yield = 0.25 g, 11%; IR (KBr): ν (Hg–Cl) 342 cm^{-1}; ^{1}H NMR (400 MHz, $CDCl_3$, 298 K): δ (ppm) = 6.81 - 6.87 (m, 1H), 7.07 (d, J = 4.0 Hz 1H), 7.34 - 7.37 (m, 1H), 7.78 (t, J = 7.8 Hz, 1H), 8.02 (d, J = 8.0 Hz, 1H), 8.61 (d, J = 4.8 Hz, 1H); ^{13}C NMR (125 MHz, $CDCl_3$, 298 K): δ (ppm) = 105.1, 120.5, 123.7, 125.1, 125.4, 138.2, 148.4, 151.7, 154.8, 162.5 (d, $^{1}J_{C\text{-}F}$ = 258.7 Hz), 163.0 (d, $^{1}J_{C\text{-}F}$ = 256.2 Hz); ^{19}F NMR (470 MHz, $CDCl_3$, 298 K): δ (ppm) = -108.3 (dd, $^{4}J_{Hg\text{-}F}$ = 248.0 Hz, $^{4}J_{F\text{-}F}$ = 8.0 Hz, 1F), -110.1 (dd, $^{4}J_{Hg\text{-}F}$ = 161.0 Hz, $^{4}J_{F\text{-}F}$ = 8.0 Hz, 1F); ^{199}Hg (89 MHz, rel. to Me_2Hg, $CDCl_3$, 298 K): δ (ppm) = -1000.0 (dd, $^{4}J_{Hg\text{-}F}$ = 248.0, 161.0 Hz).

Caution: Although we had no prior experience, mercuric chloride derivatives are potentially toxic and should be handled with care.

Thermogravimetric Analysis (TGA)

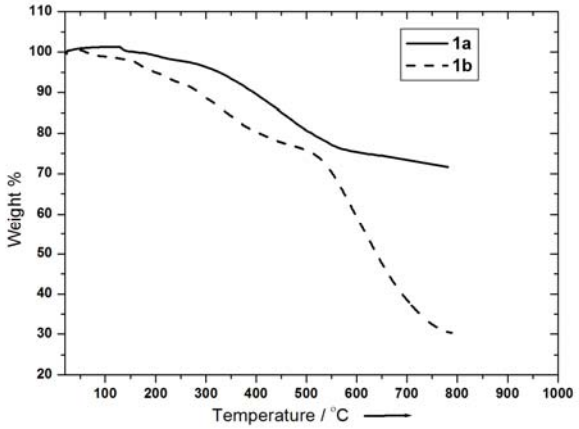

Figure S1. Thermal gravimetric traces of the complexes measured under N_2 atmosphere, rate of heating 5°C/min for **1a** and 1°C/min for **1b** from 25 °C to 800 °C.

X-ray diffraction studies of 1b, 1c and 4a.

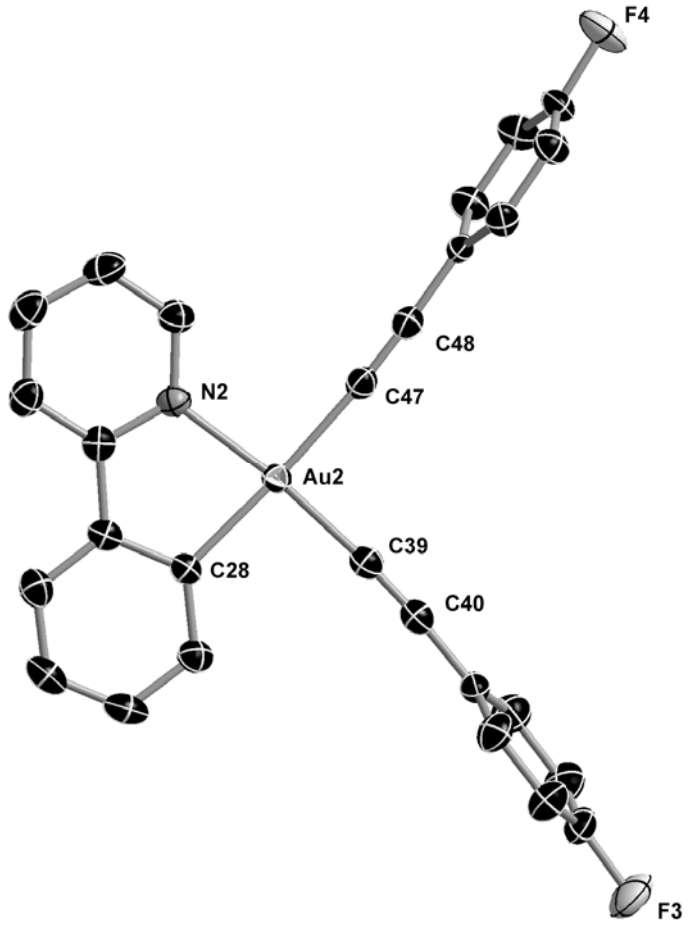

Figure S2. Thermal ellipsiod plot of **1b** (50% probability level of thermal ellipsoids) with selective atomic numbering scheme. Hydrogen atoms and solvent molecules are omitted for clarity. Selected bond lengths (Å) and angles (°): N(2)-Au(2) 2.068(2), C(28)-Au(2) 2.043(2), C(47)-Au(2) 2.031(2), C(39)-Au(2) 1.973(3), C(28)-Au(2)-N(2) 81.00(9), C(39)-Au(2)-C(47) 90.94(9), C(47)-Au(2)-N(2) 94.98(9), C(39)-Au(2)-C(28) 93.09(10).

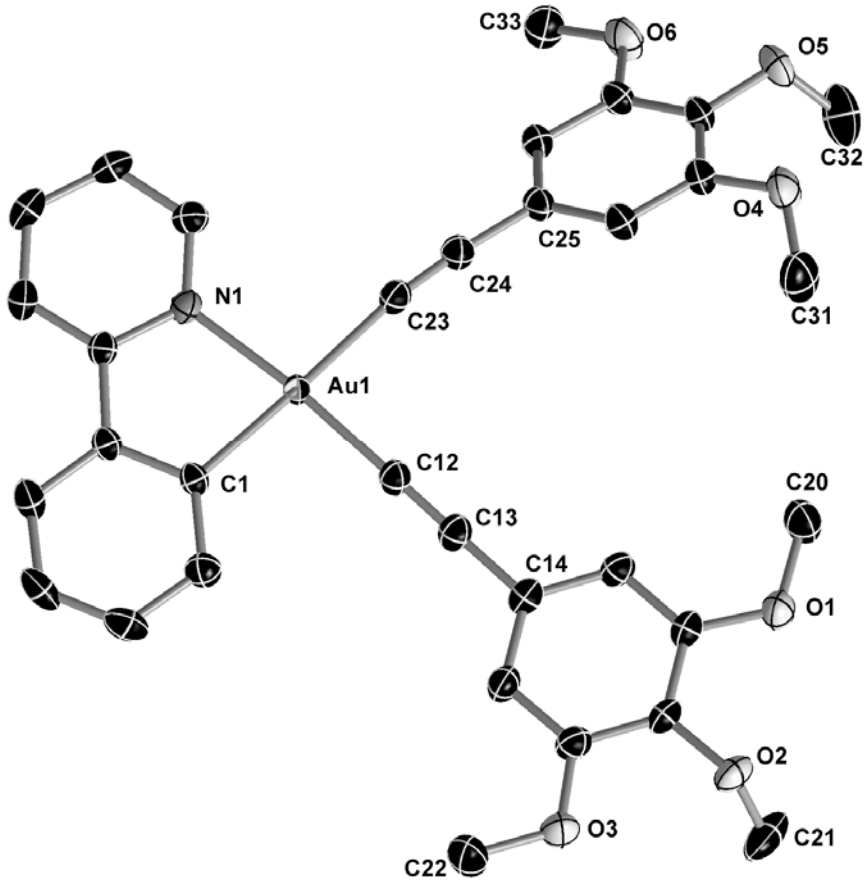

Figure S3. Thermal ellipsiod plot of **1c** (50% probability level of thermal ellipsoids) with selective atomic numbering scheme. Hydrogen atoms and solvent molecules are omitted for clarity. Selected bond lengths (Å) and angles (°): N(1)-Au(1) 2.0566(12), C(1)-Au(1) 2.0380(13), C(12)-Au(1) 1.9724(16), C(23)-Au(1) 2.0390(16), C(1)-Au(1)-N(1) 80.89(5), C(12)-Au(1)-C(1) 93.81(6), C(12)-Au(1)-C(23) 88.47(6), C(23)-Au(1)-N(1) 96.76(6).

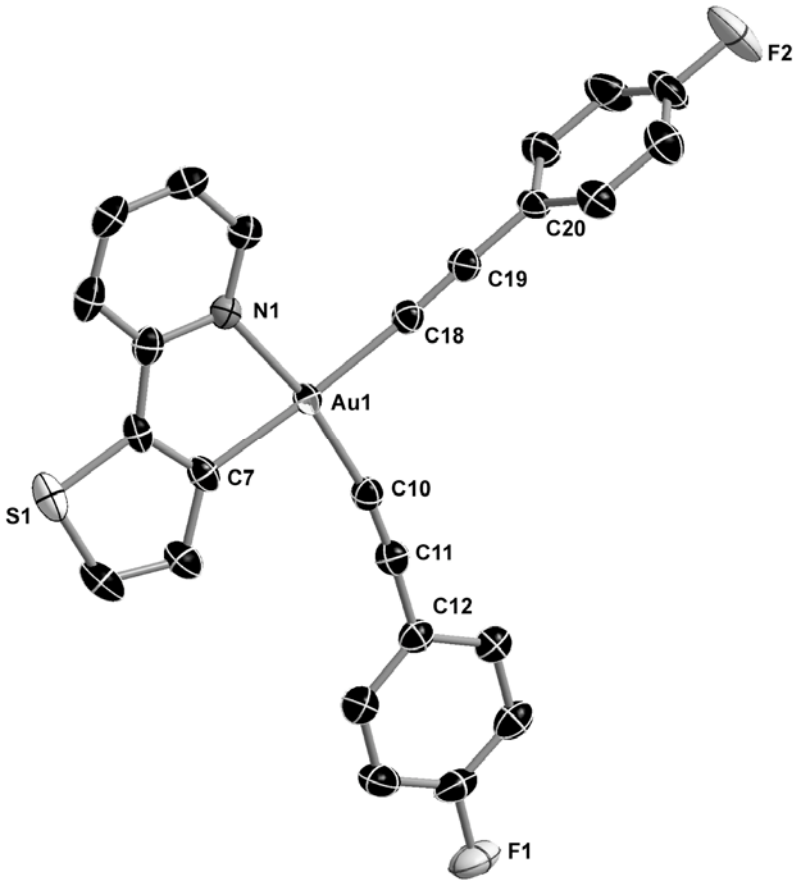

Figure S4. Thermal ellipsiod plot of **4a** (30% probability level of thermal ellipsoids) with selective atomic numbering scheme. Hydrogen atoms and solvent molecules are omitted for clarity. Selected bond lengths (Å) and angles (°): N(1)-Au(1) 2.084(3), C(7)-Au(1) 2.027(3), C(18)-Au(1) 2.033(3), C(10)-Au(1) 1.966(4), C(7)-Au(1)-N(1) 80.99(13), C(10)-Au(1)-C(18) 95.28(14), C(18)-Au(1)-N(1) 94.71(12), C(10)-Au(1)-C(7) 89.03(14).

Table S1. Crystallographic data for compounds **1a**, **1e**, **3a** and **5a**.

	1a	**1e**	**3a**	**5a**
empirical formula	$C_{27}H_{18}AuN$	$C_{33}H50AuNSi_2$	$C_{29}H_{18}AuN$	$2(C_{26}H_{16}AuF_2NS)$, CH_2Cl_2
formula weight ($g{\cdot}mol^{-1}$)	553.39	713.89	577.41	1303.80
temperature (K)	183(2)	183(2)	183(2)	183(2)
wavelength (Å)	0.71073	0.71073	0.71073	0.71073
crystal system, space group	monoclinic, *P* 2_1/c	triclinic, *P* -1	orthorhombic, *P* b c a	monoclinic, *P* 2_1/c
a (Å)	10.4792(2)	7.3589(2)	17.1690(2)	12.1145(1)
b (Å)	18.0604(2)	13.9624(4)	13.3040(1)	17.9931(1)
c (Å)	11.6604(2)	18.0915(4)	18.4488(1)	22.1153(2)
α (deg)	90	69.459(2)	90	90
β (deg)	109.518(2)	85.021(2)	90	99.232(1)
γ (deg)	90	76.161(2)	90	90
volume ($Å^3$)	2080.02(6)	1690.14(8)	4214.01(6)	4758.19(7)
Z, density (calcd) ($Mg{\cdot}m^{-3}$)	4, 1.767	2, 1.403	8, 1.820	4, 1.820
abs coefficient (mm^{-1})	7.085	4.443	6.998	6.414
F(000)	1064	724	2224	2504
crystal size (mm^3)	0.37 x 0.32 x 0.09	0.45 x 0.10 x 0.07	0.34 x 0.14 x 0.11	0.26 x 0.24 x 0.04
θ range (deg)	2.53 to 30.50	2.85 to 30.51	2.51 to 32.58	2.45 to 28.28
reflections collected	29969	31474	58657	69869
reflections unique	6351 / [R_{int} = 0.0310]	10324 / [R_{int} = 0.0357]	7663 / [R_{int} = 0.0374]	11791 / [R_{int} = 0.0428]
completeness to θ (%)	99.9	99.9	100.0	99.9
absorption correction	analytical	analytical	analytical	analytical
max/min transmission	0.551 and 0.130	0.777 and 0.224	0.499 and 0.182	0.793 and 0.293
data / restraints / parameters	5209 / 0 / 262	8324 / 0 / 492	5188 / 0 / 280	9001 / 0 / 588
goodness-of-fit on F^2	1.005	0.909	0.921	0.908
final R_1 and wR_2 indices [$I > 2\sigma(I)$]	0.0210, 0.0446	0.0269, 0.0436	0.0236, 0.0477	0.0243, 0.0401
R_1 and wR_2 indices (all data)	0.0312, 0.0459	0.0387, 0.0447	0.0463, 0.0500	0.0405, 0.0416

The unweighted R-factor is $R_1 = \sum(Fo - Fc)/\sum Fo$; $I > 2\,\sigma(I)$ *and the weighted R-factor is* $wR_2 = \{\sum w(Fo^2 - Fc^2)^2/\sum w(Fo^2)^2\}^{1/2}$

Table S2. Crystallographic data for compounds **1b**, **1c**, and **4a**.

	1b	**1c**	**4a**
empirical formula	$2(C_{27}H_{16}AuF_2N), CH_2Cl_2$	$C_{33}H_{30}AuNO_6$	$C_{25}H_{14}AuF_2NS$
formula weight ($g \cdot mol^{-1}$)	1263.68	733.55	595.41
temperature (K)	183(2)	183(2)	183(2)
wavelength (Å)	0.71073	0.71073	0.71073
crystal system, space group	triclinic, *P* -1	triclinic, *P* -1	triclinic, *P* -1
a (Å)	12.0324(2)	8.1641(1)	10.2423(2)
b (Å)	14.0679(3)	12.4453(2)	13.9037(2)
c (Å)	14.9710(3)	14.3191(2)	15.1281(2)
α (deg)	77.398(2)	93.756(1)	98.309(1)
β (deg)	71.229(2)	90.607(1)	103.044(1)
γ (deg)	72.866(2)	101.769(1)	95.233(1)
volume ($Å^3$)	2271.46(8)	1420.82(3)	2059.51(6)
Z, density (calcd) ($Mg \cdot m^{-3}$)	2, 1.848	2, 1.715	4, 1.920
abs coefficient (mm^{-1})	6.626	5.224	7.274
F(000)	1212	724	1136
crystal size (mm^3)	0.26 x 0.09 x 0.04	0.50 x 0.20 x 0.10	0.35 x 0.28 x 0.11
θ range (deg)	2.64 to 30.51	2.55 to 32.57	2.64 to 28.28
reflections collected	42000	50003	45341
reflections unique	13858 / [R_{int} = 0.0340]	10343 / [R_{int} = 0.0257]	10236 / [R_{int} = 0.0249]
completeness to θ (%)	99.9	100.0	99.9
absorption correction	analytical	analytical	analytical
max/min transmission	0.803 and 0.332	0.603 and 0.199	0.485 and 0.158
data / restraints / parameters	10032 / 0 / 586	9337 / 0 / 376	8762 / 35 / 541
goodness-of-fit on F^2	0.847	1.017	1.042
final R_1 and wR_2 indices [$I > 2\sigma(I)$]	0.0228, 0.0357	0.0157, 0.0361	0.0233, 0.0536
R_1 and wR_2 indices (all data)	0.0401, 0.0369	0.0192, 0.0364	0.0297, 0.0547

The unweighted R-factor is $R_1 = \sum(Fo - Fc)/\sum Fo$; $I > 2\,\sigma(I)$ and the weighted R-factor is $wR_2 = \{\sum w(Fo^2 - Fc^2)^2/\sum w(Fo^2)^2\}^{1/}$

X-ray diffraction details

Relevant details about the structure refinements are given in Tables S3 and S4, and selected geometrical parameters are included in the captions of the corresponding figures. Intensity data were collected at 183(2) K an Oxford Xcalibur diffractometer (4-circle kappa platform, Ruby CCD detector, and a single wavelength Enhance X-ray source with MoK_α radiation, λ = 0.71073 Å).[1] The selected suitable single crystals were mounted using polybutene oil on the top of a glass fiber fixed on a goniometer head and immediately transferred to the diffractometer. Pre-experiment, data collection, data reduction and analytical absorption corrections[2] were performed with the Oxford program suite *CrysAlisPro*.[3] The crystal structures were solved with SHELXS-97[4] using direct methods. The structure refinements were performed by full-matrix least-squares on F^2 with SHELXL-97.[4] All programs used during the crystal structure determination process are included in the WINGX software.[5] The program PLATON[6] was used to check the result of the X-ray analyses. CCDC-798717-798723 contain the supplementary crystallographic data (excluding structure factors) for this paper. These data can be obtained free of charge from The Cambridge Crystallographic Data Centre via www.ccdc.cam.ac.uk/data_request/cif.

In the crystal structure of **1e**, the phenylpyridine ligand is positionally disordered but only the N1 and C7 atoms were refined as disordered atoms, occupying the same fixed positions with identical thermal parameters. The Si^iPr_3 groups are also disordered over two positions with *sof* of about 0.5. The asymmetric unit of **4a** contains two crystallographically independent $C_{25}H_{14}AuF_2NS$ molecules. It seems that one thienylpyridine is slightly disordered over two sets of positions in an approximate ratio of 90/10 % which results in the observed positive residual peak of 2.25 e.Å^{-3} corresponding to the second position of the S2 atom. Nevertheless, we considered that the disorder is not enough to be refineable and reliable. All hydrogen positions were calculated after each cycle of refinement using a riding model, with C-H = 0.93 Å and $U_{iso}(H) = 1.2U_{eq}(C)$ for aromatic H atoms, with C-H = 0.98 Å and $U_{iso}(H) = 1.2U_{eq}(C)$ for methine H atoms, with C-H = 0.97 Å and $U_{iso}(H) = 1.2U_{eq}(C)$ for methylene H atoms, and with C-H = 0.96 Å and $U_{iso}(H) = 1.5U_{eq}(C)$ for methyl H atoms.

No classic hydrogen bonds were observed in any crystal structures.

Table S3. Summary of interplanar Au-Au distances of **1a-1c**, **1e**, **3a**, **4a** and **5a**.

Complex	Au-Au distance (Å)
[(N^C)Au(C≡CC_6H_5)$_2$] [N^C = 2-phenylpyridine] (**1a**)	6.7647(2) Å
[(N^C)Au(C≡CC_6H_4-4-F)$_2$] [N^C = 2-phenylpyridine] (**1b**)	4.7920(2) Å
[(N^C)Au(C≡C$C_9H_{11}O_3$)$_2$] [N^C = 2-phenylpyridine] (**1c**)	3.7285(1) Å
[(N^C)Au(C≡C-Si(*i*Pr)$_3$)$_2$] [N^C = 2-phenylpyridine] (**1e**)	5.2180(2) Å
[(N^C)Au(C≡CC_6H_5)$_2$] [N^C = benzo[*h*]quinoline] (**3a**)	7.6181(1) Å
[(N^C)Au(C≡CC_6H_4-4-F)$_2$] [N^C = 2-(2-thienyl)pyridine] (**4a**)	4.1468(2) Å
[(N^C)Au(C≡CC_6H_4-4-F)$_2$] [N^C = 2-(5-methyl-2-thienyl)pyridine] (**5a**)	4.3021(2) Å

Absorption and emission spectra of selected complexes (1b-1e and **2a).**

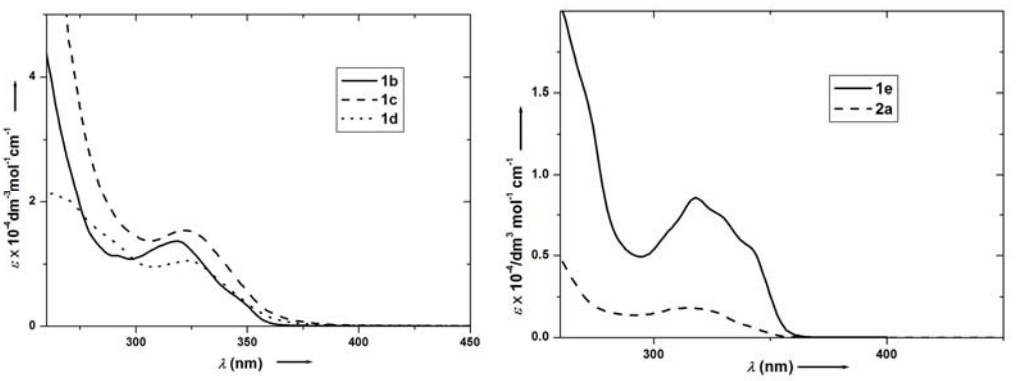

Figure S5. Electronic absorption spectra of **1b-1e** and **2a** in CH_2Cl_2 at RT.

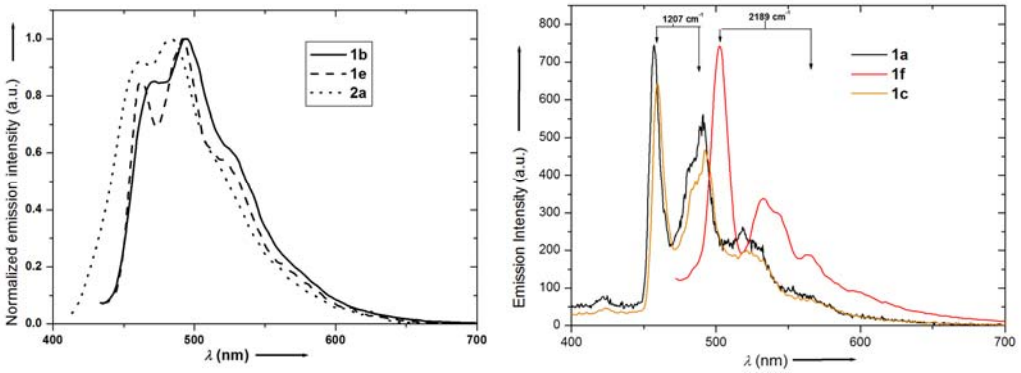

Figure S6. (*left*) Emission spectra of **1b**, **1e**, and **2a** in degassed CH_2Cl_2 at RT. (*right*) Emission spectra for selected compounds **1a**, **1c** and **1f** at 77 K in 2-MeTHF.

Cyclic voltammograms of selected complexes.

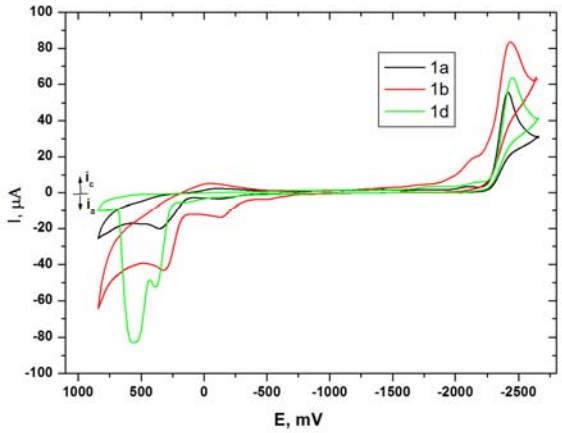

Figure S7. Cyclic voltammogram of **1a**, **1b** and **1d** in 0.1M [*n*Bu$_4$N][PF$_6$]; Au electrode; E *vs* Fc$^{0/+}$; scan rate = 100 mV/s; 20 ºC; CH_2Cl_2.

Electrochemical data of selected complexes.

Table S4. Summary of Cyclic Voltammetry for selected complexes in 0.1 M [*n*Bu$_4$N][PF$_6$]; Au electrode; E *vs* Fc$^{0/+}$; scan rate = 100 mV/s; 20 ºC, CH_2Cl_2.

Complex	Reduction $E_{p,c}$ (V)	Oxidation $E_{p,a}$ (V)
[(N^C)Au(C≡CC_6H_5)$_2$] [N^C = 2-phenylpyridine] (**1a**)	-2.41	0.36
[(N^C)Au(C≡CC_6H_4-4-F)$_2$] [N^C = 2-phenylpyridine] (**1b**)	-2.40	0.29
[(N^C)Au(C≡C$C_9H_{11}O_3$)$_2$] [N^C = 2-phenylpyridine] (**1c**)	-2.44	0.37, 0.56
[(N^C)Au(C≡CC_6H_4-C≡C-C_6H_5)$_2$] [N^C = 2-phenylpyridine] (**1f**)	-2.44	0.70
[(N^C)Au(C≡CC_6H_4-4-F)$_2$] [N^C = 2-(2-thienyl)pyridine] (**4a**)	-2.29	0.40
[(N^C)Au(C≡CC_6H_4-4-F)$_2$] [N^C = 2-(5-methyl-2-thienyl)pyridine] (**5a**)	-2.48	0.55

Computational details

All calculations were performed with the Gaussian 03 program package[7] using the hybrid functional PBE1PBE[8] in conjunction with the Stuttgart/Dresden effective core potentials (SDD) basis set[9] for the Au center augmented with one f-polarization function (exponent α = 1.050) and the standard 6-31+G(d) basis set[10] for the remaining atoms. Full geometry optimizations without symmetry constraints were carried out in the gas phase for the singlet ground states (S_0) and the lowest triplet excited states (T_1). The optimized geometries were confirmed to be potential energy minima by vibrational frequency calculations at the same level of theory, as no imaginary frequency was found. The first 10 singlet-singlet and singlet-triplet transition energies were computed at the optimized S_0 geometries, by using the time-dependent DFT (TDDFT) methodology.[11] Solvent effects were taken into account using the conductor-like polarizable continuum model (CPCM)[12] with dichloromethane as solvent for single-point calculations on all optimized gas-phase geometries.

Energies and cartesian coordinates of the optimized ground-state structure of 1a

C	2.51684542	0.53873569	0.00774091	C	-2.03489815	5.97807543	-1.15646118
C	2.93047213	1.86956258	0.01898991	H	-2.14142787	6.53504152	-2.08423425
H	2.18538548	2.65992303	0.01850191	C	-2.47948090	6.53036873	0.04472991
C	4.28838240	2.19119291	0.03135191	C	-2.34100726	5.80615156	1.22889301
H	4.59429496	3.23483684	0.03983591	H	-2.68726507	6.22840379	2.16915708
C	5.25467696	1.18451034	0.03312891	C	-1.76320086	4.54104019	1.21594900
H	6.31135915	1.43813682	0.04273091	H	-1.65806615	3.97304510	2.13596407
C	4.86264824	-0.14841256	0.02294891	C	-1.21715168	-1.04887152	-0.01903409
H	5.62414793	-0.92439001	0.02498191	C	-2.30866205	-1.60196100	-0.01689009
C	3.50032197	-0.47674389	0.01046991	C	-3.58402948	-2.24392140	-0.01468609
C	3.01366023	-1.85756575	-0.00029509	C	-4.31482461	-2.39098304	-1.20663318
C	3.81166870	-3.00583725	0.00027291	H	-3.89725238	-2.00292522	-2.13146126
H	4.89160483	-2.91045779	0.01016191	C	-5.55649002	-3.01803945	-1.20057518
C	3.22012302	-4.26072003	-0.01197909	H	-6.11028513	-3.12147217	-2.13059825
H	3.84080561	-5.15284342	-0.01160509	C	-6.09297034	-3.50887321	-0.01012009
C	1.83053285	-4.36668033	-0.02491609	C	-5.37714021	-3.36603757	1.17859300
H	1.32922132	-5.32860317	-0.03555209	H	-5.79038541	-3.74168138	2.11159507
C	1.08260539	-3.20020186	-0.02427009	C	-4.13487577	-2.74015516	1.17980200
H	-0.00378069	-3.19521630	-0.03344909	H	-3.57825867	-2.62212043	2.10542407
C	-0.21055826	1.57074817	-0.00706009	N	1.66157006	-1.99210306	-0.01181909
C	-0.71626474	2.67947451	-0.00334009	Au	0.60859590	-0.18987839	-0.00943509
C	-1.31064112	3.97697891	0.01072791	H	-2.93265843	7.51838403	0.05762891
C	-1.45514575	4.71373205	-1.17738618	H	-7.06434265	-3.99688575	-0.00837509
H	-1.11073994	4.28053584	-2.11231025				

After PCM corrections, the SCF energy is -1228.831304 a.u.

Zero-point correction=	0.365468 (Hartree/Particle)
Thermal correction to Energy=	0.390171
Thermal correction to Enthalpy=	0.391115
Thermal correction to Gibbs Free Energy=	0.304170
Sum of electronic and zero-point Energies=	-1228.436482
Sum of electronic and thermal Energies=	-1228.411779
Sum of electronic and thermal Enthalpies=	-1228.410835
Sum of electronic and thermal Free Energies=	-1228.497780

Energies and cartesian coordinates of the optimized ground-state structure of 1b

C	-1.90720300	-2.12569700	-0.02591400	C	-2.60516000	-4.46853900	-0.03032500
C	-3.24914800	-1.75076500	-0.05177600	H	-2.36706700	-5.52933400	-0.02383800
H	-3.50773700	-0.69598700	-0.06484900	C	-1.58955200	-3.50322800	-0.01757900
C	-4.25701800	-2.71602500	-0.06513000	C	-0.16630300	-3.84562400	0.00224100
H	-5.29927700	-2.40602600	-0.08620700	C	0.36272200	-5.13986300	0.01959200
C	-3.93705500	-4.07411700	-0.05336800	H	-0.30527100	-5.99386400	0.01853700
H	-4.72378400	-4.82364300	-0.06397300	C	1.73728200	-5.32639000	0.03905800

H	2.14804200	-6.33242600	0.05260500	C	1.45733600	0.14391600	-0.00857900
C	2.58215900	-4.21784000	0.04182100	C	2.51104500	0.76566000	0.00478000
H	3.66193500	-4.32065500	0.05779100	C	3.74604700	1.48105300	0.02660400
C	2.01046400	-2.95582100	0.02472100	C	4.22880400	2.04215900	1.22204400
H	2.59781300	-2.04192200	0.02694400	H	3.64433700	1.93189800	2.13064800
C	-1.28441000	0.72659600	-0.01792800	C	5.43429000	2.73448900	1.25204900
C	-1.92875000	1.76085500	-0.01270800	H	5.81462600	3.17242800	2.16988800
C	-2.67424100	2.97711700	-0.01475900	C	6.15664500	2.86452700	0.07503800
C	-3.79176900	3.13854900	0.82234500	C	5.71444700	2.32992800	-1.12598600
H	-4.08384300	2.32422300	1.47910700	H	6.30884400	2.45918400	-2.02534800
C	-4.51818900	4.32429000	0.82461600	C	4.50754500	1.63932000	-1.14459200
H	-5.38113100	4.46107500	1.46912900	H	4.14004700	1.21701600	-2.07534600
C	-4.12034700	5.34900800	-0.02114900	N	0.68182200	-2.78406900	0.00454800
C	-3.02372600	5.23015400	-0.86233600	F	-4.82320600	6.50015300	-0.02520500
H	-2.74548600	6.05862100	-1.50653100	F	7.32746300	3.53395400	0.09872500
C	-2.30186200	4.04199300	-0.85363500	Au	-0.25748500	-0.92127400	-0.0132660
H	-1.43609500	3.92738500	-1.49890800				

After PCM corrections, the SCF energy is -1426.138640 a.u.

Zero-point correction=	0.349042	(Hartree/Particle)
Thermal correction to Energy=	0.375415	
Thermal correction to Enthalpy=	0.376359	
Thermal correction to Gibbs Free Energy=	0.284598	
Sum of electronic and zero-point Energies=	-1426.759912	
Sum of electronic and thermal Energies=	-1426.733540	
Sum of electronic and thermal Enthalpies=	-1426.732596	
Sum of electronic and thermal Free Energies=	-1426.824357	

Energies and cartesian coordinates of the optimized ground-state structure of 1e

C	-1.37557800	2.99484000	-0.03636800	H	-6.42765500	-2.76122600	-1.03681900
C	-2.76779000	2.94073500	-0.06615900	H	-6.27603300	-2.64158200	-2.79616100
H	-3.26224400	1.97390400	-0.08342900	H	-5.40243100	-3.90119300	-1.92319000
C	-3.52551500	4.11252000	-0.07581500	C	-4.09745400	-1.72936100	2.73724300
H	-4.61122100	4.05167000	-0.09872700	H	-3.33338200	-0.94258300	2.76938800
C	-2.90030000	5.35971800	-0.05632000	H	-4.81198000	-1.53116000	3.54917400
H	-3.49240800	6.27093900	-0.06355400	H	-3.60116200	-2.68001300	2.96308900
C	-1.51323700	5.43542800	-0.02884000	C	-5.59774100	-0.45292200	1.17585100
H	-1.03663300	6.41250400	-0.01567900	H	-6.19030700	-0.46242400	0.25327900
C	-0.74806900	4.26138300	-0.01939200	H	-6.29242600	-0.28336600	2.01098400
C	0.71586400	4.26604200	0.00539000	H	-4.92455300	0.41321200	1.13268600
C	1.52829300	5.40401200	0.02711400	C	-3.71806100	-4.87864500	0.60930200
H	1.07484900	6.38878900	0.02706100	H	-4.63838200	-4.95532300	0.01827800
C	2.90887200	5.26966900	0.04895200	H	-3.23282100	-5.86473000	0.58977400
H	3.53982000	6.15439600	0.06569700	H	-4.01139300	-4.68609100	1.64916000
C	3.47611700	3.99667200	0.04959200	C	-1.47058500	-3.77458500	0.90937100
H	4.55057300	3.84803300	0.06623100	H	-1.66244200	-3.52525700	1.96044900
C	2.62961000	2.89985800	0.02800300	H	-0.98739700	-4.76233200	0.89365700
H	2.99140600	1.87540300	0.02822000	H	-0.75597700	-3.03934000	0.52601400
C	-1.43279500	0.07601900	-0.03781500	C	4.13613200	-4.62940800	-1.15713600
C	-2.31318900	-0.77575600	-0.04245500	H	3.74605800	-5.15532700	-0.27663000
C	1.37768400	0.01126500	-0.02060200	H	4.02628000	-5.31011300	-2.01311100
C	2.29720400	-0.80477000	-0.03026700	H	5.20989700	-4.47561400	-0.99749400
N	1.29713200	3.03788400	0.00590500	C	1.89752600	-3.59939000	-1.68934100
Au	-0.04924600	1.43917800	-0.02217800	H	1.34198600	-2.68107100	-1.90582200
Si	-3.60505000	-2.08505300	-0.06280600	H	1.79093500	-4.27520900	-2.55003900
Si	3.66839600	-2.02979600	-0.02407700	H	1.40664100	-4.08152800	-0.83529100
C	-4.52031800	-1.91138600	-1.73088100	C	2.42872900	-3.51864900	2.08373400
H	-4.89795800	-0.87645900	-1.72997200	H	2.16969300	-4.32462600	1.38765200
C	-4.80898600	-1.75008200	1.38044300	H	2.49591500	-3.96156400	3.08780500
H	-5.52559600	-2.58743500	1.38323700	H	1.59306600	-2.80822600	2.09053900
C	-2.76365400	-3.79696500	0.08812000	C	4.11950600	-1.79464300	2.78213500
H	-2.48781900	-4.06452800	-0.94474200	H	3.38009400	-0.98465400	2.82808400
C	3.37733200	-3.32011500	-1.40717900	H	4.15314500	-2.26380500	3.77579200
H	3.79961300	-2.85805900	-2.31420600	H	5.10189900	-1.34165700	2.60145900
C	5.27431700	-1.03922400	-0.34645700	C	5.24888600	-0.30926600	-1.69246600
H	5.28196400	-0.27367800	0.44667300	H	4.34525300	0.30039300	-1.81355300
C	3.74107500	-2.82194200	1.71010200	H	6.12108700	0.35211800	-1.79918200
H	4.53559400	-3.58480000	1.67078000	H	5.28094200	-1.01577800	-2.53201400
C	-3.57590900	-2.05131700	-2.92826800	C	6.55390200	-1.86919000	-0.20676900
H	-3.17093600	-3.06899600	-3.00462200	H	6.62541500	-2.62885400	-0.99552000
H	-4.10535500	-1.84534400	-3.86949300	H	7.44614600	-1.23297300	-0.29588900
H	-2.72794300	-1.36019200	-2.86180200	H	6.61562100	-2.38687000	0.75827100
C	-5.72083300	-2.85217200	-1.87105200				

After PCM corrections, the SCF energy is -2055.182849 a.u.

Zero-point correction=	0.753400	(Hartree/Particle)
Thermal correction to Energy=	0.800488	
Thermal correction to Enthalpy=	0.801432	

Thermal correction to Gibbs Free Energy= 0.667558
Sum of electronic and zero-point Energies= -2054.412867
Sum of electronic and thermal Energies= -2054.365780
Sum of electronic and thermal Enthalpies= -2054.364836
Sum of electronic and thermal Free Energies= -2054.498710

Energies and cartesian coordinates of the optimized ground-state structure of 4a

C	6.00963500	-1.64139500	-1.09482800	C	-0.10147200	-3.57723100	0.03372400
C	4.62461900	-1.51603900	-1.09930500	H	0.92021600	-3.20743400	0.02930800
C	-1.57220100	4.81815100	0.22860000	Au	-0.70003800	-0.55938800	-0.00522500
C	-1.48305300	6.20557000	0.22545200	C	-0.40850600	4.01538000	-0.03449700
F	8.05670400	-1.32221600	0.04729500	F	-0.12470600	8.13184700	-0.04768700
C	6.71328700	-1.20241200	0.03754100	C	-0.21708700	6.78681600	-0.04345800
H	-5.96784200	0.38696200	-0.03119100	C	6.08142400	-0.64350200	1.15992000
S	-4.98586100	-1.84715700	-0.00065500	C	4.69611300	-0.52280300	1.14474000
C	-5.01386900	-0.12691000	-0.02223700	C	0.85508500	4.64510600	-0.30242000
H	-2.03656200	-6.35123300	0.06751700	C	0.95665300	6.03140700	-0.30791900
H	-3.79459600	-4.59048900	0.04090800	H	4.05410000	-1.84886300	-1.97725200
H	-3.57152100	1.49286400	-0.03963200	H	6.54434100	-2.06989500	-1.95334100
C	-3.75688100	0.42476100	-0.02640000	H	6.67099600	-0.30915100	2.02381100
C	-1.75730400	-5.30102100	0.05440800	H	4.18087100	-0.08324200	2.01035300
C	-2.74195200	-4.32421500	0.03957300	H	1.75867400	4.03122300	-0.50645900
H	0.38371100	-5.66486300	0.06227600	H	1.92667300	6.52828000	-0.51328200
C	-3.25399000	-1.83637100	0.00516200	H	-2.37513500	6.83543400	0.42726100
C	-0.41269200	-4.92861900	0.05151100	H	-2.55353700	4.34279400	0.43674200
C	-2.37178100	-2.97548800	0.02238900	C	1.30449700	-0.72055900	0.00007700
C	3.94441400	-0.95770600	0.01833800	C	2.52265700	-0.83039400	0.00843000
C	-2.73246800	-0.55447900	-0.01012700	C	-0.56912200	1.37560800	-0.02241300
N	-1.05150000	-2.63510500	0.01999000	C	-0.49785100	2.59182600	-0.03128300

After PCM corrections, the SCF energy is -1747.834458 a.u.

Zero-point correction= 0.315629 (Hartree/Particle)
Thermal correction to Energy= 0.341637
Thermal correction to Enthalpy= 0.342581
Thermal correction to Gibbs Free Energy= 0.251743
Sum of electronic and zero-point Energies= -1747.491834
Sum of electronic and thermal Energies= -1747.465825
Sum of electronic and thermal Enthalpies= -1747.464881
Sum of electronic and thermal Free Energies= -1747.555719

Energies and cartesian coordinates of the optimized triplet-state structure of 1a

C	-2.32931600	1.08097300	-0.02929900	C	2.79782600	5.78010300	0.72357300
C	-2.45092800	2.45406500	-0.06556300	H	2.58294700	6.65021200	1.33930800
H	-1.55217500	3.06397100	-0.08863600	C	3.94287700	5.75320300	-0.07260500
C	-3.71205800	3.07361900	-0.07671600	C	4.21200000	4.63046900	-0.85579800
H	-3.78776400	4.15680400	-0.10876900	H	5.10379100	4.60129900	-1.47720700
C	-4.90514500	2.28410800	-0.04764800	C	3.34632800	3.54191300	-0.84572000
H	-5.87104100	2.78291800	-0.05490200	H	3.55451500	2.66403800	-1.45067600
C	-4.84639900	0.92393200	-0.01259100	C	0.94133700	-1.28747800	0.00055900
H	-5.76221500	0.34111700	0.00799900	C	1.89274400	-2.05773700	0.00966000
C	-3.55952700	0.25841000	-0.00468300	C	3.01052900	-2.94396200	0.04001500
C	-3.39340800	-1.11979400	0.02476300	C	4.00509200	-2.79964300	1.02378500
C	-4.43866600	-2.10282500	0.05252500	H	3.91001100	-2.00068100	1.75358000
H	-5.47093700	-1.76900900	0.05080200	C	5.09304600	-3.66504800	1.05973000
C	-4.14399500	-3.43807900	0.08099900	H	5.85335500	-3.54012000	1.82692100
H	-4.93676000	-4.17960400	0.10274700	C	5.21327600	-4.68660400	0.11710000
C	-2.78220000	-3.84093100	0.08379500	C	4.23482800	-4.83610700	-0.86586800
H	-2.49861800	-4.88728500	0.11114200	H	4.32391800	-5.62677900	-1.60702400
C	-1.78320800	-2.86370100	0.05384400	C	3.14273000	-3.97550300	-0.90632300
H	-0.72788100	-3.12517300	0.05480600	H	2.38276700	-4.08678600	-1.67510700
C	0.54930000	1.48261500	-0.03613100	N	-2.04990700	-1.56627400	0.02530400
C	1.29889500	2.44400600	-0.03855900	Au	-0.64782400	-0.05209100	-0.01243500
C	2.18779200	3.56033700	-0.04955400	H	6.06578000	-5.36044300	0.14667000
C	1.92611700	4.69627500	0.73604000	H	4.62259200	6.60153800	-0.08150100
H	1.03592500	4.71338600	1.35903700				

After PCM corrections, the SCF energy is -1228.730047 a.u.

Zero-point correction= 0.360972 (Hartree/Particle)
Thermal correction to Energy= 0.386274
Thermal correction to Enthalpy= 0.387219
Thermal correction to Gibbs Free Energy= 0.298482
Sum of electronic and zero-point Energies= -1228.340705
Sum of electronic and thermal Energies= -1228.315403
Sum of electronic and thermal Enthalpies= -1228.314459
Sum of electronic and thermal Free Energies= -1228.403195

Energies and cartesian coordinates of the optimized triplet-state structure of 1b

C	-2.49087700	-1.37244100	-0.02414900
C	-3.62924500	-0.59632900	-0.05304500
H	-3.53134200	0.48547400	-0.06901800
C	-4.90934300	-1.17865100	-0.06602200
H	-5.79490700	-0.55005500	-0.09191600
C	-5.05591100	-2.60124000	-0.04654600
H	-6.05425300	-3.03130000	-0.05489700
C	-3.96697500	-3.41833800	-0.01951400
H	-4.09545900	-4.49625700	-0.00629100
C	-2.63538200	-2.84542500	-0.01068200
C	-1.46626200	-3.59235000	0.00816100
C	-1.37189200	-5.02468400	0.02223500
H	-2.28650700	-5.60785000	0.01863300
C	-0.15348300	-5.64598300	0.03985400
H	-0.08498600	-6.72954900	0.05086900
C	1.02285700	-4.85175800	0.04487300
H	2.01108000	-5.29794300	0.06178200
C	0.90349300	-3.45814800	0.02961300
H	1.77674900	-2.81039800	0.03326000
C	-0.97106600	1.10570000	-0.01569400
C	-1.23489200	2.29569100	-0.01218900
C	-1.52557900	3.69223800	-0.02067700
C	-2.58526300	4.21489400	0.74083500
H	-3.18441200	3.54166000	1.34716600
C	-2.86923000	5.57620700	0.73264700
H	-3.68362500	5.99056900	1.31907100
C	-2.08506500	6.41388600	-0.04651500
C	-1.02936100	5.93918200	-0.81086500
H	-0.43880000	6.63060000	-1.40411100
C	-0.75227700	4.57693600	-0.79280500
H	0.07203200	4.18251700	-1.37938100
C	1.41894500	-0.35376200	0.00168900
C	2.61698500	-0.10451000	0.01100600
C	4.01426500	0.18450300	0.03026300
C	4.61494400	0.73911000	1.17424700
H	3.99974500	0.94968700	2.04395200
C	5.97601400	1.02170600	1.20182500
H	6.44879900	1.45083600	2.07997900
C	6.73593100	0.74789000	0.07413500
C	6.18260700	0.20463700	-1.07583000
H	6.81280400	0.01009000	-1.93829100
C	4.82048000	-0.07520200	-1.09217800
H	4.36549700	-0.49582400	-1.98428000
N	-0.26706800	-2.83910700	0.01184000
F	-2.35762800	7.73497600	-0.06003600
F	8.05695400	1.02027700	0.09602100
Au	-0.54687800	-0.79377600	-0.00735800

After PCM corrections, the SCF energy is -1427.036733 a.u.

Zero-point correction=	0.344538 (Hartree/Particle)
Thermal correction to Energy=	0.371524
Thermal correction to Enthalpy=	0.372469
Thermal correction to Gibbs Free Energy=	0.279165
Sum of electronic and zero-point Energies=	-1426.663955
Sum of electronic and thermal Energies=	-1426.636968
Sum of electronic and thermal Enthalpies=	-1426.636024
Sum of electronic and thermal Free Energies=	-1426.729328

Energies and cartesian coordinates of the optimized triplet-state structure of 1e

C	-1.36029800	2.97407900	-0.03254300
C	-2.73768900	2.93425600	-0.06101400
H	-3.23757100	1.97002300	-0.08423100
C	-3.50209000	4.11410700	-0.06036100
H	-4.58692600	4.06124200	-0.08183600
C	-2.85886300	5.39209600	-0.02859200
H	-3.46812600	6.29242100	-0.02560800
C	-1.50136500	5.49353300	-0.00249000
H	-1.02993800	6.47132000	0.02110600
C	-0.68844700	4.29302900	-0.00813100
C	0.69943700	4.29135200	0.00490500
C	1.54965300	5.44759600	0.02560400
H	1.09361400	6.43190600	0.03066100
C	2.91082900	5.31594400	0.03854800
H	3.55195700	6.19204600	0.05400900
C	3.47402100	4.01256300	0.03154500
H	4.54715300	3.85647200	0.04179300
C	2.62344900	2.90268300	0.01059300
H	3.00965200	1.88622600	0.00534500
C	-1.42276800	0.06835100	-0.04117000
C	-2.30876200	-0.77810900	-0.04256600
C	1.38765000	0.01055600	-0.03767600
C	2.30495300	-0.80818900	-0.04885900
N	1.30352200	3.01098400	-0.00336200
Au	-0.03598700	1.43537100	-0.02948100
Si	-3.61056700	-2.07632400	-0.06331500
Si	3.66073800	-2.04917700	-0.02446800
C	-4.53749300	-1.87849800	-1.72273800
H	-4.90325800	-0.83922400	-1.71009600
C	-4.80428700	-1.74273900	1.39008400
H	-5.52681700	-2.57491200	1.39513500
C	-2.78701000	-3.79801100	0.06593300
H	-2.52118700	-4.06002500	-0.97083400
C	3.35496900	-3.37009900	-1.37678400
H	3.81207400	-2.95184700	-2.28815100
C	5.28117100	-1.09213200	-0.36800000
H	5.31552700	-0.32485500	0.42248400
C	3.71994300	-2.80868600	1.72548500
H	4.48376600	-3.60264200	1.69509500
C	-3.60361000	-2.01960400	-2.92796000
H	-3.21193900	-3.04160600	-3.01587500
H	-4.13642700	-1.79871000	-3.86388700
H	-2.74651300	-1.33999300	-2.86021900
C	-5.74980600	-2.80428800	-1.86079800
H	-6.44779400	-2.71467000	-1.01890200
H	-6.31189500	-2.57901100	-2.77836800
H	-5.44351100	-3.85614500	-1.92633800
C	-4.08342800	-1.73113100	2.74192800
H	-3.31280900	-0.95070500	2.77073600
H	-4.79039900	-1.53030500	3.55984500
H	-3.59266300	-2.68626100	2.96080100
C	-5.58620200	-0.44046700	1.19326400
H	-6.18491900	-0.44599200	0.27456900
H	-6.27416500	-0.26721600	2.03328300
H	-4.90774500	0.42146400	1.14627900
C	-3.74813500	-4.87410700	0.58621600
H	-4.67273800	-4.94023900	0.00070300
H	-3.27162800	-5.86427000	0.55803700
H	-4.03292300	-4.68522100	1.62905600
C	-1.48883900	-3.79563800	0.87941300
H	-1.67183500	-3.54893600	1.93270100
H	-1.01803400	-4.78918900	0.85591700
H	-0.76766000	-3.06713400	0.49596500
C	4.06377200	-4.69473600	-1.06810300
H	3.63859200	-5.17746800	-0.17915700
H	3.94840500	-5.39953000	-1.90364000
H	5.13863800	-4.57098700	-0.89078100
C	1.87275200	-3.60960600	-1.68018300
H	1.35447600	-2.68316500	-1.94849100
H	1.75942500	-4.31867500	-2.51285900
H	1.34781200	-4.03504100	-0.81644100
C	2.38434000	-3.44665000	2.12045100
H	2.08206900	-4.24418300	1.43210200
H	2.44512200	-3.88581500	3.12655600
H	1.58032100	-2.70070400	2.13196800
C	4.14610400	-1.77679300	2.77463200
H	3.43991100	-0.93698400	2.80916800
H	4.16765300	-2.22719000	3.77731300
H	5.14457500	-1.36727600	2.57877000
C	5.25704600	-0.36634400	-1.71626100
H	4.36964100	0.26849400	-1.82646000
H	6.14602100	0.26963100	-1.83746000
H	5.25683000	-1.07607200	-2.55380800
C	6.54178200	-1.95260500	-0.24079600
H	6.58377400	-2.71708600	-1.02708800
H	7.44813800	-1.33898800	-0.34469900
H	6.60351700	-2.46741000	0.72586100

After PCM corrections, the SCF energy is -2055.081668   a.u.

Zero-point correction=	0.749661 (Hartree/Particle)
Thermal correction to Energy=	0.797031
Thermal correction to Enthalpy=	0.797975
Thermal correction to Gibbs Free Energy=	0.664589
Sum of electronic and zero-point Energies=	-2054.316329
Sum of electronic and thermal Energies=	-2054.268959
Sum of electronic and thermal Enthalpies=	-2054.268014
Sum of electronic and thermal Free Energies=	-2054.401401

Energies and cartesian coordinates of the optimized triplet-state structure of 4a

C	5.70742900	-2.26398800	-1.20693600	C	-0.82667800	-3.45571100	0.00013400
C	4.37815500	-1.85607100	-1.20481100	H	0.25027500	-3.30878100	-0.00246900
C	-0.52710100	5.04535700	0.04446900	Au	-0.80058300	-0.39464300	-0.00628500
C	-0.15243000	6.38416200	0.05310100	C	0.43693400	4.02352900	0.00240600
F	7.60661500	-2.94706000	0.00898100	F	1.56802500	7.99247400	0.02617100
C	6.31769100	-2.54951300	0.00549600	C	1.19884000	6.69552300	0.01825800
H	-5.76598800	1.58147600	-0.01380800	C	5.64708300	-2.43877300	1.21460600
S	-5.30123100	-0.85649500	-0.00320100	C	4.31805900	-2.02992100	1.20532400
C	-4.94312300	0.87699900	-0.01055400	C	1.79598900	4.38299200	-0.03191500
H	-3.27495300	-5.82655800	0.01009600	C	2.18255100	5.71826700	-0.02437100
H	-4.66247300	-3.76439900	0.00666300	H	3.88131500	-1.62362400	-2.14212700
H	-3.18669100	2.17217800	-0.01611400	H	6.27040100	-2.35998100	-2.13033900
C	-3.57134600	1.15781700	-0.01156300	H	6.16412600	-2.66816800	2.14137700
C	-2.80800200	-4.84610300	0.00687400	H	3.77503900	-1.93208100	2.14077700
C	-3.57760100	-3.70942900	0.00503000	H	2.54730500	3.59963100	-0.06432500
H	-0.75649300	-5.59822500	0.00493800	H	3.22893100	6.00667500	-0.05064200
C	-3.58704900	-1.19578900	-0.00237200	H	-0.88893300	7.18115100	0.08620500
C	-1.40007100	-4.72531700	0.00419300	H	-1.57999500	4.78022800	0.07188400
C	-2.95449000	-2.42916500	0.00076900	C	1.12656500	-0.95773700	-0.00766800
C	3.66066500	-1.73416300	-0.00181800	C	2.29555200	-1.31729300	-0.00645200
C	-2.76953300	0.03689500	-0.00707900	C	-0.27208900	1.47564900	-0.00732800
N	-1.55474500	-2.34221500	-0.00107200	C	0.05321900	2.64977800	-0.00500400

After PCM corrections, the SCF energy is -1747.750875   a.u.

Zero-point correction=	0.311962 (Hartree/Particle)
Thermal correction to Energy=	0.337584
Thermal correction to Enthalpy=	0.338528
Thermal correction to Gibbs Free Energy=	0.250152
Sum of electronic and zero-point Energies=	-1747.412256
Sum of electronic and thermal Energies=	-1747.386634
Sum of electronic and thermal Enthalpies=	-1747.385690
Sum of electronic and thermal Free Energies=	-1747.474067

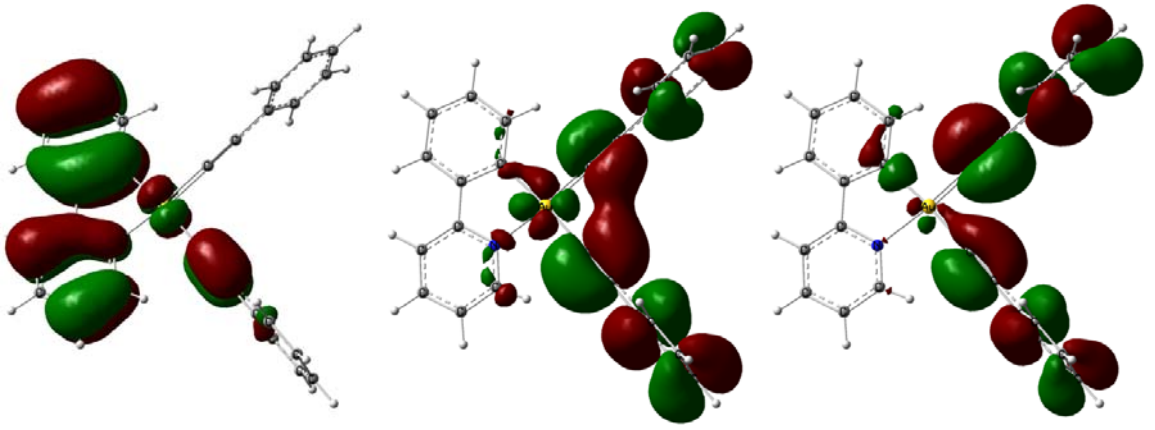

HOMO -2 HOMO -1 HOMO

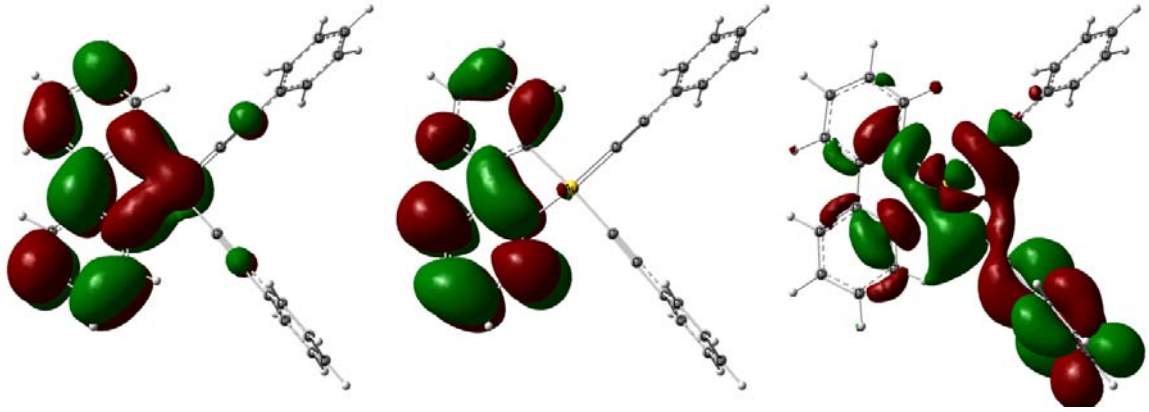

LUMO LUMO +1 LUMO +2

Energy (eV)		Composition (%)		
		ppy	Au	$(C{\equiv}CR)_2$
L+2	-1.00	16	25	59
L+1	-1.35	100	0	0
LUMO	-2.13	92	7	1
HOMO	-6.38	2	1	97
H-1	-6.46	2	5	93
H-2	-6.90	87	4	9

Figure S8. Spatial plots, energies (eV) and compositions (%) of selected frontier molecular orbitals of the ground-state of **1a**.

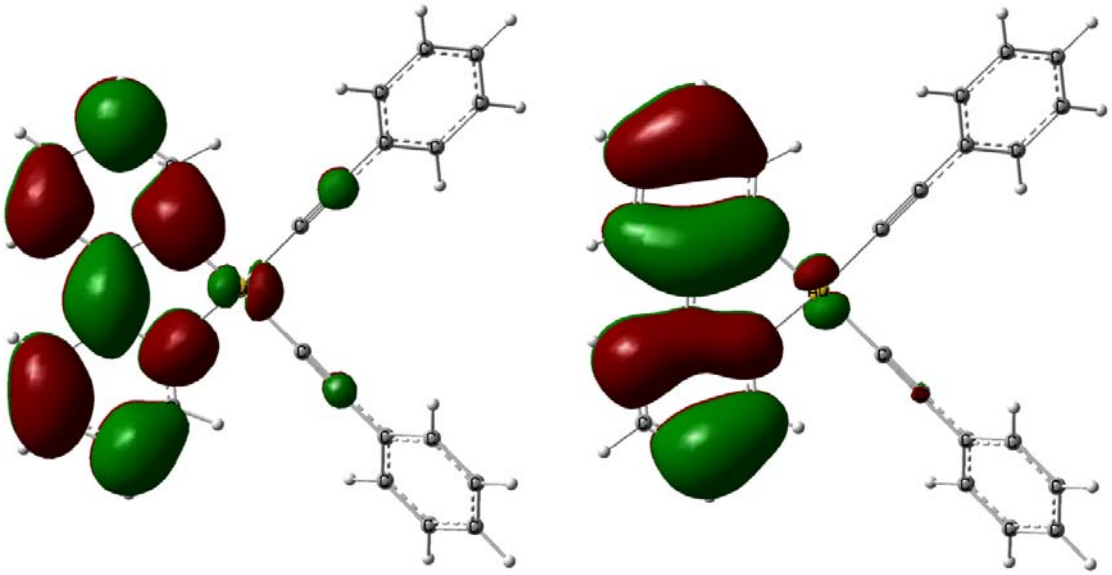

Figure S9. Singlet HOMO (top left) and singlet LUMO (top right) of the lowest triplet state of **1a**.

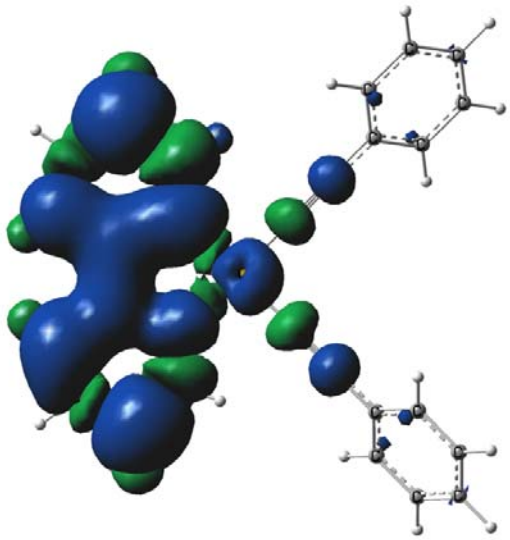

Figure S10. Triplet spin density surface of the lowest triplet state of **1a**.

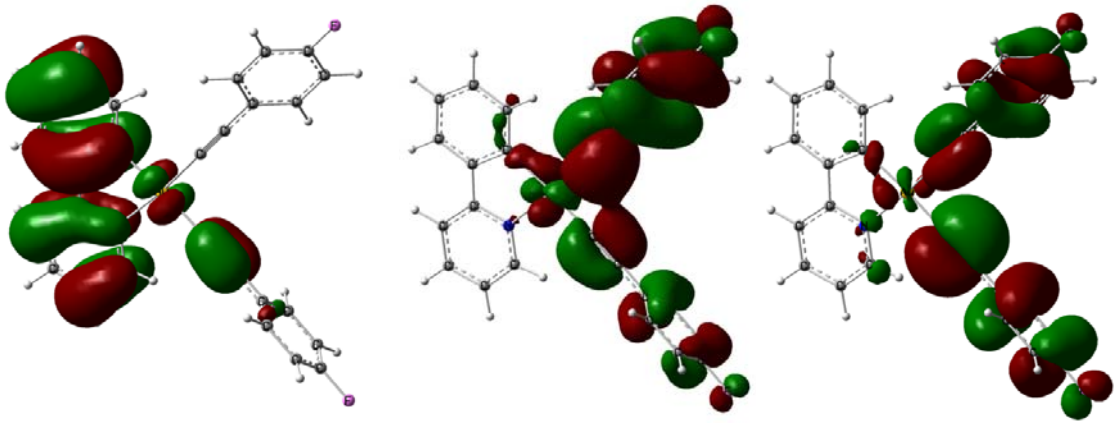

HOMO -2 HOMO -1 HOMO

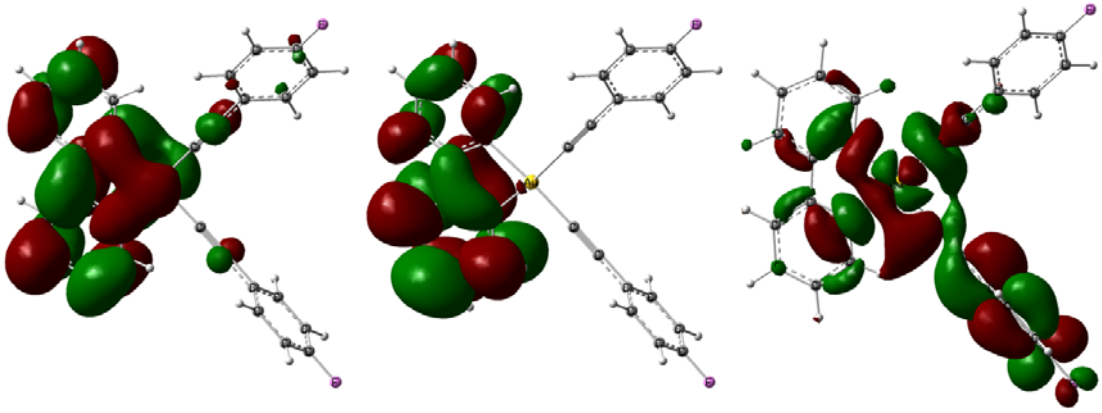

LUMO LUMO +1 LUMO +2

Energy (eV)		Composition (%)		
		ppy	Au	$(C{\equiv}CR)_2$
L+2	-1.01	22	28	50
L+1	-1.37	99	0	1
LUMO	-2.16	92	7	2
HOMO	-6.41	1	2	97
H-1	-6.46	1	5	94
H-2	-6.92	88	4	8

Figure S11. Spatial plots, energies (eV) and compositions (%) of selected frontier molecular orbitals of the ground-state of **1b**.

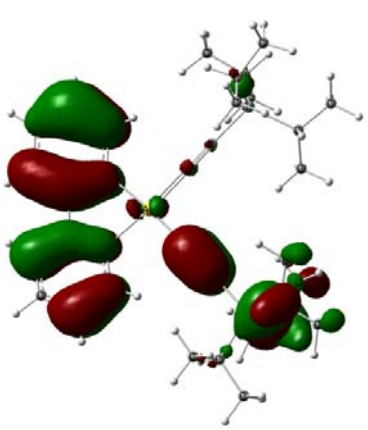

HOMO -4

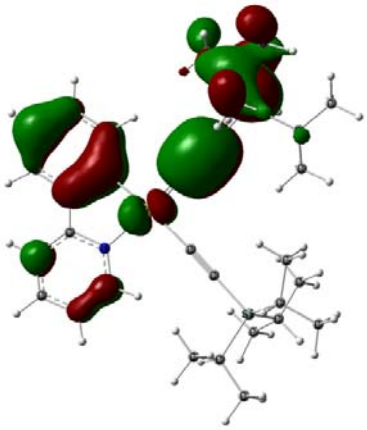

HOMO -3

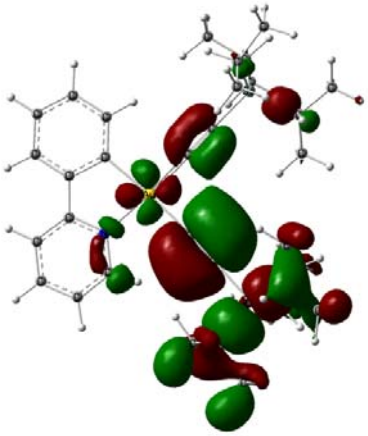

HOMO-2

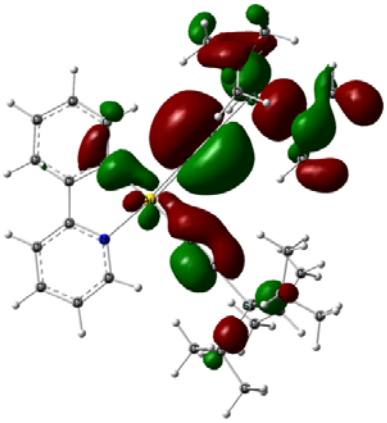

HOMO-1

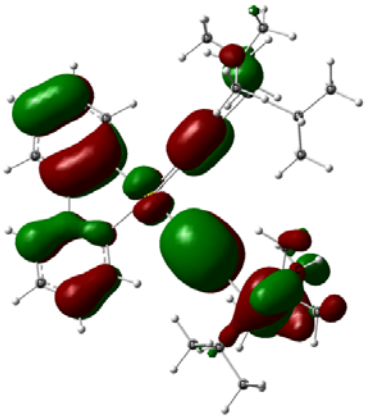

HOMO

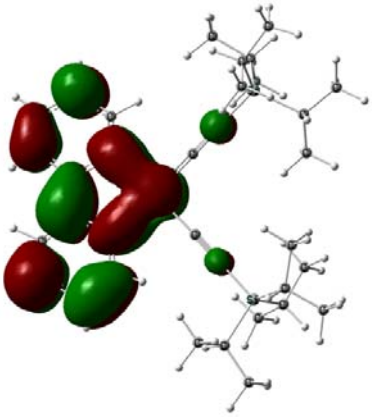

LUMO

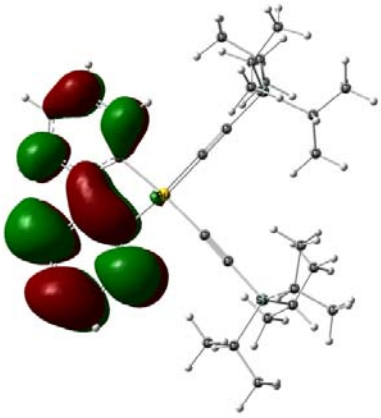

LUMO+1

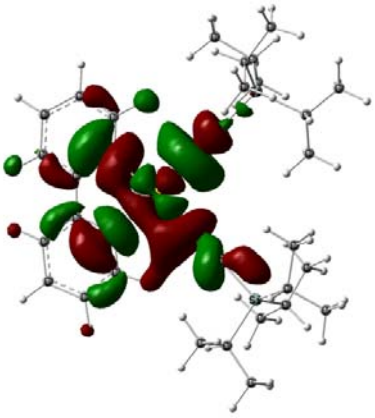

LUMO+2

Energy (eV)		Composition (%)		
		ppy	Au	$(C{\equiv}CR)_2$
L+2	-0.73	27	43	30
L+1	-1.35	100	0	0
LUMO	-2.12	92	7	1
HOMO	-6.75	28	6	66
H-1	-6.77	4	2	94
H-2	-6.86	1	5	94
H-3	-6.89	18	4	78
H-4	-7.01	67	1	32

Figure S12. Spatial plots, energies (eV) and compositions (%) of selected frontier molecular orbitals of the ground-state of **1e**.

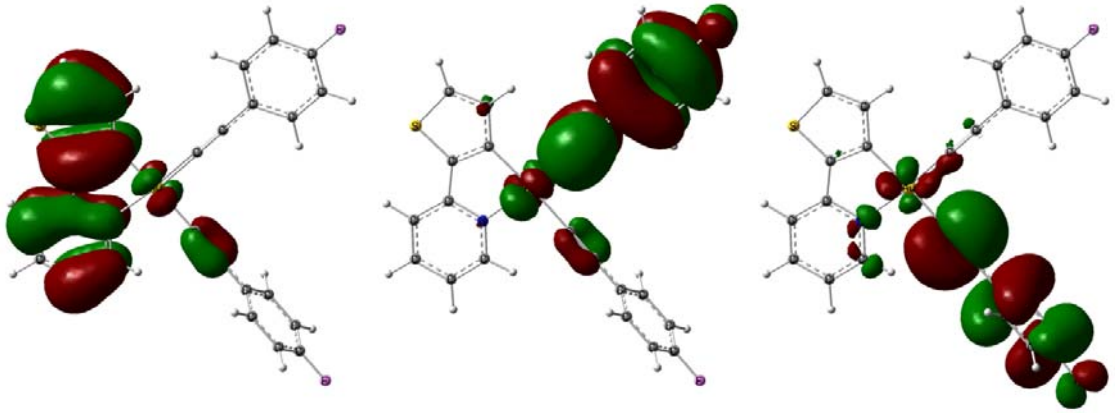

HOMO -2 HOMO -1 HOMO

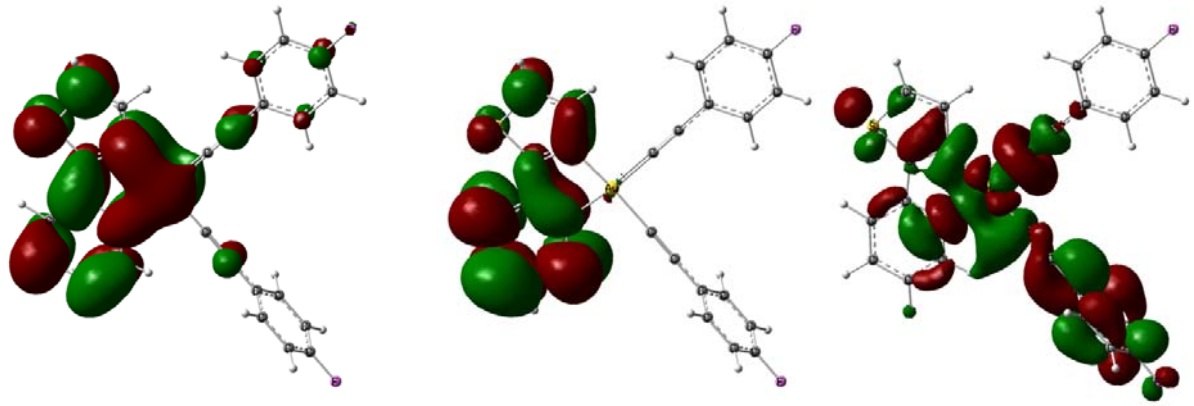

LUMO LUMO +1 LUMO +2

Orbital	Energy (eV)	MO composition (%)		
		thpy	Au	$(C{\equiv}CR)_2$
L+2	-1.13	25	30	45
L+1	-1.35	100	0	0
LUMO	-2.25	88	8	4
HOMO	-6.44	1	2	97
H-1	-6.54	2	4	94
H-2	-6.60	94	2	4

Figure S13. Spatial plots, energies (eV) and compositions (%) of selected frontier molecular orbitals of the ground-state of **4a**.

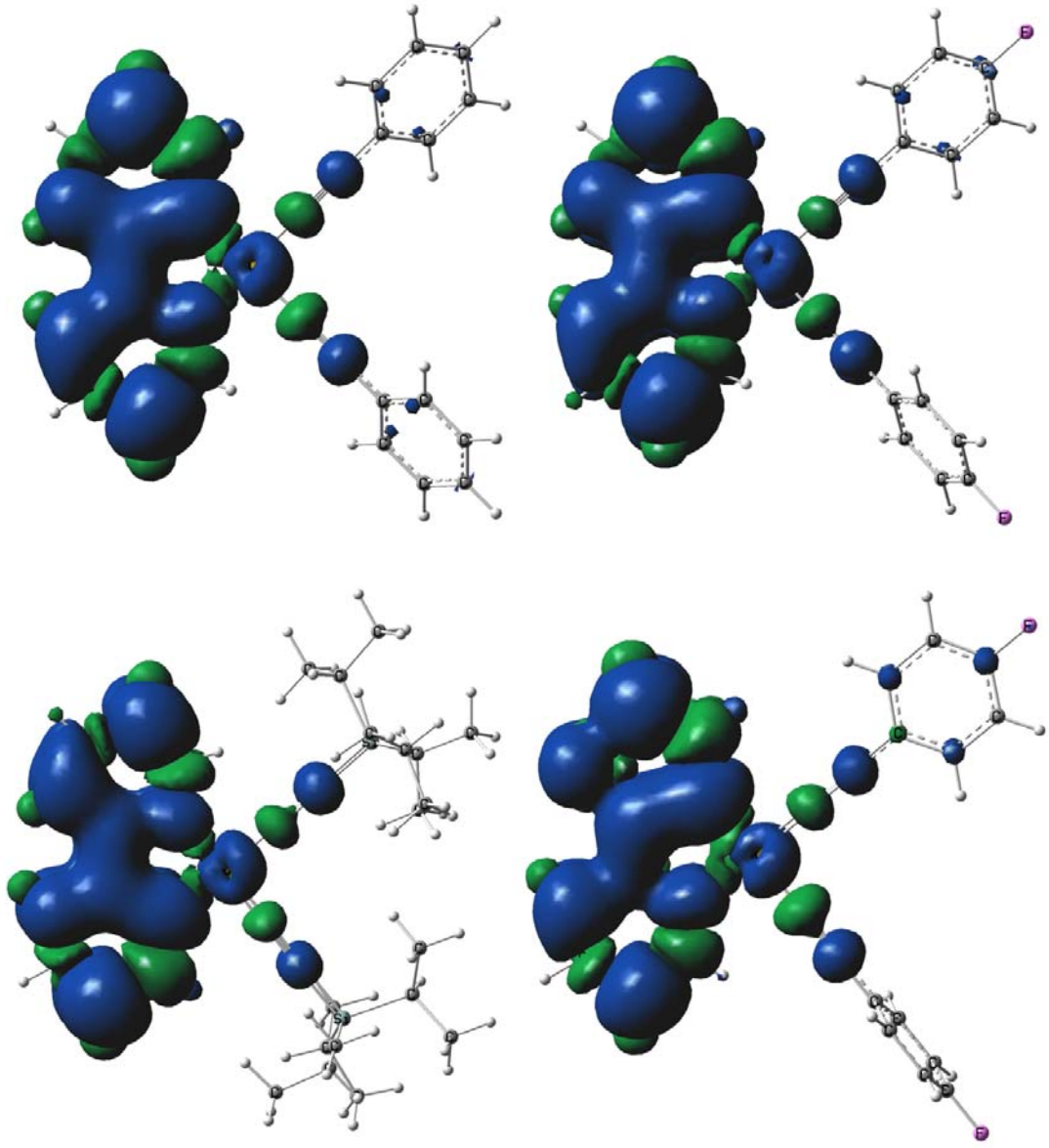

Figure S14. Triplet spin density surfaces of the lowest triplet state of **1a** (top left), **1b** (top right), **1e** (bottom left), and **4a** (bottom right).

References

[1] Xcalibur CCD System; Oxford Diffraction Ltd: Abingdon, Oxfordshire, England, 2007.

[2] Clark, R. C.; Reid, J. S. *Acta Cryst.* **1995**, *A51*, 887-897.

[3] *CrysAlisPro* (versions 1.171.32.55), Oxford Diffraction Ltd, Abingdon, Oxfordshire, England.

[4] Sheldrick, G. M. *Acta Cryst.* **2008**, *A64*, 112-122.

[5] Farrugia, L. J. *J. Appl. Cryst.* **1999**, *32*, 837.

[6] Spek, A. L. *J. Appl. Cryst.* **2003**, *36*, 7-13.

[7] Frisch, M. J.; Trucks, G. W.; Schlegel, H. B.; Scuseria, G. E.; Rob, M. A.; Cheeseman, J. R.; Montgomery Jr., J. A.; Vreven, T.; Kudin, K. N.; Burant, J. C.; Millam, J. M.; Iyengar, S. S.; Tomasi, J.; Barone, V.; Mennucci, B.; Cossi, M.; Scalmani, G.; Rega, N.; Petersson, G. A.; Nakatsuji, H.; Hada, M.; Ehara, M.; Toyota, K.; Fukuda, R.; Hasegawa, J.; Ishida, M.; Nakajima, T.; Honda, Y.; Kitao, O.; Nakai, H.; Klene, M.; Li, X.; Knox, J. E.; Hratchian, H. P.; Cross, J. B.; Bakken, V.; Adamo, C.; Jaramillo, J.; Gomperts, R.; Stratmann, R. E.; Yazyev, O.; Austin, A. J.; Cammi, R.; Pomelli, C.; Ochterski, J. W.; Ayala, P. Y.; Morokuma, K.; Voth, G. A.; Salvador, P.; Dannenberg, J. J.; Zakrzewski, V. G.; Dapprich, S.; Daniels, A. D.; Strain, M. C.; Farkas, O.; Malick, D. K.; Rabuck, A. D.; Raghavachari, K.; Foresman, J. B.; Ortiz, J. V.; Cui, Q.; Baboul, A. G.; Clifford, S.; Cioslowski, J.; Stefanov, B. B.; Liu, G.; Liashenko, A.; Piskorz, P.; Komaromi, I.; Martin, R. L.; Fox, D. J.; Keith, T.; Al-Laham, M. A.; Peng, C. Y.; Nanayakkara, A.; Challacombe, M.; Gill, P. M. W.; Johnson, B.; Chen, W.; Wong, M. W.; Gonzalez, C.; Pople, J. A. Gaussian 03 (Gaussian, Inc., Wallingford, CT, **2003**).

[8] Adamo, C.; Barone, V. *J. Chem. Phys.* **1999**, *110*, 6158.

[9] Dunning Jr, T. H.; Hay, P. J. *Modern Theoretical Chemistry*; Schaefer, H. F., III, Ed.; Plenum: New York, **1976**; Vol. 3, pp 1− 28.

[10] Ditchfield, R.; Hehre, W. J.; Pople, J. A. *J. Chem. Phys.* **1971**, *54*, 724.

[11] a) Stratmann, R. E.; Scuseria, G. E.; Frisch, M. J. *J. Chem. Phys.* **1998**, 109, 8218-24; b) Bauernschmitt, R.; Ahlrichs, R. *Chem. Phys. Lett.* **1996**, *256*, 454-64; c) Casida, M. E.; Jamorski, C.; Casida, K. C.; Salahub, D. R. *J. Chem. Phys.* **1998**, *108*, 4439-49.

[12] a) Barone, V.; Cossi, M. *J. Phys. Chem. A* **1998**, *102*, 1995-2001; b) Cossi, M.; Rega, N.; Scalmani, G.; Barone, V. *J. Comp. Chem.* **2003**, *24*, 669-81.

APPENDIX (Chapter 3)

Some of the Au(III)-σ-dialkynyl complexes bearing the *ppy*$AuCl_2$ core (**1**), and prepared according to the general procedure is presented here. It is to be noted that complexes **1g** and **1h** were also reported by Yam et. al. (ref. no 22a in main text of Publication 2) by an alternative synthetic route by the time of submission this thesis and were identical in all respects. The photophysical properties of these complexes were however not evaluated.

Experimental section.

[(N^C)AuL_2][N^C = 2-phenylpyridine, L = 1-ethynyl-4-methoxybenzene] (1g)

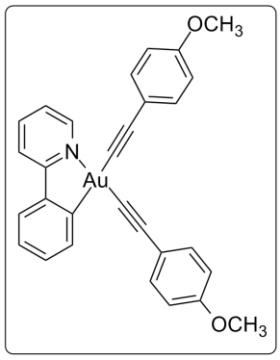

Following the general procedure, **A** (200.0 mg, 0.473 mmol) was reacted with 1-ethynyl-4-methoxybenzene (144.0 mg, 1.08 mmol) to obtain **1g** as a off-white solid which was further purified by column chromatography (neutral Al_2O_3; eluent: Hexane/EtOAc = 1/1), Yield = 160.0 mg, 55.0%. IR (KBr): ν_{max} 2120, 2167 cm^{-1}; ^1H NMR (500 MHz, CD_2Cl_2, 298 K): δ = 3.86 (s, 3H), 3.87 (s, 3H), 6.90-6.94 (m, 4H), 7.40-7.48 (m, 3H), 7.49-7.57 (m, 4H), 7.79 (dd, 7.5 Hz, 2.0 Hz, 1H), 8.00 (dd, 7.5 Hz, 2.0 Hz, 1H), 8.13 (td, 7.5 Hz, 3.0 Hz, 1H), 8.29 (dd, 7.5 Hz, 2.0 Hz, 1H), 9.71 (dd, 7.5 Hz, 2.0 Hz, 1H); $^{13}C\{^1H\}$NMR (125 MHz, CD_2Cl_2, 298 K): δ = 55.2, 55.3, 78.1, 98.5, 103.4, 113.7, 115.7, 117.9, 118.1, 120.4, 124.2, 124.9, 127.4, 131.6, 132.9, 133.0, 135.0, 135.6, 141.6, 145.5, 150.8, 156.2, 158.7, 159.0, 166.7; elemental analysis (%) calc for $C_{29}H_{22}AuNO_2$; C, 56.78; H, 3.61; N, 2.28; Found: C, 56.51; H, 3.58; N, 2.14.

[(N^C)AuL_2][N^C = 2-phenylpyridine, L= ethynyltrimethylsilane] (1h)

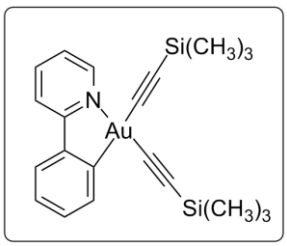

Following the general procedure, **A** (150.0 mg, 0.355 mmol) was reacted with ethynyltrimethylsilane (83.6 mg, 0.85 mmol) to obtain **1h** as a off-white solid which was further purified by column chromatography (neutral Al_2O_3; eluent: Hexane/EtOAc = 1/1), Yield = 100.0 mg, (52.0%). EI-MS: *m/z*: 568.1; $[M+Na]^+$; IR (KBr): *v*(C≡C); 2099, 2075 cm^{-1}; ^1H NMR (500 MHz, CD_2Cl_2, 298 K): δ = 0.29 (s, 9H), 0.31 (s, 9H), 7.38-7.49 (m, 3H), 7.76 (dd, *J* = 7.5, 2.0 Hz, 1H), 7.97 (d, *J* = 7.5 Hz,

1H), 8.12 (td, 7.5, 2.0 Hz, 1H), 8.19 (dd, *J* = 7.5, 2.0 Hz, 1H), 9.65 (dd, 7.5, 2.0 Hz, 1H); $^{13}C\{^{1}H\}$NMR (125 MHz, CD_2Cl_2, 298 K): δ = 0.22, 0.28, 96.6, 103.8, 108.5, 120.3, 124.0, 124.7, 127.5, 131.6, 135.8, 137.1, 141.6, 145.5, 150.6, 155.8, 166.8; elemental analysis (%) calc for $C_{21}H_{26}AuNSi_2$: C, 46.23; H, 4.80; N, 2.57; Found: C, 45.91; H, 4.99; N, 2.31.

[(N^C)AuL$_2$][N^C = 2-phenylpyridine, L = 4-ethynylpyridine] (1i)

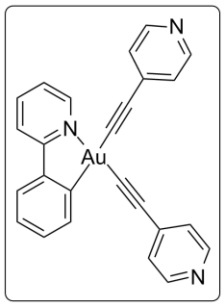

Following the general procedure, **A** (100.0 mg, 0.236 mmol) was reacted with 4-ethynylpyridine (53.5 mg, 0.51 mmol) to obtain **1i** as a light brown solid which was further purified by repeated washings with toluene. Yield = 30.0 mg (23%). EI-MS: *m/z*: 555.4 $[M]^+$; ν(C≡C); 2167.3, 2139.4 cm^{-1}; ^{1}H NMR (400 MHz, $CDCl_3$, 298 K): δ = 7.40-7.53 (m, 8H), 7.74 (d, *J* = 7.5 Hz, 1H), 7.98 (d, *J* = 7.5 Hz, 1H), 8.14 (t, *J* = 7.0 Hz, 1H), 8.23 (d, *J* = 7.5 Hz, 1H), 8.59 (t, *J* = 10.0 Hz, 3H), 9.60 (dd, 7.5 Hz, 2.0 Hz, 1H); $^{13}C\{^{1}H\}$NMR (125 MHz, CD_2Cl_2, 298 K): 97.1, 101.7, 120.6, 123.7, 123.9, 124.3, 124.4, 124.9, 125.8, 127.9, 132.0, 133.4, 133.5, 135.6, 142.1, 149.4, 149.5, 149.6, 151.0, 155.1, 166.9; elemental analysis (%) calc for $C_{25}H_{16}AuN_3$: C, 54.07; H, 2.90; N, 7.57; Found: C, 53.80; H, 2.60; N, 7.40.

[(N^C)AuL$_2$][N^C = 2-phenylpyridine, L = buta-1,3-diynyltrimethylsilane] (1j)

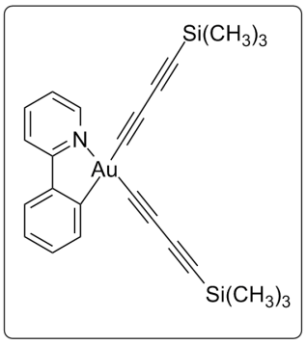

Following the general procedure, **A** (200.0 mg, 0.473 mmol) was reacted with buta-1,3-diynyltrimethylsilane (53.5 mg, 1.23 mmol) to obtain **1j** as a dark brown solid which was further purified by a short neutral Al_2O_3 plug eluted with ethyl acetate. The compound was found to be sensitive to light and was stored at -30 °C. Yield: 175.0 mg (62%); ν(C≡C); 2128.1, 2088.5 cm^{-1}; ^{1}H NMR (400 MHz, CD_2Cl_2, 298 K): δ = 0.23 (s, 9H), 0.25 (s, 9H), 7.39-7.47 (m, 2H), 7.53 (t, *J* = 6.5 Hz, 1H), 7.75 (d, *J* = 7.5 Hz, 1H), 7.77 (d, *J* = 8.0 Hz, 1H), 8.01 (d, *J* = 7.5 Hz, 1H), 8.16 (t, *J* = 8.0 Hz, 1H), 9.41 (d, *J* = 8.0 Hz, 1H); $^{13}C\{^{1}H\}$NMR (125 MHz, CD_2Cl_2, 298 K): -0.52, -0.48, 72.4, 80.8, 83.0, 83.3, 87.6, 89.9, 90.0, 110.9, 120.7, 124.6, 125.1, 127.9, 131.9, 135.6, 142.1, 145.2,

151.1, 154.4, 166.4; elemental analysis (%) calc for: $C_{25}H_{26}AuNSi_2 \cdot 1.0$ (EtOAc); C, 51.09; H, 5.03; N, 2.05; Found: C, 51.45; H, 5.11; N, 2.09.

Chapter 4.
(Benzimidazolin-2-ylidene)-Au(I)-Alkynyl Complexes: Syntheses, Structure, and Photophysical Properties

Publication 3. Garg, J. A.; Blacque, O.; Heier, J.; Venkatesan. K. *Eur. J. Inorg. Chem.* **2012**, 1750-1763

EurJIC European Journal of Inorganic Chemistry

DOI: 10.1002/ejic.201101351

(Benzimidazolin-2-ylidene)–Au^{I}–Alkynyl Complexes: Syntheses, Structure, and Photophysical Properties

Jai Anand Garg,[a] Olivier Blacque,[a] Jakob Heier,[b] and Koushik Venkatesan*[a]

Dedicated to Professor Heinz Berke on the occasion of his 65th birthday

Keywords: Gold / Aurophilicity / N-Heterocyclic carbenes / Alkynes / Luminescence / Photophysics

A series of N-heterocyclic carbene-based Au^{I}–σ-acetylide complexes of the type [(Bimz)Au–C≡CR] (Bimz = benzimidazolin-2-ylidene; R = aryl, silyl groups) (**1a**–**1l**, **2**, **3**) were prepared from the precursor [(Bimz)Au^{I}Cl] by an in situ deprotonation of the terminal alkynes. Steady-state photoluminescence studies revealed that most of these complexes exhibit phosphorescence at room temperature and in 77 K rigidified matrices. Molecular structures were determined by single-crystal X-ray diffraction studies for complexes **1a**, **1b**, **1e**, **1f**, **1h**, **1k**, and **1l**. Complexes **1f**, **1h**, and **1l** revealed weak unsupported aurophilic interactions. Cyclic voltammetry studies exhibited irreversible behavior with one oxidation peak potential ($E_{p,a}$) for most cases in the region 0.7–1.4 V. Experimental and DFT studies suggest that the nature of the emission is predominantly of intraligand character ^{3}IL(π–π*) with a slight perturbation from the metal.

Introduction

Au^{I}–σ-acetylides constitute an interesting class of linear two-coordinate d^{10}-metal–alkynyl systems that continues to be widely investigated for various applications due to their stability, rigid-rod nature, and polarizability.[1] During earlier decades, access to a variety of neutral Au^{I}–alkynyls of the type [Au(C≡CR)**L**] (**L** = tertiary phosphane, stilbene, arsine, isocyanide, or amine) were achieved by either treating [AuCl**L**] with Grignard reagents or by adding **L** to polymeric [{Au(C≡CR)}$_n$] complexes.[2] Facile and high-yielding methods that emerged later[3] paved the way for obtaining molecules with intriguing physical properties such as liquid crystallinity,[4] photoluminescence,[3g,5] and optical nonlinearity (NLO).[6] Particular attention was paid towards achieving room-temperature phosphorescence (RTP) that has promising applications in organic light-emitting diode (OLED) devices. Together with the effects arising from the "heavy-atom" nature of 5d transition metals, the photophysics of gold(I) complexes could stand uniquely modified by significant closed-shell aurophilic (Au···Au) interactions.[7] Although there has been a reasonable understanding of the luminescence properties of neutral phosphane-ligated Au^{I}–acetylides,[5o,8] relatively less effort have been devoted towards N-heterocyclic carbenes (NHCs) bearing Au^{I}–acetylides. With the increasing number of NHCs that have good π-accepting and σ-donating properties in the literature, this class of molecules can be expected to offer a greater scope for ligand-tunable photoluminescence (PL) properties.

In this context, we were interested in preparing a variety of benzimidazolyl NHC Au^{I}–acetylides and studying their PL properties. Previously, the groups of Lin[5f,9] and Gray[10] examined the PL properties of NHC gold acetylides at room temperature. Nolan and co-workers described a versatile gold(I) NHC hydroxide [Au(OH)(IPr)] [IPr = 1,3-bis(2,6-diisopropylphenyl)imidazol-2-ylidene] as a suitable synthon for the preparation of mono-, di-, and trinuclear acetylide complexes.[11] Che and co-workers recently probed the photophysics and molecular aggregation of anthracenyl-containing NHC Au^{I}–acetylides.[12] There are also some examples of such complexes from the patent literature.[13]

Results and Discussion

Various chosen terminal alkynes, either available commercially or prepared by standard Sonagashira cross-coupling protocols, were deprotonated in situ by using a NaOH/MeOH mixture and were subsequently reacted with [(Bimz)Au^{I}Cl] (Bimz = 1,3-diisopropylbenzimidazolin-2-ylidene) (**A**) under reflux conditions (Scheme 1). Complexes [(Bimz)Au^{I}**L**] [**L** = phenylethynyl (**1a**), *p*-fluorophenylethynyl (**1b**), *p*-methoxyphenylethynyl (**1c**), 3,4,5-trimeth-

[a] Institute of Inorganic Chemistry, University of Zürich, Winterthurerstrasse 190, 8057 Zürich, Switzerland
Fax: +41-44-635802
E-mail: venkatesan.koushik@aci.uzh.ch
[b] Laboratory of Functional Polymers, Empa, Swiss Federal Laboratories for Material Testing and Research, Überlandstrasse 129, 8600 Dübendorf, Switzerland

Supporting information for this article is available on the WWW under http://dx.doi.org/10.1002/ejic.201101351.

oxyphenylethynyl (**1d**), 1-ethynyl-4-phenylethynyl (**1e**), 4-pyridylethynyl (**1f**), 2-thienylethynyl (**1g**), 3-thienylethynyl (**1h**), pyren-1-ylethynyl (**1i**), 3-hydroxy-3-methylbut-1-yn-1-yl (**1j**), triisopropylsilylethynyl (**1k**), (4-ethynylphenyl)dimesitylborane (**1l**)], [{(Bimz)Au^{I}}$_2$(1,4-diethynylphenyl)] (**2**), and [{(Bimz)Au^{I}}$_3$(1,3,5-triethynylphenyl)] (**3**) were obtained as off-white to yellow powders in modest to good yields (42–92%) following easy workup and purification by column chromatography. Complex **1l** has a three-coordinate boron group incorporated in the ancillary ligand. This was chosen since it was expected to offer interesting luminescence properties because of the availability of the empty p orbital. The obtained products were stable to air and moisture under ambient conditions. An absence of signals corresponding to a free terminal acetylenic proton in the region 2.8–3.5 ppm in the ^{1}H NMR spectrum and a high-field shift of the aurated carbon ($C_{\alpha}\equiv$) in the ^{13}C NMR spectrum confirmed that the complexes were the desired σ-bonded Au^{I}–acetylide complexes. Asymmetric ν(C≡C) stretching modes of vibrations in the region 2103–2126 cm^{-1} together with the disappearance of the ν(Au–Cl) band around 340–345 cm^{-1} was also distinctly observed in the IR spectra. The ^{13}C NMR spectroscopy chemical shift for the carbenic carbon atom was found to lie in a narrow interval of 191.6–192.9 ppm, and was in a similar range to that reported in the literature.[11a] The positive-ion ESI-MS spectrum obtained for most complexes showed peaks corresponding to [M + H]$^{+}$ and [M + Na]$^{+}$ and was particularly helpful in assigning the dinuclear/trinuclear products **2** and **3**, respectively.

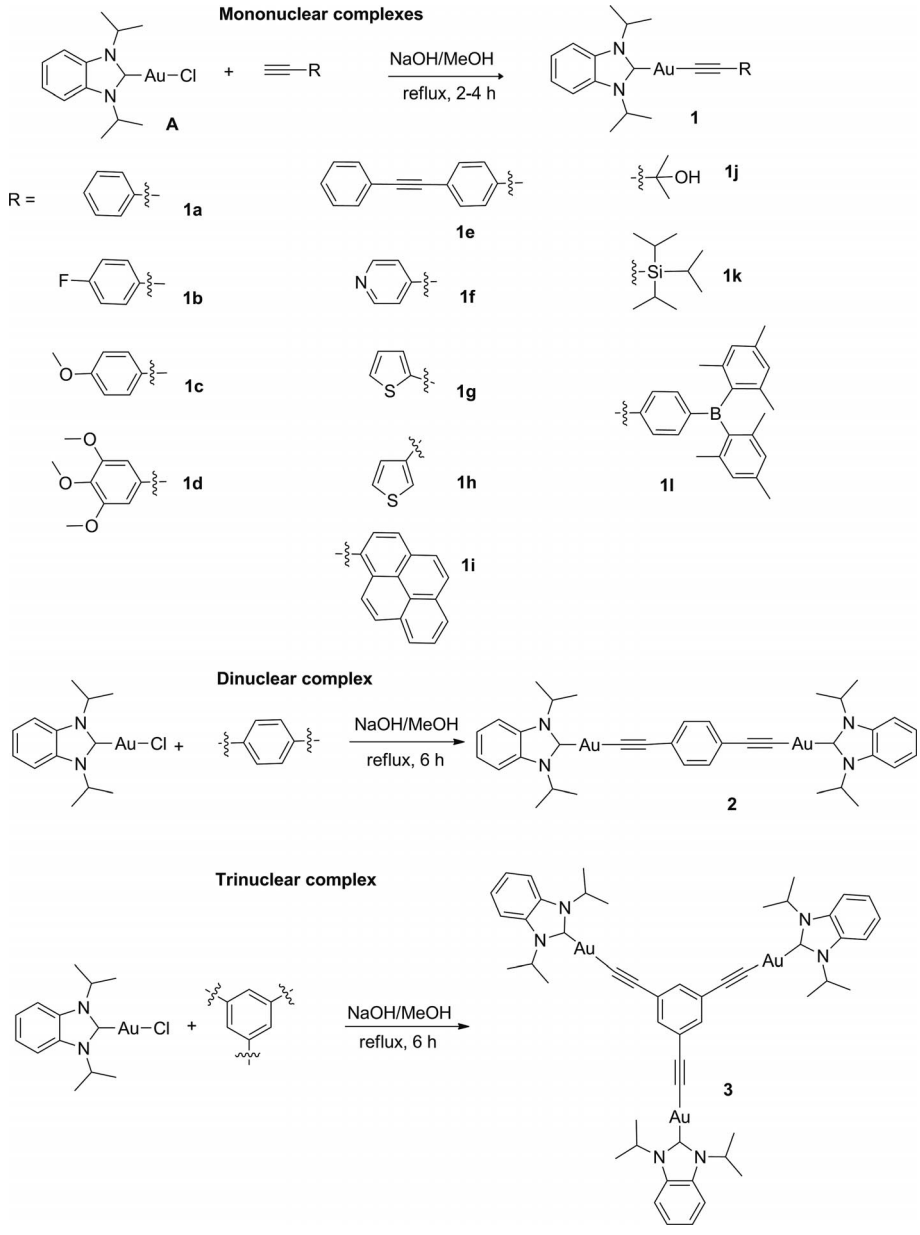

Scheme 1.

X-ray Diffraction Studies

Crystals of X-ray diffraction quality were obtained for **1a**, **1b**, **1e**, **1f**, **1h**, **1k**, and **1l** by slow evaporation of a layer of pentane over a concentrated solution of the complexes in dichloromethane at 0–5 °C. The perspective views of the complexes are shown in Figure 1 and some selected bond lengths and angles are described in Tables 1, 2, and 3. The other crystallographic details are provided in Tables 4 and 5. Further confirming the proposed structure of the complexes by NMR spectroscopy and other spectroscopic methods, the X-ray structure of these complexes revealed linear two-coordinate geometry with the gold atom flanked by the carbenic carbon atom and the substituted acetylenic carbon atom. Related systems in literature also reflect similar structural features.[8b,12] The average Au–$C_{carbene}$ bond length of 2.027 Å is marginally longer than that of the reported[14] chloride precursor [1.972(9) Å], which can be ex-

Table 1. Selected interatomic distances [Å] of complexes **1a**, **1b**, **1e**, **1f**, **1h**, **1k**, and **1l**.

Complex	Au–$C_{carbene}$	Au–C_{alkyne}	C≡C
1a	2.011(4)	2.003(4)	1.172(5)
1b	2.034(4)	2.007(4)	1.184(5)
1e	2.026(4)	1.985(4)	1.208(5)
1f	2.031(5)	1.993(5)	1.191(7)
1h	2.025(6)	2.023(6)	1.169(8)
1k	2.021(8)	1.991(8)	1.214(10)
1l	2.027(2)	1.988(2)	1.204(3)

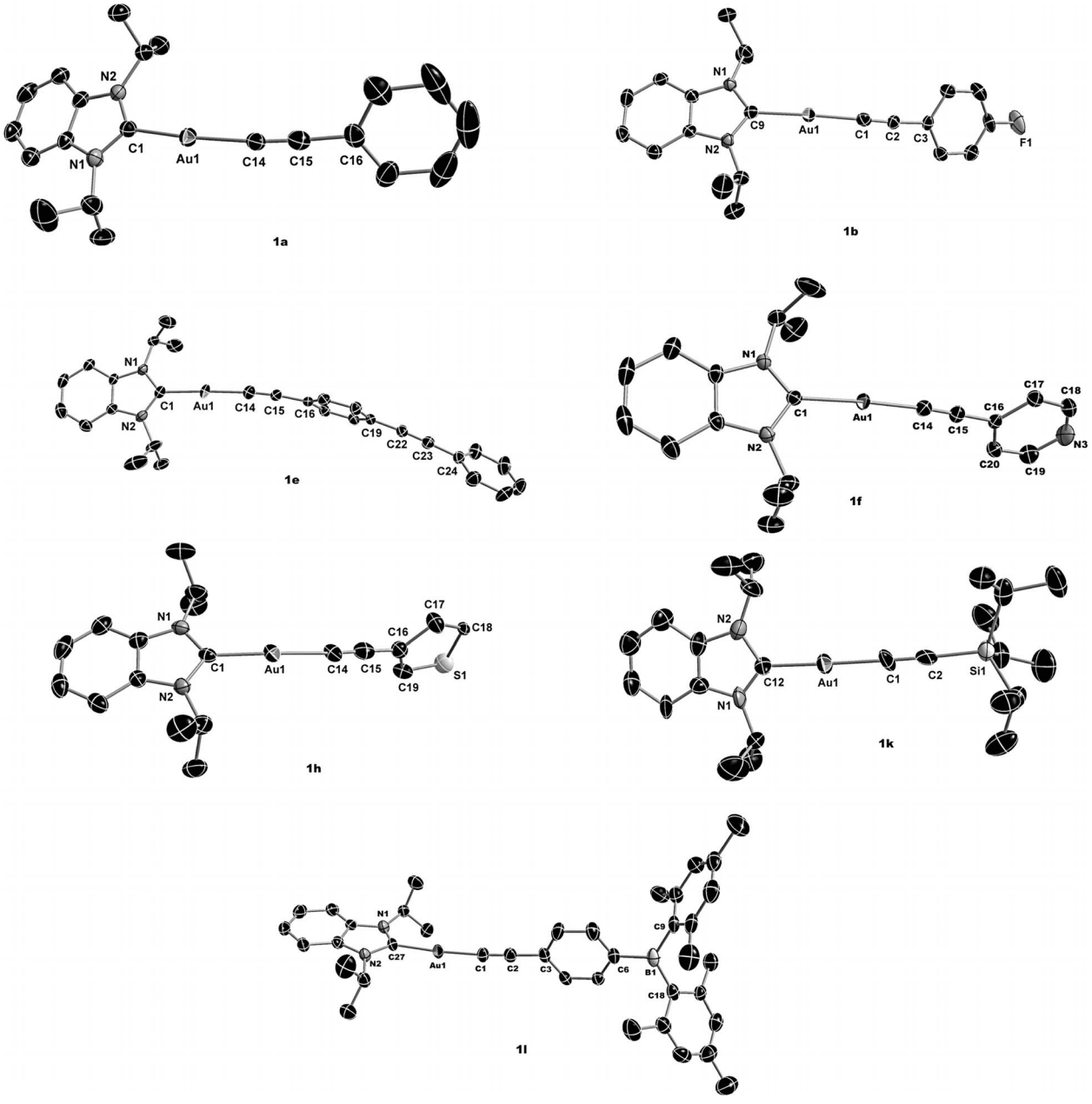

Figure 1. X-ray molecular structures of **1a**, **1b**, **1e**, **1f**, **1h**, **1k**, and **1l** with selective atomic numbering scheme. Thermal ellipsoids are drawn at the 50% probability level; hydrogen atoms and solvent molecules are omitted for clarity.

Table 2. Selected interatomic angles [°] of complexes **1a**, **1b**, **1e**, **1f**, **1h**, **1k**, and **1l**.

Complex	$C_{carbene}$–Au–C_{alkyne}	Au–C≡C	C≡C–R
1a	174.42(15)	172.7(4)	177.3(5)
1b	174.87(17)	170.5(4)	175.4(5)
1e	177.01(18)	175.0(4)	174.3(5)
1f	173.72(8)	175.6(2)	178.8(2)
1h	173.8(2)	168.8(6)	178.1(7)
1k	178.8(4)	178.1(10)	177.6(10)
1l	174.3(2)	176.0(5)	178.8(6)

Table 3. Summary of interplanar Au···Au distances [Å] of complexes **1a**, **1b**, **1e**, **1f**, **1h**, **1k**, and **1l**.

Complex	Au···Au distance [Å]
1a	7.721
1b	8.189
1e	6.516
1f	3.4074(2)
1h	3.4352(3)
1k	8.330
1l	3.4453(3)

pected because of the greater *trans* influence of the acetylenic carbon atom, however, it was within the range of related complexes described recently. The bond lengths of Au–C_{alkyne} were found to lie in the range 1.991(8)–2.023(6) Å and those of C≡C were observed between 1.191(7) and 1.204(3) Å, both of which are typically observed in the cases of internal and terminal Au^{I}–acetylides. The $C_{carbene}$–Au–C_{alkyne} valence bond angles were found to be in the range from 173.72(8)–178.8(4)°, the deviation from the ideal 180°, also observed with the other two angles (see Table 2), could be attributed to the crystal-packing forces. This kind of observation has been well documented in previously reported

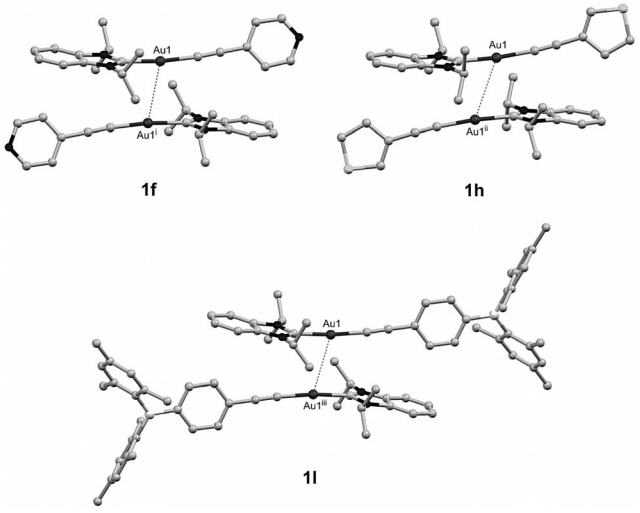

Figure 2. Head-to-tail arrangement in the crystal structures of **1f**, **1h**, and **1l** showing molecules interacting through Au···Au contacts. Symmetry codes: (i) $-x + 2, -y, -z$; (ii) $-x + 1, -y, -z + 2$; (iii) $-x + 1, -y + 1, -z + 1$.

Table 4. Crystallographic data for compounds **1a**, **1b**, **1e**, and **1f**.

	1a	**1b**	**1e**	**1f**
Empirical formula	$C_{21}H_{23}AuN_2$	$C_{21}H_{22}AuFN_2$	$C_{29}H_{27}AuN_2$	$C_{20}H_{22}AuN_3$
Formula weight [g mol^{-1}]	500.38	518.38	600.50	501.38
Temperature [K]	183(2)	183(2)	183(2)	183(2)
Wavelength [Å]	0.71073	0.71073	0.71073	0.71073
Crystal system	orthorhombic	orthorhombic	triclinic	monoclinic
Space group	*Pbca*	$P2_12_12_1$	$P\bar{1}$	$P2_1/c$
a [Å]	12.5726(2)	12.1077(3)	9.9314(3)	13.3296(2)
b [Å]	13.3647(2)	12.5146(2)	13.8448(4)	11.0859(1)
c [Å]	23.5131(3)	12.9476(2)	18.7365(4)	13.1919(2)
α [°]	90	90	90.886(2)	90
β [°]	90	90	96.356(2)	108.559(1)
γ [°]	90	90	104.457(2)	90
Volume [Å^3]	3950.88(10)	1961.86(7)	2476.84(12)	1848.00(4)
Z	8	4	4	4
Density (calcd.) [Mg m^{-3}]	1.682	1.755	1.610	1.802
Abs. coefficient [mm^{-1}]	7.450	7.512	5.958	7.966
F(000)	1936	1000	1176	968
Crystal size [mm^3]	0.44 × 0.34 × 0.28	0.20 × 0.10 × 0.06	0.60 × 0.35 × 0.25	0.50 × 0.30 × 0.05
q range [°]	2.39 to 28.28	2.8 to 30.5	2.72 to 29.13	2.64 to 30.51
Reflections collected	23389	14726	32837	36763
Reflections unique	4897/[R_{int} = 0.0524]	5975/[R_{int} = 0.046]	13316/[R_{int} = 0.028]	5635/[R_{int} = 0.0334]
Completeness to *q* [%]	100.0	99.9	99.9	99.9
Absorption correction	analytical	analytical	analytical	analytical
Max./min. transmission	0.229 and 0.119	0.695 and 0.352	0.381 and 0.123	0.657 and 0.107
Data/restraints/parameters	3302/0/221	4706/0/230	9526/19/585	5177/0/221
Goodness-of-fit on F^2	0.927	0.82	0.936	1.082
Final R_1 and wR_2 indices [$I > 2\sigma(I)$][a]	0.0275, 0.0647	0.031, 0.043	0.035, 0.075	0.0183, 0.0392
R_1 and wR_2 indices (all data)[a]	0.0501, 0.0676	0.045, 0.045	0.056, 0.078	0.0218, 0.0403
Largest diff. peak and hole [e Å^{-3}]	1.05 and –1.45	0.84 and –1.09	1.58 and –3.36	1.03 and –0.47

[a] The unweighted *R* factor is $R_1 = \Sigma(F_o - F_c)/\Sigma F_o$; $I > 2\sigma(I)$ and the weighted *R* factor is $wR_2 = \{\Sigma w(F_o^2F_c^2)^2/\Sigma w(F_o^2)^2\}^{1/2}$.

Table 5. Crystallographic data for compounds **1h**, **1k**, and **1l**.

	1h	**1k**	**1l**
Empirical formula	$C_{19}H_{21}AuN_2S$	$C_{24}H_{39}AuN_2Si$	$4(C_{39}H_{44}AuBN_2)\cdot 2(C_5H_{12})$
Formula weight [g mol^{-1}]	506.42	580.63	3138.46
Temperature [K]	183(2)	183(2)	183(2)
Wavelength [Å]	0.71073	0.71073	0.71073
Crystal system	monoclinic	orthorhombic	monoclinic
Space group	$P2_1/c$	$P2_12_12_1$	$P2_1/n$
a [Å]	12.5461(2)	16.9480(3)	8.6957(2)
b [Å]	11.2845(1)	17.2822(3)	15.5587(6)
c [Å]	13.4397(3)	17.7778(4)	29.0431(6)
α [°]	90	90	90
β [°]	108.381(2)	90	92.985(2)
γ [°]	90	90	90
Volume [Å^3]	1805.67(6)	5207.10(17)	3924.02(19)
Z	4	8	1
Density (calcd.) [Mg m^{-3}]	1.863	1.481	1.328
Abs. coefficient (mm^{-1})	8.263	5.71	3.777
F(000)	976	2320	1588
Crystal size [mm^3]	$0.29\times0.28\times0.06$	$0.24\times0.10\times0.04$	$0.32\times0.16\times0.04$
q range [°]	2.65 to 30.51	2.6 to 25.4	2.62 to 25.68
Reflections collected	15622	34918	17902
Reflections unique	5496/[R_{int} = 0.0330]	9525/[R_{int} = 0.0748]	7286/[R_{int} = 0.0427]
Completeness to q (%)	99.9	99.8	97.7
Absorption correction	analytical	analytical	analytical
Max./min. transmission	0.668 and 0.131	0.784 and 0.450	0.852 and 0.563
Data/restraints/parameters	4022/0/212	6486/6/524	5793/62/488
Goodness-of-fit on F^2	1.062	0.96	1.069
Final R_1 and wR_2 indices [$I>2\sigma(I)$][a]	0.0429, 0.1037	0.044, 0.080	0.0414, 0.0838
R_1 and wR_2 indices (all data)[a]	0.0647, 0.1085	0.073, 0.083	0.0605, 0.0911
Largest diff. peak and hole [e Å^{-3}]	3.92 and –2.88	1.30 and –0.77	0.92 and –0.61

[a] The unweighted R factor is $R_1 = \Sigma(F_o - F_c)/\Sigma F_o$; $I>2\sigma(I)$ and the weighted R factor is $wR_2 = \{\Sigma w(F_o^2F_c^2)^2/\Sigma w(F_o^2)^2\}^{1/2}$.

crystal structures.[8c] More interesting aspects were the weak unsupported[7c] intermolecular Au···Au interactions in the range 3.41–3.44 Å observed in the crystal lattices of **1f**, **1h**, and **1l** (Table 3). The crystal-packing structures (Figure 2) revealed a head-to-tail arrangement between the heterocyclic carbene and acetylene ligand of the participating molecules.

Electronic Absorption Studies

The electronic spectra of the complexes measured in dichloromethane at room temperature generally featured intense absorption peaks (Figure 3 and Table 6). The lowest energy-absorption maxima of the complexes containing phenylacetylide (**1a**) or substituted forms of phenylacetylides, namely, 4-fluoro and 4-methoxy (**1b**–**1d**) as ancillary ligands, appeared in the range 288–292 nm. Complexes bearing heteroaromatic aryl-acetylide ancillary ligands, namely, **1f**–**1h**, showed slight variations from **1a**. The absorption maxima of **1f** was found to show a hypsochromic shift to 285 nm, while **1g** and **1h** showed a much more red-shifted maxima at 291 and 300 nm, respectively. The absorption maxima of **1e** (355 nm) and **1i** (381 nm) containing *p*-phenylethynyl phenylacetylide and 2-pyrenylacetylide ligands, respectively, were observed at longer wavelengths due to the extended conjugation and increased π delocalization. These complexes also possess additionally intense high-energy absorptions that suggest strong spin-allowed transitions. The nonaryl acetylides (**1j** and **1k**) showed absorption profiles markedly similar to their carbene gold(I) chloride precursor **A**. The dinuclear **2** and trinuclear **3** gold complexes showed absorption at 291 to 294 nm, respectively. The molar extinction coefficients of the complexes were generally in the range of 10^4 dm^3 mol^{-1} cm^{-1}. Successive higher values were observed with the increase in the number of gold units as in the case of **2** and **3**.

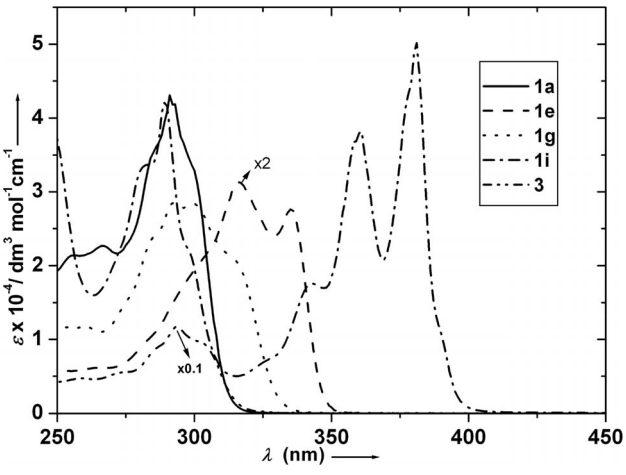

Figure 3. Electronic absorption spectra of complexes **1a**, **1e**, **1g**, **1i**, and **3** recorded in CH_2Cl_2 at 298 K.

Table 6. Photophysical properties of complexes **1a**–**l**, **2**, **3**, and **A**.

	Absorption λ_{max} [nm] (ε_{max}/[dm^3 mol^{-1} cm^{-1}])	Room-temperature solution (CH_2Cl_2) Emission λ_{max} [nm]	τ [μs]	Φ_P[a] $\times10^{-3}$	k_r [s^{-1}][b] $\times10^3$	k_{nr} [s^{-1}][c] $\times10^6$	77 K glass[d] (2-MeTHF)	E_{opt}[e] [eV]
1a	291 (43110)	423, 443	0.70	10.0	14.2	1.40	423, 485, 528	3.88
1b	281 sh (21617), 288 (27667), 298 (17076)	421, 440	0.22	6.5	29.5	4.51	415, 432, 453	3.90
1c	283 sh (30827), 292 (34178), 306 sh (27936)	428, 456	0.21	2.9	13.8	4.74	424, 487, 531	3.74
1d	283 sh (29855), 292 (34210), 306 sh (27117)	481	0.37	3.8	10.3	2.68	424, 485, 531	3.71
1e	316 (62641), 355 (55280)	513, 544	0.68	1.9	2.8	1.46	423, 447, 487, 532	3.51
1f	285 (33452)	411, 433, 449	3.75	66.0	17.6	0.24	406, 424, 444	3.93
1g	293 (28556), 300 (28431), 313 sh (21375)	525	0.26	3.0	11.5	0.38	481, 495, 515, 534	3.75
1h	291 (27356), 300 sh (22845)	371(fl), 465	1.10	2.1	–	–	429, 441, 469, 483	3.80
1i	289 (42081), 343 sh (17590), 361 (38221), 381 (50183)	nonemissive	–	–	–	–	424, 481, 540	3.05
1j	274 sh (12957), 282 (23302), 291 (25806)	416	0.70	–	–	–	416, 483, 530	4.09
1k	283 (27545), 292 (33298)	417	–	–	–	–	425, 487	4.18
1l	343 (35960)	380(fl), 481	2.9	99.0	–	–	480	3.33
2	292 sh (34457), 312 (57048), 328 (69249)	496, 528	0.40	3.2	8.0	2.49	488, 519, 529	3.48
3	293 (116810), 304 sh (92210)	445	2.31	3.1	1.34	0.43	443, 475, 489	3.74
A	280 (17982), 288 (19864)	nonemissive	–	–	–	–	422, 466, 586	4.23

[a] Photoluminescence quantum yield determined with quinine sulfate in 1 N H_2SO_4 as standard at 298 K. [b] Radiative rate constant. 2-MeTHF = 2-methyltetrahydrofuran. [c] Nonradiative rate constant. [d] Vibronic structured emission bands. [e] Optical bandgap. (fl) denotes fluorescence intensity.

Photoluminescence Studies

All complexes except **1i** displayed varied steady-state emission characteristics when measured at room temperature in dichloromethane. Selected PL profiles are shown in Figure 4 (also see Figures S1 and S2 in the Supporting Information). The Au^{I}–carbene precursor **A** was nonemissive at room temperature in dichloromethane. It is pertinent here to note that its X-ray structure determined previously[15] was devoid of aurophilic interactions, but interestingly the closely related compound with a methyl substituent on the benzimidazolyl carbene instead of the isopropyl group did possess interactions with an Au···Au distance of 3.1664(10) Å.[15] All the complexes except **1i** showed structured emission with an intense E_{0-0} band following a less intense peak in the lower-energy region; the others showed broad and structureless profiles. The influence of the electron-withdrawing or -donating abilities of the aryl acetylides in **1b**, **1c**, and **1d** on the onset of emission maxima was found to be small but nevertheless distinct; **1b** that contains an electronegative fluorine atom showed a marginal hypsochromic shift of 2 nm (see Table S1 in the Supporting Information) with respect to **1a**, whereas in **1c** the peak maxima was shifted bathochromically by 5 nm. Complex **1e** with extended π conjugation showed a significantly redshifted emission with a trend parallel to its absorption maxima. It is worth noting that the onset of emission in **1e** (513 nm) was significantly redshifted relative to that of the dinuclear complex **2** (496 nm); if **2** is considered a variant of **1e** in which one unit of ethynylbenzene was replaced by an alkynyl gold carbene unit, the electronic conjugation seems to be less effective in the lowering of the bandgap. In the case of **3**, the emission maximum at 445 nm appears not much to be affected, which perhaps can be attributed to its symmetrical nature. Also, the emission of **1g** (2-ethynylthiophene ligand) appeared at lower energies than **1h** (3-ethynylthiophene ligand), which could be understood based on the less conjugation in the latter. Complex **1i** that contains a polyaromatic pyrenyl ligand was found to be nonemissive at room temperature; this observation corresponds to the increase in the nonradiative decay rates[16] (K_{nr}) in line with the energy-gap law for π-delocalized systems. The nonaryl-ligand-bearing complexes **1j** and **1k** showed a very weak emission around 417 nm, which suggests that aryl groups can play a role in emissivity and/or emission tunability in this class of complexes. The complexes that displayed weak Au···Au interactions (**1f**, **1h**, and **1l**) in their solid-state molecular structures, however, did not reveal any appreciable additional low-energy bands assignable to metal–metal-to-ligand charge transfer (MMLCT) emissions in room-temperature fluid and in 77 K rigid media. Complex **1l** showed peak emission intensities at 481 nm in addition to a less intense residual fluorescence band at 380 nm (Figure 5). Considering the relatively high quantum yield of approximately 10% in the fluid media and the observed aurophilic-

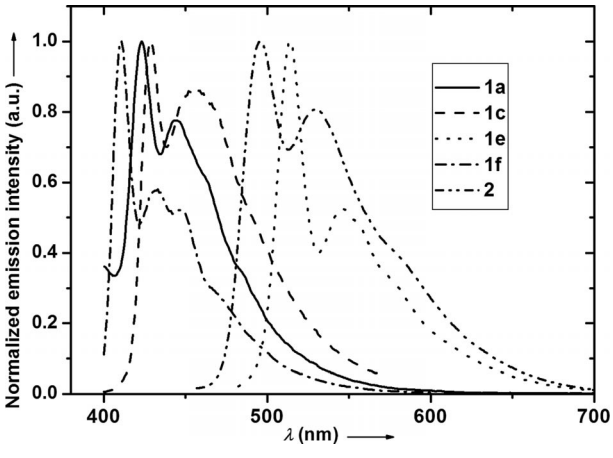

Figure 4. Emission spectra of selected complexes degassed in CH_2Cl_2 at 298 K.

ity, we chose to further investigate the PL properties of this molecule. The solid-state emission spectra of **1l** as 10% loading in polymethylmethacrylate (PMMA) showed λ_{em} at 493 nm that was redshifted by 8 nm relative to the emission trace in fluid. A similar phenomenon was observed for **1f**, which also showed weak aurophilicity (Figure 5). In the case of **1b**, where no interactions were evident from the X-ray structure analysis, the PMMA thin-film spectra appeared to replicate the solution spectra (see Figure S3 in the Supporting Information). To verify whether this could be an effect arising from Au···Au interactions, PMMA thin films with different concentration loadings were prepared and the emission spectrum was recorded for **1l** (see Figure S5 in the Supporting Information). The result showed that the onset of a bathochromic shift by 7 nm was observed in as low as 1% (wt/wt) concentration, thereafter increasing the concentration had little effect. Concentration-dependent studies were also carried out at 77 K to gain further insight into this behavior. Increasing concentrations of **1b** and **1f** (10^{-5} to 10^{-2} M) in methyl-THF showed no change in the emitting wavelengths of their strong vibronic profiles (Figure S6 in the Supporting Information). This suggested that there was no explicit effect due to metallophilic interactions in these complexes, and the observation in thin films could not be explained convincingly. The luminescence efficiencies of the complexes in the solid state were investigated by spin-coating thin films (2% PMMA loading) of **1b**, **1f**, and **1l** using an integrating-sphere setup. For the respective complexes the quantum yields were determined as 2.4, 1.0, and 27.0%. Here again, no correlation could be drawn for the influence of aurophilicity on the quantum yields. However it needs to be mentioned that **1l** shows a good quantum yield in the solid state among these monomeric Au^{I}–acetylides. Whether the effect arises purely due to boron needs further investigations. To the best of our knowledge, boron-containing Au^{I}–acetylides are sparse in the literature and are worth investigating. The 77 K emission spectra of all the complexes featured strong vibronic bands with tailing of the emission intensities over wide wavelength regions. The vibrational progression of 2200 cm^{-1} corresponding to the stretching frequency of C≡C was observed. Excited-state lifetime measurements for all the complexes showed monoexponential decay profiles, which indicated that the emission process arises from a single noninteracting excited state with lifetimes ranging between 0.2 and 3.7 μs. The quantum yields of the compounds were generally in the range of 10^{-3} percent in solution. However, higher values with an increase by an order of ten were obtained for **1a** and **1f**. The calculated K_r and K_{nr} constants, assuming the intersystem crossing to the triplet state occurs with unit efficiency, were on average 10^3 and 10^6 s^{-1}, respectively. Since K_{nr} was several orders of magnitude greater than K_r ($K_{nr} >> K_r$), it could be assumed that the nonradiative decay pathways are the major factor for lowering the quantum yields.

The emission intensities of these complexes were found to decrease two- to fivefold upon exposure to oxygen. Based on the observation that the excited-state lifetimes were in the microsecond regime along with a large Stokes shift, the origin of the emission is assigned to be from the triplet manifold. The optical bandgap calculated from the absorption edges was between 3.05 and 4.05 eV. From the preceding discussions, accounting for the fact that the subtle variations of the absorption and emission profiles are in line with our expectations following the change in the electronic nature of the ancillary acetylides, one could tentatively assume dominant ^{3}IL(π–π*) transitions governing the emission phenomenon. Also, the perturbing nature of the heavy metal could be realized as "good-enough" for efficient intersystem crossing to the triplet state as most complexes (except **1h** and **1l**) showed no residual fluorescence intensities.

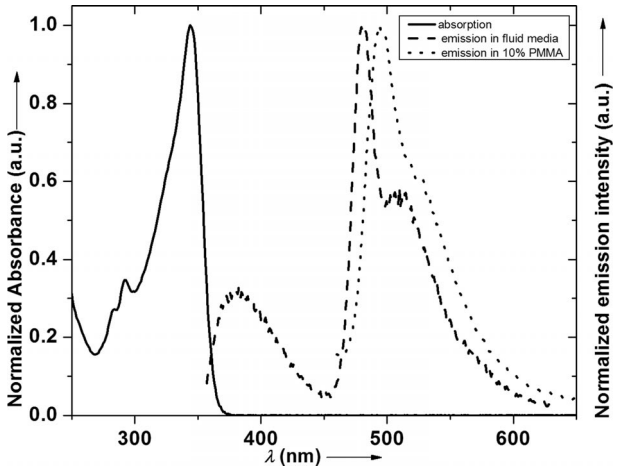

Figure 5. Absorption and emission spectra of **1l** in fluid and the solid state.

Cyclic Voltammetry

The cyclic voltammograms of **1a**–**1l**, **2**, and **3** in dichloromethane were generally characterized by a single irreversible oxidation wave in the range +0.7 to +1.4 V (vs. Ag/Ag^+). The trend of oxidation was found to correlate with the electronic nature of the acetylides thereby suggesting their origin. The electrochemical data for selected complexes are collected in Table 7. Among the various substi-

Table 7. Electrochemical data for selected complexes.[a]

Complex	Oxidation $E_{p,a}$ [V]
1a	+1.10
1b	+1.12
1c	+0.77
1d	+0.68
1e	+1.02
1f	+1.40
1g	+0.85
1h	+0.93
1k	+1.23
1l	+1.11
2	+0.88, +1.21
3	+1.00

[a] Scan rate = 100 mV s^{-1} in 0.1 M $[nBu_4][PF_6]$ (Au electrode; E versus $F_c^{0/+}$; 20 °C; CH_2Cl_2).

tuted phenyl acetylides **1a**–**1d**, the first anodic peak potentials ($E_{p,a}$) varied as **1d** < **1c** < **1a** < **1b**. For the heteroaromatic acetylides **1f**–**1h** the trend was also in line with our expectations; a larger oxidation potential was observed for **1f** containing a pyridyl group followed by **1h** and **1g**. Complexes **1k** and **1l** typically showed larger values than **1a**. No specific correlation could be ascertained for second-oxidation waves observed in **2**.

Theoretical Calculations

To better understand the absorption and emission properties of the synthesized compounds, density functional theory (DFT) calculations were carried out for selected molecules with the Gaussian 03 program package.[17] The hybrid functional PBE1PBE[18] in conjunction with the Stuttgart/Dresden effective core potentials (SDD) basis set[19] for the Au center augmented with one f-polarization function (α = 1.050) and the standard 6-31+G(d) basis set[20] for the remaining atoms was applied. The molecular structures of the electronic ground states and lowest triplet states of compounds **1a**, **1b**, **1e**, **1f**, **1l**, and **2** were exemplarily studied. On the basis of the optimized geometries, time-dependent DFT (TD-DFT) calculations[21] combined with the conductive polarizable continuum model (CPCM)[22] were used to produce the molecular orbital energy levels and compositions, the absorption spectra, and the ten lowest singlet–singlet and singlet–triplet vertical excitations (in solution in dichloromethane) with the corresponding energies, transition coefficients, and oscillator strengths. The lowest-energy absorption bands (285–291 nm) of the complexes containing phenylacetylide (**1a**), a substituted form of phenylacetylide (**1b**), and a heteroaromatic aryl acetylide ligand **1f** were found to be derived from excitations involving molecular orbitals in the narrow range of HOMO – 1 to LUMO + 1 (Table 8). These highest occupied and lowest unoccupied orbitals of the complexes are largely of ligand π/π^* character with a limited participation of the metal center. The two lowest significant singlet–singlet excitations, with oscillator strength $f > 0.015$, are $S_0 \rightarrow S_2$ (278 nm, f = 0.664) and $S_0 \rightarrow S_4$ (269 nm, f = 0.979) for **1a**, $S_0 \rightarrow S_2$ (277 nm, f = 0.619) and $S_0 \rightarrow S_3$ (268 nm, f = 0.994) for **1b**, and $S_0 \rightarrow S_2$ (277 nm, f = 0.812) and $S_0 \rightarrow S_4$ (266 nm, f = 0.763) for **1f**, which lead to calculated absorption maxima (λ_{max}) of 270–272 nm (Table 8). As already observed in a previous study,[23] the PBE1PBE/SDD 6-31+G(d) calculations systematically provide underestimated absorption maxima by only approximately 20 nm.

The major contributions to these one-electron excitations are from HOMO → LUMO + 1 and HOMO – 1 → LUMO

Table 8. Selected singlet–singlet (S_0–S_n) and singlet–triplet (S_0–T_1) excited states with TDDFT/CPCM vertical excitation energies [nm], transition coefficients, orbitals involved in the transitions, and oscillator strengths (f) for compounds **1a**, **1b**, **1e**, **1f**, **1l**, and **2** (with $f >$ 0.015).

	1a	**1b**	**1e**	**1f**	**1l**	**2**
Exp. abs., λ_{max}	291	288	355	285	343	292
Calcd. abs., λ_{max}[a]	272	270	348	271	348	323
S_0–S_n	n = 2	n = 2	n = 1	n = 2	n = 1	n = 1
	278 (0.664)	277 (0.619)	348 (2.119)	277 (0.812)	353 (1.085)	325 (2.051)
	H→L + 1 (0.65)	H→L + 1 (0.64)	H→L (0.66)	H→L (0.65)	H→L (0.65)	H→L + 2 (0.66)
	n = 4	n = 3	n = 5	n = 4	n = 2	n = 7
	269 (0.979)	268 (0.994)	277 (0.433)	266 (0.763)	343 (0.102)	276 (1.275)
	H – 1→L (0.66)	H – 1→L (0.66)	H – 1→L + 1 (0.57)	H – 1→L + 1 (0.66)	H – 1→L (0.68)	H – 2→L + 1 (0.44)
						H – 1→L (0.49)
	n = 6	n = 5	n = 6	n = 6	n = 3	
	250 (0.054)	260 (0.020)	274 (0.076)	248 (0.073)	324 (0.067)	
	H – 5→L (0.69)	H→L + 2 (0.64)	H – 2→L (0.63)	H – 2→L + 1 (0.65)	H – 2→L (0.67)	
	n = 7	n = 6	n = 8	n = 7	n = 4	
	248 (0.081)	250 (0.055)	265 (0.085)	248 (0.046)	316 (0.206)	
	H – 2→L (0.65)	H – 4→L (0.69)	H→L + 2 (0.63)	H – 3→L + 1 (0.67)	H – 3→L (0.64)	
	n = 8	n = 7	n = 10	n = 8	n = 9	
	238 (0.110)	248 (0.081)	263 (0.047)	247 (0.032)	263 (0.331)	
	H – 4→L (0.60)	H – 2→L (0.65)	H – 5→L + 1 (0.67)	H – 5→L (0.52)	H – 5→L + 1 (0.51)	
					H – 8→L (0.32)	
		n = 8		n = 9	n = 10	
		246 (0.123)		246 (0.071)	261 (0.033)	
		H – 3→L (0.59)		H – 3→L (0.66)	H – 9→L (0.62)	
		n = 10				
		232 (0.014)				
		H→L + 5 (0.59)				
Exp. em., λ_{max}	**423**, 443	**421**, 440	**513**, 544	**411**, 433, 449	481	**496**, 528
Calcd. λ_{max}[b]	442 (2.81 eV)	440 (2.82 eV)	558 (2.22 eV)	434 (2.86 eV)	492 (2.52 eV)[c]	507 (2.45 eV)[c]
T_1–S_0	417	415	534	408	485	494
	H←L+1 (0.72)	H←L + 1 (0.72)	H←L (0.76)	H←L (0.74)	H←L (0.69)	H←L + 2 (0.76)

[a] The calculated values are obtained from the TD-DFT/CPCM UV/Vis spectra drawn by Gaussview. [b] Solvent-corrected (CH_2Cl_2) energy difference between optimized ground state and lowest triplet state. [c] Energy difference obtained without zero-point energy correction.

for **1a** (Figure 6) and **1b**, and from HOMO→LUMO and HOMO – 1→LUMO + 1 for **1f**. Based upon the molecular orbital composition analysis (Table 9), the lowest $S_0 \rightarrow S_2$ excited state can be assigned as intraligand charge-transfer ^{1}ILCT [π→π*(C≡CR)] character, whereas the second-lowest $S_0 \rightarrow S_n$ (n = 3 or 4) excited state shows an admixture of ligand-to-ligand ^{1}LLCT [π(carbene)→π*(C≡CR)] and intraligand ^{1}ILCT [π→π*(carbene)] characters. It is worth noting that the metal-center participation in these frontier orbitals are at a significant level (7 to 25%, Table 9).

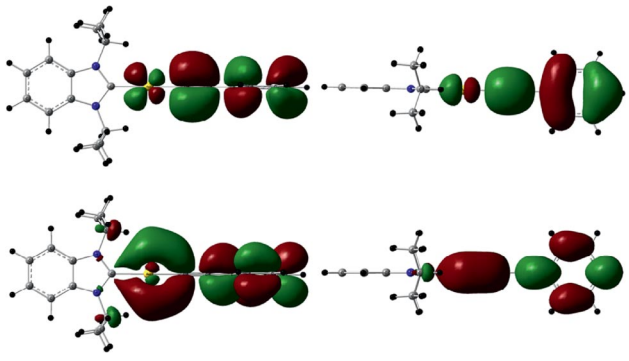

Figure 6. Isodensity plots of the HOMO (up) and LUMO + 1 (down) of the DFT-optimized ground state of **1a** (isodensity value 0.02).

The absorption maxima of **1e**, containing *p*-phenylethynyl phenylacetylide, and **1l**, containing a dimesitylborane group, were experimentally observed at longer wavelengths (355 and 343 nm, respectively) due to an extended conjugation. The redshift effect of the absorption is reproduced well by the DFT calculations with intense bands at 348 nm resulting dominantly from the HOMO→LUMO excitation for **1e** ($S_0 \rightarrow S_1$, f = 2.119) and **1l** ($S_0 \rightarrow S_1$, f = 1.085). The HOMO and LUMO of **1e** and **1l** are localized on the C≡C–R ligand with 90–96% composition and a very small participation of the metal of 4–7%. This also partly explains the observation of fluorescence in the steady-state emission of **1l**; the participation of the carbene ligand is also limited to 3–4% in this compound. The absorption phenomenon of these conjugated systems can be described as a π→π*(C≡CR) transition with an intraligand charge-transfer ^{1}ILCT character. Table 6 shows that the absorption band of the dinuclear gold complex **2** at 292 nm is contributed by the HOMO→LUMO + 2 excitation ($S_0 \rightarrow S_1$, 325 nm, f = 2.051). Table 7 shows that the HOMO is composed of 92% π[C≡C–(C_6H_4)–C≡C], 7% d(Au), and 1% π(carbene), whereas LUMO + 2 has 81% π(C≡C–C_6H_4–C≡C) and 19% d(Au). Thus the energy absorption is again dominantly originating from an excited state with a metal-perturbed ^{1}ILCT character. The calculated emissions of the complexes are given in Table 8. The lowest singlet–triplet vertical excitation ($T_1 - S_0$) energies obtained by TD-DFT are consistent with the experimental emissions (in parentheses) with 417 (423), 415 (421), 408 (411), 485 (481), and 494 (496) nm for **1a**, **1b**, **1f**, **1l**, and **2** with an absolute energy difference in the range 2–6 nm, except for the highly conjugated system **1e** for which the emission energy is overestimated by 21 nm (534 vs. 513 nm).

Table 9. Compositions [%] and energy level [eV] of selected molecular orbitals of the optimized ground states of **1a**, **1b**, **1e**, **1f**, **1l**, and **2**.

	1a				**1b**				**1e**			
MO	*E*	Carbene	Au	C≡CR	*E*	Carbene	Au	C≡CR		Carbene	Au	C≡CR
L + 5	0.00	0	100	0	–0.01	0	100	0	–0.16	50	50	0
L + 4	–0.09	100	0	0	–0.10	99	0	1	–0.30	0	0	100
L + 3	–0.14	50	50	0	–0.15	45	52	3	–0.36	0	0	100
L + 2	–0.18	0	0	100	–0.45	0	0	100	–0.51	0	33	67
L + 1	–0.94	0	21	79	–0.93	4	25	71	–1.35	79	21	0
L	–1.34	80	20	0	–1.34	70	20	10	–1.73	0	4	96
H	–6.23	1	7	92	–6.22	4	7	89	–5.94	0	4	96
H – 1	–6.78	40	16	44	–6.80	43	16	41	–6.82	45	15	40
H – 2	–7.13	100	0	0	–7.14	99	0	1	–7.07	1	6	93
H – 3	–7.29	0	0	100	–7.38	26	64	10	–7.14	100	0	0
H – 4	–7.38	58	3	39	–7.40	55	3	42	–7.42	53	3	44
H – 5	–7.38	22	64	14	–7.57	0	0	100	7.44	23	61	16

	1f				**1l**				**2**			
MO	*E*	Carbene	Au	C≡CR	*E*	Carbene	Au	C≡CR	*E*	Carbene	Au	C≡C–(C_6H_4)–C≡C
L + 5	–0.02	0	100	0	–0.10	100	0	0	–0.15	100	0	0
L + 4	–0.09	100	0	0	–0.21	25	75	0	–0.17	50	50	0
L + 3	–0.16	53	51	0	–0.34	0	1	99	–0.17	50	50	0
L + 2	–0.39	0	0	100	–0.48	6	31	63	–1.18	0	19	81
L + 1	–1.36	79	21	0	–1.32	74	17	9	–1.36	81	19	0
L	–1.42	0	10	90	–1.95	4	5	91	–1.37	81	18	1
H	–6.74	1	10	89	–6.24	3	7	90	–5.63	1	7	92
H – 1	–6.87	53	15	32	–6.50	0	0	100	–6.62	22	16	62
H – 2	–7.13	100	0	0	–6.58	1	0	99	–6.68	25	16	59
H – 3	–7.47	23	62	15	–6.65	3	2	95	–7.00	2	15	83
H – 4	–7.47	45	5	50	–6.68	0	0	100	–7.18	100	0	0
H – 5	–7.59	0	0	100	–6.93	35	14	51	–7.18	100	0	0

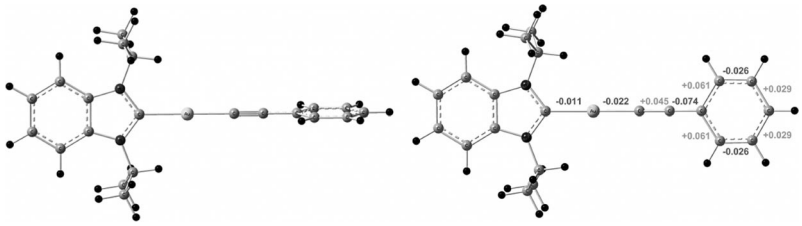

Figure 7. DFT-optimized ground state (left) and triplet state (right) of **1a**. The main differences in bond lengths (larger than 0.01 Å) between the optimized geometries are reported.

Full geometry optimizations of the low-lying triplet states of the selected compounds were carried out in the gas phase by the use of unrestricted DFT calculations. The solvent-corrected energy differences between the optimized ground state and lowest triplet state are unexpectedly not as accurate as the results of the TD-DFT calculations as indicated by the average error of 21 nm in comparison with the experimental data. It could be related to the facile rotation of the phenyl ring (or the heteroaromatic ring in **1f**) of the alkyne ligand, which is perpendicular to the plane of the carbene in the optimized ground states while both planes are coplanar in the optimized triplet states (Figure 7).

Besides that, the main changes observed in the triplet state of **1a** with respect to the ground state take place within the $AuC_{\alpha}C_{\beta}R$ moiety with shortenings of the Au–C_{α} and C_{β}–R bonds by 0.022 and 0.074 Å and a significant elongation of the central $C_{\alpha}\equiv C_{\beta}$ triple bond by 0.045 Å (Figure 7). The geometry of the DFT-optimized triplet state of **1a** corresponds well to the expected structural distortion induced by the promotion of one electron from the C≡C bonding HOMO to the C≡C antibonding LUMO + 1 of the ground state. A careful analysis of the molecular orbital diagram of the open-shell triplet state of **1a** confirm that the singly occupied molecular orbitals SOMO (α) and SOMO – 1 (α) are derived from the LUMO + 1 and HOMO orbitals of the ground state (Figure 8). The SOMO, from which the emission is produced, is localized at 88% on the alkyne ligand, 7% on the carbene ligand, and 5% on the metal center, while the SOMO – 1, where the excited electron should return, is localized at 60% on the alkyne ligand, 28% on the carbene ligand, and 12% on the metal center (Table 10). The isodensity plots of the SOMO and

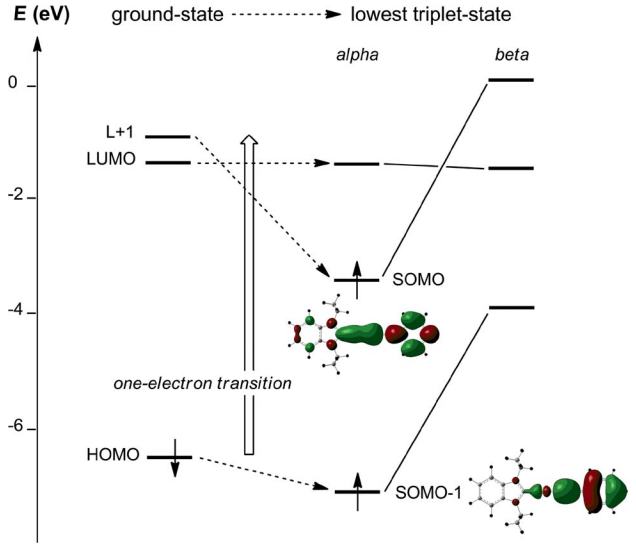

Figure 8. MO diagrams for the ground state and lowest triplet state of **1a**.

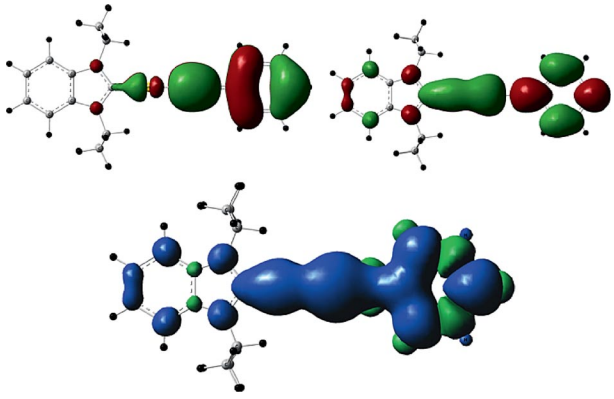

Figure 9. Isodensity plots of the singly occupied molecular orbitals SOMO (up/left) and SOMO – 1 (up/right), and the spin-density surface of the DFT-optimized triplet state of **1a** (isodensity value is 0.02 for SOMOs, and 0.0004 for the spin-density surface).

Table 10. Molecular orbital compositions [%] and energy level [eV] of the singly occupied SOMO and SOMO – 1 of the optimized triplet states of **1a**, **1b**, **1e**, **1f**, **1l**, and **2**.

	1a				**1b**				**1e**			
MO	*E*	Carbene	Au	C≡CR	*E*	Carbene	Au	C≡CR	*E*	Carbene	Au	C≡CR
SOMO	–3.30	5	7	88	–3.28	6	8	86	–3.64	2	3	95
SOMO – 1	–6.69	28	12	60	–6.65	26	11	63	–6.18	4	5	91
	1f				**1l**				**2**			
MO	*E*	Carbene	Au	C≡CR	*E*	Carbene	Au	C≡CR	*E*	Carbene	Au	C≡C–(C_6H_4)–C≡C
SOMO	–1.31	3	6	91	–3.82	0	2	98	–3.35	5	7	88
SOMO – 1	–3.75	70	10	20	–6.32	0	0	100	–6.14	10	12	78

SOMO – 1, and the spin density surface of the lowest triplet state of **1a** (Figure 9) visually identify the emission from a transition with a ^{3}ILCT character originated by the alkyne ligand. Similar orbital analyses were carried out for all DFT-studied compounds. The spin-density surfaces of the lowest triplet states of **1b**, **1e**, **1f**, **1l**, and **2** (Figure 10) point to the ^{3}ILCT nature of the emitting triplet states with a participation of 2–6% of the metal center.

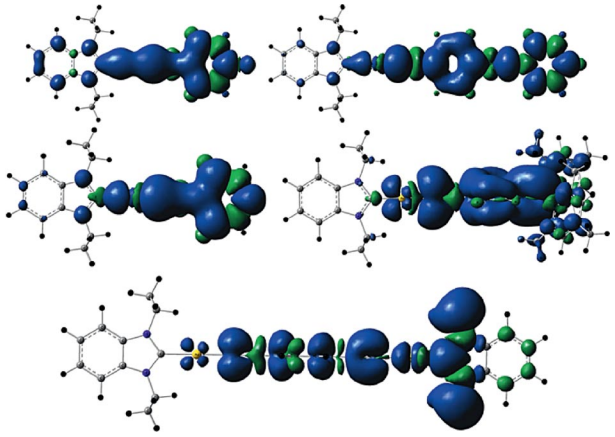

Figure 10. Spin-density surface of the DFT-optimized triplet state of **1b**, **1e**, **1f**, **1l**, and **2** (isodensity value, 0.0004) showing the origins of the emission properties.

Conclusion

The present study has investigated the variation in photophysical characteristics upon incorporation of various acetylides on benzimidazole N-heterocyclic carbene Au^{I} chloride. The effect of the metal is evident from the phosphorescent nature of the emission and is supported by theoretical calculations. Optical, electrochemical, and theoretical investigations (DFT and TD-DFT) suggest a significant dominance of the ligand character, which can be advantageously used for tuning the luminescent properties. Weak aurophilic interactions were observed in certain complexes reported in this work, however, its direct influence on modulation of the photophysical properties could not be unequivocally established among the studied examples.

Experimental Section

Material and Methods: All manipulations were carried out without special precautions for excluding air and moisture. ^{1}H and ^{13}C{^{1}H} NMR spectra were recorded on Bruker AV2-400 or AV-500 spectrometers. ^{19}F NMR spectra were recorded on either Varian Mercury or Bruker AV2-400 spectrometers. Chemical shifts (δ) are reported in parts per million (ppm) referenced to tetramethylsilane (δ = 0.00) ppm using the residual protio solvent peaks as internal standards (^{1}H NMR spectroscopy experiments) or the characteristic resonances of the solvent nuclei (^{13}C NMR spectroscopy experiments). ^{19}F NMR spectroscopy was referenced to $CFCl_3$ (δ = 0.00 ppm) ppm. Coupling constants (J) are quoted in Hertz (Hz) and the following abbreviations are used to describe the signal multiplicities: s (singlet), d (doublet), t (triplet), q (quartet), m (multiplet), dd (doublet of doublet), td (triplet of doublet), dt (doublet of triplet). Proton and carbon assignments have been made using routine one- and two-dimensional NMR spectroscopy where appropriate. IR spectra were recorded on a Perkin–Elmer 1600 Fourier Transform spectrophotometer using KBr pellets with frequencies (ν) quoted in wave numbers [cm^{-1}]. Elemental microanalysis was carried out with a Leco CHNS-932 analyzer.

Mass spectra were recorded on a Finnigan-MAT-8400 mass spectrometer. TLC analysis was performed on precoated Merck silica gel 60 F_{254} slides and visualized by luminescence quenching either at (short wavelength) 254 nm or (long wavelength) 365 nm. UV/Vis measurements were carried out on a Perkin–Elmer Lambda 19 UV/Vis spectrophotometer. Emission spectra were acquired on a Perkin–Elmer spectrophotometer using 450 W xenon-lamp excitation by exciting at the longest-wavelength absorption maxima. All samples for emission spectra were degassed by at least three freeze–pump–thaw cycles in an anaerobic cuvette and were pressurized with N_2 following each cycle. 77 K emission spectra were acquired in frozen 2-methyltetrahydrofuran (2-MeTHF) glass. Luminescence quantum yields (Φ) were determined at 298 K (estimated uncertainty ±15%) using standard methods[24] Wavelength-integrated intensities (I) of the corrected emission spectra were compared to isoabsorptive spectra of a quinine sulfate standard (Φ_r = 0.546 in 1 N H_2SO_4 air-equilibrated solution) and was corrected for the solvent refractive index. Absolute quantum yields were determined for thin-film samples coated on glass plates (2% PMMA loading) using an integrating-sphere apparatus on a Horiba Jobin Yvon spectrophotometer. The results were calculated according to the literature protocol.[25] Phosphorescence lifetimes were measured by a time-correlated single-photon counting method (TCSPC) performed on an Edinburgh FLS920 spectrophotometer, using a nF900 lamp source at 30000 Hz frequency with 15 nm excitation and 15 nm emission slit widths. Cyclic voltammograms were obtained with a voltammetric analyzer. The cell was equipped with a gold working electrode and a Pt counter electrode, and a nonaqueous reference electrode (Ag/AgCl). All sample solutions (CH_2Cl_2) were approximately 5×10^{-3} M in substrate and 0.1 M in Bu_4NPF_6, and were prepared under nitrogen. Ferrocene was subsequently added and the calibration of voltammograms was recorded.

General Procedure for the Preparation of (1,3-Diisopropylbenzimidazolin-2-ylidene)–Au^{I}–Alkynes: NaOH (7.0 equiv.) was added to the methanolic solution (ca. 20 mL) of the appropriate terminal alkynes (1.0 equiv.) and it was left at reflux. After 15 min, the (1,3-diisopropylbenzimidazoline-2-ylidene)gold(I) chloride complex (1.0 equiv.) was added to the mixture and it was stirred for 2–4 h. Once the TLC indicated the complete consumption of the starting material, the reaction mixture was concentrated. The residue thus obtained was diluted with CH_2Cl_2 and washed twice with water. The combined organic layer after separation was then dried with anhydrous Na_2SO_4 and the solvent was concentrated under vacuum to obtain the crude product. Further purification by column chromatography (Al_2O_3, hexane/EtOAc 1:1) afforded products as off-white to yellow solids. The reaction conditions and/or the work-up procedures are slightly different and are described individually where appropriate.

[(Bimz)Au^{I}(phenylethynyl)] (1a): Following the general procedure, phenylacetylene (23.4 mg, 0.23 mmol) was treated with **A** (100.0 mg, 0.23 mmol) to obtain the product as an off-white solid, Yield: 85.0 mg, 74%. IR (KBr): $\tilde{\nu}$ = (C≡C) 2115 cm^{-1}. ^{1}H NMR (500 MHz, $CDCl_3$, 298 K): δ = 1.76 (d, J = 8.5 Hz, 12 H, *i*Pr–CH_3), 5.60 (sept, J = 7.0 Hz, 2 H, *i*Pr–CH), 7.19–7.22 (m, 1 H, Ar–H), 7.26 (t, J = 5.0 Hz, 2 H, Ar–H), 7.37 (dt, J = 9.5, 3.5 Hz, 2 H,

bimz–CH), 7.54 (d, J = 5.5 Hz, 2 H, Ar–H), 7.67 (dt, J = 9.5, 3.5 Hz, 2 H, bimz–CH) ppm. ^{13}C NMR (125 MHz, $CDCl_3$, 298 K): δ = 21.8, 54.4, 105.8, 113.4, 123.6, 125.5, 126.4, 127.1, 127.8, 132.4, 132.6, 192.0 ppm. $C_{21}H_{23}AuN_2$ (500.38): calcd. C 50.41, H 4.63, N 5.60; found C 50.23, H 4.49, N 5.42.

[(Bimz)Au^{I}(*p*-fluorophenylethynyl)] (1b): Following the general procedure, *p*-fluorophenylacetylene (55.0 mg, 0.45 mmol) was treated with **A** (200.0 mg, 0.460 mmol) to obtain the product as an off-white solid; yield 190.0 mg, 80%. IR (KBr): $\tilde{\nu}$ = (C≡C) 2118 cm^{-1}. ESI-MS: m/z = 519 [M + H]$^+$. ^{1}H NMR (400 MHz, $CDCl_3$, 298 K): δ = 1.76 (d, J = 6.8 Hz, 12 H, *i*Pr–CH_3), 5.60 (sept, J = 6.8 Hz, 2 H, *i*Pr–CH), 6.95 (t, J = 6.8 Hz, 2 H, Ar–H), 7.40 (dt, J = 6.0, 2.5 Hz, 2 H, bimz–CH), 7.52 (dd, J = 5.5, 3.0 Hz, 2 H, Ar–H), 7.66 (dt, J = 6.0, 2.5 Hz, 2 H, bimz–CH) ppm. ^{13}C NMR (125 MHz, $CDCl_3$, 298 K): δ = 21.7, 54.0, 104.6, 113.1, 115.0, 121.6, 123.6, 123.8, 132.4, 132.7, 134.0, 192.0 ppm. ^{19}F NMR (282 MHz, $CDCl_3$, 298 K): δ = –115.5 (m, 1 F) ppm. $C_{21}H_{22}AuFN_2$ (518.38): calcd. C 48.66, H 4.28, N 5.40; found C 48.44, H 4.47, N 5.35.

[(Bimz)Au^{I}(*p*-methoxyphenylethynyl)] (1c): Following the general procedure, *p*-methoxyphenylacetylene (30.3 mg, 0.23 mmol) was treated with **A** (100.0 mg, 0.23 mmol) to obtain the product as a white solid; yield 96.0 mg, 79%. IR (KBr): $\tilde{\nu}$ = (C≡C) 2113 cm^{-1}. ^{1}H NMR (500 MHz, $CDCl_3$, 298 K): δ = 1.75 (d, J = 7.0 Hz, 12 H, *i*Pr–CH_3), 3.81 (s, 3 H, -OCH_3), 5.61 (sept, J = 7.0 Hz, 2 H, *i*Pr–CH), 6.81 (d, J = 8.0 Hz, 2 H, Ar–H), 7.37 (dt, J = 9.0, 3.0 Hz, 2 H, bimz–CH), 7.50 (d, J = 8.5 Hz, 2 H, Ar–H), 7.66 (dt, J = 9.0, 3.0 Hz, 2 H, bimz–CH) ppm. ^{13}C NMR (125 MHz, $CDCl_3$, 298 K): δ = 21.8, 54.0, 55.2, 105.7, 113.1, 113.4, 117.8, 123.5, 125.0, 132.7, 133.7, 158.2, 192.2 ppm. $C_{22}H_{25}AuN_2O$ (530.41): calcd. C 49.82, H 4.75, N 5.28; found C 49.48, H 4.60, N 4.88.

[(Bimz)Au^{I}(3,4,5-trimethoxyphenylethynyl)] (1d): Following the general procedure, 1,2,3-trimethoxybenzene (66.3 mg, 0.34 mmol) was treated with **A** (150.0 mg, 0.34 mmol) to obtain the product as a white solid; yield 161.0 mg, 79%. IR (KBr): $\tilde{\nu}$ = (C≡C) 2109 cm^{-1}. ESI-MS: m/z = 613 [M + Na]$^+$. ^{1}H NMR (400 MHz, $CDCl_3$, 298 K): δ = 1.74 (d, J = 7.0 Hz, 12 H, *i*Pr–CH_3), 3.85 (d, J = 7.0 Hz, 9 H), 5.58 (sept, J = 7.0 Hz, 2 H, *i*Pr–CH), 6.80 (s, 2 H, Ar–H), 7.36 (dt, J = 8.5, 3.0 Hz, 2 H, bimz–CH), 7.64 (dt, J = 8.5, 3.0 Hz, 2 H, bimz–CH) ppm. ^{13}C NMR (125 MHz, $CDCl_3$, 298 K): δ = 21.8, 54.0, 56.0, 61.0, 105.8, 109.5, 113.0, 120.6, 123.6, 126.2, 132.4, 132.6, 152.6, 192.0 ppm. $C_{24}H_{29}AuN_2O_3$ (590.47): calcd. C 48.82, H 4.95, N 4.74; found C 48.65, H 4.85, N 4.59.

[(Bimz)Au^{I}(1-ethynyl-4-phenylethynyl)] (1e): Following the general procedure, 1-ethynyl-4-(phenylethynyl)benzene (97.6 mg, 0.48 mmol) was treated with **A** (200.0 mg, 0.46 mmol) to obtain the product as a white solid; yield 221.0 mg, 80%. IR (KBr): $\tilde{\nu}$ = (Au–C≡C) 2110 cm^{-1}. ESI-MS: m/z = 601 [M + H]$^+$. ^{1}H NMR (400 MHz, $CDCl_3$, 298 K): δ = 1.73 (d, J = 7.2 Hz, 12 H, *i*Pr–CH_3), 5.60 (sept, J = 7.2 Hz, 2 H, *i*Pr–CH), 7.31–7.36 (m, 5 H, Ar–H), 7.32–7.42 (m, 2 H, bimz–CH), 7.47–7.52 (m, 4 H, Ar–H), 7.64 (dt, J = 9.5, 3.1 Hz, 2 H, bimz–CH) ppm. ^{13}C NMR (125 MHz, $CDCl_3$, 298 K): δ = 21.8, 53.9, 89.7, 90.2, 105.6, 113.0, 121.0, 123.4, 123.6, 125.6, 128.0, 128.3, 130.2, 131.1, 131.5, 132.2, 132.6, 191.8 ppm. $C_{29}H_{27}AuN_2$ (600.51): calcd. C 58.00, H 4.53, N 4.66; found C 58.29, H 4.73, N 4.68.

[(Bimz)Au^{I}(4-pyridylethynyl)] (1f): Following the general procedure, 4-ethynylpyrdine (35.5 mg, 0.34 mmol) was treated with **A** (150.0 mg, 0.34 mmol) to obtain the product as off-white solid, Column purification: Neutral Al_2O_3; eluent: EtOAc diluted with 5% MeOH; yield 100 mg, 58%. IR (KBr): $\tilde{\nu}$ = (C≡C) 2115 cm^{-1}. ESI-MS: m/z = 502 [M + H]$^+$. ^{1}H NMR (400 MHz, $CDCl_3$, 298 K): δ = 1.80 (d, J = 6.8 Hz, 12 H, *i*Pr–CH_3), 5.55 (sept, J = 7.0 Hz, 2 H, *i*Pr–CH), 7.28 (d, J = 2.8 Hz, 2 H, pyridyl Ar–H), 7.43 (dt, J = 9.5, 3.2 Hz, 2 H, bimz–CH), 7.71 (dt, J = 9.5, 3.2 Hz, 2 H, bimz–CH), 8.47 (d, J = 2.8 Hz, 2 H, pyridyl Ar–H) ppm. ^{13}C NMR (125 MHz, $CDCl_3$, 298 K): δ = 21.8, 54.0, 103.2, 113.1, 123.7, 128.6, 132.1, 132.6, 134.7, 135.4, 191.6 ppm. $C_{20}H_{22}AuN_3$ (501.38): calcd. C 47.91, H 4.42, N 8.38; found C 47.69, H 4.36, N 8.25.

[(Bimz)Au^{I}(2-ethynylthiophene)] (1g): Following the general procedure, 2-ethynylthiophene (24.8 mg, 0.23 mmol) was treated with **A** (100.0 mg, 0.23 mmol) to obtain the product as an off-white solid; yield 58.0 mg, 50%. IR (KBr): $\tilde{\nu}$ = (C≡C) 2103 cm^{-1}. ESI-MS: m/z = 507 [M + H]$^+$. ^{1}H NMR (500 MHz, $CDCl_3$, 298 K): δ = 1.71 (d, J = 7.0 Hz, 12 H, *i*Pr–CH_3), 5.61 (sept, J = 7.0 Hz, 2 H, *i*Pr–CH), 6.90 (t, J = 5.0 Hz, 1 H, Ar–H), 7.05 (d, J = 5.0 Hz, 1 H, Ar–H), 7.15 (d, J = 5.0 Hz, 1 H, Ar–H), 7.35 (dt, J = 9.0, 3.5 Hz, 2 H, bimz–ArH), 7.63 (dt, J = 9.2, 3.5 Hz, 2 H, bimz–ArH) ppm. ^{13}C NMR (125 MHz, $CDCl_3$, 298 K): δ = 21.8, 53.9, 97.7, 113.1, 123.6, 124.7, 126.0, 126.6, 130.9, 132.6, 132.8, 191.6 ppm. $C_{19}H_{21}AuN_2S$ (506.41): calcd. C 45.06, H 4.18, N 5.53; found C 44.81, H 4.08, N 5.41.

[(Bimz)Au^{I}(3-ethynylthiophene)] (1h): Following the general procedure, 3-ethynylthiophene (24.8 mg, 0.23 mmol) was treated with **A** (100.0 mg, 0.23 mmol) to obtain the product as an off-white solid, Yield: 50.0 mg, 43%. IR (KBr): $\tilde{\nu}$ = (C≡C) 2116 cm^{-1}. ^{1}H NMR (400 MHz, $CDCl_3$, 298 K): δ = 1.76 (d, J = 6.8 Hz, 12 H, *i*Pr–CH_3), 5.61 (sept, J = 6.9 Hz, 2 H, *i*Pr–CH), 7.20–7.21 (m, 2 H, Ar–H), 7.63 (dt, J = 9.0, 2.8 Hz, 2 H, bimz–CH), 7.40–7.44 (m, 1 H, Ar–H), 7.66 (dt, J = 9.0, 2.8 Hz, 2 H, bimz–CH) ppm. ^{13}C NMR (100 MHz, $CDCl_3$, 298 K): δ = 21.8, 53.9, 100.2, 113.1, 123.6, 124.0, 124.5, 126.6, 127.2, 131.1, 132.7, 192.0 ppm. $C_{19}H_{21}AuN_2S$ (506.41): calcd. C 45.06, H 4.18, N 5.53; found C 44.92, H 4.22, N 5.14.

[(Bimz)Au^{I}(pyren-1-ylethynyl)] (1i): Following the general procedure, 1-ethynylpyrene (78.0 mg, 0.34 mmol) was treated with **A** (100.0 mg, 0.23 mmol) to obtain the product as an orange-brown solid. The crude product was purified by column chromatography using neutral alumina (eluent: CH_2Cl_2/hexane 1:1); yield 87.0 mg, 60%. IR (KBr): $\tilde{\nu}$ = (C≡C) 2102 cm^{-1}. ^{1}H NMR (500 MHz, $CDCl_3$): δ = 1.76 (d, J = 6.8 Hz, 12 H, *i*Pr–CH_3), 5.60 (sept, J = 7.0 Hz, 2 H, *i*Pr–CH), 7.19 (dt, J = 9.0, 2.8 Hz, 2 H, bimz–CH), 7.48 (dt, J = 9.0, 2.8 Hz, 2 H, bimz–CH), 7.79–7.87 (m, 3 H, Ar–H), 7.95 (d, 1 H, Ar–H), 8.00–8.11 (m, 3 H, Ar–H), 8.13 (d, J = 8.5 Hz, 1 H, Ar–H), 8.84 (d, J = 8.5 Hz, 1 H, Ar–H) ppm. ^{13}C NMR ($CDCl_3$, 125 MHz, 298 K): δ = 105.0, 113.6, 124.0, 125.0, 125.2, 125.3, 125.4, 125.5, 126.4, 127.6, 127.7, 127.9, 128.0, 130.5, 131.3, 132.0, 132.8, 133.3, 136.0, 192.2 ppm. $C_{31}H_{27}AuN_2$ (624.53): calcd. 59.62, H 4.36, N,4.49; found C 59.59, H 4.54, N 4.72.

[(Bimz)Au^{I}(3-hydroxy-3-methylbut-1-yn-1-yl)] (1j): Following the general procedure, 2-methylbut-3-yn-2-ol (29.0 mg, 0.34 mmol) was treated with **A** (100.0 mg, 0.23 mmol) to obtain the product as a white solid; yield 67 mg, 60%. IR (KBr): $\tilde{\nu}$ = (C≡C) 2126 cm^{-1}. ^{1}H NMR (500 MHz, $CDCl_3$, 298 K): δ = 1.60 (s, 6 H, 2-methylbutynol –CH_3), 1.68 (d, J = 7.0 Hz, 12 H, *i*Pr–CH_3), 2.05 (s, 1 H, hydroxy–H), 5.53 (sept, J = 7.0 Hz, 2 H, *i*Pr–CH), 7.32 (t, J = 6.5 Hz, 2 H, bimz–CH), 7.61 (t, J = 6.5 Hz, 2 H, bimz–CH) ppm. ^{13}C NMR (100 MHz, $CDCl_3$, 298 K): δ = 21.7, 32.7, 53.9, 65.7, 111.0, 113.2, 116.7, 123.5, 132.6, 192.0 ppm. $C_{18}H_{25}AuN_2O$ (482.37): calcd. C 44.82, H 5.22, N 5.81; found C 44.30, H 5.00, N 5.48.

[(Bimz)Au^{I}(ethynyltriisopropylsilane)] (1k): Following the general procedure, (triisopropylsilyl)acetylene (42.0 mg, 0.23 mmol) was

treated with **A** (100.0 mg, 0.23 mmol) to obtain the product as an off-white solid; yield 110.0 mg, 82%. IR (KBr): $\tilde{\nu}$ = (C≡C) 2052 cm^{-1}. ESI-MS: *m*/*z* = 603 $[M + Na]^+$. ^1H NMR (400 MHz, $CDCl_3$, 298 K): δ = 1.17–1.19 (m, 18 H, Si–*i*Pr_3), 1.71 (d, *J* = 7.0 Hz, 12 H, *i*Pr–CH_3), 5.60 (sept, *J* = 7.0 Hz, 2 H, *i*Pr–CH), 7.35 (dt, *J* = 6.5, 2.5 Hz, 1 H), 7.65 (dt, *J* = 6.5, 3.5 Hz, 2 H) ppm. ^{13}C NMR (125 MHz, $CDCl_3$, 298 K): δ = 11.8, 19.0, 21.6, 53.8, 105.6, 113.2, 123.4, 132.6, 148.9, 192.9 ppm. $C_{24}H_{39}AuN_2Si$ (580.64): calcd. C 49.65, H 6.77, N 4.82; found C 49.41, H 6.90, N 4.66.

[(Bimz)Au^I(4-ethynylphenyl)dimesitylborane] (1l): Following the general procedure, (4-ethynylphenyl)dimesitylborane (96.7 mg, 0.27 mmol) was treated with **A** (100.0 mg, 0.23 mmol) to obtain the product as an off-white solid; yield 65.0 mg, 37.0%. IR (KBr): $\tilde{\nu}$ = (C≡C) 2110 cm^{-1}. ESI-MS: *m*/*z* = 749 $[M + H]^+$. ^1H NMR (500 MHz, $CDCl_3$, 298 K): δ = 1.78 (d, *J* = 7.5 Hz, 12 H, *i*Pr–CH_3), 2.03 (s, 12 H, mesityl–CH_3), 2.33 (s, 6 H, mesityl–CH_3), 5.53 (sept, *J* = 7.0 Hz, 2 H), 6.86 (s, 4 H, Ar–H), 7.41 (dd, *J* = 7.0, 3.5 Hz, 2 H, bimz–ArH), 7.70 (dd, *J* = 7.0, 3.5 Hz, 2 H, bimz–ArH) ppm. ^{13}C NMR (125 MHz, $CDCl_3$, 298 K): δ = 21.0, 21.7, 23.1, 105.3, 113.1, 132.7, 123.5, 128.0, 130.1, 131.3, 133.7, 136.2, 138.5, 140.6, 141.5, 143.6, 191.9 ppm. $4(C_{39}H_{44}AuBN_2)\cdot 2(C_5H_{12})$ (3138.46): calcd. C 62.58, H 5.92, N 3.74; found C 62.33, H 5.88, N 3.67.

[{(Bimz)Au^I}$_2$(1,4-diethynylbenzene)] (2): Following the general procedure, 1,4-diethynylbenzene (14.5 mg, 0.114 mmol) was treated with **A** (100.0 mg, 0.23 mmol) to obtain the product as an off-white solid; yield 90.0 mg, 42%. IR (KBr): $\tilde{\nu}$ = (C≡C) 2113 cm^{-1}. ESI-MS: *m*/*z* = 923 $[M + H]^+$. ^1H NMR (400 MHz, $CDCl_3$, 298 K): δ = 1.76 (d, *J* = 7.2 Hz, 24 H, *i*Pr–CH_3), 5.61 (sept, *J* = 7.0 Hz, 4 H, *i*Pr–CH), 7.32 (dt, *J* = 6.8, 3.2 Hz, 4 H, bimz–CH), 7.43 (s, 4 H, Ar–H), 7.67 (dt, *J* = 6.8, 3.2 Hz, 4 H, bimz–CH) ppm. ^{13}C NMR (100 MHz, $CDCl_3$, 298 K): δ = 21.9, 54.0, 106.2, 113.1, 123.4, 123.5, 128.5, 131.7, 132.7, 192.3 ppm. $C_{36}H_{40}Au_2N_4$ (922.67): calcd. C 46.86, H 4.37, N 6.07; found C 46.58, H 4.35, N 6.02.

[{(Bimz)Au^I}$_3$(1,3,5-triethynylbenzene)] (3): Following the general procedure, 1,3,5-triethynylbenzene (11.4 mg, 0.075 mmol) was treated with **A** (100 mg, 0.23 mmol) to obtain the product as an off-white solid; yield 123 mg, 40%. IR (KBr): $\tilde{\nu}$ = (C≡C) 2103 cm^{-1}. ESI-MS: *m*/*z* = 1354 $[M^+]$. ^1H NMR (500 MHz, $CDCl_3$, 298 K): δ = 1.75 (d, *J* = 6.5 Hz, 36 H, *i*Pr–CH_3), 5.62 (sept, *J* = 7.0 Hz, 6 H, *i*Pr–CH), 7.35 (dd, *J* = 6.5, 3.0 Hz, 6 H, bimz–CH), 7.56 (s, 3 H, Ar–H), 7.64 (dd, *J* = 6.5, 3.0 Hz, 6 H, bimz–CH) ppm. ^{13}C NMR (125 MHz, $CDCl_3$, 298 K): δ = 21.7, 54.0, 105.7, 113.4, 123.4, 124.7, 126.4, 128.9, 132.7, 134.8, 192.4 ppm. $C_{51}H_{57}Au_3N_6$ (1344.95): calcd. C 45.54, H 4.27, N 6.25; found C 45.20, H 4.07, N 6.25.

X-ray Diffraction Analyses: Single-crystal X-ray diffraction data were collected at 183(2) K on a Xcalibur diffractometer (Agilent Technologies, Ruby CCD detector) for all compounds using a single wavelength enhance X-ray source with Mo-K_α radiation (λ = 0.71073 Å).[26] The selected suitable single crystals were mounted using polybutene oil on the top of a glass fiber fixed on a goniometer head and were immediately transferred to the diffractometer. Pre-experiment, data collection, data reduction, and analytical absorption corrections[27] were performed with the program suite CrysAlisPro.[26] The crystal structures were solved with SHELXS-97[28] using direct methods. The structure refinements were performed by full-matrix least-squares on F^2 with SHELXL-97.[28] All programs used during the crystal-structure determination process are included in the WINGX software.[29] PLATON[30] was used to check the result of the X-ray analyses.

CCDC-855992 (for **1a**), -855993 (for **1b**), -855994 (for **1e**), -855995 (for **1f**), -855996 (for **1h**), -855997 (for **1k**), and -855998 (for **1l**) contain the supplementary crystallographic data (excluding structure factors) for this paper. These data can be obtained free of charge from The Cambridge Crystallographic Data Centre via www.ccdc.cam.ac.uk/data_request/cif.

Supporting Information (see footnote on the first page of this article): Absorption and emission spectra, cyclic voltammetry, energies, and Cartesian coordinates are presented.

Acknowledgments

We thank Prof. Frank Nüesch (EMPA) for help with solid-state luminescence measurements. Funding from University of Zürich is gratefully acknowledged.

[1] a) R. J. Puddephatt, *The Chemistry of Gold*, Elsevier, Amsterdam, **1978**; b) G. K. Anderson, *Adv. Organomet. Chem.* **1982**, *20*, 39–114; c) K. I. Grandberg, *Russ. Chem. Rev.* **1982**, 51, 249–264; d) T. E. Muller, D. M. P. Mingos, D. J. Williams, *J. Chem. Soc., Chem. Commun.* **1994**, 1787–1788; e) D. Michael, P. Mingos, J. Yau, S. Menzer, D. J. Williams, *Angew. Chem.* **1995**, *107*, 2045; *Angew. Chem. Int. Ed. Engl.* **1995**, *34*, 1894–1895; f) J. Vicente, M. T. Chicote, M. D. Abrisqueta, R. Guerrero, P. G. Jones, *Angew. Chem.* **1997**, *109*, 1252; *Angew. Chem. Int. Ed. Engl.* **1997**, *36*, 1203–1205; g) C. P. McArdle, M. J. Irwin, M. C. Jennings, R. J. Puddephatt, *Angew. Chem.* **1999**, *111*, 3571; *Angew. Chem. Int. Ed.* **1999**, *38*, 3376–3378; h) C. P. McArdle, J. J. Vittal, R. J. Puddephatt, *Angew. Chem.* **2000**, *112*, 3977; *Angew. Chem. Int. Ed.* **2000**, *39*, 3819; i) M. J. Irwin, G. C. Jia, N. C. Payne, R. J. Puddephatt, *Organometallics* **1996**, *15*, 51–57; j) M. Shiotsuka, Y. Yamamoto, S. Okuno, M. Kitou, K. Nozaki, S. Onaka, *Chem. Commun.* **2002**, 590–591; k) W. Lu, W.-M. Kwok, C. Ma, T.-L. Chris, M.-X. Zhu, C. M. Che, *J. Am. Chem. Soc.* **2011**, *133*, 31684–31696.

[2] a) G. E. Coates, C. Parkin, *J. Chem. Soc.* **1962**, 3220; b) O. M. Abu-Salah, A. A. Al-Ohaly, *Inorg. Chim. Acta* **1983**, *77*, L159.

[3] a) R. J. Cross, M. F. Davidson, *J. Chem. Soc., Dalton Trans.* **1986**, 411–414; b) R. J. Cross, M. F. Davidson, A. J. Mclennan, *J. Organomet. Chem.* **1984**, *265*, C37–C39; c) M. I. Bruce, E. Horn, J. G. Matisons, M. R. Snow, *Aust. J. Chem.* **1984**, *37*, 1163–1170; d) M. I. Bruce, M. Jevric, B. W. Skelton, M. E. Smith, A. H. White, N. N. Zaitseva, *J. Organomet. Chem.* **2006**, *691*, 361–370; e) J. Vicente, A. R. Singhal, P. G. Jones, *Organometallics* **2002**, *21*, 5887–5900; f) S. K. Bhargava, K. Kitadai, N. Mirzadeh, S. H. Priver, M. Takahashi, J. Wagler, *J. Organomet. Chem.* **2010**, *695*, 1787–1793; g) J. Vicente, M. T. Chicote, M. D. Abrisqueta, P. G. Jones, *Organometallics* **1997**, *16*, 5628–5636; h) J. Vicente, M. T. Chicote, *Coord. Chem. Rev.* **1999**, *193–5*, 1143–1161; i) O. Schuster, R. Y. Liau, A. Schier, H. Schmidbaur, *Inorg. Chim. Acta* **2005**, *358*, 1429–1441.

[4] T. Kaharu, R. Ishii, T. Adachi, T. Yoshida, S. Takahashi, *J. Mater. Chem.* **1995**, *5*, 687–692.

[5] a) A. Luquin, E. Cerrada, M. Laguna, *Gold Chemistry-Applications and Future Directions in the Life Sciences*, Wiley-VCH, Weinheim, Gemany, **2009**; b) V. W. W. Yam, E. C. C. Cheng, *Top. Curr. Chem.* **2007**, *281*, 269–309; c) M. J. Irwin, J. J. Vittal, R. J. Puddephatt, *Organometallics* **1997**, *16*, 3541–3547; d) G. C. Jia, R. J. Puddephatt, J. D. Scott, J. J. Vittal, *Organometallics* **1993**, *12*, 3565–3574; e) V. W. W. Yam, S. W. K. Choi, *J. Chem. Soc., Dalton Trans.* **1996**, 4227–4232; f) H. M. J. Wang, C. Y. L. Chen, I. J. B. Lin, *Organometallics* **1999**, *18*, 1216–1223; g) W. J. Hunks, M. A. MacDonald, M. C. Jennings, R. J. Puddephatt, *Organometallics* **2000**, *19*, 5063–5070; h) J. Vicente, M. T. Chicote, M. M. Alvarez-Falcon, P. G. Jones, *Organometallics* **2005**, *24*, 5956–5963; i) D. Li, X. Hong, C. M. Che, W. C. Lo, S. M. Peng, *J. Chem. Soc., Dalton Trans.* **1993**,

2929–2932; j) X. Hong, K. K. Cheung, C. X. Guo, C. M. Che, *J. Chem. Soc., Dalton Trans.* **1994**, 1867–1871; k) H. Xiao, Y. X. Weng, S. M. Peng, C. M. Che, *J. Chem. Soc., Dalton Trans.* **1996**, 3155–3157; l) C. M. Che, H. Y. Chao, V. M. Miskowski, Y. Q. Li, K. K. Cheung, *J. Am. Chem. Soc.* **2001**, *123*, 4985–4991; m) W. Lu, H. F. Xiang, N. Y. Zhu, C. M. Che, *Organometallics* **2002**, *21*, 2343–2346; n) H. Y. Chao, W. Lu, Y. Q. Li, M. C. W. Chan, C. M. Che, K. K. Cheung, N. Y. Zhu, *J. Am. Chem. Soc.* **2002**, *124*, 14696–14706; o) W. Lu, N. Y. Zhu, C. M. Che, *J. Organomet. Chem.* **2003**, *670*, 11–16.

[6] a) I. R. Whittall, M. G. Humphrey, M. Samoc, B. LutherDavies, *Angew. Chem.* **1997**, *109*, 386; *Angew. Chem. Int. Ed. Engl.* **1997**, *36*, 370–371; b) I. R. Whittall, M. G. Humphrey, M. Samoc, B. Luther Davies, D. C. R. Hockless, *J. Organomet. Chem.* **1997**, *544*, 189–196; c) Q. Y. Hu, W. X. Lu, H. D. Tang, H. H. Y. Sung, T. B. Wen, I. D. Williams, G. K. L. Wong, Z. Y. Lin, G. C. Jia, *Organometallics* **2005**, *24*, 3966–3973; d) R. H. Naulty, M. P. Cifuentes, M. G. Humphrey, S. Houbrechts, C. Boutton, A. Persoons, G. A. Heath, D. C. R. Hockless, B. LutherDavies, M. Samoc, *J. Chem. Soc., Dalton Trans.* **1997**, 4167–4174.

[7] a) H. Schmidbaur, *Gold Bull.* **1990**, 11–21; b) H. Schmidbaur, *Chem. Soc. Rev.* **1995**, *24*, 391; c) H. Schmidbaur, A. Schier, *Chem. Soc. Rev.* **2012**, *41*, 370–412; d) P. Pyykko, *Chem. Rev.* **1997**, *97*, 597–636; e) V. W. W. Yam, T. F. Lai, C. M. Che, *J. Chem. Soc., Dalton Trans.* **1990**, 3747–3752.

[8] a) X. X. Lu, C. K. Li, E. C. C. Cheng, N. Y. Zhu, V. W. W. Yam, *Inorg. Chem.* **2004**, *43*, 2225–2227; b) V. W. W. Yam, K. L. Cheung, S. K. Yip, K. K. Cheung, *J. Organomet. Chem.* **2003**, *681*, 196–209; c) V. W. W. Yam, S. K. Yip, L. H. Yuan, K. L. Cheung, N. Y. Zhu, K. K. Cheung, *Organometallics* **2003**, *22*, 2630–2637; d) S. K. Yip, W. H. Lam, N. Y. Zhu, V. W. W. Yam, *Inorg. Chim. Acta* **2006**, *359*, 3639–3648; e) I. O. Koshevoy, L. Koskinen, E. S. Smirnova, M. Haukka, T. A. Pakkanen, A. S. Melnikov, S. P. Tunik, *Z. Anorg. Allg. Chem.* **2010**, *636*, 795–802; f) L. Liu, W. Y. Wong, J. X. Shi, K. W. Cheah, T. H. Lee, L. M. Leung, *J. Organomet. Chem.* **2006**, *691*, 4028–4041.

[9] H. A. J. Wang, C. S. Vasam, T. Y. R. Tsai, S. H. Chen, A. H. H. Chang, I. J. B. Lin, *Organometallics* **2005**, *24*, 486–493.

[10] a) L. Gao, D. V. Partyka, J. B. Updegraff, N. Deligonul, T. G. Gray, *Eur. J. Inorg. Chem.* **2009**, 2711–2719; b) D. V. Partyka, L. Gao, T. S. Teets, J. B. Updegraff, N. Deligonul, T. G. Gray, *Organometallics* **2009**, *28*, 6171–6182.

[11] a) G. C. Fortman, A. Poater, J. W. Levell, S. Gaillard, A. M. Z. Slawin, I. D. W. Samuel, L. Cavallo, S. P. Nolan, *Dalton Trans.* **2010**, *39*, 10382–10390; b) D. Konkolewicz, S. Gaillard, A. G. West, Y. Y. Cheng, A. Gray-Weale, T. W. Schmidt, S. P. Nolan, S. Perrier, *Organometallics* **2011**, *30*, 1315–1318.

[12] A. L. F. Chow, M. H. So, W. Lu, N. Y. Zhu, C. M. Che, *Chem. Asian J.* **2011**, *6*, 544–553.

[13] a) O. Fujimura, K. Fukunaga, T. Honma, T. Machida, WO2008050733, **2008**, 16; b) O. Fujimura, K. Fukunaga, T. Honma, T. Machida, T. Takahashi, WO2006080515, **2006**, 102.

[14] L. Ray, V. Katiyar, S. Barman, M. J. Raihan, H. Nanavati, M. M. Shaikh, P. Ghosh, *J. Organomet. Chem.* **2007**, *692*, 4259–4269.

[15] L. Ray, M. M. Shaikh, P. Ghosh, *Inorg. Chem.* **2008**, *47*, 230–240.

[16] Radiative (k_r) and nonradiative (k_{nr}) decay rates were estimated from the lifetime data (τ) using the formula $k_r = \Phi_P/\tau$ and $k_{nr} = (1 - \Phi_P)/\tau$ assuming radiative rate constants do not show significant temperature dependence from 77 to 298 K and k_{isc} is considered as unity.

[17] M. J. Frisch, G. W. Trucks, H. B. Schlegel, G. E. Scuseria, M. A. Rob, J. R. Cheeseman, J. A. Montgomery Jr, T. Vreven, K. N. Kudin, J. C. Burant, J. M. Millam, S. S. Iyengar, J. Tomasi, V. Barone, B. Mennucci, M. Cossi, G. Scalmani, N. Rega, G. A. Petersson, H. Nakatsuji, M. Hada, M. Ehara, K. Toyota, R. Fukuda, J. Hasegawa, M. Ishida, T. Nakajima, Y. Honda, O. Kitao, H. Nakai, M. Klene, X. Li, J. E. Knox, H. P. Hratchian, J. B. Cross, V. Bakken, C. Adamo, J. Jaramillo, R. Gomperts, R. E. Stratmann, O. Yazyev, A. J. Austin, R. Cammi, C. Pomelli, J. W. Ochterski, P. Y. Ayala, K. Morokuma, G. A. Voth, P. Salvador, J. J. Dannenberg, V. G. Zakrzewski, S. Dapprich, A. D. Daniels, M. C. Strain, O. Farkas, D. K. Malick, A. D. Rabuck, K. Raghavachari, J. B. Foresman, J. V. Ortiz, Q. Cui, A. G. Baboul, S. Clifford, J. Cioslowski, B. B. Stefanov, G. Liu, A. Liashenko, P. Piskorz, I. Komaromi, R. L. Martin, D. J. Fox, T. Keith, M. A. Al-Laham, C. Y. Peng, A. Nanayakkara, M. Challacombe, P. M. W. Gill, B. Johnson, W. Chen, M. W. Wong, C. Gonzalez, J. A. Pople, *Gaussian 03*, revision D.01, Gaussian, Inc., Wallingford, CT, **2003**.

[18] C. Adamo, V. Barone, *J. Chem. Phys.* **1999**, *110*, 6158–6170.

[19] T. H. Dunning Jr, P. J. Hay, *Modern Theoretical Chemistry*, Plenum, New York, **1976**.

[20] R. Ditchfie, W. J. Hehre, J. A. Pople, *J. Chem. Phys.* **1971**, *54*, 724.

[21] a) R. Bauernschmitt, R. Ahlrichs, *Chem. Phys. Lett.* **1996**, *256*, 454–464; b) M. E. Casida, C. Jamorski, K. C. Casida, D. R. Salahub, *J. Chem. Phys.* **1998**, *108*, 4439–4449; c) R. E. Stratmann, G. E. Scuseria, M. J. Frisch, *J. Chem. Phys.* **1998**, *109*, 8218–8224.

[22] a) V. Barone, M. Cossi, *J. Phys. Chem. A* **1998**, *102*, 1995–2001; b) M. Cossi, N. Rega, G. Scalmani, V. Barone, *J. Comput. Chem.* **2003**, *24*, 669–681.

[23] J. A. Garg, O. Blacque, K. Venkatesan, *Inorg. Chem.* **2011**, *50*, 5430–5441.

[24] J. N. Demas, G. A. Crosby, *J. Phys. Chem.* **1971**, *75*, 991–1024.

[25] J. C. de Mello, H. F. Wittmann, R. H. Friend, *Adv. Mater.* **1997**, *9*, 230.

[26] *Agilent Technologies* (formerly Oxford Diffraction), Yarnton, England, **2011**.

[27] R. C. Clark, J. S. Reid, *Acta Crystallogr., Sect. A* **1995**, *51*, 887–897.

[28] G. M. Sheldrick, *Acta Crystallogr., Sect. A* **2008**, *64*, 112–122.

[29] L. J. Farrugia, *J. Appl. Crystallogr.* **1999**, *32*, 837.

[30] A. L. Spek, *J. Appl. Crystallogr.* **2003**, *36*, 7–13.

Received: December 2, 2011
Published Online: February 29, 2012

Eur. J. Inorg. Chem. **2012** · © WILEY-VCH Verlag GmbH & Co. KGaA, 69451 Weinheim, 2012 · ISSN 1434–1948

SUPPORTING INFORMATION

DOI: 10.1002/ejic.201101351
Title: (Benzimidazolin-2-ylidene)–Au^{I}–Alkynyl Complexes: Syntheses, Structure, and Photophysical Properties
Author(s): Jai Anand Garg, Olivier Blacque, Jakob Heier, Koushik Venkatesan*

1. Electronic absorption spectra of selected complexes **1b-1d, 1h**, **1j**, **1k**, **2** and **A.**

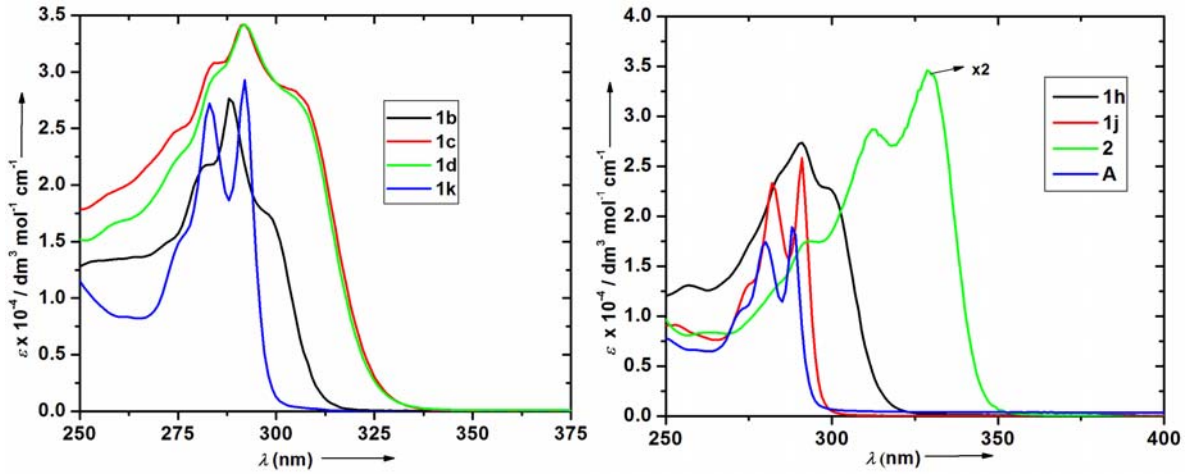

Figure S1. Electronic absorption spectra of **1b-1d**, **1h, 1j, 2** and **A** in CH_2Cl_2 at r.t.

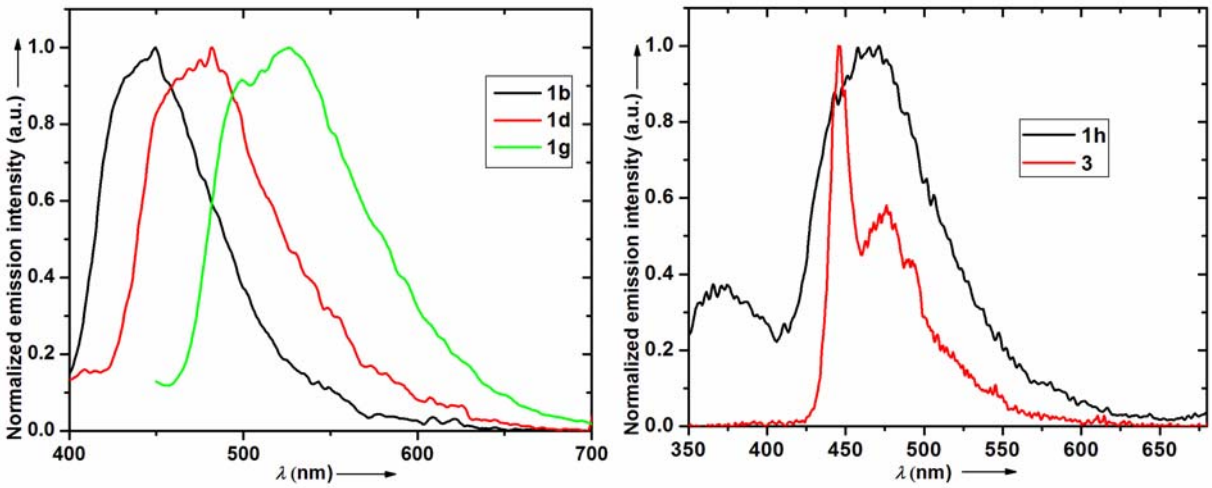

Figure S2. *Left*: Emission spectra of **1b**, **1d**, and **1g**. *Right*: Emission spectra of **1h** and **3** in degassed CH_2Cl_2 recorded at r.t.

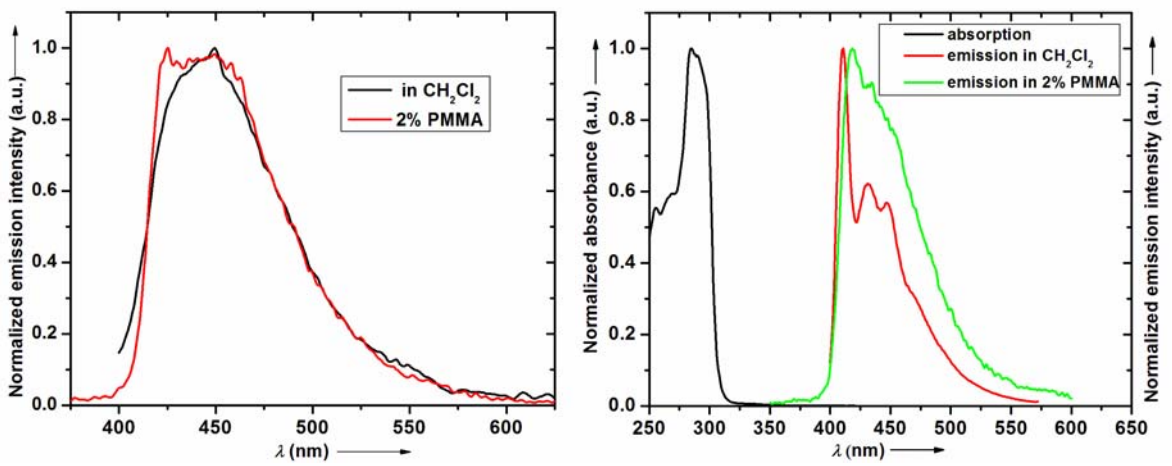

Figure S3. (*Left*) Emission spectra of **1b**. (*Right*) Absorption and Emission spectra of **1f** in CH_2Cl_2 and in thin films recorded at r.t

2. Cyclic voltammograms of selected complexes.

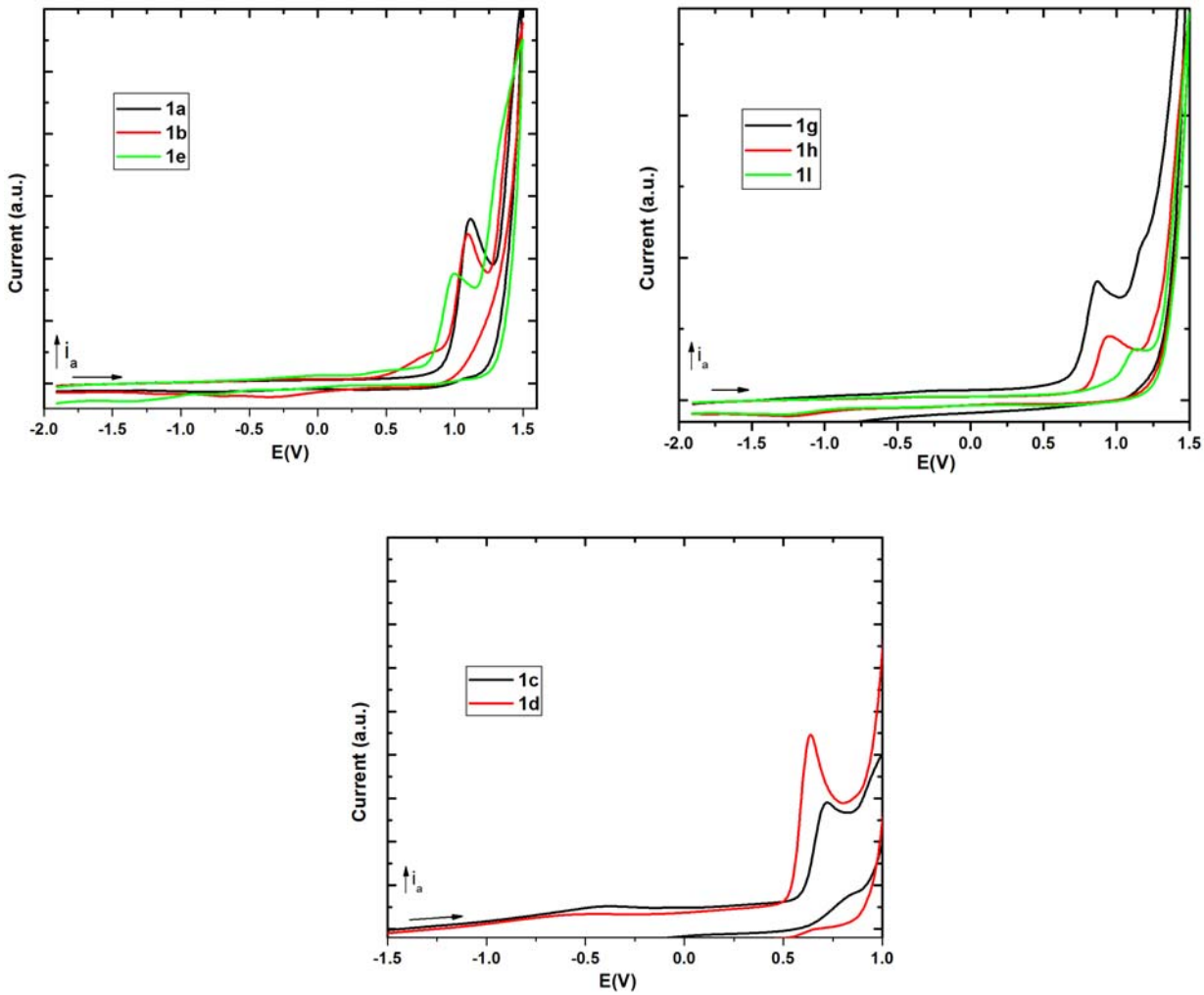

Figure S4. Cyclic voltammogram of **1a-1e**, **1g**, **1h** and **1l** in 0.1M $[nBu_4N][PF_6]$; Au electrode; E *vs* $Fc^{0/+}$; scan rate = 100 mV/s; 20 ºC; CH_2Cl_2.

3. Concentration dependent emission studies.

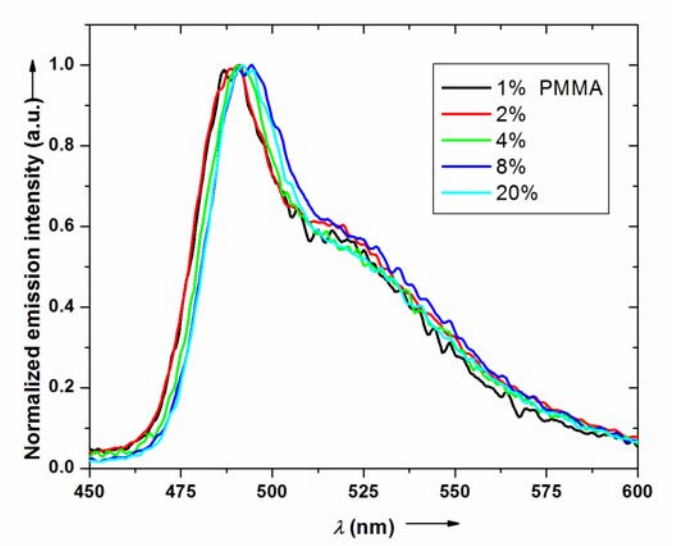

Figure S5. PL spectra recorded with various weight percent concentrations of **1f** on PMMA film.

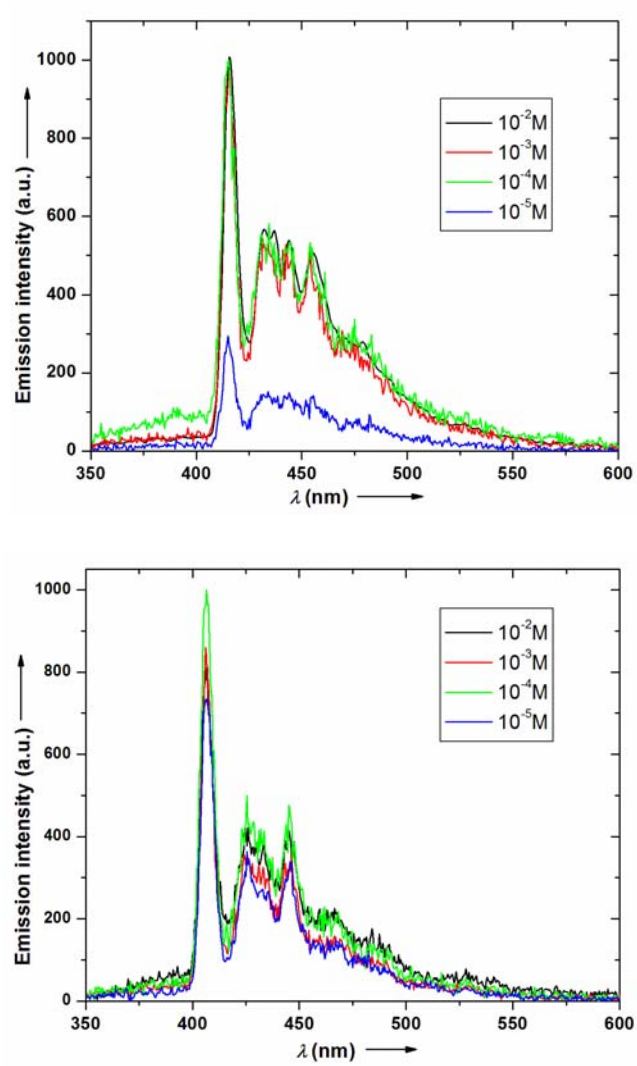

Figure S6. PL spectra of **1b** (*top*) and **1f** (*bottom*) in methyl-THF 77 K at various concentrations.

4. X-ray diffraction analyses

Single-crystal X-ray diffraction data were collected at 183(2) K on a Xcalibur diffractometer (Agilent Technologies, Ruby CCD detector) for all compounds using a single wavelength Enhance X-ray source with MoK_α radiation (l = 0.71073 Å).[1] The selected suitable single crystals were mounted using polybutene oil on the top of a glass fiber fixed on a goniometer head and immediately transferred to the diffractometer. Pre-experiment, data collection, data reduction and analytical absorption corrections[2] were performed with the program suite *CrysAlisPro*.[1] The crystal structures were solved with SHELXS-97[3] using direct methods. The structure refinements were performed by full-matrix least-squares on F^2 with SHELXL-97.[3] All programs used during the crystal structure determination process are included in the WINGX software.[4] PLATON[5] was used to check the result of the X-ray analyses. CCDC-855992 (for **1a**), CCDC-855993 (for **1b**), CCDC-855994 (for **1e**), CCDC-855995 (for **1f**), CCDC-855996 (for **1h**), CCDC-855997 (for **1k**) and CCDC-855998 (for **1l**) contain the supplementary crystallographic data (excluding structure factors) for this paper. These data can be obtained free of charge from The Cambridge Crystallographic Data Centre via www.ccdc.cam.ac.uk/data_request/cif.

[1] Agilent Technologies (formerly Oxford Diffraction), Yarnton, England, 2011.

[2] R. C. Clark, J. S. Reid, *Acta Crystallogr. Sect. A* 1995, **51**, 887 – 897.

[3] G. M. Sheldrick, *Acta Crystallogr. Sect. A* 2008, **64**, 112 – 122.

[4] L. J. Farrugia, *J. Appl. Cryst.* 1999, **32**, 837.

[5] A. L. Spek, *J. Appl. Cryst.* 2003, **36**, 7 – 13.

[6] K. Brandenburg, *DIAMOND*, Crystal Impact GbR, Bonn, Germany, 2007.

5. Computational details

Energies and cartesian coordinates of the optimized ground-state structure of 1a

C	0.00000317	0.70219824	-3.68404210	H	2.14951153	-0.00302930	7.76732981
C	-0.00000317	-0.70219824	-3.68404210	H	-2.14951153	0.00302930	7.76732981
C	0.00000141	-1.42339679	-4.87919954	H	0.00000000	0.00000000	9.01865937
C	0.00000010	-0.70126890	-6.06650772	C	0.00005422	2.46442902	-1.83170777
C	-0.00000010	0.70126890	-6.06650772	H	0.00006883	2.32802983	-0.74430579
C	-0.00000141	1.42339679	-4.87919954	C	-0.00005422	-2.46442902	-1.83170777
C	-0.00000000	-0.00000000	-1.54089151	H	-0.00006883	-2.32802983	-0.74430579
H	-0.00000289	-2.50712857	-4.89507103	C	-1.27684054	3.20340625	-2.21635123
H	-0.00000100	-1.23575063	-7.01222266	H	-1.29497406	4.17793442	-1.71726849
H	0.00000100	1.23575063	-7.01222266	H	-1.35238426	3.37888445	-3.29433092
H	0.00000289	2.50712857	-4.89507103	H	-2.16013954	2.64150650	-1.89610005
N	-0.00000010	-1.08940953	-2.35070846	C	1.27700777	3.20329159	-2.21636596
N	0.00000010	1.08940953	-2.35070846	H	1.35259402	3.37869210	-3.29434810
Au	0.00000000	0.00000000	0.48990578	H	1.29517465	4.17785336	-1.71733878
C	0.00000000	0.00000000	2.46280782	H	2.16026570	2.64136421	-1.89604291
C	0.00000000	0.00000000	3.69047932	C	-1.27700777	-3.20329159	-2.21636596
C	0.00000000	0.00000000	5.11587713	H	-1.35259402	-3.37869210	-3.29434810
C	1.20824490	-0.00170842	5.83715844	H	-1.29517465	-4.17785336	-1.71733878
C	-1.20824490	0.00170842	5.83715844	H	-2.16026570	-2.64136421	-1.89604291
C	1.20492961	-0.00169496	7.22813391	C	1.27684054	-3.20340625	-2.21635123
H	2.14582521	-0.00303987	5.28818562	H	1.29497406	-4.17793442	-1.71726849
C	-1.20492961	0.00169496	7.22813391	H	1.35238426	-3.37888445	-3.29433092
H	-2.14582521	0.00303987	5.28818562	H	2.16013954	-2.64150650	-1.89610005
C	0.00000000	0.00000000	7.93144604				

After PCM corrections, the SCF energy is -1058.27095142 a.u.

Zero-point correction=	0.393380 (Hartree/Particle)
Thermal correction to Energy=	0.417510
Thermal correction to Enthalpy=	0.418454
Thermal correction to Gibbs Free Energy=	0.336348
Sum of electronic and zero-point Energies=	-1057.853964
Sum of electronic and thermal Energies=	-1057.829834
Sum of electronic and thermal Enthalpies=	-1057.828890
Sum of electronic and thermal Free Energies=	-1057.910996

Energies and cartesian coordinates of the optimized triplet-state structure of 1a

C	0.70299065	0.00011208	-3.67473704	H	-2.16782053	0.00077463	7.75042577
C	-0.70299065	-0.00011208	-3.67473704	H	2.16782053	-0.00077463	7.75042577
C	-1.42348350	-0.00034787	-4.87033269	H	-0.00000000	-0.00000000	9.00057829
C	-0.70033783	-0.00016595	-6.05954539	C	2.46509793	-0.00003604	-1.82777557
C	0.70033783	0.00016595	-6.05954539	H	2.33315673	-0.00038917	-0.73983472
C	1.42348350	0.00034787	-4.87033269	C	-2.46509793	0.00003604	-1.82777557
C	0.00000000	0.00000000	-1.52797232	H	-2.33315673	0.00038917	-0.73983472
H	-2.50717504	-0.00055699	-4.88689862	C	3.20391582	1.27722095	-2.21285536
H	-1.23552587	-0.00033320	-7.00493240	H	4.18130405	1.29471413	-1.71911372
H	1.23552587	0.00033320	-7.00493240	H	3.37300932	1.35425938	-3.29170836
H	2.50717504	0.00055699	-4.88689862	H	2.64291988	2.15976317	-1.88888107
N	-1.09118057	-0.00004539	-2.34369758	C	3.20413724	-1.27700112	-2.21344824
N	1.09118057	0.00004539	-2.34369758	H	3.37386462	-1.35324881	-3.29224585
Au	-0.00000000	-0.00000000	0.49207129	H	4.18123242	-1.29472574	-1.71913143
C	-0.00000000	-0.00000000	2.44258515	H	2.64301069	-2.15979864	-1.89040304
C	-0.00000000	-0.00000000	3.71490504	C	-3.20413724	1.27700112	-2.21344824
C	-0.00000000	-0.00000000	5.06633663	H	-3.37386462	1.35324881	-3.29224585
C	-1.25125660	0.00040734	5.83370783	H	-4.18123242	1.29472574	-1.71913143
C	1.25125660	-0.00040734	5.83370783	H	-2.64301069	2.15979864	-1.89040304
C	-1.23091038	0.00040442	7.19786741	C	-3.20391582	-1.27722095	-2.21285536
H	-2.18670105	0.00076182	5.28188397	H	-4.18130405	-1.29471413	-1.71911372
C	1.23091038	-0.00040442	7.19786741	H	-3.37300932	-1.35425938	-3.29170836
H	2.18670105	-0.00076182	5.28188397	H	-2.64291988	-2.15976317	-1.88888107
C	-0.00000000	-0.00000000	7.91492263				

After PCM corrections, the SCF energy is -1058.16363326 a.u.

Zero-point correction=	0.389390 (Hartree/Particle)
Thermal correction to Energy=	0.414030
Thermal correction to Enthalpy=	0.414974
Thermal correction to Gibbs Free Energy=	0.331117
Sum of electronic and zero-point Energies=	-1057.754812
Sum of electronic and thermal Energies=	-1057.730171
Sum of electronic and thermal Enthalpies=	-1057.729227
Sum of electronic and thermal Free Energies=	-1057.813085

Energies and cartesian coordinates of the optimized ground-state structure of 1b

C	0.00000000	0.70216987	-3.98060904	C	-0.00000000	-0.70216987	-3.98060904

C	-0.00000082	-1.42344679	-5.17575480	H	-2.14173586	0.00122531	7.49643122
C	-0.00000089	-0.70129451	-6.36297118	C	0.00002231	2.46462275	-2.12849008
C	0.00000089	0.70129451	-6.36297118	H	0.00000725	2.32855986	-1.04104987
C	0.00000082	1.42344679	-5.17575480	C	-0.00002231	-2.46462275	-2.12849008
C	0.00000000	-0.00000000	-1.83767379	H	-0.00000725	-2.32855986	-1.04104987
H	-0.00000249	-2.50717180	-5.19167589	C	-1.27687296	3.20345591	-2.51338876
H	-0.00000247	-1.23572991	-7.30870009	H	-1.29506219	4.17811294	-2.01456736
H	0.00000247	1.23572991	-7.30870009	H	-1.35228967	3.37872574	-3.59138667
H	0.00000249	2.50717180	-5.19167589	H	-2.16024377	2.64163943	-2.19318960
N	0.00000073	-1.08942911	-2.64724416	C	1.27695940	3.20340081	-2.51335795
N	-0.00000073	1.08942911	-2.64724416	H	1.35241989	3.37864469	-3.59135688
Au	-0.00000000	0.00000000	0.19335886	H	1.29517009	4.17806678	-2.01455521
C	-0.00000000	0.00000000	2.16673483	H	2.16029698	2.64155554	-2.19311733
C	-0.00000000	0.00000000	3.39420240	C	-1.27695940	-3.20340081	-2.51335795
C	-0.00000000	0.00000000	4.81922195	H	-1.35241989	-3.37864469	-3.59135688
C	1.20726254	-0.00069136	5.54202126	H	-1.29517009	-4.17806678	-2.01455521
C	-1.20726254	0.00069136	5.54202126	H	-2.16029698	-2.64155554	-2.19311733
C	1.21357674	-0.00069263	6.93280617	C	1.27687296	-3.20345591	-2.51338876
H	2.14643267	-0.00123121	4.99660051	H	1.29506219	-4.17811294	-2.01456736
C	-1.21357674	0.00069263	6.93280617	H	1.35228967	-3.37872574	-3.59138667
H	-2.14643267	0.00123121	4.99660051	H	2.16024377	-2.64163943	-2.19318960
C	-0.00000000	0.00000000	7.60393802	F	-0.00000000	0.00000000	8.95528833
H	2.14173586	-0.00122531	7.49643122				

After PCM corrections, the SCF energy is -1157.42398877 a.u.

Zero-point correction=	0.385171 (Hartree/Particle)
Thermal correction to Energy=	0.410135
Thermal correction to Enthalpy=	0.411079
Thermal correction to Gibbs Free Energy=	0.326777
Sum of electronic and zero-point Energies=	-1157.016048
Sum of electronic and thermal Energies=	-1156.991085
Sum of electronic and thermal Enthalpies=	-1156.990140
Sum of electronic and thermal Free Energies=	-1157.074443

Energies and cartesian coordinates of the optimized triplet-state structure of 1b

C	-0.00007004	-0.70294704	-3.96987736	H	-0.00000150	2.15976914	7.48101655
C	0.00007004	0.70294704	-3.96987736	H	0.00000150	-2.15976914	7.48101655
C	0.00019421	1.42352312	-5.16545145	C	-0.00004569	-2.46525018	-2.12302522
C	0.00010303	0.70036507	-6.35457552	H	-0.00025174	-2.33359618	-1.03504014
C	-0.00010303	-0.70036507	-6.35457552	C	0.00004569	2.46525018	-2.12302522
C	-0.00019421	-1.42352312	-5.16545145	H	0.00025174	2.33359618	-1.03504014
C	0.00000000	0.00000000	-1.82328019	C	1.27717611	-3.20397340	-2.50837926
H	0.00033499	2.50721021	-5.18201244	H	1.29475909	-4.18140861	-2.01473922
H	0.00017286	1.23545612	-7.30000460	H	1.35399290	-3.37304496	-3.58722534
H	-0.00017286	-1.23545612	-7.30000460	H	2.15980620	-2.64299969	-2.18460723
H	-0.00033499	-2.50721021	-5.18201244	C	-1.27705909	-3.20405108	-2.50889826
N	0.00001183	1.09118409	-2.63873625	H	-1.35336931	-3.37320754	-3.58777234
N	-0.00001183	-1.09118409	-2.63873625	H	-1.29481810	-4.18144702	-2.01518522
Au	-0.00000000	-0.00000000	0.19703096	H	-2.15986013	-2.64309170	-2.18556823
C	-0.00000000	-0.00000000	2.14786112	C	1.27705909	3.20405108	-2.50889826
C	-0.00000000	-0.00000000	3.41944321	H	1.35336931	3.37320754	-3.58777234
C	-0.00000000	-0.00000000	4.77060332	H	1.29481810	4.18144702	-2.01518522
C	0.00000000	1.25432208	5.53751939	H	2.15986013	2.64309170	-2.18556823
C	-0.00000000	-1.25432208	5.53751939	C	-1.27717611	3.20397340	-2.50837926
C	0.00000000	1.24116808	6.90126546	H	-1.29475909	4.18140861	-2.01473922
H	0.00000000	2.19011915	4.98758834	H	-1.35399290	3.37304496	-3.58722534
C	-0.00000000	-1.24116808	6.90126546	H	-2.15980620	2.64299969	-2.18460723
H	-0.00000000	-2.19011915	4.98758834	F	-0.00000000	-0.00000000	8.92791865
C	-0.00000000	-0.00000000	7.58033254				

After PCM corrections, the SCF energy is -1157.31626489 a.u.

Zero-point correction=	0.381079 (Hartree/Particle)
Thermal correction to Energy=	0.406662
Thermal correction to Enthalpy=	0.407606
Thermal correction to Gibbs Free Energy=	0.321273
Sum of electronic and zero-point Energies=	-1156.916550
Sum of electronic and thermal Energies=	-1156.890967
Sum of electronic and thermal Enthalpies=	-1156.890023
Sum of electronic and thermal Free Energies=	-1156.976356

Energies and cartesian coordinates of the optimized ground-state structure of 1e

C	0.70215355	0.00012673	5.93948036	H	1.23571514	0.00024033	9.26751482
C	-0.70215355	-0.00012673	5.93948036	H	2.50719759	0.00047919	7.15054531
C	-1.42348074	-0.00027346	7.13461448	N	-1.08945792	-0.00018904	4.60608501
C	-0.70130718	-0.00013697	8.32177628	N	1.08945792	0.00018904	4.60608501
C	0.70130718	0.00013697	8.32177628	Au	-0.00000000	-0.00000000	1.76560917
C	1.42348074	0.00027346	7.13461448	C	0.00000000	0.00000000	-0.20742406
C	-0.00000000	-0.00000000	3.79680902	C	0.00000000	0.00000000	-1.43556184
H	-2.50719759	-0.00047919	7.15054531	C	0.00000000	0.00000000	-2.85759163
H	-1.23571514	-0.00024033	9.26751482	C	-0.00156034	1.20769701	-3.58241503

C	0.00156034	-1.20769701	-3.58241503	H	-3.37838555	-1.35298818	5.55028664
C	-0.00155603	1.20879745	-4.96813704	H	-4.17790925	-1.29592244	3.97354794
H	-0.00278203	2.14667201	-3.03632424	H	-2.64127417	-2.16080465	4.15204106
C	0.00155603	-1.20879745	-4.96813704	C	-3.20373234	1.27635020	4.47235113
H	0.00278203	-2.14667201	-3.03632424	H	-4.17835159	1.29444508	3.97348242
C	0.00000000	0.00000000	-5.68844598	H	-3.37906895	1.35159332	5.55033675
H	-0.00277290	2.14910921	-5.51262969	H	-2.64205418	2.15986027	4.15230211
H	0.00277290	-2.14910921	-5.51262969	C	0.00000000	0.00000000	-7.10925123
C	2.46475758	0.00043996	4.08738285	C	0.00000000	0.00000000	-8.32711446
H	2.32890668	0.00039059	2.99992087	C	0.00000000	0.00000000	-9.74942606
C	-2.46475758	-0.00043996	4.08738285	C	0.00038312	-1.21069343	-10.46558761
H	-2.32890668	-0.00039059	2.99992087	C	-0.00038312	1.21069343	-10.46558761
C	3.20373234	-1.27635020	4.47235113	C	0.00038232	-1.20611476	-11.85587272
H	4.17835159	-1.29444508	3.97348242	H	0.00067788	-2.14858888	-9.91740443
H	3.37906895	-1.35159332	5.55033675	C	-0.00038232	1.20611476	-11.85587272
H	2.64205418	-2.15986027	4.15230211	H	-0.00067788	2.14858888	-9.91740443
C	3.20322696	1.27753948	4.47228509	C	0.00000000	0.00000000	-12.55708486
H	3.37838555	1.35298818	5.55028664	H	0.00067777	-2.14981855	-12.39574110
H	4.17790925	1.29592244	3.97354794	H	-0.00067777	2.14981855	-12.39574110
H	2.64127417	2.16080465	4.15204106	H	0.00000000	0.00000000	-13.64405806
C	-3.20322696	-1.27753948	4.47228509				

After PCM corrections, the SCF energy is -1365.13022917 a.u.

Zero-point correction=	0.485169 (Hartree/Particle)
Thermal correction to Energy=	0.516094
Thermal correction to Enthalpy=	0.517038
Thermal correction to Gibbs Free Energy=	0.416672
Sum of electronic and zero-point Energies=	-1364.616688
Sum of electronic and thermal Energies=	-1364.585763
Sum of electronic and thermal Enthalpies=	-1364.584819
Sum of electronic and thermal Free Energies=	-1364.685185

Energies and cartesian coordinates of the optimized triplet-state structure of 1e

C	-0.70234605	0.00009104	5.92676751	C	-3.20368918	1.27736126	4.46220838
C	0.70234605	-0.00009104	5.92676751	H	-4.17932025	1.29557631	3.96528235
C	1.42355911	-0.00020107	7.12202461	H	-3.37690419	1.35276527	5.54047945
C	0.70111205	-0.00010204	8.30951868	H	-2.64226110	2.16067430	4.14118736
C	-0.70111205	0.00010204	8.30951868	C	-3.20391831	-1.27672894	4.46201338
C	-1.42355911	0.00020107	7.12202461	H	-3.37723433	-1.35222593	5.54026047
C	-0.00000000	-0.00000000	3.78355233	H	-4.17951239	-1.29473489	3.96500735
H	2.50724619	-0.00035513	7.13821860	H	-2.64260531	-2.16009503	4.14093936
H	1.23562309	-0.00017906	9.25519478	C	3.20391831	1.27672894	4.46201338
H	-1.23562309	0.00017906	9.25519478	H	3.37723433	1.35222593	5.54026047
H	-2.50724619	0.00035513	7.13821860	H	4.17951239	1.29473489	3.96500735
N	1.09005208	-0.00012105	4.59405939	H	2.64260531	2.16009503	4.14093936
N	-1.09005208	0.00012105	4.59405939	C	3.20368918	-1.27736126	4.46220838
Au	-0.00000000	-0.00000000	1.75582618	H	4.17932025	-1.29557631	3.96528235
C	0.00000000	0.00000000	-0.20779498	H	3.37690419	-1.35276527	5.54047945
C	0.00000000	0.00000000	-1.45631707	H	2.64226110	-2.16067430	4.14118736
C	0.00000000	0.00000000	-2.83282718	C	0.00000000	0.00000000	-7.06484553
C	1.23963909	-0.00008306	-3.58884123	C	0.00000000	0.00000000	-8.31023460
C	-1.23963909	0.00008306	-3.58884123	C	0.00000000	0.00000000	-9.70352470
C	1.24510210	-0.00008206	-4.94308234	C	-1.21926609	-0.00123194	-10.43399377
H	2.17345917	-0.00016611	-3.03331619	C	1.21926609	0.00123194	-10.43399377
C	-1.24510210	0.00008206	-4.94308234	C	-1.20964909	-0.00121794	-11.81881687
H	-2.17345917	0.00016611	-3.03331619	H	-2.15771417	-0.00219089	-9.88685075
C	0.00000000	0.00000000	-5.70239239	C	1.20964909	0.00121794	-11.81881687
H	2.18063917	-0.00015511	-5.49531438	H	2.15771417	0.00219089	-9.88685075
H	-2.18063917	0.00015511	-5.49531438	C	0.00000000	0.00000000	-12.52374590
C	-2.46533319	0.00028012	4.07664235	H	-2.15239116	-0.00218389	-12.36070189
H	-2.33133418	0.00034812	2.98899727	H	2.15239116	0.00218389	-12.36070189
C	2.46533319	-0.00028012	4.07664235	H	0.00000000	0.00000000	-13.61037503
H	2.33133418	-0.00034812	2.98899727				

After PCM corrections, the SCF energy is -1365.04473090 a.u.

Zero-point correction=	0.481382 (Hartree/Particle)
Thermal correction to Energy=	0.512713
Thermal correction to Enthalpy=	0.513657
Thermal correction to Gibbs Free Energy=	0.411724
Sum of electronic and zero-point Energies=	-1364.536771
Sum of electronic and thermal Energies=	-1364.505440
Sum of electronic and thermal Enthalpies=	-1364.504495
Sum of electronic and thermal Free Energies=	-1364.606429

Energies and cartesian coordinates of the optimized ground-state structure of 1f

C	0.00000000	0.70212002	-3.68168023	C	0.00000512	1.42355825	-4.87679261
C	-0.00000000	-0.70212002	-3.68168023	C	-0.00000000	-0.00000000	-1.53951551
C	-0.00000512	-1.42355825	-4.87679261	H	-0.00001102	-2.50725942	-4.89281120
C	-0.00000379	-0.70133843	-6.06381849	H	-0.00000762	-1.23569166	-7.00956894
C	0.00000379	0.70133843	-6.06381849	H	0.00000762	1.23569166	-7.00956894

H	0.00001102	2.50725942	-4.89281120	H	-0.00001592	-2.32962885	-0.74217110
N	0.00000533	-1.08951175	-2.34823268	C	-1.27690800	3.20367968	-2.21477402
N	-0.00000533	1.08951175	-2.34823268	H	-1.29517092	4.17835641	-1.71605700
Au	0.00000000	0.00000000	0.49206219	H	-1.35195824	3.37893899	-3.29274954
C	0.00000000	0.00000000	2.46576956	H	-2.16045770	2.64196921	-1.89490527
C	0.00000000	0.00000000	3.69327430	C	1.27699436	3.20361570	-2.21476529
C	0.00000000	0.00000000	5.11507843	H	1.35207620	3.37883457	-3.29274543
C	1.19620204	-0.00050883	5.85289659	H	1.29528743	4.17830723	-1.71607847
C	-1.19620204	0.00050883	5.85289659	H	2.16051215	2.64187677	-1.89485799
C	1.13600650	-0.00047923	7.24130508	C	-1.27699436	-3.20361570	-2.21476529
H	2.15264613	-0.00091746	5.33886747	H	-1.35207620	-3.37883457	-3.29274543
C	-1.13600650	0.00047923	7.24130508	H	-1.29528743	-4.17830723	-1.71607847
H	-2.15264613	0.00091746	5.33886747	H	-2.16051215	-2.64187677	-1.89485799
H	2.05574737	-0.00086503	7.82515010	C	1.27690800	-3.20367968	-2.21477402
H	-2.05574737	0.00086503	7.82515010	H	1.29517092	-4.17835641	-1.71605700
C	0.00002320	2.46502489	-1.82966894	H	1.35195824	-3.37893899	-3.29274954
H	0.00001592	2.32962885	-0.74217110	H	2.16045770	-2.64196921	-1.89490527
C	-0.00002320	-2.46502489	-1.82966894	N	0.00000000	0.00000000	7.94544769

After PCM corrections, the SCF energy is -1074.29987678 a.u.

Zero-point correction=	0.381770 (Hartree/Particle)
Thermal correction to Energy=	0.405749
Thermal correction to Enthalpy=	0.406693
Thermal correction to Gibbs Free Energy=	0.325066
Sum of electronic and zero-point Energies=	-1073.893062
Sum of electronic and thermal Energies=	-1073.869084
Sum of electronic and thermal Enthalpies=	-1073.868139
Sum of electronic and thermal Free Energies=	-1073.949766

Energies and cartesian coordinates of the optimized triplet-state structure of 1f

C	-0.00019000	-0.70265402	-3.67498221	H	0.00031301	-2.06918024	7.81673067
C	0.00019000	0.70265402	-3.67498221	H	-0.00031301	2.06918024	7.81673067
C	0.00030799	1.42361116	-4.87039628	C	-0.00009399	-2.46601517	-1.82713509
C	0.00013400	0.70080312	-6.05847439	H	-0.00057199	-2.33424317	-0.73921600
C	-0.00013400	-0.70080312	-6.05847439	C	0.00009399	2.46601517	-1.82713509
C	-0.00030799	-1.42361116	-4.87039628	H	0.00057199	2.33424317	-0.73921600
C	0.00000000	0.00000000	-1.53081004	C	1.27743311	-3.20389522	-2.21259913
H	0.00048199	2.50726724	-4.88688427	H	1.29571112	-4.18048830	-1.71751209
H	0.00021600	1.23552716	-7.00403745	H	1.35335212	-3.37492422	-3.29113821
H	-0.00021600	-1.23552716	-7.00403745	H	2.16033618	-2.64248317	-1.89040009
H	-0.00048199	-2.50726724	-4.88688427	C	-1.27683609	-3.20490023	-2.21333612
N	0.00037500	1.09097511	-2.34321009	H	-1.35190809	-3.37647223	-3.29183921
N	-0.00037500	-1.09097511	-2.34321009	H	-1.29474408	-4.18128731	-1.71783509
Au	-0.00000000	-0.00000000	0.49211512	H	-2.16035315	-2.64399019	-1.89194609
C	-0.00000000	-0.00000000	2.44235227	C	1.27683609	3.20490023	-2.21333612
C	-0.00000000	-0.00000000	3.72060736	H	1.35190809	3.37647223	-3.29183921
C	-0.00000000	-0.00000000	5.07062647	H	1.29474408	4.18128731	-1.71783509
C	0.00025700	-1.23125515	5.85626650	H	2.16035315	2.64399019	-1.89194609
C	-0.00025700	1.23125515	5.85626650	C	-1.27743311	3.20389522	-2.21259913
C	0.00017100	-1.15704416	7.22232360	H	-1.29571112	4.18048830	-1.71751209
H	0.00048401	-2.18889122	5.34437647	H	-1.35335212	3.37492422	-3.29113821
C	-0.00017100	1.15704416	7.22232360	H	-2.16033618	2.64248317	-1.89040009
H	-0.00048401	2.18889122	5.34437647	N	-0.00000000	-0.00000000	7.94151268

After PCM corrections, the SCF energy is -1074.19066834 a.u.

Zero-point correction=	0.377838 (Hartree/Particle)
Thermal correction to Energy=	0.402305
Thermal correction to Enthalpy=	0.403249
Thermal correction to Gibbs Free Energy=	0.319771
Sum of electronic and zero-point Energies=	-1073.789898
Sum of electronic and thermal Energies=	-1073.765430
Sum of electronic and thermal Enthalpies=	-1073.764486
Sum of electronic and thermal Free Energies=	-1073.847964

Energies and cartesian coordinates of the optimized ground-state structure of 1l

C	7.59147886	0.68020278	-0.17438781	C	0.21670851	-0.00002986	-0.00028270
C	7.59149723	-0.68012133	0.17459718	C	-1.20489895	-0.00002286	-0.00023145
C	8.78662145	-1.37878486	0.35338863	C	-1.92852014	1.06668471	0.56967156
C	9.97383013	-0.67927250	0.17409580	C	-1.92858805	-1.06671318	-0.57007917
C	9.97381208	0.67947328	-0.17366375	C	-3.31510873	1.06568266	0.55411262
C	8.78658525	1.37892597	-0.35306831	H	-1.38011389	1.89198944	1.01581390
C	5.44903995	-0.00001552	-0.00000202	C	-3.31517485	-1.06568955	-0.55439058
H	8.80252894	-2.42858559	0.62210901	H	-1.38023711	-1.89202490	-1.01627679
H	10.91957386	-1.19703156	0.30647347	H	-3.85043191	1.90769394	0.98890667
H	10.91954205	1.19728040	-0.30595150	H	-3.85055240	-1.90768771	-0.98914383
H	8.80246491	2.42872741	-0.62178755	C	5.73917413	2.38664514	-0.61524435
N	6.25829690	-1.05530238	0.27106655	H	4.65186858	2.25332607	-0.58313787
N	6.25826891	1.05531510	-0.27098633	C	5.73923768	-2.38666014	0.61527265
Au	3.41773335	-0.00005968	-0.00009720	H	4.65192832	-2.25338828	0.58309684
C	1.44501956	-0.00007704	-0.00018692	C	6.12522348	2.78393316	-2.03561394

H	5.62181150	3.72027908	-2.29819482	C	-6.85441058	-3.68211446	0.40298073
H	7.20253930	2.94081988	-2.15108529	C	-7.72463949	-3.84166202	-0.66908643
H	5.81019919	2.01718358	-2.75068772	H	-8.59977499	-2.84175670	-2.36055628
C	6.12011729	3.42134040	0.43775637	H	-6.68740266	-4.51849518	1.08217181
H	7.19761584	3.61241007	0.46961314	C	-5.31329021	2.41821833	-1.87512402
H	5.61992006	4.36885070	0.21139069	H	-5.93115693	2.48143331	-2.78108577
H	5.79851373	3.09694508	1.43265096	H	-4.61516259	3.26362849	-1.90320634
C	6.12029996	-3.42131717	-0.43772222	H	-4.72206523	1.50267872	-1.93803649
H	7.19781909	-3.61227548	-0.46956043	C	-8.42672535	5.14610621	0.92782869
H	5.62019492	-4.36887910	-0.21136897	H	-8.11999035	5.57868541	1.88854014
H	5.79868260	-3.09694958	-1.43262141	H	-8.20700228	5.88051319	0.14599201
C	6.12521015	-2.78395702	2.03566020	H	-9.51479617	5.01250677	0.96780234
H	5.62176621	-3.72029399	2.29821190	C	-7.56102011	0.39718563	2.26074656
H	7.20251644	-2.94086796	2.15118701	H	-8.24597767	0.72260064	3.05090496
H	5.81016378	-2.01720506	2.75072163	H	-8.00921302	-0.46655651	1.75739012
C	-4.05431952	0.00000096	-0.00010247	H	-6.64305919	0.04446721	2.74623166
B	-5.61649174	0.00000630	-0.00001348	C	-7.56132005	-0.39712736	-2.26053929
C	-6.38613745	1.36769705	0.20882543	H	-8.00945650	0.46661070	-1.75712610
C	-6.18297947	2.47628644	-0.64270124	H	-6.64341543	-0.04440214	-2.74612603
C	-7.28820738	1.52274091	1.29468522	H	-8.24636804	-0.72253675	-3.05062138
C	-6.85442185	3.68214252	-0.40289463	C	-5.31309775	-2.41822005	1.87504110
C	-7.92508130	2.74273402	1.51019023	H	-4.72183137	-1.50270219	1.93788130
C	-7.72450323	3.84171051	0.66928949	H	-5.93086620	-2.48140291	2.78107215
H	-6.68750722	4.51850838	-1.08212711	H	-4.61500204	-3.26365835	1.90305062
H	-8.59945595	2.84182901	2.36086289	C	-8.42699449	-5.14601534	-0.92747867
C	-6.38619158	-1.36766184	-0.20876823	H	-8.20633668	-5.88075947	-0.14622255
C	-7.28839847	-1.52269043	-1.29451681	H	-9.51512680	-5.01250713	-0.96616445
C	-6.18293370	-2.47626441	0.64272051	H	-8.12129927	-5.57810580	-1.88873609
C	-7.92530689	-2.74267727	-1.50995553				

After PCM corrections, the SCF energy is -1780.87036131 a.u.

Zero-point correction=	0.737132 (Hartree/Particle)
Thermal correction to Energy=	0.782885
Thermal correction to Enthalpy=	0.783830
Thermal correction to Gibbs Free Energy=	0.649970
Sum of electronic and zero-point Energies=	-1780.108521
Sum of electronic and thermal Energies=	-1780.062767
Sum of electronic and thermal Enthalpies=	-1780.061823
Sum of electronic and thermal Free Energies=	-1780.195683

Energies and cartesian coordinates of the optimized triplet-state structure of 1l

C	-7.59963507	-0.50441412	-0.48668222	C	-6.13083752	1.41519572	3.14460491
C	-7.59878543	0.50640012	0.48780552	H	-5.63283739	2.10320988	3.83574673
C	-8.79344593	1.02634659	0.98929243	H	-7.20873718	1.48733996	3.32126682
C	-9.98054989	0.50732022	0.48810332	H	-5.80950083	0.39744470	3.38829147
C	-9.98139847	-0.50203767	-0.48624330	C	4.05371209	-0.00137507	-0.00101220
C	-8.79516866	-1.02271034	-0.98779525	B	5.59767837	-0.00011011	-0.00036505
C	-5.45862059	-0.00048457	0.00023377	C	6.37586950	-1.32128258	0.41352041
H	-8.80884144	1.80614570	1.74177756	C	6.14301082	-2.54795751	-0.25348933
H	-10.92600320	0.89227914	0.85936711	C	7.34292537	-1.31385047	1.45253442
H	-10.92749850	-0.88568541	-0.85721648	C	6.85210511	-3.69856908	0.10954447
H	-8.81187934	-1.80249854	-1.74026288	C	8.01710501	-2.48494163	1.79953483
N	-6.26524452	0.78506717	0.75640295	C	7.79089677	-3.69350947	1.13754583
N	-6.26656376	-0.78491959	-0.75569152	H	6.66572364	-4.62516486	-0.43376134
Au	-3.42575040	-0.00181799	-0.00017426	H	8.74596783	-2.45290708	2.60976246
C	-1.46151155	-0.00283117	-0.00063928	C	6.37368374	1.32251671	-0.41370838
C	-0.20399622	-0.00299729	-0.00092511	C	7.34264183	1.31676006	-1.45066832
C	1.16095997	-0.00281974	-0.00124701	C	6.13810165	2.54876691	0.25361237
C	1.92482537	-0.99835873	0.74270237	C	8.01566496	2.48917207	-1.79629573
C	1.92393752	0.99320545	-0.74543627	C	6.84612937	3.70033167	-0.10766674
C	3.28188285	-0.99004580	0.73099602	C	7.78539126	3.69740297	-1.13552510
H	1.37218548	-1.74461575	1.30796346	H	8.74758531	2.45800880	-2.60376910
C	3.28098547	0.98621922	-0.73355685	H	6.65916714	4.62591644	0.43718458
H	1.37062491	1.73883359	-1.31087009	C	5.15184988	-2.67232670	-1.38469283
H	3.82818252	-1.73985931	1.29960763	H	5.39629611	-3.52987198	-2.02203409
H	3.82661638	1.73649515	-1.30219815	H	4.13038414	-2.82222688	-1.01110366
C	-5.75016503	-1.77472004	-1.71274977	H	5.12480533	-1.77889107	-2.01639911
H	-4.66223493	-1.68046139	-1.61846522	C	8.54373634	-4.93754008	1.52222363
C	-5.74718936	1.77416461	1.71329910	H	8.36616853	-5.20315682	2.57201682
H	-4.65941899	1.67841683	1.61867458	H	8.24413671	-5.79213958	0.90629359
C	-6.13376906	-1.41522383	-3.14393402	H	9.62627964	-4.80270474	1.40342264
H	-5.63691909	-2.10390944	-3.83523446	C	7.65295248	-0.06141647	2.23255067
H	-7.21181980	-1.48590366	-3.32026460	H	8.40835507	-0.25869704	3.00107196
H	-5.81112572	-0.39790781	-3.38771089	H	8.02651357	0.73930778	1.58548429
C	-6.13922250	-3.19271860	-1.31007601	H	6.76219123	0.32875410	2.73988481
H	-7.21705469	-3.36946297	-1.38266784	C	7.65814350	0.06447870	-2.22875387
H	-5.63905527	-3.90644796	-1.97296619	H	8.03505439	-0.73368236	-1.58045505
H	-5.82410459	-3.40450369	-0.28329051	H	6.76916250	-0.33035153	-2.73556089
C	-6.13443021	3.19269233	1.31074663	H	8.41278016	0.26389569	-2.99747925
H	-7.21200205	3.37089171	1.38363974	C	5.14639607	2.67060688	1.38461827
H	-5.63311335	3.90573493	1.97350732	H	5.12258153	1.77779936	2.01734225
H	-5.81930818	3.40406256	0.28387689	H	5.38756273	3.52979897	2.02097587

H	4.12444947	2.81622718	1.01070011	H	9.60452468	4.77107822	-1.59387130
C	8.52394839	4.94711396	-1.52920374	H	8.19715445	5.30909341	-2.51288007
H	8.35676960	5.75407491	-0.80779133				

After PCM corrections, the SCF energy is -1780.77770043 a.u.

Energies and cartesian coordinates of the optimized ground-state structure of 2

C	0.70202138	0.00011781	-9.43617842	H	2.64224857	2.16125123	-7.65088361
C	-0.70202138	-0.00011781	-9.43617842	C	3.20422403	-1.27645520	-7.97032098
C	-1.42375903	-0.00024852	-10.63123359	H	3.37931223	-1.35090135	-9.04828933
C	-0.70142729	-0.00012214	-11.81791965	H	4.17904145	-1.29473532	-7.47196307
C	0.70142729	0.00012214	-11.81791965	H	2.64285477	-2.16038316	-7.65091648
C	1.42375903	0.00024852	-10.63123359	C	-3.20422403	1.27645520	-7.97032098
C	0.00000000	-0.00000000	-7.29515088	H	-3.37931223	1.35090135	-9.04828933
H	-2.50742336	-0.00044525	-10.64740090	H	-4.17904145	1.29473532	-7.47196307
H	-1.23560060	-0.00021729	-12.76373043	H	-2.64285477	2.16038316	-7.65091648
H	1.23560060	0.00021729	-12.76373043	C	-3.20385304	-1.27748804	-7.97032395
H	2.50742336	0.00044525	-10.64740090	H	-4.17868784	-1.29602671	-7.47201207
N	-1.08964970	-0.00020114	-8.10258360	H	-3.37887203	-1.35199896	-9.04830034
N	1.08964970	0.00020114	-8.10258360	H	-2.64224857	-2.16125123	-7.65088361
Au	0.00000000	-0.00000000	-5.26221286	C	-0.00000000	0.00000000	3.59200476
C	0.00000000	-0.00000000	-3.29053637	C	-0.00000000	0.00000000	4.82875714
C	0.00000000	-0.00000000	-2.05877828	C	0.69041773	-0.00052235	11.02237342
C	0.00000000	-0.00000000	-0.64645620	C	-0.69041773	0.00052235	11.02237342
C	-0.00079320	-1.21457904	0.07868610	C	-1.42775573	0.00107792	12.19284375
C	0.00079320	1.21457904	0.07868610	C	-0.70065678	0.00052999	13.38408037
C	-0.00078741	-1.21521862	1.45851770	C	0.70065678	-0.00052999	13.38408037
H	-0.00140687	-2.15098971	-0.47152858	C	1.42775573	-0.00107792	12.19284375
C	0.00078741	1.21521862	1.45851770	C	-0.00000000	0.00000000	8.81927946
H	0.00140687	2.15098971	-0.47152858	H	-2.51275110	0.00189674	12.16371788
C	-0.00000000	0.00000000	2.18523212	H	-1.23304634	0.00093443	14.33117725
H	-0.00139427	-2.15133787	2.00917559	H	1.23304634	-0.00093443	14.33117725
H	0.00139427	2.15133787	2.00917559	H	2.51275110	-0.00189674	12.16371788
C	2.46579176	0.00040945	-7.58466401	N	-1.12477205	0.00084969	9.66370993
H	2.33159973	0.00038641	-6.49701167	N	1.12477205	-0.00084969	9.66370993
C	-2.46579176	-0.00040945	-7.58466401	Au	-0.00000000	0.00000000	6.79450088
H	-2.33159973	-0.00038641	-6.49701167	C	2.39450973	-0.00179380	9.30077430
C	3.20385304	1.27748804	-7.97032395	H	2.47623388	-0.00185858	8.20183995
H	4.17868784	1.29602671	-7.47201207	C	-2.39450973	0.00179380	9.30077430
H	3.37887203	1.35199896	-9.04830034	H	-2.47623388	0.00185858	8.20183995

After PCM corrections, the SCF energy is -1884.56596244 a.u.

Zero-point correction=	0.685136 (Hartree/Particle)
Thermal correction to Energy=	0.728348
Thermal correction to Enthalpy=	0.729293
Thermal correction to Gibbs Free Energy=	0.601932
Sum of electronic and zero-point Energies=	-1883.839502
Sum of electronic and thermal Energies=	-1883.796289
Sum of electronic and thermal Enthalpies=	-1883.795345
Sum of electronic and thermal Free Energies=	-1883.922706

Energies and cartesian coordinates of the optimized triplet-state structure of 2

C	10.15000975	0.82358233	0.00018307	H	7.36153161	-2.34625899	0.00020007
C	10.21742280	-0.58034478	0.00015007	C	8.56731156	3.25140148	-1.27696403
C	11.44645188	-1.24216280	0.00015207	H	8.02503352	4.20270254	-1.29431103
C	12.59897596	-0.46274371	0.00019607	H	9.63629664	3.47465552	-1.35459303
C	12.53158391	0.93673840	0.00022507	H	8.27118556	2.67509843	-2.15941209
C	11.30921781	1.60120542	0.00021607	C	8.56710057	3.25125748	1.27751317
C	8.04027562	0.01889822	0.00008907	H	9.63605962	3.47455352	1.35534517
H	11.51552491	-2.32380188	0.00012607	H	8.02478952	4.20253854	1.29485917
H	13.56912307	-0.95165572	0.00019307	H	8.27083154	2.67486643	2.15985524
H	13.45018296	1.51673547	0.00026407	C	8.87412276	-3.14842301	-1.27693202
H	11.27277776	2.68442550	0.00023207	H	9.95958484	-3.26978499	-1.35224303
N	8.90569972	-1.03136684	0.00008207	H	8.42395474	-4.14659709	-1.29550203
N	8.80138263	1.14699232	0.00013107	H	8.52671869	-2.60231098	-2.15987510
Au	6.01879842	-0.07074284	-0.00002193	C	8.87448572	-3.14859301	1.27679517
C	4.05994930	-0.13660289	-0.00016893	H	8.42407074	-4.14665310	1.29550117
C	2.80902920	-0.15564893	-0.00015593	H	9.95995081	-3.27023499	1.35163618
C	1.43651410	-0.16130496	-0.00002893	H	8.52760072	-2.60244097	2.15991724
C	0.67738207	-1.40318307	0.00032207	C	-2.80903023	-0.15555607	-0.00049293
C	0.67721101	1.08064412	-0.00026593	C	-4.05995033	-0.13642710	-0.00074593
C	-0.67743504	-1.40315511	0.00022307	C	-10.15004483	0.82348283	0.00040807
H	1.23233113	-2.33739613	0.00065907	C	-10.21738480	-0.58045028	0.00049207
C	-0.67718010	1.08066308	-0.00032693	C	-11.44637489	-1.24233636	0.00084607
H	1.23261403	2.01457320	-0.00036593	C	-12.59893796	-0.46297033	0.00108007
C	-1.43651313	-0.16125603	-0.00020193	C	-12.53161799	0.93651678	0.00096607
H	-1.23241106	-2.33735220	0.00048707	C	-11.30928692	1.60104986	0.00063507
H	-1.23254516	2.01461414	-0.00048693	C	-8.04026864	0.01891082	-0.00006593
C	8.21884056	2.49474341	0.00019907	H	-11.51538283	-2.32397945	0.00091907
H	7.13887547	2.30838737	0.00010907	H	-13.56906406	-0.95192539	0.00135007
C	8.45434671	-2.42841496	0.00004307	H	-13.45025208	1.51645880	0.00115607

```
H  -11.27289397    2.68427194    0.00058107
N   -8.90563965   -1.03139928    0.00021207
N   -8.80143873    1.14696188    0.00005307
Au  -6.01879451   -0.07062714   -0.00048293
C   -8.21900069    2.49474800   -0.00008993
H   -7.13902263    2.30847001   -0.00032893
C   -8.45421362   -2.42841938    0.00011407
H   -7.36140450   -2.34619835   -0.00011093
C   -8.56712777    3.25124405    1.27727517
H   -9.63611884    3.47430804    1.35533518
H   -8.27057372    2.67490402    2.15955624
H   -8.02501172    4.20264214    1.29451117
C   -8.56768674    3.25133705   -1.27723903
H   -8.27172971    2.67498002   -2.15971109
H   -9.63666686    3.47466105   -1.35470303
H   -8.02536373    4.20260814   -1.29473403
C   -8.87437962   -3.14849845   -1.27669103
H   -9.95986070   -3.26994248   -1.35161203
H   -8.52733862   -2.60237540   -2.15977110
H   -8.42415456   -4.14664751   -1.29540103
C   -8.87384362   -3.14856145    1.27706217
H   -8.52662661   -2.60236740    2.16003024
H   -9.95927569   -3.27023248    1.35233218
H   -8.42340657   -4.14661151    1.29564117
```

```
After PCM corrections, the SCF energy is  -1884.47595942     a.u.

Zero-point correction=                           0.519976 (Hartree/Particle)
Thermal correction to Energy=                    0.556433
Thermal correction to Enthalpy=                  0.557378
Thermal correction to Gibbs Free Energy=         0.443238
Sum of electronic and zero-point Energies=          -1724.260405
Sum of electronic and thermal Energies=             -1724.223948
Sum of electronic and thermal Enthalpies=           -1724.223004
Sum of electronic and thermal Free Energies=        -1724.337144
```

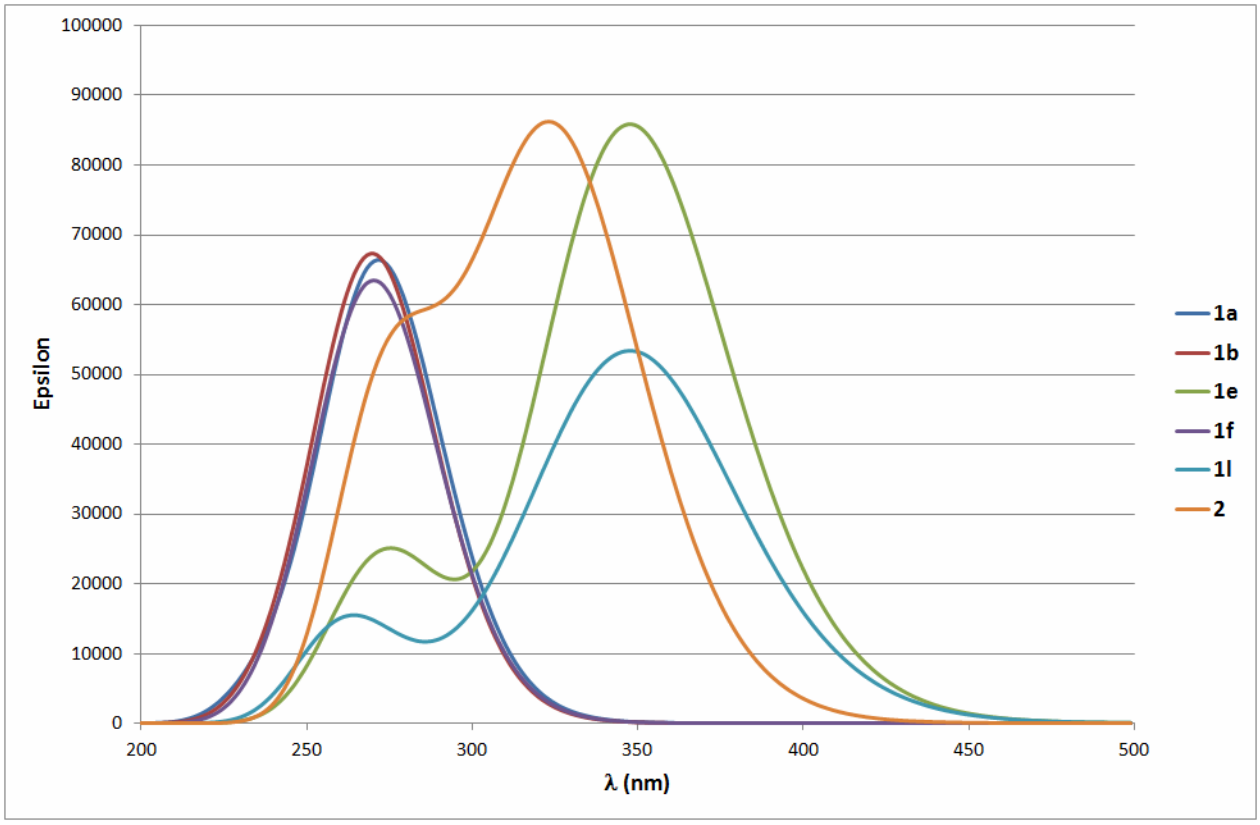

Figure S7. TD-DFT calculated absorption spectra of **1a**, **1b**, **1e**, **1f**, **1l** and **2**.

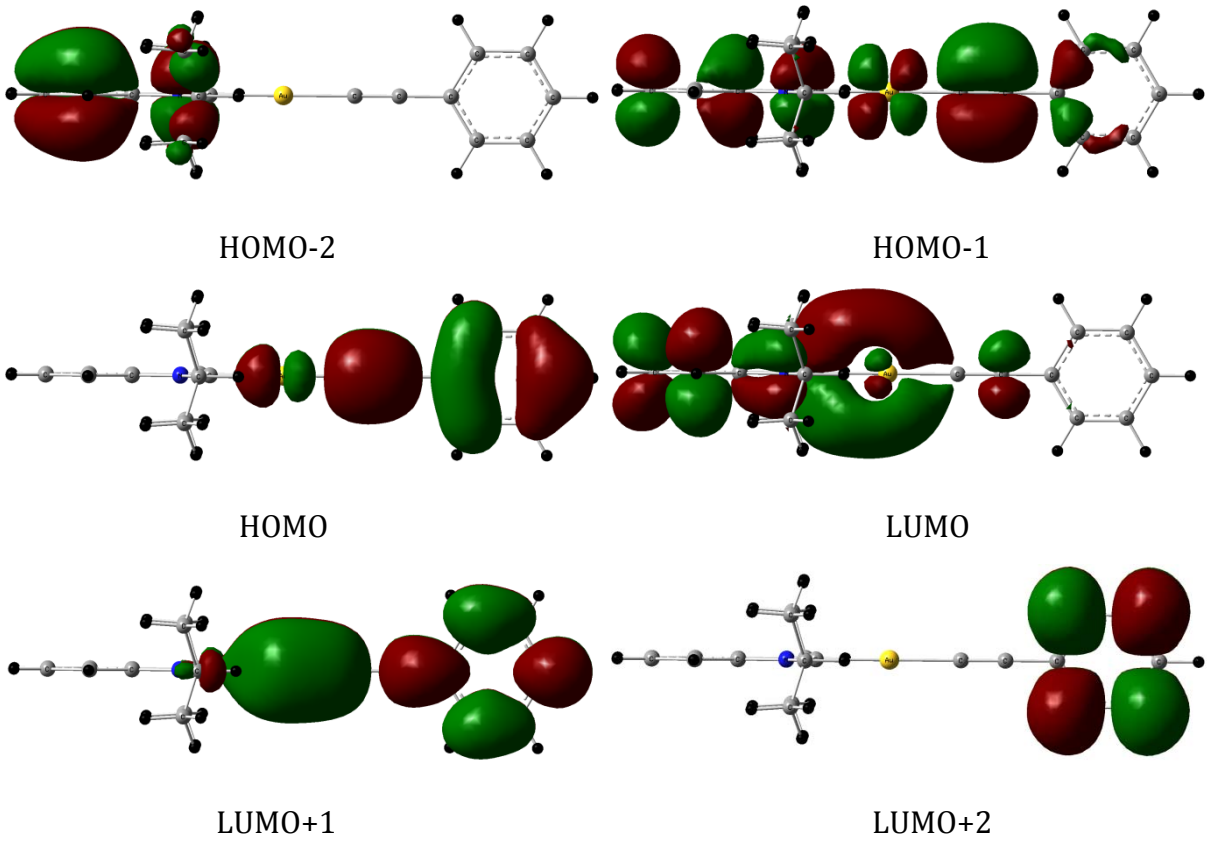

Figure S8. Selected frontier molecular orbitals of the ground-state of **1a**.

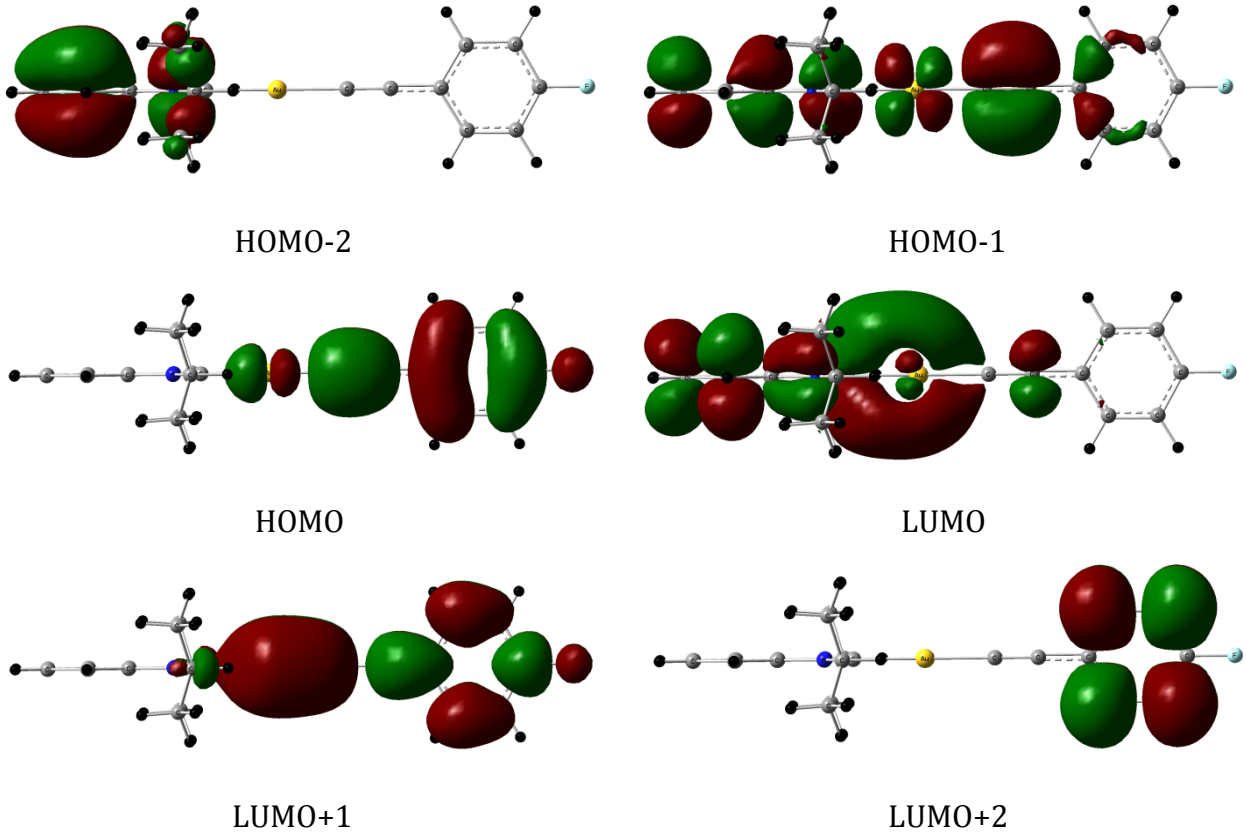

Figure S9. Selected frontier molecular orbitals of the ground-state of **1b**.

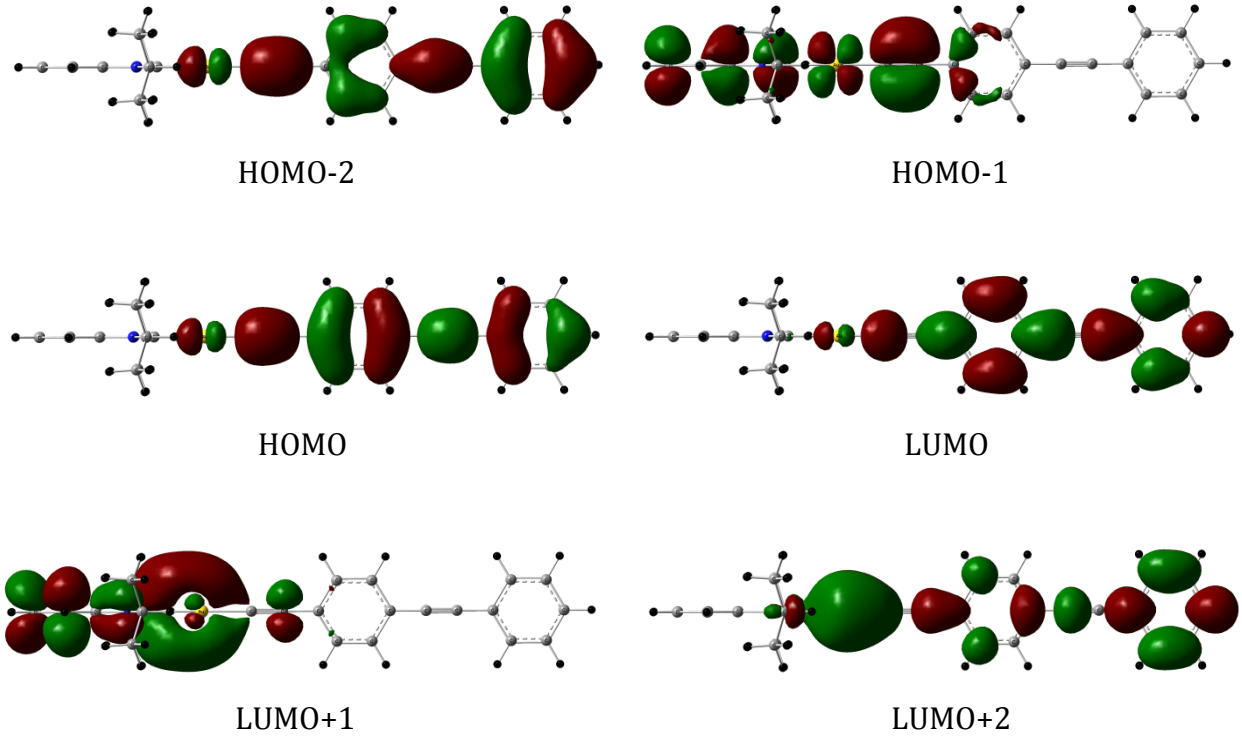

Figure S10. Selected frontier molecular orbitals of the ground-state of **1e**.

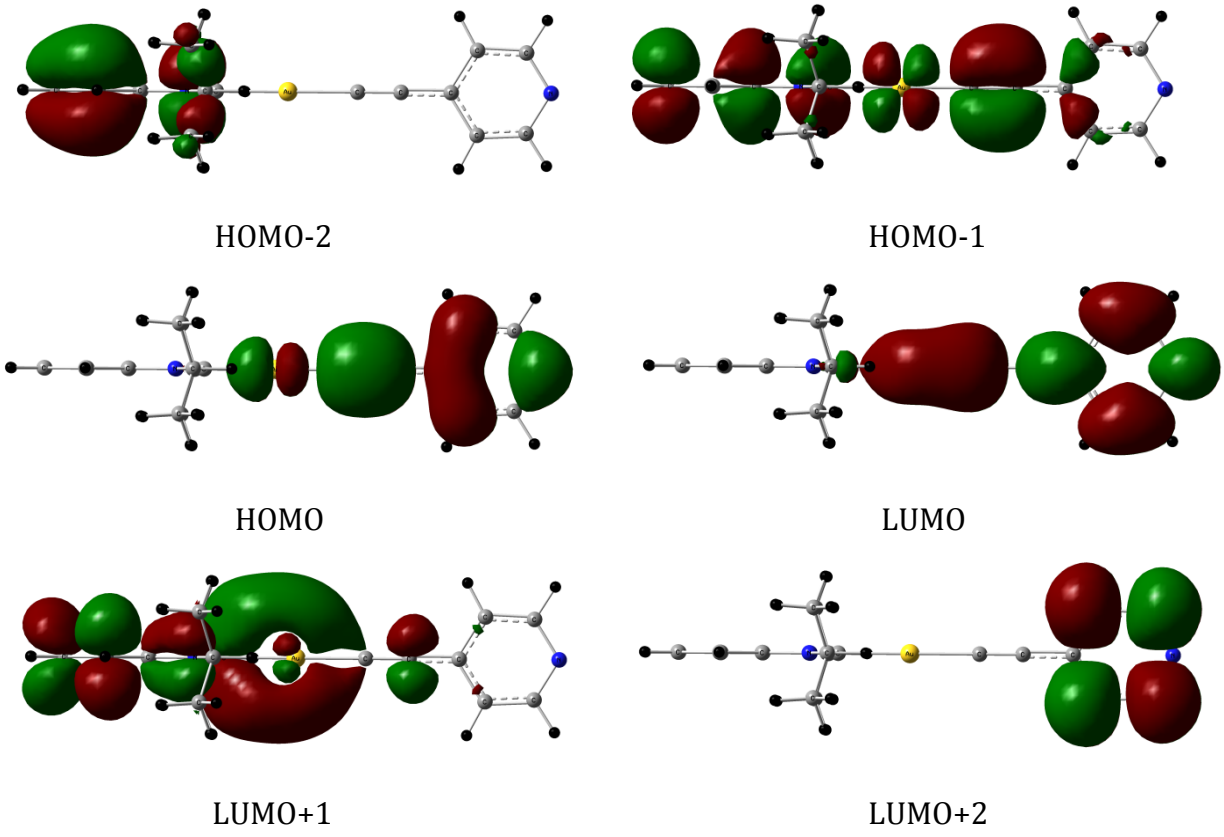

Figure S11. Selected frontier molecular orbitals of the ground-state of **1f**.

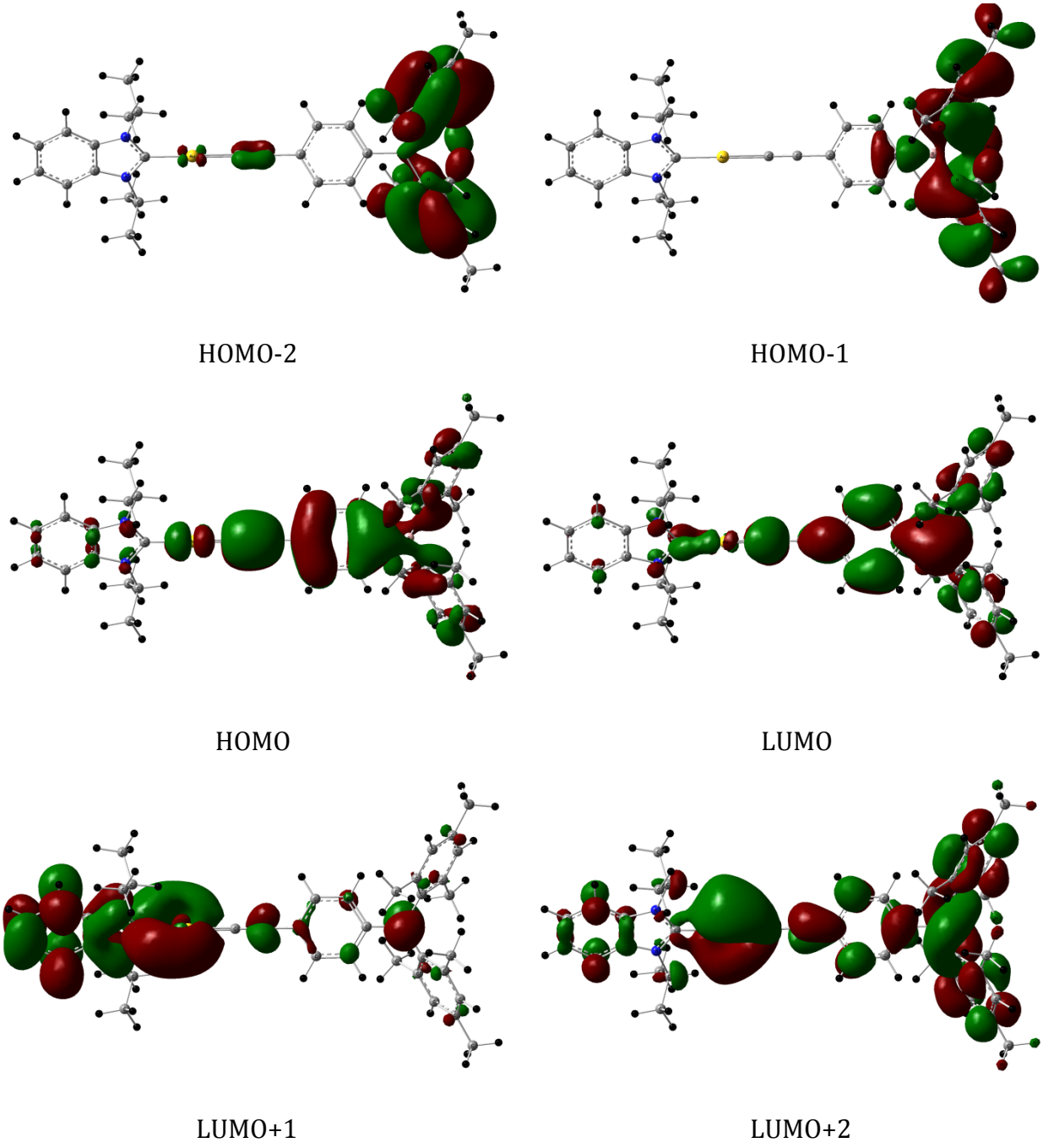

Figure S12. Selected frontier molecular orbitals of the ground-state of **1l**.

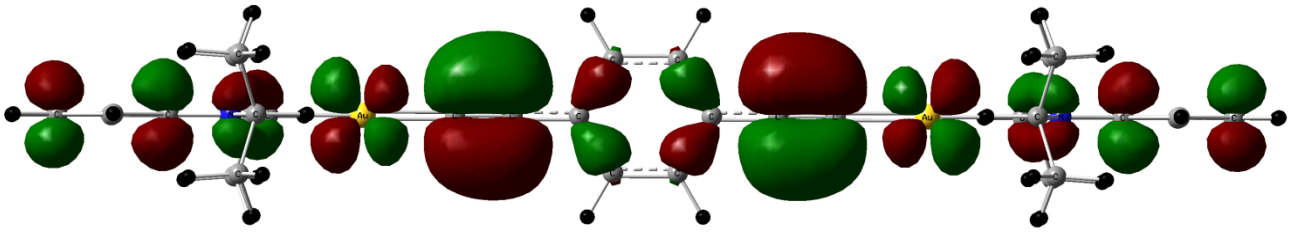

HOMO-2

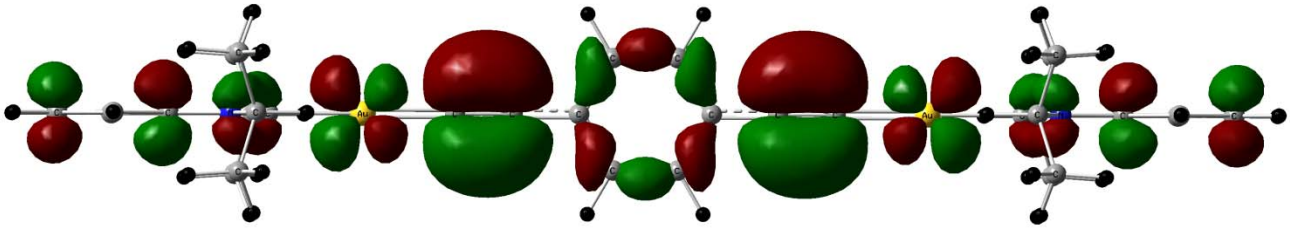

HOMO-1

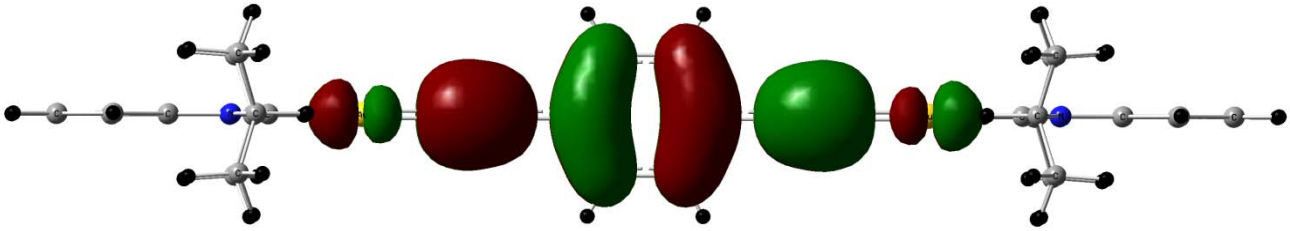

HOMO

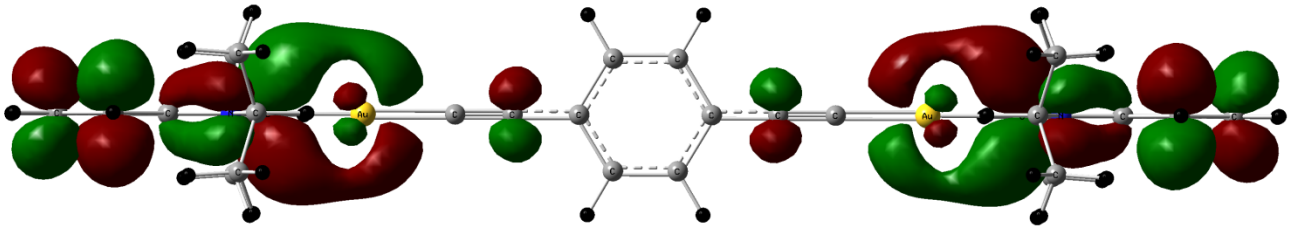

LUMO

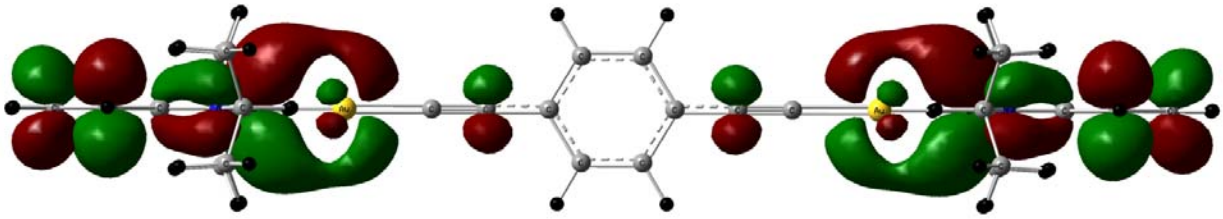

LUMO+1

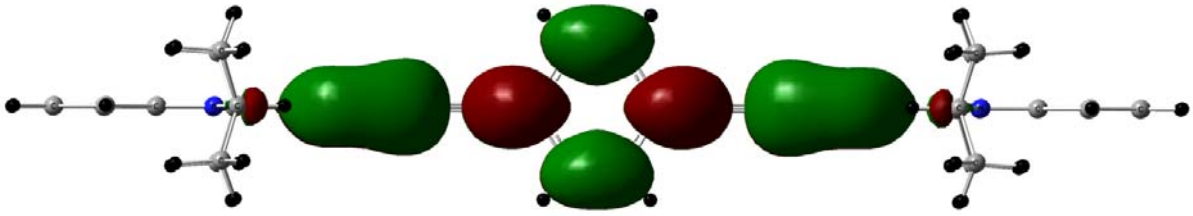

LUMO+2

Figure S13. Selected frontier molecular orbitals of the ground-state of **2**.

Chapter 5.
Gold(III) complexes containing 2-Pyridyl-*N*-heterocycles: Syntheses, Structure and Photophysical Evaluation

Gold(III) complexes containing 2-Pyridyl-*N*-heterocycles: Syntheses, Structure and Photophysical Evaluation

1.0 Abstract

Various N^N chelated Au(III) dichlorides containing 2-pyridyl-*N*-heterocycles namely pyrrole (*pypyr*$AuCl_2$), pyrazole (*pyzpyr*$AuCl_2$), triazole (*trpyr*$AuCl_2$) and tetrazole (*tetpyr*$AuCl_2$) were prepared from sodium tetrachloroaurate. Starting from these precursor dihalide complexes, the primary objective was to derive appropriate aryl substituted complexes, which can display room temperature (RT) emission. Accordingly, (2-pyridyl)pyrroleAu(III) perfluorinated diaryl complexes *viz*., *pypyr*$Au(C_6F_5)_2$ (**3c** and **4c**) were prepared by a lithiation procedure. Contrary to our expectation, **3c** and **4c** were found to be non-emissive at RT and even at cryogenic temperature (77 K). Single crystal X-ray diffraction, Cyclic voltammetry and Raman spectroscopic analyses of the complexes qualitatively suggested that the frontier orbitals in the above compounds to be closely placed for deactivation through non-radiative pathways. The unexpected modes of reactivity encountered during the study and the delocalized nature of *pypyr* ligand further supported this conjecture.

2.0 Introduction and literature overview

As stressed in the preceding chapters (1 and 2), the appropriate placement of the triplet energy manifold (E_T) and the metal-centered (MC) *d*-*d* orbital energy levels are believed to be one of the crucial factors determining the emissivity in Au(III) complexes. In this regard, carbanionic ligands are considered to be strong-enough σ-donors to destabilize antibonding *d** orbitals such that they are inaccessible during a photophysical process. Therefore, the incorporation of a cyclometalating ligand seemed to be an essential design principle in creating novel room temperature phosphorescent (RTP) Au(III) moieties. Indeed, literature presents only limited examples of RTP non-cyclometalated Au(III) molecules.[1]

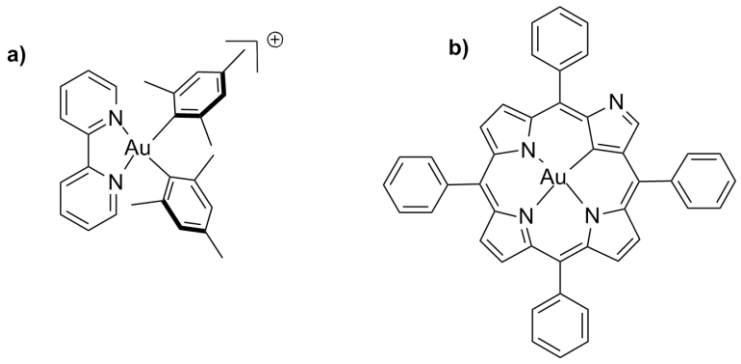

Figure 1.

Among the few, complex **a** (Figure 1) is a rare example of a mono cationic non-cyclometalated Au(III) complex which shows phosphorescence at RT in CH_3CN solution.[2] Its precursor namely $[Au(bpy)Cl_2]^+$ is non-emissive in fluid solution at RT although it shows luminescence in the solid state at RT. Unlike many metalloporphyrin complexes[3] which are known to be emissive at RT, Au(III) porphyrins are known to be emissive only in frozen media below 200 K. However, the *N*-confused tetraphenyl porphyrin (Figure 1, **b**) was found to emissive at RT in the fluid media.[4] In this case the ligation of one of the carbon atom of the pyrrole ring to the metal is believed to be responsible for its emissivity. The two above chosen examples, together with a host of other mononuclear Au(III) complexes, which were probed for photoluminescence properties seem to suggest the following points: (i) The photophysical properties as observed in the frozen, RT fluid and in the solid states are governed by several factors, and it often becomes difficult to predict the emissive phenomenon beforehand. (ii) Carbanionic σ-donating ligands, as primarily seen in cyclometalated transition-metal complexes certainly augments radiative decay, however the possibility for designing emissive complexes with other (non-cyclometalated) anionic ligands remain widely open, as could be seen from the above noted examples. In this context, our attention was first drawn towards incorporating (2-pyridyl)pyrrolide (*pypyr*) as a replacement for cyclometalated phenylpyridine (*ppy*) systems, which were investigated in Chapters 2 and 3. Due to its delocalized nature and a propensity for photoinduced tautomerization, (2-pyridyl)pyrrolide (*pypyr*) moieties have been a subject of interest in excited-state intramolecular proton transfer (ESIPT) studies.[5] In metal-organic chemistry, *pypyr* have

been typically used as neutral-anionic bidentate ligands, capable of stabilizing late transition-metal complexes in their high oxidation states and also to tune their redox properties.[6] The sterically demanding nature of *pypyr* has been utilized to achieve Si-H activation in Ir(I) and Rh(I) complexes (Figure 2, **a**-**c**).[7] With gold, the *pypyr* dimethylgold(III) complex (Figure 2, **d**), remains as a sole example reported by Vicic et al. aimed for studying the reductive elimination processes to ethane.[8]

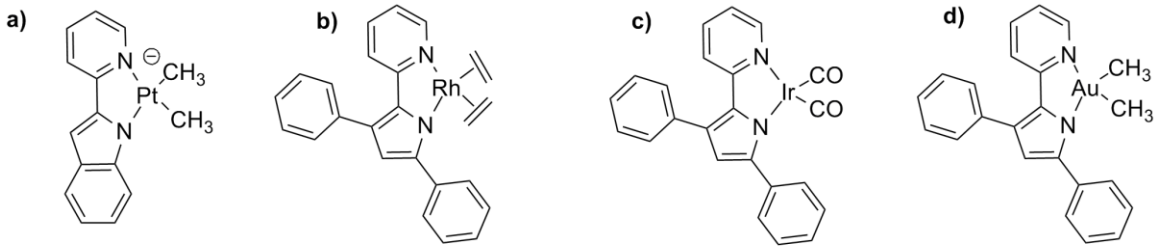

Figure 2.

From a photophysical perspective, the utility of *pypyr* ligands in phosphorescent molecules is virtually unexplored. However, in the cases of related *N*-heterocycles such as pyrazole, triazole and tetrazoles, the relative stabilization of the frontier orbitals (HOMO-LUMO) as a consequence of adding electronegative nitrogen atoms have been advantageously used in achieving blue emission. Various metal ions like Os(II), Rh(I) and Pt(II) systems (Figure 3, **a** and **b**) have utilized in this respect.[9]

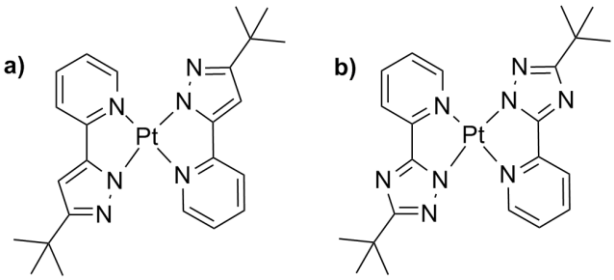

Figure 3.

An important point which needs to be taken note in this context is that; invariably in all the cases where the 2-pyridyl heterocyclic ligands have been used, the transition metal chosen for this purpose are those which predominantly exhibit increased metal percentage (^{3}MLCT dominated) in their emitting states. The photophysical evaluation of such ligands incorporated into metal ions like Au(III) and Pd(II), which normally show ligand centered emission characteristics (^{3}ILCT) have been seldom explored.[1] Therefore, we surmised that one such study would add to our existing knowledge on the importance of cyclometalating ligands and also enable comparison with non-cyclometalated carbanionic ligands such as pyrroles. Needless to mention that, creation of suitable and stable Au(III) complexes molecules in itself is a synthetically daunting task.

3.0 Results and Discussion

3.1 Synthesis of (2-pyridyl)pyrrolide (*pypyr*) class of chelates and their Au(III) complexes.

In 2001, McNeill and co-workers described an elegant protocol for the preparation of 3,5-disubstituted- and 3,4,5-trisubstituted-2-(2-pyridyl)pyrroles in one-pot fashion starting from 2-(aminomethyl)-pyridine and 1,3-diones.[10] The cyclization reaction proceeds through the (2-pyridyl)methylamine intermediate. Accordingly, a variety of symmetrically disubstituted (2-pyridyl)pyrrolides with varied aliphatic (**1a**-**3a**) and aromatic substituents (**4a**-**8a**) were prepared (Scheme 1). Compounds **5a**-**8a** are new and the procedure for synthesis of **3a** has been reported only recently.[6] It is to be noted here that the isolation of product in this reaction could be proceeded only after confirming its identity either by GC-MS or ^{1}H NMR and not merely by the disappearance of the starting material, since the reaction proceeds through well defined intermediacy of β-iminoketone which is observable by TLC.

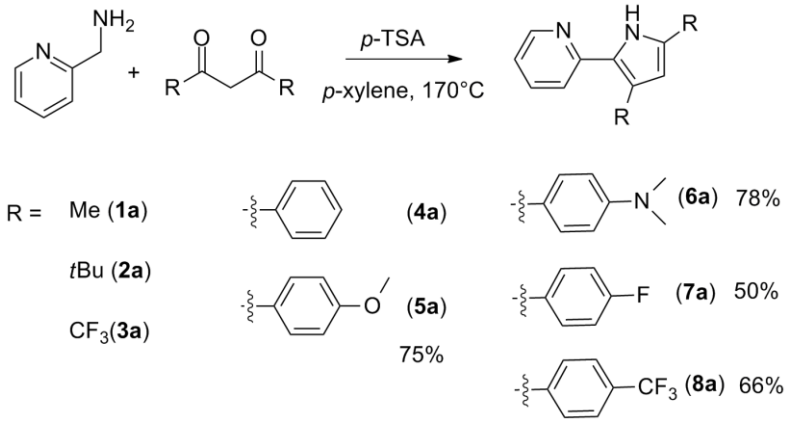

Scheme 1.

Therefore, reaction times were quite different, while **5a**-**7a** showed good conversion when heated at 170°C for 24 h, the formation of **3a** required elongated reaction time (48 h). Having synthesized the 3,5-disubstituted-2-(2-pyridyl)pyrroles incorporated with substituents having different electronic properties, we then proceeded to synthesize their corresponding Au(III) dichlorides by reacting with $NaAuCl_4 \cdot 2H_2O$. To begin with, **4a** was reacted with $NaAuCl_4 \cdot H_2O$ to afford **4b** (Scheme 2) in a yield of 87% according to the protocol described by Vicic et al.[8] A marginal improvement in the yield to 94% was realized upon using 1:2 mixture of CH_2Cl_2 and CH_3CN instead of H_2O:CH_3CN (2:1) and by prolonging the reaction time for 10 days. To our surprise, when **1a**, **2a**, **5a** and **6a** were subjected to any of the original or modified reaction conditions, the desired product could not be isolated neither at RT nor at elevated temperatures (50-60°C). Use of extraneous bases like K_2CO_3, KO*t*Bu,

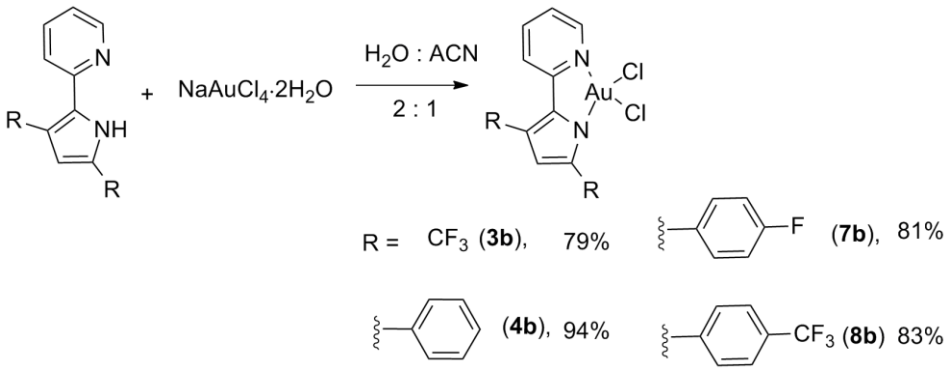

Scheme 2.

NEt_3 etc., under appropriately modified reaction conditions also failed to give the Au(III)dichlorides. In contrast, **3a**, **7a** and **8a** showed facile conversion to their respective products qualitatively suggesting the acidity of the pyrrolic proton (N*H*) to be an important contributing factor to the formation of the desired product. The reaction time in the latter cases was also considerably reduced (24 h) without much compromise on the isolated yields. In a completely deprotonated form, the lithium salt of **1a** prepared using LiHMDS described by Tilley et al.[7] failed to form the desired complex. We presume that in the cases of **1a**, **2a**, **5a** and **6a** where the pyrrolic proton is not sufficiently acidic, the coordination to the metal center happens through the nitrogen lone pair forming mono-cationic complexes as discussed by Vicic et al.[8] However, due to the complexity of the ^{1}H NMR signals and lack of crystal structure, definitive conclusions could not be drawn. Reaction of **1a** with a different precursor namely $AuCl_3$(*tht*) (*tht* = tetrahydrothiophene) was also not successful. When **5a** was lithated using *n*-BuLi at -78 °C in Et_2O and was reacted with $NaAuCl_4 \cdot 2H_2O$, the ^{1}H NMR of the crude mixture did not reveal the expected product. Instead, a reduced Au(I) monochloro complex (**5b**) was isolated after purification in a low yield of 12% (Scheme 3, **5b**). The 2 position of the pyrrole containing the Au(I)chloride was found to be connected to 4 position of free (2-pyridyl)pyrrole establishing a new C(sp^3)-C(sp^2) linkage.

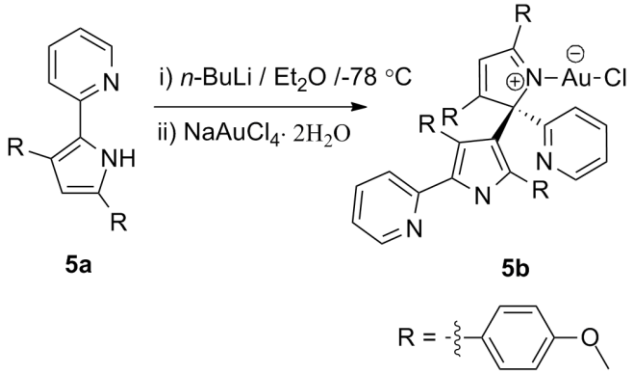

5a **5b**

Scheme 3.

X-ray structure of the product revealed the absolute configuration of the stereocentre to be of (*R*). Although the full characterization for this complex was not pursued, the structural details are informative and hence included in the discussion in the

crystallographic section (Figure 7). The ^{1}H NMR spectra of all the other isolated gold complexes (**3b**, **7b** and **8b**) depicted in scheme 2 revealed the expected downfield shifts of the α-pyridyl proton resonances in the region (9.08-9.24 ppm). Unlike in the cases of cyclometalated complexes *ppy*$AuCl_2$, the dichloride gold complexes of *pypyr* were quite soluble in moderately polar solvents like CH_2Cl_2. Owing to the non-emissive nature of the dichloride complexes (**3b**, **4b**, **7b** and **8b**), which can be attributed to the stabilization effect of electronegative chlorides on the MOs, we intended to replace the chlorides with aryl groups. Accordingly, when **4b** was reacted with stoichiometric amount of phenyllithium in Et_2O at -78°C, the dissociated free ligand (*Pypyr*-H) and the reductively homocoupled biphenyl were the sole products which were identified by GC and ^{1}H NMR analyses. Although the generation of 2,2'-biphenyl was rather unsurprising, it suggested the prior incorporation of arenes into the gold center. When **4b** was used in catalytic amount (1.0 mol%), for the same reaction, it revealed to be a promising catalyst showing an initial TON of 162. Keeping the goal in mind, further studies were not performed in these lines. Attempts to substitute the chlorides with lithiated terminal aryl alkynes also failed under various conditions. Au(III) complexes are generally oxidizing in nature and therefore any reducing reaction environment might increase the chances of reduction to either Au(I) or Au(0). Being aware of this fact, we sought to use other forms of activated nucleophiles which might yield the desired product by possible intimate transmetalation sequences. This idea was further strengthened due to the precedence of tin mediated dimethyl Au(III) species in literature[8] (Figure 2, **d**). Pursuing this strategy, the stannylated compounds like tetraphenyl tin, 2-(tributylstannyl)thiophene or trimethytin phenylacetylene were reacted with **4b** under various conditions. However all of them failed to give the expected disubstituted products. Presuming that the strong σ-donicity of the phenyl anion to be the reason for the displacement of the free-ligand, electron deficient arenes were employed to effect substitution. Indeed, upon reacting 2.0 equiv. of (perfluorophenyl)lithium with **3b** and **4b** gave the desired *pypyr*Au(III) diaryls **3c** and **4c** as air and moisture stable solids in 44% and 45% yields respectively (Scheme 4).

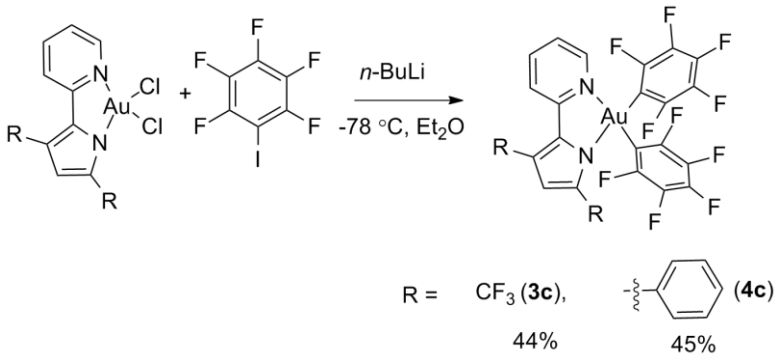

Scheme 4.

The ^{19}F NMR of **3c** and **4c** showed two inequivalent sets of three distinct resonance signals corresponding to *o*-, *m*- and *p*-fluorine atoms around the region -124.0 ppm, -156.0 ppm and -158.0 ppm. The disappearance of asymmetric stretches due to the *v*(Au-Cl) in the lower wave numbers (300-380 cm^{-1}) in IR corresponding to the gold dichloride[8] along with the observation of new bands in the region 510-582 cm^{-1} assignable to asymmetric *v*(Au-C) stretching[11] were indicative of the product formation.

3.2 Synthesis of 2-(1*H*-pyrazol-5-yl)pyridyl ligand (*pyzpyr*) and its Au(III) complex

The preparation of Au(III) dichlorides with 2-(1*H*-pyrazol-5-yl)pyridyl ligands (*pyzpyr*) was embarked. *Pyzpyr* ligands can be conveniently synthesized by an intial step of Claisen condensation of 2-acetylpyridine and methyl/ethyl esters of substituted acetic acid followed by ring closure using hydrazine.[12] In line with this protocol, a pyridyl pyrazole moiety containing CF_3 substituent at the 3-position of the pyrazole was synthesized. This trifluoromethyl substituent was deliberately chosen to enhance the acidity of proton bound to the nitrogen.

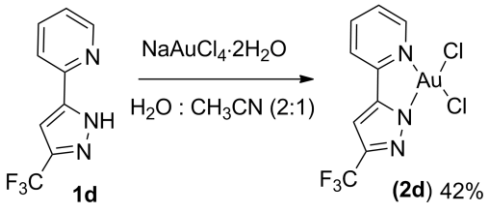

Scheme 5.

In line with our expectation, when **1d** was reacted with $NaAuCl_4 \cdot 2H_2O$ it afforded **2d** as an air and moisture stable yellow product in 42% yield (Scheme 5). The ^1H NMR studies consistently showed high field shift for the α-pyridyl proton resonating at 9.16 ppm ($\Delta\delta$ = 0.5 ppm), and a slight shift in ^{19}F NMR from -60.5 ppm to -60.3 ppm was also observed. When **2d** was reacted with (perfluorophenyl)lithium similar to Scheme 4, the isolation of the arylated product could not be achieved even though ^1H NMR and ^{19}F NMR analyses of the crude mixture suggested the presence of the product. Various dialkynylation reactions attempted on this compound also met with little success. Metathetical substitution of the chlorides to obtain more reactive triflate salts for further functionalization using AgOTf in CH_2Cl_2 also failed.

3.3 Synthesis of (1,2,4-triazol-3-yl)pyridyl ligand (*trpyr*) ligand and its Au(III) complex

Synthesis of (1,2,4-triazol-3-yl)pyridyl ligand (*trpyr*) was pursued next. Triazole derivatives have been scarcely reported in literature [13] and are unprecedented with Au(III) metal center. The scheme for the ligand synthesis is depicted below (Scheme 6) and was adopted according to the known report [14]

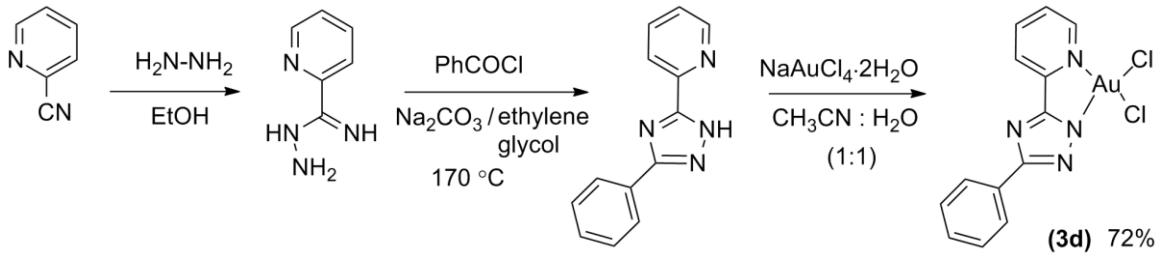

Scheme 6.

The choice of triazole ligand stemmed since they are considered to be good σ-donors and weak π-acceptors.[15] The π-electron rich five membered ring of the triazole have been perceived to enhance stabilization of the higher oxidation states due to its relatively large ligand field stabilization energy. Also, the incorporation of azoles or other *N*-heterocyclic systems like in pyrazole have been shown to avoid columnar stacking in d^8 square-planar

complexes which are detrimental to radiative photophysical processes.[9c] The formation of Au(III) dichloride in this case was rather facile and occurred at RT after stirring for 12 h. **3d** (Scheme 6) was isolated in 72% yield as a pale pink powder after recrystallization from a ternary mixture of ethyl acetate, THF and hexane in the ratio 8:1:1. The ^{1}H NMR studies of **3d** showed the expected resonances with slight downfield shifts as compared to their free ligands. Substitution by lithiation reactions were however not attempted on this complex.

3.4 Synthesis of 2-(1*H*-tetrazol-5-yl)pyridine (*trpyr*) ligand and its Au(III) complex.

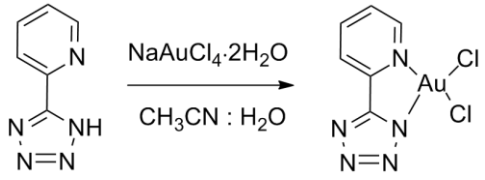

(**4d**) 68%

Scheme 7.

2-(1*H*-tetrazol-5-yl)pyridine suitable for coordination was prepared from cyano pyridine precursor described by Sharpless et al.[16] The reaction of this ligand with the gold precursor was found to proceed in good yields both at RT and at elevated temperatures (Scheme 7). A temperature of 60 °C and 12 h was found to be the optimal condition, and the product was isolated by a simple filtration step followed by trituration with CH_3CN in 68-74% yields. The structural confirmation was established by a combination of ^{1}H NMR, IR spectroscopy and XRD studies.

3.5 Photophysical and Electrochemical investigations

The arylated gold complexes **3c** and **4c** were found to be non-emissive at RT and also at 77 K. Usually at cryogenic temperatures like 4 K or 8 K, the onset of emission from the triplet state is reflected by the occurrence of three well defined peaks in the photoluminescence spectra.[17],[18] At relatively higher temperatures (even at 77 K) there exist an appreciable degree of Boltzmann population which leads to line broadening and

they behave kinetically as a single state. Raising the temperature from 77 K to RT (300 K) can significantly erode emission due to thermal deactivation which is in turn dictated by a host of factors.[19] The non-emissive nature of **3c** and **4c** even at 77 K primarily suggests a probable misappropriate placement of the triplet manifold. It is perhaps placed in close proximity with iso-energetic and interacting ligand orbitals which are known to be effective channels for radiationless vibrational relaxation. Although this may be the case, we proceeded with synthesis of other heterocyclic chelates like pyrazole (*pzpyr*-$AuCl_2$), triazole (*trpyr*-$AuCl_2$) and tetrazole (*tetpyr*-$AuCl_2$) complexes simply because, the photophysical nature of transition metal complexes are known to differ profoundly with changes in the coordination sphere. Che and co-workers have emphasized that the design of emissive molecules solely with the strategy of utilizing *5d* transition metals with strong field donor ligand may be over-simplified.[19] Although, in one hand the energy separation of *d-d* orbitals is desired to be large, but for an effective spin-orbit coupling (SOC), it is required that the occupied *d* orbitals of the metal should not be too low in energy. Keeping the fact that the *pypyr* bearing Au(III) complexes could be stabilized only with perfluorinated arenes, an explanation for the non-emissive nature of **3c** and **4c** can be sought by comparing them to cyclometalated phenyl pyridine (*ppy*) perfluorinated diaryl Au(III) complexes studied in Chapter 2. The perfluorinated phenylpyridine gold complex was found to be emissive both at RT and at 77 K rigidified matrices with the triplet energy (E_T) of 2.71 eV. It was thought that the electrochemical behavior of these complexes would shed some light on the nature of its frontier orbitals, which could further help to find reason for the non-emissive nature of *pypyr* gold complexes. Most of the literature pertaining to the cyclic voltammetry (CV) studies of cyclometalated Au(III) complexes until now have suggested predominance of ligand centered events with relatively less activity from the metal.[20] The CV of **4c** was recorded in CH_2Cl_2 at RT. It exhibited a completely irreversible behavior with two approximate quasi-reversible oxidation events and one irreversible reduction peak potential at -1.99V with respect to ferrocene. Under the same conditions the CV studies of two cyclometalated *ppy*Au(III) complexes reported in Chapter 2 namely *cis*-[(N^C)AuR_2][N^C = phenylpyridine (*ppy*)][L = C_6F_5] (Chapter 2, **2**) and *cis*-

[(N^C)AuL$_2$][N^C = 2-(5-methyl-2-thienyl)pyridine (*5m-thpy*)][L = C_6F_5] (Chapter 2, **8**) bearing perfluorinated benzenes were recorded (Figure 4).

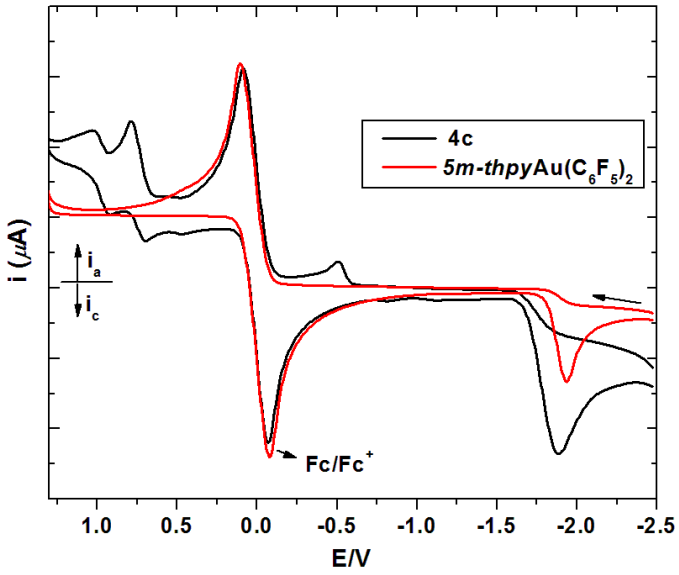

Figure 4. Cyclic voltammogram of **4c** and *5m-thpy*Au(C_6F_5)$_2$ in 0.1M [*n*Bu$_4$N][PF_6]; Au electrode; E *vs* $Fc^{+/0}$, scan rate = 100 mV/s; 20 ºC; CH_2Cl_2.

While we observed oxidation and reduction events in **4c**, the cyclometalated complexes **2** (not shown in Figure 4) and **8** showed only one well defined reduction wave. Considering no involvement of the metal, the reduction event can be assigned due to the ligand. Interestingly the reduction peak potentials ($E_{p,c}$) of **4c**, **2** [*ppy*Au(C_6F_5)$_2$] and **8** [*5m-thpy*Au(C_6F_5)$_2$] were remarkably close indicating contribution from either the pyridyl or the -C_6F_5 groups in the lowest unoccupied molecular orbital (LUMO). No oxidation events could be observed for the cyclometalated complexes within the solvent electrochemical window as against **4c** under same conditions. It could be therefore understood that the HOMO in the case of *pypyr* (**4c**) presumably from pyrrole unit is relatively more destabilized. The results qualitatively suggest a lower HOMO-LUMO gap in *pypyr* as compared to cyclometalated *ppy* gold complexes. This explanation seems more plausible because pyrroles are π-excessive in nature therefore good π-donors when compared to benzene. This can result in a number closely placed ligand π-orbitals quite similar to conjugated organic poly-aromatic systems. In fact *pypyr* moieties are known to be one among the highly delocalized systems.[6]

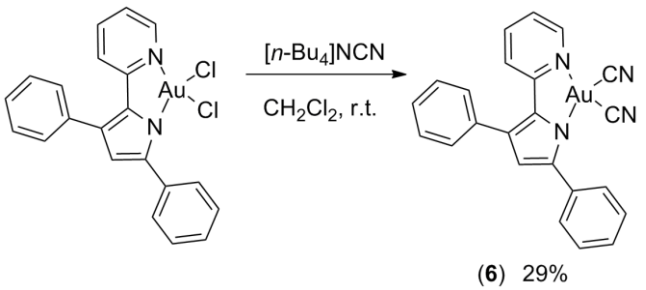

Scheme 8.

The availability of RT emissive dicyano complex namely *cis*-[(N^C)Au(CN)$_2$][N^C = phenylpyridine (*ppy*)] in the research group [21] prompted us to synthesize *pypyr*Au(CN)$_2$ to gain some understanding on the σ-donating abilities of both. Therefore, *pypyr*Au(CN)$_2$ (Scheme 8, **6**) was prepared by reacting (*n*-Bu)$_4$NCN with **4b**. As previously noted, the dissociation of the free ligand was a serious handicap among *pypyr* systems, only **4b** could be converted to its corresponding dicyano complex **6** (Scheme 8) and was completely characterized including single-crystal XRD. In the Raman spetra ν_1(C≡N) = 2098 cm^{-1} and ν_2(C≡N) = 2166 cm^{-1} were observed for **6** and ν_1(C≡N) = 2158 cm^{-1} and ν_2(C≡N) = 2177 cm^{-1} were observed for *cis*-[(N^C)Au(CN)$_2$][N^C = phenylpyridine] or *ppy*Au(CN)$_2$. From the XRD data (Table 3 and ref. 21) of both the complexes, the higher frequencies could be assigned to cyanide *trans* to pyridine. While the lower frequencies are attributable to the cyanide *trans* to the pyrrolic nitrogen in **6** and to the cyclometalated carbon in *ppy*Au(CN)$_2$ respectively. A longer bond distance of 1.131 Å for C≡N in **6** consistent with its Raman stretching frequency ν_1(C≡N) compared to a bond distance of 1.107(6) Å for C≡N in *ppy*Au(CN)$_2$ qualitatively suggests a greater σ-donation from the pyrrolic nitrogen. However, this conclusion would not support the non-emissivity of *pypyr* gold complex since *d-d* (MC) levels should be more thermally inaccessible for non-radiative decay pathways.

Concluding from both Raman and CV experiments, the following points are evident: (i) the pyrrolic nitrogen in *pypyr* is more σ-donating than the cyclometalated carbon in the studied complexes, (ii) the band-gap is lower in the case of *pypyr* as compared to *ppy*. Therefore one can speculate that metal centered *d-d* orbitals do not dictate the photophysics in this case. The non-emissive nature is primarily due to extensive

conjugated nature of the *pypyr* ligand. The $^1(\pi\pi^*)$, $^3(\pi\pi^*)$ and singlet ground levels are too close to effect non-radiative channels in line with the energy-gap law.

Adopting a different strategy to create emissive Au(III) complexes with (2-pyridyl)pyrroles, we sought to incorporate pyridyl pyrazole chelate ancillary to cyclometalated gold centre by means of substituting the chlorides in *ppy*$AuCl_2$. Such complexes can turn out to be emissive if the role of cyclometalation is decisive. Although such a method would give monocationic complexes which is outside our general theme of creating neutral emissive Au(III) molecules, we thought that it would help atleast in proving the hypothesis. **7a** was therefore lithiated using *n*-BuLi in Et_2O at -78 °C and was subsequently transferred into flask containing *ppy*$AuCl_2$. Isolation and characterization of the major product **9** by XRD revealed the attachment of the carbon from the bay region instead of the pyrrolic nitrogen initially suggesting a non-regioselective lithiation (Scheme 9). In a different attempt, **4a** was converted to its lithium salt by reacting with LiHMDS in toluene at RT by a known procedure,[6] then a subsequent stoichiometric addition of the lithated salt **4a-Li** to *ppy*$AuCl_2$ and stirring for 24 h surprisingly revealed similar monochloro gold complex **5c** (Scheme 7), which was revealed from detailed NMR studies. Elemental microanalyses and further characterization of mono chloro complexes **5c** and **9** were however not performed. The highly delocalized nature of *pypyr* anion was then thought to be a reason for the similar kinetic behavior in both the cases.

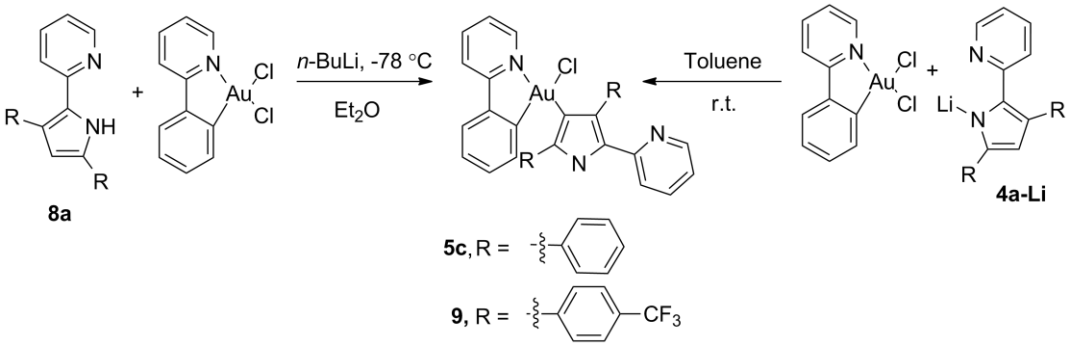

Scheme 9.

3.6 X-ray diffraction studies

Crystals suitable for diffraction of **3b**, **2d**-**4d** were obtained by the slow evaporation of pentane or Et_2O or THF in concentrated solution of the compound in CH_2Cl_2. The crystallographic and refinement details for individual complexes are presented in the appendix (Tables A1 to A3) to this chapter. The perspective views are shown in Figure 5, 6 and 7. Structural characterization of the Au(III) dichlorides revealed the metal occupying a distorted square planar position, consistent with the assignment by various other spectroscopic methods. XRD characterization was particularly helpful in confirming the monomeric nature of the complexes eliminating the possibility of bridged dichloride dinuclear species (μ-type bonding modes) although such situations are not commonly encountered in Au(III) complexes but nevertheless seen in Pt(II) cases. With the availability of structural information of the five membered *N*-heterocyclic complexes with progressive increase of nitrogen atoms, it is interesting to compare the electronic influence on the coordination geometry. The various bond lengths and angles are enumerated in Tables 1-3. A comparison of the bond distances between the heterocyclic nitrogen (N_{het}-Au) and pyridyl nitrogen (N_{pyr}-Au) to gold reveals that, in all the cases the former is shorter because of the anionic character. Notably, in the case of *pypyr* amido complex (**3b**) the difference was marginal (approx. 2.2 pm) when compared to others (**2d**-**4d**) which exhibited a difference around 6-12 pm. It is interesting to note that the situation is reversed in the case of **4b**,[8] where the anionic N to Au distance is larger than from the pyridyl nitrogen. The Au-Cl distances *trans*- to anionic nitrogen in all cases was greater than the other (*trans* to N of pyridine) due to the greater *trans-influence* effect. The N^N bite angles (Table 2) observed in the complexes, without much difference among themselves (**3b**, **2d**-**4d**) were less by an average of ten degrees from the idealized 90° owing to the various steric requirements of the chelating ligand.

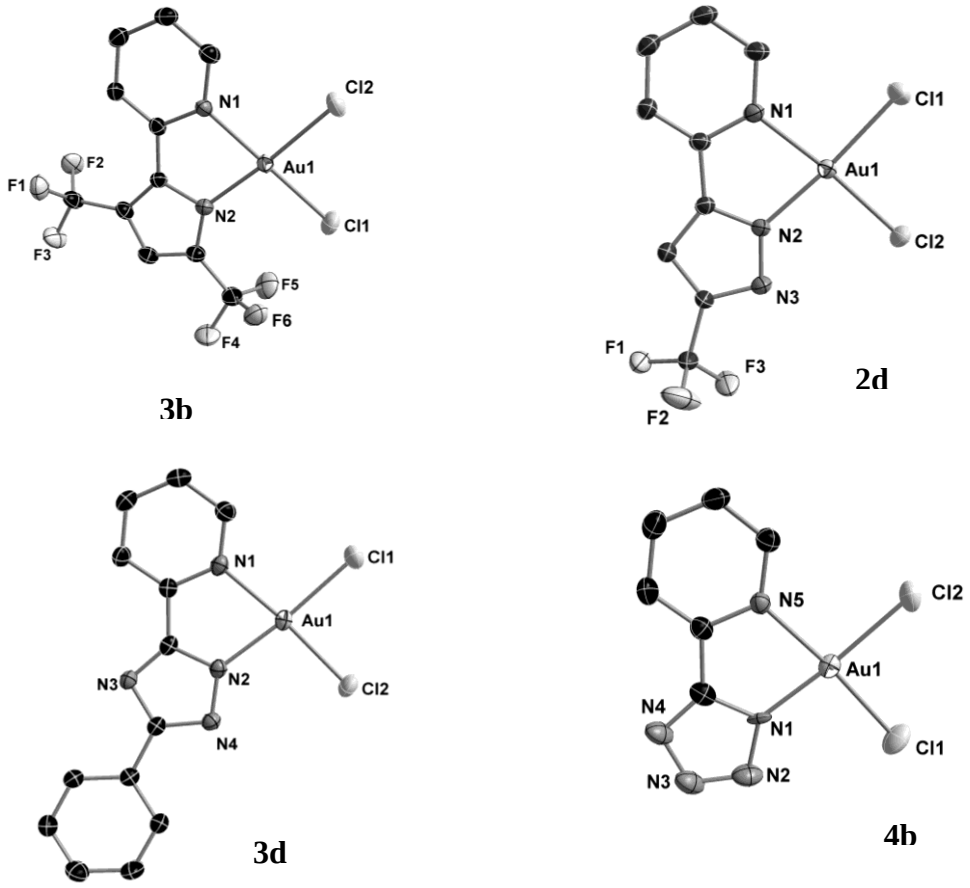

Figure 5. X-ray crystal structures of **3b**, **2d**-**4d** with selective atomic numbering scheme. Thermal ellipsoids are drawn at 50% probability level. Hydrogen atoms and solvent molecules (if any) are omitted for clarity.

Table 1. Selected bond distances (Å) of **3b**, **2d**-**4d**.

	$N_{pyridyl}$-Au	N_{het}-Au	Au-Cl[a]	Au-Cl[b]
3b	2.0418(18)	2.019(2)	2.2503(6)	2.2727(7)
2d	2.053(3)	1.993(3)	2.2582(8)	2.2698(9)
3d	2.063(3)	1.992(3)	2.2564(8)	2.2731(9)
4d	2.062(4)	1.939(4)	2.2585(13)	2.2683(13)

[a] Distance trans to pyridyl nitrogen. [b] Distance trans to anionic nitrogen

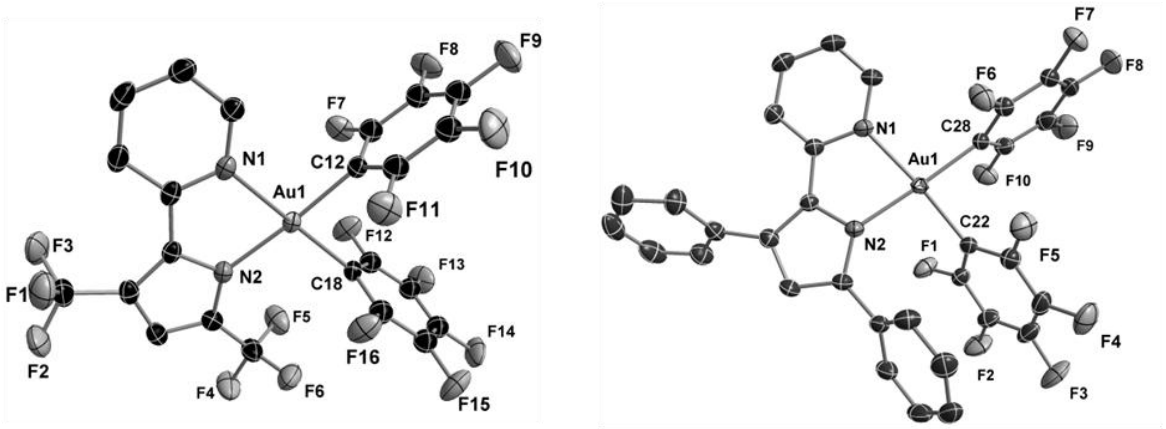

3c **4c**

Figure 6. X-ray crystal structures of **3c** and **4c** with selective atomic numbering scheme. Thermal ellipsoids are drawn at 50% probability level. Hydrogen atom and solvent molecules (if any) are omitted for clarity.

Table 2. Selected bond angles (°) of **3b**, **2d-4d.**

	N(1)-Au(1)-N(2)	**N(2)-Au(1)-Cl(2)**	**N(1)-Au(1)-Cl(1)**
3b	81.04(8)	97.80(6)	94.57(6)
2d	80.04(12)	95.14(9)	94.89(9)
3d	79.85(11)	95.13(8)	94.87(8)
	N(1)-Au(1)-N(5)	**N(1)-Au(1)-Cl(1)**	**N(5)-Au(1)-Cl(2)**
4d	80.21(14)	94.88(11)	94.59(11)
	Cl(1)-Au(1)-Cl(2)	**N(1)-Au(1)-Cl(2)**	**N(2)-Au(1)-Cl(2)**
3b	86.60(3)	176.54(6)	175.60(5)
2d	89.92(3)	175.19(8)	74.71(8)
3d	90.16(3)	174.85(8)	174.71(8)
4d	90.21(6)	174.68(11)	174.05(10)

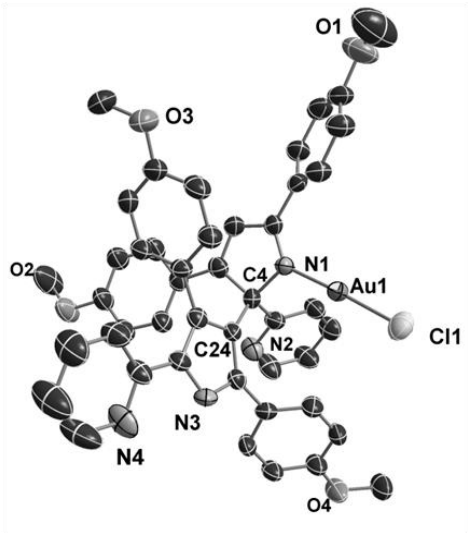

5b

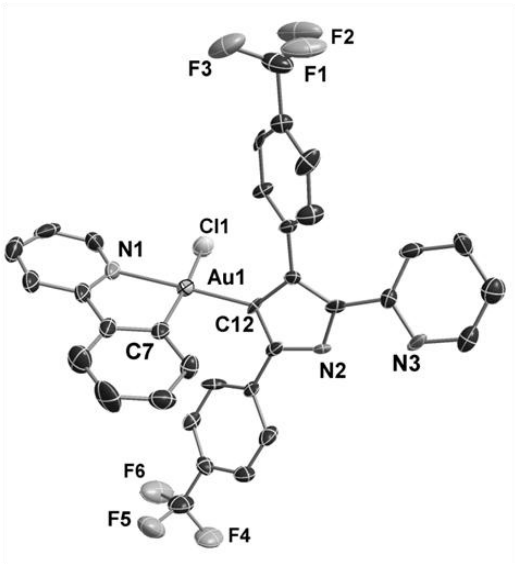

5c

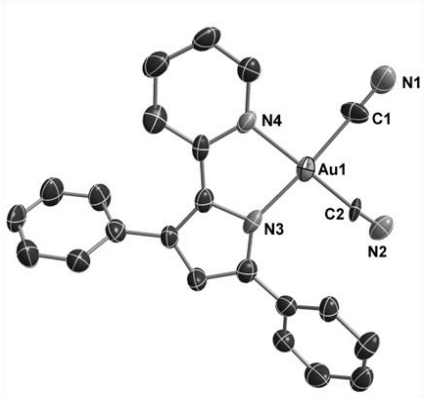

6

Figure 7. X-ray crystal structures of **5b**, **5c** and **6** with selective atomic numbering scheme. Thermal ellipsoids are drawn at 50% probability level. Hydrogen atoms and solvent molecules (if any) are omitted for clarity.

Table 3. Selected bond distances (Å) and angles (°) for **3c**-**5c** and **6.**

Complex **3c**			
C(12)-Au(1)	2.018(3)	N(1)-Au(1)	2.078(2)
C(18)-Au(1)	2.018(2)	N(2)-Au(1)	2.060(2)
N(1)-Au(1)-N(2)	79.83(9)	N(1)-Au(1)-C(12)	95.7(1)
C(12)-Au(1)-C(18)	82.83(10)	N(2)-Au(1)-C(18)	101.62(9)
N(1)-Au(1)-C(18)	176.81(9)	N2(2)-Au(1)-C(12)	175.53(9)
Complex **4c**			
N(1)-Au(1)	2.0817(17)	C(22)-Au(1)	2.011(2)
N(2)-Au(1)	2.0340(17)	C(28)-Au(1)	2.030(2)
C(22)-Au(1)-N(1)	172.91(8)	C(22)-Au(1)-C(28)	86.04(8)
C(28)-Au(1)-N(2)	177.44(7)	N(1)-Au(1)-C(28)	98.05(7)
N(1)-Au(1)-N(2)	79.60(7)	N(2)-Au(1)-C(22)	96.41(7)

Complex 5c			
N(1)-Au(1)	2.089(10)	C(12)-Au(1)	2.007(11)
Cl(1)-Au(1)	2.368(3)	C(7)-Au(1)	2.020(13)
N(1)-Au(1)-C(7)	80.7(4)	N(1)-Au(1)-Cl(1)	93.8(3)
N(1)-Au(1)-C(12)	173.3(5)	C(12)-Au(1)-Cl(1)	92.3(3)
C(7)-Au(1)-C(12)	93.4(4)	C(7)-Au(1)-Cl(1)	172.5(4)

Complex 6			
N(3)-Au(1)	1.984(12)	N(4)-Au(1)	2.066(10)
C(1)-Au(1)	1.966(16)	C(2)-Au(1)	1.982(12)
C(1)-N(1)	1.131(18)	C(2)-N(2)	1.110(16)
N(4)-Au(1)-N(3)	81.7(4)	N(4)-Au(1)-C(1)	93.9(5)
C(1)-Au(1)-C(2)	86.8(6)	C(2)-Au(1)-N(3)	97.5(5)

The Au metal ion in **5b** adopted a near linear shape with N(1)-Au(1)-Cl(1) angle of 177.28(18)°. The bond distance of the imine nitrogen of the five membered ring to Au centre N(1)-Au(1) was found to be 1.999(6) Å which is well within the normal range observed for Au(I) complexes in literature.[22] The monochloro Au(III) complex, **5c** similar to other Au(III) complexes exhibited distorted square planar arrangement. Selected metric parameters for this compound are listed in Table 3. The C(12)-Au(1) bond distance of 2.007(11) Å is comparable to those of *ppy*Au(III) aryls described in Chapters 2, 3 and in reference 21. Close intermolecular N-H···N hydrogen bonds which are common in (2-pyridyl)pyrrole compounds[5] were also observed in these complexes. It is useful to compare the bond distances of **6** (Figure 2 and Table 3) with that of *ppy*Au(CN)$_2$.While the distance between gold and the cyanide carbon *trans* to pyridine [Au-C(*sp*), 1.982 (12) Å] in **6** was remarkably close to that observed in the case of *ppy*Au(CN)$_2$. [Au-C(*sp*), 1.981(5) Å],[21] the Au-C(*sp*) bond distance *trans* to pyrrole nitrogen was lower 1.966(16) Å in **6** as compared to 2.078(5) Å in *ppy*Au(CN)$_2$ indicating stronger bond in the case of the former.

4.0 Conclusions

In summary a synthetic sequence for the preparation of various N^N chelated Au(III) dichlorides containing 2-pyridyl-*N*-heterocycles was established. The photophysical investigations on (2-pyridyl)pyrrolide Au(III) diaryl complexes suggested that, the good σ-donating properties of the ancillary chelate ligands alone is not decisive in rendering the gold complexes emissive but the appropriate placement of the energy levels of the ligand orbitals in a MO scheme becomes important. Accordingly, the extensively π-delocalized nature of the pyridyl pyrrole (*pypyr*)

ligand in the (N^N)Au(III) diaryl complex was reasoned to be the cause of its non-emissive nature despite the good σ-donating property of the pyrrolide unit.

5.0 Experimental section

5.1 General considerations

Synthetic steps requiring inert atmosphere was carried out using standard schlenk techniques under an atmosphere of dry nitrogen. The various organic ligands (*viz*., pyridylpyrroles, pyridylpyrazole, pridyltriazole and pyridyl tetrazole) were prepared according to established literature procedures and appropriately cited in the result and discussion section of the chapter. All the isolated gold complexes were stable to air and moisture and were stored at room temperature. Et_2O used in reactions was dried by distillation under N_2 atmosphere using sodium benzophenone ketyl radical prior to use. Sodium tetrachloroaurate (III) dihydrate was purchased from Strem chemicals. Commercially available reagents were purchased from Aldrich and were used as such without further purification.^{1}H and ^{13}C{^{1}H} were recorded on Bruker AV2-400 or AV-500 spectrometers. ^{19}F NMR spectra were recorded on either on Varian Mercury spectrometer or Bruker AV2-400 spectrometers. Chemical shifts (δ) are reported in parts per million (ppm) referenced to tetramethylsilane (δ 0.00) ppm using the residual protio solvent peaks as internal standards (^{1}H NMR experiments) or the characteristic resonances of the solvent nuclei (^{13}C NMR experiments). ^{19}F NMR was referenced to $CFCl_3$ (δ 0.00) ppm. Coupling constants (*J*) are quoted in Hertz (Hz) and the following abbreviations are used to describe the signal multiplicities: s (singlet); d (doublet); t (triplet); q (quartet); m (multiplet); dd (doublet of doublet); ddd (doublet of doublet of doublets); td (triplet of doublet); dt (doublet of triplet). Proton and carbon assignments have been made using routine one and two dimensional NMR spectroscopies where appropriate. Infra-red (IR) spectra were recorded on a Perkin-Elmer 1600 Fourier Transform spectrophotometer using KBr pellet with frequencies (ν) quoted in wavenumbers (cm^{-1}). Elemental microanalysis was carried out with Leco CHNS-932 analyser. Mass spectra were run on a Finnigan-MAT-8400 mass spectrometer. TLC analysis was performed on precoated Merck Silica Gel $60F_{254}$ slides and visualised by luminescence quenching either at (short wavelength) 254 nm or (long wavelength) 365 nm. Chromatographic purification of products was performed on a short column (length 15.0 cm: diameter 1.5 cm) using forced flow of eluent. UV-vis measurements were carried out on a Perkin-Elmer Lambda

19 UV/VIS spectrophotometer. Cyclic voltammograms were obtained with Metrohm 757 computrace voltammetric analyzer. The cell was equipped with a gold working electrode and a Pt counter electrode, and a non-aqueous reference electrode. All sample solutions (CH_2Cl_2) were approximately $5x10^{-3}$ M in substrate and 0.1 M in *n*-Bu_4NPF_6, and were prepared under nitrogen. Ferrocene was subsequently added and the calibration of voltammograms was performed.

5.2 Ligand precursor syntheses.

Precursor ligands **1a**-**3a** were prepared according to a known literature procedure.[10] Analogous procedures were adopted for the syntheses of **5a**, **6a** and **7a** and are described below.

2-(3,5-bis(4-methoxyphenyl)-1*H*-pyrrol-2-yl)pyridine (**5a**).

To a N_2 flushed RB-flask equipped with a Dean-Stark condenser were added *p*-xylene (100.0 mL), 1,3-bis(4-methoxyphenyl)propane-1,3-dione (1.0 g, 3.51 mmol), 2-(aminomethyl)pyridine (0.42 g, 3.90 mmol) and tosic acid. (0.189 g, 1.09 mmol) and the reaction mixture was stirred at RT for 30 min. It was then heated to reflux (~170°C) for 24 h with continuous azeotropic removal of water. The product formation was monitored by GC/MS. After completion of the reaction, the residue was purified by column chromatography using silica gel. Eluent: Hexane/EtOAc (1:1) to obtain **5a** as an off-white solid, Yield: 0.941 g (75%); ESI-MS: 357.1 $[M+H]^+$; ^{1}H NMR (500 MHz, $CDCl_3$, 298 K): δ = 3.87 (s, 3H), 3.90 (s, 3H), 6.48 (d, J = 4.8 Hz, 1H), 6.96 - 7.01 (m, 5H), 7.29 (t, J = 4.8 Hz, 1H), 7.40-7.45 (m, 3H), 7.58 (d, J = 4.8 Hz, 2H), 8.50 (d, J = 4.8 Hz, 1H), 9.85 (s, br, 1H); ^{13}C NMR (125 MHz, $CDCl_3$, 298 K): δ = 55.3, 55.4, 109.3, 114.0, 114.4, 119.4, 120.2, 125.0, 125.5, 126.3, 126.8, 129.5, 130.4, 132.8, 136.0, 148.9, 150.6, 158.6, 158.7; elemental analysis (%) calcd. for $C_{23}H_{20}N_2O_2$: C, 77.51; H, 5.66; N, 7.86. Found: C, 77.50; H, 5.61; N, 7.50.

4-(5-(4-(dimethylamino)phenyl)-2-(pyridin-2-yl)-1*H*-pyrrol-3-yl)-*N*,*N*-dimethylbenzenamine (**6a**).

Following the procedure similar to **5a**, 1,3-bis(4-(dimethylamino)phenyl)propane-1,3-dione (0.500 g, 1.61 mmol), 2-(aminomethyl)pyridine (0.19 g, 1.75 mmol) and tosic acid (0.094 g, 0.54 mmol) were refluxed in *p*-xylene (60.0 mL) for 24 h. The product was obtained as a red solid after purification by column chromatography using silica gel. Eluent: Hexane/EtOAc (1:1), Yield: 0.48 g (78%); ESI-MS: 382.0 $[M]^+$; ^{1}H NMR (500 MHz, $CDCl_3$, 298 K): δ = 3.02 (s, 6H),

3.04 (s, 6H), 6.44 (s, 1H), 6.80-6.85 (m, 4H), 6.96 (m, 1H), 7.40 (t, J = 4.8 Hz, 4H), 7.54 (d, J = 4.9 Hz, 2H), 8.50 (d, J = 4.8 Hz, 1H), 9.76 (s, br, 1H); ^{13}C NMR (125 MHz, $CDCl_3$, 298 K): δ = 40.6, 40.7, 108.6, 112.0, 112.7, 119.3, 119.7, 120.8, 120.9, 125.3, 125.4, 125.9, 129.0, 130.0, 133.5, 135.8, 148.5, 149.5, 151.0; elemental analysis (%) calcd. for $C_{25}H_{26}N_4$: C, 78.50; H, 6.85; N, 14.65. Found: C, 78.70; H, 6.71; N, 14.41.

2-(3,5-bis(4-fluorophenyl)-1*H*-pyrrol-2-yl)pyridine (7a)

Following the procedure similar to **5a**, 1,3-bis(4-fluorophenyl)propane-1,3-dione (0.800 g, 3.07 mmol), 2-(aminomethyl)pyridine (0.372 g, 3.4 mmol) and tosic acid (0.151 g, 0.87 mmol) were refluxed in *p*-xylenes (80.0 mL) for 24 h. The product was obtained as a yellow solid after purification by column chromatography using silica gel. Eluent: Hexane/EtOAc (1:1), Yield: 0.50 g (50%); ESI-MS: 332.0 $[M]^+$; ^{1}H NMR (500 MHz, $CDCl_3$, 298 K): δ = 6.55 (d, J = 3.5 Hz, 1H), 7.06 (ddd, J = 7.5 Hz, 4.0 Hz, 1.5 Hz, 1H), 7.12-7.20 (m, 4H), 7.24 (d, J = 8.5 Hz, 1.0H), 7.44-7.52 (m, 3H), 7.644 (td, J = 3.0 Hz, 6.5 Hz, 2H), 8.53 (d, J = 4.5 Hz, 1H), 10.01 (s, br, 1H); ^{13}C NMR (125 MHz, $CDCl_3$, 298 K): 109.9, 115.3, 115.5, 115.7, 116.0, 119.4, 120.8, 125.3, 125.8, 125.9, 127.7, 128.3, 130.8, 131.6, 133.0, 149.0, 150.1; elemental analysis (%) calcd. for $C_{21}H_{14}F_2N_2$: C, 75.89; H, 4.25; N, 8.43. Found: C, 75.92; H, 4.05; N, 8.07.

2-(3,5-bis(4-(trifluoromethyl)phenyl)-1*H*-pyrrol-2-yl)pyridine (8a)

Following the procedure similar to **5a**, 1,3-bis(4-(trifluoromethyl)phenyl)propane-1,3-dione (1.0 g, 2.77 mmol), 2-(aminomethyl)pyridine (0.336 g, 3.1 mmol) and tosic acid (0.160 g, 0.92 mmol) were refluxed in *p*-xylenes (100.0 mL) for 24 h. **8a** was obtained as a yellow solid after purification by column chromatography using silica gel. Eluent: Hexane/EtOAc (1:1). Yield: 0.80 g (66.0%); ^{1}H NMR (500 MHz, $CDCl_3$, 298 K): δ = 6.78 (d, J = 3.0 Hz, 1H), 7.14 (ddd, J = 7.2 Hz, 4.0 Hz, 1.5 Hz, 1H), 7.30 (d, J = 7.5 Hz, 1H), 7.53 (t, J = 7.2 Hz, 1H), 7.76-7.74 (m, 6H), 7.78 (m, 2H), 8.57 (d, J = 4.2 Hz, 1H), 10.40 (s, br, 1H); ^{13}C NMR (100 MHz, $CDCl_3$, 298 K): δ = 111.3, 120.1, 121.5, 124.1, 125.0, 125.4, 125.6, 127.6, 127.7, 127.8, 128.0, 129.4, 129.5, 131.3, 135.0, 136.4, 140.6, 149.2, 149.6; elemental analysis (%) calcd. for $C_{23}H_{14}F_6N_2$: C, 63.89; H, 3.26; N, 6.48. Found: C, 63.57; H, 3.15; N, 6.29.

2-(3,5-bis(trifluoromethyl)pyrrolyl)pyridinyl·$AuCl_2$ (3b)

To a solution of $NaAuCl_4 \cdot 2H_2O$ (70.9 mg, 0.178 mmol) in 2.0 mL of deionized water was added a solution of 2-(3,5-bis(trifluoromethyl)-1*H*-pyrrol-2-yl)pyridine (50.0 mg, 0.178 mmol) in 1.0 mL of CH_3CN. After 24 h, the product precipitated as a brown solid, which was filtered, washed with water (5.0 mL) followed by diethyl ether (8.0 mL). Yield: 50.0 mg (79%); ESI-MS: *m*/*z* 510.4 $[M\text{-}Cl]^+$; ^{1}H NMR (500 MHz, DMSO-d_6, 298 K): δ = 7.23 (s, 1H), 7.74 (t, *J* = 6.5 Hz, 1H), 8.01 (d, *J* = 8.0 Hz, 1H), 8.44 (t, *J* = 8.0 Hz, 1H), 9.24 (d, *J* = 6.0 Hz); ^{13}C NMR (125 MHz, DMSO-d_6, 298 K): 115.9, 120.1, 120.5, 124.5, 126.0, 129.6, 131.0, 134.0, 142.1, 145.5, 155.1; ^{19}F NMR (282.0 MHz, DMSO-d_6) δ = -55.4 (s, 3F), -54.2 (s, 3F); elemental analysis (%) calcd. for $C_{11}H_5AuCl_2F_6N_2$: C, 24.15; H, 0.92; N, 5.12. Found: C, 23.98; H, 0.89; N, 4.98.

2-(3,5-bis(4-fluorophenyl)-pyrrolyl)pyridinyl·$AuCl_2$ (7b)

To a solution of $NaAuCl_4 \cdot 2H_2O$ (239.0 mg, 0.60 mmol) in 12.0 mL of deionized water was added a solution of 2-(3,5-bis(4-fluorophenyl)-1*H*-pyrrol-2-yl)pyridine (200.0 mg, 0.60 mmol) in 4.0 mL of CH_3CN. After 24 h, the product precipitated as a brown solid which was filtered, washed with water (8.0 mL) followed by cold CH_3CN (8.0 mL). Yield: 292.0 mg (81%); ^{1}H NMR (500 MHz, $CDCl_3$, 298 K): δ = 6.38 (s, 1H), 7.05-7.10 (m, 3H), 7.20 (t, *J* = 9.5 Hz, 2H), 7.31 (s, 1H), 7.45 (td, *J* = 5.0 Hz, 2.5 Hz, 2H), 7.49 (td, *J* = 5.0 Hz, 2.5 Hz, 2H), 7.66 (t, *J* = 9.5 Hz, 2H), 9.08 (d, *J* = 9.5 Hz, 1H); ^{13}C NMR (125 MHz, $CDCl_3$, 298 K): δ = 114.6, 114.8, 116.1, 118.9, 120.2, 130.8, 130.9, 131.0, 131.1, 132.0, 141.4, 145.3, 146.7, 155.5, 161.6, 163.6, 163.8; elemental analysis (%) calcd. for $C_{21}H_{13}AuCl_2F_2N_2$: C, 42.09; H, 2.19; N, 4.68. Found: C, 41.81; H, 2.01; N, 4.57.

2-(3, 5-bis(4-(trifluoromethyl)-pyrrolyl)pyridinyl·$AuCl_2$ (8b)

To a solution of $NaAuCl_4 \cdot 2H_2O$ (184.0 mg, 0.463 mmol) in 12.0 mL of deionized water was added a solution of 2-(3,5-bis(4-(trifluoromethyl)-1*H*-pyrrol-2-yl)pyridine (200.0 mg, 0.462 mmol) in 4.0 mL of CH_3CN. After 24 h, the product precipitated as a brown solid, which was filtered, washed with water (8.0 mL) followed by cold CH_3CN (8.0 mL). Yield: 268.0 mg (83%); ^{1}H NMR (500 MHz, $CDCl_3$, 298 K): δ = 6.50 (s, 1H), 7.19 (t, *J* = 6.5 Hz, 1H), 7.38 (d, *J* = 7.5 Hz, 1H), 7.65-7.72 (m, 6H), 7.75-7.80 (m, 3H), 9.11 (d, *J* = 5.5 Hz, 1H); ^{13}C NMR (125 MHz, $CDCl_3$, 298 K): δ 115.9, 120.1, 120.5, 121.5, 124.0, 124.5, 125.9, 129.3, 129.5, 129.6, 131.0,

133.9, 136.4, 137.5, 138.5, 142.1, 145.5, 145.7, 155.1; ^{19}F NMR (282.0 MHz, CD_2Cl_2) δ = -57.3 (s, 3F), -58.4 (s, 3F); elemental analysis (%) calcd. for $C_{23}H_{13}AuCl_2F_6N_2$: C, 39.51; H, 1.87; N, 4.01. Found: C, 39.32; H, 1.95; N, 3.90.

[(N^N)Au(C_6H_5)$_2$][N^N = 2-(3,5-bis(trifluoromethyl)-1*H*-pyrrol-2-yl)pyridine] (3c)

n-BuLi (0.27 mL, 0.420 mmol, 1.6 M in hexanes) was added *via* syringe to a cooled (-78 °C) solution of the iodopentafluorobenzene (0.118 g, 0.39 mmol) in dry diethylether (5.0 mL) under nitrogen atmosphere and stirred for 20 min. at that temperature. It was then transferred *via* cannula into a flask containing a diethylether suspension of **3b** (0.100 g, 0.182 mmol) precooled at -78 °C. This temperature was maintained for 15 min and then the mixture was allowed to warm to RT and stirred further for 1 h. TLC examination (EtOAc/Hexane = 1/5) of the reaction mixture at this stage showed complete consumption of the starting material. The reaction was quenched by addition of water (5.0 mL) followed by extraction with CH_2Cl_2 (3 x 10.0 mL). After separation, the organic layer was dried over $MgSO_4$ and concentrated *in vacuo* to obtain the crude product. Purification by column chromatography (neutral Al_2O_3, eluent: Hexane/EtOAc (2:1) yielded the product as an orange solid. Yield: 0.065 g (44%); IR (KBR); ν_{max} 3425, 1640, 1618, 1570, 1563, 1514, 1493, 1470, 1434, 1390, 1372, 1278, 1258, 1162, 1092, 1175, 1127, 1118, 1143, 1097, 1081, 1071, 996, 974, 809, 772, 751, 742, 731, 708, 684, 661, 582 (Au-C), 511(Au-C), 466, 419 cm^{-1}; ^{1}H NMR (500 MHz, CD_2Cl_2, 298 K): δ = 7.05 (s, 1H), 7.37 (t, J = 5.5 Hz, 1H), 7.73 (d, J = 5.5,1H), 8.20 (t, J = 3.5, 1H), 8.26 (d, J = 5.5, 1H); ^{13}C{^{1}H}NMR (125 MHz, CD_2Cl_2, 298 K): 114.2, 116.9 (q, $^1J_{C\text{-}F}$ = 37.5 Hz), 119.0, 121.2, 122.3, 123.3, 124.1, 126.3, 131.2 (q, $^1J_{C\text{-}F}$ = 37.5 Hz), 137.2 (dm, $^1J_{C\text{-}F}$ = 237.0 Hz), 138.0 (dm, $^1J_{C\text{-}F}$ = 236.0 Hz), 139.1, 140.0 (dm, $^1J_{C\text{-}F}$ = 247.0 Hz), 141.1 (dm, $^1J_{C\text{-}F}$ = 249.0 Hz), 142.8, 145.4 (dm, $^1J_{C\text{-}F}$ = 229.0 Hz), 146.3, 146.5 (dm, $^1J_{C\text{-}F}$ = 230.0 Hz), 154.1; ^{19}F NMR (282 MHz, CD_2Cl_2, 298 K): δ = -57.97 (3F, CF_3), -61.0 (3F, CF_3), -123.7 (2F, *o*-C_6F_5), -124.3 (2F, *o*-C_6F_5), -154.7 (1F, *p*-C_6F_5), -156.9 (1F, *p*-C_6F_5), -160.5 (2F, *m*-C_6F_5), -163.7 (2F, *m*-C_6F_5); elemental analysis (%) calc. for $C_{23}H_5AuF_{16}N_2$: C, 34.09; H, 0.62; N, 3.46. Found: C, 33.92; H, 0.61; N, 3.33.

[(N^N)Au(C_6H_5)$_2$][N^N = 2-(3,5-diphenyl-1*H*-pyrrol-2-yl)pyridine] (4c)

n-BuLi (0.25 mL, 0.39 mmol, 1.6 M in hexanes) was added *via* syringe to a cooled (-78 °C) solution of the iodopentafluorobenzene (0.123 g, 0.39 mmol) in dry diethylether (5.0 mL) under

nitrogen atmosphere and stirred for 20 minutes at that temperature. It was then transferred *via* cannula into a flask containing a diethylether suspension of **4b** (0.100 g, 0.177 mmol) precooled at -78 °C. This temperature was maintained for 15 min and then the mixture was allowed to warm to RT and stirred further for 1 h. TLC examination (EtOAc/Hexane = 1/5) of the reaction mixture at this stage showed complete consumption of the starting material. The reaction was quenched by addition of water (5.0 mL) followed by extraction with CH_2Cl_2 (3 x 10.0 mL). After separation, the organic layer was dried over $MgSO_4$ and concentrated *in vacuo* to obtain the crude product. Purification by column chromatography (neutral Al_2O_3, eluent: Hexane/EtOAc (2:1) yielded the product as an orange solid. Yield: 0.066 g (45%); IR (KBR): ν_{max} 3430, 1610, 1549, 1512, 1485, 1467, 1382, 1346, 1322, 1269, 1248, 1234, 1162, 1071, 1024, 969, 817, 807, 768, 759, 740, 699, 677, 661, 529 (Au-C), 510(Au-C), 441, 420, 353, 333, 327, 322, 313, 297, 284, 279, 275, 271, 268, 264, 259 cm^{-1}; ESI-MS (*m/z*): 492 $[M\text{-}2(C_6F_5)]^+$; ^{1}H NMR (500 MHz, CD_2Cl_2, 298 K): δ = 6.30 (s, 1H), 6.92 (t, *J* = 8.0 Hz, 1H), 7.12 -7.17 (m, 3H), 7.26-7.28 (m, 2H), 7.42-7.45 (m, 1H), 7.49-7.55 (m, 5H), 7.62-7.65 (m, 2H); ^{13}C{^{1}H}NMR (125 MHz, CD_2Cl_2, 298 K): 115.8, 119.6, 120.1, 126.9, 127.2, 127.4, 128.5, 128.7, 129.3, 132.8, 135.0, 135.2, 136.0, 136.5 (dm, $^1J_{C\text{-}F}$ = 236.0 Hz), 137.6 (dm, $^1J_{C\text{-}F}$ = 233.0 Hz), 145.4 (dm, $^1J_{C\text{-}F}$ = 240.0 Hz), 140.5, 145.8 (dm, $^1J_{C\text{-}F}$ = 222.0 Hz), 145.9, 147.5, 156.8; ^{19}F NMR (282 MHz, CD_2Cl_2, 298 K): δ = -124.0 (2F, *o*-C_6F_5), -124.1 (2F, *o*-C_6F_5), -156.6 (1F, *p*-C_6F_5), -158.7 (1F, *p*-C_6F_5), -161.8 (2F, *m*-C_6F_5), -163.8 (2F, *m*-C_6F_5); elemental analysis (%) calcd. for $C_{33}H_{15}AuF_{10}N_2$: C, 47.96; H, 1.83; N, 3.39. Found: C, 47.54; H, 2.06; N, 3.33.

[(N^N)AuCl$_2$][N^N = 2-(3-(trifluoromethyl)-1*H*-pyrazol-5-yl)pyridine] (2d)

To a solution of $Na_2AuCl_4{\cdot}2H_2O$ (0.186 g, 0.469 mmol) in deionized water (6.0 mL) was dropwise added 2-(3-(trifluoromethyl)-1*H*-pyrazol-5-yl)pyridine (0.100 g, 0.469 mmol) dissolved in CH_3CN (2.0 mL) at RT. After 6 h, the precipitated solid was filtered and washed with water (5.0 mL). The collected solid was then dissolved in THF (15.0 mL) dried over anhyd. Na_2SO_4, solvent concentrated to get **2d** as brown solid. Yield: 95.0 mg (42%); ^{1}H NMR (500 MHz, DMSO-d_6, 298 K): δ = 7.65 (s, 1H), 7.77 (t, *J* = 9.5 Hz, 1H), 8.36 (d, *J* = 5.0 Hz, 1H), 8.46 (t, *J* = 9.5 Hz, 1H), 9.16 (d, *J* = 5.0 Hz, 1H); ^{13}C NMR (125 MHz, DMSO-d_6, 298 K): δ = 105.3, 123.0, 123.4, 125.1, 139.8, 145.2, 146.7, 150.0, 150.1; ^{19}F NMR (188 MHz, DMSO-d_6, 298 K): δ

= -60.3; elemental analysis (%) calcd. for C, 22.52; H, 1.05; N, 8.75. Found: C, 22.28; H, 1.00; N, 8.87.

[(N^N)$AuCl_2$][N^N = 2-(5-phenyl-2*H*-1,2,4-triazol-3-yl)pyridine] (3d)

To a solution of $Na_2AuCl_4 \cdot 2H_2O$ (0.179 g, 0.449 mmol) in deionized water (6.0 mL) was dropwise added 2-(5-phenyl-2*H*-1,2,4-triazol-3-yl)pyridine (0.100 g, 0.469 mmol) dissolved in CH_3CN (2.0 mL) at RT. After 30 min the yellow suspension turned orange-red and was allowed to stir for an additional 12 h. The precipitated solid was filtered and washed with water (5.0 mL) followed by cold CH_3CN (5.0 mL). The crude product thus obtained was then recrystallized from EtOAc/THF/Hexane mixture (8:1:1) to obtain **3d** as a pale pink solid. Yield: 158.6 mg (72%); ^{1}H NMR (500 MHz, DMSO-d_6, 298 K): δ = 7.45-7.48 (m, 1H), 7.50-7.53 (m, 2H), 7.89 (t, J = 6.0 Hz, 1H), 8.09 (dd, J = 6.0 Hz, 1.5 Hz, 2H), 8.33 (d, J = 7.5 Hz, 1H), 8.51 (t, J = 7.5 Hz, 1H), 9.25 (d, J = 6.0 Hz, 1H); ^{13}C NMR (125 MHz, DMSO-d_6, 298 K): δ = 124.0, 126.4, 126.8, 129.3, 129.9, 131.3, 145.6, 145.7, 147.2, 160.1, 161.3; elemental analysis (%) calc. for $C_{13}H_9AuCl_2N_4$; C, 31.92; H, 1.85; N, 11.45. Found: C, 31.78; H, 1.92; N, 11.15.

[(N^N)$AuCl_2$][N^N = 2-(1*H*-tetrazol-5-yl)pyridine] (4d)

To a solution of $Na_2AuCl_4 \cdot 2H_2O$ (0.135 g, 0.339 mmol) in deionized water (3.0 mL) was dropwise added 2-(1*H*-tetrazol-5-yl)pyridine (0.05 g, 0.339 mmol) dissolved in CH_3CN (1.0 mL) at RT and was allowed to stir for 12 h. The precipitated solids was collected by filtration and washed with water (5.0 mL) followed by cold CH_3CN (5.0 mL). The crude product thus obtained was then recrystallized from EtOAc/hexane (1:2) mixture to get **4d** as yellow solid. Yield: 0.095 g (68%); ^{1}H NMR (500 MHz, THF-d_8, 298 K): δ = 7.96 (td, J = 6.0 Hz, 2.5 Hz, 1H), 8.51-8.55 (m, 2H), 9.40 (d, J = 6.0 Hz, 1H); ^{13}C NMR (125 MHz, THF-d_8, 298 K): δ = 123.0, 126.0, 142.7, 143.9, 145.7, 159.2; elemental analysis (%) calc. for C, 17.41; H, 0.97; N, 16.92. Found: C, 17.20; H, 0.92; N, 16.70.

[(N^N)$Au(CN)_2$][N^N = 2-(3,5-diphenyl-1*H*-pyrrol-2-yl)pyridine] (6)

To a solution of [*n*-Bu_4]NCN (0.123 g, 0.458 mmol) in DCM approx. 12.0 mL was added [N^N)$AuCl_2$][N^N = 2-(3,5-diphenyl-1*H*-pyrrol-2-yl)pyridine] **4b** (0.118 g, 0.209 mmol) and stirred at RT. After 12 h, TLC monitoring showed the complete consumption of gold dichloride. Deionized water (15.0 mL) was then added to the reaction mixture and the aqueous layer was

extracted twice with DCM (2 x 10.0 mL), the combined organic phases were dried over anhydrous Na_2SO_4 and the crude product was obtained after concentration of the solvent *in vacuo*. The polar spot was then isolated by purification by column chromatography (neutral Al_2O_3; eluent: Hexane/EtOAc = 1/1), Yield: 0.033 g (dark red crystals, 29%); IR (KBr): ν_1(C≡N) 2009 cm^{-1}, ν_2(C≡N) 2053 cm^{-1}; Raman: ν_1(C≡N) 2098 cm^{-1}, ν_2(C≡N) 2166 cm^{-1}; ^{1}H NMR (500 MHz, CD_2Cl_2, 298 K): δ = 6.44 (s, 1H), 7.09-7.122 (m, 1H), 7.48-7.59 (m, 10H), 7.73-7.76 (m, 1H), 8.85 (d, J = 6.0 Hz, 2H); $^{13}C\{^1H\}$ NMR (125 MHz, CD_2Cl_2, 298 K): δ = 87.0, 102.7, 114.7, 120.2, 120.5, 120.5, 128.1, 128.2, 129.0, 129.1, 129.6, 134.5, 134.6, 135.0, 142.0, 148.7, 149.3, 156.5, 170.8; elemental analysis $C_{23}H_{15}AuN_4$ (%) calcd. for C, 50.75; H, 2.78; N, 10.29. Found: C, 51.01; H, 3.01; N, 9.98.

6.0 APPENDIX (Chapter 5)

6.1 X-ray diffraction details

Relevant details about the structure refinements are given in Tables A1, A2 and S3, and selected geometrical parameters are included in the captions of the corresponding figures. Intensity data were collected at 183(2) K an Oxford Xcalibur diffractometer (4-circle kappa platform, Ruby CCD detector, and a single wavelength Enhance X-ray source with MoK_α radiation, λ = 0.71073 Å).[23] The selected suitable single crystals were mounted using polybutene oil on the top of a glass fiber fixed on a goniometer head and immediately transferred to the diffractometer. Pre-experiment, data collection, data reduction and analytical absorption corrections[24] were performed with the Oxford program suite *CrysAlisPro*.[25] The crystal structures were solved with SHELXS-97[26] using direct methods. The structure refinements were performed by full-matrix least-squares on F^2 with SHELXL-97.[26] All programs used during the crystal structure determination process are included in the WINGX software.[27] The program PLATON[28] was used to check the result of the X-ray analyses.

In the crystal structure of **3d**, and **6** the solvent molecules of THF and ether co-crystallized with the main species in a ratio 1:2. In **6** the solvent molecule lies about a center of inversion and is disordered over two positions, some distance restraints were used to correct the geometry. In the crystal structure of **5c**, intermolecular N-H···N hydrogen bonds were observed. All hydrogen positions were calculated after each cycle of refinement using a riding model, with C-H = 0.93 Å and U_{iso}(H) = 1.2U_{eq}(C) for aromatic H atoms, with C-H = 0.98 Å and U_{iso}(H) = 1.2U_{eq}(C) for methine H atoms, with C-H = 0.97 Å and U_{iso}(H) = 1.2U_{eq}(C) for methylene H atoms, and C-H = 0.96 Å and U_{iso}(H) = 1.5U_{eq}(C) for methyl H atoms and with N-H = 0.86 Å and U_{iso}(H) = 1.2U_{eq}(N).

Table A1. Crystallographic data for compounds **2d**, **3d** and **4d.**

	2d	**3d**	**4d**
empirical formula	$C_9 H_5 Au Cl_2 F_3 N_3$	$2(C_{13} H_9 Au Cl_2 N_4), C_4 H_8 O$	$C_6 H_4 Au Cl_2 N_5$
formula weight ($g \cdot mol^{-1}$)	480.03	1050.33	414.01
temperature (K)	183(2)	183(2)	183(2)
wavelength (Å)	0.71073	0.71073	0.71073
crystal system, space group	Orthorhombic, *P* b c a	Orthorhombic, *P* b c a	Monoclinic, *P* 21/n
a (Å)	7.3451(1)	16.7302(2)	9.103(3)
b (Å)	17.1802(2)	8.6281(1) A	8.3029(5)
c (Å)	18.5318(2)	21.5433(4) A	13.6466(7)
α (deg)	90	90	90
β (deg)	90	90	105.944(14)
γ (deg)	90	90	90
volume ($Å^3$)	2338.53(5)	3109.77(8)	991.7(3)
Z, density (calcd) ($Mg \cdot m^{-3}$)	8, 2.727	4, 2.243	4, 2.773
abs coefficient (mm^{-1})	13.060	9.809	15.337
F(000)	1760	1984	752
crystal size (mm^3)	0.29 x 0.13 x 0.02	0.24 x 0.06 x 0.03	0.15 x 0.11 x 0.03
θ range (deg)	2.61 to 30.50	2.82 to 30.51	2.90 to 28.28
reflections collected	30621	26932	14597
reflections unique	3571 / [R(int) = 0.0365]	4739 / [R(int) = 0.0358]	2455 / [R(int) = 0.0428]
completeness to *θ* (%)	99.9	99.9	100.0
absorption correction	Analytical	Analytical	Analytical
max/min transmission	0.997 and 0.978	0.759 and 0.267	0.635 and 0.207
data / restraints / parameters	3265 / 0 / 163	3901 / 35 / 226	2227 / 0 / 127
goodness-of-fit on F^2	1.212	1.049	1.069
final R_1 and wR_2 indices [$I > 2\sigma(I)$]	R_1= 0.0250, wR_2 = 0.0511	R_1 = 0.0263, wR_2= 0.0438	R_1= 0.0253, wR_2= 0.0530
R_1 and wR_2 indices (all data)	R_1= 0.0291, wR_2 = 0.0524	R_1= 0.0376, wR_2= 0.0469	R_1= 0.0301, wR_2= 0.0549

The unweighted R-factor is $R_1 = \sum(Fo - Fc)/\sum Fo$; $I > 2\,\sigma(I)$ *and the weighted R-factor is* $wR_2 = \{\sum w(Fo^2 - Fc^2)^2/\sum w(Fo^2)^2\}^{1/2}$

Table A2. Crystallographic data for compounds **3b, 3c** and **4c.**

	3b	**3c**	**4c**
empirical formula	C_{11} H_5 Au Cl_2 F_6 N_2	C_{23} H_5 Au F_{16} N_2	C_{33} H_{15} Au F_{10} N_2
formula weight ($g \cdot mol^{-1}$)	547.04	810.26	826.44
temperature (K)	183(2)	183(2)	183(2)
wavelength (Å)	0.71073	0.71073	0.71073
crystal system, space group	Triclinic, *P* -1	Orthorhombic, *P* b c a	Monoclinic, *P* 21/c
a (Å)	7.4723(3)	11.3213(1)	12.9024(1)
b (Å)	9.6564(3)	17.9097(3)	16.3919(1)
c (Å)	10.1696(4	22.9576(2)	13.0368(1)
α (deg)	73.830(3)	90.0	90.0
β (deg)	75.839(3	90.0	99.430(1)
γ (deg)	76.469(3)	90.0	90.0
volume ($Å^3$)	672.42(4)	4654.91(10)	2719.96(3)
Z, density (calcd) ($Mg \cdot m^{-3}$)	2, 2.702	8, 2.312	4, 2.018
abs coefficient (mm^{-1})	11.402	6.467	5.506
F(000)	504	3040	1584
crystal size (mm^3)	0.17 x 0.09 x 0.05	0.35 x 0.17 x 0.13	0.39 x 0.29 x 0.18
θ range (deg)	2.70 to 30.51	2.53 to 30.03	2.73 to 30.51
reflections collected	12389	40680	53091
reflections unique	4107 / [R(int) = 0.0282]	6787 / [R(int) = 0.0279]	8310 / [R(int) = 0.0270]
completeness to *θ* (%)	100	99.9	99.9
absorption correction	Analytical	Analytical	Analytical
max/min transmission	0.569 and 0.265	0.497 and 0.353	0.832 and 0.688
data / restraints / parameters	3685 / 0 / 199	5792 / 0 / 379	7140 / 0 / 415
goodness-of-fit on F^2	0.997	1.095	1.054
final R_1 and wR_2 indices [$I > 2\sigma(I)$]	R_1= 0.0182, wR_2= 0.0338	R_1= 0.0242, wR_2= 0.0508	R_1= 0.0181, wR_2= 0.0444
R_1 and wR_2 indices (all data)	R_1= 0.0228, wR_2= 0.0343	R = 0.0324, wR_2= 0.0532	R_1= 0.0241, wR_2= 0.0453

The unweighted R-factor is $R_1 = \sum(Fo - Fc)/\sum Fo$; $I > 2\,\sigma(I)$ *and the weighted R-factor is* $wR_2 = \{\sum w(Fo^2 - Fc^2)^2/\sum w(Fo^2)^2\}^{1/2}$

Table A3. Crystallographic data for compounds **5b**, **5c** and **6.**

	5b	**5c**	**6**
empirical formula	$C_{46}H_{38}AuClN_4O_4$	$C_{34}H_{21}AuClF_6N_3$	$2(C_{23}H_{15}AuN_4)$, $C_4H_{10}O$
formula weight ($g \cdot mol^{-1}$)	943.22	817.96	1162.84
temperature (K)	183(2)	183(2)	183(2)
wavelength (Å)	0.71073	0.71073	0.71073
crystal system, space group	Monoclinic, *C* 2/c	Monoclinic, *P* 2/n	Triclinic, *P* -1
a (Å)	a = 28.3023(5)	13.8279(8)	4.8031(2)
b (Å)	b = 13.0945(4)	12.8274(5)	11.6531(5)
c (Å)	c = 22.2218(4)	17.6110(8)	19.9543(11)
α (deg)	90	90	75.611(4)
β (deg)	106.764(2)	100.977(5)	84.488(4)
γ (deg)	90	90	84.492(3)
volume ($Å^3$)	7885.5(3)	3066.6(3)	1073.81(9)
Z, density (calcd) ($Mg \cdot m^{-3}$)	8, 1.589	4, 1.772	1, 1.798
abs coefficient (mm^{-1})	3.849	4.950	6.872
F(000)	3760	1584	562
crystal size (mm^3)	0.24 x 0.14 x 0.11	0.12 x 0.05 x 0.03	0.20 x 0.06 x 0.02
θ range (deg)	2.68 to 25.68 deg.	2.61 to 25.35	3.10 to 25.68
reflections collected	36997	13489	8797
reflections unique	7471 / [R(int) = 0.0579]	5623 / [Rint = 0.1039]	4028 / [R(int) = 0.0510]
completeness to *θ* (%)	99.9 %	99.8	98.9
absorption correction	Analytical	Analytical	Analytical
max/min transmission	0.740 and 0.542	0.871 and 0.735	0.863 and 0.415
data / restraints / parameters	5836 / 0 / 509	3418 / 18 / 406	3174 / 33 / 299
goodness-of-fit on F^2	1.083	1.025	1.154
final R_1 and wR_2 indices [$I > 2\sigma(I)$]	R_1= 0.0606, wR_2= 0.1415	R_1= 0.0762, wR_2= 0.1071	R_1= 0.0634, wR_2= 0.1542
R_1 and wR_2 indices (all data)	R_1= 0.0813, wR_2= 0.1528	R_1= 0.1460, wR_2= 0.1276	R_1= 0.0831, wR_2= 0.1591

The unweighted R-factor is $R_1 = \sum(Fo - Fc)/\sum Fo$; $I > 2\,\sigma(I)$ *and the weighted R-factor is* $wR_2 = \{\sum w(Fo^2 - Fc^2)^2/\sum w(Fo^2)^2\}^{1/2}$

7.0 References

[1] Vogler, A.; Kunkely, H. *Coord. Chem. Rev.* **2001**, *219*, 489.

[2] Yam, V. W.-W.; Choi, S. W. K.; Lai, T. F.; Lee, W. K.; *J. Chem. Soc. Dalton Trans*. **1993**, 1001.

[3] (a) Antipas, A.; Dolphin, D.; Gouterman, M.; Johnson.; E. C. *J. Am. Chem. Soc.* **1978**, *100*, 7705. (b) Eng, M. P.; Ljungdahl. T.; Andrèasson, J.; Mårtensson, J.; Albinsson, B. *J. Phys. Chem. A*, **2005**, *109*, 1776.

[4] Toganoh, M.; Niino, T.; Furuta, H. *Chem. Commun.* **2008**, (*34*), 4070.

[5] (a) Kijak, M.; Nosenko, Y.; Singh, A.; Thummel, R. P.; Waluk, J. *J. Am. Chem. Soc.* **2007**, *129* (10), 2738. (b) Rode, M. F.; Sobolewski, A. L. *Chem. Phys.* **2008**, *347* (1-3), 413.

[6] Flores, J. A.; Andino, J. G.; Tsvetkov, N. P.; Pink, M.; Wolfe, R. J.; Head, A. R.; Lichtenberger, D. L.; Massa, J.; Caulton, K. G. *Inorg. Chem.* **2011**, *50* (17), 8121.

[7] Mcbee, J. L.; Escalada, J.; Tilley, T. D. *J. Am. Chem. Soc.* **2009**, *131* (35), 12703.

[8] Schouteeten, S.; Allen, O. R.; Haley, A. D.; Ong, G. L.; Jones, G. D.; Vicic, D. A. *J. Organomet. Chem.* **2006**, *691* (23), 4975.

[9] (a) Yu, J. K.; Hu, Y. H.; Cheng, Y. M.; Chou, P. T.; Peng, S. M.; Lee, G. H.; Carty, A. J.; Tung, Y. L.; Lee, S. W.; Chi, Y.; Liu, C. S. *Chem.–Eur. J.* **2004**, *10* (24), 6255. (b) Cheng, C. C.; Yu, W. S.; Chou, P. T.; Peng, S. M.; Lee, G. H.; Wu, P. C.; Song, Y. H.; Chi, Y. *Chem. Commun.* **2003**, (*20*), 2628. (c) Chang, S. Y.; Kavitha, J.; Li, S. W.; Hsu, C. S.; Chi, Y.; Yeh, Y. S.; Chou, P. T.; Lee, G. H.; Carty, A. J.; Tao, Y. T.; Chien, C. H. *Inorg. Chem.* **2006**, *45* (1), 137. (d) Wu, P. C.; Yu, J. K.; Song, Y. H.; Chi, Y.; Chou, P. T.; Peng, S. M.; Lee, G. H. *Organometallics* **2003**, *22* (24), 4938. (e) Fang, C. H.; Chen, Y. L.; Yang, C. H.; Chi, Y.; Yeh, Y. S.; Li, E. Y.; Cheng, Y. M.; Hsu, C. J.; Chou, P. T.; Chen, C. T. *Chem.–Eur. J.* **2007**, *13* (9), 2686. (f) Wu, L. L.; Yang, C. H.; Sun, I. W.; Chu, S. Y.; Kao, P. C.; Huang, H. H. *Organometallics* **2007**, *26* (8), 2017. (g) Stagni, S.; Colella, S.; Palazzi, A.; Valenti, G.; Zacchini, S.; Paolucci, F.; Marcaccio, M.; Albuquerque, R. Q.; De Cola, L. *Inorg. Chem.* **2008**, *47* (22), 10509. (h) Yeh, S. J.; Wu, M. F.; Chen, C. T.; Song, Y. H.; Chi, Y.; Ho, M. H.; Hsu, S. F.; Chen, C. H. *Adv. Mater.* **2005**, *17* (3), 285.

[10] Klappa, J. J.; Rich, A. E.; McNeill, K. *Org. Lett.* **2002**, *4* (3), 435.

[11] Scovell, W. M.; Stocco, G. C.; Tobias, R. S. *Inorg. Chem.* **1970**, *9* (12), 2682. (b) Adams, H. N.; Strahle, J. *Z. Anorg. Allg. Chem.* **1982**, *485* (2), 65.

[12] Thiel, W. R.; Eppinger, J. *Chem.–Eur. J.* **1997**, *3* (5), 696.

[13] Yang, C. H.; Li, S. W.; Chi, Y.; Cheng, Y. M.; Yeh, Y. S.; Chou, P. T.; Lee, G. H.; Wang, C. H.; Shu, C. F. *Inorg. Chem.* **2005**, *44* (22), 7770. (b) Lo, S. C.; Shipley, C. P.; Bera, R. N.; Harding, R. E.; Cowley, A. R.; Burn, P. L.; Samuel, I. D. W. *Chem. Mater.* **2006**, *18* (21), 5119. (c) Mak, C. S. K.; Hayer, A.; Pascu, S. I.; Watkins, S. E.; Holmes, A. B.; Kohler, A.; Friend, R. H. *Chem. Commun.* **2005**, (*37*), 4708.

[14] Orselli, E.; Kottas, G. S.; Konradsson, A. E.; Coppo, P.; Fröhlich, R.; De Cola, L.; van Dijken, A.; Büchel, M.; Börner, H. *Inorg. Chem.* **2007**, *46* (26), 11082.

[15] Browne, W. R.; Hage, R.; Vos, J. G. *Coord. Chem. Rev.* **2006**, *250* (13-14), 1653.

[16] Demko, Z. P.; Sharpless, K. B. *J. Org. Chem.* **2001**, *66* (24), 7945.

[17] Yersin, H.; Finkenzeller, W. J. in *Highly Efficient OLEDs with Phosphorescent Materials*: Ed.; Yersin, H., Wiley-VCH, Weinheim, 2007, chap. 1.

[18] Kozhevnikov, D. N.; Kozhevnikov, V. N.; Ustinova, M. M.; Santoro, A.; Bruce, D. W.; Koenig, B.; Czerwieniec, R.; Fischer, T.; Zabel, M.; Yersin, H. *Inorg. Chem.* **2009**, *48* (9), 4179.

[19] Tong, G. S. M.; Che, C. M. *Chem.–Eur. J.* **2009**, *15* (29), 7225.

[20] Koelle, U.; Laguna, A. *Inorg. Chim. Acta* **1999**, *290* (1), 44. (b) Yam, V. W.-W.; Wong, K. M. C.; Hung, L. L.; Zhu, N. *Angew. Chem. Int. Ed*. **2005**, *44*, 3107. (c) Wong, K. M. C.; Hung, L. L.; Lam, W. H.; Zhu, N.; Yam, V. W.-W. *J. Am. Chem. Soc*. **2007**, *129*, 4350. (d) Yam, V. W.-W.; Au, V. K. M.; Wong, K. M. C.; Zhu, N. *J. Am. Chem. Soc*. **2009**, *131*, 9076.

[21] Szentkuti, A. in *New Strategies for the Stabilization of Phosphorescent Monocyclometalated Gold(III)-complexes*, (Master thesis, Univ. of Zurich), 2011.

[22] Melgarejo, D. Y.; Chiarella, G. M.; Fackler, J. P. *Inorg. Chim. Acta.* **2011**, *378* (1), 297. (b) Yam, V. W.-W.; Cheung, K. L.; Yip, S. K.; Cheung, K. K. *J. Organomet.Chem.* **2003**, *681* (1-2), 196.

[23] Xcalibur CCD System; Oxford Diffraction Ltd: Abingdon, Oxfordshire, England, 2007.

[24] Clark, R. C.; Reid, J. S. *Acta Cryst.* **1995**, *A51*, 887.

[25] *CrysAlisPro* (versions 1.171.32.55), Oxford Diffraction Ltd, Abingdon, Oxfordshire, England.

[26] Sheldrick, G. M. *Acta Cryst.* **2008**, *A64*, 112.

[27] Farrugia, L. J. *J. Appl. Cryst.* **1999**, *32*, 837.

[28] Spek, A. L. *J. Appl. Cryst.* **2003**, *36*, 7.

Chapter 6.

Exploration and Development of Bulky *N*-Heterocyclic Carbene based Gold σ-Alkynyl Monomers suitable for Modular Construction of Luminescent Conjugated Polymers

Exploration and Development of Bulky *N*-heterocyclic Carbene based Gold σ-alkynyl Monomers suitable for Modular Construction of Luminescent Conjugated Polymers

1.0 Abstract

This chapter has two important goals: first is to create *N*-heterocyclic carbene coordinated late transition-metal (d^8/d^{10} systems especially with gold) σ-alkynyl organometallic units, suitable to be used as monomers for building conjugated polymers. Second, is to evaluate phosphorescent photophysical attributes of the synthesized monomers which are driven by 'heavy-metal' effect. In this regard, appropriate σ-alkynyl complexes based on Pd(II), Pt(II), Au(I)\Au(III) metal centers have been synthesized using novel synthetic routes. Triptycene has been used to design sterically imposing NHC ligand to improve the monomer characteristics (*viz.* solubility, high molecular weight etc.). The electronic and steady-state photoluminescence properties of the monomers have been studied at both 77 K and at ambient temperatures. The photoluminescence in the blue-green region exhibited by most of the monomers synthesized, are anticipated to be suitable for incorporation into conjugated polymers.

2.0 Introduction and literature overview

Exploration of room temperature phosphorescence (RTP) in late transition-metal complexes has secured a unique position among the various research areas of organometallic chemistry. Impressive progress have been made in understanding the multiple aspects of photoexcited states in such metal complexes.[1] For the reasons discussed in Chapter 1, the photodeactivation processes of the long-lived triplet (T_n) excited states has been perceived to be of immense importance. Moving forward from the photophysics of purely small organic molecular entities, numerous studies have been carried out to understand the excited state behavior of higher molecular weight fragments like dendrimers, polymers, organogels etc.[2] While this is so, such an understanding has been limited in the case of metal containing macromolecules that are phosphorescent. The lack of appropriate synthetic methodology and the unease in handling organometallic

complexes are presumably some of the key reasons. In this regard, an effort towards building novel transition metal based phosphorescent polymers was considered to be both important and attractive. As seen in the previous chapters, incorporation of gold metal stabilized with aryl acetylides and *N*-heterocyclic carbenes (NHCs) remained a central theme of our study in this chapter also, nevertheless initial studies began with exploring NHCs containing Pd(II) and Pt(II) complexes to understand the reactivity patterns along the isoelectronic series. In literature, inorganic (or) organometallic polymers built with different metals have been aimed to serve different purposes; for example, polymers constructed from main group or early transition group metals like Sn, Ni or Fe were found to display good oxidative, thermal and hydrolytic stabilities which were superior to many organic polymers.[3] Polyferrocenes were found to unify the electrochemical aspects of ferrocene itself with the facile immobilization of active centres and high functional density into polymers thereby generating novel materials for catalysis.[4] Polystannanes on the other hand were found to be semi-conductive and also exhibited liquid crystallinity.[5] There are several more and continuously surging reports of new synthetic methods for building and applications of organometallic polymeric materials.[6] Our concern for using 4d/5d transition-metals primarily arises due to aforementioned phosphorescent nature of emission and to the increased triplet excited state yield. Amongst the various types of polymers, conjugated metallopolymers provide an unique flexibility in anchoring different functional units. This aspect has resulted in the realization of polymers reflecting the characteristics of the incorporated monomers[7] and is therefore well suited for a modular approach. A survey of literature revealed two robust synthetic methodologies for the construction of soluble linear two dimensional rigid-rod conjugated polymers containing late transition metals. They are as follows,

(1) The dehydrohalogenation method developed by Hagihara and co-workers in 1978,[8] which employs a base like diethylamine in the presence of Cu(I) catalyst to couple $PtCl_2$ and aryl acetylides (Figure 1).

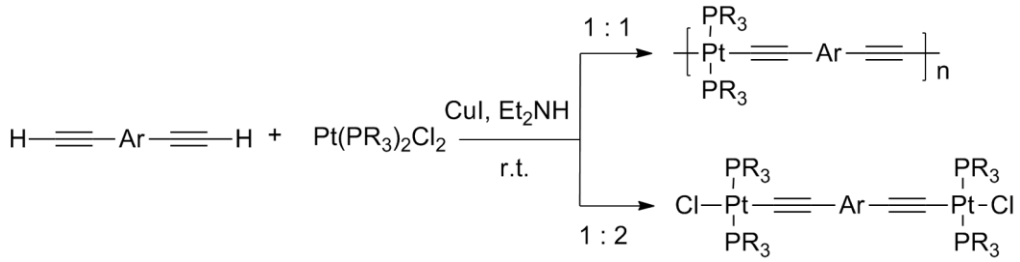

Figure 1. Synthesis of metal acetylides by dehydrohalogenation.

(2) The Hay's coupling reaction applied on metal-organic monomers, (Figure 2) which involves oxidative homocoupling of bis(terminal alkyne) complexes with Cu(I) salt as catalyst and O_2 as oxidant.[9]

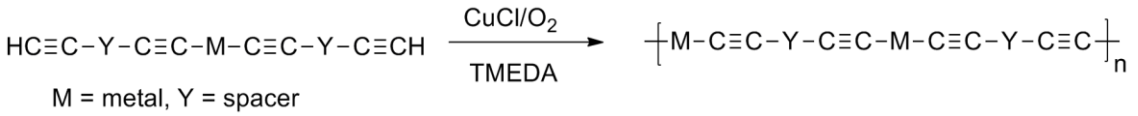

Figure 2. Oxidative homocoupling of di(terminal) acetylides.

In the first case, the reaction conditions are generally mild and the extent of polymerization relies on the exact stoichiometric ratio of the difunctional monomers involved, and in the latter case the degree of polymerization is dependent on the stoichiometry of only one monomer. Both the methods proved to be facile synthetic routes for the preparation of high molecular weight σ-bonded transition metal alkynes (metal polyynes). Depending on the bridging alkynes, the molecular weights (by gel-permeation chromatography) typically in the range of M_w = 60,000 to 160,000 for Pt(II) and around M_w = 26,000 for Pd(II) have been achieved.[10] Moreover, further proving the versatility of the dehydrohalogenation strategy, heterobimetallic metal polyynes[11] have been synthesized by reacting mixed metal momomeric units *viz*. Ru(*dppe*)$_2$ and Pd(P^nBu_3)$_2$ (Figure 3)

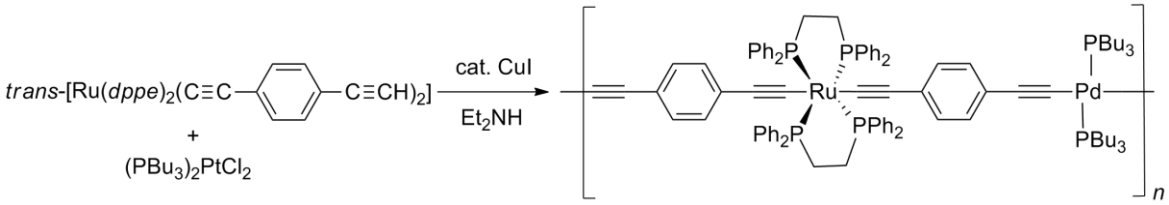

Figure 3. Heterobimetallic polymeric complex prepared *via* dehydrohalogenation method.

Heavy transition-metals such as Ir(III), Re(I) and Pt(II) have been either incorporated directly into the main chain of the polymer or covalently tethered as pendent units using such cross-coupling methods[12] (Figure 4). Owing to the triplet emitting nature of these phosphorescent polymers, they have been effectively used for sensing triplet-state analytes.[13] In contrast to the above described transition metals, a survey of literature on rigid-rod polyynes based on gold metal was found to be surprisingly sparse. Some of the earlier known methods involved either reacting $AuCl(SMe_2)$ with suitable diethynyl arenes or reactions between gold acetylide precursors and appropriate diphosphines (Figure 5, **a**).[14] In 1993, Puddephatt showed that the reaction of iso(cyanoaryl)acetylide with *t*BuC≡C–C–Au–C≡N–Ar–C≡CH with the expulsion of *tert*-butylacetylene can lead to the generation of gold polyynes (Figure 5, **b**).[15a]

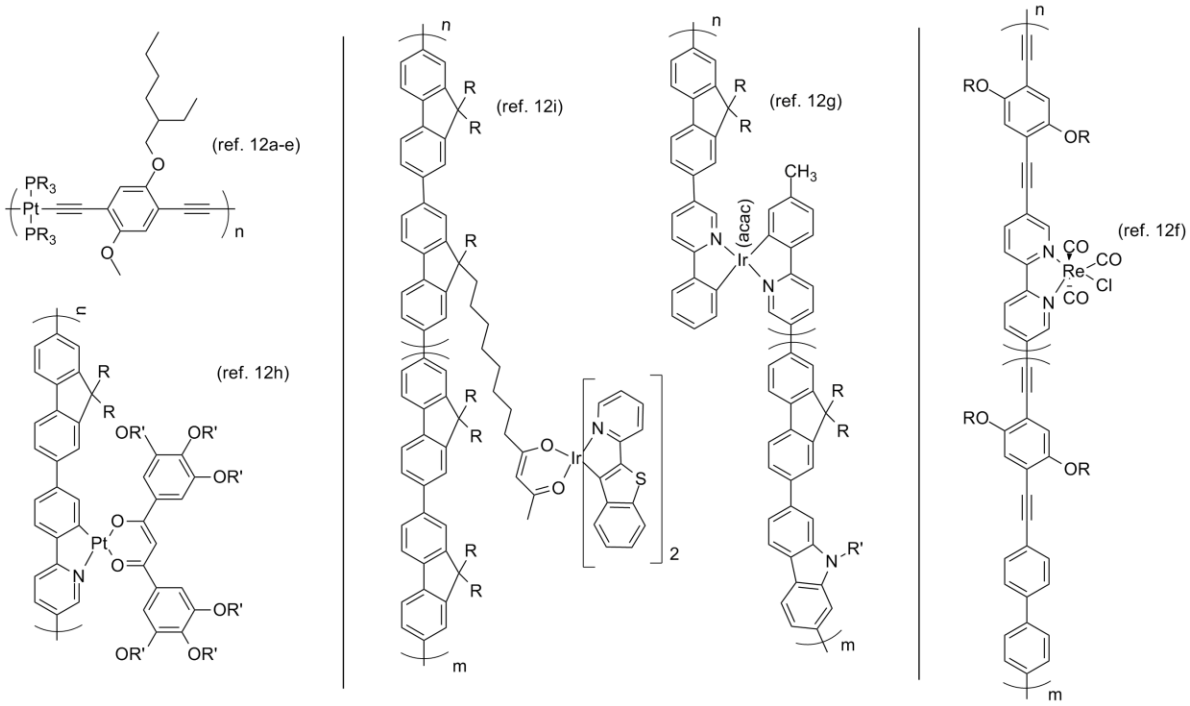

Figure 4. Examples of metallopolymers incorporated either in the main chain or tethered as side chain units.

However, the above methods yielded poorly soluble polymers limiting further investigations. In later decades, building on these methods, gold based macrocycles and dendrimers were synthesized. An account on gold polyynes until the year 1997 has been described by Puddephatt,[16] and more recently a concise review of metal alkynyl σ-complexes has been described by Long.[17]

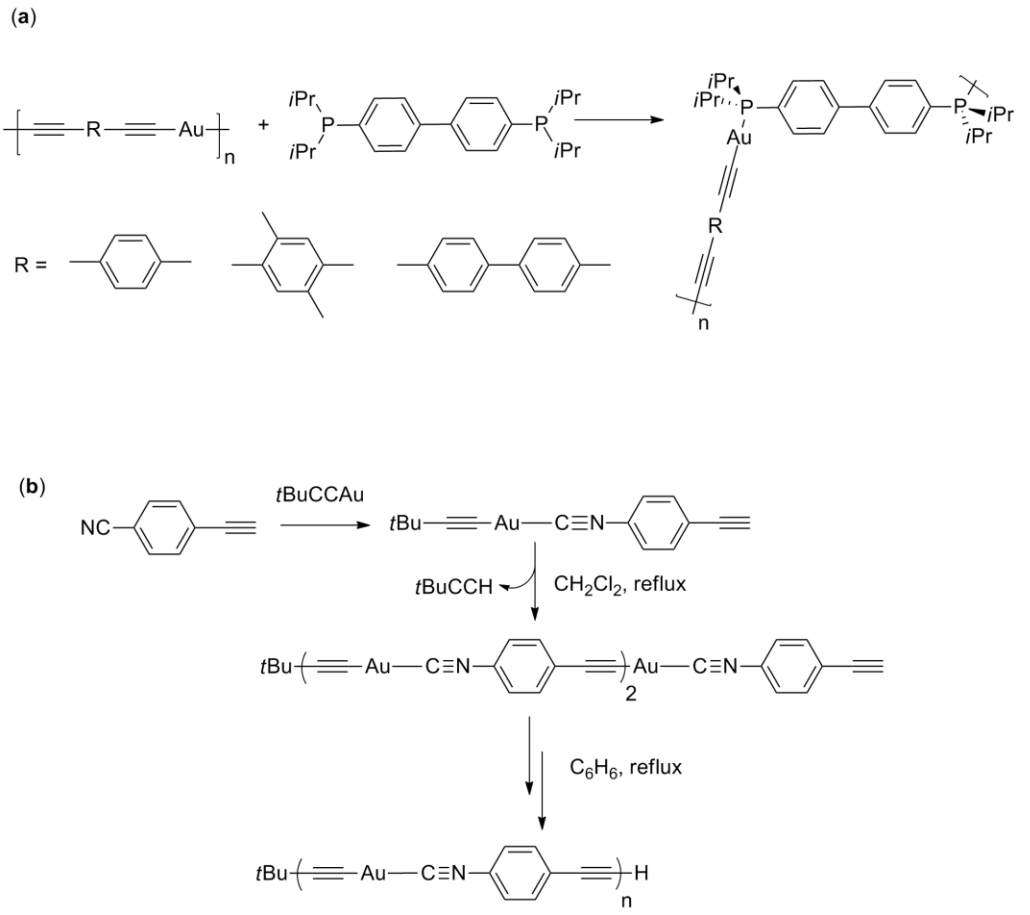

Figure 5. (**a**) Gold(I) metal polyyne obtained from aryl phosphines. (**b**) Gold polymer obtained with (isocyano)arylacetylide as bridging ligand.

2.1. Design considerations for the construction of rigid-rod polyynes

Two important design considerations need to be taken into account for a putative design of a monomer aimed for generating high molecular weight phosphorescent polymer.

(1) Avoidance of stacking (e.g. π-π) effect in the polymer unit, which is detrimental both from a solubility and photophysical perspective since it renders the polymer insoluble and also quenches the excited state.

(2) Delocalization of the triplet-excited state along the polymer backbone; this is an important criterion, which in turn depends on other factors such as the position of the metal unit in the polymeric chain (main chain or pendant) and lowest emitting state of the monomer complex itself.

So far, efforts to tackle the issue of poor solubility in transition metal polyynes have been mainly limited to altering the co-monomeric proportion of the alkynes. For example, improved solubility in the case of a Pt(II) rigid-rod acetylide was achieved using the co-monomeric mixtures of 1,3,5-triethynylbenzene and 2,5-diethynyl-*p*-xylene in various molar ratios (1:50 and 1:100) with *trans*-dichloro(bis-tri-n-butylphosphine) (Figure 6).[18]

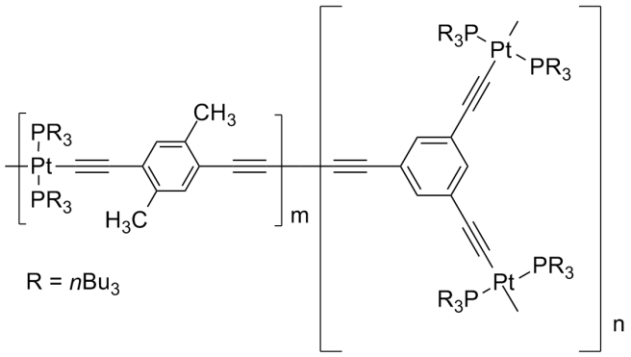

Figure 6. Example of a metallopolymer with improved solubility.

Typically molecular weights in the range M_{wt} = 27,000 to 58,000 were obtained. This method was considered not to be suitable for the present study because such type of cross-linked polymers would complicate the photophysical understanding of the polymer. An alternative strategy to improve the solubility would be to either replace the phosphine groups with sterically demanding NHCs or to use a bulky co-monomer with solubilizing chains. In literature there are very less reports of non-phosphinated ligand monomers serving as ancillary ligands for the construction of main chain organometallic polymers with d^8 or d^{10} metals.[19]

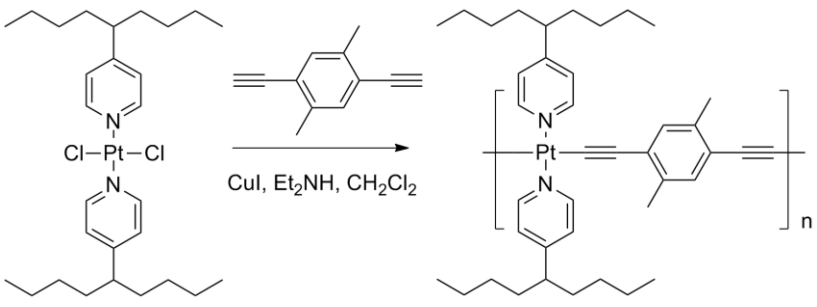

Figure 7. Example of a Pt(II) metallopolymer with alkylated pyridyl group as ancillary ligand.

In this respect, Raithby and co-workers have partly succeeded in improving the solubility by using pyridyl units containing long *n*-alkyl chain (Figure 7).[19a] Swager and co-workers have a long-term interest in iptycenes, which belong family of rigid and bridged aromatic molecules. Iptycenes incorporated into poly(phenylene ethylenes)s (PPEs) were demonstrated to be efficient fluorescent chemosensor for the detection of nitroaromatics like TNT. Yet another intriguing feature of the iptycenes is the internal free volume (IFV) defined by iptycene's aromatic side arms.

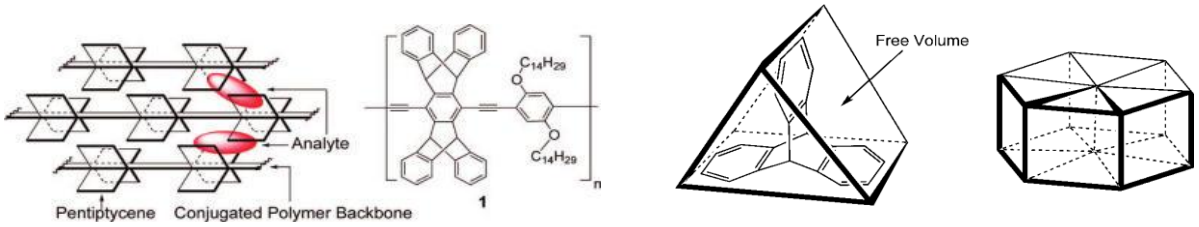

Figure 8. Iptycene based fluorescent chemosensor developed in Swager's laboratory. Figure adapted from ref. 20.

Due to these structural features, polymers containing iptycenes units were found to be resistant not only against self-quenching, but also created desired porosity for diffusion and interaction of the analyte with the polymer backbone in the solid-state (Figure 8).[20] It was thought that triptycene (a molecule belonging to iptycene family) based *N*-heterocyclic carbene coordinated to gold metal would couple the aforementioned advantages while retaining the nature of triplet excited states unique to Au(I) polyynes. Although, there are no detailed investigations until now on the photophysical behavior of either Au(I) or Au(III) polyynes, we believe that such an effort would be a good starting point. Fortunately, there exists a wealth of information about the extent of delocalization or evolution of triplet excited state in Pt(II) acetylide rigid-rod polymers (Figure 9). Extensive investigations on the topic has been performed by the groups of Köhler, [12e, 12c, 21] Rogers[22] and Schanze[23]

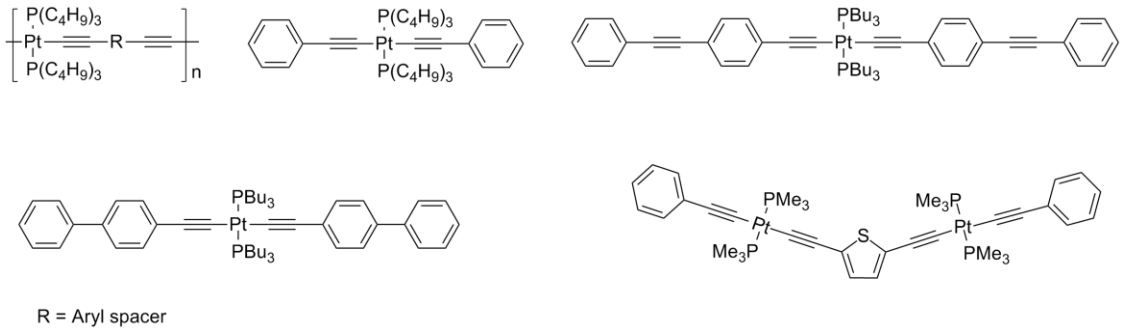

Figure 9. Examples of Pt(II) polymers/oligomers for which photophysical investigations have been carried out.[22,23]

Schanze has shown that the non-radiative decay of the triplet states in a series of platinum containing conjugated polymers obeys the energy-gap law similar to their monomer units. Also, more significantly, the triplet state was realized to be localized/restricted within one or two repeat units of the polymer chain unlike the singlet state, which appeared to be delocalized over the entire polymer backbone. Considering the above points we embarked on the synthesis of triptyceneimidazolium heterocyclic carbenes suitable for deriving organometallic precursor monomeric units. Another foreseeable advantage of using a sterically demanding ligand could be that such systems can thermodynamically favour *trans* geometry in a square planar environment which is desirable for construction of linear chain polymers.

3.0 Results and Discussion

As discussed, the use of NHC as diametrically opposite *trans* disposed ligands in a d^8 metal ions like Pd(II), Pt(II) and Au(III) was considered to be attractive. Before attempting to synthesize NHCs incorporating bulky iptycenes, it was felt necessary to establish a synthetic protocol for *trans* dialkynyl complexes with simpler units such as the imidazole or benzimidazole. In 2007, Huynh et al. reported the synthesis of *trans*-[PdX_2(*i*Pr_2-*bimz*)$_2$][*bimz* = benzimidazolin-2-ylidenes, X = Br or I] by a reaction of *N*,*N*′-diisopropylbenzimidazolium salt with $Pd(OAc)_2$ in DMSO at elevated temperatures.[24] Adopting this procedure, the *trans*-Pd(II) dibromo complexes **2a** and **2b** were prepared (Scheme 1). In order to prepare *trans*-Pd(II) bisacetylides starting from the above

dibromides, various transmetallation procedures were initially attempted. Employing tin reagents such as trimethyl(2-phenylethynyl)stannane or *in situ* generated Cu acetylides under basic pH conditions failed to give the desired product. Isomerization followed by reductive elimination is presumed to be the reason for the failure. However, lithiation of the aryl terminal acetylide at -78 °C using *n*-BuLi followed by reacting with the dibromo palladium complex **2a** in dry THF yielded the desired complex **3a** as an air and moisture stable solid.

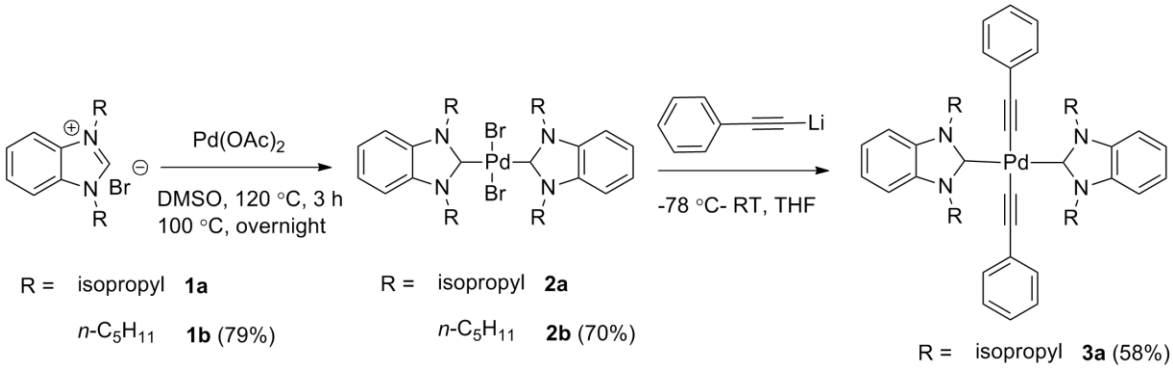

Scheme 1.

The ^{1}H NMR spectra of **3a** exhibited three sets of new resonances corresponding to the aromatic protons of the phenylacetylide between δ = 7.61 and 7.05 ppm and the ^{13}C NMR spectrum showed distinct resonances for the metal bound acetylide ligand at 112.1 (C_{α}) and at 72.5 (C_{β}) ppm. In the IR spectra a typical ν(C≡C) absorption band was observed at 2115 cm^{-1}. ESI-MS analysis evidenced the molecular fragment corresponding to the loss of one acetylenic unit (*m*/*z* = 611.2). Single crystals suitable for X-ray diffraction were obtained by slow evaporation of pentane in a concentrated solution of **3a** in CH_2Cl_2 at 5°C. As expected, the solid state molecular structure of **3a** (Figure 10) revealed the palladium ion to be positioned in a distorted square planar geometry. $C_{acetylene}$-Pd-$C_{carbene}$ bond angle was found to be 87.04(8)°, the deviation from an idealized 90° is conceivably due to steric reasons. The bond distances of Pd-C_{sp} [2.031(3) Å] and that between the acetylenic carbons [(C≡C), 1.168(3) Å] were in the range described for Pd(II) bis-phosphine bis-acetylide complexes.[25] Further, analysis of the molecular packing showed no Pd···Pd interactions, the shortest intermolecular Pd···Pd distance was measured to be

7.8076(2) Å. Concentration dependent absorption studies (range: c ~10^{-6} to 10^{-4} $M^{-1}dm^{-3}$) of **3a** in CH_2Cl_2 neither showed any change in the position of the peak maxima nor generated additional low-energy MMLCT band also excluding the possibility of Pd···Pd interactions in solution.

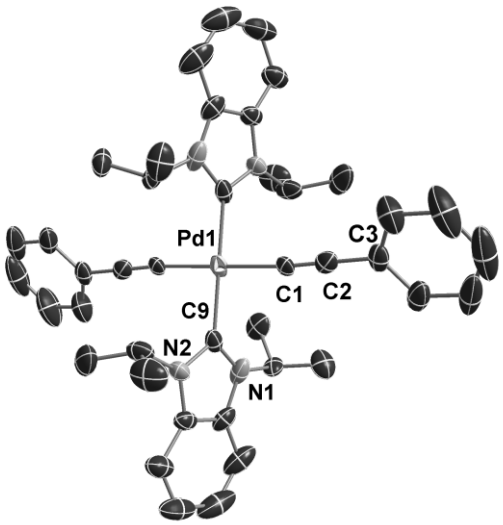

Figure 10. X-ray crystal structure of **3a** with selective atomic numbering scheme. Thermal ellipsoids are drawn at 50% probability level. Hydrogen atoms are omitted for clarity.

Table 1. Selected bond distances (Å) and angles (°) data for **3a.**

Complex **3a**			
Pd(1)-C(1)	2.031(3)	C(1)-C(2)	1.168(3)
Pd(1)-C(9)	2.021(3)	C(2)-C(3)	1.460(4)
C(9)-N(1)	1.346(3)	C(9)-N(2)	1.363(3)
C(2)-C(1)-Pd(1)	174.8(2)	C(9)-Pd(1)-C(1)	92.96(10)
C(1)-C(2)-C(3)	176.1(3)	C(9)-Pd(1)-C(9i)	180.00(6)
C(9)-Pd(1)-C(1i)	87.04(10)	N(1)-C(9)-Pd(1)	126.3(2)

As an extension of this work, various other terminal acetylides (not shown here) were successfully incorporated into **2a** by Michael Koch in the group and their electronic absorption and electrochemical behavior were also studied in detail.[26] It is pertinent to mention here that, the Pd complex with *trans* trimethylsilylacetylide ligand (TMSA) is expected to behave as a suitable monomer for preparing conjugated polymer by oxidative polymerization procedure after desilylation. The electronic absorption spectra of **3a** was similar to the halide precursor **2a** but with a slight bathochromic shift (λ_{max}= 279 nm, ε = 45600 M^{-1} cm^{-1}) due to metal coordination. Most of the known organometallic oligomers/polymers with Pd are known to be phosphorescent only at cryogenic temperatures.[27] Unsurprisingly **3a** did not display photoluminescence in a degassed fluid medium (CH_2Cl_2) at RT. In rigid glass matrices of 2-*methyl*-THF at 77 K, however emission was observed with well resolvable vibronic bands (λ_{max} = 423 nm). In continuation with the exploratory studies, we next turned our attention towards replacing the halides for alkynes in an isoelectronic Pt(II) complex bearing biscarbene ligands. In this regard, a literature survey revealed that, the desirable *trans* isomer in the preparatory procedure of a suitable precursor namely $PtBr_2$(*i*Pr_2-*bimy*)$_2$][*bimy* = benzimidazolin-2-ylidenes] could be isolated only in a meager yield of 3%.[24] The major product was the *cis* dibromo isomer with a solvent (DMSO) coordination to the metal. With this information in hand, alternative strategies to exclusively synthesize *trans* Pt(II) dihalides were attempted; treatment of the silver carbene complex [(*i*Pr_2-*bimy*)$_2$ AgBr] with either K_2PtCl_4 or allyl-chloride Pt(II) dimer complexes yielded monocationic tris-NHC platinum complexes instead as concluded from ESI-MS and ^{1}H NMR analyses. Finally, the reaction of Pt(COD)$_2$(acetylide)$_2$ (COD = 1,5-cyclooctadiene) with benzimidazolium salts in the presence of a base gave *trans*-Pt(II) bis-carbene-bisacetylides directly as demonstrated by one of the colleague in the group.[28] Aiming for the alkynyl substitution in a carbon bridged *cis*-biscarbene Pt(II) system, such as one described by Strassner and co-workers,[29] [Pt(*meim*)$_2$I$_2$][*meim* = 1,1'-dimethyl-3,3'-methylene-diimidazoline-2,2'-diylidene] was reacted with lithiated terminal arylacetylides (Scheme 2). Gratifyingly, **4** and **5** were obtained as air and moisture stable solids insoluble in non-polar solvents like cyclohexane and diethylether but sparingly soluble in THF.

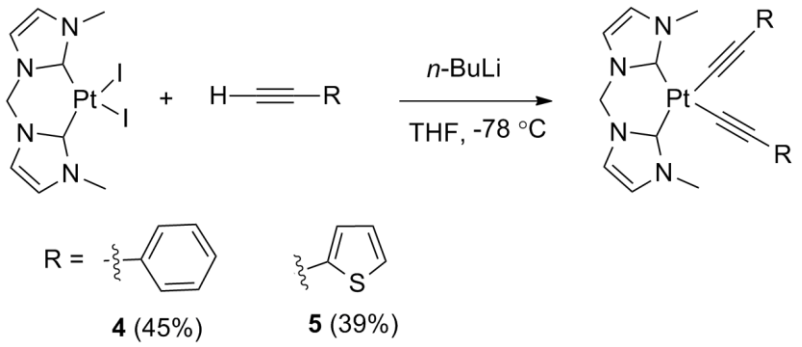

Scheme 2.

In a view to increase the lipophilicity of such Pt dialkynyl units, complexes with long *N*-alkylated chain on the NHCs were later developed in our group.[28]

Similar to what was observed for the dihalide precursor complex,[29b] the X-ray molecular structure of **4** (Figure 2) showed platinum occupying a slightly distorted quadratic square planar environment coordinated by bowl shaped NHC and acetylide anionic ligands. Selected metric parameters are collected in Table 2. Compared to the dihalide precursor the Pt-$C_{carbene}$ distances C(18)-Pt(1) = 2.029(3) Å and C(21)-Pt(1) = 2.021(3) Å measured marginally larger due to the greater *trans* influence of the acetylide ligands. The mean average distances of Pt-C_{sp} bonds (d_{avg} ~2.037 Å) and that of carbon-carbon (C≡C) acetylenic bonds (d_{avg} ~1.171 Å) were in the similar range as for the reported Pt(II) diimine bisacetylide complexes.[25] The crystal packing showed large intermolecular Pt···Pt separation to the extent of approximately 9.767 Å excluding the possibility of closed shell interactions. The valance angle subtended by the biscarbene chelate to the metal $C_{carbene}$-Pt-$C_{carbene}$ was seen to be restricted to 85.35(13)° owing to the steric requirements.

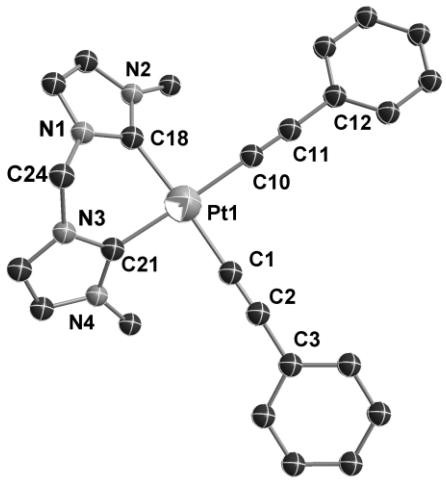

Figure 11. X-ray crystal structure of **4** with selective atomic numbering scheme. Thermal ellipsoids are drawn at 50% probability level. Hydrogen atoms and solvent molecules are omitted for clarity.

Table 2. Selected bond distances (Å) and angles (°) data of **4**.

Complex **4**			
Pt(1)-C(18)	2.029(3)	Pt(1)-C(1)	2.028(3)
Pt(1)-C(21)	2.021(3)	Pt(1)-C(10)	2.047(3)
C(1)-C(2)	1.178(5)	C(10)-C(11)	1.165(4)
C(1)-Pt(1)-C(21)	90.97(12)	C(10)-Pt(1)-C(18)	92.60(11)
C(1)-Pt(1)-C(10)	91.02(12)	C(18)-Pt(1)-C(21)	85.35(13)

Unlike the palladium diacetylide (**3a**) which were only luminescent only at 77 K, **4** and **5** exhibited photoluminescence even at RT albeit with low quantum yields. The UV-vis and PL spectra are shown in Figure 12 and various photophysical properties are enumerated in Table 3.

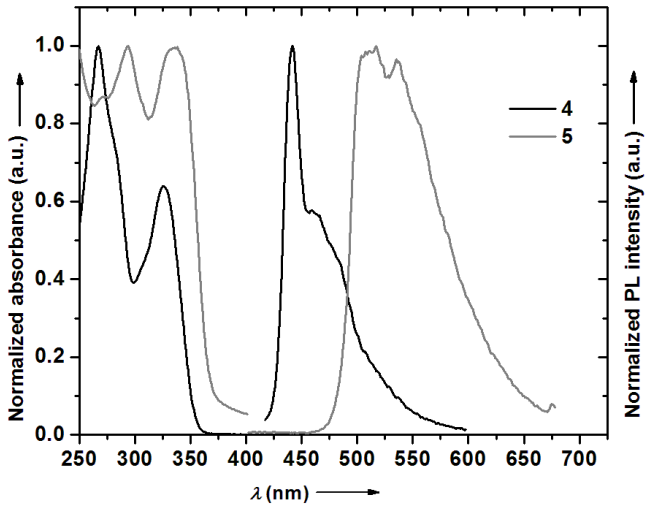

Figure 12. Normalized UV-vis spectrum and PL spectra of **4** and **5** recorded in CH_2Cl_2 at RT.

Table 3. Photophysical data of **4** and **5.**

Compd.	Room temperature solution (CH_2Cl_2)						77 K glass[b] (2-MeTHF)
	Abs. λ_{max}[nm]	PL λ_{max} [nm]	τ [ns]	Φ_{em}[a] x 10^{-2}	K_r [s^{-1}] x 10^4	K_{nr} [s^{-1}] x 10^6	
4	267, 325	441, 461 sh	26.56	5.5	207.0	35.58	437, 457 sh
5	293, 336	511, 535 sh	900.08	3.8	4.2	10.96	494, 508 sh

[a]Photoluminescence quantum yield was determined with quinine sulfate in 1 N H_2SO_4 as standard at 298 K. [b]Vibronic structured emission bands. $K_r = \Phi_P/\tau$ and $K_{nr} = (1- \Phi_P)/\tau$ were calculated assuming unit efficiency of inter system crossing.

The five to ten fold quenching of the luminescence intensity upon exposure to molecular oxygen and the large stokes shift suggested the triplet character of the lowest emitting state in these complexes. In line with our design principle and the positive outcome of the lithiation method to obtain stable *cis*-Pt(II) and *trans*-Pd(II) NHC complexes, we proceeded to synthesize triptycene fused imidazolium carbenes. The synthesis of 2,3-diaminotriptycene, the key precursor for triptycene imidazole was achieved by sequential nitration and reduction of triptycene according to a published procedure (Figure 13).[30]

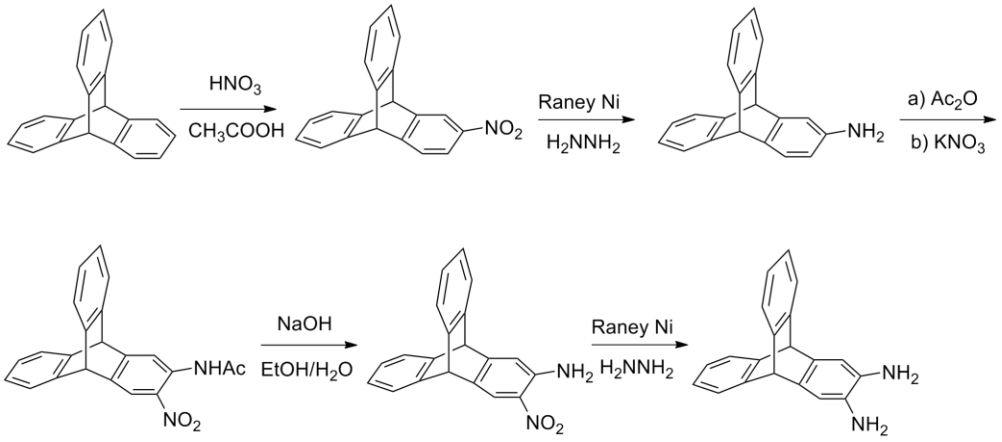

Figure 13. Synthetic steps for preparing 2,3-diaminotriptycene[30]

Although, the sequence proceeds well for milligram quantities, scale-up operations presented problems in the second step which involves the reduction of nitro group using hydrazine and with Raney-Ni as the catalyst. Employment of $SnCl_2$ in abs. EtOH at 70 °C circumvents the problem and the product could be isolated in good yields (70-75%).

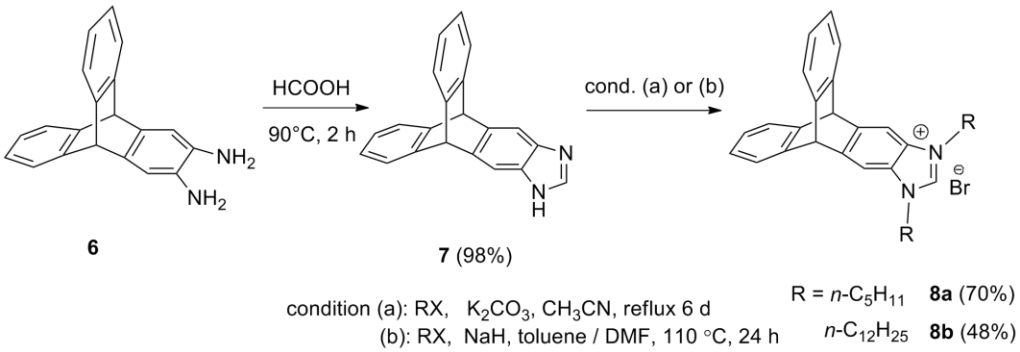

Scheme 3.

2,3-Diaminotriptycene (**6**) was condensed with formic acid to give the triptyceneimidazole (**7**) in 90% yield. *N,N'*-dialkylation reactions however presented problems in some cases; when a mild base like K_2CO_3 was employed, a mixture of mono- and di-alkylated products along with other impurities presumably the wanzlick dimerized products of the NHC[31] were obtained even after refluxing for 5 days. By prolonging the reaction time for 3 more days the desired dialkylated product could be isolated in the case of **8a** but not in the case of **8b**. Microwave reaction in DIPA at 160 °C for 0.5-1.0 h with

excess of the alkyl halide posed similar problems. Use of a stronger base like NaH in a mixture of dry toluene and DMF resolved the problem and afforded **8b** in moderate yields after repeated recrystallization from THF at 0-5°C. The chemical identites of **8a** and **8b** were confirmed by NMR, IR and elemental analyses and they served as useful starting materials for preparing different bulky monomers.

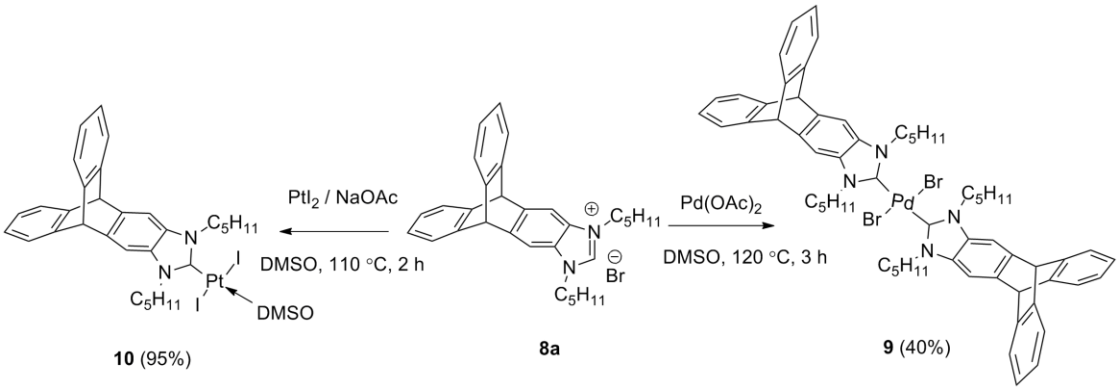

Scheme 4.

Treatment of **8a** with $Pd(OAc)_2$ in DMSO for 2 h (Scheme 4) gave **9** as yellow solid after precipitation by addition of water. ESI-MS analysis showed the molecular ion peak corresponding to loss of one bromine atom *m/z* = 1055 $[M\text{-}Br]^+$. When an aliquot of **9** in CH_3CN was treated with $AgNO_3$, the ESI-MS spectrum revealed several peaks with the characteristic isotopic distribution of the complex. Among them, peaks corresponding to the masses of **9** with either two CH_3CN instead of bromines (*m*/*z* = 1056.5) or one CH_3CN (*m*/*z* = 1094.4) were clearly observed. ^1H NNMR (NOE) studies suggested the *trans* disposition of the carbene ligands. Finally, single-crystal XRD reaffirmed the structure assignment in solution; the Pd ion was located on the crystallographic centre of inversion posing a slightly distorted square planar environment (Figure 13 and Table 4).

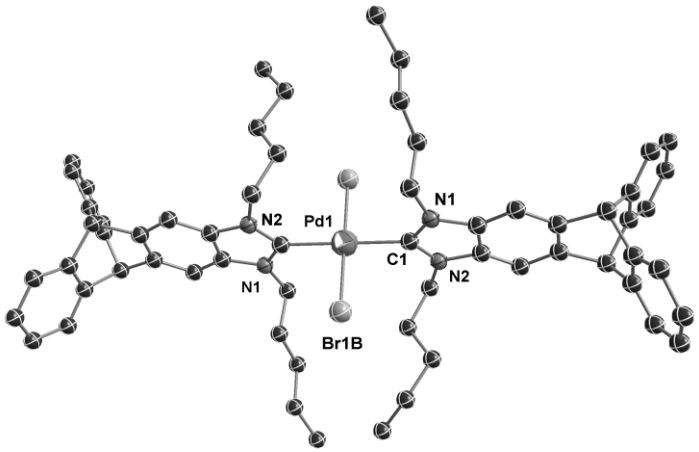

Figure 14. X-ray crystal structure of **9** with selective atomic numbering scheme. Thermal ellipsoids are drawn at 50% probability level. Hydrogen atoms and solvent molecules are omitted for clarity.

The angle defined by the Pd atom and the bromides was observed to be almost perfectly linear [Br(1B)-Pd-Br(1B) 180.0°] suggesting less steric congestion. This is advantageous from the point of further functionalization of the halides. Both the carbenic heterocyclic planes of the triptycene are oriented at an approximate torsional angle of 80.0° with respect to the plane defined by PdC_2Br_2. This value is however lower than the *trans* benzimidazole biscarbene Pd complex known in literature.[32a] The Pd-$C_{carbene}$ distances [2.037(7) Å] are much longer than those [1.947(3) Å] observed for dimeric [$PdBr_2$(${}^{i}Pr_2$-*bimy*)]$_2$ complex,[32a] which can be attributed to the less Lewis acidic nature of palladium and also the *trans* arrangement of the carbene ligands. The reaction of **8a** with PtI_2 in the presence of NaOAc in DMSO at 110 ºC gave **10** in 95% yield. Although the geometry of **10** is not unambiguously proven by single-crystal XRD, other characterizations *viz.* ^{1}H, ^{13}C NMR and elemental analysis support the proposed structure depicted in Scheme 4. IR spectrum showed the stretching band due to sulfoxide ν(S=O) appearing at 1129 cm^{-1} which is significantly shifted to higher wave numbers than observed for the free DMSO (1058 cm^{-1}).[32b] The methyl signals due to coordinated DMSO resonated at δ = 2.55 ppm in the ^{1}H NMR and irradiating them did not show any NOE effect suggesting a probable

trans arrangement to the monocarbene. The coordination mode of the sulfoxide ligand (S or O coordinated) is not certain at this point. Interestingly, **10** showed solvatochromic behaviour. A solution of **10** (orange solid) in CH_2Cl_2 was orange while in $CHCl_3$ the solution appeared to be red suggesting a probable equilibration with the corresponding bridged diiodo dimer complex. Following the success in incorporating bisacetylides as in Scheme 1, **9** was reacted with 2.3 equiv. of a lithiated alkyne (Scheme 5). The major product which was obtained was confirmed to be the mono-substituted product (**11**) by ESI-MS (*m/z*: 1705.0 $[M]^+$) and ^1H NMR studies. Increasing the equivalents of the alkynes also resulted in the same product and complete characterization of **11** was not carried out. It is presumed that the steric hindrance was main the reason for monosubstitution.

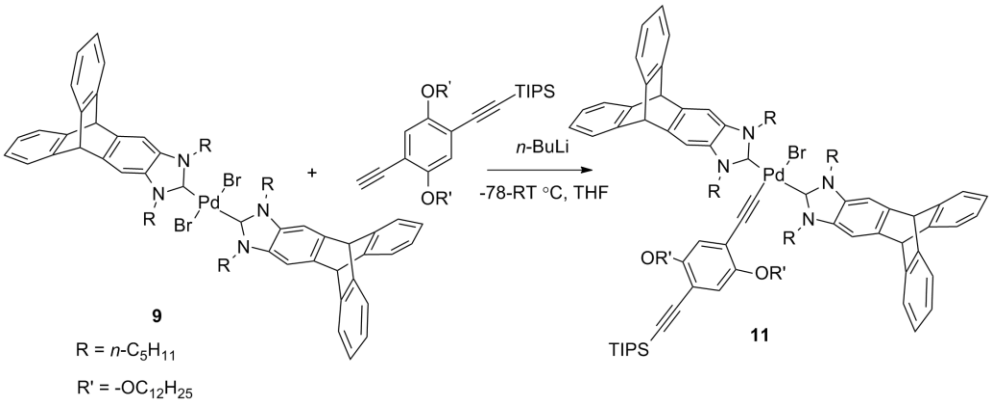

Scheme 5.

Until so far we realize that the procedure using $Pt(COD)_2(acetylide)_2$ and NHCs discussed earlier[28] to be the only other viable alternative for achieving *trans* biscarbene bisacetylide Pt(II) complexes.

3.1 Monomers suitable for construction of side chain polymers containing NHC Au(I) alkynyl complexes.

In Chapter 3, the PL properties of the less explored class of Au(I) σ-acetylides stabilized by *N*-heterocyclic carbenes were studied. Absolute phosphorescence quantum yields to the extent of 27% in the solid-state (dispersed as thin neat films on PMMA host matrix) was achieved by using benzimidazole carbene Au(I) compex with boron acetylide as an

ancillary ligand.[33a] It was also observed that the closed shell aurophilic interactions appeared to be less dominant and the triplet emission mainly originated from heavy atom perturbed ^{3}IL(π-π*) states. With this background, it was hypothesized that bulkier versions of such NHC Au(I) units incorporated as pendant units along a conjugated polymer backbone would exhibit the following: (1) phosphorescent nature of emission in the polymer, and (2) lower non-radiative decay rates, expected due to avoidance of metal to metal charge transfer (MMLCT) phenomenon. To this end, we aimed to prepare suitable triptycene based monomers containing gold metal. Owing to the tedious synthesis of triptycene fused NHCs, the intended precursors for Au(I) monomers were first prepared with benzimidazole and their photophysical properties were evaluated (Scheme 6). For *N*-dialkylation using dodecyl halides (C_{12} chains), the procedure using NaH was preferred over K_2CO_3 owing to shorter reaction time and formation of cleaner products. For the benzimidazole or triptyceneimidazole carbene Au(I) complexes (**12b**, **16a** and **16b**), the carbenic carbon attached to gold center resonated in a narrow range of δ = 177.4 to 178.2 ppm in ^{13}C NMR. In the case of **15**, the signal due to carbenic carbon appeared further downfield at 183.4 ppm due to its electron deficient nature. Single-crystals suitable for XRD analysis was obtained for **12b** (Figure 15). It was observed that the angle subtended at the gold center by the carbene and the halide ligands was close to linearity [C(1)-Au(1)-Cl(1) 176.61(18) Å]. The carbene to gold distance [C(1)-Au(1) 1.941(6) Å] and the gold to the chloride distances [Au(1)-Cl(1) 2.3089(12) Å] fall in the normal range as observed for similar complexes in literature.[34]

The yields of the triptyceneimidazolium salts **8a** (70%), **8b** (48%) (Scheme 3) were lower compared to those of benzimidazolium salts **1b** (79%) and **1c** (65%) (Scheme 6). 4,7-dibromobenzimidazole (**13**) was prepared from 3,6-dibromobenzene-1,2-diamine by condensation with formic acid. The bromine atoms in the 1,4-position of the phenyl ring in **13** was perceived to serve as a convenient handle for dehalogenative polycondensation[35] and other cross-coupling polymeric procedures.

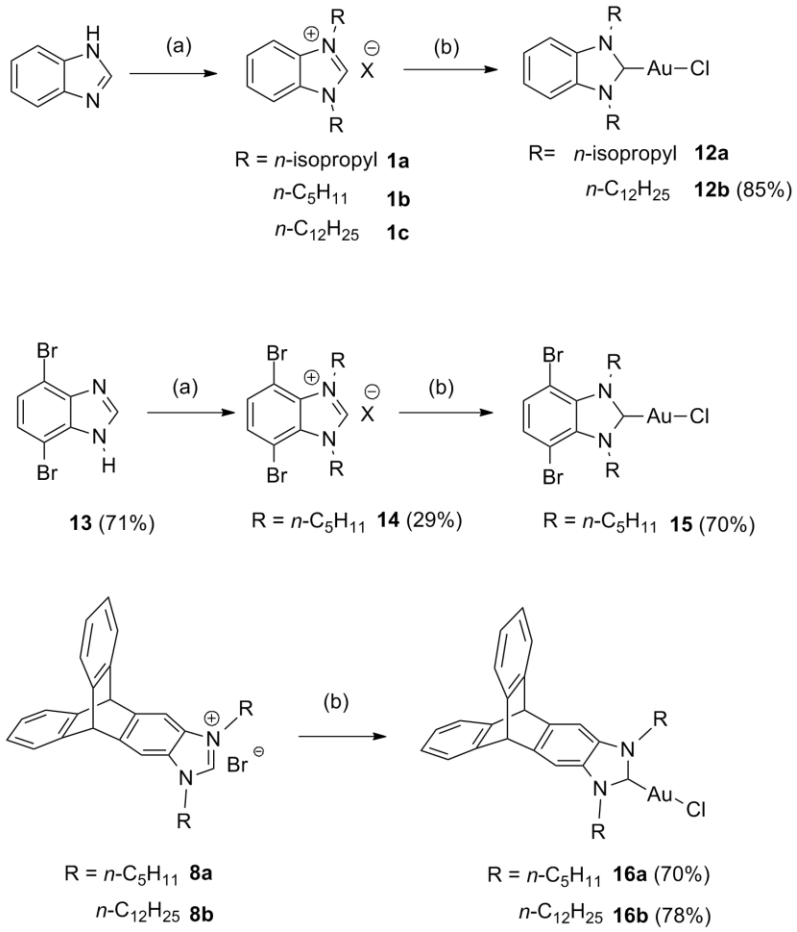

Conditions, (a): RX, K_2CO_3, CH_3CN, reflux, 6 d (or) RX, NaH, toluene / DMF, 110 °C, 24 h

(b): i) Ag_2O, CH_2Cl_2, 6 h, ii) $(SMe_2)AuCl$, CH_2Cl_2, 6 h, RT

Scheme 6.

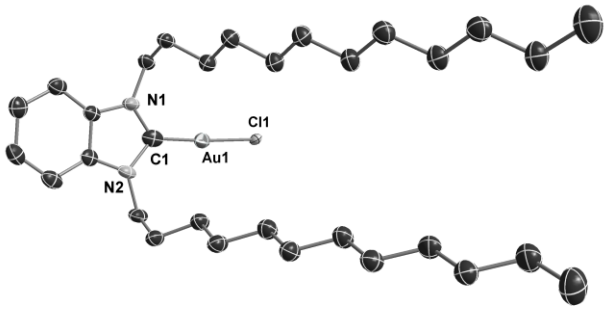

Figure 15. X-ray crystal structure of **12b** with selective atomic numbering scheme. Thermal ellipsoids are drawn at 50% probability level. Hydrogen atoms are omitted for clarity.

Complex **14** was obtained in a low yield of 29% upon alkylation using K_2CO_3 procedure. Reaction of the benzimidazolium salts (**1a**-**1c**, **14**) with Ag_2O followed by transmetallation with (SMe_2)AuCl yielded respective gold chlorides (**12a**-**12c**, **15**). The triptyceneimidazolium salts **8a** and **8b** reacted in a similar manner affording **16a** and **16b** in 70-78% yield. All attempts to grow single crystals suitable for XRD of the triptycene imidazolium gold chlorides were futile. In one of the trial reactions aimed for preparing **16b** directly from the unpurified crude starting material, where the monoalkylated triptycene imidazole was present as impurity (7-8%), we obtained crystals of monocationic gold complex **IMP1**, which was solved by XRD (Figure 16). The nitrogen of the monoalkylated triptycene imidazole was found to be coordinated to the gold center with $AuCl_2$ as the counter anion. Although this compound is unimportant for the intended goal, it does offer structural evidence for the elusive triptycene Au(I) complexes and therefore included here. As could be seen from the perspective view shown in Figure 16, the linear two-coordinate geometry is preserved from the gold chloride precursor. The gold to carbenic carbon distance [Au(1)-C(1) 1.984(9) Å] was noticed to be slightly shorter than the *trans* gold to imine nitrogen [Au(1)-N(3) 2.040(7) Å]. The valence angle defining these metal coordination sphere $C_{carbene}$-Au-N_{imine} deviated from linearity [C(1)-Au(1)-N(3) 177.3(3)°] presumably due to crystal packing forces.

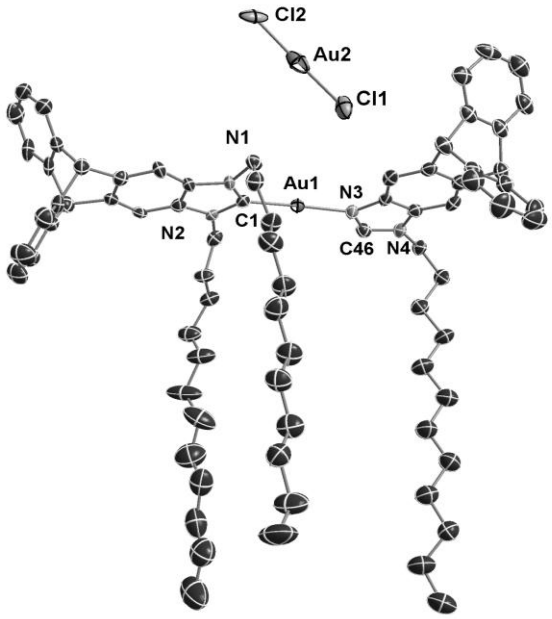

Figure 16. X-ray crystal structure of **IMP1** with selective atomic numbering scheme. Thermal ellipsoids are drawn at 50% probability level. Hydrogen atoms and solvent molecules are omitted for clarity.

Having the gold chlorides in hand, terminal acetylides **A1** and **A3** were prepared following simple Sonagashira cross-coupling and deprotection sequences as depicted in Scheme 7. **A1** is already known in literature.[35] Similarly, 2-(4-ethynylphenoxy)ethanol (**A5**) designed for lactide ring opening polymerization[36] was prepared quite easily starting from 2-(4-bromophenoxy)ethanol.

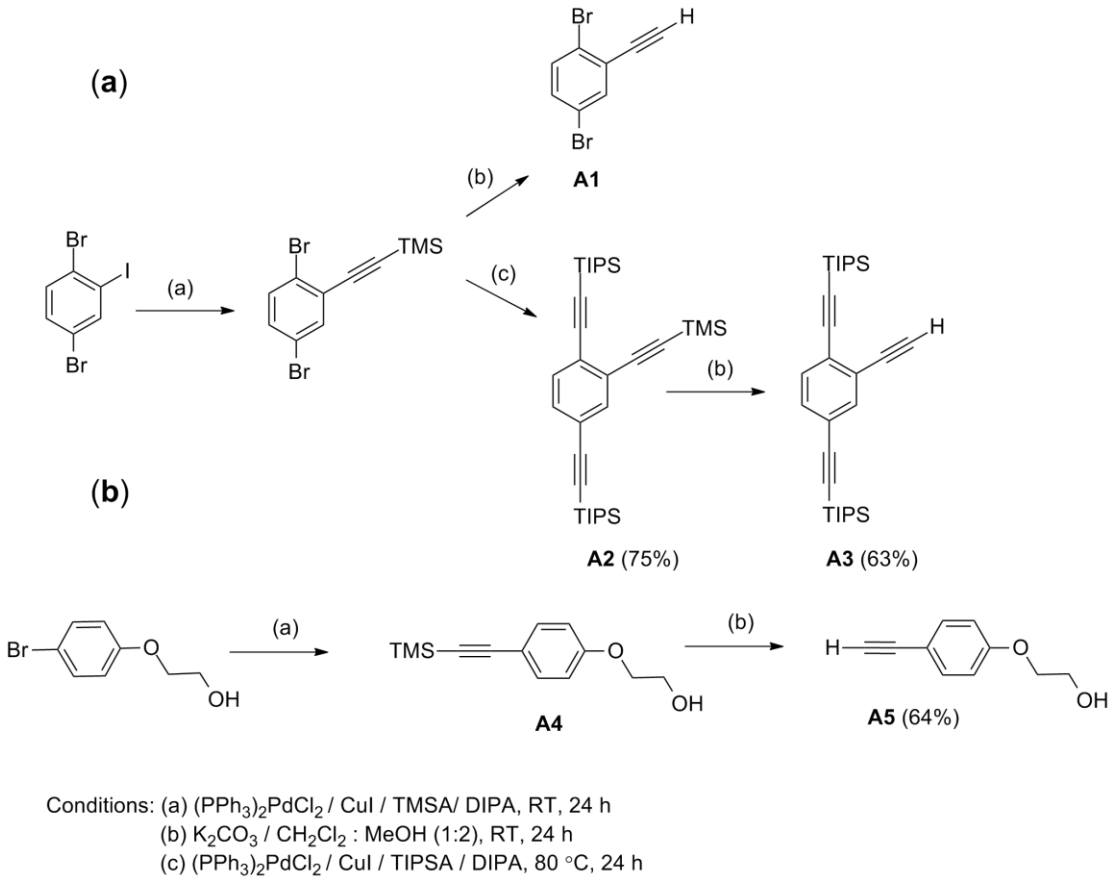

Scheme 7.

The substitution of the chloride with various acetylides (**A1**, **A3** and **A5**) was achieved by *in situ* deprotonation using 5.0 equiv. NaOH in a solvent mixture of MeOH and methyl-*tert*-butylether (Schemes 8 and 9). Use of the ether in up to 10% volume ratio with MeOH serves to enhance the solubility of the Au(I) chlorides containing long alkyl chains. The incorporation of acetylide was evidenced in ^{13}C NMR by the downfield shift of acetylenic carbon (Au-C_{sp} attached to gold in the region 134-139 ppm.

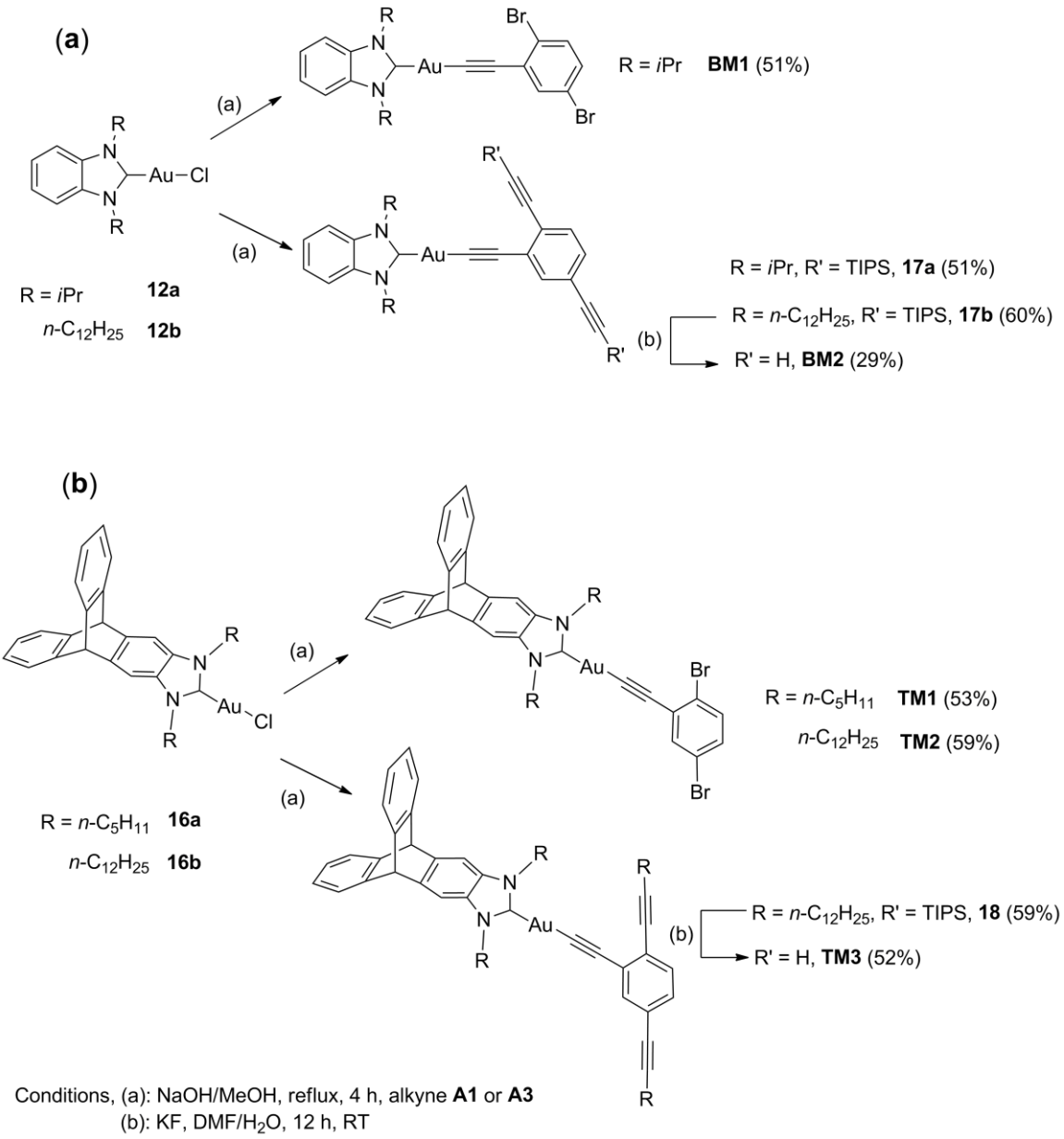

Scheme 8.

The ν(C≡C) asymmetric stretching bands in the IR, sometimes with weak intensities were observed in the range 2110-2176 cm^{-1}.The desilylation step of TIPS (Scheme 8) using the typical reagent TBAF in 1.0% H_2O posed huge problems; although the reaction seems to proceed in short time, all attempts to isolate the pure forms of the deprotected monomers were unsuccessful. Purification by column chromatography (SiO_2 or neutral Al_2O_3) led to

decomposition of the product. After screening several reagents, the reaction using KF in DMF at RT with small quantities of water proved to be successful. In the cases of **BM2**, and **TM3**, the products can be isolated by a simple addition of water and extraction of the product into diethyl ether. Although it was not possible to obtain X-ray structural characterization of the pivotal monomers (**TM2** and **TM3**), the structures were unambiguously established with the help of data from ESI, MALDI-MS, IR and elemental microanalysis (only for **TM2**) and from the internal consistencies of 1D and 2D NMR spectra. Resonances for the free acetylenic protons in ^{1}H NMR of **TM3** appeared at δ = 3.4 and 3.2 ppm. (NMR details with assignment provided in appendix). The carbenic and the acetylenic carbons appeared at δ = 193.7 and 138.5 ppm respectively. MALDI-MS analysis of **TM3** evidenced the masses corresponding to the $[M]^+$ m/z = 977.4 and also due to the loss of the acetylide fragment $[M\text{-}C_{12}H_6]^+$ m/z = 827.9. As mentioned earlier, the easily synthesized acetylide containing phenoxy ethanol **A5** could also be ligated with Au(I) chloride to yield **LM**. (Scheme 9, part **a**). This monomer can be potentially used for forming gold based lactide polymers with lesser backbone acetylide conjugation. The reaction of **15** (Scheme 6) with 1-ethynyl-4-fluorobenzene to give **17** (Scheme 9, part **b**) was however found to proceed with low yield of 17%.

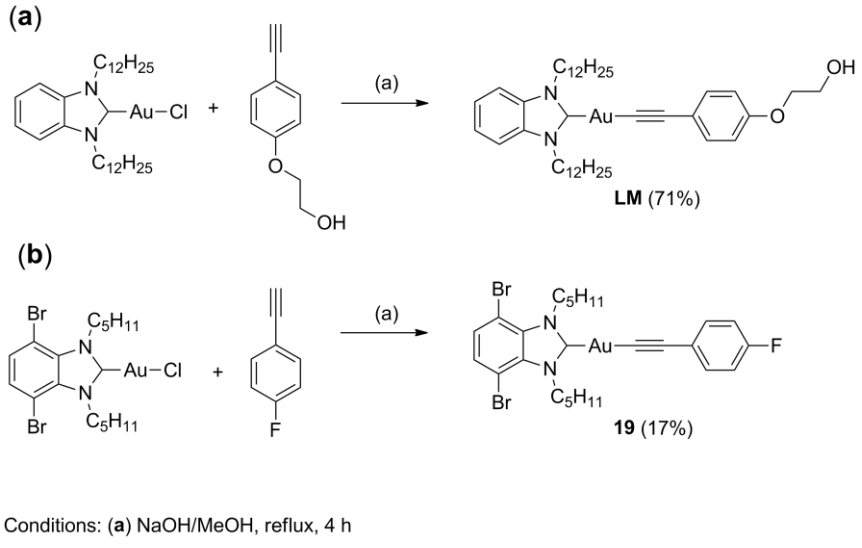

Scheme 9.

As expected, all the monomers exhibited room temperature phosphorescence (Table 4 and Figure 17) and the general photophysical behavior was quite analogous to those investigated in chapter 3. Significant is the fact that the E_{00} band maxima of the monomers were centered in the blue-green region (428-498 nm) of the electromagnetic spectrum. Therefore one might expect that the bathochromic shift induced upon polymerization with delocalization of the triplet would not be large enough to render the polymer non-emissive in accordance with the energy-gap law.

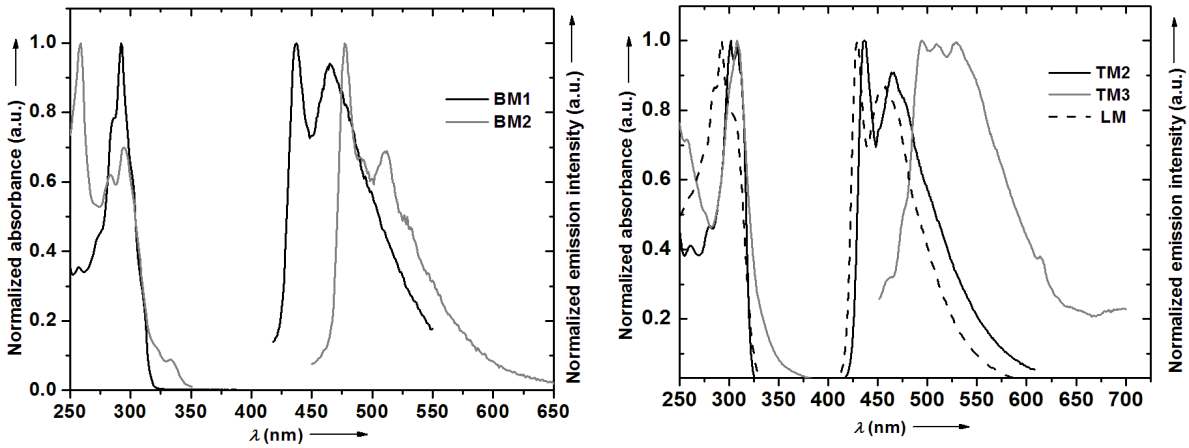

Figure 17. UV-vis and photoluminescence spectra of various monomers recorded in CH_2Cl_2 at RT.

Table 4. Photophysical data of **BM1**, **BM2**, **TM2**, **TM3** and **LM**.

complex	Room temperature solution (CH_2Cl_2)						77 K glass[b]
	Absorption λ_{max}[nm]	Emission λ_{max} [nm]	τ [μs]	Φ_{em}[a] x 10^{-2}	K_r [s^{-1}] x 10^4	K_{nr} [s^{-1}] x 10^5	(2-MeTHF)
BM1	292	436, 465 sh	0.56	0.3	0.552	17.70	425, 484, 530
BM2	259, 294	476, 510 sh	12.6	1.0	0.008	0.711	437, 472
TM2	308	437	2.28	1.3	0.57	4.32	433, 462, 476
TM3	308	495, 514	5.51	0.9	0.16	17.84	438, 480, 503
LM	295	428, 456 sh	0.61	12.0	20.0	14.4	422, 446, 483

[a] Photoluminescence quantum yield was determined with quinine sulfate in 1N H_2SO_4 as standard at 298 K. [b] Vibronic structured emission bands. $K_r = \Phi_P/\tau$ and $K_{nr} = (1- \Phi_P)/\tau$ were calculated assuming unit efficiency of inter system crossing.

3.2 Synthesis of Gold(III) Monomers by Oxidative Addition Reaction.

Yet a different direction envisaged to create luminescent Au(III) monomers was to oxidatively add dihalides such as I_2 to Au(I) complexes, which can later be substituted with alkynes. Direct oxidative addition of terminal alkynyl halide was considered to be difficult because Au(I) complexes are known to be sluggish towards activation of carbon halogen bonds.[37] The halide in the NHC gold precursor (**12a**, Scheme 8) can be replaced by perfluorophenyl group to give **20** (Scheme 10) by using pentafluorophenyl anion or by using a borylated nucleophilic equivalent like pentafluorophenylboronic acid in the presence of Cs_2CO_3.[38] The former method provided increased yield (73%) and cleaner product. Oxidative addition of I_2 was easily achieved similar to their phosphine and ylide counterparts[39] (Scheme 10). In the next step, when 2.5 equiv. of 1-ethynyl-4-fluorobenzene was lithiated and added to **21** at -78°C, the product thus obtained after column purification was interpreted to be the Au(III) complex with monosubstituted alkyne by NMR studies and IR studies. Further investigations are due to arrive at definitive conclusions about its structure. It is presumed that either the disubstituted product is sterically disfavored or undergoes reductive elimination in a kinetically fast

step. Attempts to grow single crystals of this monosubstituted gold alkyne complex were also unsuccessful. Treating the gold precursor chloride with *n*-Bu_4NCN leads to facile cyanation yielding the NHC Au(I) cyano complex **22**. In an exactly similar protocol as applied to obtain **21**, iodine was oxidatively added to **22** to achieve **24** in good yield (73%). Single crystals suitable for XRD were obtained for all the compounds (**20**, **21**, **22** and **23**) by slow evaporation of pentane in a concentrated solution of the complexes in CH_2Cl_2. The perspective views of these complexes are shown in Figure 19 and some selected bond distances and angles are collected in Table 5.

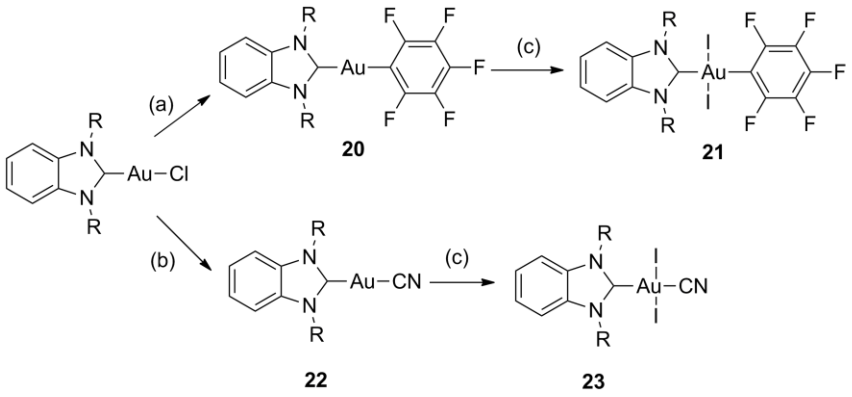

Conditions, (a): (Pentafluorophenyl)boronic acid/Cs_2CO_3/dry IPA, 50 °C, 24 h
(or) 1,2,3,4,5-pentafluoro-6-iodobenzene/*n*-BuLi, -78 °C, Et_2O, 1 h
(b): *n*-$Bu_4N^+CN^-$, CH_2Cl_2, RT, 10 h.
(c): I_2, $CHCl_3$, 5 h, RT

Scheme 10.

Both the substituted Au(I) complexes namely **20** and **22** and their corresponding oxidized products **21** and **23** were non-emissive at RT and very weakly emissive in 77 K rigidified matrices. The UV-vis spectra (Figure 18) of the of these oxidized complexes displayed typical low energy absorption bands [λ_{max} = 362 nm for **21** and 376 nm for **23**], which were absent in their corresponding Au(I) starting complexes.

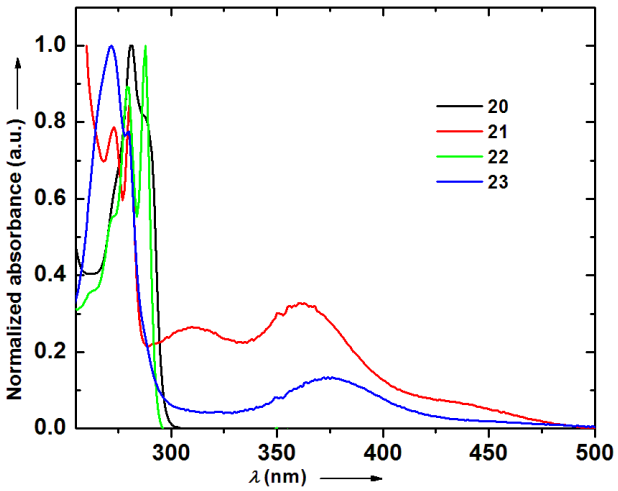

Figure 18. Normalized UV-vis spectra of **20**, **21**, **22** and **23** recorded in CH_2Cl_2 at RT.

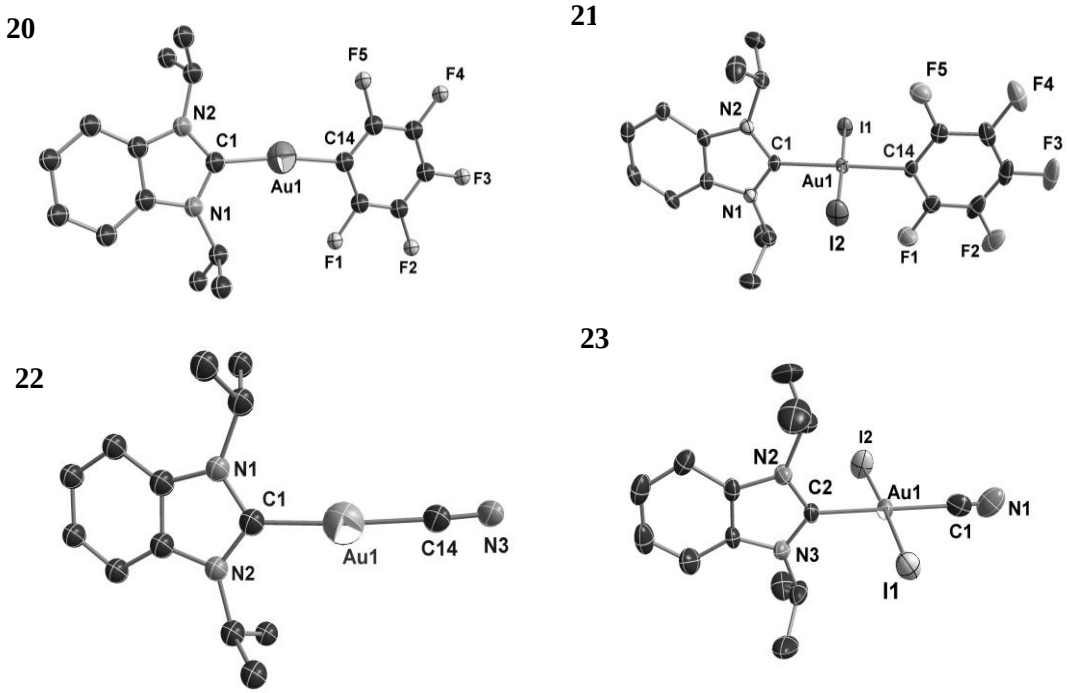

Figure 19. X-ray crystal structures of **20**, **21**, **22** and **23** with selective atomic numbering scheme. Thermal ellipsoids are drawn at 50% probability level. Hydrogen atoms are omitted for clarity.

The X-ray structures of the Au(I) complexes **20** and **22** revealed the typical linear two coordinate geometry with some deviation from ideal 180° angle. The $C_{carbene}$-Au-C_{aryl} and $C_{carbene}$-Au-C_{cyano} bond angles in **20** and **22** were 172.69(13) Å and 174.1(2) Å respectively (Table 5). After oxidation, these complexes exhibited a relatively strain free square planar geometry owing to non-sterically encumbering ligands. The benzimidazole and pentafluorophenyl rings were disposed approximately orthogonal to plane containing gold and iodine atoms (torsional angle approx. 93.7° observed in **21**). The dihedral angles defined by the least-squares mean planes comprising the benzimidazole carbene (N-$C_{carbene}$-N) and the gold iodine atoms (I-Au-I) were evaluated to be close to ideal 90° *viz.*, 89.19° for **21** and 89.59° for **23**. More interestingly, the C≡N bond distance of the cyano group in **22** was measured to be 1.132(8) Å, which is slightly larger than 0.932(9) Å found in **23**. Oxidation leads to the decrease on the π-back donating ability consequently leading to the shortening of the C≡N bond distance in **23**.

Before attempting to polymerize the vital triptycene bearing monomers, it was important to arrive at the optimal catalyst concentration and reaction conditions. In a trial reaction (Scheme 11; **a**) applying Sonagashira coupling protocol (5.0 mol% of $Pd(PPh_3)_4$ and 2.5 mol% CuI) we identified the formation of organic cross-coupled product (approx. 30% yield from ^{1}H NMR, GC-MS) due to the cleavage of Au-C_{sp} bond and coupling to the dialkynyl monomer. Also, development of violet coloration during the reaction course suggested the formation of Au(0). These observations prompted us to investigate more into optimizing the coupling conditions. In fact, literature survey revealed that phosphine Au(I) alkynes have been used as alkynyl transfer reagents in a Pd catalyzed coupling protocol.[40]

Table 5. Selected bond distances (Å) and angles (°) data of **20**, **21**, **22** and **23**.

Complex **20**			
C(1)-Au(1)	2.026(3)	Au(1)-C(14)	2.042(3)
C(1)-Au(1)-C(14)	172.69(13)		

Complex **21**			
C(1)-Au(1)	2.050(3)	Au(1)-C(14)	2.058(3)
Au(1)-I(1)	2.6037(3)	Au(1)-I(2)	2.5897(3)
C(1)-Au(1)-C(14)	179.43(15)	C(1)-Au(1)-I(1)	89.54 (9)
C(1)-Au(1)-I(2)	89.44 (9)	C(14)-Au(1)-I(1)	90.17(19)

Complex **22**			
C(1)-Au(1)	2.013(5)	Au(1)-C(14)	1.985(7)
C(14)-N(3)	1.132(8)	C(14)-Au(1)-C(1)	174.1(2)
Au(1)-C(14)-N(3)	177.4(6)		

Complex **23**			
C(2)-Au(1)	2.025(5)	Au(1)-C(1)	2.113(9)
C(1)-N(1)	0.932(9)	Au(1)-I(1)	2.6056(5)
Au(1)-I(2)	2.6133(5)	C(1)-Au(1)-C(2)	178.5(3)
C(2)-Au(1)-I(1)	88.85(16)	C(2)-Au(1)-I(2)	87.76(16)
C(1)-Au(1)-I(1)	92.53(19)	C(1)-Au(1)-I(2)	90.87(19)

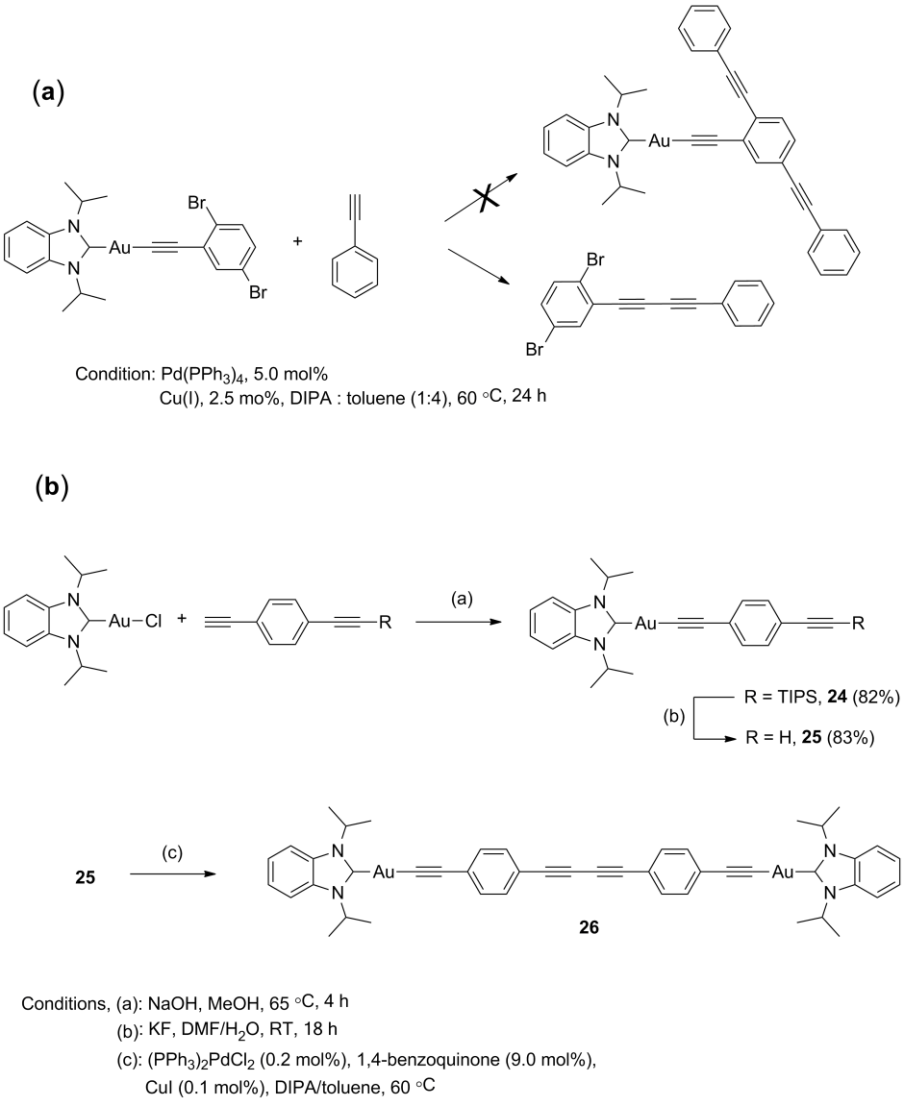

Scheme 11.

When a lower catalyst loading of 3.0 mol% of $Pd(PPh_3)_4$ and 1.0 mol% CuI was applied directly on a reaction employing triptycene dibromomonomer (**TM2**) and a dialkynyl co-monomer (Scheme 12), the major cross-coupled product that was obtained after work-up[41] turned out to be a short oligomer with approximately 1-2 repeat units based on ^1H NMR integration (see appendix for spectra). It needs to be mentioned here that no noticeable decomposition of the gold was observed in this case during the course of the reaction. The ^1H NMR of the oligomer shows characteristic aromatic resonances

corresponding to the phenyl unit of the co-monomer between δ = 6.87-7.0 ppm and the triptycene between δ = 7.28 -7.43.

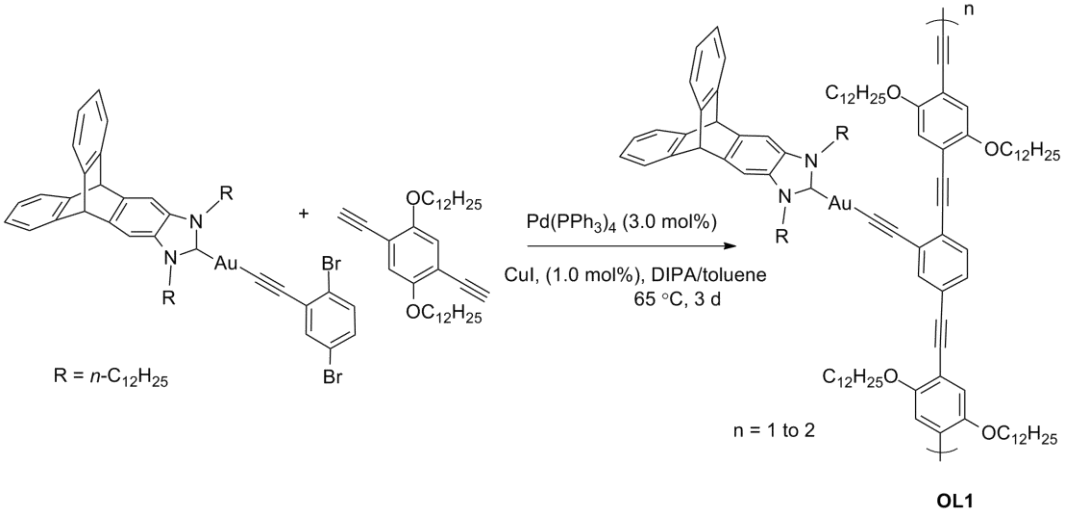

Scheme 12.

Gel permeation chromatography (GPC) to determine the molecular weight of the oligomer however was not performed. Based on the outcome of the above experiments, clearly, further studies are necessary for optimization of dehydrohalogenation procedure. To test the efficacy of the oxidative coupling procedure[42] in NHC bearing gold complexes, **25** was prepared by substitution followed by desilylation as indicated in the Scheme 11 (part **b**) starting from mono-TIPS protected 1,4-diethynylbenzene. In the presence of 1,4-benzoquinone (9.0 mol%) as oxidant and $Pd(PPh_3)_2Cl_2$ (0.2 mol%) as catalyst, complex **26** could be obtained along with approx. 5% of inseparable and unidentified impurity. The structure of **26** was confirmed by NMR and IR analyses. Although the reaction conditions are not fully optimized, the success of this method in enduring the stability of Au(I) NHC complex in the presence of palladium catalyst is considered important.

4.0 Conclusions and Outlook

In summary, the chapter has explored synthetic strategies for the creation of d^8 and d^{10} transition metal based novel rigid-rod σ-alkynyl complexes, which can be made suitable for cross-coupling or oxidative polymerization. Specifically, the following have been achieved

i) Novel *trans* bis-alkynyl bis-carbene Pd(II) complexes which are luminescent at 77 K have been synthesized.

ii) Room temperature phosphorescent *cis*-Pt(II) dialkynyl complexes have been prepared starting from bridged biscarbene ligand.

iii) Iptycene based bulky *N*-heterocyclic carbene monomers which are suitable for preparing Au(I) based luminescent cross-conjugated polymers have been prepared.

Some of the important outlooks for this project would involve extensive optimization of substrate/catalyst ratio and reaction conditions for realizing high molecular weights using **TM2** in Scheme 12. The preliminary success in the oxidative coupling protocol depicted in Scheme 11, part (**b**) also opens avenues for standardization of the reaction condition using the monomer **TM3**. Evaluation of the photophysical behavior of the oligomers which might result along the course of synthetic development is also important for predicting the properties of the desired polymer. The monomer (**LM**) shown in Scheme 9, designed for lactide ring opening polymerization is anticipated to preserve the emission wavelength of the monomer also in the polymer since it lacks acetylenic conjugation in the backbone. In this way, emission will not get quenched if the triplet happens to delocalize over several monomer units resulting in low band-gaps. Complexes **21** and **23** can serve as important starting materials for aryl or alkynyl substitution. Especially, **23** is expected to show lesser degree of isomerization/reductive elimination after incorporation of acetylides/aryl ligands, which is important during polymerization reactions.

5.0 Experimental section

5.1 General consideration

Synthetic steps requiring inert atmosphere was carried out using standard schlenk techniques under an atmosphere of dry N_2. Commercially available reagents were purchased from Aldrich or Strem chemicals and were used as such without further purification. [(SMe_2)AuCl] was prepared according to the published procedure.[15b] ^1H and $^{13}C\{^1H\}$ were recorded on Bruker AV2-400 or AV-500 spectrometers. ^{19}F NMR spectra were recorded on either on Varian Mercury spectrometer or Bruker AV2-400 spectrometers. Chemical shifts (δ) are reported in parts per million (ppm) referenced to tetramethylsilane (δ = 0.00 ppm) using the residual protio solvent peaks as internal standards (^1H NMR experiments) or the characteristic resonances of the solvent nuclei (^{13}C NMR experiments). ^{19}F NMR was referenced to $CFCl_3$ (δ = 0.00 ppm). Coupling constants (*J*) are quoted in Hertz (Hz) and the following abbreviations are used to describe the signal multiplicities: s (singlet); d (doublet); t (triplet); q (quartet); m (multiplet); dd (doublet of doublet); td (triplet of doublet); dt (doublet of triplet). Proton and carbon assignments have been made using routine one and two dimensional NMR spectroscopies where appropriate. Infra-red (IR) spectra were recorded on a Perkin-Elmer 1600 Fourier Transform spectrophotometer using KBr pellet with frequencies (ν) quoted in wavenumbers (cm^{-1}). Elemental microanalysis was carried out with Leco CHNS-932 analyser. Mass spectra were run on a Finnigan-MAT-8400 mass spectrometer. TLC analysis was performed on precoated Merck Silica Gel $60F_{254}$ slides and visualised by luminescence quenching either at (short wavelength) 254 nm or (long wavelength) 365 nm. UV-vis measurements were carried out on a Perkin-Elmer Lambda 19 UV/VIS spectrophotometer. Steady-state photoluminescence spectra were acquired on Perkin Elmer spectrophotometer using 450W Xenon lamp excitation by exciting at the longest-wavelength absorption maxima. All samples for emission spectra were degassed by at least three freeze-pump-thaw cycles in an anaerobic cuvette and were pressurized with N_2 following each cycle. 77 K emission spectra were acquired in frozen 2-methyltetrahydrofuran (2-MeTHF) glass. Luminescence quantum yields (ϕ) were determined at 298 K (estimated uncertainty ± 15%) using standard methods as described

in Chapter 2. Wavelength-integrated intensities (*I*) of the corrected emission spectra was compared to iso-absorptive spectra of quinine sulfate standard (ϕ_r = 0.546 in 1 N H_2SO_4 air-equilibrated solution) and was corrected for solvent refractive index.

1,3-Dipentylbenzimidazolium Bromide (1b)

A mixture of benzimidazole (1.18 g, 9.9 mmol) and K_2CO_3 (1.52 g, 10.9 mmol) was suspended in CH_3CN (5.0 mL) and stirred at ambient temperature for 1 h. To the suspension was added 1-bromopentane (1.85 mL, 15.0 mmol) and the reaction mixture was refluxed for 24 h. Following this, a second portion of 1-bromopentane (1.85 mL, 15.0 mmol) was added and the reaction was continued further for an additional 72 h. After removing the volatiles *in vacuo*, the residue was diluted with CH_2Cl_2 (100.0 mL) and was filtered over a celite plug. The filtrate was then solvent concentrated to give the product as a white solid. Yield: 2.67 g, 79%; ESI-MS: *m*/*z* 259 $[M\text{-}Br]^+$; ^{1}H NMR (500 MHz, $CDCl_3$, 298 K): δ = 11.41 (s, 1H, NC*H*N), 7.70 (dd, *J* = 6.0, 3.0 Hz, 2H, Ar-*H*), 7.64 (dd, *J* = 6.0, 3.0 Hz, 2H, Ar-*H*), 4.61 (t, *J* = 7.5 Hz, 4H, C_5H_{11}), 2.0 (t, *J* = 7.5 Hz, 6H, C_5H_{11}), 1.96-1.98 (m, 2H, C_5H_{11}), 1.36-1.39 (m, 7H, C_5H_{11}), 0.87 (t, 3H, *J* = 7.0 Hz, C_5H_{11}); ^{13}C{1H} NMR (125.75 MHz, $CDCl_3$, 298 K): δ = 143.4, 132.0, 127.7, 113.7, 48.3, 29.8, 29.4, 22.7, 14.4; elemental analysis (%) calc. for $C_{17}H_{27}BrN_2$: C, 60.17; H, 8.02; N, 8.26. Found: C, 59.81; H, 7.84; N, 7.99.

***trans*-dibromo-bis(*N*,*N*'-dipentylbenzimidazolin-2-ylidene)palladium(II) (2b)**

A mixture of **1b** (339.0 mg, 1.0 mmol) and $Pd(OAc)_2$ (112.2 mg, 0.5 mmol) was dissolved in DMSO (6.0 mL) and stirred at 120 °C for 3 h and then at 100 °C overnight. The obtained precipitate was filtered and washed with small portions of cold DMSO (2.0 mL) and Et_2O (5.0 mL). Drying thoroughly *in vacuo* yielded the product as an off-white powder. Yield 547.0 mg, 70%; ESI-MS: *m*/*z* = 702 $[M\text{-}Br]^+$; ^{1}H NMR (400 MHz, $CDCl_3$, 298 K): δ = 7.38 (dd, *J* = 6.0, 3.0 Hz, 4H, Ar-*H*), 7.27 (dd, *J* = 6.0, 3.0 Hz, 4H, Ar-*H*), 4.97 (td, *J* = 6.5, 2.0 Hz, 3H, C_5H_{11}), 4.81 (t, *J* = 7.5, 2H, C_5H_{11}), 4.36 (td, *J* = 6.5, 2.0 Hz, 3H, C_5H_{11}), 2.21-2.35 (m, 5H, C_5H_{11}), 1.77-1.85 (m, 3H, C_5H_{11}), 1.36-1.58 (m, 17H, C_5H_{11}), 0.92 (m, 12H, C_5H_{11}); ^{13}C{1H} NMR (125 MHz, $CDCl_3$, 298 K): δ = 181.2,

134.1, 123.3, 111.0, 49.6, 29.5, 28.6, 22.6, 14.0; elemental analysis (%) calc. for: $C_{34}H_{52}Br_2N_4Pd$: C, 52.15; H, 6.69; N, 7.16. Found: C, 51.89; H, 6.58; N, 6.91.

***trans*-[Pd(*bimz*)$_2$(C≡C-C$_6$H$_5$)$_2$][*bimz* = 1,3-diisopropylbenzimidazoline-2-ylidene] (3a)**

n-BuLi (0.27 mL, 0.75 mmol; 1.6 M soln. in hexanes) was added to phenylacetylene (36.0 mg, 0.35 mmol) in THF (9.0 mL) at -78 °C and stirred for 30 min to obtain a slightly yellow to orange colored solution. The solution was then allowed to warm up to approx. -30 °C and was added to a solution of **2a** (115.0 mg, 0.17 mmol) in THF (15.0 mL) maintained at -78 °C. After addition, the suspension was brought to RT and stirred overnight. It was then quenched with water and then extracted twice with CH_2Cl_2 (10.0 mL). The combined organic layer was dried over anhyd. Na_2SO_4 and concentrated *in vacuo* to obtain a beige colored solid which was further purified by column chromatography (silica gel, eluent: hexane/EtOAc = 8/2). Further, recrystallization of the isolated product from CH_2Cl_2/pentane afforded **3a** as a pale yellow solid. Yield: 60.0 mg, 58%; m.p: decomp < 204 °C; IR (KBr): ν(C≡C) 2106 cm^{-1}; ^{1}H NMR (500 MHz, $CDCl_3$, 298 K): δ = 7.58 (m, 4H, *bimz-H*), 7.36 (m, 4H, phenyl-*H*), 7.20 (m, 4H, *bimz*-H), 7.02 (m, 8H, phenyl-*H*), 6.93 (m, 2H, phenyl-*H*), 6.13 (sept. J = 7.1 Hz, 4H, C*H*$(CH_3)_2$), 1.86 (t, J = 7.1 Hz, 24H, C*H*$_3$); ^{13}C{1H} NMR (125.8 MHz, $CDCl_3$, 298 K): δ = 189.0 (Pd=C), 134.0, 132.7, 130.9, 129.4, 129.1, 128.6, 127.7, 124.3, 122.0, 121.6, 112.4, 107.8, 81.7, 54.0, 21.2; elemental analysis (%) calc. for $C_{58}H_{54}N_4Pd$: C, 76.26; H, 5.96; N, 6.13. Found: C, 76.38; H, 6.01; N, 6.09.

[Pt(*meim*)$_2$(C≡C-C$_6$H$_5$)$_2$] [*meim* = 1,1'-dimethyl-3,3'-methylene-diimidazoline-2,2'-diylidene] (4) *(general procedure 1)*

n-BuLi (0.25 mL, 0.39 mmol; 1.6 M soln. in hexanes) was added to phenylacetylene (41.0 mg, 0.40 mmol) in THF (9.0 mL) at -78 °C. The temperature was then gradually raised to RT and stirred for 20 min. It was then transferred into a flask containing Pt(*pmim*)$_2$I$_2$ (100.0 mg, 0.16 mmol) in THF (10.0 mL) and maintained at -78 °C. The mixture was stirred at that temperature for 20 min prior to allowing it to warm to RT. After 12 h, H_2O (10.0 mL) was added to the reaction mixture and was extracted with EtOAc (3 x 10.0 mL). The combined organic layer was dried over anhyd. Na_2SO_4, concentrated and further purified by flash column chromatography.

(silica gel, eluent: EtOAc /CH_2Cl_2 = 3/1); Yield: 41.3 mg, 45%; ESI-MS: *m*/*z* = 574 $[M]^+$; IR (KBr): ν(C≡C) = 2099 cm^{-1}; ^{1}HNMR (500 MHz, THF-d_8, 298 K): δ = 7.28 (d, 2H, *J* = 2.0 Hz, NC*H*CHN), 7.20-7.21 (4H, Ar-H and NCHC*H*N), 7.05-7.08 (m, 5H, Ar-H), 6.92 (t, 3H, *J* = 7.5 Hz), 6.08 (AB, 1H, *J* = 13.1 Hz, NCH_2N), 5.88 (AB, 1H, *J* = 13.1 Hz, NCH_2N), 4.09 (s, 6H, CH_3); ^{13}C{1H} NMR (125.0 MHz, THF-d_8, 298 K): δ = 167.0, 131.1, 129.6, 128.4, 124.7, 122.5, 120.7, 108.3, 106.8, 63.2, 37.9; elemental analysis (%) calc. for $C_{25}H_{22}N_4Pt$: C, 52.35; H, 3.87; N, 9.77. Found: C, 52.07; H, 3.89; N, 9.59.

[Pt(*meim*)$_2$(C≡C-C$_4$H$_3$S)$_2$] [*meim* = 1,1'-dimethyl-3,3'-methylene-diimidazoline-2,2'-diylidene] (5)

Following the *general procedure 1*, 2-ethynylthiophene (43.0 mg, 0.39 mmol) was lithiated and reacted with Pt(*pmim*)$_2$I$_2$ (100.0 mg, 0.16 mmol) to obtain **5** as brown solid. Yield: 37.0 mg, 39%; ESI-MS: *m*/*z* = 630 $[M+2Na]^+$; IR (KBr): ν(C≡C) = 2090 cm^{-1}; ^{1}H NMR (500 MHz, THF-d_8, 298 K): δ = 7.25 (d, 2H, *J* = 2.0 Hz, NC*H*CHN), 6.92 (m, 2H, Ar-H), 6.77 (d, 2H, *J* = 7.5 Hz, NCHC*H*N), 6.62-6.66 (m, 4H, NCHC*H*N and Ar-H), 5.82-5.91 (m, 2H, NCH_2N), 3.93 (s, 6H, CH_3); ^{13}C{1H} NMR (125.0 MHz, THF-d_8, 298 K): δ = 167.0 (*C*=Pt), 144.7 (N*C*N), 129.8, 124.6, 124.3, 122.5, 119.9 (N*C*HCHN), 119.6 (NCH*C*HN), 118.1, 111.6 (C≡C-Pt), 36.1 (CH_3); elemental analysis (%) calc. for $C_{21}H_{18}N_4PtS_2$: C, 43.07; H, 3.10; N, 9.57. Found: C, 43.54; H, 2.99; N, 9.44.

2,3-Triptyceneimidazole (**7**)

A solution of 2,3-diaminotriptycene (850.0 mg, 2.99 mmol) in 30.0 mL of deaerated formic acid was heated at 90 ºC for 2.0 h under an atmosphere of N_2. It was allowed to cool to RT, poured into ice/water and neutralized with 10% aqueous NaOH solution until precipitation was complete. The solids were collected by vacuum filtration, washed with water followed by cold THF and dried *in vacuo* to give **7** as a white solid. Yield: 865 mg, 98%; ESI-MS: *m*/*z* = 295 $[M-H]^+$; ^{1}H NMR (500 MHz, CD_2Cl_2, 298 K): δ = 8.01 (s, 1H, imidazole-*H*), 7.69 (s, 2H, Ar-*H*), 7.44-7.46 (m, 4H, Ar-*H*), 7.04-7.06 (m, 4H, Ar-*H*), 5.54 (s, 2H, bridgehead), 4.95 (s, broad, N*H*); ^{13}C{1H} NMR (125.0 MHz, CD_2Cl_2, 298 K): δ = 145.7, 140.5, 140.4, 135.0, 125.2, 123.5, 110.8, 60.3; elemental analysis (%) calc. for $C_{21}H_{14}N_2$: C, 85.69; H, 4.79; N, 9.52. Found: C, 85.50; H, 5.00; N, 9.39.

1,3-Dipentyl-2,3-triptyceneimidazolium Bromide (8a) *(general procedure 2)*

To a suspension of **7** (800.0 mg, 2.72 mmol) and K_2CO_3 (413.0 mg, 2.98 mmol) in acetonitrile (20.0 mL) was added 1-bromopentane (1.31 g, 8.6 mmol) and refluxed with vigorous stirring. After 24 h, an equal amount of 1-bromopentane was added and the reaction was continued for 6 days. The resulting suspension was filtered over celite and the filter cake was washed with CH_2Cl_2 (20.0 mL). Removal of the solvent *in vacuo* afforded the crude product as a white solid, which was further purified by recrystallization in ethanol. Yield: 980.0 mg, 70%; ESI-MS: *m*/*z* = 435 $[M\text{-}Br]^+$; ^{1}H NMR (500 MHz, CD_2Cl_2, 298 K): δ = 11.3 (s, 1H, imidazole-*H*), 7.40-7.38 (dd, *J* = 5.4, 2.8 Hz, 4H, Ar-*H*), 7.08 (s, 2H, Ar-*H*), 7.01-7.00 (dd, *J* = 5.4, 2.8 Hz, 4H, Ar-H), 5.43 (s, 2H, bridgehead), 3.78 (t, 4H, *J* = 7.5 Hz), 1.66-1.68 (m, 4H), 1.52-1.53 (m, 2H), 1.30-1.32 (m, 6H), 0.87 (t, 6H, *J* = 6.5 Hz); ^{13}C{1H} NMR (125.0 MHz, CD_2Cl_2, 298 K): δ = 154.4, 145.7, 138.4, 126.4, 125.0, 123.3, 104.1, 54.3, 41.0, 28.8, 28.0, 22.3, 13.7; elemental analysis (%) calc. for $C_{31}H_{35}BrN_2$: C, 72.22; H, 6.84; N, 5.43. Found: C, 71.99; H, 6.94; N, 5.63.

1,3-Didodecyl-2,3-triptyceneimidazolium bromide (8b) *(general procedure 3)*

Sodium hydride (36.0 mg, 60 wt%, 0.91 mmol) was washed twice with dry hexane (4.0 mL) in a RB-flask under N_2 atmosphere. Dry toluene (10.0 mL) and **7** (200.0 mg, 0.68 mmol) were added successively and suspension was heated initially at 110 °C for 1 h. It was then allowed to cool to RT, and 1-bromododecane (411.0 mL, 1.70 mmol) was added *via* syringe. The suspension was re-heated to 110 °C and maintained at that temperature for 1.5 h. Dry DMF (6.0 mL) was then added and the reaction was continued for 6 h at 110 °C then at 60 °C for 4 h. Upon completion of the reaction, the suspension was allowed to cool to RT, diluted with toluene (15 mL) and *t*-BuOH (2.0 mL) and filtered under vacuum. The filter cake was washed with minimal water and cold THF. Repeated recrystallization of the solids thus obtained in THF afforded **8b** as an off-white solid. Yield: 235.0 mg, 48%; ESI-MS: *m*/*z* = 631.0 $[M\text{-}Br]^+$; ^{1}H NMR (500 MHz, $CDCl_3$, 298 K): δ = 11.4 (s, 1H, imidazole-*H*), 7.64 (s, 2H), 7.47-7.48 (m, 4H, Ar-*H*), 7.07-7.09 (m, 4H, Ar-*H*), 5.63 (s, 2H, bridgehead), 4.54 (t, 4H, *J* = 7.5 Hz, alkyl), 1.97 (t, 4H, *J* = 7.5 Hz, alkyl), 1.25-1.35 (m, 36H, alkyl), 0.88 (t, 6H, *J* = 6.5 Hz, alkyl-C*H*$_3$); ^{13}C{1H} NMR

(125.0 MHz, $CDCl_3$, 298 K): δ = 145.4, 143.7, 142.3, 128.9, 126.1, 124.0, 108.1, 53.9, 47.6, 31.9, 29.7, 29.6, 29.5, 29.4, 29.3, 29.2, 29.1, 29.0, 26.5, 14.1; elemental analysis (%) calc. for $C_{45}H_{63}BrN_2$: C, 75.92; H, 8.92; N, 3.94. Found: C, 74.90; H, 8.39; N, 3.84.

***trans*-dibromo-bis(1,3-dipentyl-2,3-triptyceneimidazolium)palladium(II) (9)**

A mixture of **8a** (200.0 mg, 0.389 mmol) and $Pd(OAc)_2$ (43.5 mg, 0.191 mmol) was dissolved in 15.0 mL of DMSO and heated at 120 ºC for 3 h. It was then allowed to cool to RT and precipitated by addition of water (20.0 mL). The precipitate was filtered washed with small portions of water and cold THF and dried thoroughly *in vacuo* to give **9** as a yellow solid. Yield: 176.0 mg, 40%; ESI-MS: *m*/*z* = 1157.3 $[M+Na]^+$, 1175.3 $[M+CH_3CN]^+$; ^{1}H NMR (500 MHz, $CDCl_3$, 298 K): δ = 7.42 (dd, *J* = 3.0, 2.0 Hz, 8H, aryl), 7.40 (s, 4H, aryl), 7.03 (dd, *J* = 3.0, 2.0 Hz, 8H, aryl), 5.52 (s, 4H, bridgehead), 4.70 (t, *J* = 7.5 Hz, 8H, alkyl), 2.2 (t, *J* = 7.5 Hz, 8H, alkyl), 1.46-1.57 (m, 16H, alkyl), 0.96-1.0 (m, 12H, alkyl); ^{13}C{1H} NMR (125.0 MHz, $CDCl_3$, 298 K): δ = 180.6, 144.9, 140.6, 132.1, 125.7, 123.6, 106.1, 54.0, 48.5, 41.1, 29.2, 22.4, 14.1; elemental analysis (%) calc. for $C_{62}H_{68}Br_2N_4Pd$: C, 65.58; H, 6.04; N, 4.93. Found: C, 65.23; H, 5.89; N, 4.55.

(1,3-dipentyl-2,3-triptyceneimidazolin-2-ylidene)(dimethylsulfoxide)platinum(II) (10)

To a solution of **8a** (51.0 mg, 0.10 mmol) in 2.0 mL of DMSO was added PtI_2 (45.0 mg, 0.1 mmol) and NaOAc (16.4 mg, 0.2 mmol), and the mixture was stirred at 110 ºC for 2 h. It was cooled to RT and precipitated by addition of water. The solids were collected by vacuum filtration, washed with water and dried under vacuum to give **10** as yellow powder. Yield: 62.0 mg, 95%; ^{1}H NMR (500 MHz, $CDCl_3$, 298 K): δ = 7.40-7.42 (m, 8H, aryl), 7.32 (s, 4H, aryl), 6.97-6.99 (m, 8H, aryl), 5.63 (s, 4H, bridgehead), 3.75 (broad, 8H, alkyl), 1.57-1.58 (m, 8H, alkyl), 1.19-1.27 (m, 20H), 0.81(t, 12H, *J* = 7.5 Hz, alkyl); ^{13}C{1H} NMR (125.0 MHz, $CDCl_3$, 298 K): δ = 154.2, 146.3, 139.0, 126.0, 125.3, 123.9, 105.0, 53.0, 28.7, 28.0, 22.1, 14.4; elemental analysis (%) calc. for $C_{33}H_{40}I_2N_2OPtS$: C, 41.22; H, 4.19; N, 2.91. Found: C, 41.55; H, 4.27; N, 2.70.

[1,3-didodecylbenzimidazol-2-ylidene]AuCl (12b) *(general procedure 4)*

A mixture of 1,3-didodecylbenzimidazolium bromide (100.0 mg, 0.187 mmol) and Ag_2O (21.6 mg, 0.093 mmol) in CH_2Cl_2 (15.0 mL) was stirred for 6 h at RT and was then filtered over a celite plug. The filtrate was then transferred into a CH_2Cl_2 (5.0 mL) solution of $(SMe_2)AuCl$ (51.1 mg, 0.173 mmol) and stirred for 6 h at RT. The precipitated AgBr was filtered over celite, and the solvent was evaporated *in vacuo* to obtain the crude product. Washing the crude product with cold pentane (5.0 mL) afforded **12b** as a white solid. Yield: 102 mg, 85%; ESI-MS: *m*/*z* = 455.5 $[M\text{-}Cl]^+$; ^{1}H NMR (500 MHz, $CDCl_3$, 298 K): δ = 7.49 (dd, 2H, *J* = 6.0, 3.0 Hz, *o*-C_6H_4), 7.44 (dd, 2H, *J* = 6.0, 3.0 Hz, *m*-C_6H_4), 4.48 (t, *J* = 7.0 Hz, 4H, alkyl), 1.94 (quint, *J* = 7.0 Hz, 4H, alkyl), 1.23-1.43 (m, 36H, alkyl), 0.896 (t, *J* = 7.0 Hz, 6H, alkyl); ^{13}C{1H} NMR (125.0 MHz, $CDCl_3$, 298 K): δ = 178.0, 133.1, 124.3, 111.5, 49.0, 32.0, 30.0, 29.7, 29.6, 29.5, 29.2, 29.4, 29.3, 26.8, 22.7, 14.2; elemental analysis (%) calc. for $C_{31}H_{54}AuClN_2$: C, 54.18; H, 7.92; N, 4.08. Found: C, 53.95; H, 7.79; N, 4.01.

4,7-dibromo-1*H*-benzo[*d*]imidazole (13)

Following the same procedure as described for obtaining triptyceneimidazole (**7**), 3,6-dibromobenzene-1,2-diamine (100.0 mg, 0.37 mmol) was reacted with 5.0 mL of deareated formic acid to obtain **13** as an off-white solid. Yield: 81.0 mg, 71%; ESI-MS: *m*/*z* = 275.8 $[M]^+$; ^{1}H NMR (400 MHz, DMSO-d_6, 298 K): δ = 13.2 (broad, 1H), 8.36 (s, 1H), 7.35 (s, 2H); ^{13}C{1H} NMR (100 MHz, DMSO-d_6, 298 K): δ = 144.0, 132.7, 126.2, 113.7; elemental analysis (%) calc. for: $C_7H_4Br_2N_2$: C, 30.47; H, 1.46; N, 10.15. Found: C, 30.25; H, 1.70; N, 10.01.

[1,3-didodecyl[4,7-dibromo-1*H*-benzo[*d*]imidazolium]bromide (14)

Following the *general procedure 2*; **13** (100.0 mg, 0.36 mmol) was treated with 1-bromopentane (0.27 mL, 2.16 mmol) in two equal portions in the presence of K_2CO_3 (54.6 mg, 0.40 mmol) to obtain **14** as a white solid. Yield: 52.2 mg, 29%; ESI-MS: *m*/*z* = 417.0 $[M\text{-}Br]^+$; ^{1}H NMR (400 MHz, $CDCl_3$, 298 K): δ = 11.92 (s, 1H, NC*H*N), 7.63 (s, 2H, aryl), 4.97 (t, *J* = 7.5 Hz, 4H, alkyl), 2.07 (quint, *J* = 7.5 Hz, 4H, alkyl), 1.40-1.47(m, 8H, alkyl), 0.91 (t, *J* = 7.5 Hz, 6H, alkyl); ^{13}C{1H} NMR (125.0 MHz, $CDCl_3$, 298 K): δ

= 146.8, 132.8, 130.7, 105.8, 49.7, 31.4, 28.1, 22.1, 13.8; elemental analysis (%) calc. for: $C_{17}H_{25}Br_3N_2$: C, 41.07; H, 5.07; N, 5.64; Found: C, 40.68; H, 4.90; N, 5.37.

1,3-dipentyl-[4,7-dibromobenzimidazolylidene]AuCl (15)

Following *general procedure 4*; **14** (100.0 mg, 0.20 mmol) was initially reacted with Ag_2O (23.1 mg, 0.10 mmol) and subsequently with $(SMe_2)AuCl$ (56.0 mg, 0.19 mmol) to obtain **15** as white solid. Yield: 98.2 mg, 70.0%; ^{1}H NMR (500 MHz, $CDCl_3$, 298 K): δ = 7.45 (s, 2H, aryl), 4.93 (t, J = 7.5 Hz, 4H, alkyl), 1.94 (quint, J = 7.5 Hz, 4H, alkyl), 1.40-1.58 (m, 8H, alkyl), 0.95 (t, J = 7.5 Hz, 6H, alkyl); ^{13}C{1H} NMR (125.0 MHz, $CDCl_3$, 298 K): δ = 183.4, 132.2, 130.6, 104.2, 50.8, 31.9, 28.4, 22.2, 14.0; elemental analysis (%) calc. for: $C_{17}H_{24}AuBr_2ClN_2$: C, 31.48; H, 3.73; N, 4.32. Found: C, 31.69; H, 3.92; N, 4.14.

1,3-dipentyl[triptyceneimidazolylidene]AuCl (16a)

Following *general procedure 4*; **8a** (130.0 mg, 0.252 mmol) was initially reacted with Ag_2O (30.0 mg, 0.129 mmol) and subsequently with $(SMe_2)AuCl$ (61.8 mg, 0.210 mmol) to obtain **16a** as white solid. Yield: 119.0 mg, 70%; ESI-MS: m/z = 631.2 $[M\text{-}Cl]^+$; ^{1}H NMR (400 MHz, $CDCl_3$, 298 K): 7.45-7.47 (dd, 4H, J = 5.4, 2.2 Hz, 4H, Ar-*H*), 7.29 (s, 2H, Ar-*H*), 7.06-7.08 (dd, 4H, J = 5.4, 2.2 Hz, 4H, Ar-*H*), 5.58 (s, 2H, bridgehead), 4.39 (t, 4H, J = 7.5 Hz, alkyl), 1.86-1.93 (m, 4H, alkyl), 1.35-1.46 (m, 8H, alkyl), 0.92 (t, 6H, J = 4.0 Hz, alkyl-C*H*$_3$); ^{13}C{1H} NMR (100.0 MHz, $CDCl_3$, 298 K): 177.4, 144.5, 142.5, 130.6, 125.7, 123.8, 107.0, 54.02, 49.0, 29.6, 28.8, 22.3, 13.9; elemental analysis (%) calc. for: $C_{31}H_{34}AuClN_2$ (%): C, 55.82; H, 5.14; N, 4.20. Found: C, 55.29; H, 5.64; N, 3.99.

1,3-didodecyl[triptyceneimidazolylidene]AuCl (16b)

Following *general procedure 4*; **8b** (250.0 mg, 0.351 mmol) was initially reacted with Ag_2O (40.6 mg, 0.175 mmol) and subsequently with $(SMe_2)AuCl$ (97.2 mg, 0.33 mmol) to obtain **16b** as a white solid. Yield: 236.0 mg, 78%; ESI-MS: m/z = 631.5 $[M\text{-}AuCl]^+$; ^{1}H NMR (400 MHz, $CDCl_3$, 298 K): δ = 7.45-7.47 (dd, 4H, J = 5.2, 2.0 Hz, 4H, Ar-*H*), 7.29 (s, 2H, Ar-*H*), 7.09-7.06 (dd, 4H, J = 5.4, 3.2 Hz, 4H, Ar-*H*), 5.57 (s, 2H, bridgehead), 4.40 (t, 4H, J = 7.5 Hz, alkyl), 1.86-1.93 (m, 4H, alkyl), 1.28-1.36 (m, 36H,

alkyl), 0.92 (t, 6H, J = 6.8 Hz, alkyl-CH_3); ^{13}C{1H} NMR (100.0 MHz, $CDCl_3$, 298 K): δ = 177.5, 144.5, 142.5, 130.6, 125.7, 123.8, 107.0, 54.03, 49.0, 32.0, 29.9, 29.7, 29.6, 29.5, 29.4, 29.3, 29.2, 26.8, 22.7, 14.1; elemental analysis (%) calc. for $C_{45}H_{62}AuClN_2$: C, 62.60; H, 7.24; N, 3.24; Found: C, 63.00; H, 6.90; N, 2.97.

1,4-bis(2-(triisopropylsilyl)ethynyl)-2-(2-(trimethylsilyl)ethynyl)benzene (**A2**)

A mixture containing 1,4-dibromo-2-ethynylbenzene **A1** (630.0 mg, 1.89 mmol), triisopropylsilylacetylene (0.86 mL, 3.84 mmol), bis(triphenylphosphine)palladium(II) chloride (66.6 mg, 0.09 mmol) and CuI (18.0 mg, 0.09 mmol) in DIPA (50.0 mL) was initially degassed for 15 min and then stirred at 80 °C under N_2 for 24 h. After being cooled to RT, the mixture was diluted with CH_2Cl_2 (80.0 mL) and was then washed with water (3 x 100.0 mL). The organic layer was collected and filtered through celite plug. The filtrate was evaporated *in vacuo* and the resulting solids were purified by column chromatography (neutral Al_2O_3, eluent: Hexane/ethyl acetate = 5/1) to afford **A2** as beige solid. Yield: 770.0 mg, 75%; ^{1}H NMR (400 MHz, $CDCl_3$, 298 K): δ = 7.65 (d, J = 2.4 Hz, 1H, aryl), 7.44 (d, J = 7.5 Hz, 1H, aryl), 7.33 (dd, J = 7.5, 2.2 Hz, aryl), 1.25 (s, 30H, (CH_3)$_3$CHSi), 1.10 (s, 6H, (CH$_3$)$_3$CHSi), 0.23 (s, 9H, CH_3Si); ^{13}C{1H} NMR (100.0 MHz, $CDCl_3$, 298 K): δ = 136.7, 136.1, 132.7, 132.3, 131.3, 125.6, 125.5, 105.7, 105.0, 102.6, 98.8, 97.0, 93.3, 18.8, 18.6 11.3, 0.2; elemental analysis (%) calc. for $C_{33}H_{54}Si_3$: C, 74.08; H, 10.17; Found: C, 73.99; H, 9.89.

2-ethynyl-1,4-bis(2-(triisopropylsilyl)ethynyl)benzene (A3)

K_2CO_3 (837.0 mg, 139.0 mmol) was added to a solvent mixture of CH_2Cl_2 (8.0 mL) and MeOH (16.0 mL) containing **A2** (675.0 mg, 1.26 mmol) and was stirred at RT for 24 h. It was then concentrated *in vacuo*, diluted with CH_2Cl_2 (30.0 mL) and washed with water (3 x 10.0 mL). The combined organic layer was dried over anhyd. $MgSO_4$, and solvent concentrated to afford the crude product. It was further purified by flash chromatography, (silica gel, eluent: EtOAc/hexane: 1/5) to yield compound **A3** as a light brown fluffy solid which tends to sublimate. Yield: 380.0 mg, 65%; ^{1}H NMR (400 MHz, $CDCl_3$, 298 K): δ = 7.70 (d, J = 2.2 Hz, 1H, aryl), 7.44 (d, J = 7.5 Hz, 1H, aryl), 7.34 (dd, J = 7.5, 2.3 Hz, aryl), 3.25 (s, 1H, (C≡CH), 1.20 (s, 36H, (CH_3)$_3$CHSi), 1.10 (s, 6H, (CH$_3$)$_3$CHSi);

$^{13}C\{1H\}$ NMR (100.0 MHz, $CDCl_3$, 298 K): δ = 135.8, 132.2, 131.6, 126.2, 125.0, 123.3, 105.5, 104.5, 97.4, 93.6, 81.5, 19.0, 11.23; elemental analysis (%) calc. for $C_{30}H_{46}Si_2$: C, 77.85; H, 10.02; Found: C, 78.14; H, 9.71.

2-(4-(2-(trimethylsilyl)ethynyl)phenoxy)ethanol (A4)

A mixture of 2-(4-bromophenoxy)ethanol (850.0 mg, 3.91 mmol), bis(triphenylphosphine) palladium(II) chloride (274.8 mg, 0.39 mmol) and CuI (37.2 mg, 0.19 mmol) in diisopropylamine (25.0 mL) was degassed for 15 min followed by the addition of trimethylsilylacetylene (1.0 mL, 7.04 mmol). After stirring the reaction mixture for 24 h at RT, the reaction mixture was filtered over celite bed. The filtrate was then concentrated, diluted with CH_2Cl_2 (50.0 mL) and washed with water (20.0 mL). The organic layer was dried over anhyd. Na_2SO_4 and concentrated to yield the crude product **A4**, which was directly desilylated following the same procedure as described for **A3**. The compound **A5** was obtained as a waxy light brown solid after column purification (silica gel, eluent: Hexane/EtOAc : 5/1) which slowly turns reddish brown after few days. Selected data for **A4**: ESI-MS: *m*/*z* = 319 $[M+H]^+$; Data for **A5**: Overall yield: 409.0 mg, 64%, IR (KBr): 2104 ν(C≡C), 3285 ν(OH) cm^{-1}; ESI-MS: *m*/*z* = 184.8 $[M+Na]^+$; ^1H NMR (500 MHz, $CDCl_3$, 298 K): δ = 7.34 (d, 2H, *J* = 8.0 Hz, aryl), 6.77 (d, 2H, *J* = 8.0 Hz, aryl), 4.00 (t, 2H, *J* = 4.5 Hz, C*H*$_2$), 3.87 (t, 2H, *J* = 4.5 Hz, C*H*$_2$), 2.91 (s, 1H, C≡C*H*); $^{13}C\{1H\}$ NMR (125.0 MHz, $CDCl_3$, 298 K): δ = 159.6, 134.2, 115.3, 84.0, 76.5, 70.0, 62.0; elemental analysis (%) calc. for $C_{10}H_{10}O_2$: C, 74.06; H, 6.21; Found: C, 73.90; H, 5.94.

[(*Bimz*)Au(I)(1,4-dibromo-2-ethynylbenzene)] (BM1) *(general procedure 5)*

The general procedure described in Chapter 3[33a] is adopted here. Accordingly, [*N*,*N'*-diisopropylbenzimidazolin-2-ylidene]AuCl (**12a**) (100.0 mg, 0.230 mmol) was reacted with 1,4-dibromo-2-ethynylbenzene **A1** (83.6 mg, 0.32 mmol) to obtain **BM1** as a white solid. Yield: 77.0 mg, 51%; IR (KBr): ν(C≡C) 2119 cm^{-1}; ESI-MS: *m*/*z* 658 $[M+H]^+$; ^1H NMR (500 MHz, $CDCl_3$, 298 K): δ = 7.74 (d, 1H, *J* = 2.5 Hz, dibromo-aryl) 7.67 (dt, 2H, *J* = 6.0 Hz, 3.0 Hz, *bimz*-C*H*), 7.40 (d, 1H, *J* = 6.0 Hz, dibromo-aryl), 7.37 (dt, 2H, *J* = 6.0 Hz, 3.0 Hz, *bimz*-C*H*), 7.17 (dd, 1H, *J* = 6.0, 2.5 Hz, dibromo-aryl), 5.58 (sept, 2H, *J*

= 7.0 Hz, ^{i}Pr-C*H*), 1.74 (d, 12H, *J* = 7.0 Hz, ^{i}Pr-CH_3); ^{13}C NMR (125 MHz, $CDCl_3$, 298 K): δ = 191.6, 136.5, 133.2, 133.1, 132.6, 130.5, 129.4, 124.0, 123.8, 120.2, 113.2, 102.3, 54.0, 21.8; elemental analysis (%) calc. for $C_{21}H_{21}AuBr_2N_2$: C, 38.32; H, 3.22; N, 4.26; Found: C, 38.15; H, 3.40; N, 4.01.

[(*Bimz*)Au(I)(2-ethynyl-1,4-bis(2-(triisopropylsilyl)ethynyl)benzene)] (17a)

Following the *general procedure 5*, [*N,N'*-diisopropylbenzimidazolin-2-ylidene]AuCl (**12a**) (100.0 mg, 0.230 mmol) was reacted with 2-ethynyl-1,4-bis(2-(triisopropylsilyl)ethynyl)benzene (**A3**) (138.4 mg, 0.29 mmol) to obtain **17a** as a white solid. Yield: 102.0 mg, 51%; IR (KBr): *ν*(C≡C) 2153.0, 2114.3 cm^{-1}; ESI-MS: *m*/*z* 862.0 $[M+H]^+$, 883.4 $[M+Na]^+$; ^{1}H NMR (500 MHz, $CDCl_3$, 298 K): δ = 7.70 (dt, 2H, *J* = 6.5 Hz, 3.0 Hz, *bimz*-C*H*), 7.60 (s, 1H, aryl-C_6H_3), 7.41 (dt, 2H, *J* = 6.5 Hz, 3.0 Hz, *bimz*-C*H*), 7.23 (dd, 1H, *J* = 6.0, 2.5 Hz, aryl-C_6H_3), 5.52 (sept, 2H, *J* = 7.0 Hz, ^{i}Pr-C*H*), 1.81 (d, 12H, *J* = 7.0 Hz, ^{i}Pr-CH_3), 1.21 (s, 36H, $(CH_3)_3$CHSi), 1.17 (s, 6H, $(CH_3)_3$C*H*Si); ^{13}C NMR (125 MHz, $CDCl_3$, 298 K): δ = 192.0, 137.5, 137.0, 136.2, 135.7, 132.7, 131.1, 129.0, 128.6, 125.6, 123.5, 123.1, 106.3, 102.2, 95.4, 92.3, 27.0, 21.7, 18.7, 18.6, 11.4, 11.3; elemental analysis (%) calc. for $C_{43}H_{63}AuN_2Si_2$: C, 59.98; H, 7.37; N, 3.25; Found: C, 59.12; H, 7.09; N, 3.07.

[(*n-dodecylbimz*)Au(I)(2-ethynyl-1,4-bis(2-(triisopropylsilyl)ethynyl)benzene)] (17b)

Following the *general procedure 5*, [1,3-didodecylbenzimidazol-2-ylidene]AuCl (**12b**) (67.0 mg, 0.097 mmol) was reacted with **A3** (58.7 mg, 0.126 mmol) to obtain **17b** as a white solid. Yield: 65.0 mg, 60%; ESI-MS: *m*/*z* 1136 $[M+Na]^+$; ^{1}H NMR (400 MHz, CD_2Cl_2, 298 K): δ = 7.61 (dd, 1H, *J* = 6.5 Hz, 2.0 Hz, aryl-C_6H_3), 7.53-7.55 (m, 2H, *bimz*-C*H*), 7.45-7.48 (m, 2H, *bimz*-C*H*), 7.40 (d, 1H, *J* = 7.5 Hz, aryl-C_6H_3), 7.23(dd, 1H, *J* = 6.5 Hz, 2.0 Hz, aryl-C_6H_3), 4.54 (t, 4H, *J* = 7.2 Hz, alkyl), 2.02 (quint, 4H, *J* = 7.2 Hz, alkyl), 1.28-1.29 (m, 8H, alkyl), 1.18-1.24 (m, 70H, alkyl and $(CH_3)_3$C*H*Si), 0.90 (t, 6H, *J* = 6.5 Hz, alkyl-CH_3); ^{13}C NMR (100 MHz, CD_2Cl_2, 298 K): δ = 193.4, 136.0, 135.7, 133.4, 132.2, 131.6, 129.1, 128.6, 126.1, 125.5, 124.9, 123.9, 122.9, 111.4, 106.4, 105.4, 104.4, 95.3, 81.5, 48.5, 31.9, 30.1, 29.6, 29.3, 26.8, 22.7, 18.8, 18.4, 13.9, 11.3;

elemental analysis (%) calc. for $C_{61}H_{99}AuN_2Si_2$: C, 65.79; H, 8.96; N, 2.52; Found: C, 65.40; H, 8.80; N, 2.20.

[(*n-dodecylbimz*)Au(I)(1,2,4-triethynylbenzene)] (BM2) *(general procedure 6)*

KF (100.0 mg, 1.72 mmol) was added to the TIPS protected complex (**17b**) (244.0, 0.219 mmol) dissolved in a solvent mixture containing DMF (40.0 mL), THF (4.0 mL) and deionized water (0.3 mL). The reaction mixture was stirred for 12 h at RT. Upon completion of the reaction by TLC, it was diluted with 100.0 mL of deionized water and extracted with 3 x 50.0 mL of Et_2O. The combined organic layers was then dried over anhyd. $MgSO_4$ and concentrated *in vacuo* to obtain a pasty solid, which was triturated with pentane to obtain **BM2** as white solid. Yield: 52.0 mg, 29%; IR (KBr): ν(C≡C) 2151.5, 2112.1 cm^{-1}; ^{1}H NMR (400 MHz, $CDCl_3$, 298 K): δ = 7.71 (d, 1H, *J* = 3.2 Hz, aryl-C_6H_3), 7.46-7.51 (m, 2H, *bimz*-C*H*), 7.42-7.44 (m, 3H, *bimz*-C*H* and aryl-C_6H_3), 7.25-7.28 (dd, 1H, *J* = 6.5, 1.6 Hz, *bimz*-C*H* and aryl-C_6H_3), 4.53 (t, 4H, *J* = 7.5 Hz, alkyl), 3.4 (s, 1H, C≡C*H*), 3.13 (s, 1H, C≡C*H*), 1.97 (quint, 4H, *J* = 7.5 Hz, alkyl), 1.38-1.45 (m, 36H, alkyl), 0.90 (t, 6H, *J* = 6.5 Hz, alkyl-CH_3); ^{13}C NMR (125 MHz, $CDCl_3$, 298 K): δ = 194.3, 139.1, 137.1, 136.6, 134.0, 132.8, 132.7, 131.1, 129.8, 129.6, 127.4, 127.1, 125.4, 124.6, 122.6, 121.4, 111.9, 102.7, 83.6, 82.5, 79.0, 49.2, 32.5, 30.7, 30.2, 30.0, 29.8, 27.4, 23.3, 14.8; elemental analysis (%) calc. for $C_{43}H_{59}AuN_2$: C, 64.48; H, 7.43; N, 3.50; Found: C, 64.72; H, 7.23; N, 3.30.

[(*n-pentyltripimz*)Au(I)(1,4-dibromo-2-ethynylbenzene)] (TM1)

Following the general procedure, 1,3-dipentyl[triptyceneimidazolylidene]AuCl (**16a**) (50.0 mg 0.075 mmol) was reacted with **A1** (19.4 mg, 0.075 mmol) to obtain **TM1** as a white solid. Yield: 35.0 mg, 53%; IR (KBr): ν(C≡C) 2116.1 cm^{-1}; ^{1}H NMR (300 MHz, $CDCl_3$, 298 K): δ = 7.67 (d, 1H, *J* = 2.5 Hz, aryl-C_6H_3), 7.42-7.45 (m, 4H, tript-aryl), 7.39 (d, 1H, *J* = 8.5 Hz, aryl-C_6H_3), 7.13 (d, 1H, *J* = 8.5 Hz, aryl-C_6H_3), 7.03-7.06 (m, 4H, tript-aryl), 5.55 (d, 2H, bridgehead), 4.42 (t, 4H, *J* = 7.5 Hz, alkyl), 1.90 (quint, 4H, *J* = 7.0 Hz, alkyl), 1.30-1.41 (m, 8H, alkyl), 0.91 (t, 6H, *J* = 5.5 Hz, alkyl); ^{13}C NMR (125.5 MHz, CD_2Cl_2, 298 K): δ = 193.4, 146.0, 145.4, 142.4, 138.7, 136.6, 133.5, 131.2, 130.4, 125.9, 124.0, 123.7, 120.6, 107.4, 104.4, 54.1, 48.9, 30.0, 29.0, 26.8, 22.7, 14.1;

elemental analysis (%) calc. for $C_{39}H_{37}AuBr_2N_2$: C, 52.60; H, 4.19; N, 3.15; Found: C, 52.85; H, 4.24; N, 3.09.

[(*n-dodecyltripimz*)Au(I)(1,4-dibromo-2-ethynylbenzene)] (TM2)

Following the *general procedure 5*, 1,3-didodecyl[triptyceneimidazolylidene]AuCl (**16b**) (300.0 mg 0.34 mmol) was reacted with **A1** (108.3 mg, 0.41 mmol) to obtain **TM2** as a white solid. Yield: 131.0 mg, 35%; IR (KBr): ν(C≡C) 2116.6 cm^{-1}; ^{1}H NMR (300 MHz, $CDCl_3$, 298 K): δ = 7.68 (d, 1H, J = 2.5 Hz, aryl-C_6H_3), 7.42-7.44 (m, 4H, tript-aryl), 7.38 (d, 1H, J = 8.5 Hz, aryl-C_6H_3), 7.13 (d, 1H, J = 8.3 Hz, aryl-C_6H_3), 7.03-7.05 (m, 4H, tript-aryl), 5.56 (d, 2H, bridgehead), 4.42 (t, 4H, J = 7.0 Hz, alkyl), 1.90 (quint, 4H, J = 7.0 Hz, alkyl), 1.34-1.64 (m, 36H, alkyl), 0.21 (t, 6H, J = 6.8 Hz, alkyl-CH_3); ^{13}C NMR (75.5 MHz, $CDCl_3$, 298 K): δ = 193.1, 144.4, 142.2, 138.1, 136.6, 133.0, 130.2, 129.4, 125.6, 123.8, 123.7, 120.0, 107.1, 103.6, 54.0, 48.6, 32.0, 30.0, 29.7, 29.6, 29.5, 29.4, 29.3, 29.1, 26.8, 22.7, 14.1; elemental analysis (%) calc. for $C_{53}H_{65}AuBr_2N_2$: C, 58.57; H, 6.03; N, 2.58; Found: C, 58.46; H, 5.98; N, 2.54.

[(*n-dodecyltripimz*)Au(I)(2-ethynyl-1,4-bis(2(triisopropylsilyl)ethynyl)benzene)] (18)

Following the *general procedure 5*, 1,3-didodecyl[triptyceneimidazolylidene]AuCl (**16b**) (201.0 mg, 0.292 mmol) was reacted with **A3** (176.1, 0.38 mmol) to obtain **18** as a pale green solid. 230 mg, 59%; ESI-MS: m/z 1289.8 $[M+H]^+$; ^{1}H NMR (400 MHz, $CDCl_3$, 298 K): δ = 7.64 (d, 1H, J = 3.2 Hz, aryl-C_6H_3), 7.30-7.41 (dd, 1H, J = 5.2, 2.0 Hz, tript-aryl), 7.41 (d, 1H, J = 4.2 Hz, aryl-C_6H_3), 7.10 (d, 1H, J = 4.2 Hz, aryl-C_6H_3), 6.80-6.90 (dd, 4H, J = 5.2, 2.0 Hz, tript-aryl), 4.40 (t, 4H, J = 7.2 Hz, alkyl), 1.8 (quint, 4H, J = 7.5 Hz, alkyl), 1.20-1.31 (m, 36H, alkyl), 1.20 (s, 6H, (CH_3)$_3$CHSi), 1.10 (s, 36H, (CH_3)$_3$CHSi), 0.97 (t, 6H, J = 6.8 Hz, alkyl-CH_3); ^{13}C NMR (75.0 MHz, $CDCl_3$, 298 K): δ = 193.7, 144.5, 142.0, 136.5, 136.4, 136.0, 131.9, 130.8, 128.8, 125.8, 125.6, 123.7, 122.6, 107.1, 106.7, 106.4, 102.6, 95.2, 91.8, 54.1, 54.0, 48.6, 31.9, 30.2, 29.6, 29.3, 26.9, 22.7, 19.0, 18.6, 14.1, 11.5, 11.3; elemental analysis (%) calc. for $C_{75}H_{107}AuN_2Si_2$: C, 69.84; H, 8.36; N, 2.17; Found: C, 69.49; H, 8.05; N, 2.14.

[(*n-dodecyltripimz*)Au(I)(1,2,4-triethynylbenzene)] (TM3)

Following the *general procedure 6*, **19** (13.0 mg, 0.01 mmol) was treated with KF (6.0 mg, 0.001 mmol) in a solvent mixture of DMF (5.0 mL), THF (0.5 mL) and deionized water (0.1 mL) to yield **TM3** as a white solid. Yield: 5.1 mg, 52%; ESI-MS and MALDI-MS: *m*/*z* 977.5 $[M]^+$; IR (KBr): ν(C≡C) 2153.6, 2110.9 cm^{-1}; ^{1}H NMR (500 MHz, $CDCl_3$, 298 K): δ = 7.53 (d, 1H, *J* = 1.5 Hz, aryl-C_6H_3), 7.48 (s, 2H, tript-aryl), 7.43-7.46 (dd, 4H, *J* = 5.5, 2.0 Hz, aryl-C_6H_3), 7.38 (d, 1H, *J* =10.0 Hz, aryl-C_6H_3), 7.23 (d, 1H, *J* =10.0 Hz, aryl-C_6H_3), 7.03-7.05 (dd, 4H, tript-aryl), 5.56 (d, 2H, bridgehead), 4.42 (t, *J* = 7.0 Hz, alkyl), 3.43 (s, 1H, C≡C*H*), 3.20 (s, 1H, C≡C*H*), 1.90 (quint, 4H, *J* = 7.0 Hz, alkyl), 1.64-1.34 (m, 42H, alkyl), 0.21 (t, 6H, *J* = 6.8 Hz, alkyl); ^{13}C NMR (125 MHz, $CDCl_3$, 298 K): δ = 193.7, 145.0, 142.4, 138.5, 136.5, 132.8, 131.2, 129.7, 129.4, 125.9, 124.6, 124.0, 122.4, 107.4, 101.7, 83.2, 83.0, 81.8, 79.0, 54.1, 49.0, 32.2, 30.1 ,29.9, 29.8, 29.7, 29.6, 29.5, 27.0, 23.0, 14.2. Elemental analysis was not performed due to limited availability of the sample; other supporting data are provided in the appendix.

[(*n-dodecylbimz*)Au(I)(2-(4-ethynylphenoxy)ethanol)] (LM)

Following the *general procedure 5*, 1,3-didodecyl[benzimidazolylidene]AuCl (**12b**) (190.0 mg, 0.27 mmol) was reacted with **A5** (62.6 mg, 0.386 mmol) to obtain **LM** as a white solid, Yield: 160.0 mg, 71%; ESI-MS: *m*/*z* 801.5 $[M+H]^+$; IR (KBr): ν(OH) 3438, ν(C≡C) 2115 (w) cm^{-1}; ^{1}H NMR (300 MHz, $CDCl_3$, 298 K): δ = 7.50 (dd, 2H, *J* = 6.0, 3.0 Hz, aryl-C_6H_4), 7.41 (dd, 2H, *J* = 6.0, 3.0 Hz, aryl-C_6H_4), 7.34 (dt, 2H, *J* = 6.5 Hz, 3.0 Hz, *bimz*-C*H*), 6.79 (dt, 2H, *J* = 6.5 Hz, 3.0 Hz, *bimz*-C*H*), 4.51 (t, 4H, *J* = 5.5 Hz, alkyl), 4.05 (t, 2H, *J* = 4.2 Hz, CH_2), 3.91 (t, 2H, *J* = 4.2 Hz, CH_2), 1.96 (quint, 4H, *J* = 5.5 Hz, alkyl), 1.24-1.38 (m, 36H, alkyl), 0.87 (t, 6H, *J* = 6.8 Hz, alkyl); ^{13}C NMR (125.0 MHz, $CDCl_3$, 298 K): δ = 194.6, 157.8, 134.3, 134.2, 132.9, 127.2, 124.5, 119.0, 116.9, 114.6, 113.9, 105.7, 70.0, 69.7, 62.0, 49.2, 32.5, 30.8, 30.2, 30.1, 29.9, 27.4, 23.3, 14.7; elemental analysis (%) calc. for $C_{41}H_{63}AuN_2O_2$: C, 60.58; H, 7.81; N, 3.45; Found: C, 60.34; H, 7.74 ; N, 3.29.

1,3-dipentyl-(4,7-dibromobenzimidazolylidene)Au(I)(1-ethynyl-4-fluorobenzene)] (19)

Following the *general procedure 5*, 1,3-dipentyl[triptyceneimidazolylidene]AuCl (**15)** (25.0 mg 0.038 mmol) was reacted with 1-ethynyl-4-fluorobenzene (7.4 mg, 0.06 mmol) to obtain **19** as a white solid, which was further purified by column chromatography (silica gel, eluent: EtOAc/hexane = 3/1). Yield: 5.0 mg, 17%; IR (KBr): ν(C≡C) 2115.8 cm^{-1}; ^{1}H NMR (500 MHz, $CDCl_3$, 298 K): δ = 7.50 (dd, J = 8.5 Hz, 3.5 Hz, 2H, Ar-H), 7.43 (s, 2H, bimz-C*H*), 6.96 (t, J = 8.5 Hz, 2H, Ar-H), 4.92 (t, 4H, J = 7.5 Hz, alkyl), 1.94 (quint, 4H, J = 7.0 Hz, alkyl), 1.39-1.49 (m, 8H, alkyl), 0.93 (t, 6H, J = 5.5 Hz, alkyl); ^{13}C NMR (125 MHz, $CDCl_3$, 298 K): δ = 198.3, 183.3, 162.5, 160.5, 134.0, 132.5, 130.4, 121.4, 115.1, 104.1, 50.4, 31.9, 28.4, 22.3, 14.0; elemental analysis (%) calc. for $C_{25}H_{28}AuBr_2FN_2 \cdot 1.0$(EtOAc): C, 42.46; H, 4.42; N, 3.41; Found: C, 42.30; H, 4.10; N, 3.35.

[(*Bimz*)Au(I)(pentafluorobenzene)] (20)

Procedure using perfluorophenylboronic acid.

Analogous to the procedure described in reference 38a: **12a** (100.0 mg, 0.23 mmol) was added to suspension containing Cs_2CO_3 (150.0 mg, 0.46 mmol) and perfluorophenylboronic acid (73.0 mg, 0.34 mmol) in dry isopropanol (10.0 mL). The mixture was stirred at 50 °C for 24 h. After cooling, the solvent was evaporated under vacuum and the residue was extracted with toluene, filtered over celite and concentrated. The residue was triturated with pentane and re-extracted into toluene after concentration. Vapor diffusion of pentane resulted in the precipitation of **20** as white solid. Yield: 84.0 mg, 65%; UV-vis [λ (nm), CH_2Cl_2, RT]: 282, 289; ^{1}H NMR (500 MHz, $CDCl_3$, 298 K): δ = 7.67 (dt, J = 9.5 Hz, 3.0 Hz, 2H, *bimz*-C*H*), 7.37 (dt, J = 9.5 Hz, 3.0 Hz, 2H, *bimz*-C*H*), 5.60 (sept, J = 7.0 Hz, 2H, ^{i}Pr-C*H*), 1.85 (d, J = 8.5 Hz, 12H, ^{i}Pr-CH_3); ^{13}C NMR (125.0 MHz, $CDCl_3$, 298 K): δ = 192.8, 149.5 (dm, $^{1}J_{C\text{-}F}$ = 250.0 Hz), 138.5 (dm, $^{1}J_{C\text{-}F}$ = 250.0 Hz), 137.0 (dm, $^{1}J_{C\text{-}F}$ = 250.0 Hz), 132.8, 123.8, 112.6, 53.0, 22.4; ^{19}F NMR (282 MHz, $CDCl_3$, 298 K): -117.4 (d, 2F, $^{3}J_{F\text{-}F}$ = 20.5 Hz, *o*-C_6F_5), -161.4 (t, 1F, $^{3}J_{F\text{-}F}$ = 20.2 Hz, *p*-

C_6F_5), -164.6 (t, 2F, $^3J_{F\text{-}F}$ = 20.4 Hz, *m*-C_6F_5); elemental analysis (%) calc. for $C_{19}H_{18}AuF_5N_2$: C, 40.30; H, 3.20; N, 4.95; Found: C, 40.05; H, 3.17; N, 4.82.

Alternate procedure by lithiation.

Pentafluorophenyl iodide (67.7 mg, 0.23 mmol) in Et_2O (5.0 mL), was lithiated using *n*-BuLi (1.6 M in hexanes) (14.7 mg, 0.23 mmol) at -78 °C and was stirred for 20 min before transferring into a RB-flask containing **12a** (100.0 mg, 0.23 mmol). The mixture was then allowed to rise to RT and stirred for 1 h before quenching with water. Extraction of the crude mass with CH_2Cl_2 (3 x 10.0 mL) and washing with deionized water gave **23** as a white solid. Yield: 95.0 mg, 73%.

[(*Bimz*)Au(III)I_2(pentafluorobenzene)] (21)

To a chloroform (20.0 mL) solution of **20** (100.0 mg, 0.17 mmol), was added I_2 (24.0 mg, 0.187 mmol) and stirred for 5 h at RT. The solvent was removed *in vacuo* and the residue was washed with hexane (4 x 15.0 mL). Purification by flash column chromatography (silica gel, eluent: EtOAc/hexane = 1/3) yielded **21** as a red crystalline solid. Yield: 110.0 mg, 69%; UV-vis [λ (nm), CH_2Cl_2, RT]: 271, 280, 311, 362; ^{1}H NMR (500 MHz, $CDCl_3$, 298 K): δ = 7.64 (dt, *J* = 9.5 Hz, 3.0 Hz, 2H, *bimz*-C*H*), 7.31 (dt, *J* = 9.5 Hz, 3.0 Hz, 2H, *bimz*-C*H*), 5.14 (sept, *J* = 7.0 Hz, 2H, ^{i}Pr-C*H*), 1.72 (d, *J* = 7.0 Hz, 12H, ^{i}Pr-CH_3); ^{13}C NMR (100 MHz, $CDCl_3$, 298 K): δ = 162.6, 146.04 (dm, $^1J_{C\text{-}F}$ = 227.0 Hz), 140.4 (dm, $^1J_{C\text{-}F}$ = 245.0 Hz), 137.7 (dm, $^1J_{C\text{-}F}$ = 251.2 Hz), 134.2, 124.6, 114.6, 54.5, 21.0; ^{19}F NMR (282 MHz, $CDCl_3$, 298 K): -121.3 (d, 2F, $^3J_{F\text{-}F}$ = 21.3 Hz, *o*-C_6F_5), -159.6 (t, 1F, $^3J_{F\text{-}F}$ = 20.0 Hz, *p*-C_6F_5), -164.0 (t, 2F, $^3J_{F\text{-}F}$ = 20.0 Hz, *m*-C_6F_5); elemental analysis (%) calc. for $C_{19}H_{18}AuF_5I_2N_2$; C, 27.83; H, 2.21; N, 3.42. Found: C, 27.15; H, 2.02; N, 3.13.

[(*Bimz*)Au(I)(C≡N)] (22)

n-Bu_4NCN (67.0 mg, 0.25 mmol) was added to a solution of **12a** (100.0 mg, 0.23 mmol) in CH_2Cl_2 (10.0 mL) and was stirred for 10 h at RT. Deionized water (15.0 mL) was added to the reaction mixture and was extracted with CH_2Cl_2 (2 x 15.0 mL), the combined organic layers were then dried *in vacuo* and the residue was triturated with pentane (15.0 mL) to yield the crude product as an off-white solid which further purified

by column chromatography (silica gel, eluent: EtOAc). Yield: 70.0 mg, 71%; UV-vis [λ (nm), CH_2Cl_2, RT]: 279, 288; IR (KBr): ν(C≡C): 2144 cm^{-1}; ^{1}H NMR (500 MHz, $CDCl_3$, 298 K): δ = 7.63 (dt, 2H, *J* = 6.5 Hz, 3.0 Hz, *bimz*-C*H*), 7.40 (dt, 2H, *J* = 6.5 Hz, 3.0 Hz, *bimz*-C*H*), 5.60 (sept, *J* = 7.0 Hz, 2H, ^{i}Pr-C*H*), 1.78 (d, 12H, *J* = 7.0 Hz, ^{i}Pr-CH_3); ^{13}C NMR (125 MHz, $CDCl_3$, 298 K): δ = 187.0, 152.0, 132.5, 124.2, 113.0, 53.8, 22.2; elemental analysis (%) calc. for $C_{14}H_{18}AuN_3$: C, 39.54; H, 4.27; N, 9.88; Found: C, 39.68; H, 4.32; N, 9.59.

[(*Bimz*)Au(III)I_2(C≡N)] (23)

Following the procedure as described for **21**; I_2 (60.0 mg, 0.47 mmol) was reacted with **22** (100.0, 0.23 mmol) to yield **23** as a red solid after purification. Yield: 71.0 mg, 74%; UV-vis [λ (nm), CH_2Cl_2, RT]: 271, 376; IR (KBr): ν(C≡C): 2171.2 cm^{-1}; ^{1}H NMR (500 MHz, $CDCl_3$, 298 K): δ = 7.77 (dt, 2H, *J* = 6.5 Hz, 3.0 Hz, *bimz*-C*H*), 7.45 (dt, 2H, *J* = 6.5 Hz, 3.0 Hz, *bimz*-C*H*), 5.01 (sept, *J* = 7.0 Hz, 2H, ^{i}Pr-C*H*), 1.78 (d, 12H, *J* = 7.0 Hz, ^{i}Pr-CH_3); ^{13}C NMR (125 MHz, $CDCl_3$, 298 K): δ = 147.1, 133.4, 124.5, 114.2, 109.8, 54.5, 20.0; elemental analysis (%) calc. for $C_{14}H_{18}AuI_2N_3$: C, 24.76; H, 2.67; N, 6.19; Found: C, 24.48; H, 2.82; N, 6.04.

[(*Bimz*)Au(I)(2-(4-ethynylphenyl)ethynyl)triisopropylsilane)] (24)

Following the *general procedure 5*, **12a** (100.0 mg, 0.23 mmol) was reacted with (2-(4-ethynylphenyl)ethynyl)triisopropylsilane (71.4 mg, 0.25 mmol) to obtain **24** as a white solid. Yield: 129.0 mg, 82%; IR (KBr): ν(C≡C): 2112.0, 2150.1 cm^{-1}; ^{1}H NMR (500 MHz, $CDCl_3$, 298 K): δ = 7.48 (dt, 2H, *J* = 6.0 Hz, 3.0 Hz, *bimz*-C*H*), 7.28-7.30 (m, 1H, C_6H_4), 7.18-7.21 (m, 3H, *bimz*-C*H* and C_6H_4), 7.10 (s, 2H, C_6H_4), 5.40 (sept, *J* = 7.0 Hz, 2H, ^{i}Pr-C*H*), 1.57 (d, 12H, *J* = 7.0 Hz, ^{i}Pr-CH_3), 0.97 (s, 3H, $(CH_3)_3$C*H*Si), 0.96 (s, 18H, $(CH_3)_3$CHSi); ^{13}C NMR (125 MHz, $CDCl_3$, 298 K): δ = 191.9, 132.6, 132.1, 131.9, 131.6, 129.9, 125.6, 123.6, 121.3, 113.1, 107.3, 105.6, 91.3, 79.9, 53.9, 21.9, 18.7, 11.3; elemental analysis (%) calc. for $C_{32}H_{43}AuN_2Si$: C, 56.46; H, 6.37; N, 4.12; Found: 56.64; H, 6.32; N, 4.04.

[(*Bimz*)Au(I)(1,4-diethynylbenzene] (25)

Following the *general procedure 6*, **24** (50.0 mg, 0.073 mmol) was treated with KF (20.0 mg, 0.34 mmol) in a solvent mixture of DMF (10.0 mL) and deionized water (0.1 mL) to yield **25** as white solid. Yield: 32.0 mg, 83%; ν(C≡C): 2114, 2101 cm^{-1}; ^{1}H NMR (500 MHz, $CDCl_3$, 298 K): δ = 7.55 (dt, 2H, *J* = 6.0 Hz, 3.0 Hz, *bimz*-C*H*), 7.36-7.38 (m, 1H, C_6H_4), 7.25-7.27 (m, 3H, *bimz*-C*H* and C_6H_4), 7.10 (s, 2H, C_6H_4), 5.47 (sept, *J* = 7.0 Hz, 2H, ^{i}Pr-C*H*), 3.01(s, 1H, C≡C*H*), 1.63 (d, 12H, *J* = 7.0 Hz, ^{i}Pr-CH_3); ^{13}C NMR (125 MHz, $CDCl_3$, 298 K): δ = 191.8, 132.6, 132.2, 131.7, 130.4, 126.2, 123.6, 119.7, 113.1, 105.3, 83.9, 77.9, 53.9, 21.1; elemental analysis (%) calc. for $C_{23}H_{23}AuN_2$: C, 52.68; H, 4.42; N, 5.34; Found: C, 52.30; H, 4.14; N, 5.20.

Preparation of the triptycene based oligomer (OL1)

TM2 (35.0 mg, 0.032 mmol), 1,4-bis(dodecyloxy)-2,5-diethynylbenzene (16.57 mg, 0.033 mmol), CuI (0.1 mg) and $Pd(PPh_3)_4$ (1.1 mg, 0.951 μM) were placed in a Schlenk tube equipped with a stir bar, the flask was evacuated and backfilled with N_2 before the addition of degassed toluene/diisopropylamine (2:1, *v/v*, 8.0 mL) under N_2 atmosphere. The tube was sealed and heated at 65 °C for 3 days. The reaction mixture was then cooled to RT and the solvents were evaporated under reduced pressure. The residue was diluted with CH_2Cl_2 (10.0 mL) and washed with water and satd. NH_4Cl followed by brine. The organic layer was then dried over anhyd. Na_2SO_4 and solvent concentrated under vacuum. The residue was dissolved in minimum amount of chloroform and reprecipitated in methanol successively for three times to yield **OL1** as a green solid. Yield: 20.0 mg (33%); ^{1}H NMR (500 MHz, $CDCl_3$, 298 K): δ = 7.61-7.62 (m, 2H, phenyl-*H*), 7.28-7.36 (m, 9H, tript and phenyl-*H*), 7.28-7.31 (m, 2H, phenyl-*H*), 6.91-6.98 (m, 9H, tript and phenyl-*H*), 6.83-6.87 (m, 2H, phenyl-*H*), 5.42 (s, 2H, bridgehead), 4.33-4.36 (m, alkyl), 3.88-3.94 (m, 12H, alkyl), 1.17-1.83 (m, 17H, alkyl), 1.10-1.20 (m, 90H, alkyl), 0.75-0.80 (m, 30H, alkyl); UV-vis [λ (nm), CH_2Cl_2, RT]: 307, 410.

6.0 APPENDIX (Chapter 6).

6.1 X-ray diffraction details

Relevant details about the structure refinements are given in Tables A1, A2 and A3, and selected geometrical parameters are included in the captions of the corresponding figures. Intensity data were collected at 183(2) K an Oxford Xcalibur diffractometer (4-circle kappa platform, Ruby CCD detector, and a single wavelength Enhance X-ray source with MoK_α radiation, λ = 0.71073 Å).[43] The selected suitable single crystals were mounted using polybutene oil on the top of a glass fiber fixed on a goniometer head and immediately transferred to the diffractometer. Pre-experiment, data collection, data reduction and analytical absorption corrections[44] were performed with the Oxford program suite *CrysAlisPro*.[45] The crystal structures were solved with SHELXS-97[46] using direct methods. The structure refinements were performed by full-matrix least-squares on F^2 with SHELXL-97.[46] All programs used during the crystal structure determination process are included in the WINGX software.[47] The program PLATON[48] was used to check the result of the X-ray analyses.

In **3a** the molecule lies on a center of inversion which led to refine only half of the atoms. One of the isopropyl group was refined as positionally disordered. In the case of **4**, one solvent molecule (CH_2Cl_2) co-crystallized with the platinum species in a ratio 1:1. The Pd center in **9** was found to be located on a center of inversion. The Br ligands are disordered over two positions with *sof* of 0.538 (11) and 0.462 (11), one C_5H_{12} chain is disordered at 80% over two sets of sites with *sof* of 0.646 (8) and 0.354 (8), the terminal CH_3 group of the second C_5H_{12} chain is disordered over two positions with *sof* of 0.791 (19) and 0.209 (19), while the solvent molecule of CH_2Cl_2 is disordered over two sets of positions with *sof* of 0.289 (9) and 0.211 (9). Many restraints (126) had to be used to correct the geometry of the disordered components (DFIX) and the anisotropic thermal parameters of the corresponding non-H atoms (SIMU). The crystal lattice of **21** was found to contain two crystallographically independent molecules in the asymmetric unit. For all the moleules, the hydrogen positions were calculated after each cycle of refinement using a riding model, with C-H = 0.93 Å and U_{iso}(H) = 1.2U_{eq}(C) for aromatic H atoms, with C-H = 0.98 Å and U_{iso}(H) = 1.2U_{eq}(C) for methine H atoms,

with C-H = 0.97 Å and U_{iso}(H) = 1.2U_{eq}(C) for methylene H atoms, and C-H = 0.96 Å and U_{iso}(H) = 1.5U_{eq}(C) for methyl H atoms and with N-H = 0.86 Å and U_{iso}(H) = 1.2U_{eq}(N).

Table A1. Crystallographic data for compounds **3a**, **4** and **9.**

	3a	**4**	**9**
empirical formula	C_{42} H_{46} N_4 Pd	C_{26} H_{24} Cl_2 N_4 Pt	C_{62} H_{68} Br_2 N_4 Pd, C H_2 Cl_2
formula weight (g·mol^{-1})	713.23	658.47	1220.33
temperature (K)	183(2)	183(2)	183(2)
wavelength (Å)	0.71073	0.71073	0.71073
crystal system, space group	Monoclinic, *P* 21/c	Orthorhombic, *P* n a 21	Monoclinic, *P* 21/c
a (Å)	11.4324(3)	15.9627(2)	17.3468(7)
b (Å)	7.8076(2)	13.3843(1)	12.8200(7)
c (Å)	21.7470(6)	11.5235(1)	15.9441(8)
α (deg)	90	90	90
β (deg)	104.914(3)	90	104.466(5)
γ (deg)	90	90	90
volume (Å^3)	1875.74(9)	2461.99(4)	3433.3(3)
Z, density (calcd) (Mg·m^{-3})	2, 1.263	4, 1.777	2, 1.180
abs coefficient (mm^{-1})	0.528	5.938	1.547
F(000)	744	1280	1252
crystal size (mm^3)	0.15 x 0.11 x 0.05	0.26 x 0.15 x 0.09	0.22 x 0.15 x 0.05
θ range (deg)	2.78 to 26.37	2.33 to 30.51	2.56 to 25.00
reflections collected	15500 3776	30852	19428
reflections unique	3776 [R(int) = 0.0562]	7390 [R(int) = 0.0523]	6033 [R(int) = 0.0623]
completeness to *θ* (%)	98.4	100.0	99.7
absorption correction	Analytical	Analytical	Analytical
max/min transmission	0.98 and 0.95	0.63 and 0.36	0.933 and 0.770
data / restraints / parameters	3776 / 3 / 248	7390 / 1 / 300	3093 / 126 / 427
goodness-of-fit on F^2	0.946	0.953	1.015
final R_1 and wR_2 indices [$I > 2\sigma(I)$]	0.0377, 0.0647	0.0224, 0.0454	0.0892, 0.2368
R_1 and wR_2 indices (all data)	0.0815, 0.0722	0.0294, 0.0464	0.1658, 0.2940
Largest diff. peak and hole (e/Å^3)	0.344/ -0.377	1.075/ -0.575	0.853/ -0.898

The unweighted R-factor is $R_1 = \sum(Fo - Fc)/\sum Fo$; $I > 2\ \sigma(I)$ and the weighted R-factor is $wR_2 = \{\sum w(Fo^2 - Fc^2)^2/\sum w(Fo^2)^2\}^{1/2}$

Table A2. Crystallographic data for compounds **12b**, **IMP1** and **20.**

	12b	**IMP1**	**20**
empirical formula	C_{31} H_{54} Au Cl N_2	2(C_{78} H_{100} Au N_4), C_5 H_{12}, 2(C H Cl_3), 2(Au Cl_2)	$C_{19}H_{18}AuF_5N_2$
formula weight ($g \cdot mol^{-1}$)	687.18	3427.81	566.32
temperature (K)	183(2)	183(2)	183(2)
wavelength (Å)	0.71073	0.71073	0.71073
crystal system, space group	Triclinic, *P* -1	Triclinic, *P* -1	Monoclinic, *P*21/n
a (Å)	9.1423(2)	12.9177(4)	12.2833 (2)
b (Å)	9.7408(2)	18.8328(6)	9.8200 (2)
c (Å)	19.7946(5)	19.6647(6)	16.2597 (3)
α (deg)	93.707(2)	65.095(3)	90
β (deg)	93.280(2)	75.177(3)	106.546 (2)
γ (deg)	113.576(2)	71.550(3)	90
volume ($Å^3$)	1605.59(6)	4074.1(2)	1880.06 (6)
Z, density (calcd) ($Mg \cdot m^{-3}$)	2, 1.421	1, 1.397	4, 2.001
abs coefficient (mm^{-1})	4.685	3.803	7.88
F(000)	700	1734	1080
crystal size (mm^3)	0.34 x 0.16 x 0.10	0.25 x 0.11 x 0.09	0.43 x 0.37 x 0.03
θ range (deg)	2.56 to 26.37	2.46 to 25.35	2.6 to 32.7
reflections collected	22805	37956	19303
reflections unique	6575 / [R(int) = 0.0456]	14879 / [R(int) = 0.0703]	5737 / [R(int) = 0.049]
completeness to *θ* (%)	99.9	99.9	99.9
absorption correction	Analytical	Analytical	Analytical
max/min transmission	0.685 and 0.377	0.775 and 0.576	0.113 and 0.782
data / restraints / parameters	5533 / 0 / 318	10345 / 140 / 905	5737 / 0 / 248
goodness-of-fit on F^2	1.046	1.040	1.040
final R_1 and wR_2 indices [$I > 2\sigma(I)$]	0.0432, 0.1139	0.0722, 0.1558	0.028
R_1 and wR_2 indices (all data)	0.0506, 0.1158	0.1123, 0.1758	0.063
Largest diff. peak and hole ($e/Å^3$)	2.847/ -1.237	3.835/ -1.875	2.06/ -1.31

The unweighted R-factor is $R_1 = \sum(Fo - Fc)/\sum Fo$; $I > 2\ \sigma(I)$ and the weighted R-factor is $wR_2 = \{\sum w(Fo^2 - Fc^2)^2/\sum w(Fo^2)^2\}^{1/2}$

Table A3. Crystallographic data for compounds **21**, **22** and **23**

	21	**22**	**23**
empirical formula	$C_{19}H_{18}AuF_5I_2N_2$	$C_{14}H_{18}AuN_3$	$4(C_{14}H_{18}AuI_2N_3)$, CH_2Cl_2
formula weight ($g \cdot mol^{-1}$)	820.12	425.28	5602.50
temperature (K)	183(2)	183(2)	183(2)
wavelength (Å)	0.71073	0.71073	0.71073
crystal system, space group	Orthorhombic, *A* b a 2	Monoclinic, *P* 21/n	Tetragonal, *P* 43 21 2
a (Å)	14.7212(1)	9.8821(1)	9.20500(10)
b (Å)	41.3918(3)	7.7641(1)	9.20500(10)
c (Å)	14.9026(1)	19.3338(3)	48.6998(11)
α (deg)	90	90	90
β (deg)	90	98.871(1)	90
γ (deg)	90	90	90
volume ($Å^3$)	9080.71(11)	1465.65(3)	4126.43(13)
Z, density (calcd) ($Mg \cdot m^{-3}$)	16, 2.400	4, 1.927	1, 2.255
abs coefficient (mm^{-1})	9.248	10.024	10.185
F(000)	6016	808	2548
crystal size (mm^3)	0.37 x 0.19 x 0.06	0.36 x 0.16 x 0.03	0.12 x 0.12 x 0.06
θ range (deg)	2.73 to 30.51	2.48 to 28.28	2.54 to 29.56
reflections collected	81425	20745	37024
reflections unique	13746 / [R(int) = 0.0369]	3638 / [R(int) = 0.0364]	5789 / [R(int) = 0.0490]
completeness to *θ* (%)	99.9	99.9	99.9
absorption correction	Analytical	Analytical	Analytical
max/min transmission	0.645 and 0.138	0.927 and 0.532	0.557 and 0.404
data / restraints / parameters	12094 / 1 / 531	3049 / 0 / 167	5191 / 5 / 213
goodness-of-fit on F^2	1.040	1.081	1.132
final R_1 and wR_2 indices [$I > 2\sigma(I)$]	0.0192, 0.0402	0.0323, 0.0773	0.0314, 0.0733
R_1 and wR_2 indices (all data)	0.0241, 0.0409	0.0410, 0.0796	0.0380, 0.0759
Absolute structure parameter	-0.0018(18).	-	-0.004(6)
Largest diff. peak and hole ($e/Å^3$)	0.770/ -0.841	4.102/ -2.343	1.055 and -1.058

The unweighted R-factor is $R_1 = \sum(Fo - Fc)/\sum Fo$; $I > 2\,\sigma(I)$ *and the weighted R-factor is* $wR_2 = \{\sum w(Fo^2 - Fc^2)^2/\sum w(Fo^2)^2\}^{1/2}$

6.2 NMR spectroscopic details of TM3.

^{1}H NMR and ^{13}C NMR spectra recorded in CD_2Cl_2 (293 K).

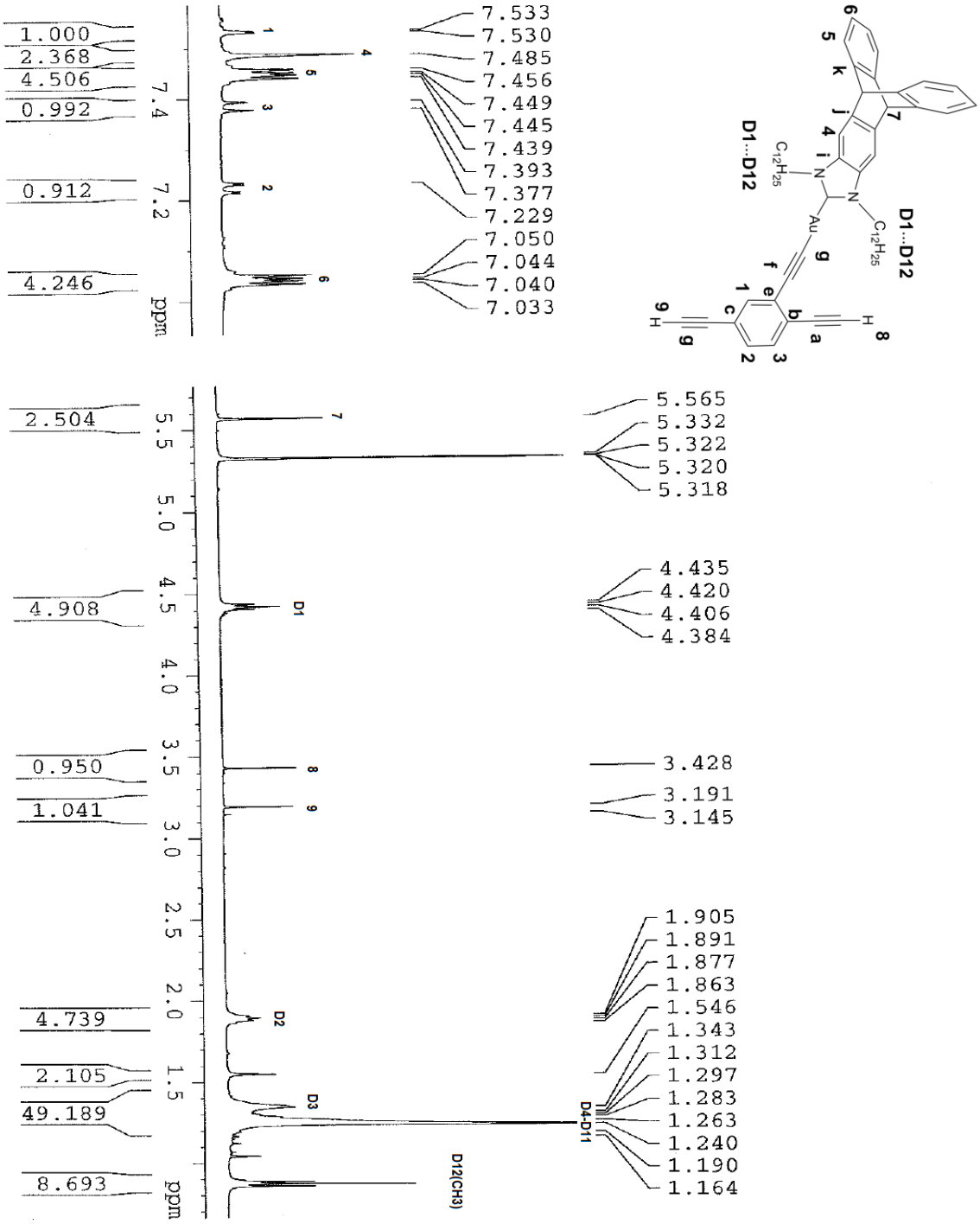

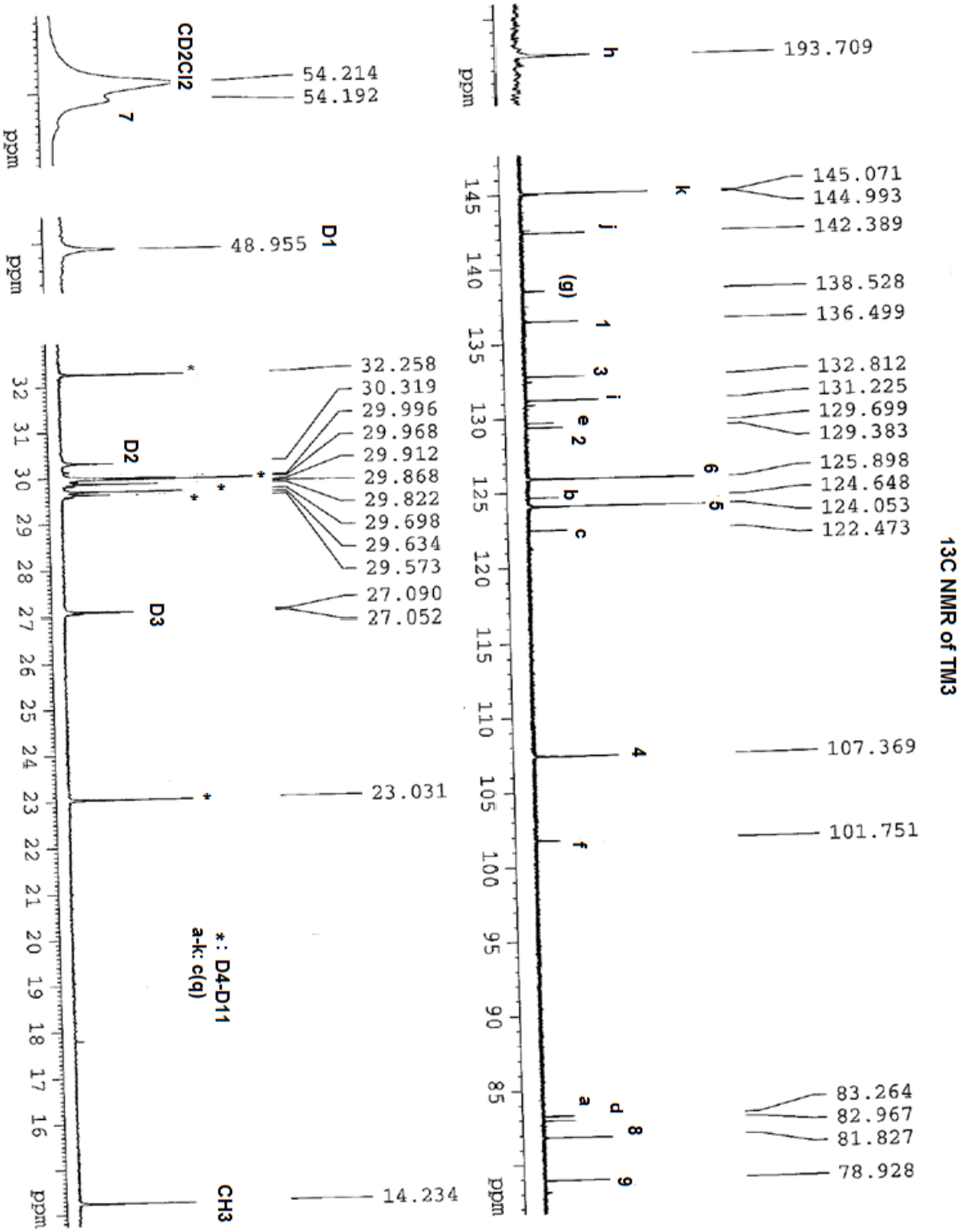
13C NMR of TM3
193.709
145.071
144.993
142.389
138.528
136.499
132.812
131.225
129.699
129.383
125.898
124.648
124.053
122.473
107.369
101.751
83.264
82.967
81.827
78.928
54.214
54.192
48.955
32.258
30.319
29.996
29.968
29.912
29.868
29.822
29.698
29.634
29.573
27.090
27.052
23.031
14.234
CD2Cl2
D1
D2
D3
CH3
*: D4-D11
a-k: c(q)
ppm

^{1}H-COSY spectra recorded in CD_2Cl_2 (293 K)

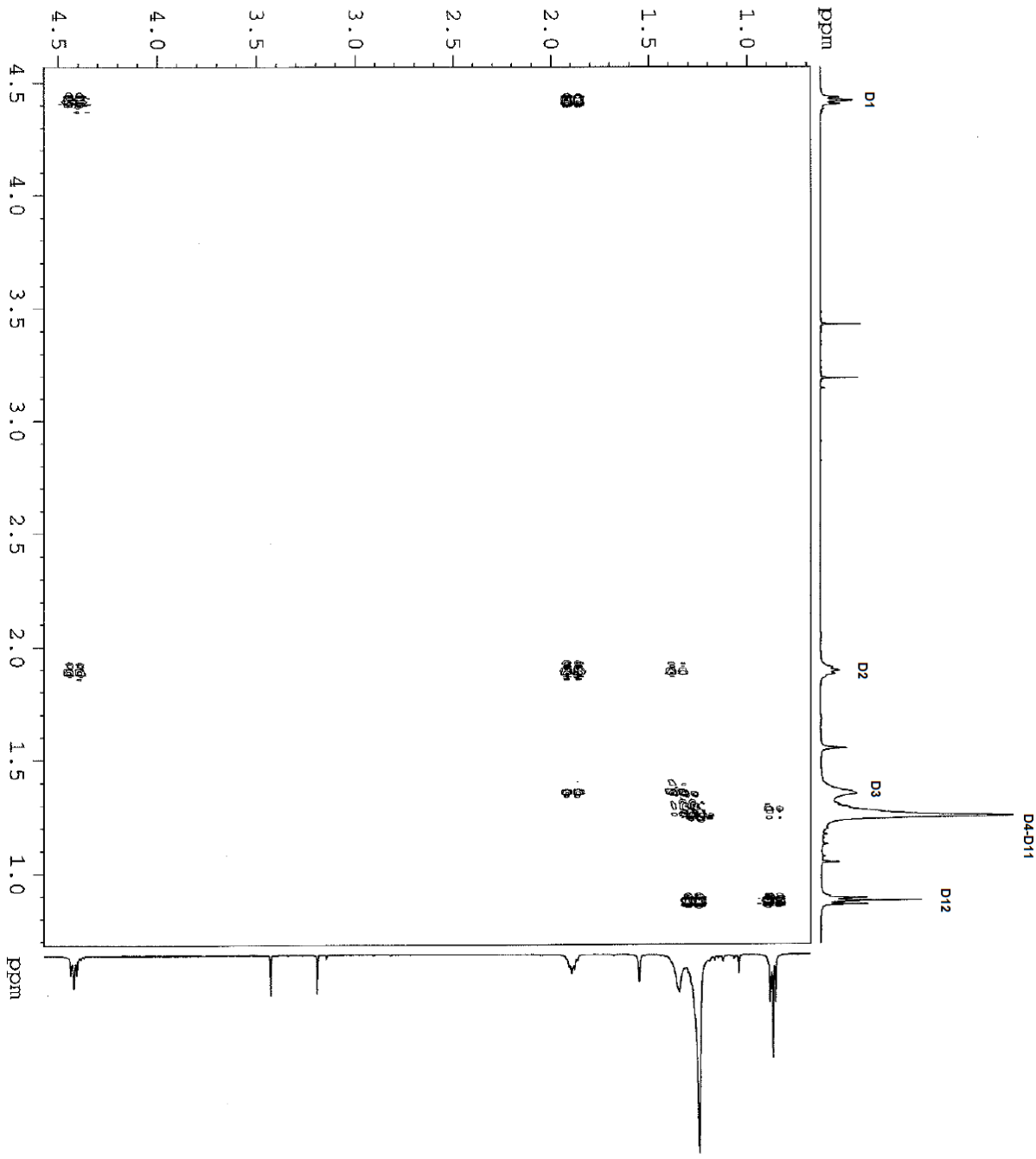

C, H-Correlation spectra in CD_2Cl_2 (293 K)

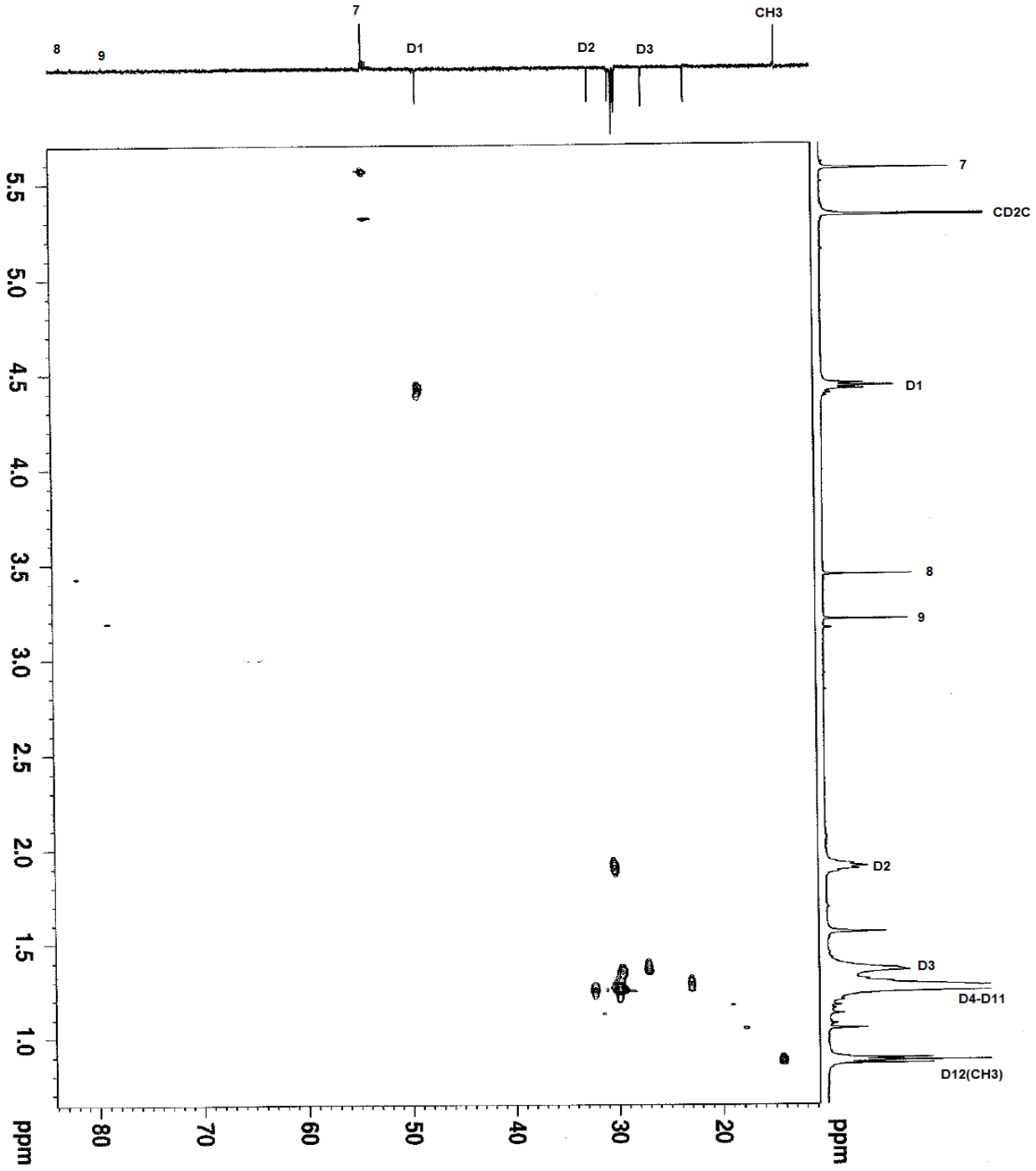

6.3 Mass spectrometry details of TM3

Positive ESI-MS spectrum.

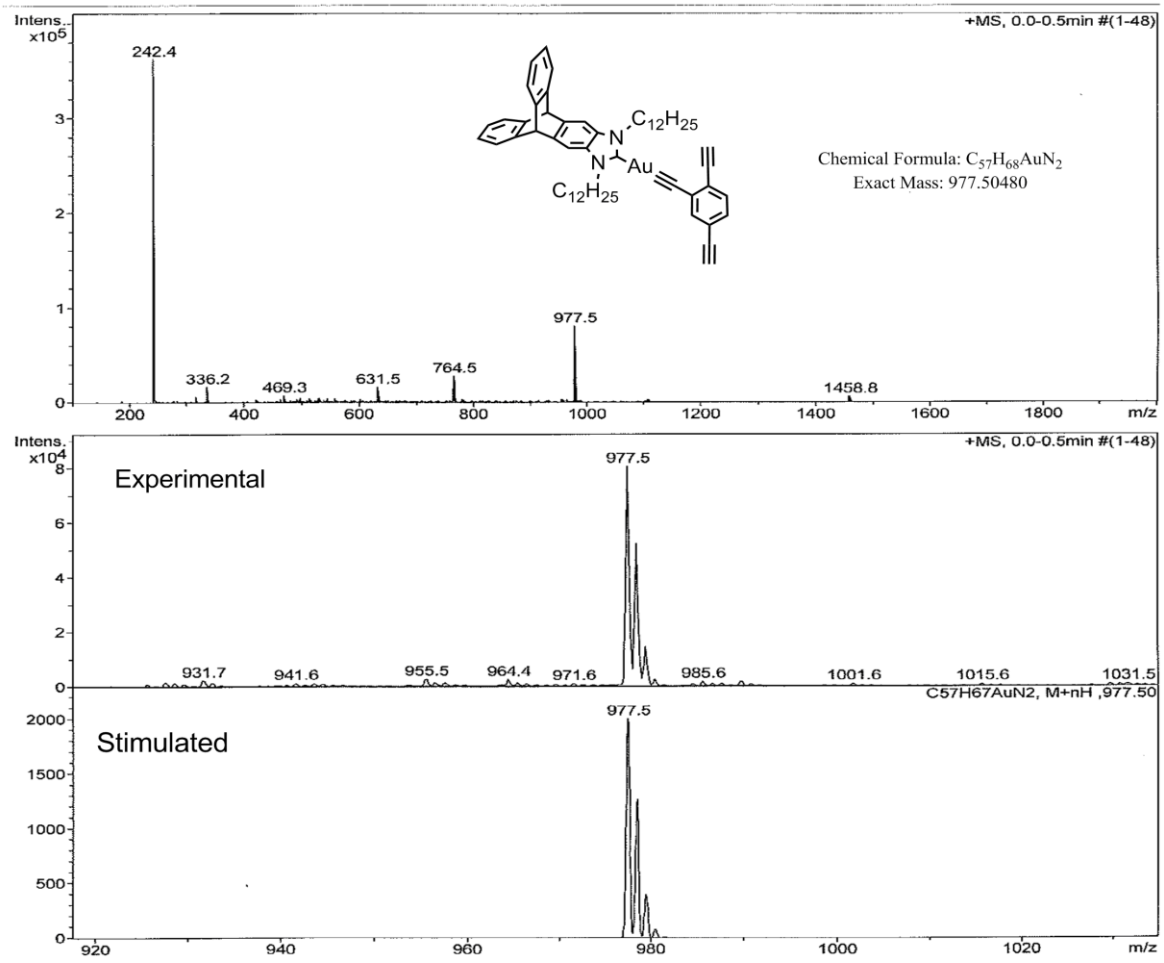

MALDI-TOF spectrum.

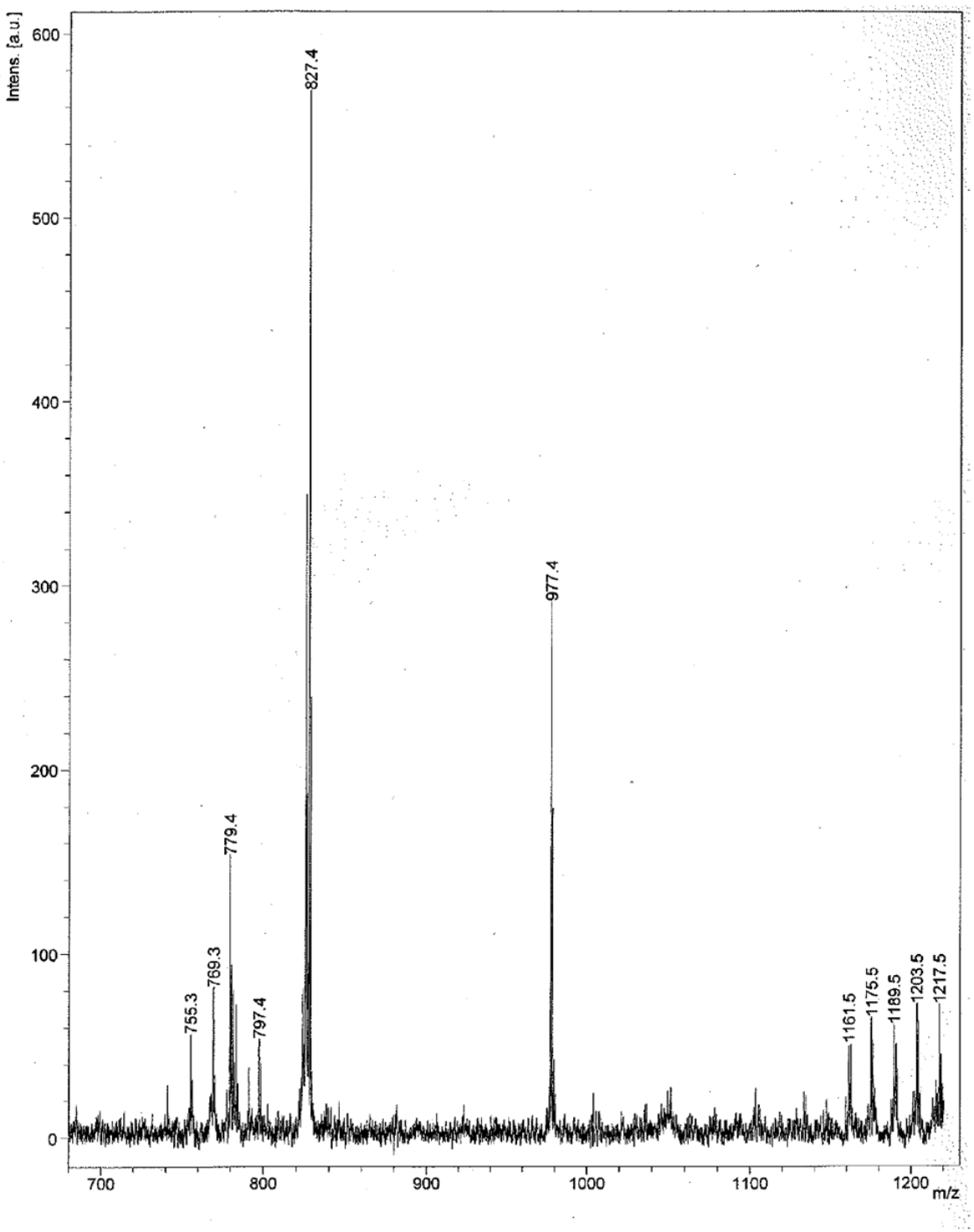

6.4 NMR spectroscopic details of OL1

^1H NMR spectra recorded in CD_2Cl_2 (293 K).

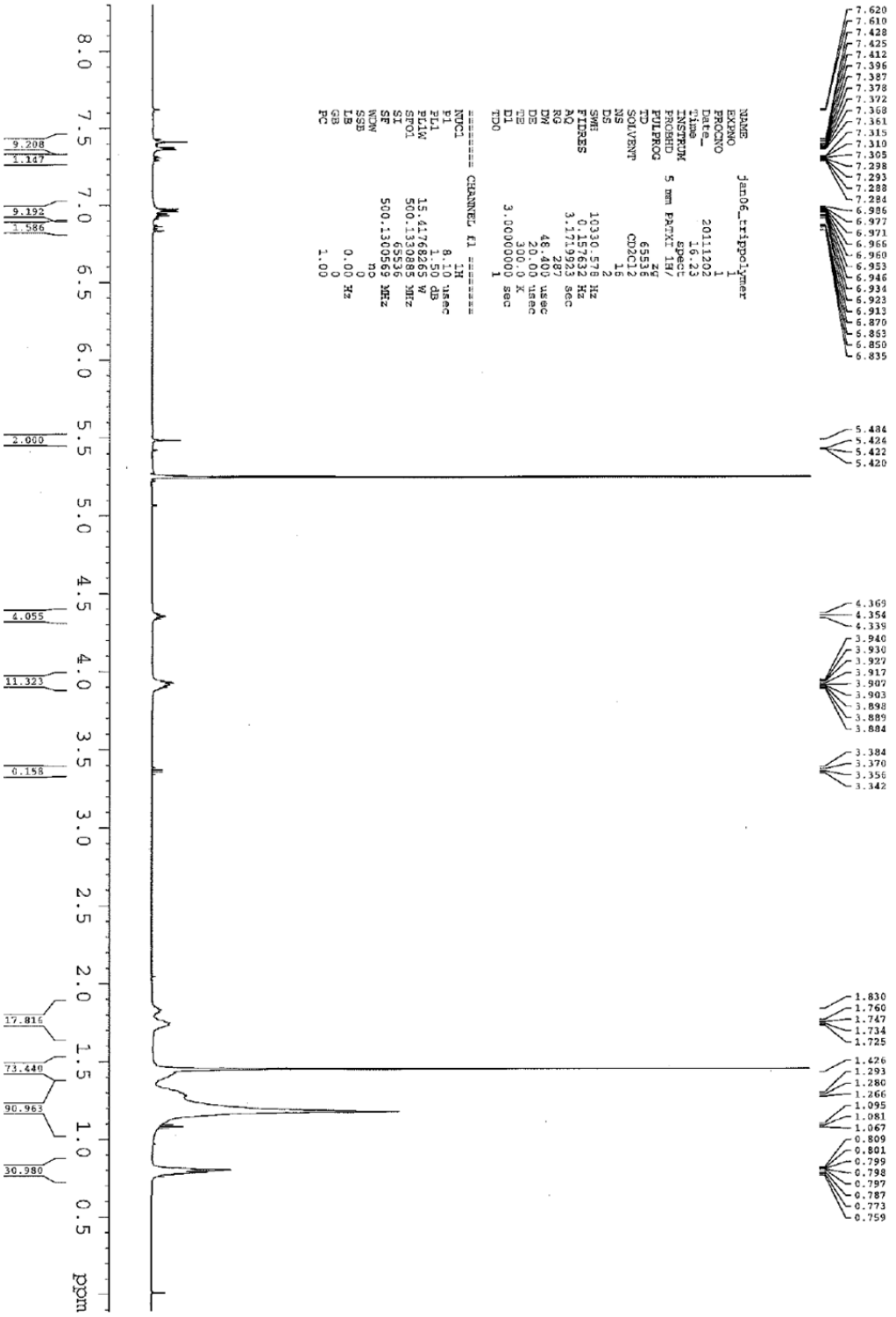

7.0 References

[1] (a) Balzani, V.; Carassiti, V. In *Photochemistry of Coordination Compounds*; Academic Press: New York, 1970. (b) *Concepts of Inorganic Photochemistry*; Adamson, A.W.; Fleischauer, P.D. Eds.; Wiley Interscience: New York, 1975. (c) Porter, G. B. *J. Chem. Educ.* **1983**, *60* (10), 785. (d) Hoffman, M. Z. *J. Chem. Educ.* **1983**, *60* (10), 784. (e) Roundhill, D. M. In *Photochemistry and Photophysics of Metal Complexes (Modern Inorganic Chemistry)*; Plenum press: 1994.

[2] (a) Rabek, J. F. In *Mechanisms of photophysical processes and photochemical reactions in polymers: theory and applications*; Wiley: 1987. (b) Turro, N. J. In *Modern molecular photochemistry*; Benjamin-Cummings: Menlo Park, CA, 1978. (c) Guillet, J. E. In *Polymer Photophysics and Photochemistry*; Cambridge University Press: 1985. (d) Lakowicz, J. R. In *Principles of Fluorescence Spectroscopy*; Springer: 2006.

[3] Archer, R. D. In *Inorganic and Organometallic polymers*; John Wiley and Sons: 2001.

[4] (a) Paquet, C.; Cyr, P. W.; Kumacheva, E.; Manners, I. *Chem. Mat.* **2004**, *16* (24), 5205. (b) Amer, W. A.; Wang, L.; Amin, A. M.; Ma, L. A.; Yu, H. J. *J. Inorg. Organomet. Polym.* **2010**, *20* (4), 605.

[5] Choffat, F.; Kaeser, S.; Wolfer, P.; Schmid, D.; Mezzenga, R.; Smith, P.; Caseri, W. *Macromolecules* **2007**, *40* (22), 7878.

[6] (a) Manners, I. *Angew. Chem., Int. Ed. Engl.* **1996**, *35* (15), 1603. (b) *Frontiers in Transition Metal-Containing Polymers*; Abd-El-Aziz, A. S., Manners, I., Eds.; John Wiley and Sons: 2007.

[7] *Photophysics and Photochemistry of Metal-containing polymers*; Abd-El-Aziz, A S.; Carraher, C. E.; Harvey, P. D.; Pittman, C. U., Zeldin, M., Eds.; John Wiley and Sons, 2007.

[8] (a) Sonogashira, K.; Fujikura, Y.; Yatake, T.; Toyoshima, N.; Takahashi, S.; Hagihara, N. *J. Organomet. Chem.* **1978**, *145*, 101. (b) Hagihara, N.; Sonagashira,

K.; Takahashi, S. *Adv. Polym. Sci.* **1980**, 40, 149. (c) Nast, R. *Coord. Chem. Rev.* **1982**, *47* (1-2), 89.

[9] (a) Hay, A. S.; Blanchard, H. S.; Endres, G. F.; Eustance, J. W. *J. Am. Chem. Soc.* **1959,** *81* (23), 6335. (b) Hay, A. S. *J. Polym. Sci.* A-1, **1969**, *7*, 1625.

[10] (a) Takahashi, S.; Murata, E.; Sonogashira, K.; Hagihara, N. *J. Polym. Sci. Polym. Chem. Educ.* **1980**, *18* (2), 661. (b) Sonogashira, K.; Ohga, K.; Takahashi, S.; Hagihara, N. *J. Organomet. Chem.* **1980**, *188* (2), 237.

[11] Lavastre, O.; Even, M.; Dixneuf, P. H.; Pacreau, A.; Vairon, J. P. *Organometallics* **1996**, *15* (6), 1530.

[12] (a) Chawdhury, N.; Köhler, A.; Friend, R. H.; Younus, M.; Long, N. J.; Raithby, P. R.; Lewis, J. *Macromolecules* **1998**, *31* (3), 722. (b) Wittmann, H. F.; Friend, R. H.; Khan, M. S.; Lewis, J. *J. Chem. Phys.* **1994**, *101* (4), 2693. (c) Köhler, A.; Wilson, J. S.; Friend, R. H.; Al-Suti, M. K.; Khan, M. S.; Gerhard, A.; Bässler, H. *J. Chem. Phys.* **2002**, *116* (21), 9457. (d) Younus, M.; Köhler, A.; Cron, S.; Chawdhury, N.; Al-Mandhary, M. R. A.; Khan, M. S.; Lewis, J.; Long, N. J.; Friend, R. H.; Raithby, P. R. *Angew. Chem. Int. Ed.* **1998**, *37* (21), 3036. (e) Wilson, J. S.; Köhler, A.; Friend, R. H.; Al-Suti, M. K.; Al-Mandhary, M. R. A.; Khan, M. S.; Raithby, P. R. *J. Chem. Phys.* **2000**, *113* (17), 7627. (f) Ming, Z.; Ping, L.; Wang, X. M.; Lin, H.; Hong, X.; Wu, Z.; Bing, Y.; Liu, L. L.; Li, Y.; Min, Y.; Ma, Y. G.; Feng, J. K.; Wang, D. J.; Tamai, N. *J Phys Chem B* **2004**, *108* (35), 13185. (g) Sandee, A. J.; Williams, C. K.; Evans, N. R.; Davies, J. E.; Boothby, C. E.; Köhler, A.; Friend, R. H.; Holmes, A. B. *J. Am. Chem. Soc.* **2004**, *126* (22), 7041. (h) Thomas, S. W. III.; Yagi, S.; Swager, T. M. *J. Mater. Chem.* **2005**, *15* (27-28), 2829. (i) Evans, N. R.; Devi, L. S.; Mak, C. S. K.; Watkins, S. E.; Pascu, S. I.; Köhler, A.; Friend, R. H.; Williams, C. K.; Holmes, A. B. *J. Am. Chem. Soc.* **2006**, *128* (20), 6647.

[13] (a) Lowry, M. S.; Bernhard, S. *Chem.–Eur J.* **2006**, *12* (31), 7970. (b) Briñas, R. P.; Troxler, T.; Hochstrasser, R. M.; Vinogradov, S. A. *J. Am. Chem. Soc.* **2005**, *127* (33), 11851. (c) Thomas, S. W. III.; Venkatesan, K.; Müller, P.; Swager, T. M. *J. Am. Chem. Soc.* **2006**, *128* (51), 16641.

[14] Jia, G. C.; Puddephatt, R. J.; Scott, J. D.; Vittal, J. J. *Organometallics* **1993**, *12* (9), 3565.

[15] (a) Jia, G. C.; Payne, N. C.; Vittal, J. J.; Puddephatt, R. J. *Organometallics* **1993**, *12* (12), 4771. (b) Brandys, M. C.; Jennings, M. C.; Puddephatt, R. J. *J. Chem. Soc. Dalton* **2000**, *24*, 4601.

[16] Puddephatt, R. J. *Chem. Commun.* **1998**, (10), 1055-1062 and references therein.

[17] Long, N. J.; Williams, C. K. *Angew. Chem. Int. Ed.* **2003**, *42* (23), 2586.

[18] Khan, M. S.; Schwartz, D. J.; Pasha, N. A.; Kakkar, A. K.; Lin, B.; Raithby, P. R.; Lewis, J. *Z. Anorg. Allg. Chem.* **1992**, *616* (10), 121.

[19] (a) Adams, C. J.; James, S. L.; Raithby, P. R. *Chem. Commun.* **1997**, 2155. (b) James, S. L.; Younus, M.; Raithby, P. R.; Lewis, J. *J. Organomet. Chem.* **1997**, *543*, 233. (c) Adams, C. J.; Raithby, P. R. *J. Organomet. Chem.* **1999**, *578*, 178.

[20] (a) Swager, T. M. *Acc. Chem. Res.* **2008**, *41* (9), 1181-1189. (b) Mullen, K.; Swager, T. M. *Acc. Chem. Res.* **2008**, *41* (9), 1085.

[21] (a) Wilson, J. S.; Chawdhury, N.; Al-Mandhary, M. R. A.; Younus, M.; Khan, M. S.; Raithby, P. R.; Köhler, A.; Friend, R. H. *J. Am. Chem. Soc.* **2001**, *123*, 9412.

[22] Rogers, J. E.; Cooper, T. M.; Fleitz, P. A.; Glass, D. J.; McLean, D. G. *J. Phys. Chem. A* **2002**, *106*, 10108.

[23] (a) Silverman, E. E.; Cardolaccia, T.; Zhao, X. M.; Kim, K. Y.; Haskins-Glusac, K.; Schanze, K. S. *Coord. Chem. Rev.* **2005**, *249* (13-14), 1491. (b) Liu, Y.; Jiang, S.; Glusac, K.; Powell, D. H.; Anderson, D. F.; Schanze, K. S. *J. Am. Chem. Soc.* **2002**, *124*, 12412. (c) Glusac, K.; Kose, M. E.; Jiang, H.; Schanze, K. S. *J. Phys. Chem. B* **2007**, *111*, 929.

[24] Han, Y.; Huynh, H. V.; Tan, G. K. *Organometallics* **2007**, *26* (18), 4612.

[25] Yam, V. W.-W.; Tao, C. H.; Zhang, L. J.; Wong, K. M. C.; Cheung, K. K. *Organometallics* **2001**, *20* (3), 453.

[26] Koch, M.; Garg, J. A.; Blacque, O.; Venkatesan, K. *J. Organomet. Chem.* **2012**, *700*, 154.

[27] (a) Neve, F.; Crispini, A.; Di Pietro, C.; Campagna, S. *Organometallics* **2002**, *21* (17), 3511. (b) Harvey, P. D.; Gray, H. B. *J. Am. Chem. Soc.* **1988**, *110* (7), 2145.

[28] Zhang, Y. Z.; Garg, J. A.; Michelin, C.; Fox, T.; Blacque, O.; Venkatesan, K. *Inorg. Chem.* **2011**, *50* (4), 1220.

[29] (a) Unger, Y.; Zeller, A.; Taige, M. A.; Strassner, T. *Dalton Trans*. **2009**, 4786. (b) Ahrens, S.; Strassner, T. *Inorg. Chim. Acta* **2006**, *359*, 4789. (c) Unger, Y.; Zeller, A.; Ahrens, S.; Strassner, T. *Chem. Commun*. **2008**, 3263. (d) Unger, Y.; Meyer, D.; Strassner, T. *Dalton Trans.* **2010**, *39*, 4295.

[30] Chong, J. H.; MacLachlan, M. J. *Inorg. Chem.* **2006**, *45* (4), 1442.

[31] (a) Wanzlick, H. W.; Schikora. *Angew. Chem. Int. Ed.* **1960**, *72* (14), 494. (b) Lemal, D. M.; Lovald, R. A.; Kawano, K. I. *J. Am. Chem. Soc.* **1964**, *86* (12), 2518. (c) Kirmse, W. *Angew. Chem. Int. Ed.* **2010**, *49* (47), 8798.

[32] (a) Han, Y.; Huynh, H. V.; Koh, L. L. *J. Organomet. Chem.* **2007**, *692* (17), 3606. (b) Forel, T.; Tranquille, M. *Spectrochim. Acta Part A*, **1970**, *26*, 1023

[33] (a) Garg, J. A.; Blacque, O.; Heier, J.; Venkatesan, K. *Eur. J. Inorg. Chem.* **2012**, *11*, 1750. (b) Ray, L.; Katiyar, V.; Barman, S.; Raihan, M. J.; Nanavati, H.; Shaikh, M. M.; Ghosh, P. *J. Organomet. Chem.* **2007**, *692* (20), 4259.

[34] (a) Kanbara, T.; Yamamoto, T. *Chem. Lett.* **1993**, (3), 419. (b) Yamamoto, T.; Usui, M.; Ootsuka, H.; Iijima, T.; Fukumoto, H.; Sakai, Y.; Aramaki, S.; Yamamoto, H. M.; Yagi, T.; Tajima, H.; Okada, T.; Fukuda, T.; Emoto, A.; Ushijima, H.; Hasegawa, M.; Ohtsu. *Macromol. Chem. Phys.* **2010**, *211* (19), 2138.

[35] Xu, B. B.; Lu, M.; Kang, J. H.; Wang, D.; Brown, J.; Peng, Z. H. *Chem. Mat.* **2005**, *17* (11), 2841.

[36] Zhang, G.; Chen, J.; Payne, S. J.; Kooi, S. E.; Demas, J. N.; Fraser, C. L. *J. Am. Chem. Soc.* **2007**, *129* (29), 8942.

[37] Lauterbach, T.; Livendahl, M.; Rosellon, A.; Espinet, P.; Echavarren, A. M. *Org. Lett.* **2010**, *12* (13), 3006.

[38] (a) Partyka, D. V.; Zeller, M.; Hunter, A. G.; Gray, T. G. *Angew. Chem. Int. Ed.* **2006**, *45*, 8188. (b) Partyka, D. V.; Updegraff, J. B.; Zeller, M.; Hunter, A. D.; Gray, T. G. *Organometallics* **2009**, *28* (6), 1666.

[39] (a) Usón, R.; Laguna, A.; Pardo, *J. Syn. React. Inorg. Met.-Org. Chem*. **1974**, *4*, 499. (b) Usón, R.; Laguna, A.; Laguna, M.; Gimeno, M. C.; Depablo, A.; Jones, P. G.; Meyerbase, K.; Erdbrugger, C. F. *J. Organomet. Chem.* **1987**, *336* (3), 461.

[40] Man, W. Y.; Bock, S.; Zaitseva, N. N.; Bruce, M. I.; Low, P. J. *J. Organomet. Chem.* **2011**, *696* (10), 2172.

[41] Zhao, D. H.; Swager, T. M. *Org. Lett.* **2005**, *7* (20), 4357.

[42] (a) Williams, V. E.; Swager, T. M, *Macromolecules* **2000**, *33* (11), 4069. (b) Williams, V. E.; Swager, T. M., *J. Polym. Sci. Polym. Chem.* **2000**, *38*, 4669.

[43] Xcalibur CCD System; Oxford Diffraction Ltd: Abingdon, Oxfordshire, England, 2007.

[44] Clark, R. C.; Reid, J. S. *Acta Cryst.* **1995**, *A51*, 887.

[45] *CrysAlisPro* (versions 1.171.32.55), Oxford Diffraction Ltd, Abingdon, Oxfordshire, England.

[46] Sheldrick, G. M. *Acta Cryst.* **2008**, *A64*, 112.

[47] Farrugia, L. J. *J. Appl. Cryst.* **1999**, *32*, 837.

[48] Spek, A. L. *J. Appl. Cryst.* **2003**, *36*, 7.

Chapter 7.

β-Iminoenamine-BF_2 Complexes: Aggregation-induced Emission and Pronounced Effects of Aliphatic Ring on and Radiationless deactivation

β-Iminoenamine-BF_2 Complexes: Aggregation-induced Emission and Pronounced Effects of Aliphatic Ring on and Radiationless deactivation

1.0 Abstract

β-Iminoenamine boron difluorides constitute an interesting and emerging class of boron based dye molecules. Herein presented are the synthesis, photophysical and electrochemical attributes of a series of molecules containing an aromatic fused alicylic/ hetero-alicyclic ring built into the *β*-iminoenamine chromophoric backbone. The compounds exhibited large Stokes-shifts (86-121 nm) with low emission quantum yields in fluid media at RT, whereas relatively higher values were seen in the solid-state. Aggregation-induced emission (AIE) was also observed in some of the tested compounds. Single crystal XRD analyses revealed lack of interplanar π-π interactions, which is presumed to be avoided due to non-planarity of the alicyclic component of the molecule.

2.0 Authors and attribution

This work is a part of collaborative effort between the groups of Venkatesan and Kabilan.[1] The entire work has been submitted as a full paper.[2] The synthesis and characterization of all the new compounds have been performed in the group of Kabilan. The contribution of the author (me) is confined to the structural characterization (single crystal XRD) of some of the synthesized compounds and the detailed photophysical investigations. For the sake of continuity, the synthetic scheme leading to the compounds that were photophysically investigated is also outlined here.

3.0 Introduction

Stable tetracoordinate organo-boron complexes are of scientific interest due to their potential utility as functional luminophores for an array of applications.[3] This is further evident from the enormous amount of research directed towards boron-dipyrromethene (BODIPY) class of molecules. Incorporation of boron atom is perceived to stabilize the N^N monoanionic chelating ligand by an effective delocalization of the negative charge. Although BODIPY dyes have evolved as a privileged class molecules for a wide variety

of applications,[4] the solid-state luminescence properties in most of its derivatives have been found to be poor when compared to that in solution primarily owing to quenching of emission due to intermolecular π-π stacking interactions. A prominent strategy to avoid such quenching has been to introduce a sterically imposing substituent at the *meso*-carbon of the dipyrrin core.[5] Apart from the dipyrrin framework, several groups have focused attention in developing new classes of boron based fluorophores to achieve superior solid-state luminescence properties. The groups of Yamaguchi,[3d,6b,6c] Wang[3a,3b,6a] and Piers[3e,6d] have developed highly luminescent fluorophores based on boron. In this chapter, we have aimed to explore the photophysical nature of yet a different class, namely the β-iminoenamine boron difluorides with a fused aliphatic ring unit. They are akin to popular "nacnac" ligands, or the β-diketiminate systems, with a formal ''formal'' 6-membered ring with a chelating μ^2-H proton bridged to the nitrogen atoms.[7] The initial choice of this chelate ligand was due to the following reasons: (1) Desymmetrization of the chromophoric coordination sphere about the nitrogen bound to boron atom (unlike in the case of BODIPY dyes) has been recently realized to effect larger Stokes-shifts.[6d] (2) Introduction of aliphatic ring in the chromophoric backbone can disrupt deleterious stacking interations due to its non-planar conformation. (3) Ease of functional group modifications, which can eventually modulate the ground/excited states leading to intriguing luminescence properties. Previously, Gardinier et al. has elegantly compared the electronic properties of difluoroboron complexes bearing β-diketonate, β-ketoiminate, and β-diiminate ligands[8] which bears close resemblance to the system under investigation. Similarly, Mu et al., has investigated the photoluminescence (PL) properties of anilido-imine BF_2 compounds.[9] The observed luminescence in this case was attributed to π/π^* transition of their conjugated anilido-imine ligands. Very recently, Piers et al. has described similar compounds exhibiting large Stokes-shift and good photostability.[6d] Here in this work, the basic skeleton of the borylated β-iminoenamine encompassed with either 1,2-dihydronapthalene or 2*H*-chromene or 2*H*-thiochromene in its chromophoric backbone is exploited. Functional variations of the substituent on the aromatic rings and also changes in the heteroatom of the fused aliphatic cycle afforded novel compounds with tunable emission properties. As expected, some of the synthesized

compounds exhibited bright luminescence in the crystalline state and in aggregated state in solution (AIE phenomenon) but were nearly non-emissive in various dissolved fluid media. Combined photophysical, NMR and single crystal X-ray diffraction studies have suggested that the aliphatic part of the molecule is primarily responsible for the varied photophysical behavior of this class of compounds.

4.0 Results and Discussion

4.1 Synthesis and characterization

Iminoenamines suitable for complexation were realized in two steps starting from the appropriate α-tetralone/(2*H*)-benzopyranone/(2*H*)-benzthiopyranones (Scheme 1). Vilsmeier-haack formylation of the ketones furnished their respective *β*-chlorovinyl aldehydes (**1a-1e**), which upon reacting with 2.0 equiv. of substituted aryl amines in the presence of PTSA gave the desired iminoenamines (**2a-2n**) in the yield range of 65-92%. This route was previously established in the groups of the of Balasubramanian[10] and Kabilan et al.[1] and was previously utilized for the synthesis of condensed heterocycles like acridines/quinolines.[10]

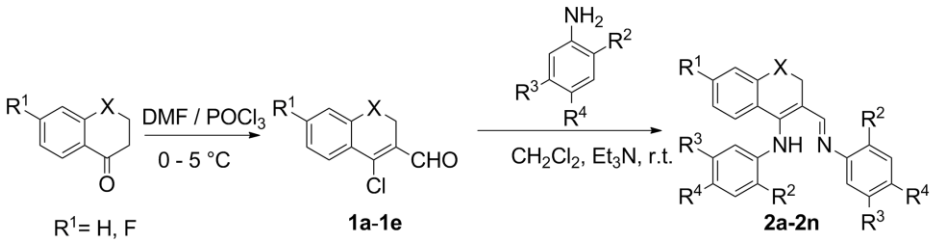

X	R^1	
C	H	**1a**
	F	**1b**
O	H	**1c**
	F	**1d**
S	H	**1e**

X	R^1	R^2	R^3	R^4	
C	H	H	H	OMe	**2a**
	H	H	H	NO_2	**2b**
	H	H	H	F	**2c**
	F	H	H	F	**2d**
	F	H	H	OMe	**2e**
	F	H	H	NO_2	**2f**

X	R^1	R^2	R^3	R^4	
O	H	H	H	H	**2g**
	H	H	H	OMe	**2h**
	H	H	H	NO_2	**2i**
	H	H	H	F	**2j**
	H	H	F	H	**2k**
	F	H	F	I	**2l**
	F	H	H	Me	**2m**
S	F	H	H	OMe	**2n**

Scheme 1.

We envisaged that the iminoenamines which are potential systems for electrocyclic ring closure should readily react with Lewis acidic $BF_3{\cdot}Et_2O$ to form stable boron compounds. As expected, reaction with $BF_3{\cdot}Et_2O$ in the presence of excess quantity of a base like Et_3N or DIPA (also to scrub the nascent HF generated) yielded the desired products in modest to good yields of 70-95% (Scheme 2). The reaction was also found to proceed with the hydrochloride salt of the iminoenamines in a one-pot sequence, which does not require prior neutralization. All the products **3a-3f**, **4a-g** and **5** were air and moisture stable and were fully characterized by ^1H, ^{13}C NMR and HRMS experiments. The key diagnostic features in the ^1H NMR of these boron compounds includes the disappearance of the signal intensity due to the proton of the free amine and coupling between iminomethine and boron with $^3J_{H\text{-}B}$ around 3.7 Hz. Broad multiplets in ^{11}B NMR and ^{19}F NMR due to the coupling between boron and fluorine atoms were also observed.

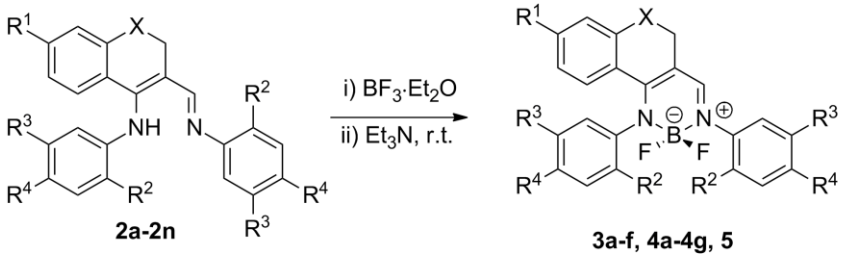

X	R^1	R^2	R^3	R^4	
C	H	H	H	OMe	**3a**
	H	H	H	NO_2	**3b**
	H	H	H	F	**3c**
	F	H	H	F	**3d**
	F	H	H	OMe	**3e**
	F	H	H	NO_2	**3f**

X	R^1	R^2	R^3	R^4	
O	H	H	H	H	**4a**
	H	H	H	OMe	**4b**
	H	H	H	NO_2	**4c**
	H	H	H	F	**4d**
	H	H	F	H	**4e**
	F	H	F	I	**4f**
	F	H	H	Me	**4g**
S	H	H	H	OMe	**5**

Scheme 2.

4.2 X-ray diffraction studies

Diffraction quality single crystals of compounds **3d**, **3e**, **4c** and **4d** were obtained by slow evaporation of concentrated solution of the compounds in ethanol. The perspective views

of their molecular structures are shown in Figure 1. As expected, the coordinatively saturated boron adopts a pseudo-tetrahedral geometry on the plane defined by the imine and amido nitrogen flanked by the two fluorine atoms above and below the plane. Selected bond distances and bond angles are provided in the appendix section along with other relevant crystallographic data (Table A1 and A2, appendix). The N_{imine}-B-N_{amido} bite angles were in expected range in comparison with the anilido-imine complexes previously reported.[6d,9] Similar to boron-dipyrromethene compounds,[4] the mean average distances of the boron atom to nitrogen of the imine B(1)-N(1) = 1.54 Å and to amine nitrogen B(1)-N(2) = 1.55 Å were close suggesting an effective delocalization of the positive charge of the iminium. The aliphatic ring in all the three cases adopted puckered conformation due to the sp^3 hybridized nature carbon or oxygen with the atoms exhibiting torsional angles approximately in the range 55.8 - 59.2°. Also, the dihedral angles between the mean planes defined by N bonded arene and the boron heterocycle was invariably greater than 35° (Table A1, appendix). These facts evidence low elements of symmetry and planarity in these molecules. Closer examination of the crystal packing structures revealed more interesting aspects. Although no specific pattern of arrangement or arene π-π stacking was evident (closest π-π interplanar distance was greater than 3.8 Å), significant intermolecular CH···F, CH···π interactions[4i,11] were observed in the lattices of these compounds, especially in **3e** CH···F distances in the order of ~2.4 Å were observed. In addition to conferring increased stability, these interactions could affect photophysically relevant electronic states of the molecule.

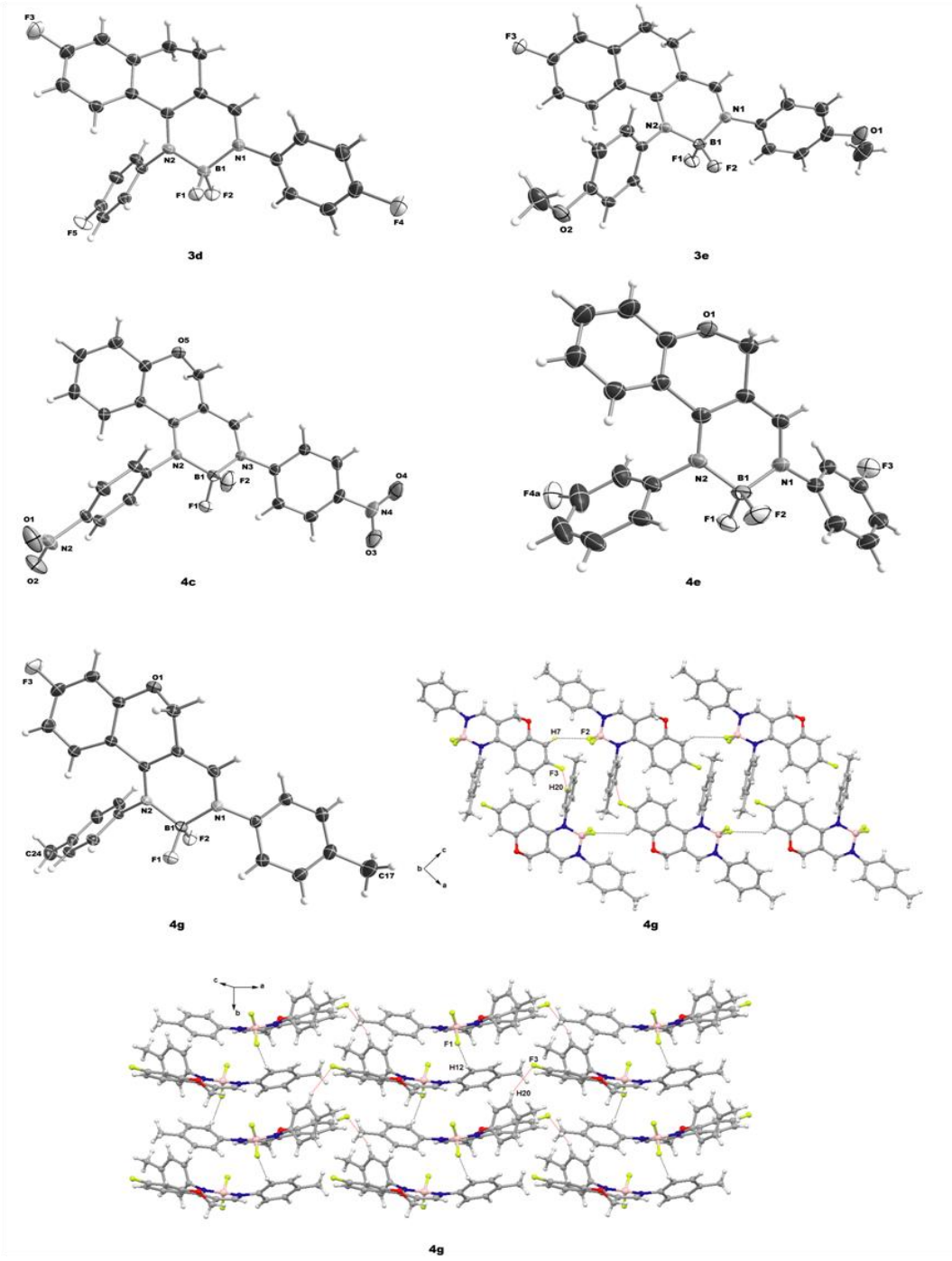

Figure 1. X-ray structures with selective atomic numbering scheme. Thermal ellipsoids are shown at 50% probability and crystal packing diagram of **4g.**

4.3 Photophysical studies

All the compounds were generally characterized by a well separated low energy intense absorption band appearing in the range 410-445 nm (Table 1, Figure 2 and Figures A1 in the appendix) with molar extinction coefficient of the order 10^4 $M^{-1}cm^{-1}$. In addition, less intense bands indicating lower transition probability were also observed in the wavelength interval 249-352 nm.

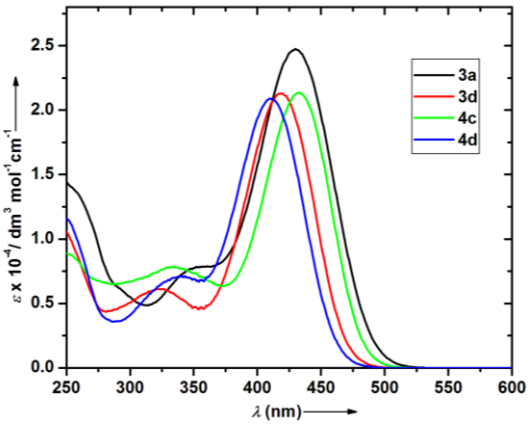

Figure 2. Electronic absorption spectra of **3a**, **3d**, **4c** and **4d.**

Steady-state emission spectra measured in CH_2Cl_2 at RT showed very weak emission intensities with low quantum yields in the range of 10^{-2} to 10^{-4}. Compound **5** containing sulfur was completely non-emissive in CH_2Cl_2 at RT presumably due to heavy atom photoinduced electron transfer.[12]

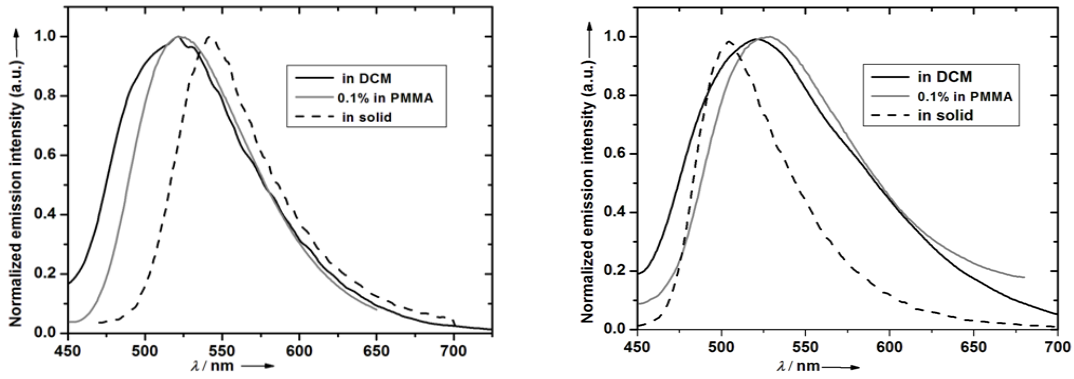

Figure 3. Emission spectra of **3d** (*left*) and **4e** (*right*) in CH_2Cl_2, thin films and solid-state.

The other emission profiles were Gaussian shaped, broad and approximately resembled the absorption bands (Figure 3 and Figure A2 in appendix). In the solid state, the emission profiles were featured to be relatively narrower and red-shifted. However, in the cases of **3c**, **4a**, **4d**, **4e** and **4g** a distinct blue shift was observed. The observed Stokes-shifts were in an extraordinary range (86-121 nm) as compared to the typical 7-15 nm shift observed in the case BODIPY derivatives. Earlier observations with anilido-amine systems [3b],[9] also revealed similar trend which can be attributed due to the deviation from the core C_2-symmetric nature as found in the dipyrrin chelates. Solvatochromic studies performed on **3d** and **4e**, showed moderate hypsochromic shifts by ~3-4 nm (Figure A3 in appendix) upon increasing the polarity *viz*., moving from benzene to THF to acetonitrile. It could be therefore surmised that the dipole moment of the ground state is more pronounced than the excited state. In CH_2Cl_2 solution at RT the quantum yields were low (Table 1); using more viscous solvents like DMSO or ethylene glycol showed no improvement. Nevertheless, it was interesting to see the solid crystals of most compounds illuminated brightly when irradiated with a hand-held UV-lamp (excitation approx. 365 nm, Figure A4 in the appendix). The absolute quantum yield of **3e** in the solid state (crystalline form) was found to be 2.4% when measured by an integrating sphere apparatus. This value is certainly way higher than that observed in CH_2Cl_2 (Table 1). In the solid state, one would normally expect electron-transfer quenching due to exciton-phonon coupling originating from close inter-atomic distances as proposed by Langhals et al.[13] As discussed earlier, compounds for which single crystal XRD were examined, for example **3e** did show CH···F and CH···π interactions but was devoid of π-π interactions. The presence of former type of interactions and absence of π-π interactions were presumed to have some influence on the quantum yield by altering the ground state properties of the luminophore.

Table 1. Photophysical properties of compounds **3a-g**, **4a-g** and **5**.

	RT solution (CH_2Cl_2)					Emission at RT [d] λ_{max}[nm]		E_{opt} [f]
	Absorption λ_{max}[nm] (ε_{max}/[$dm^3mol^{-1}cm^{-1}$])	PL λ_{emiss}[nm]	τ [ns]	Φ_f [a] x 10^{-3}	Stokes shift[b]	solid (Φ_f^{solid})[c]	PMMA (Φ_f^{PMMA})[d]	(eV)
3a	348 (7706), 429 (24996)	541	0.3, 6.5	0.97	112	562	544	2.47
3b	337 (14111), 447 (33670)	531	-[e]	6.20	84	555	538	2.44
3c	317(7061), 421(22590)	522	0.6, 4.0	3.70	101	512	514	-
3d	324 (6168), 418 (21372)	520	1.3, 9.1	2.61	102	543 (6.0)	522	2.59
3e	345 (6371), 427 (20701)	540	2.0	0.57	116	552 (2.4)	547	2.48
3f	339 (1295), 445 (36301)	531	-[e]	54.01	86	-	545	2.45
4a	338 (5221), 412 (15870)	515	-[e]	4.10	103	506	510	-
4b	337 (7971), 418 (24464)	539	0.9, 8.0	0.78	121	553 (6.4)	539	2.53
4c	335 (7849), 433 (21294)	534	-[e]	3.15	101	538 (0.003)	540	2.51
4d	340 (7041), 410 (20904)	522	0.7, 17.0	3.20	112	496	527 (6.4)	2.62
4e	344 (7511), 413 (22715)	518	0.4, 6.3	6.65	105	504	527 (10.0)	2.62
4f	331 (8433), 413 (31059)	523	0.6	6.91	110	526	514 (5.7)	-
4g	328 (7550), 411 (26740)	521	0.1	3.60	110	503	511 (1.0)	-
5	352 (12541), 428 (31510)	-	-	-	-	566	-	2.49

[a]Quantum yield (QY) determined with fluorescein in 1 N NaOH as standard. [b]Calculated from the difference between the absorption and emission maxima. [c]QY determined in the solid state. [d]QY determined from PMMA thin films with 2% doped concentration. [e]multi exponential decay. [f]Optical band-gap calculated from the absorption edges.

To verify this hypothesis we recorded the absorption spectra of **3e**, **4a**, **4c**, **4d** and **4g** in the solid state by using diffuse reflectance method. Bathochromic shifts of various extents (5-72 nm) were observed (Figure A5 in the appendix). For example the largest change in the absorption maximum (λ_{max}) was found for **4c** that showed a significant shift from 433 nm in CH_2Cl_2 to 505 nm in the solid state. Such phenomenon has been previously attributed to an increase in exciton coupling.[14] To unravel if similar

beneficial self-organizing aggregates can be triggered in the fluid media, we further carried out experiments with **4d** as an exemplary compound. To a dissolved solution of **4d** in THF, the PL spectra were obtained with increasing volumetric ratio of deionized water as shown in Figure 4. A steady increase in the relative emission intensity was observed with the increase of water fraction due to the formation of partially soluble aggregates.

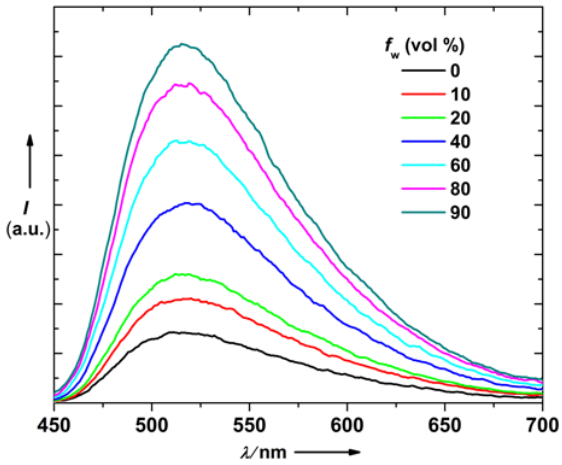

Figure 4. PL spectra of **4d** in THF/H_2O mixtures (1.0 x 10^{-5} M, excited at 410.0 nm) with different volumetric fractions of H_2O (f_w).

At 80 to 90% (v/v) ratios, the tiny aggregates of the compound were visible as tiny specks when observed under the UV lamp (Figure A4, appendix). Similar phenomenon was also observed for **4c** (Figure A6, appendix). This observation is also consistent with the phenomenon of Aggregation-induced Emission (AIE). Aprahamian et al. have recently reported AIE phenomenon in BF_2-hydrazone complexes.[15] In order to gain more insight on this, increasing weight percent concentrations of **4d** were doped onto thin films with PMMA as the host matrix. The quantum yield obtained with 2.0, 4.0, 10.0 and 40.0 wt% loadings were 6.4, 5.0, 4.0 and 2.0 x 10^{-3} percent respectively, indicating a trend opposite to induced aggregation in solution.

Based on the observations of the two above experiments the following tentative conclusions can be drawn; firstly, the increased luminescence observed by slow

incremental precipitation (AIE phenomenon) probably occurs because of photophysically favorable pre-organization due to spontaneous forces of self-organization and secondly, under forced situations such as doping small weight% of the dye in PMMA, similar phenomenon need not be observed due to the possibility of molecular motions in the matrix. The solid-state molecular structures revealed a significant loss of planarity in the molecule, adding to this, one can also expect single bond free rotation of the arenes about the nitrogen atoms in solution. We reasoned that these symmetry lowering factors can contribute more importantly to the lowering of QYs in solution. However, it was intriguing to note that the anilido difluoride system recently reported showed good quantum yields in solution[6d] despite having similar *N*-bonded arenes. A notable variation which is unique to the current system is that it incorporates acyclic ring (benzopyran or chromene) in the chelating backbone. It was therefore hypothesized that the rapid conformational changes (ring-flipping) at ambient temperature could significantly contribute in accelerating the rates of non-radiative decay. Supporting this notion, low variable temperature (VT) -NMR recorded for **4e** at 233 K revealed de-coalescence of resonance corresponding to that of the methylene protons at δ = 4.87 ppm due to the 'frozen-out' conformation (see Figure 5(a), bracketed region). Further, VT photoluminescence of **4b** (in 2-*methyl* THF) under rigorous exclusion of oxygen was also undertaken. As shown in Figure 5(b), the compound exhibited maximum relative intensity at 77 K, which decreases with increase in temperature. Even at 175 K, most of the emission intensity is lost, further confirming that conformational dynamics is a key factor responsible for quenching of fluorescence intensity in these classes of molecules. In order to further clarify the photoluminescence behavior of the compounds in the crystalline state and in PMMA matrix, we chose to measure the absolute quantum yields of selected complexes namely **3d**, **3e** and **4b** both in PMMA thin films (2 wt% doped) and as neat solid material.

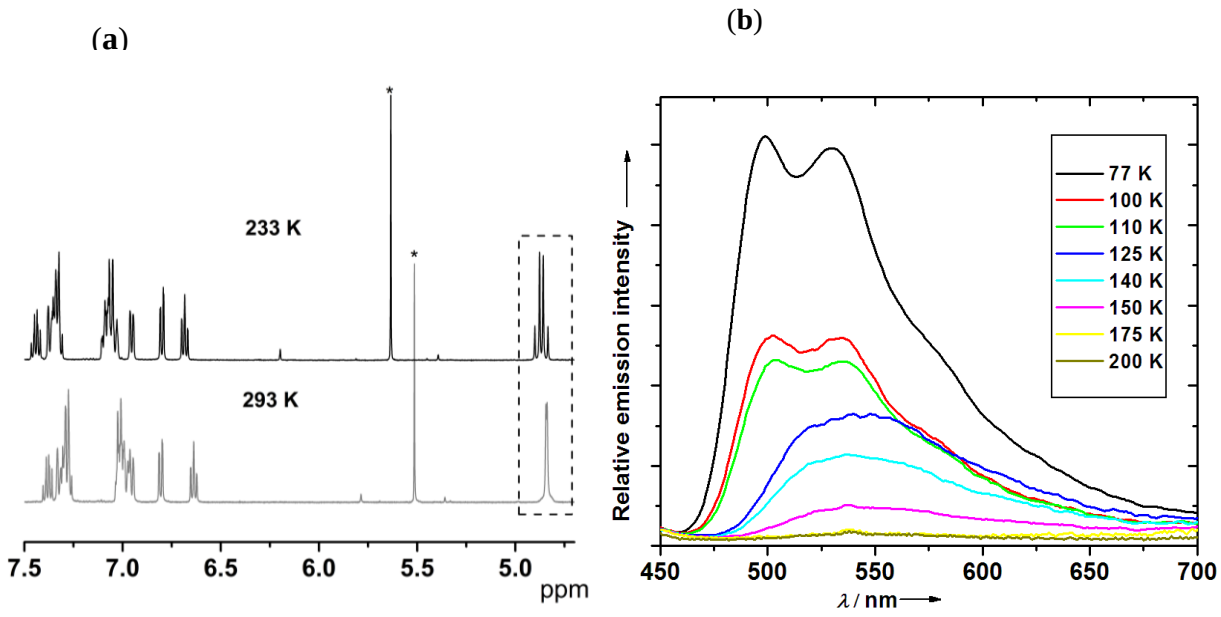

Figure 5. (**a**) Low VT-NMR of **4e** in THF-d_8, (*) denotes solvent impurity (CH_2Cl_2). (**b**) VT-photoluminescence spectrum of **4b** recorded in 2-*methyl*-THF.

In the PMMA matrix quantum yields of 2.4%, 1.6% and 1.7% were obtained for **3d**, **3e** and **4b** respectively. In the case of neat solids, marginally incremental values of 6.0%, 2.4% and 6.4% respectively was observed. It is presumed that, although the QYs increases roughly a tenfold in moderately rigid PMMA matrix as compared to solution, the molecular motions are not entirely restricted and therefore it still exhibits a lower value as compared to that in solid state. Such unrestricted molecular motions have been accounted previously.[16] The excited-state lifetime for many compounds could be best fitted bi-exponentially comprising of a short sub-nanosecond and longer nanosecond terms. Such bi-exponential decay has been observed for aggregation-induced luminophores displaying flipping kinetics.[17]

4.4 Electrochemical studies

In order to correlate band-gap and Stokes-shift, cyclic voltammetry studies were carried out for selected compounds **3b**-**3d**, **3f**, **4a**, **4c**, **4e** and **4g**. Most compounds exhibited a prominent roughly quasi-reversible first reduction wave; the anodic portion of the wave

was notably less intense than expected. An example is shown in Figure 6 and the rest are shown in the supporting information (Figure A7, appendix). Irreversible oxidation peak potential, within the electrochemical window of CH_2Cl_2 was observed for **3c** and **4c**, the other less prominent oxidation waves could not be assigned with certainty. Among the compounds with dihydronapthalene backbone (**3b**-**3d**, **3f**) those containing *p*-nitrophenyl attached to nitrogen namely **3b** and **3f**, displayed lower negative reduction peak potentials -1.43 V and -1.46 V when compared to **3c** and **3d** containing fluorine as the substituent (Table 2). Among the chromene derivatives (**4a**, **4c**, **4e** and **4g**), compound **4a** with no substituent on the phenyl ring showed peak potential at -1.95 V. Compared to this, **4c** with *p*-nitro, **4e** with *m*-fluorine groups showed relative ease of reduction with potentials -1.45 V and -1.80 V respectively. **4g** containing methyl substituent showed a cathodic shift with reduction potential at -1.98 V as expected. From the onset of the first reduction peak, the LUMO values were calculated[15] to range between -2.82 eV to -3.36 eV for the measured compounds.

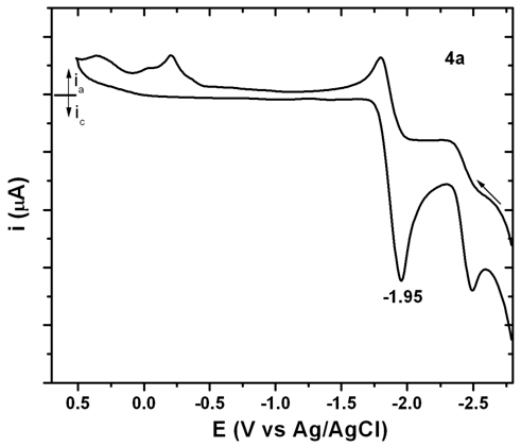

Figure 6. Cyclic voltammaogram of **4a** with Fc in 0.1M [nBu$_4$N][PF_6]; Au electrode; scan rate = 100 mV/s; 20 ºC; CH_2Cl_2; LUMO [eV] = $-(E_{red} - E_{Fc/Fc+} + 4.8)$.[18]

Table 2. Electrochemical data of **3b**-**3d**, **3f**, **4a**, **4c**, **4e**, **4g**.

	Reduction $E_{p,c}$ (V)	Oxidation $E_{p,a}$ (V)	LUMO[a] [eV]
3b	-1.43	-	-3.36
3c	-1.93	+1.02	-2.87
3d	-1.98	-	-2.82
3f	-1.46	-	-3.34
4a	-1.95	-	-2.85
4c	-1.45	+1.37	-3.35
4e	-1.80	-	-3.02
4g	-1.98	-	-2.82

[a]LUMO [eV] = -(E_{red} - $E_{Fc/Fc+}$ + 4.8).

5.0 Conclusions

The synthesis, photophysical and electrochemical aspects of a novel class of β-diketiminato boron difluoride molecule with an aromatic fused alicyclic/hetero-alicyclic ring unit have been studied. They were found to display large Stokes-shift as compared to the popular boron-dipyyromethene complexes. The solid state emission quantum yields were found to be superior as compared to those in the fluid media at RT. From various experiments it is understood that, the inclusion of a non-planar aliphatic core improves the solid state emission by preventing π-π stacking, on the other hand, in fluid media it simultaneously expedites non-radiative pathways due to the rapid conformational motions. The significant CH···F, CH···π interactions is believed to alter the ground state of the molecule to certain extent apart from enhancing the structural rigidity of the compound. Emission due to the formation of insoluble aggregates was also observed in some of the tested compounds.

6.0 APPENDIX (Chapter 7)

6.1 General considerations

UV-vis spectra in the solution were recorded on a Cary-3Bio UV-vis spectrometer and diffuse reflectance measurements were carried out on Perkin-Elmer Lambda 35 spectrometer. Emission spectra were acquired on Perkin Elmer LS50B spectrophotometer using 450W Xenon lamp excitation by exciting at the longest-wavelength absorption maxima. All samples for emission spectra were degassed with N_2 before measurement. Luminescence quantum yields (ϕ) was determined at 298 K (estimated uncertainity ± 15%) using standard methods,[19] wavelength-integrated intensities (I) of the corrected emission spectra was compared to iso-absorptive spectra of Fluorescein standard (ϕ_r = 0.79 in 0.1 M NaOH air-equilibrated solution) and was corrected for solvent refractive index. Absolute quantum yields were determined for thin-film samples (or) solid samples dispersed on glass plates using an integrating-sphere apparatus (Horiba Jobin Yvon spectrophotometer). The results were calculated according to the literature protocol.[20] Excited state lifetimes were measured by time-correlated single photon counting method (TCSPC) performed on an Edinburgh FLS920 spectrophotometer, using nF900 lamp source at 30000 Hz frequency with 15 nm excitation and 15 nm emission slit widths. Low variable temperature photoluminescence spectra were acquired in frozen 2-methyltetrahydrofuran (2-methyl-THF) glass from the same instrument. Cyclic voltammograms were obtained with Metrohm 757 computrace voltammetric analyzer. The cell was equipped with a gold working electrode and a Pt counter electrode, and a non-aqueous reference electrode. All sample solutions (CH_2Cl_2) were approximately 5.0 x 10^{-3} M in substrate and 0.1 M in n-Bu_4NPF_6, and were prepared under nitrogen. Ferrocene was subsequently added and the voltammograms were calibrated.

6.2 Electronic absorption spectra in solution.

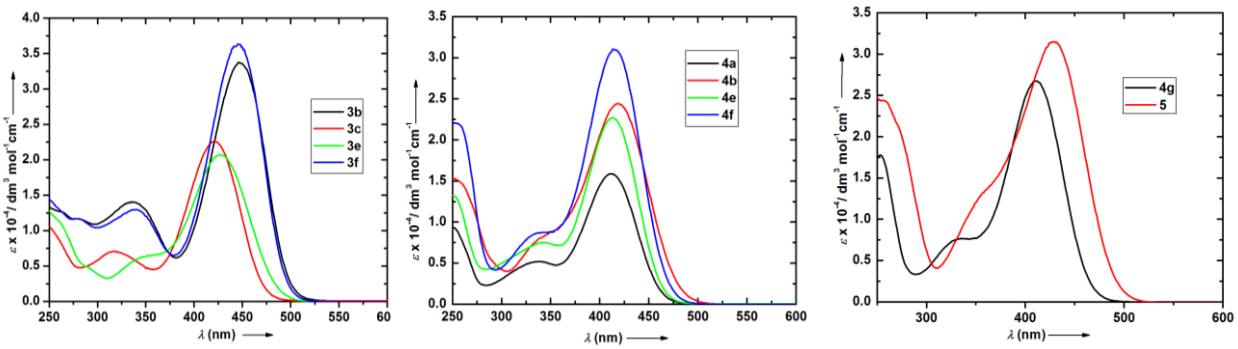

Figure A1. Electronic absorption spectra of selected compounds (**3b**, **3c**, **3e**, **3f**, **4a**, **4b**, **4e**, **4f, 4g** and **5**) in CH_2Cl_2 at RT.

6.3 Photoluminescence spectra.

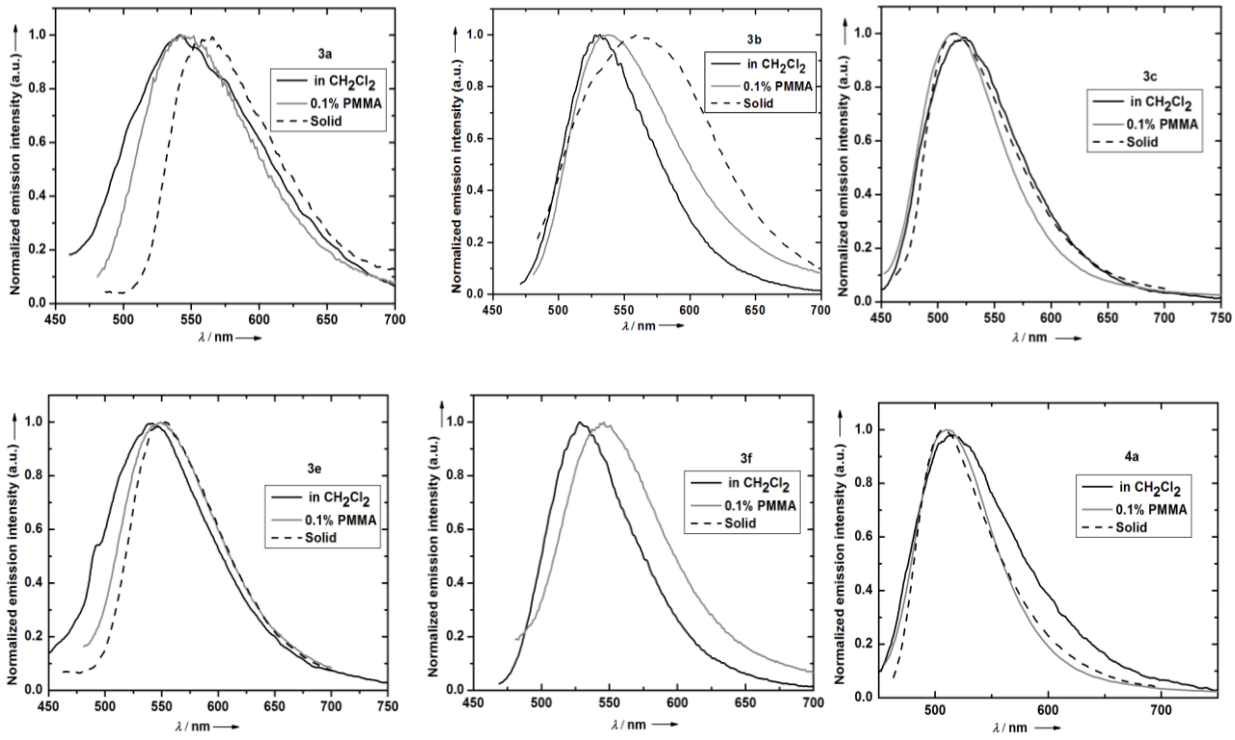

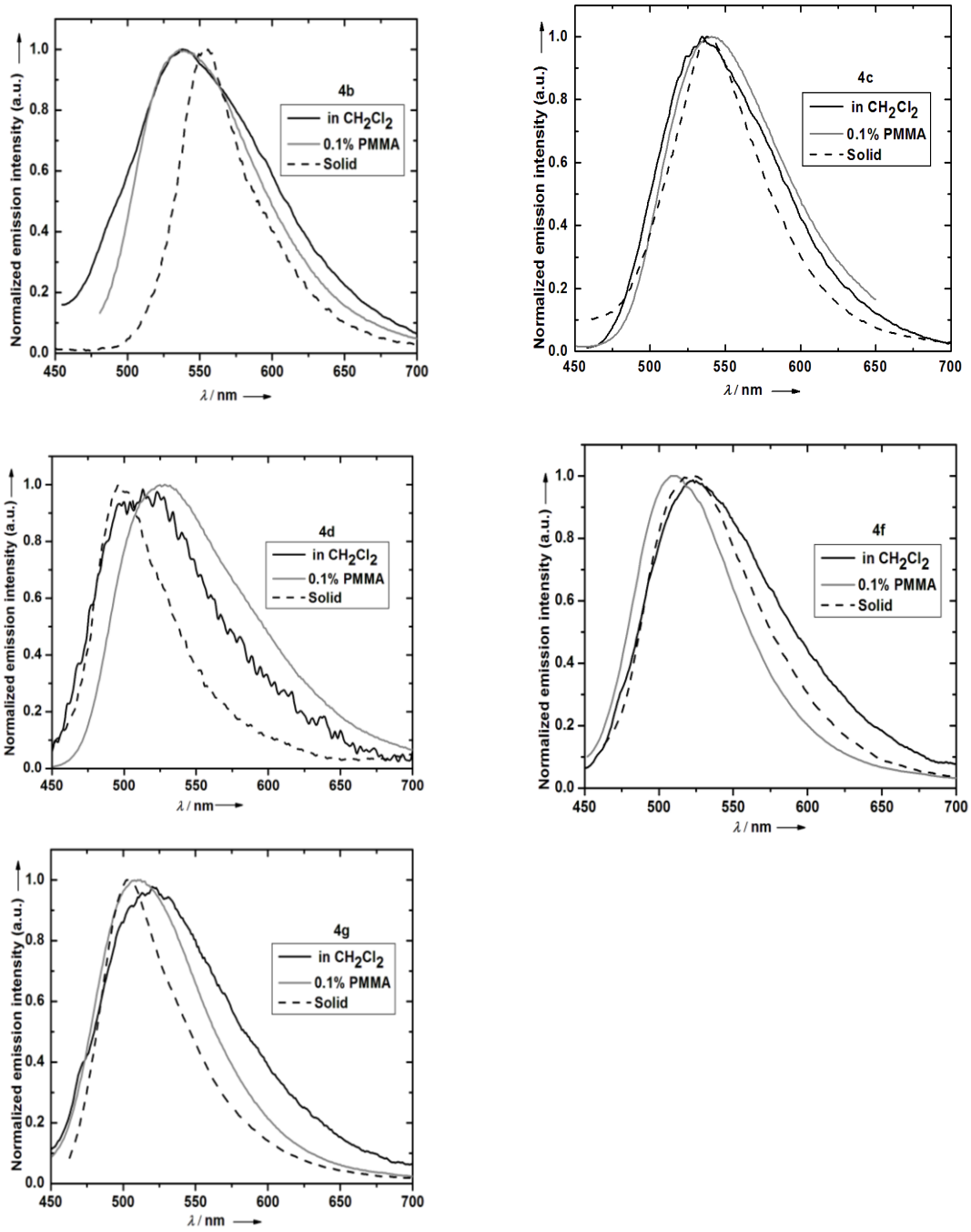

Figure A2. Emission spectra of selected compounds (**3a-3c**, **3e**, **3f**, **4a**-**4d**, **4f** and **4g**) degassed CH_2Cl_2, PMMA thin film and in the solid state.

6.4 Solvatochromic studies.

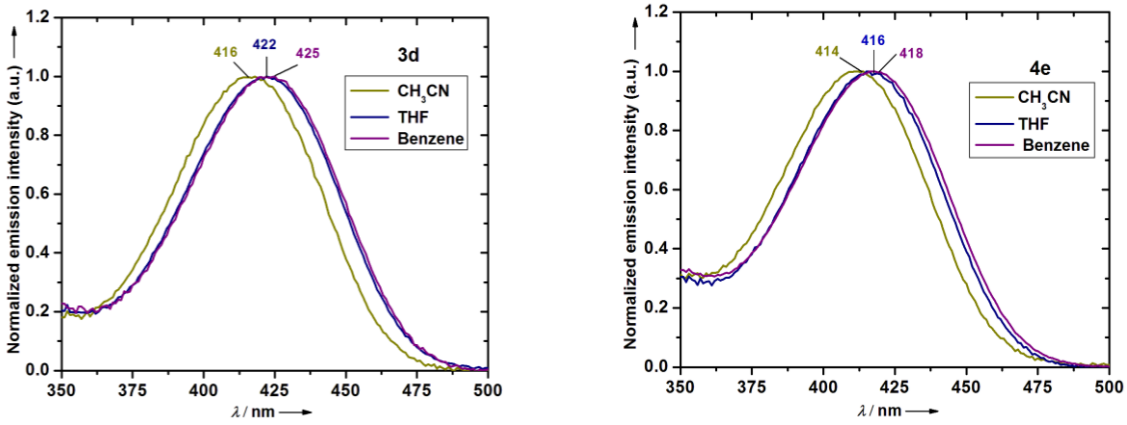

Figure A3. Electronic absorption spectra of **3d** (*left*) and **4e** (*right*) in CH_3CN, THF and benzene.

(**a**)

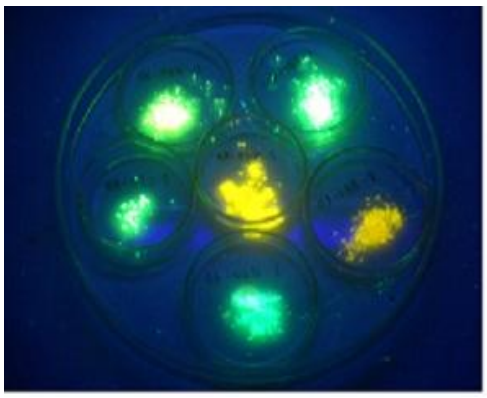

(**b**)

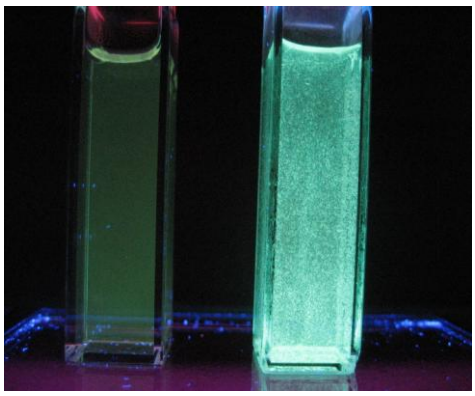

Figure A4. (**a**) Picture of solid state illumination of selected boron compounds excited with UV lamp (365 nm). (**b**) Picture of aggregation-induced emission of **4d** with 0% (v/v) H_2O fraction in the left cuvette and 80% (v/v) of H_2O in the right cuvette - excited with UV lamp (365 nm).

6.5 Electronic absorption spectra in solid-state (by Diffuse Reflectance).

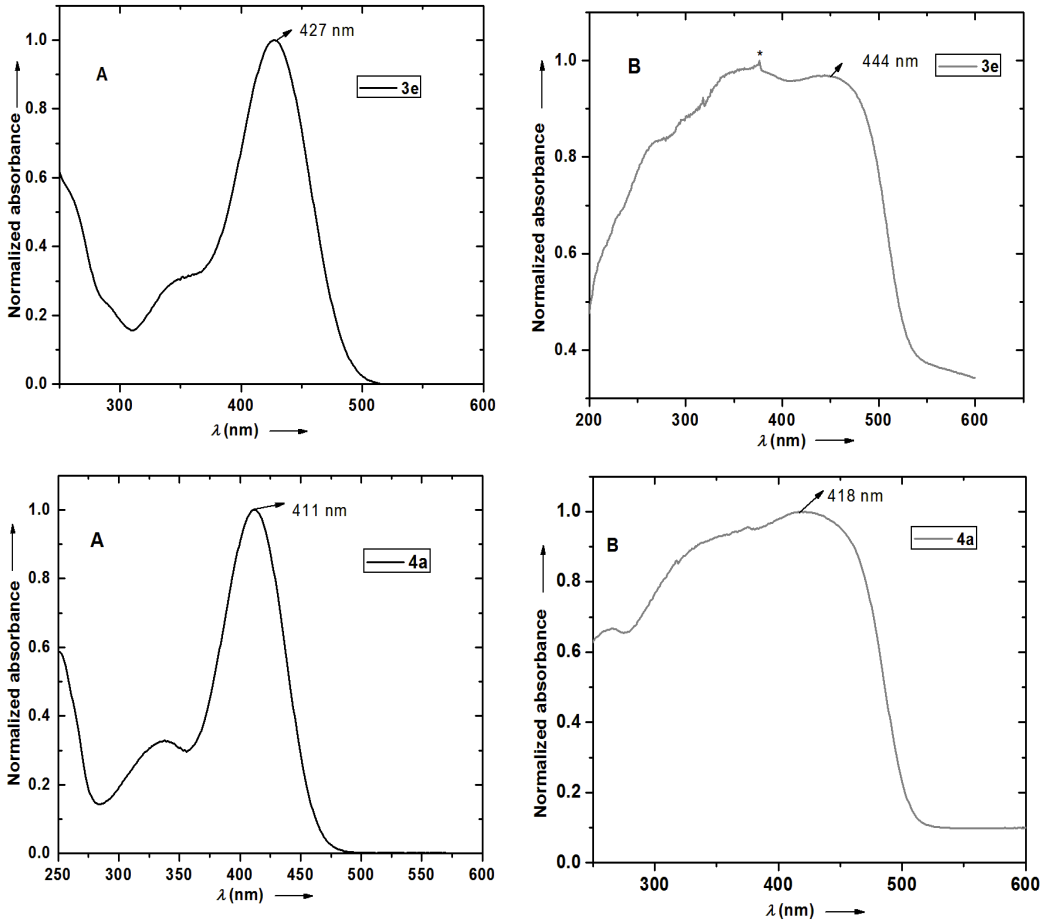

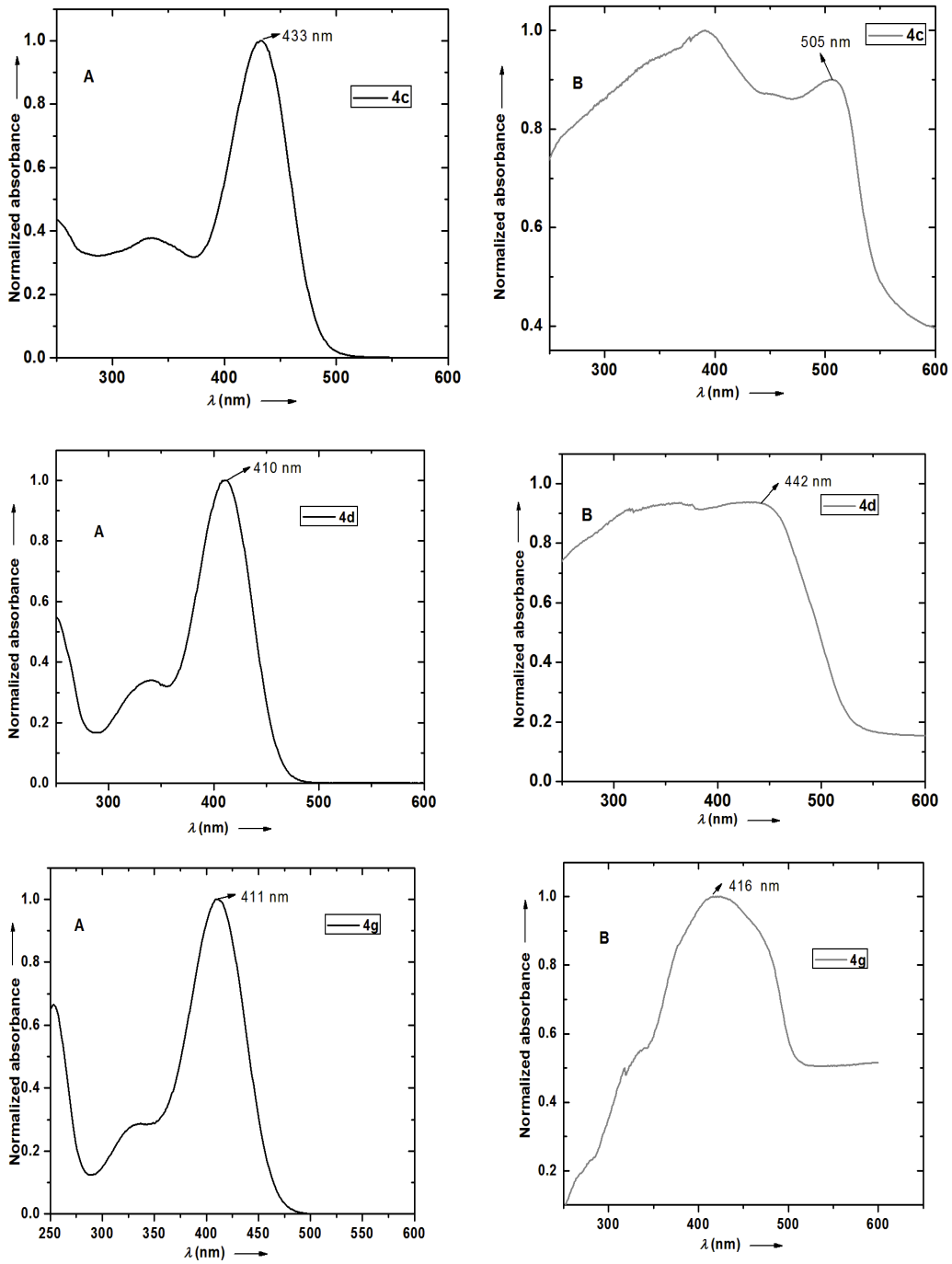

Figure A5. (*Left*): Normalized UV-vis profiles recorded in CH_2Cl_2 at RT for comparison (spectral charts **A**). (*Right*): Electronic absorption spectra of selected solid samples (**3e**, **4a**, **4c**, **4d** and **4g**) recorded by diffuse reflectance method (spectral charts **B**). *denotes instrumental artefact.

6.6 Aggregation-induced Emission (AIE) study on 2b.

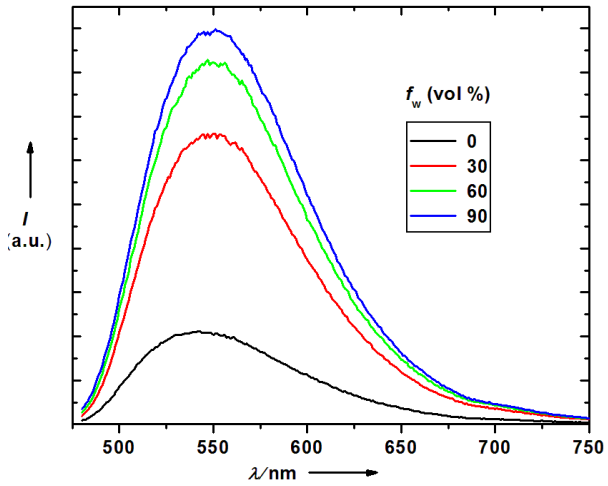

Figure A6. Photoluminescence spectra of **2b** in THF/H_2O mixtures (c = 1.0 x 10^{-5} M, excited at 447.0 nm) with different volumetric fractions of H_2O (f_w).

6.7 X-ray crystallographic details.

Table A1. Selected bond distances (Å) and angles (°).

Complex **3d.**			
B(1)-F(1)	1.3959(18)	B(1)-F(2)	1.3903(18)
B(1)-N(1)	1.551(2)	B(1)-N(2)	1.552(2)
N(1)-B(1)-N(2)	109.03(11)	F(1)-B(1)-F(2)	107.63(12)
C(2)-C(4)-C(5)-C(6)	55.34 (17)		
dihedral angle between the least-squares planes 1 and 2*			54.75(6)
**plane 1 = C3-N2-B1-C18, plane 2 = C18-C19-C20-C21-C22-C23*			

Complex **3e.**			
B(2)-F(4)	1.375(4)	B(2)-F(5)	1.395(4)
B(2)-N(4)	1.540(3)	B(2)-N(3)	1.556(3)
N(3)-B(2)-N(3)	107.5(2)	F(4)-B(2)-F(5)	110.3(2)
B(1)-F(1)	1.391(4)	B(1)-F(2)	1.390(3)
B(1)-N(1)	1.542(4)	B(1)-N(2)	1.550(3)
N(1)-B(1)-N(2)	108.1(2)	F(1)-B(1)-F(2)	109.6(2)

Torsional angles. C(2)-C(4)-C(5)-C(6) 57.5(3)

C(27)-C(29)-C(30)-C(31) 55.0(3)

dihedral angle between the least-squares planes 1a and 2a* 46.73(11)

dihedral angle between the least-squares planes 1b and 2b* 51.28(12)

**plane 1a = C3-N2-B1-C19, plane 2a = C19-C20-C21-C22-C23-C24, plane 1b = C28-N4-B2-C44, and plane 2b = C44-C45-C46-C47-C48-C49*

Complex **4c**			
B(1)-F(1)	1.392(3)	B(1)-F(2)	1.388(3)
B(1)-N(3)	1.546(3)	B(1)-N(1)	1.564(2)
N(1)-B(1)-N(3)	109.86(14)	F(1)-B(1)-F(2)	109.45(16)

Torsional angle C(14)-C(15)-O(5)-C(18) 59.22(18)

Dihedral angle: mean plane 1: C(16)-N(1)-B(1)-C1 77.84(6)

mean plane 2: C1-C(2)-C(3)-C4-C5-C6

Complex **4e**			
B(1)-F(1)	1.381(2)	B(1)-F(2)	1.394(2)
B(1)-N(1)	1.544(2)	B(1)-N(2)	1.568(2)
N(1)-B(1)-N(2)	108.51(12)	F(1)-B(1)-F(2)	109.50(13)
Torsional angle. C(2)-C(4)-O(1)-C(5) 59.16(17)			
Dihedral angle. mean plane 1: C(3)-N(2)-B(1)-C17 mean plane 2: C17/C22			62.86(7)

Complex **4g**			
B(1)-F(1)	1.3994(17)	B(1)-F(2)	1.3870(16)
B(1)-N(1)	1.5432(17)	B(1)-N(2)	1.5626(17)
N(1)-B(1)-N(2)	108.89(10)	F(1)-B(1)-F(2)	109.06(10)
Torsional angle. C(2)-C(4)-O(1)-C(5) 55.77(15)			
Dihedral angle. mean plane 1: C(3)-N(2)-B(1)-C18 mean plane 2: C18/C23			78.49(5)

Table A2. *Crystallographic data for compounds* **3d**, **3e**, **4c**, **4e** and **4g**.

	3d	**3e**	**4c**
empirical formula	$C_{23}H_{16}BF_5N_2$	$C_{25}H_{22}BF_3N_2O_2$	$C_{22}H_{15}BF_2N_4O_5$
formula weight ($g \cdot mol^{-1}$)	426.19	450.26	464.19
temperature (K)	183(2)	183(2)	183(2)
wavelength (Å)	0.71073	0.71073	0.71073
crystal system, space group	monoclinic, $P\ 2_1/c$	triclinic, P -1	orthorhombic, $P\ n\ a\ 2_1$
a (Å)	9.1811(3)	9.7583(4)	14.9386(5)
b (Å)	24.8437(5)	14.3235(6)	5.5933(1)
c (Å)	9.3799(3)	16.1431(9)	23.1884(8)
α (deg)	90	100.301(4)	90
β (deg)	117.306(4)	103.513(4)	90
γ (deg)	90	96.317(3)	90
volume ($Å^3$)	1901.08(12)	2131.19(17)	1937.53(10)
Z, density (calcd) ($Mg \cdot m^{-3}$)	4, 1.489	4, 1.403	4, 1.591
abs coefficient (mm^{-1})	0.122	0.106	0.127
F(000)	872	936	952
crystal size (mm^3)	0.43 x 0.17 x 0.11	0.34 x 0.06 x 0.03	0.46 x 0.34 x 0.10
θ range (deg)	2.63 to 28.27	2.64 to 26.37	2.73 to 30.51
reflections collected	11185	24320	16664
reflections unique	4716 / R_{int} = 0.0245	8706 / R_{int} = 0.0638	5768 / R_{int} = 0.0292
completeness to θ (%)	99.9	99.9	100.0
absorption correction	analytical	analytical	analytical
max/min transmission	0.987 and 0.967	0.997 and 0.980	0.988 and 0.960
data / restraints / parameters	3759 / 0 / 280	5199 / 0 / 599	4931 / 1 / 307
goodness-of-fit on F^2	1.029	1.038	1.047
final R_1 and wR_2 indices [$I > 2\sigma(I)$]	0.0449, 0.0945	0.0678, 0.1001	0.0437, 0.0963
R_1 and wR_2 indices (all data)	0.0612, 0.1043	0.1310, 0.1183	0.0554, 0.1033
largest diff. peak and hole ($e \cdot Å^{-3}$)	0.273 and -0.251	0.224 and -0.259	0.254 and -0.218

The unweighted R-factor is $R_1 = \sum(Fo - Fc)/\sum Fo$; $I > 2\sigma(I)$ and the weighted R-factor is $wR_2 = \{\sum w(Fo^2 - Fc^2)^2/\sum w(Fo^2)^2\}^{1/2}$

	4e	**4g**
empirical formula	$C_{24}H_{15}BF_4O$	$C_{24}H_{20}BF_3N_2O$
formula weight ($g \cdot mol^{-1}$)	406.17	420.23
temperature (K)	183(2)	183(2)
wavelength (Å)	0.71073	0.71073
crystal system, space group	monoclinic, $P\,2_1/c$	monoclinic, $P\,2_1/n$
a (Å)	14.9370(6)	13.9081(3)
b (Å)	8.6228(3)	8.2320(3)
c (Å)	15.4666(6)	17.5333(4)
α (deg)	90	90
β (deg)	110.333(4)	98.086(2)
γ (deg)	90	90
volume ($Å^3$)	1867.95(12)	1987.46(10)
Z, density (calcd) ($Mg \cdot m^{-3}$)	4, 1.444	4, 1.404
abs coefficient (mm^{-1})	0.114	0.105
F(000)	832	872
crystal size (mm^3)	0.48 x 0.21 x 0.10	0.52 x 0.14 x 0.05
θ range (deg)	2.68 to 28.28	2.74 to 30.51
reflections collected	13139	33031
reflections unique	4641 / R_{int} = 0.0295	6061 / R_{int} = 0.0378
completeness to θ (%)	100.0	100.0
absorption correction	analytical	analytical
max/min transmission	0.989 and 0.968	0.994 and 0.956
data / restraints / parameters	3488 / 0 / 281	4807 / 0 / 282
goodness-of-fit on F^2	1.048	1.021
final R_1 and wR_2 indices [$I > 2\sigma(I)$]	0.0671, 0.1961	0.0494, 0.1210
R_1 and wR_2 indices (all data)	0.0879, 0.2121	0.0661, 0.1307
largest diff. peak and hole ($e \cdot Å^{-3}$)	0.735 and -0.241	0.280 and -0.322

The unweighted R-factor is $R_1 = \sum(Fo - Fc)/\sum Fo$; $I > 2\sigma(I)$ and the weighted R-factor is $wR_2 = \{\sum w(Fo^2 - Fc^2)^2/\sum w(Fo^2)^2\}^{1/2}$

6.8 Cyclic voltammograms of selected complexes

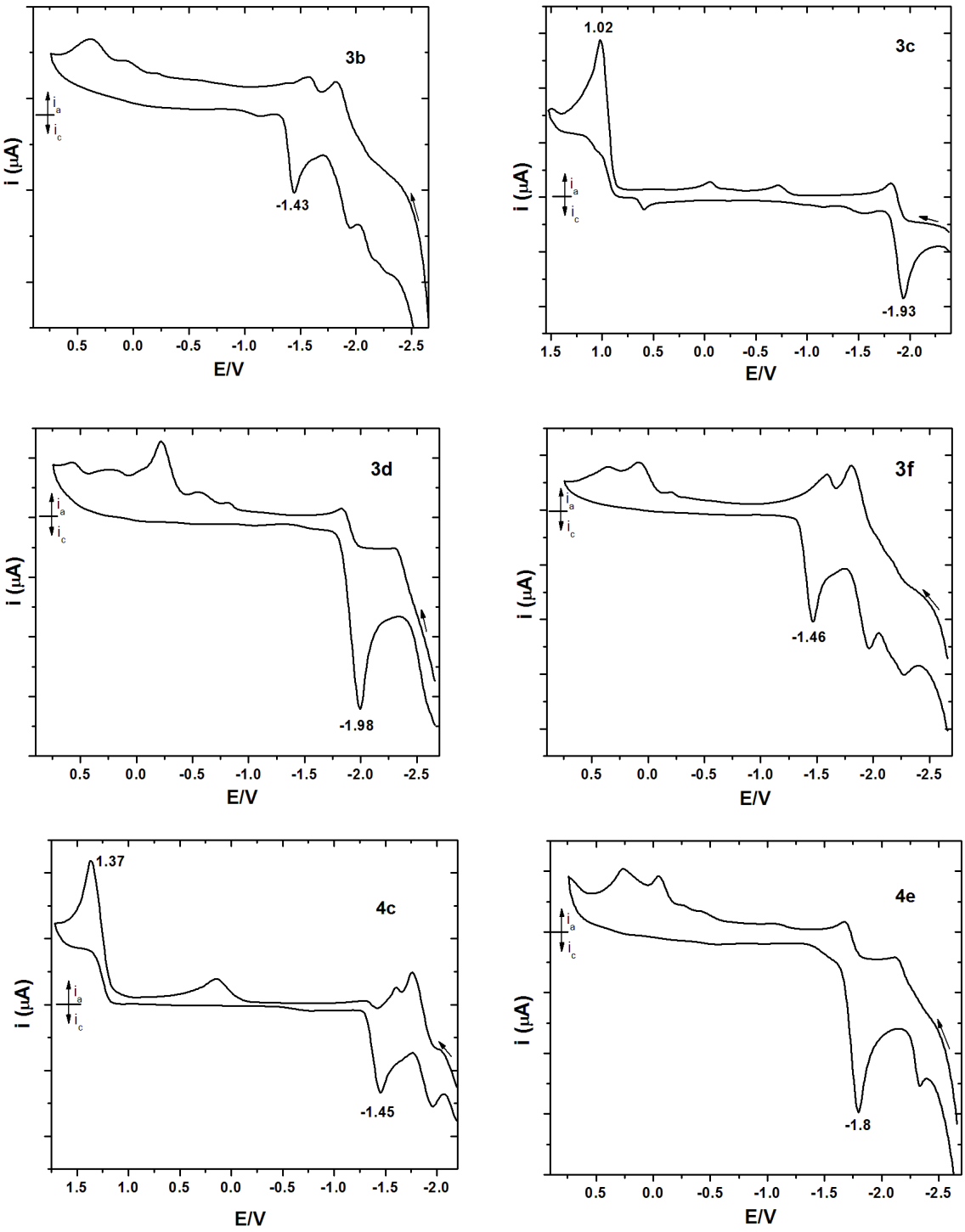

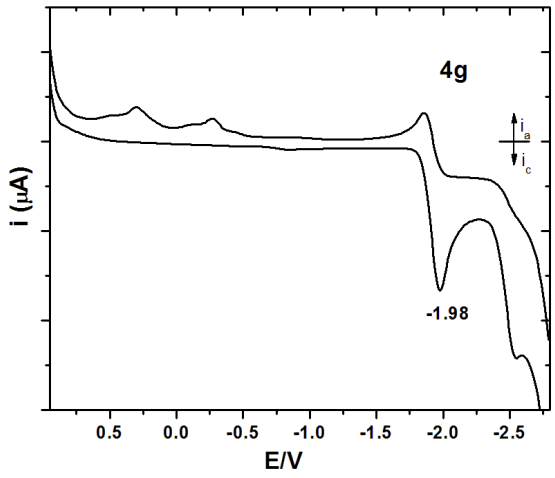

Figure A7. Cyclic voltammogram of **3b**-**3d**, **3f**, **4c**, **4e** and **4g** in 0.1M [nBu_4N][PF_6]; Au electrode; E *vs* $Fc^{0/+}$; scan rate = 100 mV/s; 20 ºC; CH_2Cl_2.

7.0 References

[1] Karthikeyan P.; Kabilan S. *Department of Chemistry, Annamalai University, Annamalai Nagar, Chidambaram - 608 002, India*.

[2] Karthikeyan. P.; Garg, J. A.; Blacque, O.; Saiganesh, R.; Kabilan. S.; Balasubramanian. K. K.; Venkatesan. K. *Submitted.*

[3] (a) Rao, Y.-Li.; Wang, S. *Inorg. Chem.* **2011**, *50* (24), 12263. (b) Wang, S. *Coord. Chem. Rev*. **2001**, *215*, 79. (c) Entwistle, C. D.; Marder, T. B. *Angew. Chem. Int. Ed.* **2002**, *41*, 2927. (b) Entwistle, C. D.; Marder, T. B. *Chem. Mater.* **2004**, *16*, 4574. (d) Fukazawa, A.; Yamaguchi, S. *Chem.–Asian J.* **2009**, *4*, 1386. (e) Piers, W. E.; Bourke, S. C.; Conroy, K. D. *Angew. Chem. Int. Ed*. **2005**, *44*, 501.

[4] For selected papers see (a) Ulrich, G.; Ziessel, R.; Harriman, A. *Angew. Chem. Int. Ed.* **2008**, *47*, 1184. (b) Loudet, A.; Burgess, K. *Chem. Rev.* **2007**, *107*, 4891. (c) Umezawa, K.; Nakamura, Y.; Makino, H.; Citterio, D.; Suzuki, K. *J. Am. Chem. Soc.* **2008**, *130*, 1550. (d) Killoran, J.; Allen, L.; Gallagher, J. F.; Gallagher, W. M.; O'Shea, D. F. *Chem. Commun.* **2002**, 1862. (e) Gorman, A.; Killoran, J.; O'Shea, C.; Kenna, T.; Gallagher, W. M.; O'Shea, D. F. *J. Am. Chem. Soc.* **2004**, *126*, 10619. (f) Ziessel, R.; Ulrich, G.; Harriman, A. *New J. Chem.* **2007**, *31*, 496. (g) Benniston, A. C.; Copley, G. *Phys. Chem. Chem. Phys.* **2009**, *11* (21), 4124. (h) Boens, N.; Leen, V.; Dehaen, W. *Chem. Soc. Rev.* **2012**, *41* (3), 1130. (i) Bellier, Q.; Pegaz, S.; Aronica, C.; Le Guennic, B.; Andraud, C.; Maury, O. *Org. Lett.* **2011**, *13* (1), 22.

[5] Ozdemir, T.; Atilgan, S.; Kutuk, I.; Yildirim, L. T.; Tulek, A.; Bayindir, M.; Akkaya, E. U. *Org. Lett.* **2009**, *11* (10), 2105.

[6] (a) Rao, Y.; Amarne, H.; Wang, S. *Coord. Chem. Rev.* **2012**, *256*, 759. (b) Neue, B.; Fröhlich. R.; Wibbeling, B.; Fukazawa, A.; Wakamiya, A.; Yamaguchi, S.; Würthwein, E.-U. *J. Org. Chem.* **2012**, *77*, 2176. (c) Hayashi, Y.; Obata, N.; Tamaru, M.; Yamaguchi, S.; Matsuo, Y.; Saeki, A.; Seki, S.; Kureishi, Y.; Saito, S.; Yamaguchi, S.; Shinokubo, H. *Org. Lett.* **2012**, *14* (3), 866. (d) Araneda J. F.;

Piers, W. E.; Heyne, B.; Parvez, M.; McDonald, R. *Angew. Chem. Int. Ed.* **2011**, *50*, 12214.

[7] Bourget-Merle, L.; Lappert, M. F.; Severn, J. R. *Chem. Rev.* **2002**, *102* (9), 3031.

[8] Macedo F. P.; Gwengo. C.; Sergey L. V.; Smith M. D.; Gardinier J. R. *Eur. J. Inorg. Chem.* **2008**, 3200.

[9] (a) Liu, X. M.; Gao, W.; Mu, Y.; Li, G. H.; Ye, L.; Xia, H.; Ren, Y.; Feng, S. H.; *Organometallics* **2005**, *24*, 1614. (b) Liu, X. M.; Xia, H.; Gao, W.; Ye, L.; Mu, Y.; Su, Q.; Ren, Y. *Eur. J. Inorg. Chem.* **2006**, 1216. (c) Ren, Y.; Liu, X. M.; Gao, W.; Xia, H.; Ye, L.; Mu, Y. *Eur. J. Inorg. Chem.* **2007**, 1808. (d) Li, Z.; Dong, Y. Q.; Mi, B. X.; Tang, Y. H.; Haussler, M.; Tong, H.; Dong, Y. P.; Lam, J. W. Y.; Ren, Y.; Sung, H. Y.; Wong, K. W.; Gao, P.; Williams, I. D.; Kwok, H. S.; Tang, B. Z. *J. Phys. Chem. B* 109, **2005**, 10061.

[10] (a) Balasubramanian, K. K.; Bindumadhavan, G. V.; Nair, M.; Venugopalan, B. *Synthesis* **1977**, 611. (b) Swaminathan, K. S.; Ganesh, R. S.; Venkatachalam, C. S.; Balasubramanian, K. K. *Tetrahedron Lett.* **1983**, *24*, 3653. (c) Karthikeyan, P.; Rani, A. M.; Saiganesh, R.; Balasubramanian, K. K.; Kabilan, S. *Tetrahedron* **2009**, *65*, 811. (d) Saiganesh, R.; Balasubramaian, K. K. *Modern Approaches to the Synthesis of O- and N-Heterocycles, Research signpost*: 2007; Vol. 3, pp 365.

[11] Thalladi, V. R.; Weiss, H. C.; Blaser, D.; Boese, R.; Nangia, A.; Desiraju, G. R. *J. Am. Chem. Soc.* **1998**, *120* (34), 8702.

[12] *Photoinduced Electron Transfer*; Fox, M. A.; Chanon, M., Eds.; Elsevier: Amsterdam, 1988.

[13] Langhals, H.; Potrawa, T.; Nöth, H.; Linti, G. *Angew. Chem. Int. Ed.* **1989**, *28*, 478.

[14] Saito, S.; Nakakura, K.; Yamaguchi, S. *Angew. Chem. Int. Ed.* **2011**, *51*,714-717.

[15] Yang. Y.; Su. X.; Carroll. C.; Aprahamian. I. *Chem. Sci.* **2012**, *3*, 610.

[16] Czerwieniec, R.; Yu, J. B.; Yersin, H. *Inorg. Chem.* **2011**, *50* (17), 8293.

[17] Ren, Y.; Lam, J. W.; Dong, Y.; Tang, B. Z.; Wong, K. S. *J. Phys. Chem. B.* **2005**, *109*, 1135.

[18] Pommerehne, J.; Vestweber, H.; Guss, W.; Mahrt, R. F.; Bässler, H.; Porsch, M.; Daub, J. *Adv. Mater.* **1995**, *7*, 551. The LUMO levels were estimated based on the fact that the reduction potential ($E_{1/2}$) of ferrocene corresponds to 4.80 eV.

[19] Demas, J. N.; Crosby, G. A.; *J. Phys. Chem.* **1971**, *75*, 991.

[20] deMello, J. C.; Wittmann, H. F.; Friend, R. H. *Adv. Mater.* **1997**, *9* (3), 230.

SUMMARY

Metal-organic complexes continue to evoke interest in applications that demand light emission. Although, photoluminescent (PL) transition metal complexes are known for decades, there are only a handful of 'privileged fragments' particularly with Ir(III) and Pt(II) metal centers, which are compatible with the current fabrication processes in a device such as OLED. Earlier, the emissive material in OLED comprised of purely organic molecules, which were typically fluorescent in nature at the operational temperature. Recently, the fact that phosphorescent metal-organic complexes can quadruple the luminous efficiency of OLEDs has stimulated a lot of research interest in this topic. The ability of 4d/5d transition metals to exhibit profound spin-orbit coupling (SOC) in a phenomenon termed 'Heavy-metal' atom effect is mainly responsible for the improved efficiency. In this regard, the use of heavier metal ions such as Ir(III) and Pt(II) encompassed in a coordination sphere of cyclometalated organic ligand have been identified to generate appropriate excited state lifetime suitable for incorporation into light emitting devices. From a molecular orbitals (MO) perspective, the realization of short and optimal lifetime in the sub/microsecond regime (ca. 0.5-20 μs) has been directly attributed to the contribution from the metal in the lowest emitting excited state. Therefore, the popularity of Ir(III) and Pt(II) fragments is due to the increased metal-to-ligand charge transfer (MLCT) characteristics. In stark contrast, all the precedent literature on Au(I)/Au(III) complexes have emphasized the domination of ligand centered emission characteristics. Adding to this, the under-exploration of photoluminescence in gold complexes can be further ascribed to the following prevalent notions: (i) The presence of non-emissive low-lying 'd-d' ligand field states of anti-bonding character (ii) Low thermodynamic stability of the incumbent molecules due to the strong electrophilicity and oxidizing nature of gold.

In 2005, Yam and co-workers, demonstrated room temperature phosphorescence (RTP) in a family of cyclometalated tridentate (C^N^C)Au(III) complexes suitable for incorporation into devices. The use of strong σ-donating carbanionic ligands (C^-) was hypothesized to be the reason for this phenomenon.

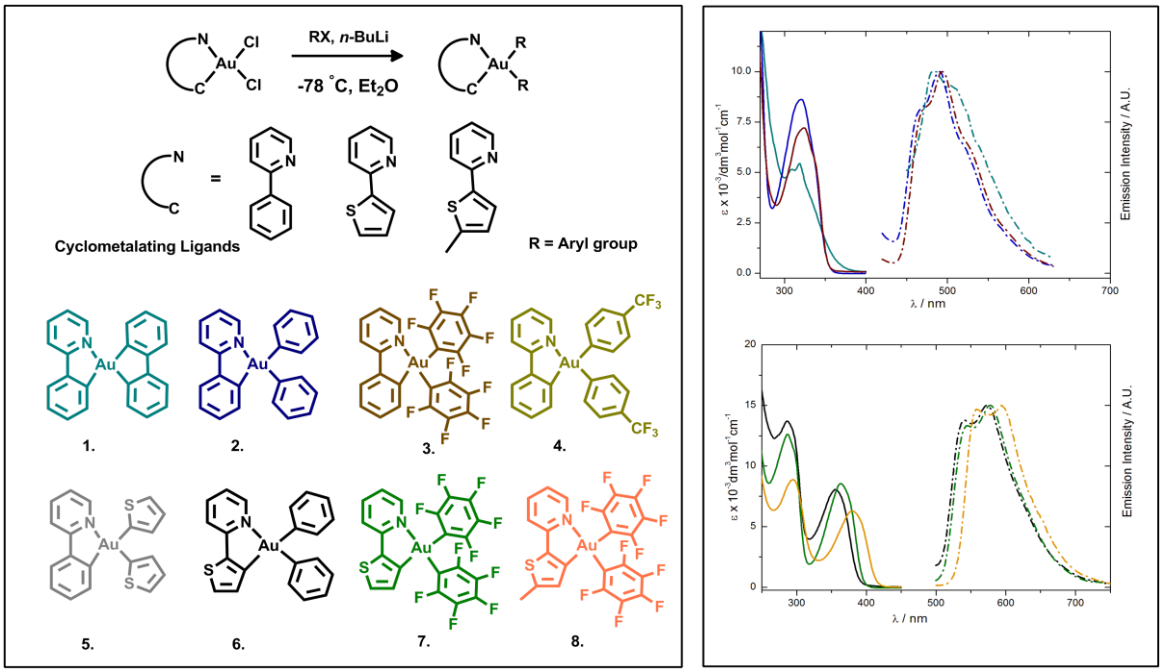

Figure 1. Some examples of synthesized complexes (*left*) and UV-vis and PL profiles in degassed CH_2Cl_2 at RT with uniform color codes (*right*).

In pursuant with the working hypothesis of creating cyclometalated gold complexes enriched with metal-carbon bonds, a novel class of neutral cyclometalated Au(III) complexes of the type *cis*-[(N^C)AuL$_n$] (L = aryl, n = 1, 2) with a bidentate core was synthesized (Figure 1, *left*) for the first time (Chapter 2).

To the best of our knowledge, the method of substitution, using aryl cabanions generated *via* a halogen exchange lithiation strategy has not been performed in cyclometalated Au(III) chemistry until this work. The stability of these complexes was found to be dependent on the nature of aryl ligands. Complexes containing fluorinated groups, for example **3**, **4**, **7** and **8** (Figure 1) were found to be more stable as compared to the non-fluorinated ones and showed no signs of decomposition either in fluid or in solid-state. Since reductive elimination is conceivably the major decomposition pathway in these *cis* disposed diaryl complexes, some theoretical insights were gained. Using DFT calculations, the transition states encountered during the intramolecular reductive elimination process of **3** were compared against **2**. The results clearly revealed that the C-

C bond formation in **2** occurs in an earlier stage than **3**. Thereafter, incorporation of ligands containing fluorinated groups was adopted as a general strategy in the stabilization of such classes of Au(III) complexes. In line with our expectations, most of the complexes synthesized exhibited RTP. These were the first known neutral monocyclometalated diaryl complexes which were emissive at room temperature and amenable for emission tunability by changing the cyclometalated cores. The excited state life-times was found to lie in the appropriate range of 0.33 - 4.4 μs, however the quantum yields in fluid media at RT were in the low order of 1.0 - 9.5 x 10^{-3}. To have a better understanding of the emission process, the nature of the excited state was investigated in detail both experimentally and theoretically (TD-DFT calculations). From DFT calculation it was inferred that, for most complexes (except in **1**) the frontier orbitals involved in dominant excitations were exclusively located on the C^N portion of the cyclometalated ligands and were responsible for intra ligand charge transfer (ILCT) type of transition. The quantum yield of certain complexes (**4** and **7**) measured in the solid-state as thin films (2% wt/wt doped on PMMA host matrix) was found to be 2.1% and 2.0% respectively. These values are roughly higher by a factor of ten when compared to their quantum yields in fluid media.

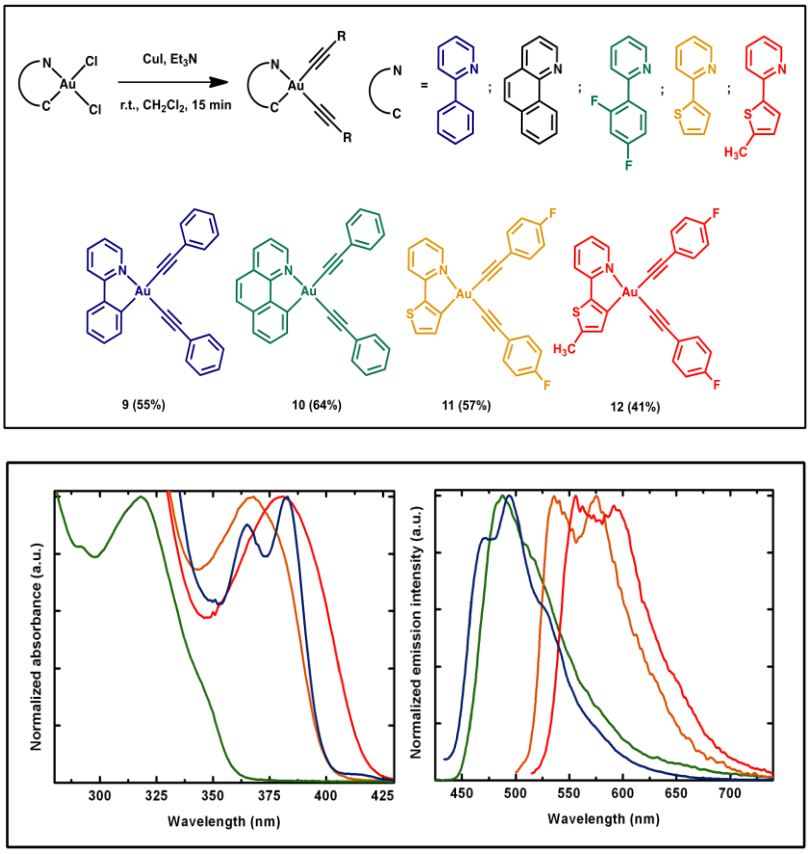

Figure 2. Selected examples of the synthesized gold(III) dialkynyl complexes (*top*). UV-vis and PL profiles recorded in degassed CH_2Cl_2 at RT represented with uniform colour codes (*bottom*).

As a logical extension of this family of complexes (Chapter 3), neutral monocyclometalated Au(III) complexes incorporating σ-alkynyl ligands of the type [Au(C^N)(C≡CR)$_2$] were next synthesized using metathetical substitution involving CuI/DIPA at RT. (Figure 2). Here again, most of the synthesized complexes showed long-lived tunable phosphorescence emission at RT with excited state life times ranging between 1.4 -19.1 μs. The quantum yields were of the order of 10^{-2}, which were higher than their diaryl counterparts. Various photophysical experiments and DFT studies qualitatively suggested limited participation of the metal and alkynyl ligands in the lowest energy emitting state. The nature of the emission was found to be mainly governed by metal-perturbed ^{3}IL(π-π*) transitions originating from the cyclometalated

part of the molecule, and its variation afforded facile tuning of the emission wavelengths. Electrochemical studies - CV measurements of selected complexes showed irreversible redox behavior with near equivalent cathodic peak potential ($E_{p,c}$) for same type of C^N cores. Further, the large electrochemical band gap and metal silent redox attributes supported the experimental observation of limited participation of the metal in the emission process.

With numerous new *N*-heterocyclic carbene ligands with good σ-donating and also π-accepting properties reported in literature, the photophysical properties of a recent class of NHC-ligated Au(I) σ-alkynyl complexes were then investigated (Chapter 4). Different chosen terminal alkynes were deprotonated *in situ* by using a NaOH/MeOH mixture and were subsequently reacted with [(*Bimz*)Au(I)Cl][*Bimz* = 1,3-diisopropylbenzimidazolin-2-ylidene] to form mononuclear, dinuclear and trinuclear Au(I) σ-acetylide complexes. Some selected examples are shown in Figure 3.

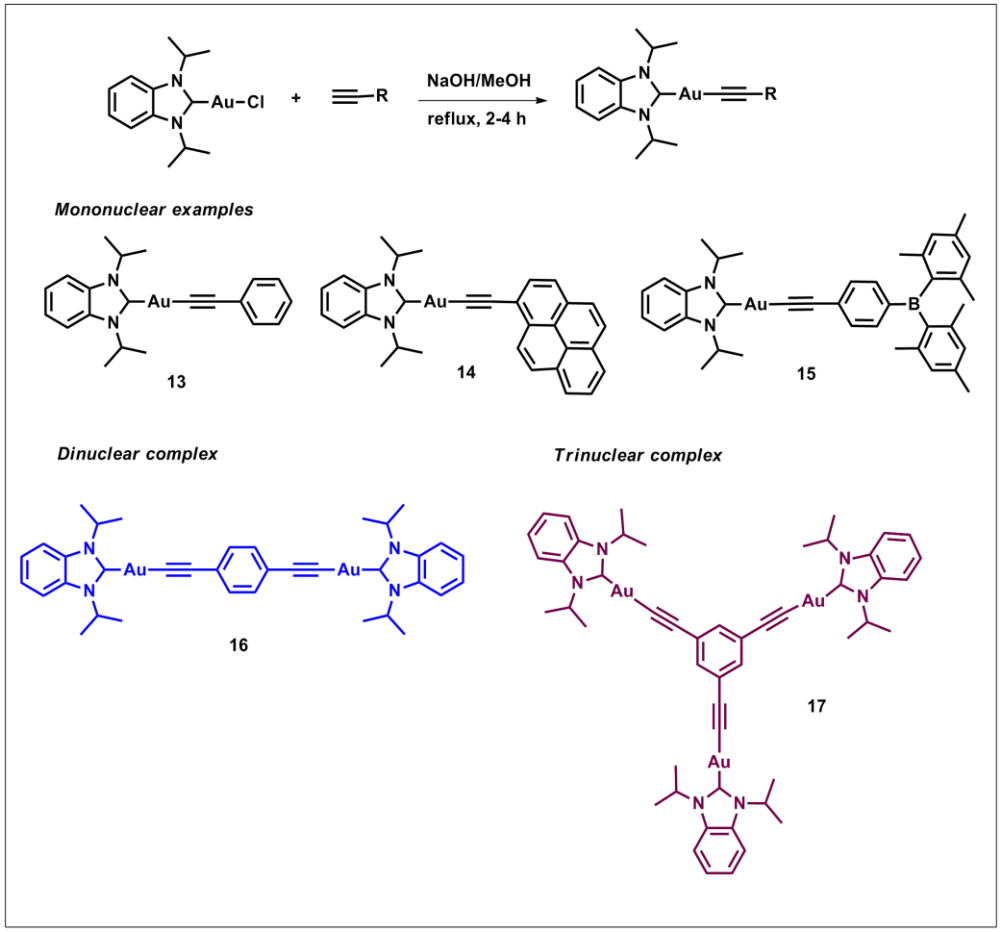

Figure 3. Selected examples of synthesized NHC-Au(I) alkynyl complexes.

The photophysical investigations in this case also revealed the predominant ligand centered nature of emission. However, unlike the case of Au(III) alkynyl complexes, they were found to be quite dependent on the electronic nature of the incorporated acetylides. Since some of the complexes showed unsupported Au···Au (aurophilic) interactions to the extent of ~3.4 Å, several experiments were conducted to verify if this phenomenon had any influence in the solid state quantum yields measured in PMMA thin films. However, no correlation could be drawn. The boron containing complex **15** (Figure 3) showed a remarkable quantum yield of 27% in thin films which is unprecedented in such a class of mononuclear σ-Au(I) acetylide complex with a neutral ligand. TD-DFT calculation revealed that the lowest $S_0 \rightarrow S_2$ excited state transition was of ^{1}ILCT [π-π^*(C≡CR)] character, whereas the second-lowest $S_0 \rightarrow S_n$ (n = 3 or 4) excited state shows

an admixture of ligand-to-ligand ^{1}LLCT [π(carbene)-π*(C≡CR)] and intraligand ^{1}ILCT [π-π*(carbene)] characters. Unlike the previously described Au(III) complexes the metal-center participation in these frontier orbitals were calculated to be at a significant level in the range of 7 to 25%. This was consistent with the experimental observation of improved quantum yields and excited state lifetimes in the sub microsecond regime when recorded at RT.

The next study (Chapter 5) was prompted by the curiosity of testing the photoluminescence behavior of Au(III) complexes containing 2-pyridyl-*N*-heterocycles which precluded cyclometalation. Different N^N chelated Au(III) dichlorides containing 2-pyridyl-*N*-heterocycles namely pyrrole (*pypyr*$AuCl_2$), pyrazole (*pyzpyr*$AuCl_2$), triazole (*trpyr*$AuCl_2$) and tetrazole (*tetpyr*$AuCl_2$) were prepared (Figure 4). Similar to (C^N)Au(III) diaryl complexes in chapter 2, certain (N^N)Au(III) diaryl complexes were prepared and this enabled a direct comparison of the effect of cycloauration. Unlike the cyclometalated complexes encountered in chapter 2, the 2-pyridylpyrrolide Au(III) perfluorodiaryl complexes (Figure 6, **18** and **19**) were completely non-emissive both at RT and at 77 K. Also, the complex with cyanide ligands instead of aryl ligand which was expected to increase the charge transfer character of the metal (MLCT) owing to its π-accepting nature was found to be non-emissive. From a combination of NMR, Raman and electrochemical studies, it is suggested that the high π-delocalization in 2-pyridyl pyrrolide complex such as **18** is responsible for emission quenching due to non-radiative pathways.

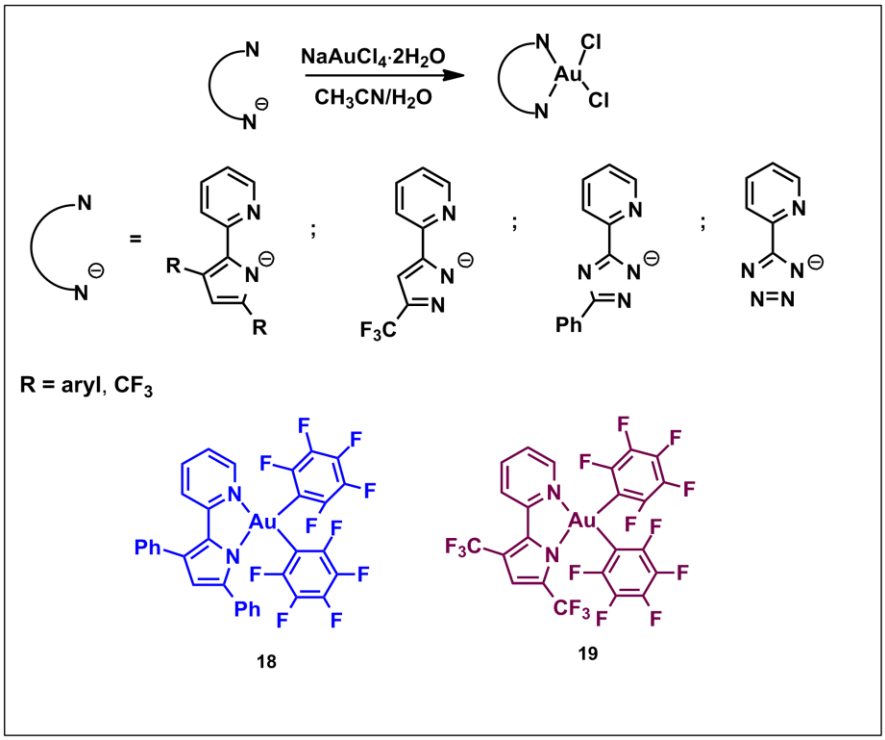

Figure 4. Selected examples of synthesized (N^N)Au(III) diaryl complexes.

With the knowledge acquired from the photophysical behavior of NHC bearing Au(I) acetylide complexes in chapter 4, the possibility for incorporation of such complexes as organometallic monomers units in conjugated polymers was probed in chapter 5. Initial synthetic exploration led to the generation of two novel classes of d^8 square planar complexes involving isoelectronic Pd(II) and Pt(II) metal ions (Figure 5). The novel NHC ligated *trans*-Pd(II) diacetylide complex **20** was luminescent only at 77 K, while the Pt(II) biscarbene bisacetylide complexes of type **21** were emissive both at 77 K and at RT albeit low quantum yields.

In line with our design hypothesis of creating a highly soluble and non-stacking NHC coordinated Au(I) alkynyl monomers, novel synthetic routes were developed to create bulky triptycene based NHC ligand. Following which, it was successfully incorporated into gold using the silver carbene transmetalation route. Further, acetylide incorporation was achieved by the

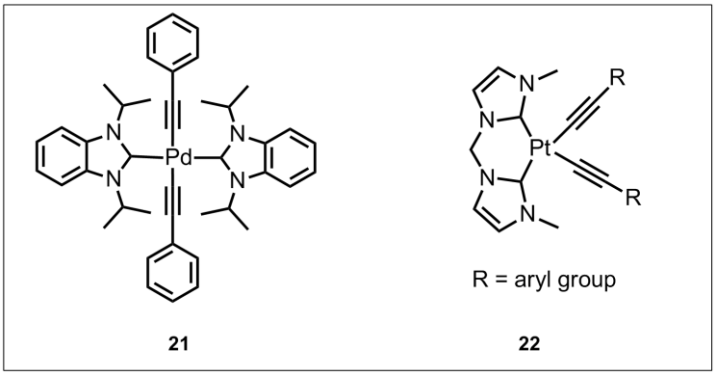

Figure 5. Examples of NHC bearing Pd(II) and Pt(II) σ-alkynyl complexes synthesized.

conditions optimized in chapter 4. Two exemplary and pivotal monomers thus prepared are shown in Figure 6. Complexes **23** and **24** are considered to be suitable for extension as conjugated polymers with palladium mediated cross-coupling and oxidative coupling methods respectively. Some preliminary optimization work has also been carried out in this regard.

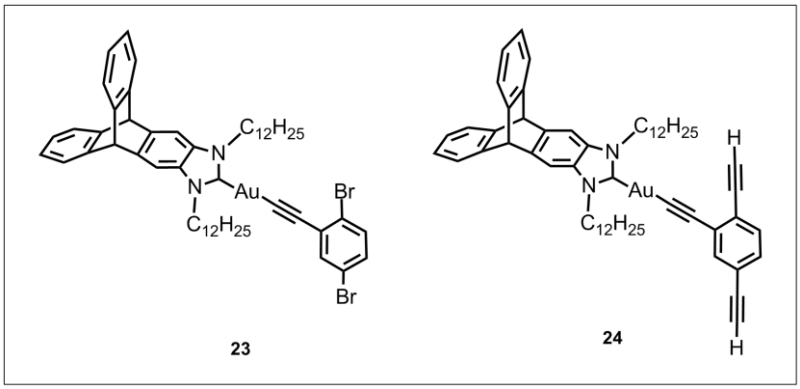

Figure 6. Selected examples of triptycene NHC based Au(I) monomers.

In an isolated study, Chapter 7 details investigations into the photophysical aspects *β*-iminoenamine boron difluoride complexes. The basic skeleton of the investigated complex is represented in figure 7.

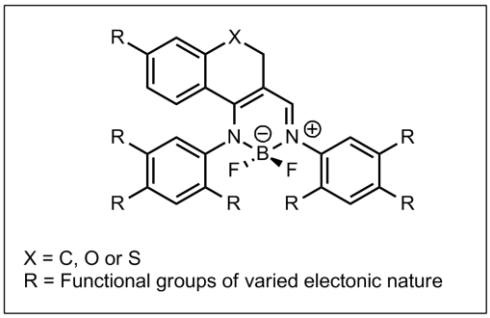

Figure 7. Basic skeleton of the boron difluoride complexes investigated.

These classes of compounds were chosen for investigation because of the following prominent reasons: (1) the use of dissymmetric chromophoric N^N chelating ligand (unlike in the case of popular BODIPY dyes) has been recently realized to effect greater Stokes-shift. (2) Use of aliphatic ring in chromophoric backbone was anticipated to disrupt deleterious π-π stacking effects due to its non-planar conformation. This is expected to be advantageous for emission in the solid state. The evaluated complexes indeed showed fluorescence in the solid state but were nearly non-emissive in the fluid media. Systematic investigations using a combination of low VT-NMR and VT-photoluminescence studies suggested that the rapid conformational motion (ring-flipping) to be the major pathway of non-radiative decay. The boron complexes also constitute a novel class of molecules showing aggregation - induced emission (AIE) phenomenon.

In conclusion, the dissertation work has mainly contributed to the basic understanding of the photophysical aspects of certain class gold complexes in its oxidation state +I and +III. The knowledge acquired herein is expected to help towards improved design and implementation of stable gold metal organic fragments in light emitting devices.

ABSTRACT

Organo transition-metal complexes are being continuously researched for various optoelectronic properties. They are expected to play an important role in energy interconversion schemes like light energy to electrical energy and vice versa. Phosphorescent transition metal-organic complexes are known for decades, however, there are only a select class of cyclometalated Ir(III) and Pt(II) complexes which are known to deliver the quantum efficiency needed for practical application in a optoelectronic device. The improved efficiency is because of strong spin-orbit coupling (SOC) phenomenon which is enhanced to a significant degree due to contribution of the heavy metal in a photophysical relaxation process. Although, gold is a heavy element with a strong spin-orbit coupling potential, it is still under-explored in this regard. Some of the limiting factors includes its strong oxidizing nature, low lying metal centered'd-d' ligand-field states and the overall instability. In this work, research effort has been directed towards overcoming these associated drawbacks. The overriding goal of this dissertation work has been to gain deeper understanding of the photophysical processes in certain class of organogold complexes along with judicious synthetic design. Novel classes of stable and charge neutral monocyclometalated gold(III) complexes comprising of diaryl and diacetylide ligands complexes that are photoluminescent at room temperature have been developed. Non-cyclometalated monoanionic gold(III) fragments containing different nitrogen heterocycles have been synthesized and their photophysical behavior have been evaluated. *N*-heterocyclic carbene coordinated gold(I) alkynyl complexes have been prepared and its photophysical attributes have also been studied systematically. Moreover, these fragments have been synthetically modified to suit for incorporation in conjugated polymers, which are expected to be phosphorescent in nature. In conclusion the work has contributed to the field of organo gold complexes and its application towards light emitting devices.

Zusammenfassung

Organische Übergangsmetallkomplexe werden fortlaufend auf Grund ihrer verschiedenen optoelektronischen Eigenschaften untersucht. Es wird von ihnen erwartet, eine wichtige Rolle in der Umwandlung von Lichtenergie zu elektrischer Energie und umgekehrt zu spielen. Obwohl phosphoreszierende organische Übergangsmetallkomplexe seit Jahrzehnten bekannt sind, erreichen nur wenige Klassen von cyclometallierten Ir(III)- und Pt(II)-Komplexen Quantenausbeuten, die für praktische Anwendungen in optoelektronischen Apparaten nötigt sind. Die erhöhte Effizienz dieser Molekülklassen ist in der starken Spin-Bahn-Kopplung begründet, welche zu einem wesentlichen Grad durch die Beteiligung des Schwermetalls in dem photophysikalischen Relaxationsprozess verstärkt werden. Obwohl Gold ein Schwermetall mit starkem Spin-Bahn-Kopplungspotential ist, wurde es bislang unter diesem Aspekt nur wenig untersucht. Einige der limitierenden Faktoren umfassen seine stark oxidierende Natur, energetisch tiefliegende metallbasierte „d-d"-Ligandenfeldzustände und die allgemeine Instabilität. In der vorliegenden Arbeit wurde Forschungsaufwand betrieben, um diese Nachteile zu überwinden. Das vorrangige Ziel dieser Dissertationsarbeit ist gewesen, neben dem anspruchsvollen synthetischen Design, ein tieferes Verständnis der photophysikalischen Prozesse in bestimmten Organogoldkomplexen zu erlangen. Neue Klassen von stabilen und ladungsneutralen monocyclometallierten Gold(III)-Komplexen wurden entwickelt. Diese enthalten Diaryl- und Diacetylid-Liganden und zeigen Photolumineszenz bei Raumtemperatur. Nicht-cyclometallierte mono-anionische Gold(III)-Fragmente mit verschiedenen Stickstoff-Heterozyklen wurden synthetisiert und ihr photophysikalisches Verhalten untersucht. N-heterozyklische carben-koordinierte Gold(I)-Alkinkomplexe wurden hergestellt und ihre photophysikalischen Eigenschaften wurden ebenfalls systematisch untersucht.

Zusätzlich wurden diese Fragmente synthetisch modifiziert, um in konjugierte Polymere eingebaut werden zu können, von welchen dann erwartet wird Phosphoreszenz zu zeigen. Schlussendlich hat diese Arbeit zum Bereich der Organogoldkomplexe und ihrer Anwendung hinsichtlich lichtemmitierender Apparate beigetragen.

ACKNOWLEDGEMENTS

I am deeply indebted to many, who helped me in different ways throughout the dissertation work, and without whom it could not have been achieved. First, I thank my supervisor Dr. Koushik Venkatesan for admitting me in his research group. Right from the day one in Zurich, Dr. Koushik has been immensely supportive in all the aspects of my Ph.D life. He is a passionate group leader with a lot of zeal for new ideas in chemistry. I will not forget the long hours of constructive research discussions and his constant inspiration during the highs and lows of my research days.

I thank Prof. Heinz Berke for his unflinching encouragement and support. I really loved his lectures on organometallic chemistry during my course-work and the group excursions. I am also indebted to Prof. Roger Alberto for his valuable support throughout my Ph.D work. Thanks are also due to Prof. Cristina Nevado for accepting to be in my thesis evaluation committee.

I profoundly thank Dr. Olivier Blacque for his huge contribution; all the XRD structure determination and theoretical calculation in the thesis had been performed by him and it helped me to understand my chemistry better. Also, I express my gratitude to Dr. Thomas Fox for NMR support, Dr. Ferdinand Wild for MS measurements, Heinz and Barbara Spring for elemental microanalyses. A lot of thanks are due to Ms. Beatrice Schpihtig, Susanna Sprokkereef, Nathalie Fichter, Dr. Jae Kuoung Pak for their help with the administrative tasks and Mr. Manfred Jöhri for computer related assistance.

I have learned so much from the group members of Prof. Berke and Koushik. Their support and invaluable friendship has helped towards the successful completion of my thesis work in various inexplicable ways. In that respect, I thank all my friends Samir, Subrata, Rajesh, Sergey, Carolina, Rajkumar, Anne, Yuzhen, Gabriel Grieco, Szentkuti, Michael, Franziska, Pascal, Bachman, Dybov and Yangfeng. Thanks a lot also for making my stay in Zurich unforgettable.

I also thank Raúl Balnco Bazaco - an exchange student of Dr. Koushik for support during the initial months of Ph.D. I thank Silvia Rocha from the organic department for her patient help

with the fluorimeter equipment. I express my gratitude to all the undergraduate short-time project students who rendered help at various points of my Ph.D.

I extend my thanks to some of our collaborators, Prof. K. K. Balasubramanian and P. Karthikeyan for their kind cooperation and help.

Financial support from the funds of Förschungs kredit, UZH and Univ. of Zurich (ACI) is highly acknowledged.

Everything would not have been possible without the grace of the almighty God and equally enough patience and endurance from my parents Saraswathi Bai, Narayana Rao and loving sister Jaya Bhavani. Thanks to all of them.

List of metal complexes

- [N^C = 2-(5-methyl-2-thienyl)pyridine][$AuCl_3$]
- [N^C = 2-(5-methyl-2-thienyl)pyridine][$AuCl_2$]
- *cis*-[(N^C)AuL][N^C = 2-phenylpyridine, L = 2,2'-biphenyl]
- *cis*-[(N^C)AuL_2][N^C = 2-phenylpyridine, L = C_6H_5]
- *cis*-[(N^C)AuL_2][N^C = 2-phenylpyridine, L = C_6F_5]
- *cis*-[(N^C)AuL_2][N^C = 2-phenylpyridine, L = C_6H_4-CF_3-*p*]
- *cis*-[(N^C)AuL_2][N^C = 2-phenylpyridine, L = C_4H_3S]
- *cis*-[(N^C)AuL_2][N^C = 2-(2-thienyl)pyridine, L = C_6H_5]
- *cis*-[(N^C)AuL_2][N^C = 2-(2-thienyl)pyridine, L = C_6F_5]
- *cis*-[(N^C)AuL_2][N^C = 2-(5-methyl-2-thienyl)pyridine, L = C_6F_5]
- [N^C = 2-(benzo[*b*]thiophen-2-yl)pyridine][$AuCl_3$]
- [N^C = 2-(benzo[*b*]thiophen-2-yl)pyridine][$AuCl_2$]
- *cis*-[(N^C)AuL_2][N^C = 2-phenylpyridine, L = 1,2,3-trimethoxybenzene]
- *cis*-[(N^C)AuClL][N^C = 2-phenylpyridine, L = naphthalene]
- [(N^C)$AuCl_2$][N^C = 2-(2,4-difluorophenyl)pyridine]
- [(N^C)$AuCl_2$][N^C = benzo[*h*]quinoline][$AuCl_2$]
- [(N^C)AuL_2][N^C = 2-phenylpyridine, L = phenylacetylene]
- [(N^C)AuL_2][N^C = 2-phenylpyridine, L = 1-ethynyl-4-fluorobenzene]
- [(N^C)AuL_2][N^C = 2-phenylpyridine, L = 5-ethynyl-1,2,3-trimethoxybenzene]
- [(N^C)AuL_2][N^C = 2-phenylpyridine, L = 2-ethynylthiophene]
- [(N^C)AuL_2][N^C = 2-phenylpyridine, L = ethynyltrisopropylsilane]
- [(N^C)AuL_2][N^C = 2-phenylpyridine, L = 1-ethynyl-4-(phenylethynyl)benzene]
- [(N^C)AuL_2][N^C = 2-phenylpyridine, L= ethynyltrimethylsilane]
- [(N^C)AuL_2][N^C = 2-phenylpyridine, L = 4-ethynylpyridine]
- [(N^C)AuL_2][N^C = 2-phenylpyridine, L = buta-1,3-diynyltrimethylsilane]
- [(N^C)AuL_2][N^C = 2-phenylpyridine, L = 1-ethynyl-4-methoxybenzene]
- (3,5-difluoro-2-(pyridin-2-yl)phenyl)Hg(II)Cl

- [(N^C)AuL_2][N^C = 2-(2,4-difluorophenyl)pyridine, L = phenylacetylene]
- [(N^C)AuL_2][N^C = benzo[*h*]quinoline, L = phenylacetylene]
- [(N^C)AuL_2][N^C = 2-(2-thienyl)pyridine, L = 1-ethynyl-4-fluorobenzene]
- [(N^C)AuL_2][N^C = 2-(5-methyl-2-thienyl)pyridine, L = 1-ethynyl-4-fluorobenzene]
- [(*Bimz*)Au(I)L][*Bimz* = 1,3-diisopropylbenzimidazoline-2-ylidene, L = phenylethynyl]
- [(*Bimz*)Au(I)L][*Bimz* = 1,3-diisopropylbenzimidazoline-2-ylidene, L = *p*-fluorophenylethynyl]
- [(*Bimz*)Au(I)L][*Bimz* = 1,3-diisopropylbenzimidazoline-2-ylidene, L = *p*-methoxyphenylethynyl]
- [(*Bimz*)Au(I)L][*Bimz* = 1,3-diisopropylbenzimidazoline-2-ylidene, L = 3,4,5-trimethoxyphenylethynyl)]
- [(*Bimz*)Au(I)L][*Bimz* = 1,3-diisopropylbenzimidazoline-2-ylidene, L = 1-ethynyl-4-phenylethynyl]
- [(*Bimz*)Au(I)L][*Bimz* = 1,3-diisopropylbenzimidazoline-2-ylidene, L = 4-pyridylethynyl]
- [(*Bimz*)Au(I)L][*Bimz* = 1,3-diisopropylbenzimidazoline-2-ylidene, L = 4-ethynylphenyl)dimesitylborane]
- [(*Bimz*)Au(I)L][*Bimz* = 1,3-diisopropylbenzimidazoline-2-ylidene, L = 4-pyridylethynyl]
- [{(*Bimz*)Au(I)}$_2$(*Bimz* = 1,3-diisopropylbenzimidazoline-2-ylidene, L = 1,4-diethynybenzene)]
- [{(*Bimz*)Au(I)}$_3$(*Bimz* = 1,3-diisopropylbenzimidazoline-2-ylidene, L = 1,3,5-triethynylbenzene)]
- 2-(3,5-bis(trifluoromethyl)pyrrolyl)pyridinyl·$AuCl_2$
- 2-(3,5-bis(4-fluorophenyl)-pyrrolyl)pyridinyl·$AuCl_2$
- 2-(3, 5-bis(4-(trifluoromethyl)-pyrrolyl)pyridinyl·$AuCl_2$
- [(N^N)Au(C_6H_5)$_2$][N^N = 2-(3,5-bis(trifluoromethyl)-1*H*-pyrrol-2-yl)pyridine]
- [(N^N)Au(C_6H_5)$_2$][N^N = 2-(3,5-diphenyl-1*H*-pyrrol-2-yl)pyridine]
- [(N^N)$AuCl_2$][N^N = 2-(3-(trifluoromethyl)-1*H*-pyrazol-5-yl)pyridine]
- [(N^N)$AuCl_2$][N^N = 2-(5-phenyl-2*H*-1,2,4-triazol-3-yl)pyridine]
- [(N^N)$AuCl_2$][N^N = 2-(1*H*-tetrazol-5-yl)pyridine]

- [(N^N)Au(CN)$_2$][N^N = 2-(3,5-diphenyl-1*H*-pyrrol-2-yl)pyridine]
- *trans*-dibromo-bis(*N*,*N*-dipentylbenzimidazolin-2-ylidene)Pd(II)
- *trans*-[Pd(*bimz*)$_2$(C≡C-C$_6$H$_5$)$_2$][*bimz* = 1,3-diisopropylbenzimidazoline-2-ylidene]
- [Pt(*meim*)$_2$(C≡C-C$_6$H$_5$)$_2$][*meim* = 1,1'-dimethyl-3,3'-methylene-diimidazoline-2,2'-diylidene]
- [Pt(*meim*)$_2$(C≡C-C$_4$H$_3$S)$_2$] [*meim* = 1,1'-dimethyl-3,3'-methylene-diimidazoline-2,2'-diylidene]
- *trans*-dibromo-bis(1,3-dipentyl-2,3-triptyceneimidazolium)Pd(II)
- [1,3-didodecylbenzimidazol-2-ylidene]AuCl
- 1,3-dipentyl-[4,7-dibromobenzimidazolylidene]AuCl
- 1,3-dipentyl[triptyceneimidazolylidene]AuCl
- 1,3-didodecyl[triptyceneimidazolylidene]AuCl
- [(*Bimz*)Au(I)L][*Bimz* = 1,3-diisopropylbenzimidazoline-2-ylidene, L = 1,4-dibromo-2-ethynylbenzene]
- [(*Bimz*)Au(I)L][*Bimz* = 1,3-diisopropylbenzimidazoline-2-ylidene, L = 2-ethynyl-1,4-bis(2-(triisopropylsilyl)ethynyl)benzene]
- [(*n-dodecylbimz*)Au(I)(2-ethynyl-1,4-bis(2-(triisopropylsilyl)ethynyl)benzene)] *n-dodecylbimz* = 1,3-didodecyl[benzimidazolylidene]
- [(*n-dodecylbimz*)Au(I)(1,2,4-triethynylbenzene)] [*n-dodecylbimz* = 1,3-didodecyl[benzimidazolylidene]
- [(*n-pentyltripimz*)Au(I)(1,4-dibromo-2-ethynylbenzene)][*n-pentyltripimz* = 1,3-dipentyl[triptyceneylidene]
- [(*n-dodecyltripimz*)Au(I)(1,4-dibromo-2-ethynylbenzene)][*n-dodecyltripimz* = 1,3-didodecyl[triptyceneylidene]
- [(*n-dodecyltripimz*)Au(I)(2-ethynyl-1,4-bis(2(triisopropylsilyl)ethynyl)benzene)][*n-dodecyltripimz* = 1,3-didodecyl[triptyceneylidene]
- [(*n-dodecyltripimz*)Au(I)(1,2,4-triethynylbenzene)][*n-dodecyltripimz* = 1,3-didodecyl[triptyceneylidene]

- [(*n-dodecylbimz*)Au(I)(2-(4-ethynylphenoxy)ethanol)][*n-dodecylbimz* = 1,3-didodecyl[benzimidazolylidene]
- 1,3-dipentyl-(4,7-dibromobenzimidazolylidene)Au(I)(1-ethynyl-4-fluorobenzene)]
- [(*Bimz*)Au(I)(pentafluorobenzene)][*Bimz* = 1,3-diisopropylbenzimidazoline-2-ylidene]
- [(*Bimz*)Au(III)I_2(pentafluorobenzene)][*Bimz* = 1,3-diisopropylbenzimidazoline-2-ylidene]
- [(*Bimz*)Au(I)(C≡N)][*Bimz* = 1,3-diisopropylbenzimidazoline-2-ylidene]
- [(*Bimz*)Au(III)I_2(C≡N)][*Bimz* = 1,3-diisopropylbenzimidazoline-2-ylidene]
- [(*Bimz*)Au(I)L][*Bimz* = 1,3-diisopropylbenzimidazoline-2-ylidene, L = (2-(4-ethynylphenyl)ethynyl)triisopropylsilane)]
- [(*Bimz*)Au(I)L][*Bimz* = 1,3-diisopropylbenzimidazoline-2-ylidene, L = 1,4-diethynylbenzene)]

N. JAI ANAND GARG

Room 34-H-30, Institute of Inorganic Chemistry, University of Zürich

Winterthurerstrasse 190, CH-8057, Zürich, Switzerland

+41-044-6354706, jai.anand@aci.uzh.ch, njagarg@gmail.com

Education

June 2008 – present

Ph.D Chemistry., University of Zurich, Switzerland (June 2008 - present)

Thesis: *Syntheses and photophysical studies of Au(I) and Au(III) metal-organic complexes*.

Advisor: Dr. Koushik Venkatesan, sub-group of Prof. Dr. Heinz Berke.

June 1999 – 2001

M.Sc. Chemistry, Sri Sathya Sai Institute of Higher Learning, Andhra Pradesh, India (1999 – 2001).

May 1996 – 1999

B.Sc. Chemistry, Sri Sathya Sai Institute of Higher Learning, Andhra Pradesh, India (1996 – 1999).

Professional Experience

July 2003 – 2008

Shasun Research Centre: R & D division of an Indian pharmaceutical company. Chennai - 600048, India. URL: *www.shasun.com.*

- Involved in process optimization, planning and executing multistep organic syntheses of Active Pharmaceutical Ingredients (API's) and custom synthesis.

Research Experience

June 2008 – present — Ph.D student in Institute of Inorganic Chemistry, University of Zürich, Switzerland.

- Involved in syntheses of cyclometalated/non-cyclometalated organogold complexes
- Evaluation of solution and solid-state photophysics of small molecule gold complexes.
- Led advanced level inorganic projects for graduate and undergraduate students during the graduate stay.

July 2002 – 2003 — Project Assistant,

Department of Biophysics, University of Madras.

- Involved in extraction, purification and characterization of active ingredients of natural products *(viz. Garcinia mangostana)*

June 1999 – 2001 Masters student

Sri Sathya Sai Institute of Higher Learning, India

- Master thesis entitled '*Preparation of m-phenylenediamine and its azo derivatives- an exploratory study'*

Publications

[1] **Garg**, **J**. **A**.; Blacque, O.; Fox, T.; Venkatesan, K. "Stable and tunable phosphorescent neutral cyclometalated Au(III) diaryl complexes." *Inorg. Chem.* **2010**, *49*, 11463-11472.

[2] Zhang, Y.; **Garg, J**. **A**.; Michelin, C.; Fox, T.; Blacque, O.; Venkatesan, K. "Synthesis and luminescent properties of *cis* Bis-*N*-heterocyclic carbene platinum(II) bis-arylacetylide complexes." *Inorg. Chem*. **2011**, *50*, 1220-1228.

[3] **Garg**, **J**. **A.**; Blacque, O.; Fox, T.; Venkatesan, K. "Syntheses and photophysical properties of luminescent mono-cyclometalated gold(III) *cis*-dialkynyl complexes," *Inorg. Chem.* **2011**, *50*, 5430-5441.

[4] **Garg**, **J**. **A**.; Blacque, O.; Heier, J.; Venkatesan. K. "Benzimidazolin-2-ylidene Au(I) alkynyl complexes-syntheses, structure and photophysical properties," *Eur. J. Inorg. Chem.* **2012**, 1750-1763

[5] Koch, M.; **Garg**, **J**. **A**.; Blacque, O.; Venkatesan. K. "*Trans* bis-*N*-heterocyclic carbene bis-acetylide palladium(II) complexes", *J. Organomet. Chem.*, **2012**, *700*, 154-159.

[6] Karthikeyan, P.; **Garg**, **J**. **A**.; Saiganesh, R.; Kabilan, K.; Balasubramanian, K. K.; Blacque, O.; Venkatesan. K. "β-Iminoenamine-BF_2 Complexes: Aggregation-induced Emission and Pronounced Effects of Aliphatic Ring on and Radiationless Deactivation." *Submitted*

[7] Karthikeyan, P.; **Garg**, **J**. **A**.; Saiganesh, R.; Kabilan, K.; Balasubramanian, K. K. "Azahexatriene Ring Closure: Cyclization of (N-aryl)-(2H)-4-Chlorobenzopyran-3-carboxaldimines to Benzopyrano[4,3-b]quinolines – A Mechanistic and Synthetic study." *Submitted*

[8] Venkatesan, K.; **Garg, J. A**. "Cyclometalated Au(III) Complexes Suitable for Electroluminescent Devices" EP Patent Application EP10190765(10/11/2010).